

Coral Reefs and Sea-Level Change: Quaternary Records and Modelling

Edited by
Gilbert F. Camoin
and Nadine Hallmann

Series Editor
Elias Samankassou

Special Publication 49
of the International
Association of
Sedimentologists

IAS
INTERNATIONAL ASSOCIATION OF SEDIMENTOLOGISTS

CORAL REEFS AND SEA-LEVEL CHANGE: QUATERNARY RECORDS AND MODELLING

A publication of the International Association of Sedimentologists

Coral Reefs and Sea-Level Change: Quaternary Records and Modelling

EDITED BY

Gilbert F. Camoin

Aix Marseille University, CNRS, IRD, INRAE, CEREGE, CEREGE, Europôle Méditerranéen de l'Arbois, BP80, 13545 Aix-en-Provence cedex 4, France

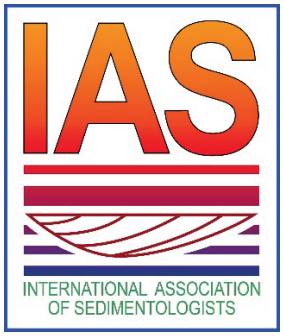
Nadine Hallmann

Aix Marseille University, CNRS, IRD, INRAE, CEREGE, CEREGE, Europôle Méditerranéen de l'Arbois, BP80, 13545 Aix-en-Provence cedex 4, France

SERIES EDITOR

Elias Samankassou

Department of Earth Sciences, University of Geneva, Rue des Maraichers 13, CH-1205 Geneva, Switzerland



The editors of this volume gratefully acknowledge the support of the Society of Sedimentary Geology (SEPM), in particular that of Howard Harper, Executive Director, Theresa Scott, Associate Director and Business Manager, and Michele Tomlinson, Managing Editor of SEPM Special Publications. The Series Editor thanks Adam Corres for the careful editing.

This edition first published 2022 ©2022 by International Association of Sedimentologists, an international non-profit organisation.

Registered address: International Association of Sedimentologists, c/o Ghent University, Department of Geology, Campus Sterre, Building S8, Krijgslaan 281, 9000 Gent, Belgium.

The right of the authors to be identified as the authors of this work has been asserted in accordance with the UK Copyright, Designs and Patents Act 1988.

All rights reserved. No part of this publication may be reproduced, stored in a retrieval system, or transmitted, in any form or by any means, electronic, mechanical, photocopying, recording or otherwise, except as permitted by the UK Copyright, Designs and Patents Act 1988, without prior permission of the publisher.

Designations used by companies to distinguish their products are often claimed as trademarks. All brand names and product names used in this book are trade names, service marks, trademarks or registered trademarks of their respective owners. The publisher is not associated with any product or vendor mentioned in this book. The publication is designed to provide accurate and authoritative information in regard to the subject matter covered. It is sold on the understanding that the publisher is not engaged in rendering professional services. If professional advice or other expert assistance is required, the services of a competent professional should be sought.

A catalogue record for this book is available from the British Library.

ISBN 978-1-7398845-1-2

Contents

Coral Reefs and Sea-Level Change: Quaternary Records and Modelling. A Window Into the Future. i
Camoin, G.F. and Hallmann, N.

Quaternary coral, coralline algal and vermetid assemblages as sea-level indicators: a review.
Braga, J.-C., Humblet, M., Ramos, D.A.E., Dechnik, B. and Webster, J.M. 1

Microscale evolution of reefal microbialites.
Koyano, S., Shiraishi, F., Miyairi, Y., Yokoyama, Y. and Fujita, K. 39

New insights on the Late Quaternary evolution of Abrolhos reefs, Eastern Brazilian Shelf.
Vieira, L.S., Bastos, A.C., Dechnik, B., Braga, J.-C., Moura, R.L., D'Agostini, D.P., Moraes, F.C. and Webster, J.M. 69

Late Pleistocene-Holocene Evolution of Malé Island (North Malé Atoll Rim, Republic of Maldives).
Yildirim, T., Droxler, A.W., Gischler, E., Naar, D.F., Yokoyama, Y., Montagna, P. and Pons-Branchu, E. 101

Shelf-edge deglacial reef establishment and subsequent partial demise: Response to distinct pulses of sea-level rise associated with environmental changes.
Harper, B.B., Droxler, A.W., Webster, J.M., Montagna, P., Yokoyama, Y., Humblet, M., Jorry, S.J., Beaufort, L., Tachikawa, K., Bard, E. and Pons-Branchu, E. 141

How reefs drown: A case study from the Northwest Hawaiian Islands.
Toomey, M., Sandstrom, M., Magette, E. and Cronin, T. 173

Reef growth history at intermediate to mesophotic depths since the end of the Last Glacial period along the Great Barrier Reef shelf edge.
Humblet, M., Webster, J.M., Yokoyama, Y., Braga, J.-C., Fujita, K., Iryu, Y., Fallon, S.J. and Thompson, W.G. 189

Coral reef development and sea-level changes over the past 50,000 years: new evidence from the north-west shelf of Australia.
Webster, J.M., Dechnik, B., Sanborn, K., Yokoyama, Y., Braga, J.-C., Renema, W., Humblet, M., Beaman, R.J., Nothdurft, L.D., Webb, G.E., Zhao, J.-X., Murphy, R.J., Gallagher, S.J., O'Leary, M. and Paumard, V. 215

Neogene and Quaternary reef terraces of Mangaia, Rarotonga and Aitutaki (southern Cook Islands, South Pacific) revisited: gauges of sea-level change and island uplift?
Gischler, E., Meyer, G., Braga, J.-C., Riechelmann, S., Immenhauser, A. and Eisenhauer, A. 275

CORAL REEFS AND SEA-LEVEL CHANGE: QUATERNARY RECORDS AND MODELLING. A WINDOW INTO THE FUTURE.

GILBERT F. CAMOIN* and NADINE HALLMANN*

**Aix Marseille University, CNRS, IRD, INRAE, CEREGE, CEREGE, Europôle Méditerranéen de l'Arbois, BP80, 13545 Aix-en-Provence cedex 4, France*

INTRODUCTION

Trying to better predict the timing and the magnitude of future sea-level rise and the related changes in the hydrological cycle are the most pressing challenges for human societies due to uncertainties concerning the vulnerability and sensitivity of ice sheets to global warming. Geological records during past higher and/or rising sea-levels can provide a baseline of utmost importance to enable future projections with improved accuracy and to better evaluate the impact of rising sea-level on coastal ecosystems. Over the last four decades, considerable progress has been made in understanding the significance of fossil coral reef systems as unique archives of past sea-level, climatic and environmental changes that extend far beyond instrumental records. The re-construction of the impact of these changes on the development, architecture and composition of fossil coral systems provides the opportunity to develop projections regarding the response of coastal systems to future climatic changes, especially during periods typified by rapid sea-level rise and short-term climate excursions.

Following their initial investigations on exposed terraces (Broecker *et al.*, 1968), fossil coral reefs from former sea-level highstands, especially the Last Interglacial period (Marine Isotopic Stage - MIS 5) and the penultimate Interglacial (Marine Isotopic Stage – MIS - 7) from various regions have been used as an independent test of the orbital forcing theory of climate change (e.g. Huon Peninsula, Bermuda, Red Sea; see review in Camoin & Webster, 2015a,b).

Over the last 30 years, a significant advance regarding the use of coral reef records of sea-level and climate changes on various time scales has been made through the drilling of modern coral reef systems. These studies have primarily concerned the reconstruction of Holocene sea-level change and reef development, a time window characterised by rising sea-level (see review in Camoin & Webster, 2015a). However, because the amplitude of Quaternary sea-level changes was in the order of 120 m, the investigation of relict reef features related to former interglacial periods, as well as glacial stages and glacial–interglacial transitions, was made possible by deeper drilling on continental margins and oceanic islands in New Caledonia (Coudray, 1976; Montaggioni *et al.*, 2011), Funafuti (e.g. Ohde *et al.*, 2002), Belize (e.g. Gischler *et al.*, 2010; Purdy *et al.*, 2003) and on the Australian Great Barrier Reef (e.g. Braithwaite & Montaggioni, 2009; Braithwaite *et al.*, 2004), as well as offshore drilling in Barbados (Fairbanks, 1989; Bard *et al.*, 1990; Gallup *et al.*, 2002). Long vertical and deviated drill holes that were carried out throughout the margin of the

©2022 International Association of Sedimentologists

Moruroa atoll, French Polynesia, have provided the unique opportunity to document sea-level changes and reef development on reef systems related to highstands (Holocene, stages 5, 7 and 9) and lowstands (stages 2, 4 and 8) (Camoin *et al.*, 2001; Braithwaite & Camoin, 2011).

The last deglacial sea-level rise (21–6 ka) has been documented in continuous coral reef sequences drilled offshore Barbados (Fairbanks, 1989; Bard *et al.*, 1990; Fairbanks *et al.*, 2005; Peltier & Fairbanks, 2006), Tahiti (IODP Expedition 310; Camoin *et al.*, 2007, 2012; Deschamps *et al.*, 2012; Camoin & Webster, 2015a,b) and the Australian Great Barrier Reef (IODP Expedition 325; Webster *et al.*, 2011, 2018; Yokoyama *et al.*, 2018; Camoin & Webster, 2015a,b). The two IODP expeditions were focused on the reconstruction of sea-level, climatic and environmental changes and the reef response to sea-level and coeval environmental changes during the Last Deglaciation, as described in IODP Proposal #519 (see Camoin *et al.*, 2007). In addition, the Tahiti and Great Barrier Reef IODP expeditions have provided valuable information regarding sea-level positions and insights into the climate system for older periods, such as MIS 3 and the transition between MIS 6 and 5 (Camoin *et al.*, 2007; Thomas *et al.*, 2009; Fujita *et al.*, 2010; Ménabréaz *et al.*, 2010; Webster *et al.*, 2011, 2018; Gischler *et al.*, 2013).

This volume includes case studies dealing with coral reef records of sea-level and environmental changes and the response of coral reef systems to changes affecting their environment at different time scales during the last glacial cycle, from the Last Interglacial (MIS 5) through the Mid-to Late Holocene. They also tackle topics of general interest such as the significance of coralgal communities as archives of sea-level and environmental changes and reef drowning processes.

Coral reef records of sea-level and environmental changes

The use of fossil coral reefs to provide reliable geological estimates of past relative sea-levels relies on the accurate reconstruction of palaeo-water depth during their growth; and precise dating. Over the last three decades, fossil coral reefs have played a pivotal role in Quaternary palaeoceanographic and palaeoclimatologic reconstructions by providing absolute sea-level positions that could be compared to sea-level data derived from isotope and trace element analysis of deep-sea sediment cores.

Tropical reef corals can be dated accurately using multiple dating techniques, including ^{14}C, U/Th, $^{87}/^{86}Sr$, U/Pb and magneto-stratigraphy, which is mandatory to determine positions, the timing and course of Quaternary sea-level changes.

Biological communities associated with tropical coral reef systems have strict ecological requirements. They are generally confined within narrow ecological niches in sufficiently specific depth ranges to be useful as absolute sea-level indicators.

Interpretation of the depth and environmental distribution of fossil reef assemblages relies on the occurrence, zonation and ecology of their modern counterparts, preferably close to the studied fossil reef, and the presumption that similar factors have controlled their distribution in the fossil record. This approach also requires a more quantitative understanding of the distribution of modern reef biota. Earlier reconstructions, such as the Barbados reef record from the Last Deglaciation (Fairbanks,

1989; Bard *et al.*, 1990; Fairbanks *et al.*, 2005; Peltier & Fairbanks, 2006), have been based on the significance of monospecific assemblages of the coral *Acropora palmata*, which is thought to have grown within 5 m of sea-level on shallow reef crests (Lighty *et al.*, 1982). However, other investigations have demonstrated that *Acropora palmata* colonies can live at depths greater than 5 m in modern environments, commonly at 10–5 m (Goreau & Wells, 1967; Hubbard, 2009) and down to 24 m (Zimmer *et al.*, 2006). It seems probable that the modern spatial zonation of this coral species appears as a consequence of the sea-level stability for several millennia and cannot, therefore, be strictly applicable to the conditions that prevailed during the last deglacial sea-level rise (Bard *et al.*, 2016). This casts doubt on the reliability of palaeo-water depth interpretations that have been considered to reconstruct the Barbados sea-level record. More generally, this may question the reliability of other records based on monospecific coral assemblages in similar environmental conditions. Over the last 25 years, whole reef assemblages, including corals and associated biota (i.e. coralline algae, vermetid gastropods and encrusting foraminifera) have increasingly been used to constrain more accurately palaeowater depths and other important environmental parameters (Montaggioni *et al.*, 1997; Cabioch *et al.*, 1999a; Montaggioni, 2005; Abbey *et al.*, 2011, 2013; Camoin *et al.*, 2012; Bard *et al.*, 2016). The Tahiti and Great Barrier Reef sea-level records illustrate the benefit of using whole reef assemblages to reconstruct the water depth and depositional environments during reef development (Camoin *et al.*, 2007, 2012; Abbey *et al.*, 2011, 2013; Webster *et al.*, 2011, 2018).

- Quaternary coral, coralline algal and vermetid assemblages as sea-level indicators: a review, by *Braga, J.-C., Humblet, M., Ramos, D.A.E., Dechnik, B.* and *Webster, J.M.*

In their paper, Braga *et al.* (this vol.) review the significance of corals, coralline algae and vermetid gastropods as indirect relative sea-level indicators in the fossil record, which relies on the information available on the habitats of their living counterparts and the accurate identification of fossil corals and coralline algae at the species or species-group level. They test the reliability of coral, coralline algal and vermetid assemblages that have been extensively used in RSL reconstructions in the light of data from the Ocean Biogeographical Information System and other recently published data. They focus primarily on the Indo-Pacific province, where the occurrence of robust-branching and high-energy encrusting coral assemblages typifies the first 10 m of the water column, when identified by several species, and to the first 6 m when corals are encrusted by thick plants of the coralline alga *Porolithon* gr. *onkodes* and/or dense assemblages of vermetid gastropods on coral and coralline algal surfaces. Concerning the Western Atlantic-Caribbean province, they state that *Acropora palmata* is the most precise RSL marker and no additional components of fossil assemblages improve its palaeodepth information.

In their conclusion, Braga and colleagues emphasise the need to realise quantitative surveys of the modern reef ecology, the acquisition of extensive information of the physical environment at sites close to the studied fossil reefs and the extensive sampling of fossil reefs with cores/sections distributed across different palaeo-environments.

Reef-dwelling organisms are sensitive to subtle ecological changes affecting their environment, such as light conditions, turbidity, water energy and nutrient levels. Environmental changes during coral reef development are frequently reflected by variations in the composition of reef communities that can potentially happen on a short time scale. Since their first description in the postglacial reef sequence of Tahiti (Montaggioni & Camoin, 1993; Camoin & Montaggioni, 1994), microbial fabrics (microbialites) have been the subject of many studies, which demonstrated that these features correspond to an important biological indicator of environmental changes involving increased alkalinity and nutrient availability in interstitial waters bathing the subsurface of the living reef framework (Camoin & Montaggioni, 1994; Camoin *et al.*, 1999, 2006; Camoin & Seard, 2011). Microbialites have been commonly reported in primary cavities ('endostromatolites'; see Seard *et al.*, 2011) from several Late Pleistocene to Holocene reef frameworks, in which they can represent a significant structural and volumetric component (Camoin *et al.*, 1999, 2006; Seard *et al.*, 2011). However, it seems probable that they have played a significant role in reef accretion in deeper-water compartments of Quaternary reef systems (Camoin *et al.*, 2006; Humble*t al.*, this volume), implying that further studies will be needed to better constrain the roles of microbial features in Quaternary reefs. In addition, microbial communities should be also investigated in modern reef environments to evaluate their potential role in reef responses to future sea-level changes.

- Microscale evolution of reefal microbialites, by *Koyano, S., Shiraishi, F., Miyairi, Y., Yokoyama, Y.* and *Fujita, K*.

In their paper, Koyano *et al.* (this vol.) investigate the evolution of reefal microbialites that developed in primary cavities from middle Holocene reefs cored offshore Okinawa Island, south-west Japan. Factors controlling mesofabric transitions, particularly from laminated to digitate microbialites, and the microscale formation process in relation to microbial communities have not yet been fully understood.

Sedimentological observations and radio-carbon dating results demonstrate that coralgal reef framework growth in a high-energy, shallow-water environment was followed by encrusting foraminifers and metazoans, coevally with macro-bioerosion and micro-bioerosion of coralgal frameworks, then finally by the development of microbialites, first in intraskeletal pores and borings and then as structureless and digitate crusts in cryptophotic, semi-closed primary cavities. Microbialite development is thought to have terminated within a few hundred years after the death of underlying coral colonies. The authors interpret this evolution as being driven by progressive changes related to reduced light and water circulation in the primary cavities during Holocene sea-level rise. They also discuss the microfabric of reefal microbialites, which primarily consists of *in situ* precipitated peloids that are probably formed by coccoid sulfate-reducing bacteria in anoxic environments.

Quaternary sea-level coral reef records and reef response to sea-level and environmental changes

The study of fossil reef outcrops and drill cores have allowed accurate records to be obtained of sea-level changes and to better understand the stratigraphic response of reef systems on a wide range of frequencies, from millennial-scale to hundreds of thousands of years, so far most reliably over the last 125 ka (see Camoin & Webster, 2015a). So far, few data including U-series ages based on coral reef records older than the Last Interglacial (ca 125 ka) can be considered as reliable. Although most of the former fossil reef studies have focused on the reconstruction of sea-level and, to a lesser extent, environmental changes, many of them included valuable information regarding coral reef composition, architecture and accretion patterns.

The development of reef systems involves a complex interplay between multiple parameters, including the rate and amplitude of sea-level change, as well as changes in local physico-chemical parameters (e.g. water temperature and salinity, turbidity, nutrient concentration and exposure to wave energy) and the composition of reef communities (Camoin & Webster, 2015a). The response of reef communities to sea-level and environmental changes is reflected by changes in depositional processes, and/or growth styles, and changes in the composition of coralgal assemblages. Homogeneous composition of framework facies within a given sequence may indicate the persistence of uniform environmental conditions. In contrast, repeated abrupt facies changes are interpreted to indicate lateral displacements of coral communities (Montaggioni, 2005). Lateral displacements and spatial variations in reef composition have been documented in drilling transects carried out on reef slopes from Tahiti (Camoin *et al.*, 2012) and the Great Barrier Reef (Webster *et al.*, 2018) at a sufficiently close spacing to fully capture their spatial heterogeneity. However, additional similar studies in various settings will be needed to clarify the nature and origin of the processes involved in these lateral displacements and to improve our knowledge concerning past and future modes of reef response to sea-level and coeval environmental changes on various time scales.

The papers included in this volume and related to this research topic provide an overview of recent advances in sea-level records and reef response to sea-level and environmental changes during 1) periods typified by rapid sea-level rise and short-term climate excursions, i.e. the Last Deglaciation (21–6 ka), 2) periods characterised by unstable sea-level and climatic conditions at millennial scale, i.e. Marine Isotopic Stage 3 (MIS 3; 60–29 ka); and 3) periods characterised by short-term, low magnitude sea-level oscillations, i.e. the Mid to Late Holocene and the Last Interglacial. All these scenarios are of utmost importance to assess coral reef responses to sea-level and environmental changes on various time scales and to contribute to any prediction concerning the future evolution of coral reef systems.

Shallow drilling through modern reef systems has provided chiefly the opportunity to document reef development patterns over the last 10,000 years. or fewer, and to demonstrate a marked variability in local Holocene sea-levels (Pirazzoli, 1991). Two distinct patterns of relative sea-level change and reef growth have been identified as a

consequence of ice-sheet unloading and redistribution of water masses in the global ocean (Milne & Mitrovica, 2008; Lambeck *et al.*, 2010), in the Pacific and Indian oceans and in the Atlantic, respectively (see reviews in Montaggioni, 2005; Woodroffe & Webster, 2014 and Camoin & Webster, 2015a). The thickness of Holocene reef sequences is generally controlled by the topography of pre-Holocene foundations (Camoin & Webster, 2015a). It has been established that the initiation of modern Indo-Pacific reef growth occurred between 7.6 and 9 ka in the Western Indian Ocean (Camoin *et al.*, 2004) and at 13.92 ka in Tahiti, where an expanded (87 m-thick) continuous reef sequence developed at nearly constant reef accretion rates (11 mm yr^{-1} on average) until 6 ka, when sea-level reached its present position (Bard *et al.*, 1996, 2010; Montaggioni *et al.*, 1997; Camoin *et al.*, 1999, 2012; Cabioch *et al.*, 1999b). The stabilisation of sea-level at its present position at around 6 ka in most Indo-Pacific regions is thought to have followed the disappearance of many large Northern Hemisphere ice sheets. However, there are still uncertainties regarding the volume of additional water, particularly from Antarctica, that has been added to the oceans during the past few millennia (Yokoyama *et al.*, 2012; Hallmann *et al.*, 2018). It has been recently established that a glacio-eustatic contribution of 1.5 to 2.5 m since 5.5 ka was most probably sourced from the Antarctic ice sheet based on Mid-Holocene to Late-Holocene coral reef records from French Polynesia (Hallmann *et al.*, 2018, 2020).

- New insights on the Late Quaternary evolution of Abrolhos reefs, Eastern Brazilian Shelf, by *Vieira, L.S., Bastos, A.C., Dechnik, B., Braga, J.-C., Moura, R.L., D'Agostini, D.P., Moraes, F.C.* and *Webster, J.M.*

In their paper, Vieira *et al*. (this vol.) document the development of two Holocene coralgal shallow reefs, which started to grow roughly coevally (between 6.8 and 6.4 ka) at different depths and with different coral assemblages in highly turbid waters, with a significant terrigenous sediment input on the Abrolhos shelf (Eastern Brazil), which encompasses the largest reef province in the South Atlantic. It relies on the study of two long boreholes of 20 and 50 m-long. The authors demonstrate that different environmental and topographic controls could have acted spatially in different ways, resulting in different timing of 'turn-off' phases (4 and 1.2 ka). Unlike other reef sequences worldwide, both reefs do not exhibit a clear shallowing upward sequence of reef builders and shift in builder assemblage during Holocene sea-level rise, maybe as a consequence of high turbidity levels, lack of hydrodynamic energy and distinctive reef morphology and coral habitats.

- Late Pleistocene-Holocene Evolution of Malé Island (North Malé Atoll Rim, Republic of Maldives), by *Yildirim, T., Droxler, A.W., Gischler, E., Naar, D.F., Yokoyama, Y., Montagna, P. and Pons-Branchu, E.*

The paper by Yildrim *et al.* (this vol.) focuses on the Holocene evolution of Malé island (Maldives), reconstructed based on the study of two boreholes up to 35 m-long and multi-beam bathymetric data. They describe a Holocene reef sequence unconformably overlying karstified late Pleistocene reef units that grew on 25 m from 8.2 to 6.5 ka,

protected behind a karstified late Pleistocene reef remnant, to form the northern margin of a newly formed lagoon that was later infilled between 5.5 and 4.5 ka. The authors conclude that the accretion of the discontinuous North Malé Atoll rim was intermittent. Short intervals of coral reef edification during peak interglacials are separated by relatively long periods of partial dissolution during glacial and subglacial exposure, when sea-level fell below the average depths of North Malé Atoll lagoon (46–64 m) and reached lowstands of 120–130 m below present sea-level.

The drilling of relict reef systems occurring on modern reef slopes has significantly advanced the understanding of the timing and course of the last deglacial sea-level rise (21–6 ka) and their relationships with ice-sheet dynamics. The study of these coral reef records is of prime importance to constrain the timing and magnitude of rapid sea-level changes, to better understand the processes associated with ice-sheet instability, and to unravel the reef response to rapid sea-level rise and short-term climate excursions during this time window. The Last Deglaciation is often seen as a potential recent analogue for environmental changes that our Planet may face in the near future, as a consequence of ocean thermal expansion and the melting of polar ice sheets related to a warming Earth.

It has been previously established that the Last Glacial Maximum terminated at around 19 ka (Clark *et al.*, 2009) with a sharp rise in sea-level at a rate of about 30 mm yr^{-1} for at least 500 years, based on various records from different sedimentary settings (Yokoyama & Esat, 2011). So far, the time window encompassing the inferred '19 ka meltwater pulse' has been documented only in two reef systems: Barbados (Bard *et al.*, 1990) and the Great Barrier Reef (Webster *et al.*, 2018; Yokoyama *et al.*, 2018). The Great Barrier Reef coral reef record has demonstrated that, in contrast to non-coral-based records that were previously used, a more gradual sea-level rise averaging 3.5 mm yr^{-1} has occurred between 21 ka (onset of the deglaciation) and 16.5 ka (Yokoyama *et al.*, 2018), thus demonstrating that the nature, timing and amplitude of events at around 19 ka are still not adequately constrained. Coral reef systems encompassing this time window will therefore require further studies.

- Shelf-edge deglacial reef establishment and subsequent partial demise: Response to distinct pulses of sea-level rise associated with environmental changes, by *Harper, B.B., Droxler, A.W., Webster, J.M., Montagna, P., Yokoyama, Y., Humblet, M., Jorry, S.J., Beaufort, L., Tachikawa, K., Bard, E. and Pons-Branchu, E.*

The paper by Harper *et al.* (this vol.) aims at documenting the development and demise of a coralgal reef system that thrived along the south-east Papua New Guinea Peninsula outer shelf during the Last Deglaciation. The authors especially describe a core that was retrieved at 111 m below present sea-level, exhibiting coral colonies that are interpreted as remnants of a coralgal reef dated to 19.4 ka and which is thought to have developed on a lowstand shelf-edge delta during the initial pulse of the Last Deglaciation. The authors interpret the distinct transition from shallow-water framework corals to deeper-water foliaceous corals as resulting from the partial reef drowning and back-stepping associated with MWP-1A (14.65 ka).

The Barbados coral reef record has suggested that, over the last 15,000 years, global sea-level rise did not occur uniformly but was

characterised by several centuries of extreme rise in sea-level of up to 40 to 50 mm yr^{-1} over 300 to 500 years. These episodes have been identified as 'meltwater pulses MWP 1A and MWP 1B' at 14.08 to 13.61 ka and 11.4 to 11.1 ka, respectively (Fairbanks, 1989; Bard *et al.*, 1990; Fairbanks *et al.*, 2005; Peltier & Fairbanks, 2006) and have been interpreted as resulting from massive, rapid discharges of freshwater related to catastrophic ice-sheet collapse. These pulses are thought to have induced periods characterised by the lack of significant reef accretion and the occurrence of classic reef-drowning signatures (Blanchon & Shaw, 1995; Montaggioni, 2005).

Coral reef records obtained during the Tahiti and Great Barrier Reef IODP expeditions represent unique archives to determine the course of the last deglacial sea-level rise. In particular, they cast doubt on the timing, magnitude and even the occurrence of meltwater pulses previously identified in the Barbados record. Maximum growth rates exceeding 10 mm yr^{-1} were recorded during an accelerated rise in sea-level averaging 46.6 mm yr-1 between 14.65 and 14.3 ka BP (Deschamps *et al.*, 2012), thus corresponding to the so-called 'MWP-1A', but with different timing than that reported in the Barbados record. The associated sea-level rise was of 16±2 m in amplitude (Deschamps *et al.*, 2012; Bard *et al.*, 2016), in good agreement with reef growth modelling results (Seard *et al.*, 2013). In contrast, the younger meltwater pulse, MWP-1B, was not evidenced in the Tahiti (Camoin *et al.*, 2012; Bard *et al.*, 2016) and Great Barrier Reef records (Webster *et al.*, 2018; Yokoyama *et al.*, 2018). However, despite the implementation of these two IODP expeditions, additional drill transects across submerged late Pleistocene and Holocene reef systems from different ocean basins, tectonic settings and latitudes, at variable distances from formerly glaciated regions ('nearfield' *vs* 'far-field') are required to better constrain the abrupt and significant environmental changes that accompanied the last deglacial sea-level rise on a global scale (i.e. meltwater pulses, Younger Dryas and 8.2 ka cold events).

The Tahiti and Great Barrier Reef records have allowed for the first time the reconstruction in unprecedented detail of reef responses to abrupt and significant environmental changes that accompanied the last deglacial sea-level rise, through the analysis of reef growth modes, reef architecture and changes in reef communities. Special attention has been given to time windows encompassing the meltwater pulses (Camoin *et al.*, 2012; Webster *et al.*, 2018). More generally, such records are of pivotal importance to better understand the respective role of the various parameters involved in reef-drowning processes that were commonly reported throughout the geological column. This knowledge is also necessary to better evaluate the potential impact of future sea-level, climatic and environmental changes associated to global warming on reef development.

- How reefs drown: A case study from the Northwest Hawaiian Islands, by *Toomey, M., Sandstrom, M., Magette, E.* and *Cronin, T.*

The paper by Toomey *et al.* (this vol.) revisits the processes that have driven the drowning of reef and carbonate platform systems forming deeply submerged seamounts across ocean basins. The authors focus on Midway Atoll (Northwest Hawaiian Islands) and reconstruct its depositional

history through the study of a 499 m-long drill core. They demonstrate how marginal conditions for carbonate production and wave erosion have shaped its depositional history. This includes its initiation in the early Miocene followed by a long hiatus and a new development phase during the Pleistocene when carbonate production was often outpaced by wave erosion. This results in the formation of distinctive morphological features that are shared with some other carbonate islands at mid-latitudes but are not typical of Central Pacific atolls, more generally, or guyots. They conclude that abrupt sea-level rise may provide a more plausible mechanism for atoll/guyot drowning in the geologic past than marginal environmental conditions for carbonate production, as previously hypothesised.

The drilling strategy that was defined for the Tahiti and Great Barrier Reef IODP expeditions has involved transects of drill holes along modern reef slopes. It has allowed the reconstruction of reef development in all compartments of reef systems (shallow-water [<10 m] *vs* intermediate [10–30 m] and mesophotic [~30–150 m] depths) where reef responses to sea-level rise may vary greatly (see Abbey *et al.*, 2013). Such a holistic approach is mandatory to analyse responses of whole reef systems to sea-level and environmental changes. So far, most studies have been focused on shallow-water communities and further research should therefore incorporate deeper water reef compartments to fulfill these objectives.

- Reef growth history at intermediate to mesophotic depths since the end of the Last Glacial period along the Great Barrier Reef shelf edge, by *Humblet, M., Webster, J.M., Yokoyama, Y., Braga, J.-C., Fujita, K., Iryu, Y., Fallon, S.J. and Thompson, W.G.*

The paper by Humblet *et al.* (this vol.) examines the responses of reef communities that developed at palaeo-water depths greater than 20 m to sea-level change and other environmental perturbations from the end of the Last Glacial period through the Last Deglaciation. It is based on the study of lithologies and biotic components combined with a new robust chronostratigraphic framework in drill cores that were collected along the shelf edge of the modern Great Barrier Reef during IODP Expedition 325.

The authors identify two episodes of reef growth characterised by abundant microbialite crusts and distinct coral assemblages, one during Marine Isotope Stage (MIS) 2 (27–25 ka) and the other at the onset of the last deglacial sea-level rise (19.5–18.5 ka), at palaeo-water depths from 30 to 60 m and 20 to 30 m, respectively. A major episode of reef demise, seemingly linked to reduced water quality combined with rapid deglacial sea-level rise, is evidenced at ca. 17 ka. Reef ecosystems dominated by microbialites and corals developed at intermediate and mesophotic depths. They grew vertically at maximum rates of 2 to 5 mm yr^{-1}, over a period of rapid environmental change during the transition from MIS 3 to MIS 1.

The Tahiti and Great Barrier Reef IODP expeditions have documented reef deposits older than the Last Deglaciation and referred to MIS 3 (Thomas *et al.*, 2009; Gischler *et al.*, 2013; Webster *et al.*, 2018; Yokoyama *et al.*, 2018) as well as MIS 6 and its transition to MIS 5 (Thomas *et al.*, 2009; Ménabréaz *et al.*, 2010). The collected data have brought

valuable sea-level data concerning specific time windows, including the first coral-based sea-level estimate during the fully glacial portion of MIS 6 (Thomas *et al.*, 2009). However, further studies are needed to reconstruct sea-level changes and their impact on reef development during these periods.

- Coral reef development and sea-level changes over the past 50,000 years: new evidence from the north-west shelf of Australia, by *Webster, J.M., Dechnik, B., Sanborn, K., Yokoyama, Y., Braga, J.-C., Renema, W., Humblet, M., Beaman, R.J., Nothdurft, L.D., Webb, G.E., Zhao, J.-X., Murphy, R.J., Gallagher, S.J., O'Leary, M. and Paumard, V.*

The paper by Webster *et al.* (this vol.) concerns sea-level change and reef development on Australia's north-west shelf over the past 50,000 years. It is mainly focused on reef systems that have developed in this region during Marine Isotopic Stage 3 (MIS 3; 60-29 ka), a period characterised by unstable sea-level and climatic conditions and that has been largely unexplored, despite the documentation of few well-dated MIS 3 submerged reefs in regions where sea-level reconstruction is not biased by tectonic activity, especially offshore Tahiti (Thomas *et al.*, 2009) and the Great Barrier Reef (Gischler *et al.*, 2013; Webster *et al.*, 2018; Yokoyama *et al.*, 2018). The morphology, facies distribution and coralgal assemblages of 10–15 m-thick MIS 3 (45.95–39.23$_{\pm}$0.2 ka) coral reef-dominated systems that occur at depths ~63–75 m below present sea-level are detailed for the first time. The authors demonstrate that, apart from on a few isolated and more distal locations, these MIS 3 reef systems were unable to fully re-establish after platform exposure during MIS 2 and subsequent reflooding during the Last Deglaciation, either due to too rapid sea-level rise or unfavourable environmental conditions.

Reef records of past higher sea-levels provide an essential baseline for developing projections regarding the response of modern coastal systems to future sea-level rise.

Besides the studies focused on the Last Interglacial period (MIS 5) and the penultimate Interglacial (MIS 7) from exposed reef terraces in Huon Peninsula, Papua New Guinea, Barbados, Sumba and the Red Sea (see reviews in Camoin & Webster, 2015a,b and Hallmann *et al.*, 2021 for tropical Pacific islands), the mid-late Holocene corresponds to the most recent window into natural variability prior to the Anthropocene (Hallmann *et al.*, 2020). The reconstruction of regional Holocene sea-level trends is required to investigate this time window but, so far, such an approach has been barely developed (Hallmann *et al.*, 2018).

- Neogene and Quaternary reef terraces of Mangaia, Rarotonga and Aitutaki (southern Cook Islands, South Pacific) revisited: gauges of sea-level change and island uplift?, by *Gischler, E., Meyer, G., Braga, J.-C., Riechelmann, S., Immenhauser, A. and Eisenhauer, A.*

The paper by Gischler *et al.* (this vol.) reports on a study carried out on reef systems that developed during periods of sea-level highstands, from the mid-Miocene to the Late Holocene, in the southern Cook Islands, where they form prominent elevated terraces (makatea). This study provides valuable information regarding the reconstruction of former sea-levels, including:

- Pleistocene highstands as old as 2.28 Ma that occur between mid-Miocene reef systems and the lowest coastal reef terrace of

Marine Isotope Stage (MIS) 5e (see review in Hallmann *et al.*, 2021);

- Late Holocene reef terraces, indicating a higher-than-present sea-level of at least +1 m.

This study also demonstrates that the difficulties to obtain an accurate reconstruction increase with the age of the relevant deposits due to the uncertainties related to the influence of various processes, including uplift, subsidence and glacial isostatic adjustment. The late Miocene age of reef deposits on Rarotonga raises important issues as it exceeds the age of subaerially exposed volcanic rocks on this island, thus suggesting that the fossil reef could have formed on an older submarine volcanic high or, alternatively, that the Sr dating cannot be considered as accurate.

REFERENCES

Abbey, E., Webster, J.M., Braga, J.C., Jacobsen, G.E., Thorogood, G., Thomas, A.L., Camoin, G., Reimer, P.J. and **Potts, D.C.** (2013) Deglacial mesophotic reef demise on the Great Barrier Reef. *Palaeogeogr. Palaeoclimatol. Palaeoecol.*, **392**, 473–494.

Abbey, E., Webster, J., Braga, J.C., Sugihara, K., Wallace, C., Iryu, Y., Potts, D., Done, T., Camoin, G. and **Seard, C.** (2011) Variation in deglacial coralgal assemblages and their palaeoenvironmental significance: IODP Expedition 310, Tahiti Sea-level. *Global Planet. Change*, **76**, 1–15.

Bard, E., Hamelin, B., Arnold, M., Montaggioni, L.F., Cabioch, G., Faure, G. and **Rougerie, F.** (1996) Deglacial sea-level record from Tahiti corals and the timing of global meltwater discharge. *Nature*, **382**, 241–244.

Bard, E., Hamelin, B. and **Delanghe-Sabatier, D.** (2010) Deglacial meltwater pulse 1B and Younger Dryas sea-levels revisited with boreholes at Tahiti. *Science*, 327, 1235–1237.

Bard, E., Hamelin, B., Deschamps, P. and **Camoin, G.** (2016) Comment on "Younger Dryas sea-level and meltwaterpulse 1B recorded in Barbados reefalcrest coral Acropora palmata" by N. A. Abdul *et al. Palaeoceanography*, **31**, 1603–1608.

Bard, E., Hamelin, B. and **Fairbanks, R.G.** (1990) U/Th ages obtained by mass spectometry in corals from Barbados. Sea-level during the past 130,000 years. *Nature*, **346**, 456–458.

Blanchon, P. and **Shaw, J.** (1995) Reef-drowning during the last deglaciation: evidence for catastrophic sea-level rise and ice-sheet collapse. *Geology*, **23**, 4–8.

Braga, J.C., Humblet, M., Ramos, D.A.E., Dechnik, B. and Webster, J.M. Quaternary coral, coralline algal and vermetid assemblages as sea-level indicators: a review. In: *Coral Reefs and Sea-Level Change: Quaternary Records and Modelling* (Eds G.F. Camoin and N. Hallmann), *Int. Assoc. Sedimentol. Spec. Publ*., **49** (this volume), 1–38.

Braithwaite, C.J.R. and **Camoin, G.** (2011) Diagenesis and sealevel change: Lessons from Moruroa, French Polynesia. *Sedimentology*, **58**, 259–284.

Braithwaite, C.J.R., Dalmasso, H., Gilmour, M.A., Harkness, D.D., Henderson, G.M., Kay, R.L.F., Kroon, D., Montaggioni, L.F. and **Wilson, P.A.** (2004) The Great Barrier Reef: The chronological record from a new borehole. *J. Sed. Res*., **74**, 298–310.

Braithwaite, C.J.R. and **Montaggioni, L.F.** (2009) The Great Barrier Reef: a 700,000 year diagenetic history. *Sedimentology*, **56**, 1591–1622.

Broecker, W.S., Thurber, D.L., Goddard, J., Ku, T.L., Matthews, R.K. and **Mesolella, K.J.** (1968) Milankovitch hypothesis supported by precise dating of coral reef and deep-sea sediments. *Science*, 159, 297–300.

Cabioch, G., Camoin, G. and **Montaggioni, L.F.** (1999b) Post-glacial growth history of a French Polynesian barrier reef tract, Tahiti, central Pacific. *Sedimentology*, **46**, 985–1000.

Cabioch, G., Montaggioni, L.F., Faure, G. and **Laurenti, A.** (1999a) Reef coralgal assemblages as recorders of palaeobathymetry and sea-level changes in the Indo-Pacific province. *Quatern. Sci. Rev.*, **18**, 1681–1695.

Camoin, G., Cabioch, G., Eisenhauer, A., Braga, J.-C., Hamelin, B. and **Lericolais, G.** (2006) Environmental significance of microbialites in reef environments during the Last Deglaciation. *Sed. Geol.*, **185**, 277–295.

Camoin, G.F., Ebren, P., Eisenhauer, A., Bard, E. and **Faure, G.** (2001) A 300,000-yr coral reef record of sea-level changes, Mururoa Atoll (Tuamotu archipelago French Polynesia). *Palaeogeogr. Palaeoclimatol. Palaeoecol.*, **175**, 325–341.

Camoin, G.F., Gautret, P., Montaggioni, L.F. and **Cabioch, G.** (1999) Nature and environmental significance of microbialites in Quaternary reefs: the Tahiti paradox. *Sed. Geol.*, **126**, 271–304.

Camoin, G.F., Iryu, Y., McInroy, D. and **the Expedition 310 scientists** (2007) *Proceedings of the Integrated Ocean Drilling Program,* 310 Tahiti Sea-Level Change, Integrated Ocean Drilling Program Management International, Inc., College Station, TX. doi:10.2204/iodp.proc.310.101.2007.

Camoin, G.F. and **Montaggioni, L.F.** (1994) High energy coralgal-stromatolite frameworks from Holocene reefs (Tahiti, French Polynesia). *Sedimentology*, **41**, 655–676.

Camoin, G.F., Montaggioni, L.F. and **Braithwaite, C.J.R.** (2004) Late glacial to post glacial sea-levels in the Western Indian Ocean. *Mar. Geol.*, **206**, 119–146.

Camoin, G.F. and **Seard, C.** (2011) Genesis of microbialites as contemporaneous framework components of deglacial coral reefs, Tahiti (IODP 310) – Comment. *Facies*, **58**, 163–165.

Camoin, G.F., Seard, C., Deschamps, P., Webster, J.M., Abbey, E., Braga, J.C., Iryu, Y., Durand, N., Bard, E., Hamelin, B., Yokoyama, Y., Thomas, A.L., Henderson, G.M. and **Dussouillez, P.** (2012) Reef response to sea-level and environmental changes during the last deglaciation: Integrated Ocean Drilling Program Expedition 310, Tahiti Sea-level. *Geology*, **40**, 643–646.

Camoin, G.F. and **Webster, J.M.** (2015a) Coral reef response to Quaternary sea-level and environmental changes: State of the science. *Sedimentology*, **62**, 401–428.

Camoin, G.F. and **Webster, J.M.** (2015b) Coral reefs and sea-level change. In: *Earth and Life Processes Discovered From Subseafloor Environments* (Eds R. Stein, D. Blackman, F. Inagaki and H.-C. Larsen). *Dev. Mar. Geol.*, **7**, Elsevier, 395–441.

Clark, P.U., Dyke, A.S., Shakun, J.D., Carlson, A.E., Clark, J., Wohlfarth, B., Mitrovica, J.X., Hostetler, S.W. and **McCabe, A.M.** (2009) The Last Glacial Maximum. *Science*, **325**, 710–714.

Coudray, J. (1976) Recherches sur le Néogène et le Quaternaire marins de la Nouvelle Calédonie. Contribution de l'étude sédimentologique à la connaissance de l'histoire géologique post-éocène de la Nouvelle-Calédonie. *Expédition Française sur les Récifs Coralliens de Nouvelle Calédonie*, v. **8**. Fondation Singer-Polignac, Paris, 276 pp.

Deschamps, P., Durand, N., Bard, E., Hamelin, B., Camoin, G., Thomas, A., Henderson, G., Okuno, J. and **Yokoyama, Y.** (2012) Ice sheet collapse and sea-level rise at the Bølling warming 14,600 yr ago. *Nature*, **483**, 559–564.

Fairbanks, R.G. (1989) A 17,000-year glacio-eustatic sea-level record: influence of glacial melting rates on the Younger Dryas event and deep-ocean circulation. *Nature*, **342**, 637–642.

Fairbanks, R.G., Mortlock, R.A., Chiu, T., Cao, L., Kaplan, A., Guilderson, T.P., Fairbanks, T.W., Bloom, A.L., Grootes, P.M. and **Nadeau, M.** (2005) Radiocarbon calibration curve spanning 0 to 50,000 years BP based on paired $^{230}Th/^{234}U/^{238}U$ and ^{14}C dates on pristine corals. *Quatern. Sci. Rev.*, **24**, 1781–1796.

Fujita, K., Omori, A., Yokoyama, Y., Sakai, S. and **Iryu, Y.** (2010) Sea-level rise during Termination II inferred from large benthic foraminifers: IODP Expedition 310, Tahiti Sea-level. *Mar. Geol.*, **271**, 149–155.

Gallup, C.D., Cheng, H., Taylor, F. W. and **Edwards, R. L.** (2002) Direct Determination of the Timing of Sea-level Change During Termination II. *Science*, **295**, 310–313.

Gischler, E., Ginsburg, R.N., Herrlez, J.O. and **Prasad, S.** (2010) Mixed carbonates and siliciclastics in the Quaternary of southern Belize: Pleistocene turning points in reef development controlled by sea-level change. *Sedimentology*, **57**, 1049–1068.

Gischler, E., Meyer, G., Braga, J.-C., Riechelmann, S., Immenhauser, A. and **Eisenhauer, A.** Neogene and Quaternary reef terraces of Mangaia, Rarotonga, and Aitutaki (southern Cook Islands, south Pacific) revisited: gauges of sea-level change and island uplift? In: *Coral Reefs and Sea-Level Change: Quaternary Records and Modelling* (Eds G.F. Camoin and N. Hallmann), *Int. Assoc. Sedimentol. Spec. Publ.*, **49** (this volume), 275–317.

Gischler, E., Thomas, A.L., Droxler, A.W., Webster, J.M., Yokoyama, Y., Schöne, B.R. and **Porta, G.D.** (2013) Microfacies and diagenesis of older Pleistocene (pre-last glacial maximum) reef deposits, Great Barrier Reef, Australia (IODP Expedition 325): A quantitative approach. *Sedimentology*, **60**, 1432–1466.

Goreau, T.F. and **Wells, J.W.** (1967) The shallow water scleractinia of Jamaica: revised list of species and their vertical distribution range. *Bull. Mar. Sci.*, **17**, 442–453.

Hallmann, N., Camoin, G., Eisenhauer, A., Botella, A., Milne, G.A., Vella, C., Samankassou, E., Pothin, V., Dussouillez, P., Fleury, J. and **Fietzke, J.** (2018) A high-precision sea-level curve for the SW Pacific from coral microatolls. *Nature Comm.*, DOI: 10.1038/s41467-017-02695-7.

Hallmann, N., Camoin, G., Eisenhauer, Samankassou, E., Vella, C., A., Botella, A., Milne, G.A., Pothin, V., Dussouillez, P., Fleury, J., Fietzke, J. and **Goepfert, T.** (2020) Reef response to sea-level and environmental changes in the Central South Pacific over the past 6000 years. *Global Planet. Change*, **195**, 103357.

Hallmann, N., Camoin, G., Webster, J.M. and **Humblet, M.** (2021) A standardized database of Marine Isotopic Stage 5e sea-level proxies on tropical Pacific Islands. In: *WALIS – the World Atlas of Last Interglacial Shorelines*, A. Rovere *et al.* (Eds). Earth System Science Data, Copernicus Publications, 2021, **13** (6), 2651−2699;10.5194/essd−13−2651−2021

Harper, B.B., Droxler, A.W., Webster, J.M., Montagna, P., Yokoyama, Y., Humblet, M., Jorry, S.J., Beaufort, L., Tachikawa, K., Bard, E. and **Pons-Branchu, E.** Shelf-edge deglacial reef establishment and subsequent partial demise: Response to distinct pulses of sea-level rise associated with environmental changes. In: *Coral Reefs and Sea-Level Change: Quaternary Records and Modelling* (Eds G.F. Camoin and N. Hallmann), *Int. Assoc. Sedimentol. Spec. Publ*., **49** (this volume), 141–171.

Hubbard, D.K. (2009), Depth-related and species-related patterns of Holocene reef accretion in the Caribbean and Western Atlantic: A critical assessment of existing models. In: *Perspectives in Carbonate Geology: A Tribute to the Career of Robert Nathan Ginsburg* (Eds P. Swart, G. P. Eberli, and J. McKenzie), *Int. Assoc. Sedimentol. Spec. Publ*., **41**, 1–18.

Humblet, M., Webster, J.M., Yokoyama, Y., Braga, J.C., Fujita, K., Iryu, Y., Fallon, S.J. and **Thompson, W.G.** Reef growth history at intermediate to mesophotic depths since the end of the Last Glacial period along the Great Barrier Reef shelf edge. In: *Coral Reefs and Sea-Level Change: Quaternary Records and Modelling* (Eds G.F. Camoin and N. Hallmann), *Int. Assoc. Sedimentol. Spec. Publ*., **49** (this volume), 189–214.

Koyano, S., Shiraishi, F., Miyairi, Y., Yokoyama, Y. and **Fujita, K.** Microscale evolution of reefal microbialites. In: *Coral Reefs and Sea-Level Change: Quaternary Records and Modelling* (Eds G.F. Camoin and N. Hallmann), *Int. Assoc. Sedimentol. Spec. Publ*., **49** (this volume), 39–67.

Lambeck, K., Woodroffe, C.D., Antonioli, F., Anzidei, M., Gehrels, W.R., Laborel, J. and **Wright, A.J.** (2010) Palaeoenvironmental records, geophysical modeling, and reconstruction of sea-level trends and variability on centennial and longer timescales. In: *Understanding Sea-Level Rise and Variability* (Eds J. Church, P.L. Woodworth, T. Aarup and W.S. Wilson), pp. 61–121. Wiley-Blackwell, Chichester.

Lighty, R.G., Macintyre, I.G. and **Stuckenrath, R.** (1982) *Acropora palmata* reef Framework: a reliable indicator of sea-level in the western atlantic for the past 10,000 years. *Coral Reefs*, **1**, 125–130.

Ménabréaz, L., Thouveny, N., Camoin, G. and **Lund, S.P.** (2010) Palaeomagnetic record of the Late Pleistocene reef sequence of Tahiti (French Polynesia): a contribution to the chronology of the deposits. *Earth Planet. Sci. Lett*., **294**, 58–68.

Milne, G.A. and **Mitrovica, J.X.** (2008) Searching for eustasy in deglacial sea-level histories. *Quatern. Sci. Rev.*, **27**, 2292–2302.

Montaggioni, L.F. (2005) History of Indo-Pacific coral reef systems since the last glaciation: development patterns and controlling factors. *Earth Sci. Rev*., **71**, 1–75.

Montaggioni, L.F., Cabioch, G., Camoin, G.F., Bard, E., Ribaud-Laurenti, A., Faure, G., Déjardin, P. and **Récy, J.** (1997) Continuous record of reef growth over the past 14 k.y. on the mid-Pacific island of Tahiti. *Geology*, **25**, 555–558.

Montaggioni, L.F., Cabioch, G., Thouveny, N., Frank, N., Sato, T. and **Sémah, A.M.** (2011) Revisiting the Quaternary development history of the western New Caledonian shelf system: From ramp to barrier reef. Mar. Geol., **280**, 57–75.

Montaggioni, L.F. and **Camoin, G.F.** (1993) Stromatolites associated with coralgal communities in Holocene high energy reefs. *Geology*, **21**, 149–152.

Ohde, S., Greaves, M., Masuzawa, T., Buckley, H. A., VanWoesik, R., Wilson, P. A., Pirazzoli, P. A. and **Elderfield, H.** (2002) The chronology of Funafuti atoll: revisiting an old friend, *Proceed. Roy. Soc. A*, **458**, 2289–2306.

Peltier, W.R. and **Fairbanks, R.G.** (2006) Global glacial ice volume and Last Glacial Maximum duration from an extended Barbados sea-level record. *Quatern. Sci. Rev*., **25**, 3322–3337.

Pirazzoli, P.A. (1991) *World Atlas of Holocene Sea-level Changes*. Oceanogr. Ser., vol. **58**. Elsevier, Amsterdam, 300 pp.

Purdy, E.G. Gischler, E. and **Lomando, A.J.** (2003) The Belize margin revisited. 2. Origin of Holocene antecedent topography. *Intern. J. Earth Sci*., **92**, 552–572.

Seard, C., Camoin, G., Yokoyama, Y., Matsuzaki, H., Durand, N., Bard, E., Sépulcre, S. and **Deschamps, P.** (2011) Microbialite development patterns in the last deglacial reefs from Tahiti (French Polynesia; IODP Expedition #310): implications on reef framework architecture. *Mar. Geol.*, **279**, 63–86.

Seard, C., Borgomano, J., Granjeon, D. and **Camoin, G.** (2013) Impact of environmental parameters on coral reef development and drowning: Forward modelling of the last deglacial reefs from Tahiti (French Polynesia). *Sedimentology*, **60**, 1357–1388.

Thomas, A.L., Henderson, G.M., Deschamps, P., Yokoyama, Y., Mason, A.J., Bard, E., Hamelin, B., Durand, N. and **Camoin, G.** (2009) Penultimate deglacial sea-level timing from uranium/thorium dating of Tahitian corals. *Science*, **324**, 1186–1189.

Toomey, M., Sandstrom, M., Magette, E. and **Cronin, Th.** How reefs drown: A case study from the Northwest Hawaiian Islands. In: *Coral Reefs and Sea-Level Change: Quaternary Records and Modelling* (Eds G.F. Camoin and N. Hallmann), *Int. Assoc. Sedimentol. Spec. Publ*., **49** (this volume), 173–188.

Vieira, L.S., Bastos, A.C., Dechnik, B., Braga, J.C., Moura, R.L., D'Agostini, D.P., Moraes, F.C., Webster, J.M. New insights on the Late Quaternary evolution of Abrolhos reefs, Eastern Brazilian Shelf. In: *Coral Reefs and Sea-Level Change: Quaternary Records and Modelling* (Eds G.F. Camoin and N. Hallmann), *Int. Assoc. Sedimentol. Spec. Publ*., **49** (this volume), 69–100.

Webster, J.M., Braga, J.-C, Humblet, M., Potts, D.C., Iryu, Y., Yokoyama, Y., Fujita, K., Bourillot, R., Esat, T.M., Fallon, S., Thompson, W.G., Thomas, A.L., Kan, H., McGregor, H.V., Hinestrosa, G., Obrochta, S.P. and **Lougheed, B.C.** (2018) Response of the Great Barrier Reef to sea-level and environmental changes over the past 30,000 years. *Nature Geosci*., https://doi.org/10.1038/s41561-018-0127-3

Webster, J.M., Dechnik, B., Sanborn, K., Yokoyama, Y., Braga, J.C., Renema, W., Humblet, M., Beaman, R., Nothdurft, L., Webb, G., Zhao, J.-X., Murphy, R., Gallagher, S., O'Leary, M. and **Paumard, V.** Coral reef development and sea-level changes over the past 50,000

years: new evidence from the northwest shelf of Australia. In: *Coral Reefs and Sea-Level Change: Quaternary Records and Modelling. A Window Into the Future* (Eds G.F. Camoin and N. Hallmann), *Int. Assoc. Sedimentol. Spec. Publ*., **49** (this volume), 215–273.

Webster, J.M., Yokoyama, Y., Cotterill, C. and **Expedition 325 Scientists** (2011) *Proceedings of the Integrated Ocean Drilling Program,* 325 Expedition Reports Great Barrier Reef Environmental Changes, Integrated Ocean Drilling Program Management International, Inc., for the Integrated Ocean Drilling Program.

Woodroffe, C.D. and **Webster, J.M.** (2014) Coral reefs and sea-level change. *Mar. Geol.*, **352**, 248–267.

Yildrim, T., Droxler, A.W., Gischler, E., Naar, D.F., Yokoyama, Y., Montagna, P. and **Pons-Branchu, E.** Late Pleistocene-Holocene Evolution of Malé Island (North Malé Atoll Rim, Republic of Maldives). In: *Coral Reefs and Sea-Level Change: Quaternary Records and Modelling. A Window Into the Future* (Eds G.F. Camoin and N. Hallmann), *Int. Assoc. Sedimentol. Spec. Publ*., **49** (this volume), 101–140.

Yokoyama, Y. and **Esat, T.M.** (2011) Global climate and sea-level-enduring variability and rapid fluctuations over the past 150,000 years. *Oceanography*, **24**, 54–69.

Yokoyama, Y., Esat, T.M., Thompson, W.G., Webster, J.M., Miyairi, Y., Sawada, C., Aze, T., Matsuzaki, H., Okuno, J., Fallon, S., Braga, J.-C, Humblet, M., Iryu, Y., Potts, D.C., Fujita, K., Suzuki, A. and **Kan, H.** (2018) Rapid glaciation and a two-step sea-level plunge into the Last Glacial Maximum. *Nature*, **559**, 603-607. https://doi.org/10.1038/s41586-018-0335-4

Yokoyama, Y., Okuno, J., Miyairi, Y., Obrochta, S., Demboya, N., Makino, Y. and **Kawahata, H.** (2012) Holocene sea-level change and Antarctic melting history derived from geological observations and geophysical modeling along the Shimokita Peninsula, northern Japan. *Geophys. Res. Lett*., **39**, L13502.

Zimmer, B., Precht, W., Hickerson, E. and **Sinclair, J.** (2006) Discovery of *Acropora palmata* at the Flower Garden Banks National Marine Sanctuary, northwestern Gulf of Mexico, *Coral Reefs*, **25**, 192–192.

IAS (2022) Coral Reefs and Sea-Level Change: Quaternary Records and Modelling, 1–38

Quaternary coral, coralline algal and vermetid assemblages as sea-level indicators: a review

JUAN C. BRAGA[*], MARC HUMBLET[†], DINO ANGELO E. RAMOS[*], BELINDA DECHNIK[‡] and JODY M. WEBSTER[‡]

[*]*Departamento de Estratigrafía y Paleontología, Universidad de Granada, Campus Fuentenueva, 18002, Granada, Spain.*
[†]*Department of Earth and Planetary Sciences, Nagoya University, Nagoya 464-8601, Japan.*
[‡]*Geocoastal Research Group, University of Sydney, Sydney, Australia.*

ABSTRACT

Corals, coralline algae and vermetid gastropods are indirect (marine limiting) relative sea-level (RSL) indicators. The precision in sea-level reconstruction based on fossils of those organisms depends on the probable palaeodepth in which they grew. Constraining such palaeodepth depends, in turn, on the available information about the habitats of their living counterparts. Diverse genera, species and species assemblages of corals, coralline algae and vermetid gastropods have historically been proposed as reliable indicators of narrow, shallow depth ranges. However, the increased information on depth distribution of marine benthos in the last two decades has challenged some early assumptions about depth ranges of taxa considered diagnostic of precise palaeodepths. Here, the authors test the reliability of coral, coralline algal and vermetid assemblages that have been extensively used in RSL reconstructions in the light of data from Ocean Biogeographical Information System (OBIS) and other recently published data. In the Indo-Pacific province, these data support the use of the robust-branching and the shallow, high-energy encrusting coral assemblages with a 0 to 10 m uncertainty. In both cases many component species have unimodal distributions and both median and average water depths are shallower than 10 m. The reliability of these coral assemblages as indicative of shallow water depths is strengthened when corals are encrusted by thick plants of the coralline alga *Porolithon* gr. *onkodes*. According to OBIS data, coralline algae of this species group in the Indo-Pacific are restricted to very shallow waters (95% probability of occurrence shallower than 0.2 m and in 99.6% of records shallower than 6 m). However, such a narrow depth range and the overall scarce data on coralline algal species in the OBIS database are questionable due to difficulties of coralline algal species identification with the naked eye. A comprehensive survey of the modern distribution of coralline algae at One Tree Reef (southern Great Barrier Reef) indicates that *P*. gr. *onkodes* has a log-normal distribution with median depth of less than 5 m and 95% of occurrence probability of thick crusts (>0.2 mm) shallower than 8.8 m. Data on modern distribution of vermetids are scarce. In the OBIS database, vermetid species are reported from relatively wide depth ranges. However, relatively high densities (>10 individuals per m^2) on coral and coralline algal surfaces only occur from above mean low tide to some 6 m depth. In the Western Atlantic-Caribbean province *Acropora palmata* is the most precise RSL marker and no additional components of fossil assemblages

©2022 International Association of Sedimentologists

improve its palaeodepth information. The confident use of coralgal and vermetid assemblages as RSL indicators relies on the identification of fossil corals and coralline algae at the species or species-group level. The scarcity of available data highlights the need for further studies on distribution of coralline algal species and vermetid in modern coral reefs from a variety of oceans and reef settings.

INTRODUCTION

In the last two decades, an extraordinary research effort has focused on Quaternary sea-level variations, from local relative sea-level (RSL) at particular time intervals to eustatic sea-level (ESL) changes throughout time and their relationships to Earth climate. The elaboration of schemes to categorise past RSL indicators have been applied to thousands of sites worldwide. This has led to the accurate definitions of the type and precision of potential RSL markers and to the development of standardised protocols for palaeo-RSL reconstructions (Rovere *et al.*, 2016). According to those protocols, several landforms can be used as precise indicators of past RSL position (Rovere *et al.*, 2016), while only a few fossil biogenic structures, such as vermetid trottoirs, can be considered accurate markers of ancient RSL (Laborel, 1986).

Marine fossils in growth position, or *in situ*, evidence a marine or lower limit (marine limiting) for the RSL uncertainty (Rovere *et al.*, 2016), but the amount of uncertainty (i.e. vertical error) depends on the probable depth position of the fossil at the time of its growth. Consequently, fossils of organisms that live in narrow depth ranges would be the most appropriate to estimate RSL at the time they grew. Obviously, the use of particular taxa, from high-order groups to species, for RSL reconstruction depends on the knowledge about their modern habitat depth ranges, which has been improving with increasing data on distribution of marine species.

Some groups of zooxanthellate corals have traditionally been considered key fossils for RSL reconstructions due to the presumed shallow habitats with narrow depth ranges of their living species (Lighty *et al.*, 1982; Davies & Montaggioni, 1985; Fairbanks, 1989; Cabioch *et al.*, 1999; Montaggioni, 2005; Montaggioni & Braithwaite, 2009; Woodroffe & Webster, 2014; Camoin & Webster, 2015). They also have a high potential for precise, radiometric dating using U-series and radiocarbon; and a worldwide distribution in the tropical/subtropical regions, in which many areas are far-field with glacio-isostatic adjustment (GIA) minimised (Hibbert *et al.*, 2016).

Corals may play a secondary role as RSL indicators in uplifting areas or in stable regions for records of ESL higher than present-day, such as the Last Interglacial (MIS5e). In both cases, precise geomorphic RSL indicators, including coral-reef terraces are usually available (Rovere *et al.*, 2016). In such instances, the dating potential of corals would be more relevant than their palaeodepth meaning. However, in subsiding areas and for periods of ESL lower than present-day, landforms can be less conclusive or even absent and RSL reconstruction needs to be based on sedimentological and palaeontological data from drill cores or collected from the sea floor via ROV, submersible or dredging.

In these cases, individual coral genera and species, and coral assemblages, have been used to estimate palaeodepth of fossil reef deposits and to subsequently reconstruct RSL changes (e.g. Fairbanks, 1989; Bard *et al*., 1996; Deschamps *et al*., 2012; Yokoyama *et al*., 2018). In Quaternary reefs, palaeodepth has been estimated based on the known depth distributions of living members of the same coral taxon or assemblage. This approach has been applied using single species, such as

Acropora palmata in the Caribbean reefs (e.g. Lighty *et al.*, 1982; Fairbanks, 1989 Bard *et al.*, 2016; Mortlock *et al.*, 2016) or assemblages defined by a combination of component species and their morphology (e.g. Nakamori, 1986; Pirazzoli & Montaggioni, 1988; Bard *et al*., 1996; Yokoyama *et al*., 2018). Logically, the depth ranges of the involved taxa have historically been estimated according to the ecological information, in some cases limited, available at that time.

As stated by Hibbert *et al.* (2016), in the last two decades the increasing use of autonomous underwater vehicles (AUV) and improvements in diving technology (rebreathers, mixed air gases) have extended the depth range of surveys on the distribution of corals species. Many of these surveys cover mesophotic reefs, which mainly occur at depth ranges of 30 to 40 m but can extend down to 150 m (Hinderstein *et al.*, 2010) and have been the subject of intense research in recent years. This new ecological information is partly published in a number of papers (for example Muir *et al.*, 2015), although most of the available data come from the Ocean Biogeographical Information System (OBIS, https://obis.org) and IUCN (International Union for Conservation of Nature; https://www.iucnredlist.org). The available information on coral ecology and biogeography shows that occurrence and reliability of coral RSL indicators vary geographically between localities within oceans and between oceans. Even within localities, coral depth ranges might change depending on geomorphology, energy and sediment input (Done, 1982; Braithwaite, 2016). On the other hand, this knowledge on the environmental distribution of reef builders, including their depth ranges, is crucial to reconstruct the response of reef ecosystems to spatio-temporal variations in global to local environmental parameters, such as climate, sea-level, water quality, and turbidity in the past (Blanchon *et al.*, 2009; Camoin *et al.*, 2012; Woodroffe & Webster, 2014; Camoin & Webster, 2015; Toth *et al.*, 2015; Webster *et al.*, 2018).

The accuracy and usefulness of coral RSL indicators can be improved by adding depth-related information about co-existing coralline algae (CAA) and vermetid gastropods. Palaeodepth interpretations based on CAA and vermetids, which are common encrusters contributing to reef growth, have been used to reconstruct RSL from fossil reefs (Davies & Montaggioni, 1985; Pirazzoli & Montaggioni, 1988; Bard *et al.*, 1996; Camoin *et al.*, 2001; Cabioch *et al.*, 2003; Abbey *et al.*, 2011; Deschamps *et al.*, 2012; Dechnik *et al.*, 2015; Gischler *et al.*, 2016; Dechnik *et al.*, 2017; Gischler *et al.*, 2018b; Webster *et al.*, 2018; Yokoyama *et al.*, 2018; Humblet *et al.*, 2019). The living and fossil representatives of these two groups have received less attention than corals and the available literature on the depth ranges of the reef-related species is relatively scarce and concentrated in a few geographic areas (Adey, 1986; Dechnik *et al.*, 2017; Humblet *et al.*, 2019 and references therein). The OBIS database includes a number of tropical/subtropical species of both groups but in many cases the records are too few to be of statistical significance. As shown below, despite these limitations, CCA and vermetid gastropods show potential to improve the accuracy of RSL reconstruction based on coral indicators.

The reliability of coralgal assemblages (coral and CCA) and vermetids in reef deposits as RSL indicators also depends on the feasibility of distinguishing *in situ* framework from allochthonous rubble. In the latter case it is crucial to understand the palaeoenvironmental setting in which the rubble accumulated. Protocols or suites of criteria have been proposed to reduce uncertainties regarding the autochthony of reef components since the early works on

corals as palaeo-RSL indicators (Lighty *et al.*, 1982; Montaggioni *et al.*, 1997; Montaggioni & Faure, 1997; Camoin *et al.*, 2001; Webster & Davies, 2003; Blanchon & Perry, 2004).

Based on worldwide records of living corals included in OBIS, Hibbert *et al.* (2016) suggest that corals are 'depth-generalists', with restricted depth ranges only when individual species are considered. Consequently, they suggest that fossil corals should be identified at the species level to reduce uncertainty in RSL reconstructions. Using OBIS and IUCN databases, Hibbert *et al.* (2016, 2018) assessed modern depth distribution of coral species previously used in RSL reconstructions, questioning blanket assumptions of coral palaeodepth interpretations and providing depth-range parameters, such as median depth, maximum depth, and probability distribution with confidence intervals for individual coral taxa.

Following a similar approach, in this paper the authors use publications on coral reef ecology, OBIS and IUCN databases to assess the reliability and precision of reef-builder assemblages as RSL markers. The authors explore the potential of the coralgal/vermetid assemblages to provide improved constraints and consistency in palaeo-RSL reconstruction based on these important reef builders. This review is particularly focused on the CCA and vermetid components of the assemblages, which have not been comprehensively incorporated into previous assessments.

METHODS

A primary source of data and interpretations included in this review is the literature about depth distribution and potential use for RSL reconstruction of living coral, CCA and vermetid assemblages. Following an historical sequence, the authors focused on papers and monographs proposing biotic zonations of corals, CCA and vermetids in modern reefs. Within the information included in those works, the authors have concentrated on assemblages of these organisms that were considered the best indicators of shallow depths and, consequently, the most precise markers of RSLs. We also refer to published reports on Quaternary reefs applying the occurrence of particular coral, coralline algal and vermetid assemblages to reconstruct RSL. The examined works are listed in the Supplementary table, detailing location, age, reef habitat, depth/palaeodepth, assemblage components and source of information for palaeodepth interpretation. The data included in the table consists of verbatim quotes from the primary papers.

The authors also used data in the Ocean Biogeographical Information System (OBIS, https://obis.org, October 2021) on depth distribution of genera and species of corals (in the Indo-Pacific province), CCA and vermetid gastropods that are reported in the literature as the most precise RSL indicators (Table 1). The R package robis version 2.3.11 (Provoost & Bosch, 2017) was used to download the occurrence data for the selected species of corals, coralline algae and vermetids. The following parameters from the OBIS records were used to filter the data for analyses: basis of record, minimum and maximum depths of the record in metres, and occurrence remarks. The authors only used human observations (basis of record), with a difference between maximum and minimum depths of 1 metre for corals and 3 metres for CCA and vermetids; and used the occurrence remarks to find and remove duplicate records. A larger min/max depth range was used for observations on CCA and vermetids to increase the number of records available for the analyses. Duplicates were identified particularly for records associated with the National Institutes for Water and Atmospheric Research (NIWA), which refers

to other OBIS datasets in most instances. Depth outliers were also excluded from the data analyses. A total of 54 species and 3 genera of corals, 6 species of CCA and 2 species and 1 genus of vermetids were examined from OBIS. The number of filtered records per species ranged from 18 (*Acropora palmerae*) to 2954 (*Pocillopora damicornis*). The authors calculated summary statistics and found the best-fitting distribution for each species using the R package fitdistrplus version 1.1-3 (Delignette-Muller & Dutang, 2015). All the depth data was increased by 0.01 to eliminate zero values and allow the testing of more distributions. The normal, log-normal, logistic, exponential, Weibull and gamma distributions were fitted and the distribution with the lowest Akaike information criterion (AIC) value was selected as the best-fit. Since the authors were primarily interested in the deepest habitat for each species, they used a one-tailed approach and calculated the value of the 95 percentile ($p<0.05$) from the chosen distribution (Tables 2 and 3). The percentage of records shallower than 6 m are presented; a depth traditionally considered to be the lower limit of high-energy shallow-water coral assemblages (Montaggioni & Braithwaite, 2009 and references therein). Of the coral species analysed, 23 were found to have bimodal distributions with a significant amount of deep-water (mesophotic) records. They fit poorly with all the distributions tested and are omitted from the results.

For CCA and vermetids. the authors also present new data on the depth distribution of living taxa recorded at One Tree Reef in the southern Great Barrier Reef (GBR), which were partly reported in the supplementary material in Dechnik *et al.* (2017). In that study, CCA sampled from 0 to 30 m depth were identified in the lab with the help of optical microscopy and SEM, reducing the uncertainty of taxon identification common in field surveys. In addition, vermetid abundance was estimated in CCA crust sections as is usually observed at fossil reef outcrops and drill cores. Data from the IUCN Red List on depth limits of coral species characteristic of coral assemblages considered the best RSL indicators are included in Table 2 (International Union for Conservation of Nature Red List; https://www.iucnredlist. org).

Although most records in the OBIS database are updated to the most recent classification schemes, for corals the authors have used the latest scheme defining the families Merulinidae, Montastraeidae and Diploastraeidae (Huang *et al.*, 2014), Lobophylliidae (Huang *et al.*, 2016) and Mussidae in the Atlantic Ocean (Budd *et al.*, 2012). The classification of Veron (2000) is followed for other families. The updated taxonomy for CCA used here can be found in ALGAEBASE (https://www.algaebase.org) as well as in specific papers referred to in the CCA section. For vermetids, the scheme in WORMS has been used herein (2021, https://www.marinespecies.org), which does include the taxonomy proposed by Golding *et al.* (2014).

Table 1. Most precise palaeo-RSL indicators according to literature on the distributions of modern coral, coralline algal and vermetid assemblages/taxa. Only the shallowest assemblages (< 10 m depth) of each group are included. See Supplementary table for information on deeper assemblages in the literature. Taxonomic names in brackets reflect later modifications of the nomenclature by Huang *et al.* (2014) for the families Merulinidae, Montastraeidae and Diploastraeidae, Huang *et al.* (2016) for the Lobophylliidae & Veron (2000) for other families. MLSL: mean low sea-level; MHSL: mean high sea-level.

Coral assemblages	Depth range	Environment	References
Atlantic/Caribbean *Acropora palmata*	0 to 5 m	High-energy reef crest	Lighty *et al.*, 1982; Hibbert *et al.*, 2016, 2018
Indo-Pacific Robust-branching coral assemblage. Charecterised by *Acropora* gr. *robusta: A. robusta, A. danai* (= *A. abrotanoides*), *A. abrotanoides, A. palmerae; Acropora (Isopora) palifera; A.* gr. *humilis: A. humilis, A. digitifera, A. gemmifera); A. latistella*, and pocilloporids (*Pocillopora damicornis, P. eydouxi* (=*P. grandis*), *P. verrucosa, P. meandrina, Stylophora pistillata, S. mordax* (= *S. pistillata*). Subordinate associated domal (*Porites lutea*, *P. lobata, Leptoria phrygia, Platygyra daedala, Goniastrea retiformis, Goniastrea favulus, Favia stelligera* (=*Goniastrea stelligera*), *Favia* (=*Dipsastraea*) *spp., Psammocora* sp., *Astreopora* sp., *Montipora* sp., platy (*Millepora platyphylla*), tabular (*A. hyacinthus*), columnar (*Porites annae*) and encrusting (*Montipora tuberculosa*, *Echinopora gemmacea*) assemblages.	0 to 6 m	High-energy, windward margins (upper forereef to outer reef flat zones)	Montaggioni, 2005, Montaggioni & Braithwaite, 2009
High-energy encrusting coral assemblage. According to the region considered, this may include the acroporids *Montipora monasteriata, M. capitata, M. undata, M. patula, M. danai*, the agariciids *Leptoseris mycetoseroides*,	0 to 10 m	High-energy reef crests, outer and inner slopes of ocean-facing fringing reefs, mid-shelf to inner-shelf	

speciosa, the pectiniid (= lobophylliids) *Echinophyllia aspera*, the faviids (= incertae sedis) *Leptastrea purpurea,* (merulinids) *Echinopora lamellosa*, *E. gemmacea, Cyphastrea serailia, C. microphthalma, C. ocellina*, the poritid *Alveopora daedala*, the merulinid *M. ampliata*; may be mixed with dome-shaped faviids (= merulinids), i.e.*F.* (=*D.*) *pallida, F.* (=*D.*) *speciosa, Oulophyllia crispa*, acroporids, i.e. *A. myriophthalma, Astreopora ocellata, Astreopora* spp., poritids, i.e. *Porites lutea, P. lobata, Goniopora lobata, G. columna*), mussids (= lobophylliids) (*Lobophyllia corumbosa, L. hemprichii, Acanthastrea echinata*), associated with finely branching (*Acropora echinata*, *Seriatopora hystrix*) or with meandroid forms (*Plerogyra sinuosa*). Also free-living corals (*Fungia* spp., *Halomitra* sp., *Herpolitha* sp.).			
<u>Coralline algal assemblages</u>			
Atlantic/Caribbean			
Porolithon antillarum (as *Porolithon pachydermum*)	0 to 3 m	High energy reef crest	Martindale, 1992
and *Lithophyllum kaiseri* (as *Lithophyllum congestum*)	0 to 6 m		Adey, 1986
Extensive framework of algal ridge	close to/slightly above MLSL		Adey & Burke, 1976, 1977
Porolithon gr. *onkodes, Melyvonnea erubescens* (as *Mesophyllum erubescens*)	2 to 5 m		Jesionek *et al.*, 2016; Amado-Filho *et al.*, 2018
Indo-Pacific			
P. onkodes and *Neogoniolithon*	0 to 10 m		Adey, 1986; Iryu *et al.*, 1995
P. onkodes (as *Hydrolithon onkodes*) and *Neogoniolithon*	0 to 6 m		Cabioch *et al.*, 1999
<u>Vermetids</u>			
Atlantic			
Dendropoma corrodens	MLSL	Rims of cup reefs Bermuda	Thomas & Stevens, 1991

Dendropoma sp.	Above MHSL	Raised reef rim Atol das Rocas	Gherardi & Bosence, 2001
Vermetus irregularis (as *'Dendropoma irregulare'*	Intertidal	Reef edge Abrolhos	Tamega *et al.,* 2014; Spotorno-Oliveira *et al.*, 2015
Indo-Pacific			
Ceraesignum maximum (as Dendropoma maximus)	0 to 6 m	Upper forereef to outer reef flat zones	Cabioch *et al.,* 1999; Montaggioni, 2005; Montaggioni & Braithwaite, 2009
Densities of *Ceraesignum maximum* > 10/m^2	0 to 6 m	Reef flat and upper forereef	Hughes & Lewis, 1974; Zvuloni *et al.,* 2008; Zuschin *et al.*, 2001

Table 2. Modern depth range, average depth of Indo-Pacific coral species characteristic of the 'Robust-branching' and 'High-energy encrusting' coral assemblages (Montaggioni, 2005) with gamma and unimodal best-fit probability distributions. Species arranged according to family ascriptions. Data from OBIS (accessed October 2021). The species depth-range in the IUCN database are also included.

Coral species	**Number of observations**	**Min. Depth (m)**	**Max. Depth (m)**	**Mean (m)**	**Median (m)**	**SD**	**Value at 95 percentile (m)**	**% records shallower than 6 m**	**Records shallower than 6 m**	**Best Fit Distribution**	**IUCN depth range (m)**
Robust branching assemblage											
Acropora aspera	57	0,0	65.0	4.2	3.0	8.6	16.2	89.5	51	gamma	0-5
A. digitifera	208	0,0	45.0	3.8	3.0	5.8	13.0	89.9	187	gamma	0-12
A. gemmifera	131	0,0	15.0	3.9	4.0	3.0	13.6	82.4	108	gamma	1-15
A. humilis	300	0,0	46.0	6.4	3.0	10.0	24.9	78.0	234	gamma	0-11
A. hyacinthus	344	0,0	38.5	4.1	3.0	3.2	10.8	81.1	279	Weibull	5-20
A. latistella	148	0,0	15.0	4.0	3.0	2.6	9.5	86.5	128	Weibull	3-20
A. monticulosa	30	0,0	9.0	2.9	2.0	2.8	11.9	86.7	26	gamma	1-12
A. nasuta	225	0,0	60.0	4.5	3.0	4.9	14.3	77.3	174	gamma	3-15
A. palmerae	18	0,0	15.0	2.4	0.0	4.2	15.5	77.8	14	log-normal	0-12
Isopora palifera	254	0,0	46.0	5.8	3.0	8.2	20.9	75.6	192	gamma	2-20

Montipora tuberculosa	148	0,0	40.0	6.1	4.0	7.8	22.8	67.6	100	gamma	0-40
Favites flexuosa	194	0.0	16.0	4.0	3.0	3.3	15.0	73.2	142	gamma	1-20
Goniastrea favulus	128	0.0	10.0	3.5	3.0	2.3	7.3	91.4	117	normal	0-15
Leptoria phrygia	240	0.0	54.0	5.3	3.0	8.5	20.9	75.8	182	gamma	0-30
Pocillopora damicornis	2954	0.0	98.0	6.7	3.0	14.5	31.3	77.6	2292	gamma	1-20
Porites annae	105	0.0	40.0	6.5	4.0	9.2	25.3	71.4	75	gamma	0.5-30
High-energy encrusting assemblage											
Acropora microphthalma	201	1.0	13.0	4.8	5.0	2.6	9.7	74.1	149	gamma	5-20
Montipora danae	90	0.0	48.0	5.0	4.0	5.8	18.4	73.3	66	gamma	0-40
Montipora monasteriata	62	0.0	48.0	4.7	3.0	6.9	20.9	72.6	45	gamma	1-40
Montipora undata	87	0.0	11.0	4.3	5.0	3.1	16.4	74.7	65	gamma	2-30
Cyphastrea microphthalma	109	0.0	40.0	4.1	2.0	7.0	17.7	87.2	95	gamma	0-30
C. serailia	263	0.0	30.0	4.9	4.0	4.8	16.3	74.9	197	gamma	0-50
Echinopora lamellosa	245	0.0	52.0	5.5	4.0	7.9	18.9	76.3	187	gamma	1-40
Merulina ampliata	257	0.0	52.0	5.8	5.0	7.3	20.0	69.3	178	gamma	0-50
Echinophyllia aspera	154	0.0	60.0	6.0	5.0	6.5	17.9	69.5	107	exponential	3-40
Lobophyllia corymbosa	136	0.0	16.0	6.0	6.0	3.2	11.3	55.9	76	normal	2-40
L. hemprichii	317	0.0	30.0	5.4	5.0	3.3	12.0	68.1	216	Weibull	1-50
Goniopora columna	58	0.0	24.3	5.0	5.0	4.0	12.0	86.2	50	gamma	2-15
G. lobata	19	0.0	12.0	4.2	4.0	2.8	12.5	84.2	16	exponential	2-10
Porites lutea	877	0.0	52.0	5.9	0.0	14.7	4.6	85.6	751	log-normal	0-30
Seriatopora hystrix	286	0.0	62.0	6.8	6.0	6.1	16.4	57.7	165	gamma	1-20
Pachyseris speciosa	223	0.0	30.0	6.6	6.0	4.7	16.6	57.4	128	Weibull	4-25

RESULTS

Coral assemblages

Western Atlantic/Caribbean

Modern

Acropora palmata has been widely used as the main, mostly single past RSL indicator (Table 1 and Supplementary table) since the work of Lighty *et al.* (1982), who proposed a depth range of <1 to 5 m for frameworks of this species based on many previous observations of different authors across the Western Atlantic. The applicability of *A. palmata* as a RSL indicator using modern depth distribution data of the species at regional to local scales has been largely detailed by Hibbert *et al.* (2016, 2018). A more precise RSL reconstruction can be attained when the *A. palmata* records are characterised with additional observations on facies and taphonomy. Colonies of *A. palmata* are considered indicative of reef crest/flat facies formed in less than 2 m depth when covered by thick crusts of CCA (Blanchon & Perry, 2004; Stathakopoulos *et al.*, 2020). In the Caribbean no assemblage/multispecies approach would improve the results that could be obtained by using *A. palmata* alone. A few papers (Ludwig *et al.*, 1996; Fruijtier *et al.*, 2000) suggested that the optimum growth depth of other corals, such as *Orbicella annularis* (as *Montastraea annularis*) and *Pseudodiploria strigosa* (as *Diploria strigosa*), and *Colpophyllia* sp. is restricted to shallow water and can be used as palaeo-RSL indicator. However, other authors question any narrow depth distribution of Caribbean corals, other than *A. palmata,* to the point of considering all of them 'deep-water corals' (Khan *et al.*, 2017). However, species of *Pseudodiploria* (formerly known as *Diploria clivosa* and *D. strigosa*), have unimodal distributions with median and average values above 10 m, according to the OBIS database.

Fossil

Mesolella (1967) observed in the Pleistocene reef terraces in Barbados a coral zonation similar to that described in modern Caribbean reefs. Accordingly, he interpreted that the top of the zone characterised by *Acropora palmata* with thick CCA crusts indicates the palaeo-mean low tide level. Since then, many studies have used the occurrence of *A. palmata* to reconstruct RSL and infer ESL (for example Fairbanks, 1989; Blanchon *et al.*, 2009; Muhs *et al.*, 2011; Abdul *et al.*, 2016; Khan *et al.*, 2017; Stathakopoulos *et al.*, 2020) or to interpret palaeowater depth of reef deposits (see Supplementary table).

Indo-Pacific province

Modern

Coral assemblages characterised by coral morphology and taxonomic composition, together with other encrusters, are typical of distinct environments with a defined depth range and can be used for reconstructing palaeo-RSL. Davies & Montaggioni (1985) reported the results of a discussion panel in the 5th International Coral Reef Congress in Tahiti that summarised the knowledge at that time on reef growth and sea-level change. Following unpublished data of Faure (1982), they suggested that common species of *Acropora*, such as *A. abrotonoides* (as *A. abrotonoides* and *A. danai*) and *A. robusta*), are indicative of waters shallower than 10 m. Davies & Montaggioni (1985) also proposed that detailed vertical zonations of coral assemblages, such as those published by Done (1982) could have regional applicability for RSL reconstructions. The robust-branching coral assemblage (community, facies) was proposed as particularly precise, typical of upper forereef to outer reef flat settings and palaeodepths of less than 6 m (Montaggioni & Faure, 1997; Cabioch *et al.*, 1999; Montaggioni, 2005, Table 1). Components can change depending on the region although dominant taxa,

namely *Acropora robusta-danai* group, *A. humilis* group and *Pocillopora verrucosa* are common in all reported localities. Other coral assemblages, such as the tabular branching community, dominated by *Acropora hyacinthus, A. cytherea and Montastrea* or a domal *Porites* community, were considered less precise indicators of deeper slope environments, outer reef flats or windward settings in lagoons (Camoin *et al.*, 1997; Montaggioni & Faure, 1997). This community/assemblage scheme was followed by Cabioch *et al.* (1999) who defined reef-building assemblages that can be used as reliable palaeo-RSL markers throughout the Indo-Pacific region (Supplementary table). These authors provided more detailed accounts of coral species belonging to each assemblage and stressed that components and distribution of these assemblages can vary according to local environmental conditions (e.g. irradiance, water energy) (Supplementary table). Montaggioni (2005), in his analysis of coral assemblages in the Indo-Pacific, maintained the assemblages proposed by Montaggioni & Faure (1997) and Cabioch *et al.* (1999) and added three more coral-dominated facies: arborescent-coral, foliaceous-coral and encrusting-coral facies (Table 1).

Montaggioni & Braithwaite (2009) in their synthesis of Quaternary reefs follow the scheme of Montaggioni (2005) to define coral zonation in the Indo-Pacific province. These authors acknowledge that coral growth forms, reflecting environmental conditions, are more diagnostic in terms of zonation than species composition due to the overlap of species distributions, referring to works by Braithwaite (1971); Rosen (1971, 1975), Pichon (1978) and Riegl & Piller (2000). According to Montaggioni (2005) and Montaggioni & Braithwaite (2009), the robust-branching-coral assemblage, characteristic of windward reef margins, represents the most precise palaeo-RSL marker based on fossil corals, indicating coral growth shallower than 6 m. The domal, the tabular–branching, arborescent and foliaceous coral assemblage can extend to depths of 15 to 20 m. The encrusting coral assemblage is limited to the top 10 m in high-energy settings, although components of this assemblage (e.g., *Pachyseris speciosa*, *Leptoseris*, *Echinophyllia*) can be dominant on reef slopes deeper than 20 m. The distributions of assemblages might vary independently of depth, due to other factors such as wave energy (Rosen, 1971) and, locally, water temperature and turbidity (Braithwaite, 2016). In any case, on steeper slopes or more turbid inner-shelf reefs, the coral assemblages adapted to lower irradiance may extend into shallower parts of the reef slope (Done, 1982; Montaggioni & Braithwaite, 2009).

Quantitative surveys were conducted at One Tree Reef, southern Great Barrier Reef, by Dechnik *et al.* (2017) to investigate the distribution of corals, CCA and vermetid gastropods between 0 and 30 m in two contrasting wave-energy settings (i.e. windward and leeward slopes). *Acropora* gr. *humilis*, *A. robusta* and encrusting *Isopora* are dominant from 0 to 6 m on the windward margin and *A*. gr. *humilis* and columnar *Isopora* are dominant from 0 to 3 m on the leeward margin. *Pocillopora* is common in both settings. These results are consistent with descriptions of the shallowest reef margin assemblages elsewhere in the Indo-Pacific province. Coral assemblages defined by Dechnik *et al.* (2017) below 6 m are characterised by massive *Porites*, associated with tabular *Acropora* down to 20 m, and from 20 to 30 m with encrusting *Montipora* on the windward margin and *Seriatopora* and *Lobophyllia* on the leeward margin.

The available data in OBIS on depth distributions of component species of the assemblages believed to have the narrowest and shallowest range, i.e. the robust-

branching and the shallow, high-energy subtype of the encrusting coral assemblages of Montaggioni (2005), strongly supports their use as palaeo-RSL markers (Table 2, Figs 1 and 2).

Regarding the robust-branching assemblage, taking into account the OBIS database, whilst a few typical species such as *Acropora robusta* and *Acropora abrotanoides, Pocillopora grandis* (= *P. eydouxi*) and *Goniastrea retiformis* have a polymodal or bimodal distributions with wide depth range (0 to 55 m), many other component species, such as *A. humilis, A. aspera, A. nasuta, A. hyacinthus, A. latistella, A. gemmifera and A. palmerae, Isopora palifera, Pocillopora damicornis, Leptoria phrygia, Favites flexuosa* and *Goniastrea favulus* have unimodal distributions and median and average depths of records shallower than 10 m (Table 2, Fig. 1). However, it is noted that the bimodal distribution of *Acropora robusta* is not supported by the published literature. Muir & Pichon (2019) do not identify *A. robusta* as a mesophotic reef-building coral species and Muir *et al.* (2015) describe this species as exclusively shallow in North-East Australia. However, morphologically similar species, i.e., *A. abrotanoides* and *A. intermedia* (Wallace, 1999), were reported from the upper mesophotic zone in the Tuamotu Islands (Muir & Pichon, 2019) and American Samoa (Montgomery *et al.*, 2019), respectively.

Establishing precise probabilities of finding two or more of these species together in a defined depth range (for example the 0-6 m assumed in many papers as typical depth range for the assemblage) is difficult as the relative frequency of the species is highly variable and only provided in relatively few available data sets. However, the remarkable coincidence of mode, median and average depths of many component species suggest that the robust-branching coral assemblage when defined by several species is a reliable indicator of palaeodepths shallower than 10 m (Fig.7; Table 2). In the case of *A. hyacinthus*, *A. latistella* and *G. favulus*, according to their probability distributions 95% of the records would be shallower than about 10 m. In addition, as an average, more than 80% of the records of the assemblage components are shallower than 6 m (Table 2).

In the case of the high-energy subtype of encrusting coral assemblage (Montaggioni, 2005), according to OBIS data, some component species, such as *Montipora capitata*, *M. patula, Leptastraea purpurea* and *Leptoseris mycetoceroides* have bimodal distributions and occur both in shallow and mesophotic reefs. However, the majority of species assigned to this assemblage (*Montipora monasteriata, M. danae, M. undata, Pachyseris speciosa, Echinophyllia aspera*, *Echinopora lamellosa, Cyphastrea microphthalma, C. serailia, Merulina ampliata and Porites lutea*) mainly occur in shallow depths, with modes and medians well above 10 m and theoretical distributions with 95% of records shallower than 10 m in a few cases (*A. microphthalma* and *P. lutea*) (Table 2, Fig. 2). As an average, 73% of records of the components of this assemblage are shallower than 6 m.

Ideally, the depth distributions of the species should be based on local to regional surveys encompassing a wide depth range in the vicinity of the study site (Dutton *et al.*, 2015; Hibbert *et al.*, 2016; Dechnik *et al.*, 2017; Chutcharavan & Dutton, 2020).

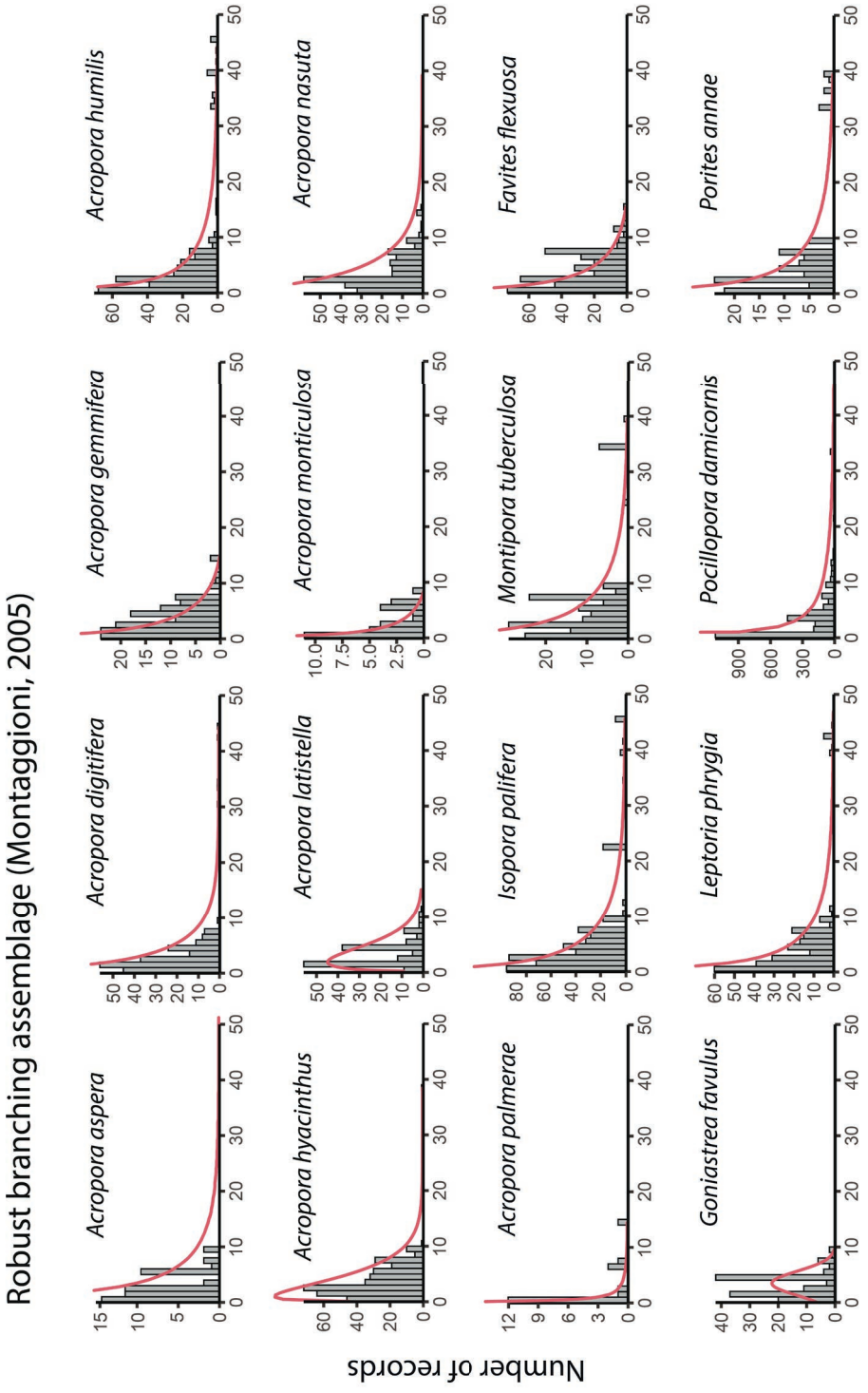


Fig. 1. Modern depth distributions for 16 Indo-Pacific coral species characteristic of the ‘ Robust-branching coral assemblage’ with gamma and unimodal theoretical depth distributions according to OBIS database (accessed October 2021). Species arranged according to family ascriptions. Depth bins = 1 m. Red lines: best fit distribution. See Table 2 for descriptive statistics.

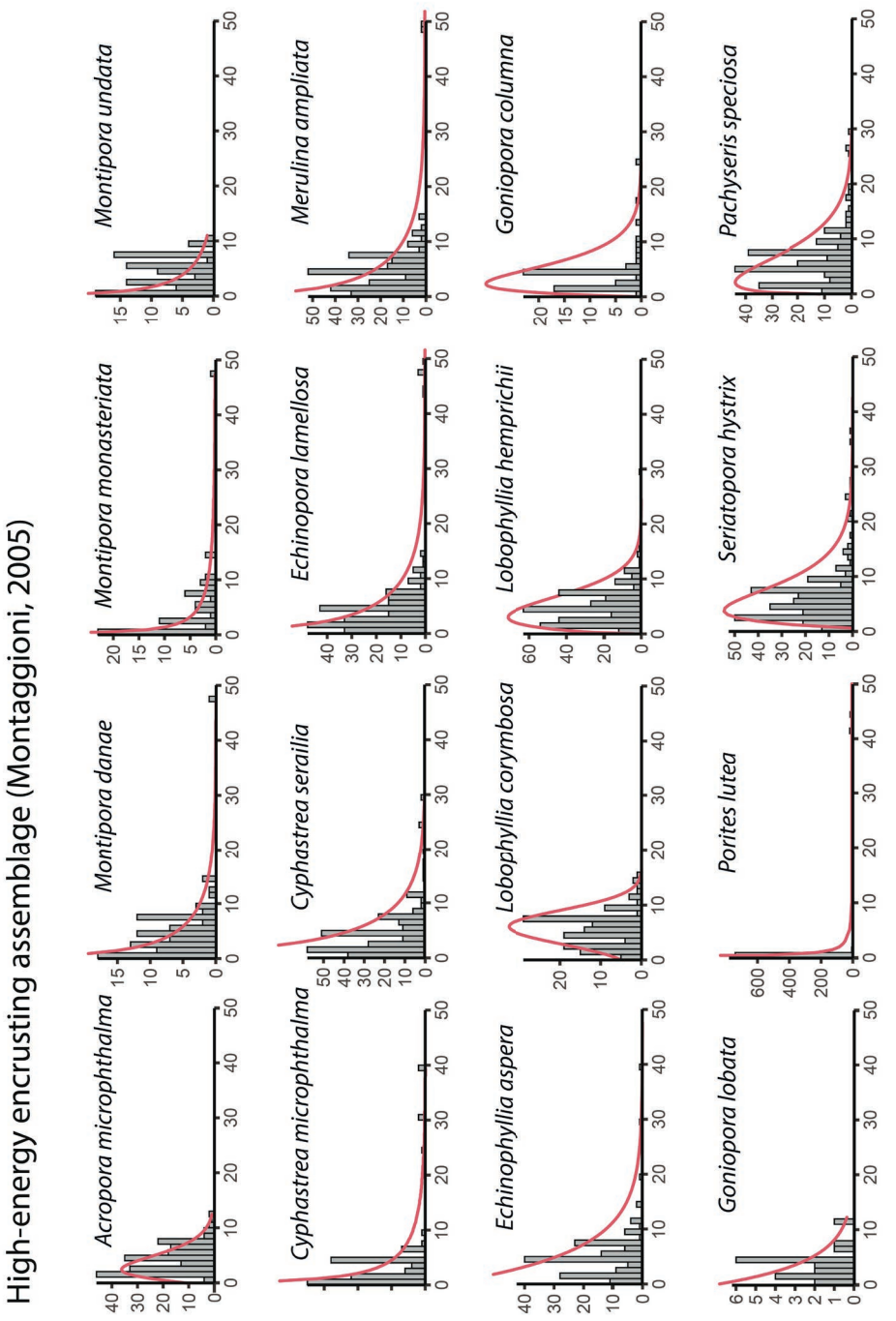


Fig. 2. Modern depth distributions for 16 Indo-Pacific coral species characteristic of the ‘ High-energy encrusting coral assemblage’ with gamma and unimodal theoretical depth distributions according to OBIS database (accessed October 2021). Species arranged according to family ascriptions. Depth bins = 1 m. Red lines: best fit distribution. See Table 2 for descriptive statistics.

Fossil

Nakamori (1986) assigned the Pleistocene coral assemblages in the Ryukyu Islands to a series of communities corresponding to living coral communities that are characteristic of different environments in fringing reefs in the archipelago. Nakamori (1986) considered two of those fossil communities (Community A, composed of branching *Acropora, Montipora* and hemispherical *Porites* and Community B, formed by tabular *Acropora*) indicative of reef crests developed almost at sea-level. Following a similar approach, Pirazzoli & Montaggioni (1988) proposed that the co-occurrence of *A. abrotonoides* (as *Acropora danae = A. danai*) and *Acropora robusta,* together with distinct CCA and vermetids (see below) in the Holocene reef deposits from Tahiti corresponds to the modern 'interlocking framework' at the reef margin in the island. Therefore, it would be characteristic of water depths shallower than 3 m. The coral-assemblage approach was systematised in several papers dealing with deglacial and Holocene deposits from the western Indian Ocean and Tahiti (Camoin *et al.*, 1997; Montaggioni *et al.*, 1997; Montaggioni & Faure, 1997, Supplementary table).

In the Ryukyu Islands, following the work of Nakamori (1986), palaeo-RSL reconstructions for Pleistocene and Holocene reefs were based on observation of depth distributions of coral assemblages in living reefs fringing the islands (Iryu *et al.*, 1995; Nakamori *et al.*, 1995; Wallace, 1999) or direct observations on living reefs near the Quaternary reefs, suggesting high-precision (less than 2 m in some cases) RSL indicators (Webster *et al.*, 1998; Sagawa *et al.*, 2001; Kayanne *et al.*, 2002; Sugihara *et al.*, 2003; Hongo & Kayanne, 2009, 2011).

With slight variations in their palaeodepth meaning, the coral assemblages proposed by Montaggioni and co-authors in the 90s and 2000s have been used as palaeo-RSL indicators in reconstructions of reef development and RSL curves based on reef cores or samples collected from the sea floor in diverse localities across the Indo-Pacific. In particular the occurrence of the robust-branching coral assemblage has been considered indicative of palaeodepths varying from 0–5 m to 0–10 m (Bard *et al.*, 1996; Galewsky *et al.*, 1996; Camoin *et al.*, 2001; Cabioch *et al.*, 2003; Webster & Davies, 2003; Camoin *et al.*, 2004; Webster *et al.*, 2004b; Frank *et al.*, 2006; Andersen *et al.*, 2008; Thomas *et al.*, 2009; Andersen *et al.*, 2010; Bard *et al.*, 2010; Shen *et al.*, 2010; Abbey *et al.*, 2011; Deschamps *et al.*, 2012; Dechnik *et al.*, 2015; Gischler *et al.*, 2016; Dechnik *et al.*, 2017; Gischler *et al.*, 2018a; b; Webster *et al.*, 2018; Yokoyama *et al.*, 2018; Humblet *et al.*, 2019; Webster *et al.*, this volume). In addition to the depth distribution proposed by Montaggioni's group, these papers refer to other works on Indo-Pacific coral ecology (see references in Supplementary table).

Coralline algae

Coralline algae are a group of red algae (Rhodophyta) that secrete calcium carbonate, high-Mg calcite, in their cell walls. They belong to four different, phylogenetically related orders (Corallinales, Hapalidiales, Sporolithales and Corallinapetrales) in the class Floridophyceae (Jeong *et al.*, 2020). From an anatomical point of view, corallines can be geniculate (articulated) with uncalcified portions in their body, or non-geniculate, possessing a thallus (body) fully calcified except at the very surface. The non-geniculate or crustose coralline algae (CCA) are common in modern coral reefs (Fig. 3) and related habitats, encrusting hard substrates or as unattached nodules called rhodoliths. They are major builders (Adey *et al.*, 1982; Bosence, 1983, 1991; Littler & Littler, 1984) and contribute significantly to

reef health and biodiversity, playing a role as settlement inducers of coral larvae (Morse *et al.*, 1996; Nelson, 2009; Vermeij *et al.*, 2011).

The first extensive synthesis of CCA as RSL indicators was presented by Adey (1986). This author considered CCA assemblages as precise indicators of palaeo-RSL in tropical areas, with ±2 m resolution near mean low sea-level and increasing uncertainty with increasing depth. This optimistic view is not fully supported by data on CCA distribution gathered since then but these data corroborate the potential of fossil CCA to estimate past RSL.

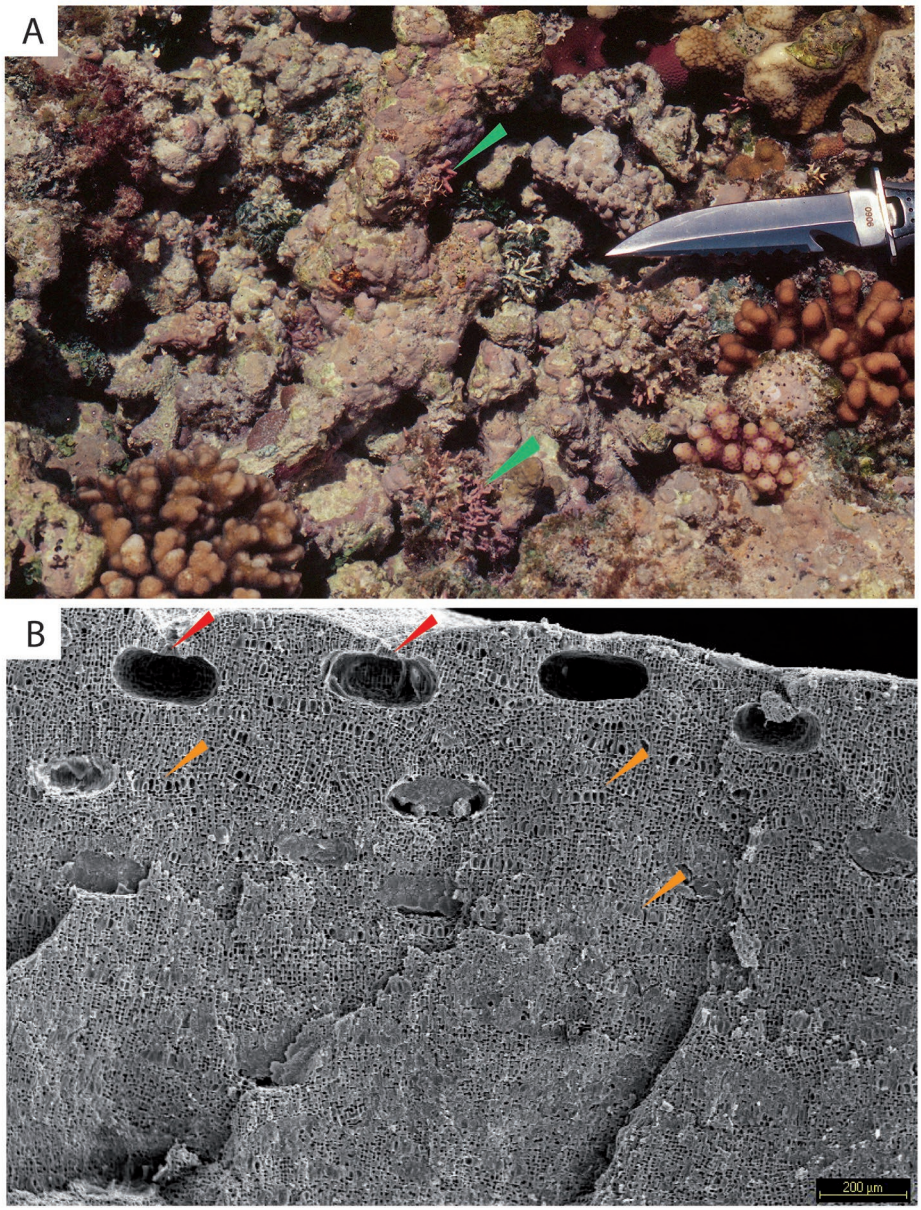


Fig. 3. *Porolithon* gr. *onkodes*. A) thick crusts of *P.* gr. *onkodes* (pink to purple surfaces) covering dead coral and rubble with some branching plants of *Lithophyllum* gr. *kotschyanum* (green arrowheads). B) SEM image of plants from the same locality showing the main diagnostic morphoanatomical characters of *P.* gr. *onkodes*: uniporate conceptacles (red arrowheads) and fields of trichocytes (orange arrowheads). Leeward coralgal rim, One Tree Reef, southern Great Barrier Reef, Australia.

Atlantic-Caribbean

Modern

Based on previous work of Adey (1975), Davies & Montaggioni (1985) considered CCA (*Lithophyllum kaiseri* and *Porolithon antillarum*, as *Lithophyllum congestum* and *Porolithon pachydermum*, respectively) reliable indicators of depths of 1 to 2 m. Adey (1986) described algal ridges as distinct features, consisting of massive carbonate frameworks built largely by CCA with foundations on coral reefs or other type of rocky substrate. Caribbean algal ridges extend from +2 m above mean sea-level to -6 m (Adey & Burke, 1976, 1977) but extensive framework develops only close to or slightly above mean low sea-level. These ridges are composed of *Lithophyllum kaiseri* and *Porolithon antillarum* (as *Lithophyllum congestum* and *Porolithon pachydermum* in Adey, 1986, respectively) and *Neogoniolithon*, with cryptic species of *Paragoniolithon* (currently considered a synonym of *Neogoniolithon*) (Table 1), *Hydrolithon, Sporolithon, Mesophyllum* and *Lithothamnion* (Adey, 1986). According to this author, on coral reefs in all oceans, thick (several cm scale) CCA encrustations are typical of less than 6 m, whereas deeper CCA are thin and leafy. Regarding taxonomic composition, assemblages dominated by *Porolithon* with cryptic *Hydrolithon* and *Neogoniolithon* occur in less than 10 m. *Neogoniolithon* (including *Paragoniolithon*) characterises assemblages in depths from 10 to 30 m and *Hydrolithon* dominates assemblages deeper than 30 m (Adey, 1986). On the other hand, friable fringing reefs/trottoirs of *Neogoniolithon strictum* are typical of very shallow water in protected areas of the Bahamas and Florida (Adey, 1986). A few years later, Martindale (1992) published a precise zonation of CCA in modern reefs in Barbados. Thick crusts of *Porolithon* sp. (*P. ?antillarum* as *P. ?pachydermum*) and *Lithophyllum* sp. (*L. ?kaiseri* as *L. ?congestum*) dominate in illuminated, shallow substrates (0 to 3 m). Thinner crusts of lithophylloids (as *Tenarea* sp.) predominate in slightly deeper water (3 to 8 m) and thin crusts of *Neogoniolithon* sp. and lithophylloids cover the well-lit surfaces between 8 and 16 m. Thin, foliaceous crusts of *Hydrolithon* sp., *Mesophyllum* sp. and *Lithothamnion* sp. characterise cryptic and deeper settings (20 to 50 m).

Following Geister (1977), Montaggioni & Braithwaite (2009) identify a CCA-dominated community, formed by 1 to 3 m-thick crusts of CCA and sparse corals in the most exposed reef crests in the Western Altlantic-Caribbean province.

In the Abrolhos reefs in the eastern Brazilian shelf, Jesionek *et al.* (2016) and Amado-Filho *et al.* (2018), consider *Porolithon gr. onkodes* and *Melyvonnea erubescens* indicative of depths between 2 and 5 m (Table 1), whilst *Dawsoniolithon* gr. *conicum* (as *Pneophyllum conicum*) is found above 15 m.

One of the robust clades in the phylogram of the *P. onkodes* group proposed by Gabrielson *et al.* (2018) comprises the holotype of *Porolithon antillarum* and the lectotype of *P. onkodes* f. *pachydermun* (i.e. the type of *P. pachydermum*, the ecological equivalent of the Indo-Pacific *P. onkodes* – see below – in the Caribbean, Adey 1986). The Atlantic *P. antillarum* and *P. pachydermum* were considered morphologically indistinguishable from and younger synonyms of *P. onkodes* by Maneveldt & Keats (2014). Despite the morpho-anatomical similarity and traditional interpretations of ecological equivalence (Adey, 1979, 1986; Martindale, 1992), the depth distribution of *P. antillarum* (including *P. pachydermum* as a younger synonym) according to OBIS database is substantially different from the one of *P. onkodes* (Table 3, Fig. 4). While the latter is restricted to the upper few metres (see below), *P. antillarum*

is reported in 31 records in a depth range from 3 to 80 m and with average depths of 29 m ± 19.3 sd.

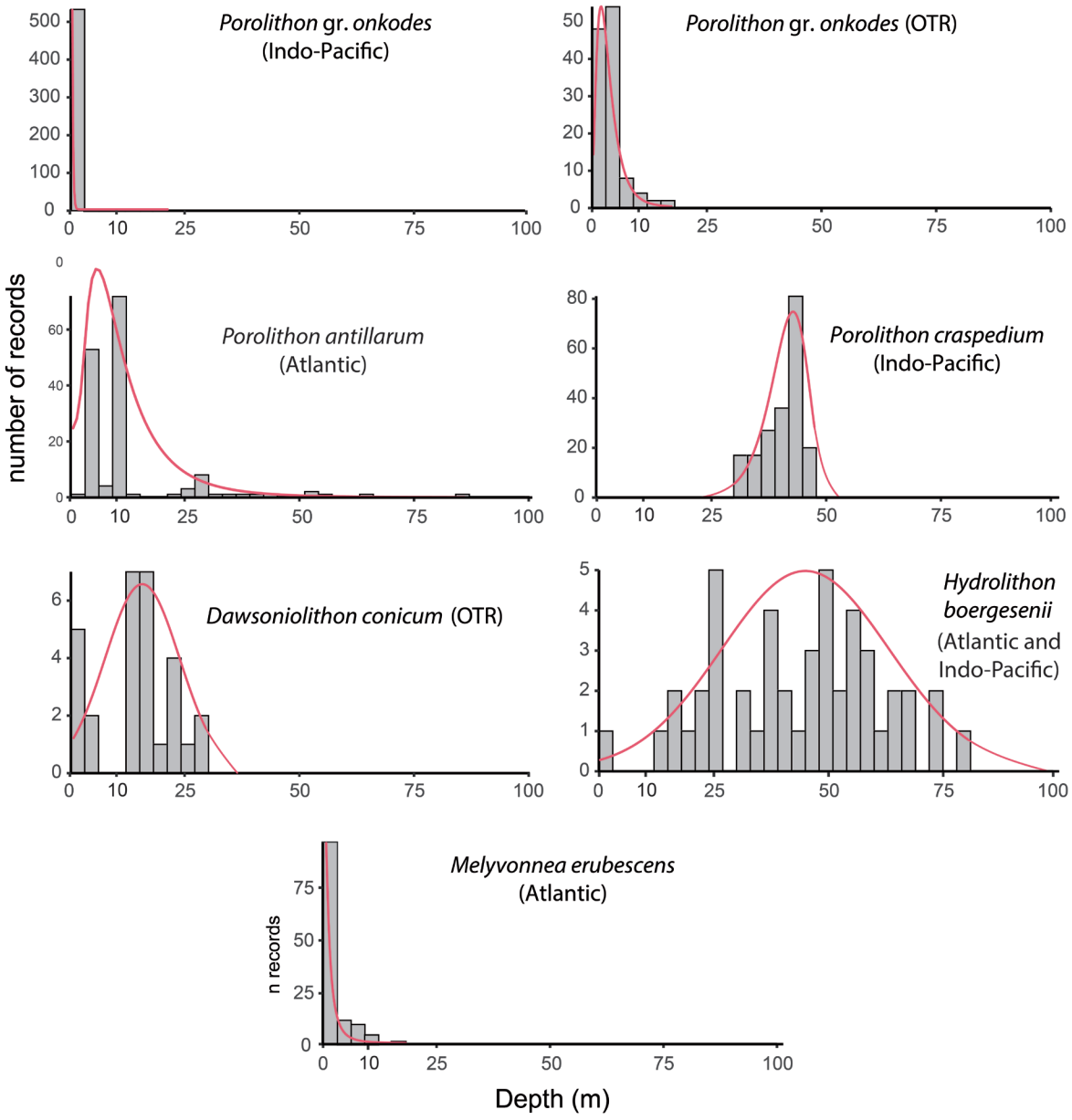


Fig. 4. Modern depth distributions of coralline algal species common in coral reefs with enough data in the OBIS database (accessed October 2021) to be statistically significant; and distributions in One Tree Reef (OTR) of significant species according to Dechnik *et al.* (2017). Depth bins =3 m. Red lines: best fit distribution. See Table 3 for descriptive statistics.

Table 3. Modern depth range, median depth and depth for maximum 95% confidence interval (95% shallower records) of coralline algal species common in coral reefs with enough data for statistical analysis in the OBIS database (accessed October 2021) and distributions in One Tree Reef (OTR) of significant species according to Dechnik *et al.* (2017). Vermetid taxa used as palaeo-RSL indicators in coral reefs with enough data for statistical analysis in OBIS (accessed October 2021).

Taxon	Number of observations	Min. Depth (m)	Max. Depth (m)	Mean (m)	Median (m)	SD	Value at 95 percentile (m)	% records shallower than 6 m	Records shallower than 6 m	Best fit Distribution
Coralline Algae										
Hydrolithon boergesenii (Atlantic and Indo-Pacific)	47	0.0	79.0	44.1	46.0	18.2	73.6	2.1	1	normal
Porolithon craspedium (Indo-Pacific)	198	32.0	48.0	41.3	42.5	4.0	46.5	0.0	0	Weibull
Porolithon antillarum (Atlantic)	153	2.0	85.0	12.4	10.5	12.4	29.1	35.3	54	log-normal
Porolithon onkodes (Indo-Pacific)	536	0.0	19.0	0.1	0.0	1.0	0.2	99.6	534	log-normal
Melyvonnea erubescens (Atlantic)	121	0.0	17.0	2.0	0.5	3.2	5.5	88.4	107	log-normal
Coralline Algae One Tree Reef										
Dawsoniolithon conicum (OTR)	29	0.0	27.4	14.3	16.4	7.8	27.1	24.1	7	normal
Porolithon onkodes (OTR)	118	1.0	16.6	4.1	3.5	2.8	8.8	86.4	102	log-normal
Vermetids										
Ceraesignum maximum (Indo-Pacific)	310	8.0	28.0	12.6	12.0	1.9	15.1	0.0	0	logistic
Dendropoma spp. (Atlantic)	97	0.0	91.0	3.9	0.8	12.1	9.7	85.6	83	log-normal
Dendropoma spp. (incl. *C. maximum*)	406	0.0	91.0	10.5	12.0	7.1	19.8	20.4	83	logistic

Fossil

In the Western Atlantic-Caribbean province, Mesolella (1967) considered thick crusts of CCA typical of the shallowest reef crest (mean low sea-level) in the Pleistocene reef zonation in Barbados. Despite this early report and the pioneer work of Adey & Burke (1976, 1977) and Adey (1986) on algal ridges, CCA have only rarely been used as palaeo-RSL indicators in the western Atlantic and Caribbean Quaternary reefs. Martindale (1992), based on his own observations in modern reefs in Barbados (see above), interpreted thick crusts of *Porolithon* and *Lithophyllum* in Pleistocene reefs in the island as indicative of very shallow, high energy settings. Blanchon *et al.* (2002) report *Porolithon* and *Lithophyllum* associated with *A. palmata* in reef-crest deposits (<5 m depth) in the Holocene of Grand Cayman. In the Holocene of Yucatan, Blanchon & Perry (2004) interpret *A. palmata* branches encrusted by cm-thick CCA, especially *Porolithon*, as indicative of reef crest/flat facies formed in less than 2 m depth, according to their own observations in the nearby modern reef. Blanchon & Eisenhauer (2001) and Blanchon *et al.* (2009) report an encruster association of thick CCA, vermetids and the foraminifer *Homotrema rubrum* as a very shallow (<1 m) facies in the LIG deposits of Barbados and Yucatan, respectively. In Saint Croix, Virgin Islands, also in LIG deposits, Toscano *et al.* (2012) include crusts of CCA and *H. rubrum* as indicators of shallow water (<5 m). In the southern Atlantic, the occurrence of *Porolithon* gr. *onkodes* and *Melyvonnea erubescens* is used by Vieira *et al.* (this volume) as shallow palaeo-RSL indicators (<5 to 10 m) in the LIG and Holocene reefs in the Abrolhos shelf in eastern Brazil (see Supplementary table).

Indo-Pacific

Modern

Davies & Montaggioni (1985) suggested that CCA ridges mainly formed by *P. onkodes* and *Porolithon gardineri* are precise indicators of mean low water springs (±0.5 m) in the Pacific Ocean. According to Adey (1986), mainly based on Adey *et al.* (1982), genera in Indo-Pacific CCA assemblages show distributions similar to those in the Caribbean. *Porolithon* and *Neogoniolithon* dominate assemblages in less than 10 m (Table 1). *Neogoniolithon* (including *Paragoniolithon*) replaces *Porolithon* down to 20 to 25 m and *Hydrolithon* dominates assemblages deeper than 30 m; *Lithothamnion, Mesophyllum* and *Sporolithon* (as *Archaeolithothamnium*) are the most common CCA below 50 m. In the Ryukyu Islands, Iryu *et al.* (1995) recorded a dominance of *Porolithon onkodes* (as *Hydrolithon onkodes*), *Lithophyllum* and *Dawsoniolithon conicum* (as *Neogoniolithon conicum*) in the upper 10 m. The proportion of *Neogoniolithon* substantially increases from 10 to 20 m and *Hydrolithon* and *Mesophyllum* mainly occur below 20 m.

Cabioch *et al.* (1999) considered thick crusts of *Porolithon* cf. *onkodes* (as *Hydrolithon*) and *Neogoniolithon* cf. *fosliei* characteristic of depth less than 6 m (Table 1), whereas thinner crusts dominated by *Lithophyllum* and *Mesophyllum* would indicate depths of 6 to 15 m (see Supplementary table). Additional data on species depth distributions were published in accounts of local CCA assemblages (for example CCA on Heron Reef in the Great Barrier Reef, Ringeltaube & Harvey, 2000) and algal guides, such as the one of Payri *et al.* (2000), for French Polynesia; and Littler & Littler (2003) for South Pacific reefs.

Rasser & Piller (1996; 1997) recognised a different CCA assemblage as a potential palaeodepth indicator in living reefs in the northern Red Sea. These authors observed an

association of *Lithophyllum kotschyanum*, together with *P. onkodes* (as *Hydrolithon*) and *Neogoniolithon brassica-florida* encrusting corals, forming rhodoliths or frameworks on the intertidal or shallow subtidal reef flat. Another association, characterised by *P. onkodes* extends down to 15 m (Rasser & Piller, 1997).

Among the facies recognisable in the Indo-Pacific coral reefs, Montaggioni (2005) distinguished a 'Coralline algal facies' formed by crusts of *P. onkodes* (as *Hydrolithon*), *Neogoniolithon* spp., *Mesophyllum* sp. and *Lithophyllum* sp., associated with encrusting foraminifers, vermetid gastropods and serpulids. The crusts can reach up to 2 m in thickness in windward reef crests and flats, and lagoonal patches exposed to high turbulence, being thinner in more sheltered areas. According to Montaggioni (2005), *Porolithon* cf. *onkodes* also forms thick crusts in the 'Robust-branching coral facies' typical of depths shallower than 6 m; and CCA crusts 1 to 10 cm-thick occur in windward reef flats of the 'Domal coral facies'. Montaggioni & Braithwaite (2009) include calcareous alga-dominated communities equivalent to the 'Coralline algal facies' of Montaggioni (2005) in their zonation scheme of Indo-Pacific reefs.

Molecular work suggests that at least 20 distinct cryptic CCA species are passing under the name *Porolithon onkodes* following morphological diagnostic characters (Gabrielson *et al.*, 2018). Nevertheless, in the Indo-Pacific the available data on *P. onkodes* distribution reflect the distribution of CCA with a morphoanatomy traditionally included in *P. onkodes* (herein referred as *Porolithon* gr. *onkodes*), characterised by smooth encrusting plants with common horizontal fields of trichocytes becoming buried in the thallus (Maneveldt & Keats, 2014).

According to the OBIS records, the probability depth distribution of *P. onkodes* is log-normal with most records at 0 m depth and with a 95% being shallower than 0.2 m (Table 3, Fig. 4). However, this distribution is probably biased by disproportionate dominance of shallow water surveys. In one of the few quantitative analyses of CCA distributions, Dean *et al.* (2015) only acknowledge a small effect of depth on composition of CCA assemblages on the Great Barrier Reef. However, they report that relative proportions of *P. onkodes* decreases from around 51% of total CCA species in sites shallower that 5 m to 14% below this depth, with no further data on depth ranges of the species.

In a systematic sampling of CCA both in the windward and leeward sides of One Tree Reef (GBR), *P.* gr. *onkodes* ranges from 1 to 27.5 m below mean sea-level (median: 3.6 m, mean: 4.7 m±4.1 sd, Dechnik *et al.*, 2017). The theoretical log-normal distribution based on 124 samples indicates that 95% of samples are shallower than 10.5 m. However, if only thick plants (thicker than 0.2 mm) are considered, as it is the common procedure in palaeo-RSL estimates, 95% of samples are shallower than 8.8 m (data from Dechnik *et al.*, 2017) (Table 3, Fig. 4).

Porolithon craspedium, whose common depth range according to phycologists is shallower than 20 m (Littler & Littler, 2003; Maneveldt & Keats, 2016), in the OBIS database (as *Hydrolithon craspedium*) is only reported below 30 m (32.5 to 46.5 m range, average 41.3 m±4 sd) (Table 3, Fig. 4). This example and the biased record of *P.* gr. *onkodes* suggest that the OBIS records of CCA species are questionable, probably due to the extreme difficulty of *in situ* identification of CCA taxa. The external morphology of many species is convergent and, without the aid of a hand lens and in many cases of optical or scanning electron

microscopy, no confident identification is possible.

Regarding CCA species that are characteristic or secondary components of assemblages with wider depth ranges, OBIS data on their depth distributions with statistical significance are very scarce. Among the few taxa with more than 30 records, *Melyvonnea erubescens* was found in the upper 20 m, whereas *Hydrolithon boergesenii* extends down to 80 m (Fig. 4). According to the OBIS database *Lithophyllum* gr. *prototypum* is restricted to 0 m. However, this species and species that can be included in this species group, such as *Titanoderma tessellatum,* have been observed at greater depths (down to 40 m, Littler & Littler, 2003). *Dawsoniolithon* gr. *conicum*, with no significant OBIS data, on One Tree Reef ranges down to 27 m, with maximum frequency from 10 to 20 m (as *'Pneophyllum' conicum*, Dechnik *et al.*, 2017; Fig. 4).

Fossil

Pirazzoli & Montaggioni (1988) used the occurrence of *Porolithon onkodes* and *Neogoniolithon fosliei* to support their interpretation of massive branching *Acropora* facies with vermetids as a shallow water (<3 m) indicator in Tahiti Holocene reefs. In these same reefs, Montaggioni *et al.* (1997) include thick crusts (>2 cm) of *Porolithon onkodes* and minor *Neogoniolithon fosliei* as diagnostic components of the shallow water (<6 m) coralgal assemblage (robust branching community). Thinner crusts of *Neogoniolithon, Lithophyllum* (also as *Dermatolithon*) and *Lithothamnion* (as *Mesophyllum prolifer*) species would prevail in deeper assemblages with rare or absent *P. onkodes* (Supplementary table).

Thick crusts of *P. onkodes* (as *Hydrolithon onkodes* in several papers) have been considered the main component (and diagnostic) of CCA assemblages characteristic of shallow water depths (<10 m) in a number of papers dealing with Indo-Pacific Quaternary records based either on samples collected on the sea floor (Camoin *et al.*, 2004; Webster *et al.*, 2004b; a, 2006, 2009; Cabioch *et al.*, 2008; Sanborn *et al.*, 2017; Hallmann *et al.*, 2020) or from drill cores (Camoin *et al.*, 2001, 2004, 2012; Cabioch *et al.*, 2003; Braga & Aguirre, 2004; Abbey *et al.*, 2011; Dechnik *et al.*, 2015, 2017; Gischler *et al.*, 2016, 2018b; a, this volume; Webster *et al.*, 2018, this volume; Yokoyama *et al.*, 2018; Humblet *et al.*, 2019; Montaggioni & Martin-Garin, 2020). In other cases, *P. onkodes* was considered indicative of a wider depth range (0 to 20 m, Iryu *et al.*, 2010) (Supplementary table).

Frameworks of branching *L. kotschyanum* have been interpreted as indicative of very shallow subtidal palaeoenvironments in Pleistocene (MIS 7 and 5) reefs in the Danakil Depression, Afar, Ethiopia, a basin connected to the Red Sea in its Quaternary evolution (Jaramillo-Vogel *et al.*, 2019).

The palaeowater depth to be interpreted from all *in situ* CCA fossil assemblages is the shallowest depth range of the co-occurring species. When the framework substrate on which they grew is overshadowed by new coral growth, shallow-water species that grew on well-illuminated surfaces can be overgrown by species characteristic of less illuminated habitats, which are the same as the deeper ones as light intensity is a major controlling factor on CCA distribution (Martindale, 1992; Abbey *et al.*, 2011).

Vermetids

Vermetids (Family Vermetidae, Class Gastropoda) include species of sessile, suspension-feeding, irregularly coiled marine snails living in warm temperate and tropical oceans (Golding *et al.*, 2014). They attach to hard substrates, including CCA, dead and living coral (Fig. 5) and have deleterious effects on reef building corals by reducing

their skeletal growth and survival (Zvuloni *et al.*, 2008; Shima *et al.*, 2010, 2013).

Laborel (1986) presented an exhaustive synthesis of the applicability of vermetid bioconstructions as RSL indicators. However, these bioconstructions, which are precise markers of upper subtidal to low intertidal transition, usually form on rocky shorelines and do not develop on actively growing coral reefs. In coral reefs, vermetids attach to hard substrates commonly encrusting CCA but they remain as secondary components of the reef-building, encrusting community.

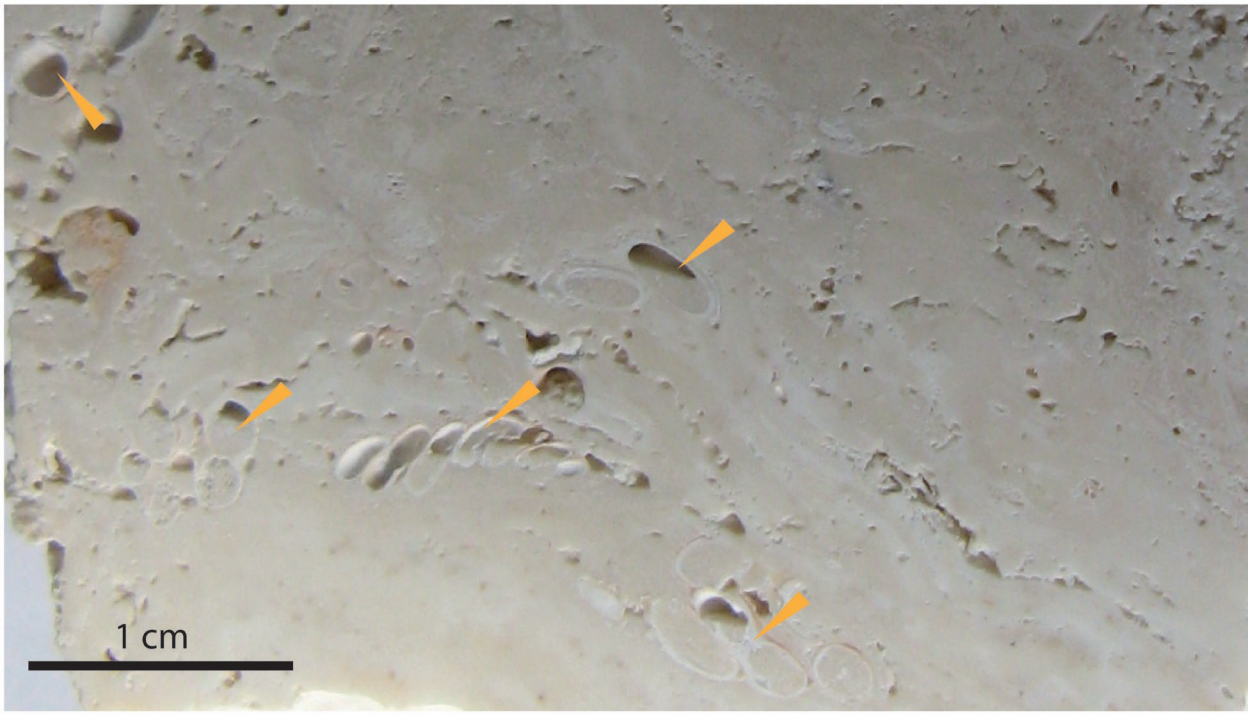


Fig. 5. Vermetid gastropods (orange arrowheads) intergrown with coralline algae in leeward coral framework, Holocene, One Tree Reef, southern Great Barrier Reef, Australia.

Atlantic/Caribbean

Modern

The gregarious vermetid *Dendropoma corrodens* is an abundant component in rims of cup reefs and constructional lips that develop at mean low tide level in Bermuda. *Dendropoma* densities are about 3000 individuals per m^2 in average with a high variance (Thomas & Stevens, 1991; Table 1).

Dendropoma sp. was identified as the most abundant framework builder after CCA in the raised reef rim both in the windward and leeward sides of Atol das Rocas in Brazil (Gherardi & Bosence, 2001). In the fringing reefs of Abrolhos Archipelago in the eastern Brazilian shelf, '*Dendropoma' irregulare* (uncertain generic placement = *Vermetus irregularis*, Golding *et al.*, 2014) is an important component, together with *Porolithon antillarum* (as *P. pachydermum*) of reef edges, which at high tide have an average depth of 2 m and are subaerially exposed at low tide (Tâmega *et al.*, 2014; Spotorno-Oliveira *et al.*, 2015; Table 1).

Fossil

In the Caribbean, the occurrence of abundant *Dendropoma* was used by Blanchon & Eisenhauer (2001) as indicative of palaeodepths of <1 m (lower quarter of tidal range) in LIG deposits (*A. palmata* rudstone)

from Barbados. The presence of vermetids and CCA and the foraminifer *H. rubrum* encrusting clasts of *A. palmata* was also considered characteristic of mean lower water in MIS 5e reefs from Yucatán (Blanchon *et al.*, 2009). Dechnik *et al.* (2019) suggest a palaeodepth of <1 m for corals heavily encrusted by thick CCA and vermetids in the Holocene reefs in eastern Brazil (Supplementary table).

Indo-Pacific

Modern

In their comprehensive work on coralgal assemblages of the Indo-Pacific as RSL indicators, Cabioch *et al.* (1999) suggested that the vermetids *Dendropoma maximus*, currently named *Ceraesignum maximum* and *Serpulorbis annulatus*, are commonly associated with the robust branching coral facies and can be considered indicative of depths shallower than 5 m (Table 1). The name *Serpulorbis annulatus* is not currently accepted; the specific name *annulatus* is either applied to serpulid worms in the genus *Filogranula* (*F. annulata*) or considered synonym of *Dendropoma corrodens*. However, none of those taxa occur in the Pacific (WoRMS, World Register of Marine Species, 2021). According to Cabioch *et al.* (1999), the assemblage robust branching coral/*Porolithon* (as *Hydrolithon*)/vermetids (Reef edge -RE- assemblage) is characteristic of near-surface environments, <6 m. Montaggioni (2005) and Montaggioni & Braithwaite (2009) describe the association of vermetids with CCA in the 'coralline algal facies' in reef crests and reef flats. Montaggioni (2005) also refers to the abundance of vermetids in the robust-branching coral facies, characteristic of high-energy setting (0 to 6 m) and in the heavily encrusted subfacies of the domal coral facies, developing in windward reef flats (Table 1).

Depth distributions of living vermetids listed in OBIS seem to question the use of their occurrence as an indicator of very shallow water depth. Although members of the family Vermetidae have been mainly recorded in the shallower 20 m, they are most frequent from 10 to 20 m and extend down to depths of hundreds of metres (Table 3, Fig. 6). The genus *Dendropoma*, mentioned as indicative of very shallow water, was also most commonly identified from 10 to 20 m depth, both considering only the species currently included in the genus or taking into account others, such as *C. maximum*, that were included in the genus before relatively recent taxonomic revisions (Golding *et al.*, 2014). Individual species reported as restricted to 0 to 6 m, such as *C. maximum* (as *D. maximum*), for example in Cabioch *et al.* (1999), have also been mainly recorded below 10 m depth (Table 3, Fig. 6).

However, the OBIS inventories do not adequately reflect the abundance of the recorded taxa in the surveyed site and, therefore, relying upon modern depth distributions registered in OBIS overlooks the role of organisms as facies builders/components and the environmental/palaeoenvironmental significance of those facies. The vermetid formations in the low-intertidal/subtidal transition are well known in the Mediterranean, Brazilian and Caribbean shorelines (Laborel, 1986; Angulo *et al.*, 2006; Suguio *et al.*, 2013). In a similar way, *Dendropoma gregarium* forms benches in the intertidal zone in the Hawaiian Islands, with densities up to 60,000 individuals per m^2 (Hadfield *et al.*, 1972, as *D. gregaria*). However, the densities of non-gregarious vermetids associated to coral reefs are much lower than those outstanding concentrations. In the Red Sea north of Jeddah (Saudi Arabia) densities of about 22 individuals per m^2 of *C. maximum* (as *D. maximum*) characterise the outer reef flat (Hughes & Lewis, 1974). Also in the Red Sea, in the Gulf of Aqaba, the highest density of *C. maximum* was found on

the upper 1 m of the vertical wall at the seaward margin of the reef flat. At this margin, the average density measured by Ribak *et al.* (2005) was 6 individuals per m^2 and increased to 14 individuals per m^2 in a later study in the same area by Zvuloni *et al.* (2008). *C. maximum* occurred on the reef flat and was rare in the shallow lagoon but was absent deeper than 3 m (Ribak *et al.*, 2005). *C. maximum* (as *D. maximum*) is also nearly restricted to reef flats in the Bay of Sarfaga (Red Sea, Egypt) where it has average densities of 20 individuals per m^2, whereas its occurrence in other reef settings is anecdotal (Zuschin *et al.*, 2001). Average densities of 17 individuals per m^2 (up to 165 per m^2) were observed at the top of patch reefs in the Moorea lagoon before a mass mortality in 2015 (Brown *et al.*, 2016). However, little information is available on how to translate surface densities observed in modern ecological surveys to individuals per volume or per area perpendicular to the depositional surface of reef framework, which is the common approach used in the observation of vermetids in drill cores and fossil reef outcrops (Fig. 5). In an attempt to provide this kind of information, in One Tree Reef vermetid abundance was estimated in line transects, perpendicular across the CCA crusts. Vermetid densities higher than 5 individuals per cm are restricted to the shallower 6 m, both in the windward and leeward sides (Dechnik *et al.*, 2017), supporting the use of vermetid abundance as a RSL indicator in the Great Barrier Reef Quaternary records.

In short, vermetid gastropods live in modern oceans in a wide depth range and according to OBIS inventories no species is restricted to a narrow shallow-water zone. However, according to published records including abundance estimates mentioned above, relatively high densities of vermetids (>10 individuals per m^2) in coral/CCA reef communities only occur in shallow depths, from above mean low tide to some 6 m depth.

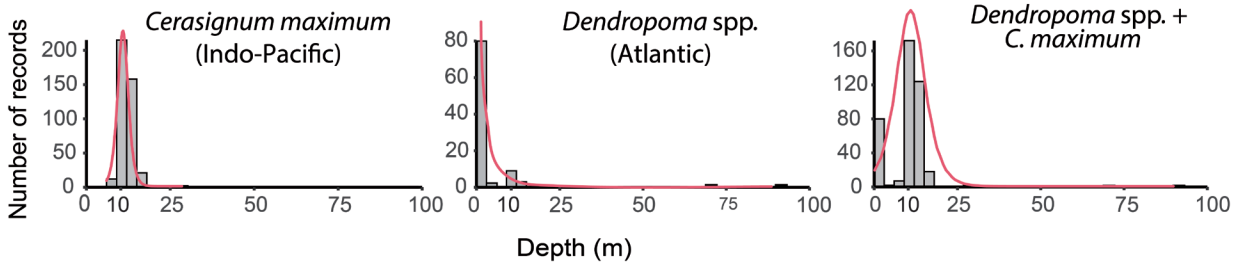


Fig. 6. Modern depth distributions of vermetid gastropod taxa used in palaeo-RSL reconstructions in coral reefs. Depth bins =3 m. Red lines: best fit distribution. See Table 3 for descriptive statistics.

Fossil

The occurrence of *Serpulorbis annulatus* (see comment above) in cores from Holocene reefs in Tahiti was used by Pirazzoli & Montaggioni (1988) to interpret palaeodepths of less than 3 m (Table 1). In cores from deglacial and Holocene reefs in the same Tahitian locality, Bard *et al.* (1996) considered the assemblage of robust-branching corals, CCA and vermetids indicative of depths <6 m. The abundance of vermetids in association with *P. onkodes* has been considered evidence to support a shallow palaeodepth (less than 10 m, usually less than 6 m) in the interpretation of coralgal assemblages from dill cores of Indo-Pacific Pleistocene and Holocene reefs (Camoin *et al.*, 2001; Cabioch *et al.*, 2003; Abbey *et al.*, 2011; Deschamps *et al.*, 2012; Dechnik *et al.*, 2015, 2017; Gischler *et al.*, 2016, 2018a; Webster *et al.*, 2018, this volume; Yokoyama *et al.*, 2018; Humblet *et al.*, 2019; Supplementary table).

CONCLUDING REMARKS

The validity of the coral assemblages as palaeodepth indicators in Quaternary reefs depends on the depth distributions of their modern component species. In the Western Atlantic-Caribbean province *A. palmata* is the most precise RSL marker and no assemblage approach improves its results (Hibbert *et al.*, 2016; Stathakopoulos *et al.*, 2020).

In the Indo-Pacific province, the available OBIS data on depth ranges of component species support the use of two assemblages considered indicative of narrow, shallow palaeodepth ranges with a 10 m uncertainty. In the case of the robust-branching assemblage (Table 1) many component species, such as *Acropora humilis, A. aspera, A. nasuta, A. hyacinthus, A. lastitella, A. gemmifera* and *A. palmerae*, *Isopora palifera, Pocillopora damicornis, Leptoria phrygia, Favites flexuosa* and *Goniastrea favulus* have unimodal distributions and median and average depths of records shallower than 10 m (Table 2, Figs 1 and 7). An average of more than 80% of records of assemblage components are shallower than 6 m (Table 2, Figs 1 and 7). According to their probability distributions, 95% of the records of *A. hyacinthus*, *A. latistella* and *G. favulus* are shallower than about 10 m.

In the case of the high-energy subtype of the encrusting coral assemblage (Montaggioni, 2005), according to OBIS data many of its species (*Acropora microphthalma, Montipora monasteriata, M. danae, M. undata, Pachyseris speciosa, Echinophyllia aspera*, *Echinopora lamellosa, Cyphastrea microphthalma, C. serailia, Merulina ampliata and Porites lutea*) are restricted to shallow depths, with modes and medians well above 10 m (Table 2, Figs 2 and 7). As an average, 73% of records of the components of this assemblage are shallower than 6 m. In the case of *P. lutea* and *A. microphthalma*, 95% of occurrence probability is shallower than 10 m (Table 2, Figs 2 and 7). These overlapping mode, median and average depths suggest that both the robust-branching and the high-energy encrusting coral assemblages can be reliable indicators of palaeodepths shallower than 10 m when identified by several species (Table 2, Fig. 7).

The reliability of the robust-branching and high-energy coral assemblages as indicative of shallow depths is reinforced when corals are associated with thick crusts of *P.* gr. *onkodes*. According to OBIS data, CCA of this group are restricted to very shallow waters with theoretically 95% of records shallower than 0.2 m and 99.6% of records shallower than 6 m (Table 3, Figs 4 and 7). However, these data and, in general, the few data concerning CCA species in OBIS are questionable due to either biased sampling or to difficulties of identifying CCA species without the aid of lab-based optical and electronic microscopy. Sampling and subsequent microscopical examination of living CCA on One Tree Reef indicates that *P.* gr. *onkodes* has a log-normal distribution with median depth of 3.5 m, 95% of occurrence probability of thick crusts are shallower than 8.8 m and 86.4% of records are shallower than 6 m (Table 3, Figs 4 and 7).

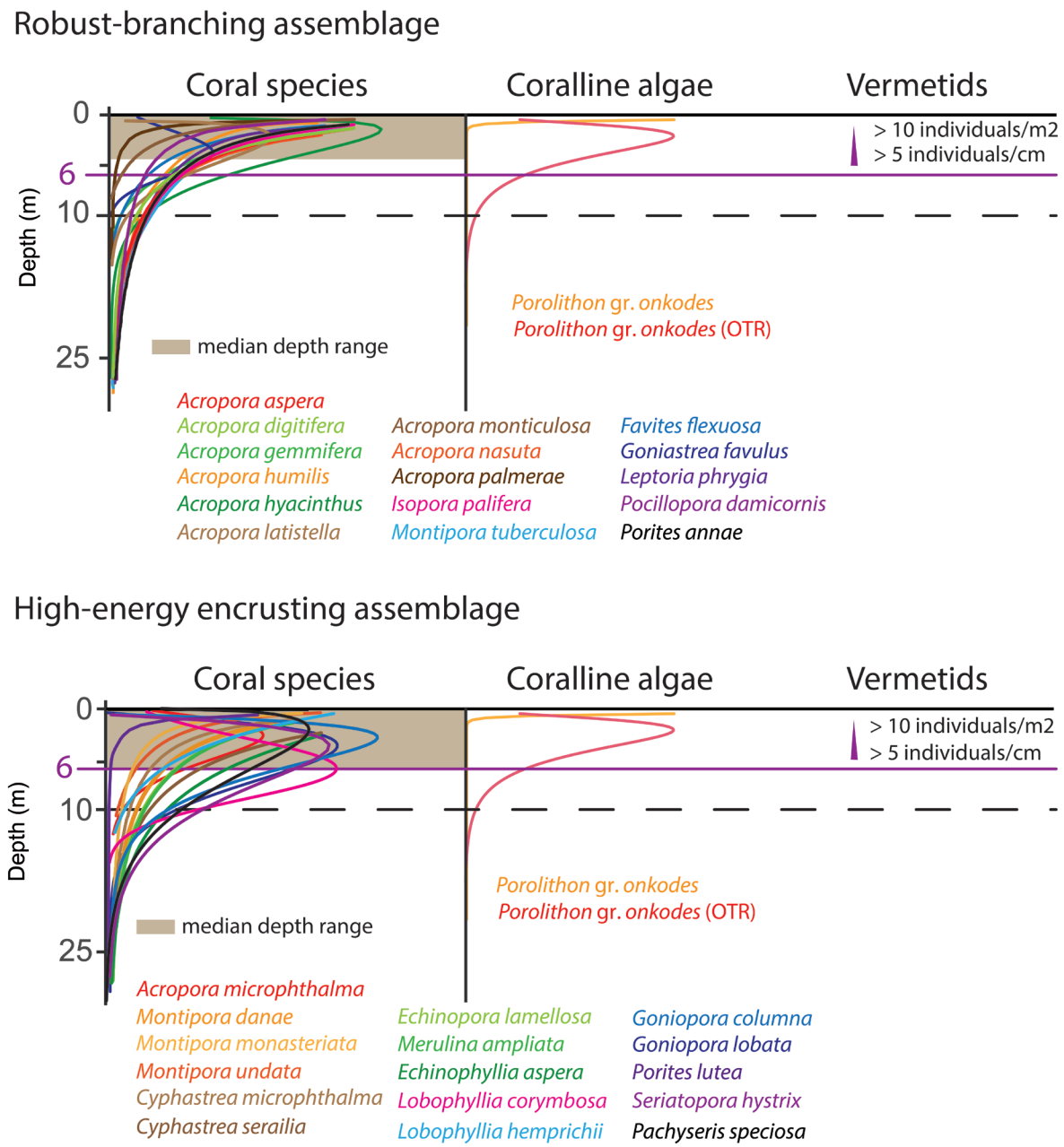


Fig. 7. Probability depth distributions of Indo-Pacific species (different colour lines) with gamma and unimodal best fits characteristic of 'Robust-branching' and 'High-energy encrusting' coral assemblages according to OBIS data (accessed October 2021). Note the coincidence of mode and median depths (ranges of median depths in pale brown rectangle) well above 10 m. Distribution of the CCA *Porites* gr. *onkodes* according to OBIS (accessed October 2021) and surveys by Dechnik *et al.* (2017) at One Tree Reef (OTR). Purple line marks the depth above which vermetid densities of >10 individuals per m^2 or >5 individuals per cm in line transects perpendicular to crusts have been reported in coral reefs.

The presence of relatively high densities of vermetids, common in shallow-water coralgal assemblages, seems to indicate palaeodepths less than 6 m, but data on modern distributions of vermetid densities are scarce. In the OBIS database vermetid species are recorded in wide depth ranges (Table 3). However, when abundance of

vermetid individuals is taken into account, relatively high densities (>10 individuals per m^2 on coral and CCA surfaces and >5 individuals per cm in CCA sections) only occur from above mean low tide to some 6 m depth.

The accurate use of coralgal and vermetid assemblages as RSL indicators requires the identification of fossil corals and CCA at the species or species-group level. There is need of studies on distributions of CCA species and vermetid in modern coral reefs worldwide (Woodroffe & Webster, 2014).

The coralgal approach would be reinforced by quantitative surveys of the modern reef ecology, including spatial distributions of coral and CCA species, as well as extensive information of the physical environment at locations close to the studied fossil reefs (Hongo & Kayanne, 2010; Dutton *et al.*, 2015; Hibbert *et al.*, 2016; Chutcharavan & Dutton, 2020). Comparison with modern depth distributions of nearby reef community components allows precising the depth ranges of fossil assemblages (Webster *et al.*, 1998; Sagawa *et al.*, 2001; Kayanne *et al.*, 2002; Sugihara *et al.*, 2003; Hongo & Kayanne, 2009, 2011; Dutton *et al.*, 2015; Vyverberg *et al.*, 2018). However, *a priori* there are no reasons to assume that past conditions, even in the Holocene, were the same as the present-day. Extensive sampling of fossil reefs with cores/sections distributed across different palaeoenvironments, in parallel with the generation of dense chronologic data sets represents a robust strategy to understand fossil reef architecture, spatio-temporal variations in coralgal assemblages and better assess their RSL significance.

ACKNOWLEDGEMENTS

Financial support of this research was provided by the Australian Research Council (grant DP120101793) and Junta de Andalucía, Spain (Research group RNM 190). DAER work is supported by EU Marie Skłodowska Curie Actions, grant 813360, 4D-REEF. We are very grateful to two anonymous reviewers whose comments helped to substantially improve the first version of the paper.

REFERENCES

Abbey, E., **Webster, J.M.**, **Braga, J.C.**, **Sugihara, K.**, **Wallace, C.C.**, **Iryu, Y.**, **Potts, D.C.**, **Done, T.J.**, **Camoin, G.F.** and **Seard, C.** (2011) Variation in deglacial coralgal assemblages and their paleoenvironmental significance: IODP Expedition 310, "Tahiti Sea Level." *Global Planet. Change*, **76**, 1–15.

Abdul, N.A., **Mortlock, R.A.**, **Wright, J.D.** and **Fairbanks, R.G.** (2016) Younger Dryas Sea-Level and Meltwater Pulse 1B Recorded in Barbados Reef-Crest Coral Acropora palmata. *Paleoceanography*, **31**, 330–344.

Adey, W.H. (1975) The algal ridges and coral reefs of St. Croix: their structure and Holocene development. *Atoll Res. Bull.*, **187**, 1–67.

Adey, W.H. (1979) Crustose coralline algae as microenvironmental indicators for the Tertiary. In: *Historical Biogeography, Plate Tectonics and the Changing Environment* (Eds A. Boucot and J. Gray), *Oregon State University Press*, Corvallis, 459–464.

Adey, W.H. (1986) Coralline algae as indicators of sea-level. In: *Sea-Level Research: a manual for the collection and evaluation of data* (Ed. O. van de Plassche), *Springer Netherlands*, Dordrecht, 229–280.

Adey, W.H. and **Burke, R.B.** (1976) Holocene bioherms (algal ridges and bank-barrier reefs) of the eastern Caribbean. *Geol. Soc. Am. Bull.*, **87**, 95–109.

Adey, W.H. and **Burke, R.B.** (1977) Holocene Bioherms of Lesser Antilles—Geologic Control of Development. In: *Reefs and Related Carbonates - Ecology and Sedimentology, AAPG Studies in Geology* (Eds S.H. Frost, M.P. Weiss and J. Saunders), *AAPG*, Tulsa, OK, **4**, 67–81.

Adey, W.H., **Townsend, R.** and **Boykins, W.** (1982) The Crustose Coralline Algae (Rhodophyta: Corallinaceae) of the Hawaiian Islands. *Smithsonian Institution Press*, Washington, D.C., 74 pp.

Amado-Filho, G.M., **Bahia, R.G.**, **Mariath, R.**, **Jesionek, M.B.**, **Moura, R.L.**, **Bastos, A.C.**, **Pereira-Filho, G.H.** and **Francini-Filho, R.B.** (2018) Spatial and temporal dynamics of the abundance of crustose calcareous algae on the southernmost coral reefs of the western Atlantic (Abrolhos Bank, Brazil). *Algae*, **33**, 85–99.

Andersen, M.B., **Stirling, C.H.**, **Potter, E.-K.**, **Halliday, A.N.**, **Blake, S.G.**, **McCulloch, M.T.**, **Ayling, B.F.** and **O'Leary, M.** (2008) High-precision U-series measurements of more than 500,000 year old fossil corals. *Earth Planet. Sci. Lett.*, **265**, 229–245.

Andersen, M.B., **Stirling, C.H.**, **Potter, E.-K.**, **Halliday, A.N.**, **Blake, S.G.**, **McCulloch, M.T.**, **Ayling, B.F.** and **O'Leary, M.J.** (2010) The timing of sea-level high-stands during Marine Isotope Stages 7.5 and 9: Constraints from the uranium-series dating of fossil corals from Henderson Island. *Geochim. Cosmochim. Acta*, **74**, 3598–3620.

Angulo, R.J., **Lessa, G.C.** and **Souza, M.C. de** (2006) A critical review of mid- to late-Holocene sea-level fluctuations on the eastern Brazilian coastline. *Quatern. Sci. Rev.*, **25**, 486–506.

Bard, E., **Hamelin, B.**, **Arnold, M.**, **Montaggioni, L.**, **Cabioch, G.**, **Faure, G.** and **Rougerie, F.** (1996) Deglacial sea-level record from Tahiti corals and the timing of global meltwater discharge. *Nature*, **382**, 241–244.

Bard, E., **Hamelin, B.** and **Delanghe-Sabatier, D.** (2010) Deglacial meltwater pulse 1B and Younger Dryas sea levels revisited with boreholes at Tahiti. *Science*, **327**, 1235–1237.

Bard, E., **Hamelin, B.**, **Deschamps, P.** and **Camoin, C.** (2016) Comment on"Younger Dryas sea level and meltwaterpulse 1B recorded in Barbados reefalcrest coral *Acropora palmata*" by N. A. Abdul *et al*. *Paleoceanography*, **31**, 1603–1608.

Blanchon, P. and **Eisenhauer, A.** (2001) Multi-stage reef development on Barbados during the Last Interglaciation. *Quatern. Sci. Rev.*, **20**, 1093–1112.

Blanchon, P., **Eisenhauer, A.**, **Fietzke, J.** and **Liebetrau, V.** (2009) Rapid sea-level rise and reef back-stepping at the close of the last interglacial highstand. *Nature*, **458**, 881–884.

Blanchon, P., **Jones, B.** and **Ford, D.C.** (2002) Discovery of a submerged relic reef and shoreline off Grand Cayman: further support for an early Holocene jump in sea level. *Sed. Geol.*, **147**, 253–270.

Blanchon, P. and **Perry, C.T.** (2004) Taphonomic differentiation of *Acropora palmata* facies in cores from Campeche Bank Reefs, Gulf of México. *Sedimentology*, **51**, 53–76.

Bosence, D.W.J. (1983) Coralline algal reef frameworks. *J. Geol. Soc. London.*, **140**, 365–376.

Bosence, D.W.J. (1991) Coralline algae : mineralization, taxonomy and palaeoecology. In: *Calcareous Algae and Stromatolites* (Ed. R. Riding), *Springer*, Berlin/Heidelberg, 98–113.

Braga, J.C. and **Aguirre, J.** (2004) Coralline algae indicate Pleistocene evolution from deep, open platform to outer barrier reef environments in the northern Great Barrier Reef margin. *Coral Reefs*, **23**, 547–558.

Braithwaite, C.J.R. (1971) Seychelles reefs: structure and development. In: *Symposium of the Zoological Society of London* (Eds D.R. Stoddart and C.M. Yonge), London, **28**, 39–63.

Braithwaite, C.J.R. (2016) Coral-reef records of Quaternary changes in climate and sea-level. *Earth-Sci. Rev.*, **156**, 137–154.

Brown, A.L., **Frazer, T.K.**, **Shima, J.S.** and **Osenberg, C.W.** (2016) Mass mortality of the vermetid gastropod *Ceraesignum maximum*. *Coral Reefs*, **35**, 1027–1032.

Budd, A.F., **Fukami, H.**, **Smith, N.D.** and **Knowlton, N.** (2012) Taxonomic classification of the reef coral family Mussidae (Cnidaria: Anthozoa: Scleractinia). *Zool. J. Linn. Soc.*, **166**, 465–529.

Cabioch, G., **Banks-Cutler, K.A.**, **Beck, W.J.**, **Burr, G.S.**, **Corrège, T.**, **Lawrence Edwards, R.** and **Taylor, F.W.** (2003) Continuous reef growth during the last 23calkyr BP in a tectonically active zone (Vanuatu, SouthWest Pacific). *Quatern. Sci. Rev.*, **22**, 1771–1786.

Cabioch, G., **Montaggioni, L.F.**, **Faure, G.** and **Ribaud-Laurenti, A.** (1999) Reef coralgal assemblages as recorders of paleobathymetry and sea level changes in the Indo-Pacific province. *Quatern. Sci. Rev.*, **18**, 1681–1695.

Cabioch, G., **Montaggioni, L.F.**, **Frank, N.**, **Seard, C.**, **Sallé, E.**, **Payri, C.**, **Pelletier, B.** and **Paterne, M.** (2008) Successive reef depositional events along the Marquesas foreslopes (French Polynesia) since 26 ka. *Mar. Geol.*, **254**, 18–34.

Camoin, G.F., **Colonna, M.**, **Montaggioni, L.F.**, **Casanova, J.**, **Faure, G.** and **Thomassin, B.A.** (1997) Holocene sea level changes and reef development in the southwestern Indian Ocean. *Coral Reefs*, **16**, 247–259.

Camoin, G.F., **Ebren, P.**, **Eisenhauer, A.**, **Bard, E.** and **Faure, G.** (2001) A 300 000-yr coral reef record of sea level changes, Mururoa Atoll (Tuamotu Archipelago, French Polynesia). *Palaeogeogr. Palaeoclimatol. Palaeoecol.*, **175**, 325–341.

Camoin, G.F., **Montaggioni, L.F.** and **Braithwaite, C.J.R.** (2004) Late glacial to post glacial sea levels in the Western Indian Ocean. *Mar. Geol.*, **206**, 119–146.

Camoin, G.F., **Seard, C.**, **Deschamps, P.**, **Webster, J.M.**, **Abbey, E.**, **Braga, J.C.**, **Iryu, Y.**, **Durand, N.**, **Bard, E.**, **Hamelin, B.**, **Yokoyama, Y.**, **Thomas, A.L.**, **Henderson, G.M.** and **Dussouillez, P.** (2012) Reef response to sea-level and environmental changes during the last deglaciation: Integrated Ocean Drilling Program Expedition 310, Tahiti Sea Level. *Geology*, **40**, 643–646.

Camoin, G.F. and **Webster, J.M.** (2015) Coral reef response to Quaternary sea-level and environmental changes: State of the science. *Sedimentology*, **62**, 401–428.

Chutcharavan, P.M. and **Dutton, A.** (2020) A global compilation of U-series dated fossil coral sea-level indicators for the Last Interglacial Period (MIS 5e). *Earth Syst. Sci. Data Discuss.*, 1–41.

Davies, P.J. and **Montaggioni, L.F.** (1985) Reef growth and sea level change: the environmental signature. In: *Proceedings of the 5th International Coral Reef Congress*, Tahiti, **3**, 477–515.

Dean, A.J., **Steneck, R.S.**, **Tager, D.** and **Pandolfi, J.M.** (2015) Distribution, abundance and diversity of crustose coralline algae on the Great Barrier Reef. *Coral Reefs*, **34**, 581–594.

Dechnik, B., **Bastos, A.C.**, **Vieira, L.S.**, **Webster, J.M.**, **Fallon, S.**, **Yokoyama, Y.**, **Nothdurft, L.**, **Sanborn, K.**, **Batista, J.**, **Moura, R.** and **Amado-Filho, G.** (2019) Holocene reef growth in the tropical southwestern Atlantic: Evidence for sea level and climate instability. *Quatern. Sci. Rev.*, **218**, 365–377.

Dechnik, B., **Webster, J.M.**, **Davies, P.J.**, **Braga, J.C.** and **Reimer, P.J.** (2015) Holocene "turn-on" and evolution of the Southern Great Barrier Reef: Revisiting reef cores from the Capricorn Bunker Group. *Mar. Geol.*, **363**, 174–190.

Dechnik, B., **Webster, J.M.**, **Webb, G.E.**, **Braga, J.C.**, **Zhao, J.-X.**, **Duce, S.** and **Sadler, J.** (2017) The evolution of the Great Barrier Reef during the last interglacial period. *Global Planet. Change*, **149**, 53–71.

Delignette-Muller, M.L. and **Dutang, C.** (2015) fitdistrplus: An R Package for Fitting Distributions. *J. Stat. Softw.*, **64**, 1–34.

Deschamps, P., **Durand, N.**, **Bard, E.**, **Hamelin, B.**, **Camoin, G.F.**, **Thomas, A.L.**, **Henderson, G.M.**, **Okuno, J.** and **Yokoyama, Y.** (2012) Ice-sheet collapse and sea-level rise at the Bølling warming 14,600 years ago. *Nature*, **483**, 559–564.

Done, T.J. (1982) Patterns in the distribution of coral communities across the central Great Barrier Reef. *Coral Reefs*, **1**, 95–107.

Dutton, A., **Webster, J.M.**, **Zwartz, D.**, **Lambeck, K.** and **Wohlfarth, B.** (2015) Tropical tales of polar ice: evidence of Last Interglacial polar ice sheet retreat recorded by fossil reefs of the granitic Seychelles islands. *Quatern. Sci. Rev.*, **107**, 182–196.

Fairbanks, R.G. (1989) A 17,000-year glacio-eustatic sea level record: influence of glacial melting rates on the Younger Dryas event and deep-ocean circulation. *Nature*, **342**, 637–642.

Faure, G. (1982) Recherche sur les peuplements de Scléractiniaires des récifs coraliens de l'Archipel des Mascareignes (Océan Indien Occidental). D.Sc. thesis, University of Marseille.

Frank, N., **Turpin, L.**, **Cabioch, G.**, **Blamart, D.**, **Tressens-Fedou, M.**, **Colin, C.** and **Jean-Baptiste, P.** (2006) Open system U-series ages of corals from a subsiding reef in New Caledonia: Implications for sea level changes and subsidence rate. *Earth Planet. Sci. Lett.*, **249**, 274–289.

Fruijtier, C., **Elliott, T.** and **Schlager, W.** (2000) Mass-spectrometric 234U-230Th ages from the Key Largo Formation, Florida Keys, United States: Constraints on diagenetic age disturbance. *Geol. Soc. Am. Bull.*, **112**, 267–277.

Gabrielson, P.W., **Hughey, J.R.** and **Diaz-Pulido, G.** (2018) Genomics reveals abundant speciation in the coral reef building alga Porolithon onkodes (Corallinales, Rhodophyta). *J. Phycol.*, **54**, 429–434.

Galewsky, J., **Silver, E.A.**, **Gallup, C.D.**, **Edwards, R.L.** and **Potts, D.C.** (1996) Foredeep tectonics and carbonate platform dynamics in the Huon Gulf, Papua New Guinea. *Geology*, **24**, 819–822.

Geister, J. (1977) The influence of wave exposure on the ecological zonation of Caribbean coral reefs. In: *Proceedings of 3rd International Coral Reef Symposium Vol. 2: Geology* (Ed. D.L. Taylor), Rosenstiel School of Marine and Atmospheric Science, Miami, Florida, 23–29.

Gherardi, D.F.M. and **Bosence, D.W.J.** (2001) Composition and community structure of the coralline algal reefs from Atol das Rocas, South Atlantic, Brazil. *Coral Reefs*, **19**, 205–219.

Gischler, E., **Hudson, J.H.**, **Humblet, M.**, **Braga, J.C.**, **Eisenhauer, A.**, **Isaack, A.**, **Anselmetti, F.S.** and **Camoin, G.F.** (2016) Late Quaternary barrier and fringing reef development of Bora Bora (Society Islands, south Pacific): First subsurface data from the Darwin-type barrier-reef system. *Sedimentology*, **63**, 1522–1549.

Gischler, E., **Hudson, J.H.**, **Humblet, M.**, **Braga, J.C.**, **Schmitt, D.**, **Isaack, A.**, **Eisenhauer, A.** and **Camoin, G.F.** (2018a) Holocene and Pleistocene fringing reef growth and the role of accommodation space and exposure to waves and currents (Bora Bora, Society Islands, French Polynesia). *Sedimentology*, **66**, 305–328.

Gischler, E., **Humblet, M.**, **Braga, J.C.** and **Eisenhauer, A.** (2018b) Last interglacial reef facies and late Quaternary subsidence in the Maldives, Indian Ocean. *Mar. Geol.*, **406**, 34–41.

Gischler, E., **Meyer, G.**, **Braga, J.C.**, **Riechelmann, S.**, **Immenhauser, A.** and **Eisenhauer, A.** Neogene and Quaternary reef terraces of Mangaia, Rarotonga, and Aitutaki (southern Cook Islands, south Pacific) revisited: gauges of sea-level change and island uplift? In: *Coral Reefs and Sea-Level Change: Quaternary Records and Modelling. A Window Into the Future* (Eds G.F. Camoin and N. Hallmann), *Int. Assoc. Sedimentol. Spec. Publ*., **49** (this volume), 275–317.

Golding, R.E., **Bieler, R.**, **Rawlings, T.A.** and **Collins, T.M.** (2014) Deconstructing *Dendropoma*: a systematic revision of a world-wide worm-snail group, with descriptions of new genera (Caenogastropoda: Vermetidae). *Malacologia*, **57**, 1–97.

Hadfield, M.G., **Kay, E.A.**, **Gillette, M.U.** and **Lloyd, M.C.** (1972) The vermetidae (Mollusca: Gastropoda) of the Hawaiian Islands. *Mar. Biol.*, **12**, 81–98.

Hallmann, N., **Camoin, G.F.**, **Eisenhauer, A.**, **Samankassou, E.**, **Vella, C.**, **Botella, A.**, **Milne, G.A.**, **Pothin, V.**, **Dussouillez, P.**, **Fleury, J.**, **Fietzke, J.** and **Goepfert, T.** (2020) Reef response to sea-level and environmental changes in the central south Pacific over the past 6000 years. *Global Planet. Change*, **195**, 103357.

Hibbert, F.D., **Rohling, E.J.**, **Dutton, A.**, **Williams, F.H.**, **Chutcharavan, P.M.**, **Zhao, C.** and **Tamisiea, M.E.** (2016) Coral indicators of past sea-level change: a global repository of U-series dated benchmarks. *Quatern. Sci. Rev.*, **145**, 1–56.

Hibbert, F.D., **Williams, F.H.**, **Fallon, S.** and **Rohling, E.J.** (2018) A database of biological and geomorphological sea-level markers from the Last Glacial Maximum to present. *Sci. Data*, **5**, 180088.

Hinderstein, L.M., **Marr, J.C.A.**, **Martinez, F.A.**, **Dowgiallo, M.J.**, **Puglise, K.A.**, **Pyle, R.L.**, **Zawada, D.G.** and **Appeldoorn, R.** (2010) Theme section on "Mesophotic Coral Ecosystems: Characterization, Ecology and Management." *Coral Reefs*, **29**, 247–251.

Hongo, C. and **Kayanne, H.** (2009) Holocene coral reef development under windward and leeward locations at Ishigaki Island, Ryukyu Islands, Japan. *Sed. Geol.*, **214**, 62–73.

Hongo, C. and **Kayanne, H.** (2010) Holocene sea-level record from corals: Reliability of paleodepth indicators at Ishigaki Island, Ryukyu Islands, Japan. *Palaeogeogr. Palaeoclimatol. Palaeoecol.*, **287**, 143–151.

Hongo, C. and **Kayanne, H.** (2011) Key species of hermatypic coral for reef formation in the northwest Pacific during Holocene sea-level change. *Mar. Geol.*, **279**, 162–177.

Huang, D., **Arrigoni, R.**, **Benzoni, F.**, **Fukami, H.**, **Knowlton, N.**, **Smith, N.D.**, **Stolarski, J.**, **Chou, L.M.** and **Budd, A.F.** (2016) Taxonomic classification of the reef coral family Lobophylliidae (Cnidaria: Anthozoa: Scleractinia). *Zool. J. Linn. Soc.*, **178**, 436–481.

Huang, D., **Benzoni, F.**, **Fukami, H.**, **Knowlton, N.**, **Smith, N.D.** and **Budd, A.F.** (2014) Taxonomic classification of the reef coral families Merulinidae, Montastraeidae and Diploastraeidae (Cnidaria: Anthozoa: Scleractinia). *Zool. J. Linn. Soc.*, **171**, 277–355.

Hughes, R.N. and **Lewis, A.H.** (1974) On the spatial distribution, feeding and reproduction of the vermetid gastropod *Dendropoma maximum*. *J. Zool.*, **172**, 531–547.

Humblet, M., **Potts, D.C.**, **Webster, J.M.**, **Braga, J.C.**, **Iryu, Y.**, **Yokoyama, Y.**, **Bourillot, R.**, **Séard, C.**, **Droxler, A.**, **Fujita, K.**, **Gischler, E.** and **Kan, H.** (2019) Late glacial to deglacial variation of coralgal assemblages in the Great Barrier Reef, Australia. *Global Planet. Change*, **174**, 70–91.

Iryu, Y., **Nakamori, T.**, **Matsuda, S.** and **Abe, O.** (1995) Distribution of marine organisms and its geological significance in the modern reef complex of the Ryukyu Islands. *Sed. Geol.*, **99**, 243–258.

Iryu, Y., **Takahashi, Y.**, **Fujita, K.**, **Camoin, G.F.**, **Cabioch, G.**, **Matsuda, H.**, **Sato, T.**, **Sugihara, K.**, **Webster, J.M.** and **Westphal, H.** (2010) Sealevel history recorded in the Pleistocene carbonate sequence in IODP Hole 310-M0005D, off Tahiti. *Isl. Arc*, **19**, 690–706.

IUCN The IUCN Red List of Threatened Species. In: *IUCN Red List of Threatened Species*. https://www.iucnredlist.org/. Accessed 8 Feb 2021.

Jaramillo-Vogel, D., **Foubert, A.**, **Braga, J.C.**, **Schaegis, J.C.**, **Atnafu, B.**, **Grobety, B.** and **Kidane, T.** (2019) Pleistocene sea-floor fibrous crusts and spherulites in the Danakil Depression (Afar, Ethiopia). *Sedimentology*, **66**, 480–512.

Jeong, S.Y., **Nelson, W.A.**, **Sutherland, J.E.**, **Peña, V.**, **Gall, L.L.**, **Diaz-Pulido, G.**, **Won, B.Y.** and **Cho, T.O.** (2020) Corallinapetrales and Corallinapetraceae: A new order and family of coralline red algae including *Corallinapetra gabrielii* comb. nov. J Phycol. doi: https://doi.org/10.1111/jpy.13115

Jesionek, M.B., **Bahia, R.G.**, **Hernández-Kantún, J.J.**, **Adey, W.H.**, **Yoneshigue-Valentin, Y.**, **Longo, L.L.** and **Amado-Filho, G.M.** (2016) A taxonomic account of non-geniculate coralline algae (Corallinophycidae, Rhodophyta) from shallow reefs of the Abrolhos Bank, Brazil. *Algae*, **31**, 317–340.

Kayanne, H., **Yamano, H.** and **Randall, R.H.** (2002) Holocene sea-level changes and barrier reef formation on an oceanic island, Palau Islands, western Pacific. *Sed. Geol.*, **150**, 47–60.

Khan, N.S., **Ashe, E.**, **Horton, B.P.**, **Dutton, A.**, **Kopp, R.E.**, **Brocard, G.**, **Engelhart, S.E.**, **Hill, D.F.**, **Peltier, W.R.**, **Vane, C.H.** and **Scatena, F.N.** (2017) Drivers of Holocene sea-level change in the Caribbean. *Quatern. Sci. Rev.*, **155**, 13–36.

Laborel, J. (1986) Vermetid gastropods as sea-level indicators. In: *Sea-Level Research: a manual for the collection and evaluation of data* (Ed. O. van de Plassche), *Springer Netherlands*, Dordrecht, 281–310.

Leão, Z.M.A.N., **Kikuchi, R.K.P.** and **Engelberg, E.F.** (1997) Internet guide to the corals and hydrocorals of Brazil. http://www.cpgg.ufba.br/guia-corais/. Accessed 8 Feb 2021.

Lighty, R.G., **Macintyre, I.G.** and **Stuckenrath, R.** (1982) *Acropora palmata* reef framework: a reliable indicator of sea level in the western atlantic for the past 10,000 years. *Coral Reefs*, **1**, 125–130.

Littler, D.S. and **Littler, M.M.** (2003) South Pacific reef plants: a diver's guide to the plant life of south Pacific coral reefs. *Offshore Graphics, Inc.*, Washington, D.C., 331 pp.

Littler, M.M. and **Littler, D.S.** (1984) Relationships between macroalgal functional form groups and substrata stability in a subtropical rocky-intertidal system. *J. Exp. Mar. Biol. Ecol.*, **74**, 13–34.

Ludwig, K.R., **Muhs, D.R.**, **Simmons, K.R.**, **Halley, R.B.** and **Shinn, E.A.** (1996) Sea-level records at ~ 80 ka from tectonically stable platforms: Florida and Bermuda. *Geology*, **24**, 211–214.

Maneveldt, G.W. and **Keats, D.W.** (2014) Taxonomic review based on new data of the reef-building alga *Porolithon onkodes* (Corallinaceae, Corallinales, Rhodophyta) along with other taxa found to be conspecific. *Phytotaxa*, **190**, 216–249.

Maneveldt, G.W. and **Keats, D.W.** (2016) Taxonomic review based on new morpho-anatomical data of the algae *Porolithon craspedium* and *P. gardineri* (Corallinaceae, Corallinales, Rhodophyta) and comments on other taxa ascribed to the genus. *Phytotaxa*, **289**, 1–35.

Martindale, W. (1992) Calcified epibionts as palaeoecological tools: examples from the Recent and Pleistocene reefs of Barbados. *Coral Reefs*, **11**, 167–177.

Mesolella, K.J. (1967) Zonation of uplifted Pleistocene coral reefs on Barbados, West Indies. *Science*, **156**, 638–640.

Montaggioni, L.F. (2005) History of Indo-Pacific coral reef systems since the last glaciation: Development patterns and controlling factors. *Earth-Sci. Rev.*, **71**, 1–75.

Montaggioni, L.F. and **Braithwaite, C.J.R.** (2009) Quaternary coral reef systems: history, development processes and controlling factors, 1st edn. *Elsevier Science Ltd.*, 532 pp.

Montaggioni, L.F., **Cabioch, G.**, **Camoin, G.F.**, **Bard, E.**, **Laurenti, A.R.**, **Faure, G.**, **Déjardin, P.** and **Récy, J.** (1997) Continuous record of reef growth over the past 14 k.y. on the mid-Pacific island of Tahiti. *Geology*, **25**, 555–558.

Montaggioni, L.F. and **Faure, G.** (1997) Response of reef coral communities to sea-level rise: a Holocene model from Mauritius (Western Indian Ocean). *Sedimentology*, **44**, 1053–1070.

Montaggioni, L.F. and **Martin-Garin, B.** (2020) Quaternary development history of coral reefs from West Indian islands: a review. *Int. J. Earth Sci.*, **109**, 911–930.

Montgomery, A.D., **Fenner, D.**, **Kosaki, R.K.**, **Pyle, R.L.**, **Wagner, D.** and **Toonen, R.J.** (2019) American Samoa. In: *Mesophotic Coral Ecosystems* (Eds Y. Loya, K.A. Puglise and T.C.L. Bridge), *Springer International Publishing*, New York, 387–407.

Morse, A.N.C., **Iwao, K.**, **Baba, M.**, **Shimoike, K.**, **Hayashibara, T.** and **Omori, M.** (1996) An ancient chemosensory mechanism brings new life to coral reefs. *Biol. Bull.*, **191**, 149–154.

Mortlock, R.A., **Abdul, N.A.**, **Wright, J.D.** and **Fairbanks, R.G.** (2016) Reply to comment by E. Bard *et al.* on "Younger Dryas sea level and meltwater pulse 1B recorded in Barbados reef crest coral *Acropora palmata*" by N. A. Abdul *et al. Paleoceanography*, **31**, 1609–1616.

Muhs, D.R., **Simmons, K.R.**, **Schumann, R.R.** and **Halley, R.B.** (2011) Sea-level history of the past two interglacial periods: new evidence from U-series dating of reef corals from south Florida. *Quatern. Sci. Rev.*, **30**, 570–590.

Muir, P., **Wallace, C.**, **Bridge, T.C.L.** and **Bongaerts, P.** (2015) Diverse staghorn coral fauna on the mesophotic reefs of north-east Australia. *PLOS ONE*, **10**, e0117933.

Muir, P.R. and **Pichon, M.** (2019) Biodiversity of reef-building, Scleractinian corals. In: *Mesophotic Coral Ecosystems* (Eds Y. Loya, K.A. Puglise and T.C.L. Bridge), *Springer International Publishing*, New York, 589–620.

Nakamori, T. (1986) Community structures of Recent and Pleistocene hermatypic corals in the Ryukyu Islands, Japan. *Sci. Rep. - Tohoku Univ. Second Ser. Geol.*, **56**, 71–133.

Nakamori, T., **Iryu, Y.** and **Yamada, T.** (1995) Development of coral reefs of the Ryukyu Islands (southwest Japan, East China Sea) during Pleistocene sea-level change. *Sed. Geol.*, **99**, 215–231.

Nelson, W.A. (2009) Calcified macroalgae – critical to coastal ecosystems and vulnerable to change: a review. *Mar. Freshw. Res.*, **60**, 787–801.

Payri, C.E., **De Ramon N'Yeurt, A.** and **Orempuller, J.** (2000) Algues de Polynésie Française / algae of French Polynesia. *Au Vent de Îles*, Singapore, 320 pp.

Pichon, M. (1978) Recherches sur les peuplements a dominance d'anthozoaires dans les recifs coralliens de Tulear. *Atoll Res. Bull.*, **222**, 1–447.

Piller, W.E. and **Rasser, M.** (1996) Rhodolith formation induced by reef erosion in the Red Sea, Egypt. *Coral Reefs*, **15**, 191–198.

Pirazzoli, P.A. and **Montaggioni, L.F.** (1988) The 7,000 year sea-level curve in French Polynesia: geodynamic implications for mid-plate volcanic islands. In: *Proceedings of the 6th International Coral Reef Symposium*, Townsville, 467–472.

Provoost, P. and **Bosch, S.** (2017) "robis: R Client to access data from the OBIS API". *Ocean Biogeographic Information System. Intergovernmental Oceanographic Commission of UNESCO*.

Rasser, M. and **Piller, W.E.** (1997) Depth distribution of calcareous encrusting associations in the northern Red Sea (Safaga, Egypt) and their geological implications. In: *Proceedings of the 8th International Coral Reef Symposium*, **1**, 743–748.

Ribak, G., **Heller, J.** and **Genin, A.** (2005) Mucus-net feeding on organic particles by the vermetid gastropod *Dendropoma maximum* in and below the surf zone. *Mar. Ecol. Prog. Ser.*, **293**, 77–87.

Riegl, B. and **Piller, W.E.** (2000) Reefs and coral carpets in the northern Red Sea as models for organism-environment feedback in coral communities and its reflection in growth fabrics. *Geol. Soc. London. Spec. Publ.*, **178**, 71–88.

Ringeltaube, P. and **Harvey, A.** (2000) Non-geniculate coralline algae (Corallinales, Rhodophyta) on Heron Reef, Great Barrier Reef (Australia). *Bot. Mar.*, **43**, 431–454.

Rosen, B.R. (1971) Principal features of reef coral ecology in shallow water environments of Mahe, Seychelles. In: *Symposia of the Zoological Society of London* (Eds D.R. Stoddart and C.M. Yonge), London, **28**, 103–183.

Rosen, B.R. (1975) The distribution of reef corals. *Rep. Underw. Assoc.*, **1**, 2–16.

Rovere, A., **Stocchi, P.** and **Vacchi, M.** (2016) Eustatic and relative sea level changes. *Curr. Clim. Change Rep.*, **2**, 221–231.

Sagawa, N., **Nakamori, T.** and **Iryu, Y.** (2001) Pleistocene reef development in the southwest Ryukyu Islands, Japan. *Palaeogeogr. Palaeoclimatol. Palaeoecol.*, **175**, 303–323.

Sanborn, K.L., **Webster, J.M.**, **Yokoyama, Y.**, **Dutton, A.**, **Braga, J.C.**, **Clague, D.A.**, **Paduan, J.B.**, **Wagner, D.**, **Rooney, J.J.** and **Hansen, J.R.** (2017) New evidence of Hawaiian coral reef drowning in response to meltwater pulse-1A. *Quatern. Sci. Rev.*, **175**, 60–72.

Shen, C.-C., **Siringan, F.P.**, **Lin, K.**, **Dai, C.-F.** and **Gong, S.-Y.** (2010) Sea-level rise and coral-reef development of Northwestern Luzon since 9.9ka. *Palaeogeogr. Palaeoclimatol. Palaeoecol.*, **292**, 465–473.

Shima, J.S., **Osenberg, C.W.** and **Stier, A.C.** (2010) The vermetid gastropod *Dendropoma maximum* reduces coral growth and survival. *Biol. Lett.*, **6**, 815–818.

Shima, J.S., **Phillips, N.E.** and **Osenberg, C.W.** (2013) Consistent deleterious effects of vermetid gastropods on coral performance. *J. Exp. Mar. Biol. Ecol.*, **439**, 1–6.

Spotorno-Oliveira, P., **Figueiredo, M.A.O.** and **Tâmega, F.T.S.** (2015) Coralline algae enhance the settlement of the vermetid gastropod *Dendropoma irregulare* (d'Orbigny, 1842) in the southwestern Atlantic. *J. Exp. Mar. Biol. Ecol.*, **471**, 137–145.

Stathakopoulos, A., **Riegl, B.M.** and **Toth, L.T.** (2020) A revised Holocene coral sea-level database from the Florida reef tract, USA. *PeerJ*, **8**, e8350.

Sugihara, K., **Nakamori, T.**, **Iryu, Y.**, **Sasaki, K.** and **Blanchon, P.** (2003) Holocene sea-level change and tectonic uplift deduced from raised reef terraces, Kikai-jima, Ryukyu Islands, Japan. *Sed. Geol.*, **159**, 5–25.

Suguio, K., **Barreto, A.M.F.**, **Oliveira, P.E. de**, **Bezerra, F.H.R.** and **Vilela, M.C.S.H.** (2013) Indicadores de variações holocênicas do nível do mar ao longo da costa dos estados de Pernambuco e Paraíba, Brasil. *Geol. USP Sér. Científica*, **13**, 141–152.

Tâmega, F.T.S., **Riosmena-Rodriguez, R.**, **Mariath, R.** and **Figueiredo, M.** (2014) Nongeniculate coralline red algae (Rhodophyta: Corallinales) in coral reefs from Northeastern Brazil and a description of *Neogoniolithon atlanticum* sp. nov. *Phytotaxa*, **190**, 277–298.

Thomas, A.L., **Henderson, G.M.**, **Deschamps, P.**, **Yokoyama, Y.**, **Mason, A.J.**, **Bard, E.**, **Hamelin, B.**, **Durand, N.** and **Camoin, G.F.** (2009) Penultimate deglacial sea-level timing from Uranium/Thorium dating of Tahitian corals. *Science*, **324**, 1186–1189.

Thomas, M.L.H. and **Stevens, J.-A.** (1991) Communities of constructional lips and cup reef rims in Bermuda. *Coral Reefs*, **9**, 225–230.

Toscano, M.A., **Macintyre, I.G.** and **Lundberg, J.** (2012) Last interglacial reef limestones, northeastern St. Croix, US Virgin Islands—evidence of tectonic tilting and subsidence since MIS 5.5. *Coral Reefs*, **31**, 27–38.

Toth, L.T., **Aronson, R.B.**, **Cobb, K.M.**, **Cheng, H.**, **Edwards, R.L.**, **Grothe, P.R.** and **Sayani, H.R.** (2015) Climatic and biotic thresholds of coral-reef shutdown. *Nat. Clim. Change*, **5**, 369–374.

Vermeij, M.J.A., **Dailer, M.L.** and **Smith, C.M.** (2011) Crustose coralline algae can suppress macroalgal growth and recruitment on Hawaiian coral reefs. *Mar. Ecol. Prog. Ser.*, **422**, 1–7.

Veron, J.E.N. (2000) Corals of the World. *Aust. Inst. Mar. Sci.*, Townsville.

Vieira, L.S., Bastos, A.C., Dechnik, B., Braga, J.C., Moura, R.L., D'Agostini, D.P., Moraes, F.C., Webster, J.M. New insights on the Late Quaternary evolution of Abrolhos reefs, Eastern Brazilian Shelf. In: *Coral Reefs and Sea-Level Change: Quaternary Records and Modelling. A Window Into the Future* (Eds G.F. Camoin and N. Hallmann), *Int. Assoc. Sedimentol. Spec. Publ*., **49** (this volume), 69–100.

Vyverberg, K., **Dechnik, B.**, **Dutton, A.**, **Webster, J.M.**, **Zwartz, D.** and **Portell, R.W.** (2018) Episodic reef growth in the granitic Seychelles during the Last Interglacial: Implications for polar ice sheet dynamics. *Mar. Geol.*, **399**, 170–187.

Wallace, C.C. (1999) Staghorn Corals of the World. *CSIRO Publishing*, Australia, 421 pp.

Webster, J.M., **Braga, J.C.**, **Clague, D.A.**, **Gallup, C.**, **Hein, J.R.**, **Potts, D.C.**, **Renema, W.**, **Riding, R.**, **Riker-Coleman, K.**, **Silver, E.** and **Wallace, L.M.** (2009) Coral reef evolution on rapidly subsiding margins. *Global Planet. Change*, **66**, 129–148.

Webster, J.M., **Braga, J.C.**, **Humblet, M.**, **Potts, D.C.**, **Iryu, Y.**, **Yokoyama, Y.**, **Fujita, K.**, **Bourillot, R.**, **Esat, T.M.**, **Fallon, S.**, **Thompson, W.G.**, **Thomas, A.L.**, **Kan, H.**, **McGregor, H.V.**, **Hinestrosa, G.**, **Obrochta, S.P.** and **Lougheed, B.C.** (2018) Response of the Great Barrier Reef to sea-level and environmental changes over the past 30,000 years. *Nat. Geosci.*, **11**, 426–432.

Webster, J.M., **Clague, D.A.**, **Braga, J.C.**, **Spalding, H.**, **Renema, W.**, **Kelley, C.**, **Applegate, B.**, **Smith, J.R.**, **Paull, C.K.**, **Moore, J.G.** and **Potts, D.C.** (2006) Drowned coralline algal dominated deposits off Lanai, Hawaii; carbonate accretion and vertical tectonics over the last 30 ka. *Mar. Geol.*, **225**, 223–246.

Webster, J.M., **Clague, D.A.**, **Riker-Coleman, K.**, **Gallup, C.**, **Braga, J.C.**, **Potts, D.C.**, **Moore, J.G.**, **Winterer, E.L.** and **Paull, C.K.** (2004a) Drowning of the - 150 m reef off Hawaii: A casualty of global meltwater pulse 1A? *Geology*, **32**, 249–252.

Webster, J.M. and **Davies, P.J.** (2003) Coral variation in two deep drill cores: significance for the Pleistocene development of the Great Barrier Reef. *Sed. Geol.*, **159**, 61–80.

Webster, J.M., **Davies, P.J.** and **Konishi, K.** (1998) Model of fringing reef development in response to progressive sea level fall over the last 7000 years – (Kikai-jima, Ryukyu Islands, Japan). *Coral Reefs*, **17**, 289–308.

Webster, J.M., Dechnik, B., Sanborn, K., Yokoyama, Y., Braga, J.C., Renema, W., Humblet, M., Beaman, R., Nothdurft, L., Webb, G., Zhao, J.-X., Murphy, R., Gallagher, S., O'Leary, M. and **Paumard, V.** Coral reef development and sea-level changes over the past 50,000 years: new evidence from the northwest shelf of Australia. In: *Coral Reefs and Sea-Level Change: Quaternary Records and Modelling. A Window Into the Future* (Eds G.F. Camoin and N. Hallmann), *Int. Assoc. Sedimentol. Spec. Publ*., **49** (this volume), 215–273.

Webster, J.M., **Wallace, L.M.**, **Silver, E.**, **Potts, D.C.**, **Braga, J.C.**, **Renema, W.**, **Riker-Coleman, K.** and **Gallup, C.** (2004b) Coralgal composition of drowned carbonate platforms in the Huon Gulf, Papua New Guinea; implications for lowstand reef development and drowning. *Mar. Geol.*, **204**, 59–89.

Woodroffe, C. and **Webster, J.M.** (2014) Coral reefs and sea-level change. *Mar. Geol.*, **352**, 248–267.

WoRMS Editorial Board (2021) WoRMS - World Register of Marine Species. http://www.marinespecies.org/. Accessed 8 Feb 2021.

Yokoyama, Y., **Esat, T.M.**, **Thompson, W.G.**, **Thomas, A.L.**, **Webster, J.M.**, **Miyairi, Y.**, **Sawada, C.**, **Aze, T.**, **Matsuzaki, H.**, **Okuno, J.**, **Fallon, S.**, **Braga, J.C.**, **Humblet, M.**, **Iryu, Y.**, **Potts, D.C.**, **Fujita, K.**, **Suzuki, A.** and **Kan, H.** (2018) Rapid glaciation and a two-step sea level plunge into the Last Glacial Maximum. *Nature*, **559**, 603–607.

Zuschin, M., **Hohenegger, J.** and **Steininger, F.** (2001) Molluscan assemblages on coral reefs and associated hard substrata in the northern Red Sea. *Coral Reefs*, **20**, 107–116.

Zvuloni, A., **Armoza-Zvuloni, R.** and **Loya, Y.** (2008) Structural deformation of branching corals associated with the vermetid gastropod *Dendropoma maxima*. *Mar. Ecol. Prog. Ser.*, **363**, 103–108.

Supplementary tables and figures for papers in this volume can be found on the IAS website: https://www.sedimentologists.org/books

IAS (2022) Coral Reefs and Sea-Level Change: Quaternary Records and Modelling, 39–67

Microscale evolution of reefal microbialites

SHO KOYANO[†], FUMITO SHIRAISHI[‡], YOSUKE MIYAIRI[§], YUSUKE YOKOYAMA[§] and KAZUHIKO FUJITA[†,¶,*]

[†]*Physics and Earth Sciences Course, Graduate School of Engineering and Science, University of the Ryukyus, 1 Senbaru, Nishihara, Okinawa 903-0213, Japan.*
[‡]*Earth and Planetary Systems Science Program, Hiroshima University, 1-3-1 Kagamiyama, Higashihiroshima, Hiroshima 739-8526, Japan.*
[§]*Atmosphere and Ocean Research Institute* and *Department of Earth and Planetary Sciences, The University of Tokyo, 5-1-5 Kashiwanoha, Kashiwa 277-8564, Japan.*
[¶]*Department of Physics and Earth Sciences, Faculty of Science* and *Tropical Biosphere Research Center, University of the Ryukyus, 1 Senbaru, Nishihara, Okinawa 903-0213, Japan.*
**Corresponding author: K. Fujita. E-mail address: fujitaka@sci.u-ryukyu.ac.jp*

ABSTRACT

Reefal microbialites are crusts and infills of microbialites developed within primary cavities of late Quaternary coralgal reef frameworks. In spite of many previous studies, factors controlling mesofabric transitions, particularly from laminated to digitate microbialites but as well as the microscale formation process in relation to microbial communities, have not yet been fully understood. Furthermore, there are still controversies regarding age differences between reef framework growth and microbialite formation. The authors have discussed the macroscale evolution of primary cavities as well as the microscale evolution of reefal microbialites obtained in a middle Holocene reef core drilled off Okinawa Island, south-west Japan, based on petrographic observations using light and scanning electron microscopy with energy dispersive X-ray spectroscopy and radiocarbon (^{14}C) ages of corals and reefal microbialites. The authors' petrographic observations show that coralgal reef framework growth was followed by encrusting foraminifers and metazoans, coevally with macro-bioerosion and microbioerosion of coralgal frameworks, then finally infilled with an intraskeletal and boring-filling microbialite (IBFM) and encrusted by reefal microbial crusts (RMCs), including structureless and digitate microbialites. The observed macroscale evolution was probably driven in response to progressive changes to reduced light and water circulation in the primary cavities associated with middle Holocene transgression and reef formation. The microfabric of reefal microbialites consists of primary *in situ* precipitated peloids (spherical micritic clots), voids (primary pores) and allochthonous detrital grains (bioclastic and siliciclastic) fallen from upper reef surfaces. IBFM geopetally infilled inside bioeroded cavities soon after the bioerosion of coralgal frameworks. RMCs have a two-layered microfabric succession, which is composed of the alternation of dense peloidal aggregates and laterally aligned voids in the lower part and the mixing of peloidal aggregates and irregularly and vertically developed voids in the upper part. The authors speculate that the repeated occurrences of laterally aligned voids in the lower part may imply the intermittent pauses of peloidal formation, while peloids accumulated on the irregular outer surfaces may result in the formation of vertically

©2022 International Association of Sedimentologists

developed voids and digitate surfaces in the upper part. These peloids are probably formed by coccoid sulfate-reducing bacteria in anoxic environments developed by the degradation of bacterial biofilms and organic matters, allowing sulfate reduction and increasing alkalinity, therefore carbonate precipitation. The two-layered microfabric succession generally observed in RMCs may reflect spatial-temporal oxic/anoxic variations in interstitial water and the degree of sulfate ion supply by the gradual closing of primary cavities.

Keywords: Holocene, microbialite, microstructure, peloid, sulfate reduction

INTRODUCTION

Reefal microbialites are crusts and infills of microbialites developed within primary cavities of late Quaternary coralgal reef frameworks (Camoin *et al.*, 2006; Humblet *et al.*, this volume). They represent the last stage of encrustation of coralgal framework developments and are as much as 20 cm-thick (e.g. Montaggioni & Camoin, 1993; Camoin *et al.*, 1999; Seard *et al.*, 2011). Up to 80% of the reef structure are locally constituted by the reefal microbialites, suggesting an important role in strengthening reef frameworks (Montaggioni & Camoin, 1993; Webb, 1996; Camoin *et al.*, 1999; Seard *et al.*, 2011). The reefal microbialites have been previously recognised as inorganic carbonates (Macintyre & Marshall, 1988; Macintyre, 2011) but now have been widely interpreted as microbial carbonates (Riding 2011).

Mesoscale fabrics of reefal microbialites that are recognisable in visual examination include laminated microbialite, digitate microbialite, structureless microbialite, intraskeletal and boring-filling microbialite (IBFM) and microbialite-coated debris (e.g. Braga *et al.*, 2019). IBFM is the first fabric to develop in skeletal voids and borings of coralgal frameworks. It is usually followed by structureless and laminated microbialites, then locally overlain by digitate microbialite (e.g. Camoin *et al.*, 1999; Seard *et al.*, 2011; Braga *et al.*, 2019). Although key factors for microbialite development in primary cavities involve decreasing light and energy conditions as well as increasing nutrients and alkalinity (e.g. Camoin *et al.*, 1999; Westphal *et al.*, 2010), factors controlling mesofabric transitions particularly from laminated to digitate microbialites have not yet been fully understood.

Microscale fabrics of reefal microbialites that are observed under a microscope are generally composed of dense clotted to peloidal micrites with voids and subordinate silt-sized detrital grains (e.g. Camoin & Montaggioni, 1994; Westphal *et al.*, 2010; Fujita *et al.*, 2020). Peloids (spherical micritic clots) are recognised as products of the microbially mediated precipitation of high-magnesium calcite (HMC) within and around active clumps of coccoid bacteria (Chafetz, 1986; Reitner *et al.*, 2000; Riding, 2000; Shiraishi *et al.*, 2017). However, it is still unclear which type of coccoid bacteria are involved in the peloidal formation of reefal microbialites. Lipid biomarker and stable sulfur isotope results confirmed that sulfate-reducing bacteria played an intrinsic role in the precipitation of reefal microbialites and similar microbial carbonates (Lyons *et al.*, 1984; Kempe, 1990; Reitner *et al.*, 2000; Heindel *et al.*, 2010; Heindel *et al.*, 2012; Gischler *et al.*, 2017; Braga *et al.*, 2019). However, it is unclear what kind of microfabric was produced by sulfate-reducing bacteria. In addition, the remnants of calcified cyanobacterial filaments (Camoin & Montaggioni, 1994; Cabioch *et al.*, 2006) and microbioerosion traces (ichnotaxa) produced by phototrophic (cyanobacteria, chlorophytes) and heterotrophic microborers

(bacteria, fungi) have been observed in reefal microbialites (Heindel *et al.*, 2009a; Heindel *et al.*, 2009b). However, the role of these microboring endoliths for the microfabric formation is not yet clear. Although it is very difficult to extract microbial remains from fossil reefal microbialites due to a rapid decay of microbial colonies, microstructural observations may provide a key to understand the microscale evolution of reefal microbialites formed by the interaction of microbial growth and metabolism, cell surface properties and extracellular polymeric substances (EPS).

In addition, there are still controversies regarding age differences between reef framework growth and microbialite formation (Camoin & Seard, 2011). Heindel *et al.* (2009b) and Westphal *et al.* (2010) considered that reefal microbialites might developed coevally with coralgal communities, based on their radiocarbon (^{14}C) age measurements for the pairs of corals and encrusting microbialites from the top of the succession, while the corals from the base of the succession are 600 to 700 yr older than the encrusting microbialites. Seard *et al.* (2011) carried out comparative ^{14}C dating using the density separation of carbonate minerals to elucidate age offsets between coralgal communities and microbialites. They demonstrated that reefal microbialites developed a few hundred years after coralgal communities in shallow-water environments, while slope microbialites grew a few thousands of years later in significantly deeper water conditions after the demise of coralgal communities (Camoin *et al.*, 2006). Other studies considered that reefal microbialites developed either coeval with coralgal communities (Braga *et al.*, 2019) or 100 to 500 yr after coralgal communities (Gischler *et al.*, 2008; Jell & Webb, 2012). More dating studies are necessary to explain their age offsets and the growth rates of RMCs.

In this paper, the authors aim to discuss the macroscale evolution of primary cavities and the microscale evolution of reefal microbialites, based on the petrographic observations using light and scanning electron microscopy, as well as measurements of ^{14}C age offsets between corals and reefal microbialites.

MATERIALS AND METHODS

Studied setting and materials

The Ryukyu Archipelago is a curved island arc separated from the East China Sea shelf by the Okinawa Trough back-arc basin in the west and from the Philippine Sea Plate by the Ryukyu Trench in the east (Fig. 1A). Okinawa Island is the largest island exposed on the middle part of the Ryukyu Archipelago (Fig. 1B). The basement rocks of Okinawa Island are composed chiefly of Mesozoic and Palaeozoic metamorphic and sedimentary rocks, exposed on the northern part of the island, while the southern part of Okinawa Island is composed of late Cenozoic siliciclastic rocks of slope to forearc basin called the Shimajiri Group and of Quaternary reef-complex deposits and associated non-marine deposits called the Ryukyu Group (Iryu *et al.*, 2006). The island is surrounded predominantly by fringing reefs enclosing a back-reef shallow lagoon or moat, with few exceptions of barrier reefs and patch reefs (Kan, 2011).

Reefal microbialites for this study were obtained in a Holocene reef core (inner core diameter ca. 46 mm; down to 8 m core depth; 87% recovery) drilled on the Naha New Port Pier, south-west of Okinawa Island, where an offshore patch reef had been landfilled (3 m above present mean sea-level; 26°14'59.4"N, 127°40'15.1"E; Fig. 1C). The lithology and age of core materials have been described in Fujita *et al.* (2020). Briefly, except for landfill deposits in the upper part of core (0 to 2.8 m in depth), the drilled core succession from 2.8 to 7.9 m-deep is composed of coral skeletal frameworks partly filled with unconsolidated bioclastic sediments. ^{14}C ages of coral colonies oriented upward indicate that the drill core is

Middle Holocene in age (younger than 7540 mean cal yr BP) and mostly developed between 7500 and 6700 mean cal yr BP.

Five core slabs, where reefal microbialites were typically developed, were selected from 3.0 to 6.9 m in core depth: NH4-13-01, NH4-13-02 (5.04 to 5.15 m), NH4-16 (5.42 to 5.45 m), NH4-17 (5.54 to 5.59 m) and NH4-23 (6.40 to 6.48 m; Figs 2 and S1). These slabs were polished and colour-scanned to examine the reef framework succession.

Microstructure observations

Petrographic thin sections were prepared from the selected slabs and observed using light microscopy under transmitted light. Two rectangular blocks (each 25 to 30 mm in length, ~5 mm in width, ~5 mm in thickness) were cut along the reef framework succession (Fig. 2). The block sections were immersed in 5% H_2O_2 to remove organic matters until no bubbles were released, ultrasonicated with Milli-Q water and air-dried. To obtain a cast section, the methods of Heindel *et al.* (2009a) were followed. One of the block sections was impregnated with epoxy resin under vacuum condition and dried at 60° C. The surface was polished to remove epoxy resin, ultrasonicated with Milli-Q water and air-dried. Then, the surface was etched in 5% HCl for 30 seconds, washed in Milli-Q water and air-dried.

The surfaces of both unetched and etched block sections were sputter-coated with gold-palladium and analysed using scanning electron microscopy (SEM; Hitachi, S-3000N and Hitachi, TM3030). SEM images were mainly obtained by a backscattered electron detector. The observations were made at the acceleration voltage of 15 to 20 kV, the emission current of 40 to 44 μA and the filament saturation of 81 to 88. The major elemental composition of crystals and grains were analysed by an energy dispersive X-ray spectrometer (EDX) attached with the SEM (Edax, Genesis-4000 and Bruker Axs K.K, Quantax 70). The analyses were made at the magnification of ×1000 to 3000, the acceleration voltage of 15 to 20 kV, the emission current of 0.5×10^{-9} A and the dead time of 7 to 12%.

Radiocarbon dating

To obtain the formation age of reefal microbialites and the age offsets between corals and reefal microbialites, a pair of a coral and a reefal microbialite in the same slab (four slabs except NH4-13 due to complicated encrustation of coralline algae and reefal microbialites inside the primary cavities of coral branches) were cut and ^{14}C dated using a single-stage of Accelerator Mass Spectrometry (YS–AMS) at the Atmosphere and Ocean Research Institute at the University of Tokyo, Japan. Prior to the ^{14}C measurement, original mineralogy was confirmed with X-ray diffraction (XRD) analysis. Then, coral and reefal microbialite samples were cleaned with Milli-Q water and a chemical pre-treatment was performed with HCl to avoid surface contamination. The graphitisation method was employed to convert CO_2 extracted from samples into graphite, in the presence of H_2, using Fe powder as a catalyst (for more details on the method see Yokoyama *et al.*, 2007). Conventional ^{14}C ages were calibrated to calendar ages using OxCal v.4.3 (https://c14.arch.ox.ac.uk/oxcal.html) using the Marine13 curve (Reimer *et al.*, 2013). $\Delta R = 29 \pm 18$ yr was used as the local reservoir correction of the Ryukyu Islands (Yoneda *et al.*, 2007). The age offsets between corals and reefal microbialites were calculated from the midpoint of the 1σ range of conventional ^{14}C ages, following the methods in Seard *et al.* (2011).

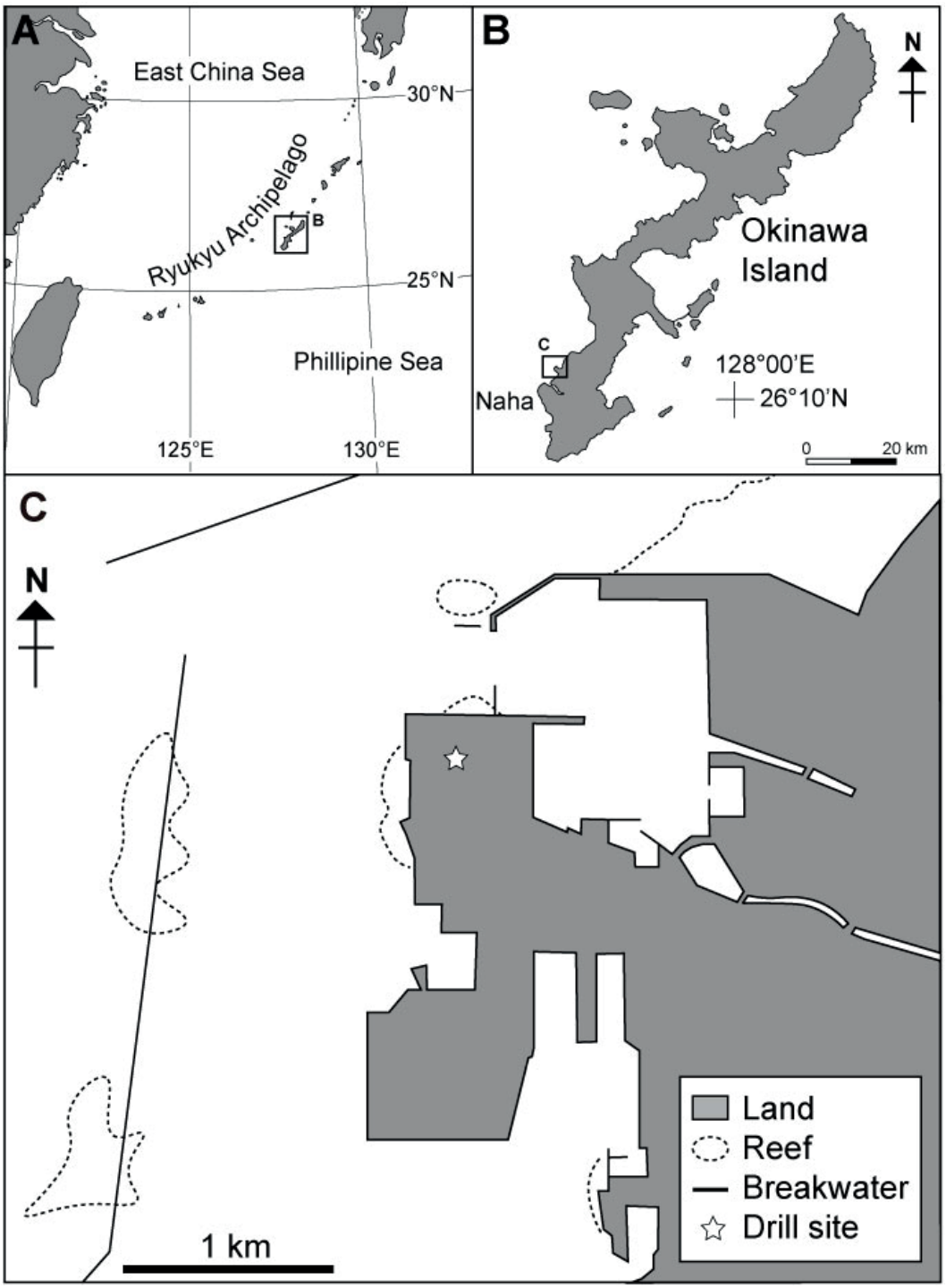


Fig. 1. Location maps of the study area. A: Ryukyu Archipelago, B: Okinawa Island, C: Naha New Port Pier, showing a drill site.

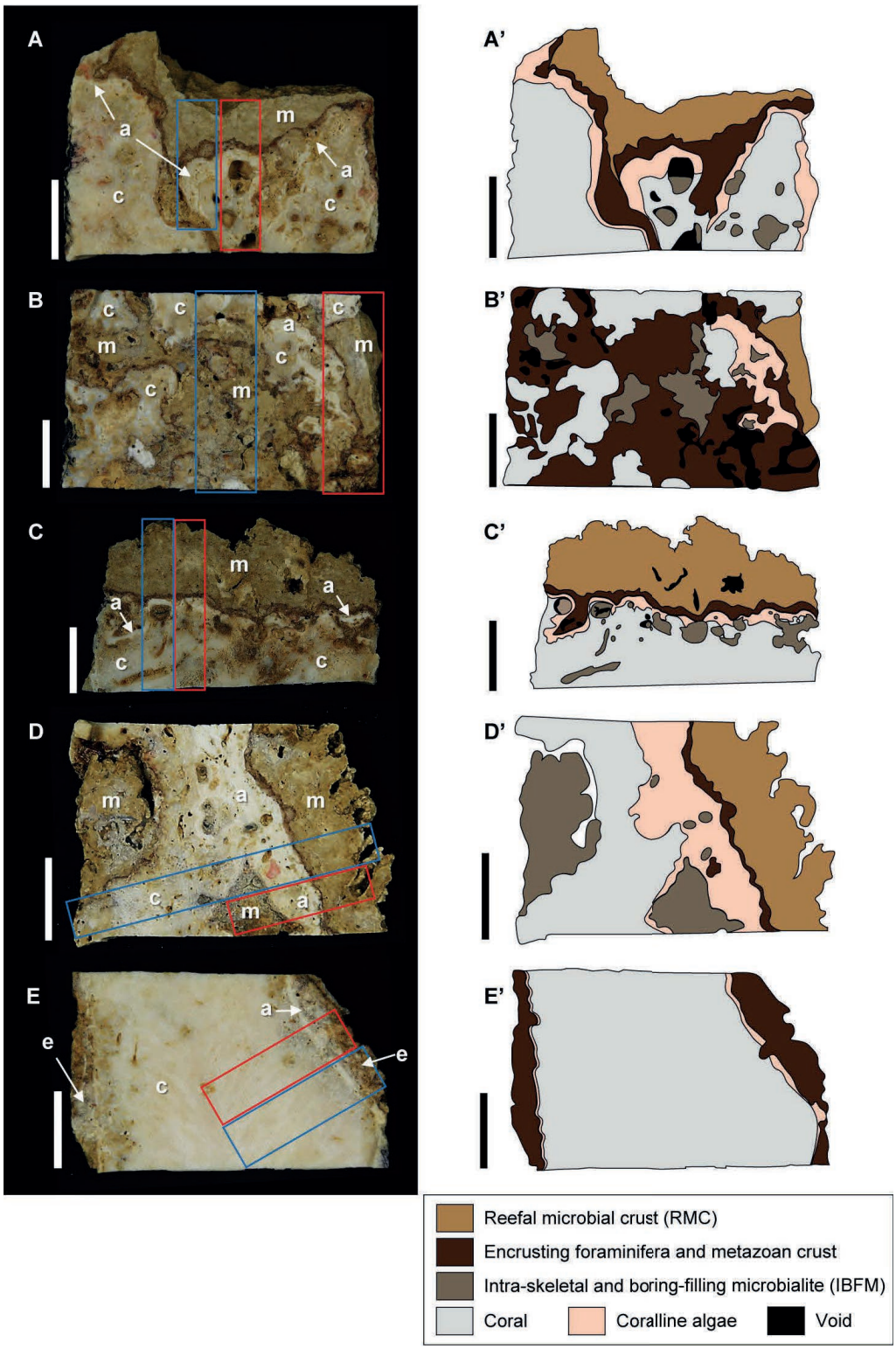


Fig. 2. Photographs (left) and sketches (right) of slabs from core NH4. A, A': NH4-13-01, B, B': NH4-13-02, C, C': NH4-16, D, D': NH4-17, E, E': NH4-23. Blue and red rectangular frames indicate cut and etched surface parts used for SEM-EDX observations, respectively. a: crustose coralline algae, c: coral, e: encrusting foraminifera and metazoan crust, m: reefal microbialite. Scale bar = 1 cm.

DESCRIPTIONS

Macroscale succession

Surfaces of coral colonies are encrusted with thin crusts (several mm-thick) of crustose coralline algae (CCA; Fig. 2). Coral skeleton and CCA are heavily bioeroded by macroborers (Fig. 2A to D). CCA are overlain by encrusting foraminifers and metazoans, such as bryozoans and worms, and finally by 4 to 14 mm-thick, brownish, non-skeletal, fine-grained microbialite crusts, which are referred to as reefal microbial crusts (RMCs; Riding, 2011; Fig. 2A to D). The surface of the RMCs is either flat (Fig. 2A and B) or knobby (club shaped/digitate; Fig. 2C and D). The RMCs are generally clotted and structureless, followed by dendritic mesofabric toward the surface (Fig. 2C and D), while a few crusts are weakly laminated horizontally (Fig. 2A) and laterally (Fig. 2B). IBFM infills primary cavities among branching coral colonies (Fig. 2B), as well as bored cavities generated by macroborers in the skeleton of corals and CCA (Fig. 2A, C and D). Encrusting foraminiferal crusts (Fig. 2E) are composed mainly of *Carpenteria* sp., with inter-skeletal and intra-skeletal spaces filled with sand-sized grains and micrites.

Microscale succession and detail of reefal microbialites

Coral skeleton and CCA are heavily bioeroded by macroborers and endolithic microborers (Fig. 3A and B). Filamentous microbioerosion traces can also be extensively observed around the boundary between coral skeleton and CCA crust (Fig. 4A to C) as well as in coral skeleton (Fig. 4D to F).

Bored cavities of coral skeleton, CCA and chambers of encrusting foraminifers are partially and totally infilled with IBFM, which is composed of peloidal aggregates of 20 to 50 μm in diameter, subordinate with bioclastic and siliciclastic detrital grains (Fig. 3C to H; Fig. 5A and B). The surfaces of peloids are surrounded by euhedral, braded HMC crystals 2 to 4 μm in width and 4 to 10 μm in length (Fig. 5C and D). Etched casts of IBFM have many hollows with rounded or polygonal shapes of <100 μm in diameter, which are moulds of bioclasts (Fig. 5E and F). Silicate mineral grains of <100 μm in diameter are rarely incorporated in these casts. Acicular aragonite crystals of 1 to 4 μm in width and 8 to 12 μm in length are rarely found as spherulites on the surface and inside bored cavities of coral skeleton (Fig. 5G and H). Not all bioeroded cavities in coral skeleton are infilled with peloidal aggregates or acicular aragonite spherulites.

RMCs are composed primarily of dense aggregates of peloids associated with voids and bioclastic and siliciclastic grains (Fig. 6A and B). Voids are aligned either laterally in the lower part (Figs 6C and 7A) or irregularly and vertically in the upper part (Figs 6E and 7D). Laterally aligned voids are surrounded by peloidal aggregates of 10 to 40 μm in diameter (Fig. 6D, 7B), which incorporate silicate mineral grains and aragonitic bioclasts (~100 μm in diameter; Fig. 7C). Irregularly and vertically developed voids are glued with micritic and peloidal aggregates of 20 to 50 μm in diameter (Figs 6F and 7E), which incorporate silicate mineral (quartz) grains (Fig. 7F) and bioclasts (~100 μm in diameter). Filamentous microbioerosion traces can be observed in relatively large bioclasts (Fig. 6G and H).

Etched surfaces of RMCs are composed of crystallite parts and epoxy-resin cast parts (Fig. 8A). Crystallites consist of the dense aggregation of micrite of <1 μm in diameter, which incorporates bioclasts of 30 to 100 μm in diameter and rarely silicate mineral grains of 30 to 50 μm in diameter (Fig. 8B). Epoxy-resin casts are characterised by two textural patterns: laminated (Fig. 8C) and irregular (Fig. 8E). Laminated casts are interlayered with crystallites, whilst irregular casts are mixed with crystallites. As observed in IBFM, both laminated and irregular casts have many

hollows with rounded or polygonal shapes of <100 μm in diameter, which are moulds of bioclasts (Fig. 8D and F). Silicate mineral grains of <50 μm in diameter are rarely incorporated in these casts. Filamentous microbioerosion traces with thin (2 to 3 μm in diameter) and thick (6 to 7 μm in diameter) galleries can be observed beneath the moulds of bioclasts (Fig. 8G). Similar filamentous microbioerosion traces of 6 to 7 μm in diameter can be rarely observed on crystallites (Fig. 8H).

The microbioerosion traces observed in coral skeleton, CCA and bioclasts in IBFM and RMCs are identified to at least 5 ichnotaxa. The ichnotaxa include *Fascichnus dactylus* (Radtke, 1991), *Eurygonum nodosum* (Schmidt, 1992) and *Scolecia filosa* (Radtke, 1991), which are produced by phototrophic cyanobacteria. *Fascichnus dactylus* is characterised by radiating bundles of long galleries 2 to 4 μm in diameter (Figs 4C, 8H and S4A), which is found in coral skeleton, CCA and bioclasts in IBFM and RMCs (Table 1). *Eurygonum nodosum* is characterised by bifurcated galleries with lateral swellings (Figs 4F, 8G and S4B), which is found in all of the substrates above. *Scolecia filosa* is characterised by 'spaghetti-like' curved, thin and long individual galleries forming large networks (Figs 4C, F, 8G and S4C), which is the most common ichnotaxa and found in all the substrates. The remaining two ichnotaxa are *Scolecia serrata* (Fig. S4D) and *Scolecia* cf. *serrata* (Fig. S4E), which are produced by unknown heterotrophs. *Scolecia serrata* is characterised by thin serrate micro-sculpture parallel to the substrate surface, while *S.* cf. *serrata* is different from *S. serrata* in having slightly thicker galleries and spherical aggregates resembling 'bags of wool'. *Scolecia serrata* is found in bioclasts in IBFM and RMCs, while *S.* cf. *serrata* is found on coral skeleton and in bioclasts in IBFM.

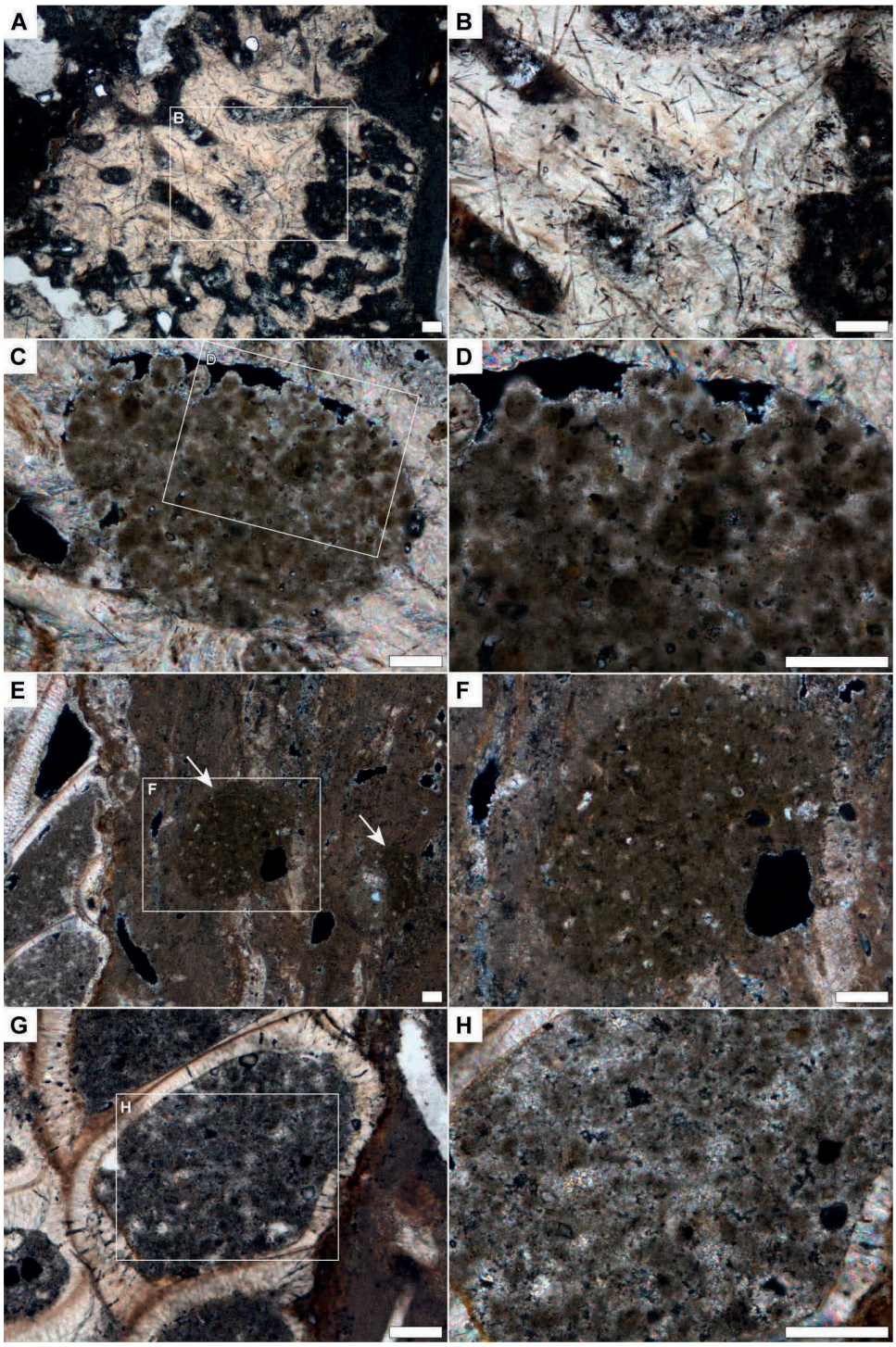


Fig. 3. Thin-section micrographs of intraskeletal and boring-filling microbialite (IBFM). A: dense micritic aggregates inside bored spaces of coral skeleton (sample NH4-17), B: close up of A showing filamentous microbioerosion traces inside coral skeleton, C: peloidal aggregates inside the bored cavity of coral skeleton (sample NH4-23), D: close up of C showing dense peloidal aggregates, E: peloidal aggregates (arrow) inside the bored cavity of crustose coralline algae (sample NH4-17), F: close up of E, showing mixed peloidal and agglutinated microfabric, G: peloidal aggregates inside chambers of an encrusting foraminifer (sample NH4-17), H: close up of G. Scale bar = 100 μm.

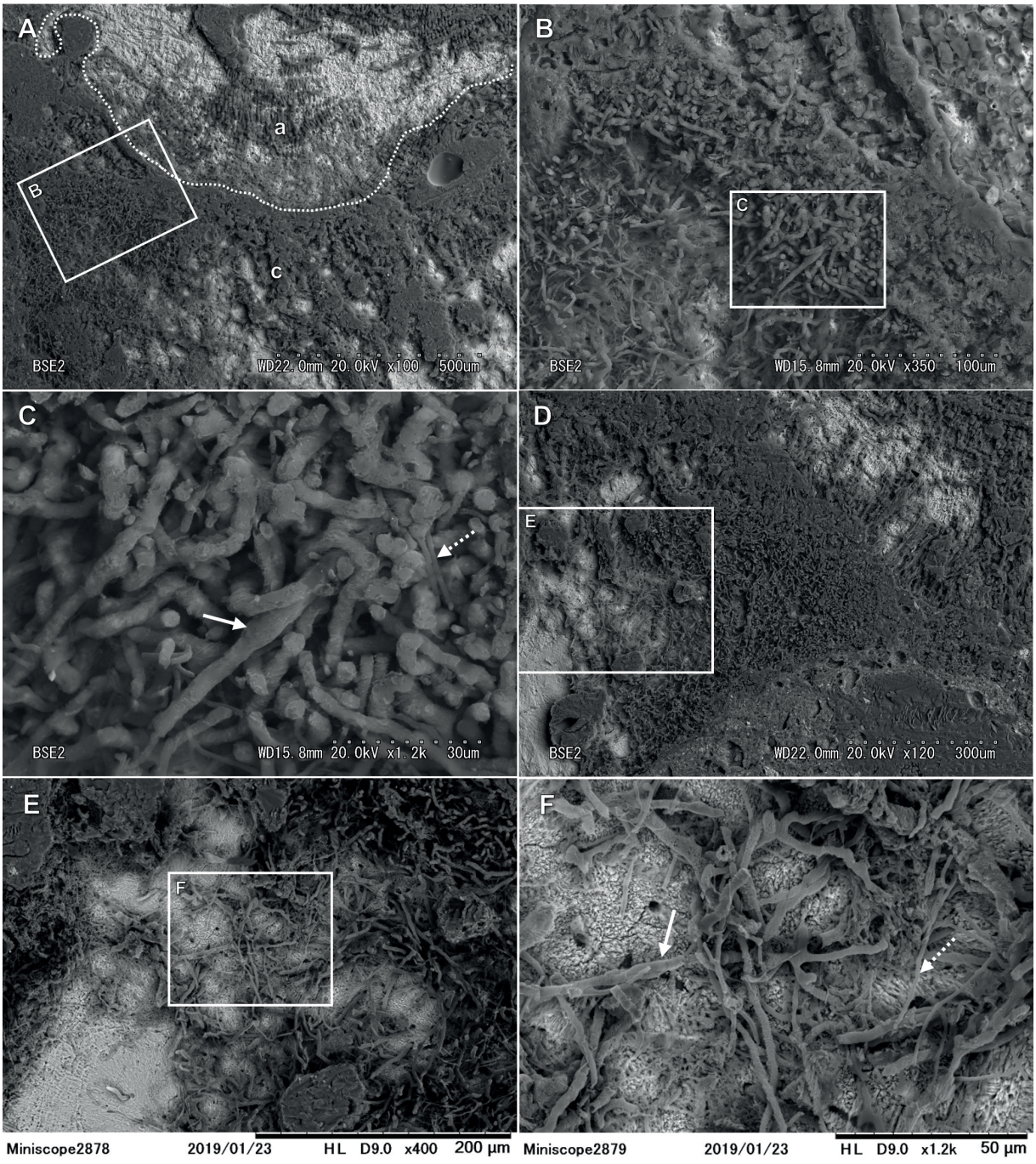


Fig. 4. SEM images of microbioerosion traces (Ichnotaxa) observed in etched surfaces. A: microbioerosion traces around the boundary between crustose coralline algae (a) and a coral (c; sample NH4-16), B: close up of image A, C: Ichnotaxa *Fascichnus dactylus* (solid line arrow) and *Scolecia filosa* (dot line arrow), observed in the close up of image B, D: microbioerosion traces in coral skeleton (sample NH4-16), E: close up of image D, F: Ichnotaxa *Eurygonum nodosum* (solid line arrow) and *Scolecia filosa* (dot line arrow), observed in the close up of image E.

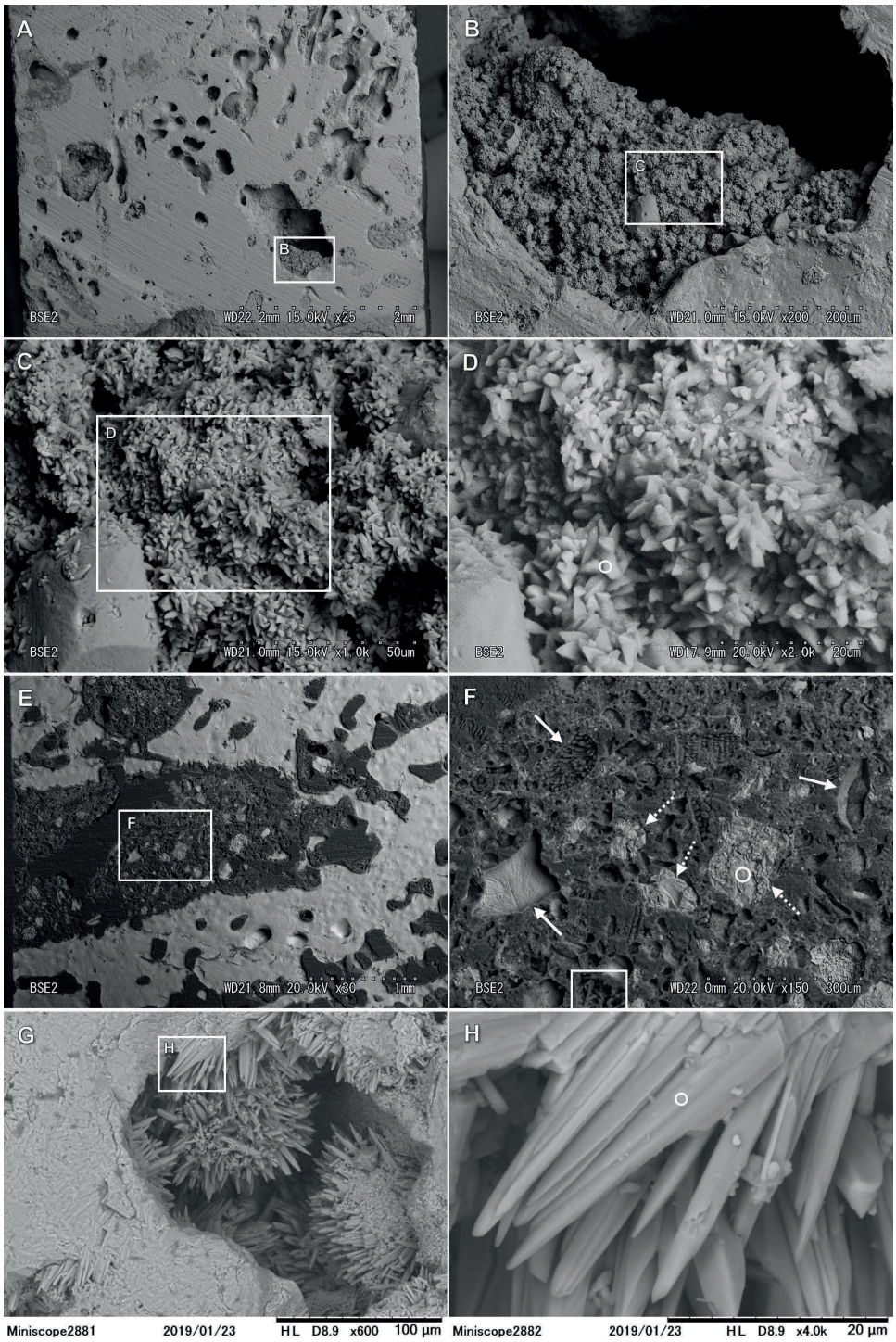


Fig. 5. SEM images of cut and etched surfaces of coral skeleton. A: bored cavities in coral skeleton (sample NH4-17), B: peloidal aggregates filled in the bottom of a bored cavity, observed in the close up of image A, C: bladed high-magnesium calcite, observed in the close up of image B, D: close up of image C, E: casts in a cavity of a bioeroded coral skeleton (sample NH4-16), F: moulds of bioclasts (solid line arrow) and silicate minerals (dot line arrow), observed in the close up of image E. G: acicular aragonite spherulites observed in a cavity of bioeroded coral skeleton (sample NH4-17), H: close up of image G. See Figs S2 and S3 for the elemental spectrum of crystals (D, F, H, circled parts), examined by SEM-EDX qualitative spot analysis.

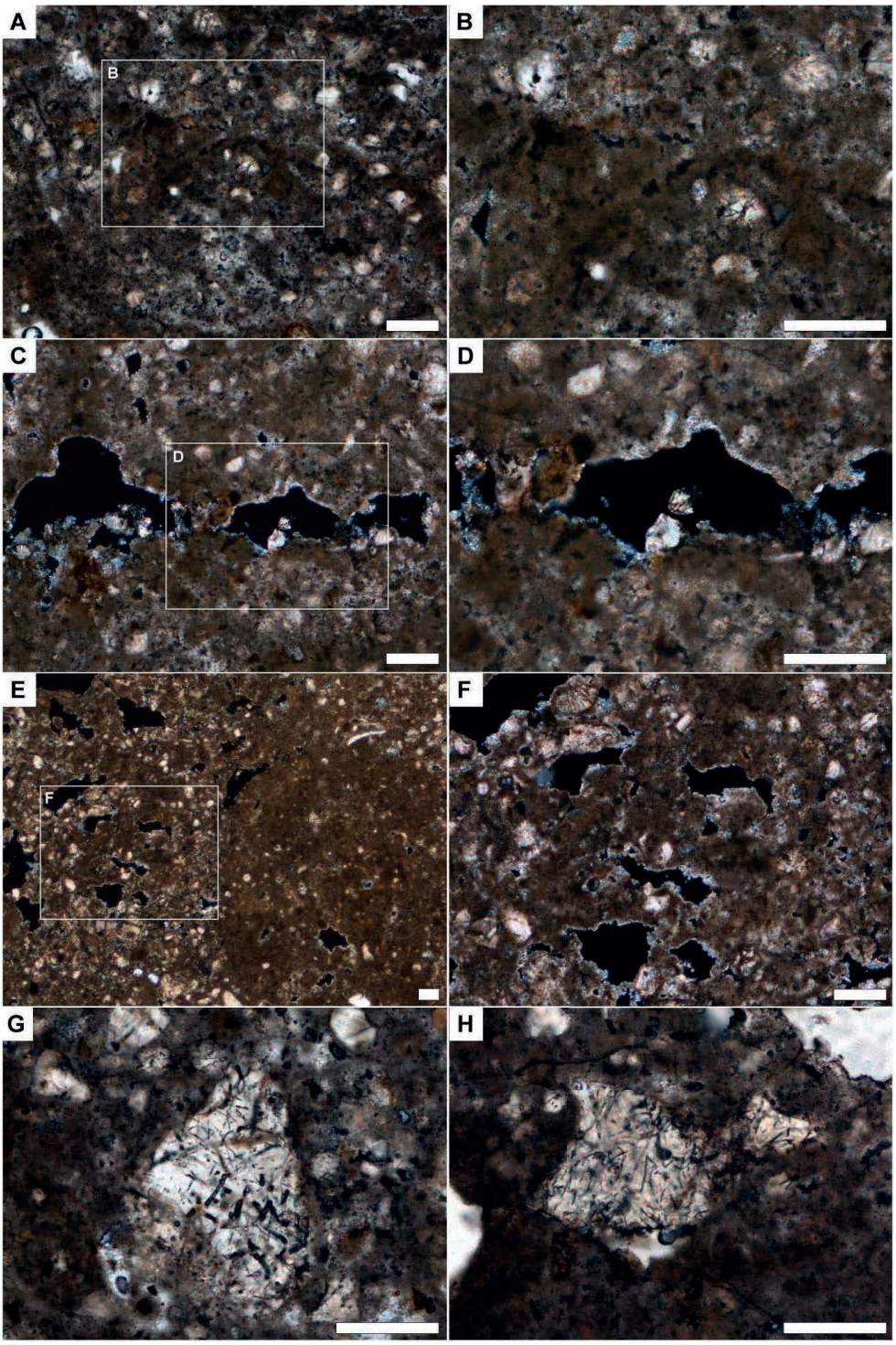


Fig. 6. Thin-section micrographs of a reefal microbial crust (RMC; sample NH4-16). A: dense peloidal aggregates associated with detrital grains in the lower part, B: close up of A, C: the lower part of the RMC showing laterally aligned voids surrounded by peloids, D: Close up of C, E: the upper part (top, leftward) of the RMC showing irregular (left) and dense (right) peloidal distribution, F: close up of mixed peloidal and agglutinated microfabric with irregular and vertical voids, G, H: a microbored bioclast incorporated in the RMC. Scale bar = 100 μm.

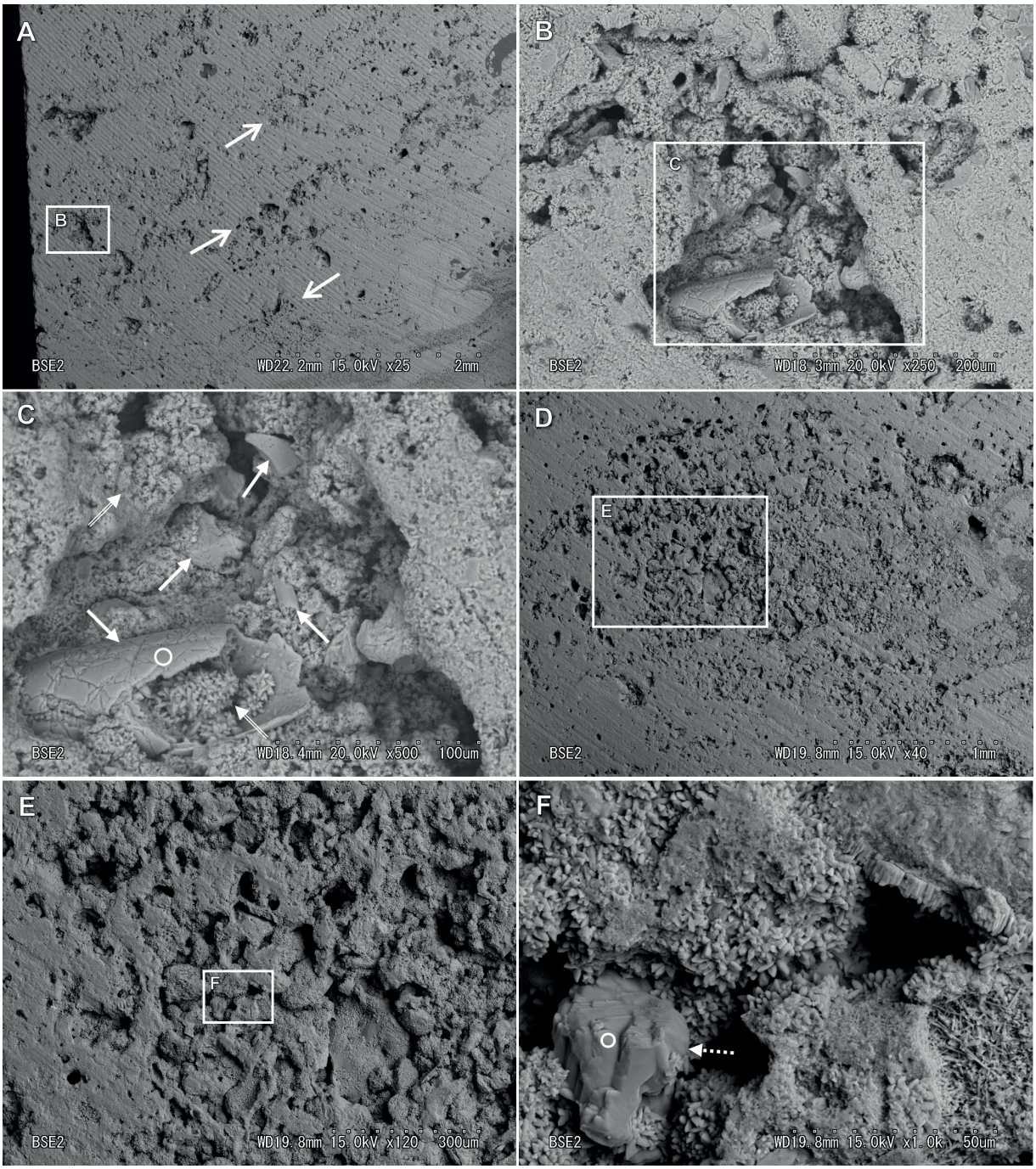


Fig. 7. SEM images of cut surfaces of a reefal microbial crust (RMC; sample NH4-17). A: laterally aligned voids (solid line arrow), B: close up of image A, C: peloids (double line arrow) and bioclasts (solid line arrow), observed in the close up of image B. D: irregular voids (sample NH4-16), E: close up of image D, F: silicate mineral (dot line arrow) in irregular voids, observed in the close up of image E. See Fig. S2 for the elemental spectrum of detrital grains (C, F, circled parts), examined by SEM-EDX qualitative spot analysis.

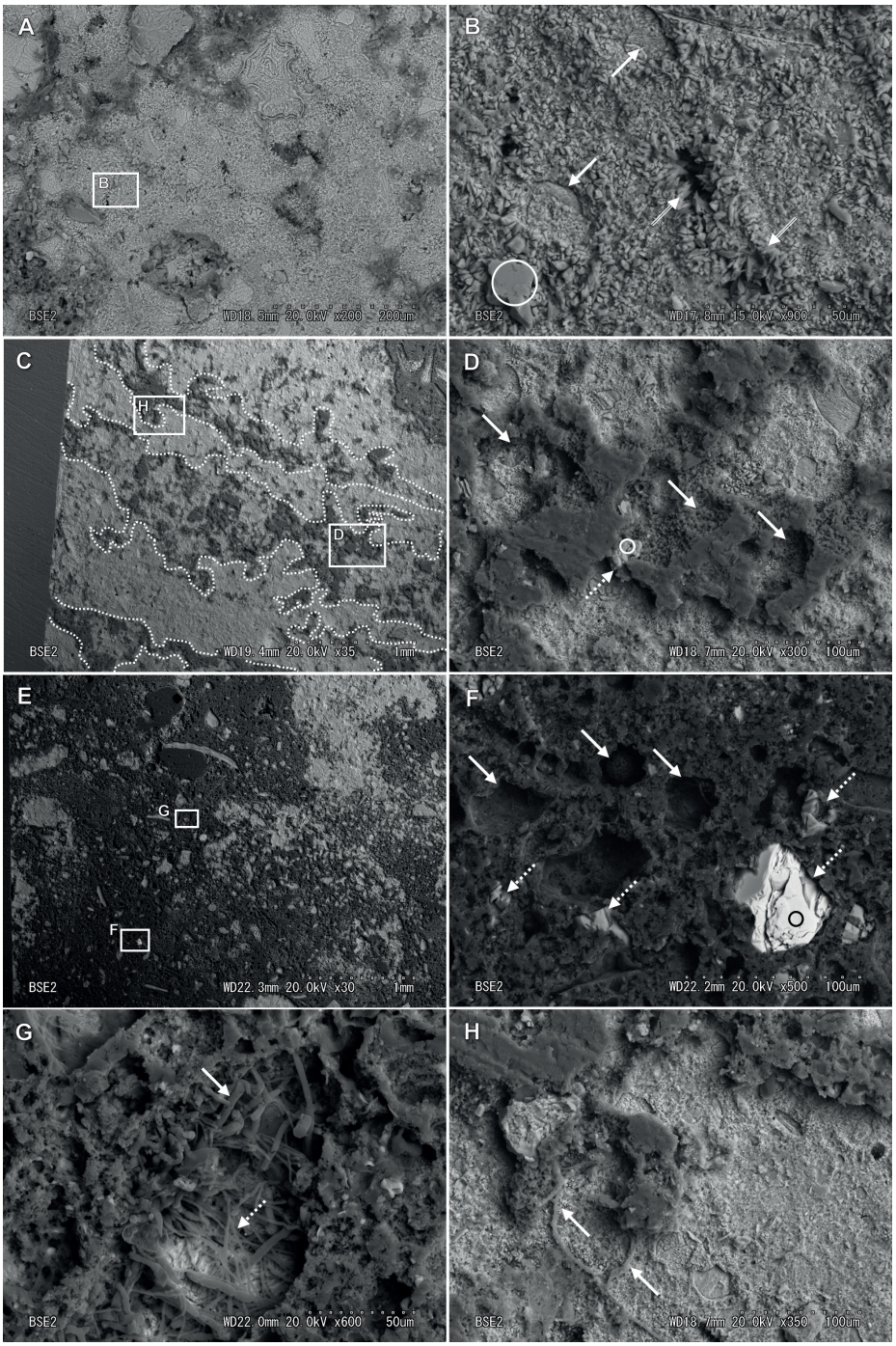


Fig. 8. SEM images of etched surfaces of reefal microbial crusts (RMCs). A: dense crystallites (sample NH4-13-01), B: micrites (double line arrow) and bioclasts (solid line arrow) found in dense crystallites, observed in the close up of image A, C: laminated casts (surrounded by dot lines; sample NH4-17), D: moulds of bioclasts (solid line arrow) and a silicate mineral (dot line arrow) in laminated casts, observed in the close up of image C, E: irregular casts (sample NH4-16), F: moulds of bioclasts (solid line arrow) and silicate minerals (dot line arrow), observed in the close up of image E, G: Ichnotaxa *Eurygonum nodosum* (solid line arrow) and *Scolecia filosa* (dot line arrow), observed in the close up of image E of Fig. 8 (sample NH4-16), H: Ichnotaxon *Fascichnus dactylus* (solid line arrow) near the boundary between laminated casts and crystallites, observed in the close up of image C of Fig. 8 (sample NH4-17).

RESULTS AND DISCUSSION

Macroscale evolution of primary cavities

The macroscale succession of primary cavities started from the death of corals, followed by CCA encrustation (Fig. 9A and B). Coral ^{14}C ages measured in this study range from 7453 to 7246 mean cal yr BP (Table 2), which are consistent with those measured in a previous study (Fujita *et al.*, 2020) and correspond to the period of Middle Holocene transgression in the Ryukyus (Kan, 2011; Kawana, 2011). These coralgal assemblages indicating a high-energy, shallow-water environment (Fujita *et al.*, 2020) imply that reef frameworks developed continuously to catch-up with rising sea-levels. Rapid reef framework development probably resulted in producing more primary cavities within coralgal frameworks. The coralgal reef frameworks were then overlain by heterotrophic foraminifers (mainly *Carpentaria* sp.) and metazoans (bryozoans and worms), indicating gradual changes to light-deficient environments in the primary cavities (Fig. 9C).

Coevally with foraminiferal and metazoan encrustation, the reef frameworks were heavily bioeroded by boring metazoans (e.g. sponge, worms, bivalves) and microorganisms, indicating some periods of exposure of reef framework surfaces before starting microbialite formation (Fig. 9C). Bioerosion generally increases under conditions causing coral tissue death because the great majority of endolithic borers attack dead coral skeletons (Glynn, 1997). Higher bioerosion tends to occur when vertical reef accretion is at its extremes (its lowest and highest limits; Patterson *et al.*, 2020). Since the majority of endolith bioeroders are suspension or filter feeders (Glynn, 1997), changes to mesotrophic environments (i.e. increases in nutrients and organic matter) in the primary cavities probably tend to favour increases in bioeroders.

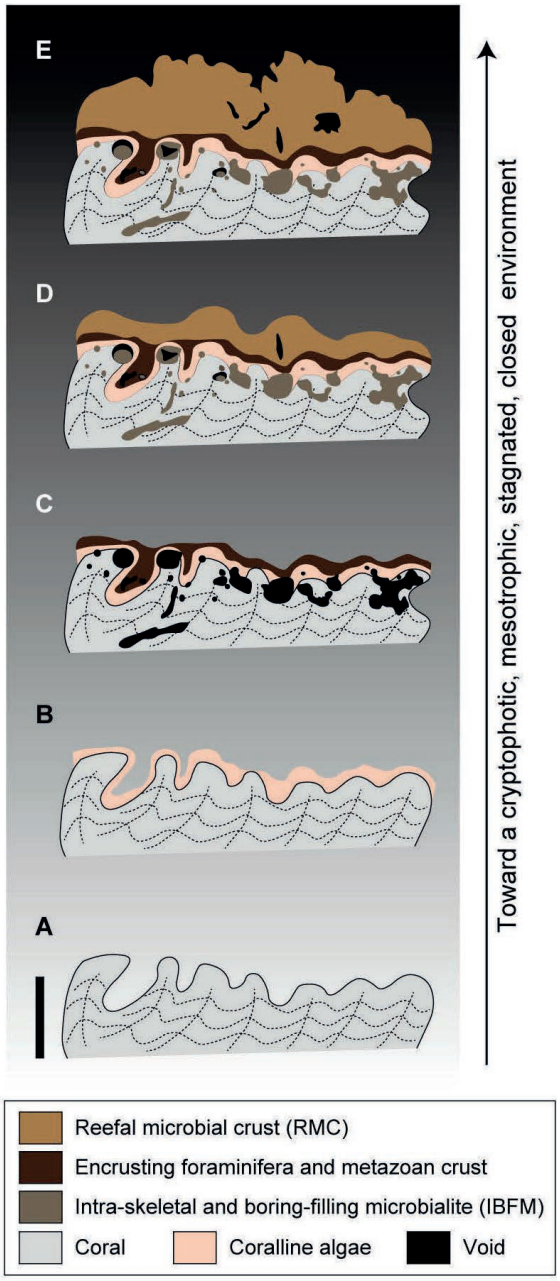


Fig. 9. Macroscale evolution of primary cavities. A: death of corals, B: encrustation of crustose coralline algae, C: bioerosion and encrustation of foraminifers and metazoans, D: voids infilled with intraskeletal and boring-filling microbialite (IBFM) and encrustation of structureless microbialite, E: development of digitate microbialite crust. Sketches based on the material in Fig. 2C. Scale bar = 1 cm.

Phototrophic (cyanobacterial) and heterotrophic microbioerosion traces were found in coral skeleton, indicating that microbioerosion was also active after the death of corals. Photic zonation criteria based on Heindel *et al.* (2009b) suggest that *F. dactylus* and *E. nodosum* are ichnotaxa that belong to a shallow eulittoral/sublittoral (shallow euphotic zone II/III) to somewhat deeper sublittoral bathymetry (deep euphotic zone). The occurrence of corresponding cyanobacterial microborers (*Hyella caespitosa* for *F. dactylus* and *Mastigocoleus testarum* for *E. nodosum*) indicates a bathymetric range from 0 to 6 m (Chazottes *et al.*, 2009). The cyanobacterial trace *S. filosa* is known from all euphotic zones (Chazottes *et al.*, 2009; Heindel *et al.*, 2009b). *Scolecia serrata* indicates no direct palaeobathymetric significance (Heindel *et al.*, 2009b). These ichnotaxa indicate a photic environment but probably include a dysphotic or cryptophotic (i.e. shaded but not entirely aphotic; Heindel *et al.*, 2009b) environment. Therefore, intense microbioerosion probably occurred during progressive changes from light-efficient to light-deficient environments in the primary cavities.

The cavities of bioeroded coral skeleton and intraskeletal voids were then filled with IBFM (Fig. 9D). Coevally, surfaces of encrusting foraminifers and metazoans were covered with structureless microbialite crusts (Fig. 9D), followed by digitate microbialite crusts (Fig. 9E). At this time, the primary cavities became cryptophotic, mesotrophic, stagnated, semi-closed environments, which were not favourable for photophilic organisms to colonise but probably favourable for microbial communities.

^{14}C ages of RMCs are always younger than underlying coral ^{14}C ages (Table 2). Age offsets between corals and RMCs are several hundred years, while the age offset between a coral and an encrusting foraminiferal crust (NH4-23) is shorter than those of the coral-RMC relationships. The result is consistent with those from Tahitian coral-microbialite relationships, which range from 100 to 500 yr (Seard *et al.*, 2011), although Heindel *et al.* (2009b) and Westphal *et al.* (2010) considered that Tahitian RMCs developed coevally with coralgal frameworks. The coral-RMC age offsets as well as the vertical depth offsets between corals and RMCs with similar ages (at least 1 to 1.5 m in depth apart) also support the conclusion by Seard *et al.* (2011) that RMCs developed in the primary cavities of coralgal frameworks at some distances beneath the living reef surfaces. The age offset is also partly attributed to measuring bulk RMC samples with detrital grains in this study. Seard *et al.* (2011) demonstrated that the ages obtained on bulk microbialite samples were younger than those obtained on the separated HMC fractions of peloidal aggregates. Therefore, the age offsets between the HMC fraction ('pure' microbialite) and the underlying coral are probably smaller than those obtained in this study. However, even if we consider the above problems and measurement errors, the results herein clearly show that RMCs developed within a few hundred years after coralgal communities, as in Tahitian RMCs (Camoin & Seard, 2011; Seard *et al.*, 2011). Although the authors have not measured ^{14}C ages of IBFM observed in bioeroded cavities in coral skeleton, these also probably developed soon after the bioerosion of coralgal reef frameworks.

The inferred macroscale evolution in the primary cavities was driven in response to progressive changes from a photic, well-circulated, oligotrophic, open environment to a cryptophotic, stagnated, mesotrophic closed environment in primary cavities. Previous studies (Fujita *et al.*, 2020) discussed that multiple factors, including both local and global origins associated with Holocene transgression and reef formation, probably constrained the development of reefal microbialites in the study area. Since the study area was located off the mouth of river and not

surrounded by fringing reefs at ca. 7 ka, marginal reef frameworks were directly exposed to terrigenous sediment input by river runoff. Such conditions probably induced increasing nutrient availability and alkalinity as well as decreasing light and energy conditions within the primary cavities, as suggested in previous studies (Camoin *et al.*, 1999; Heindel *et al.*, 2009b; Heindel *et al.*, 2012). Relatively elevated sea water carbonate saturation corresponding with relatively low levels of atmospheric CO_2 is partly attributed to microbialite formation during Middle Holocene (Riding *et al.*, 2014).

Microscale evolution of reefal microbialites

Reefal microbialites are composed of peloids, voids and silt-sized detrital grains (bioclastic and siliciclastic). Peloids are spherical micritic clots of ~50 μm in diameter, surrounded by euhedral HMC crystals. These euhedral crystals are interpreted as the progressive transformation of initially smooth, rounded crystallites that are associated with bacterial biofilms, into larger and euhedral scalenohedra during active microbialite accretion (Webb *et al.*, 1998). Therefore, peloids are probably primary, *in situ* precipitated deposits associated with microbial activities, as suggested by many previous studies (e.g. Chafetz, 1986; Reitner, 1993; Camoin & Montaggioni, 1994). Voids are primary pores, which are not yet filled with cements. These voids are surrounded by peloids and were probably formed with active *in situ* peloid accumulation. Bioclastic and siliciclastic detrital grains are allochthonous because no biological production and bioerosion were active during peloid accumulation and there were no sources for siliciclastic rocks around the primary cavities. Phototrophic (cyanobacterial) and heterotrophic microbioerosion traces were observed in bioclasts in reefal microbialites. Since most microbioerosion traces are exclusively observed in coral skeleton and CCA, and microbioerosion traces in reefal microbialites are confined only to bioclasts, these microbored bioclasts are probably products fallen from bioeroded upper reef surfaces and accumulated into primary cavities during microbialite formation.

IBFM partially or totally develops in bored cavities of coral skeleton and CCA as well as intraskeletal spaces of foraminifers and metazoans (Fig. 10A). Soon after the bioerosion of coralgal reef frameworks (Fig. 10B), peloids were precipitated and geopetally infilled inside bioeroded cavities (Fig. 10C). Allochthonous detrital grains were rarely accumulated and trapped with peloids. IBFM formation terminated because the cavities were finally infilled with peloids and/or conditions favouring peloid precipitation changed (Fig. 10D). Although acicular aragonite spherulites indicating secondary crystals of diagenetically altered coral skeleton is rarely observed in bioeroded cavities of coral skeleton, not all bioeroded cavities were infilled with either IBFM or aragonite spherulites, implying both chemically and microbially heterogeneous environments in the cavities. Braga *et al.* (2019) suggested that IBFM is the first fabric to develop in skeletal voids and borings. Although the authors have no ^{14}C ages of IBFM, it is speculated that IBFM and RMCs developed coevally inside and outside the reef frameworks, respectively.

RMCs are the last encrustation of primary cavities. The relatively thin RMCs with generally structureless mesofabrics are microstructurally composed of the alternation of dense peloidal aggregates (crystallites) and laterally aligned voids in the lower part (Fig. 11A) and the mixing of peloidal aggregates and irregularly and vertically developed voids in the upper part (Fig. 12A).

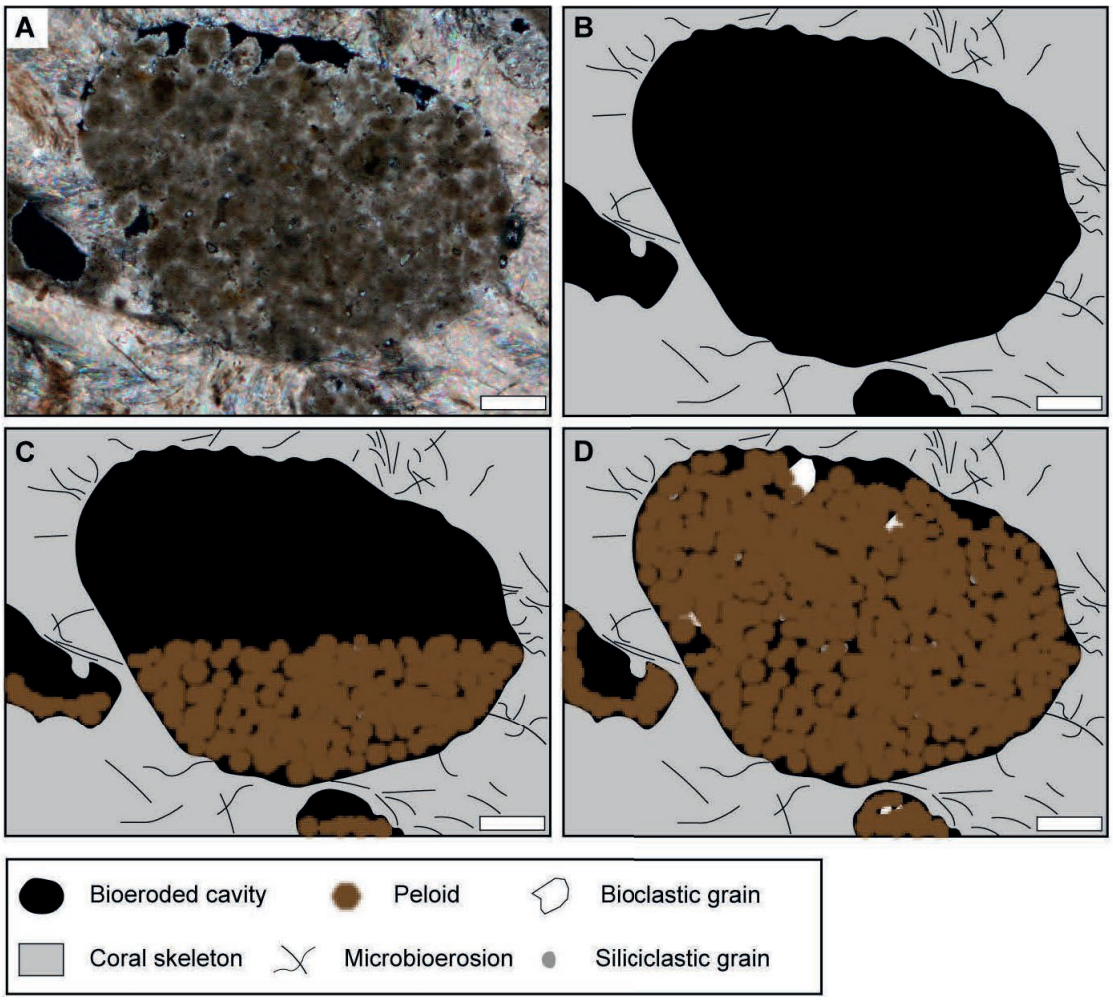


Fig. 10. Microscale evolution of intraskeletal and boring-filling microbialite (IBFM). A: thin-section micrographs of dense peloidal aggregates inside bored cavities of coral skeleton (the image identical with Fig. 3C), B: bioerosion of coral skeleton by macro-bioeroders and micro-bioeroders, C: accumulation of *in situ* precipitated peloids, D: cavities infilled with peloids and detrital grains. Scale bar = 100 μm.

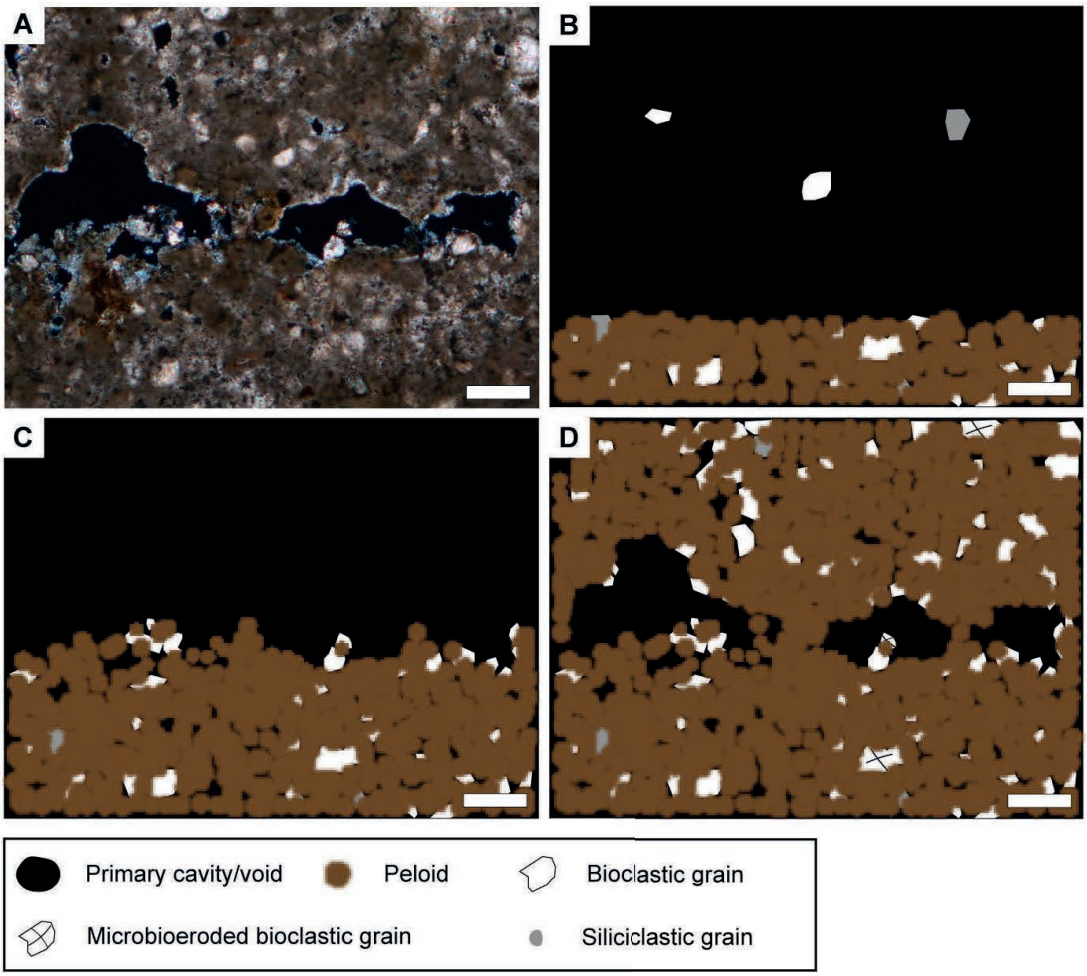


Fig. 11. Microscale evolution of the laminated microfabric of reefal microbial crusts (RMCs). A: the lower part of RMCs showing laterally aligned voids surrounded by peloids (the image identical with Fig. 6C), B: accumulation of *in situ* precipitated peloids and detrital grains, C: a pause of peloid precipitation and accumulation, D: formation of laterally aligned voids and restart of accumulation of peloids and detrital grains. Scale bar = 100 μm.

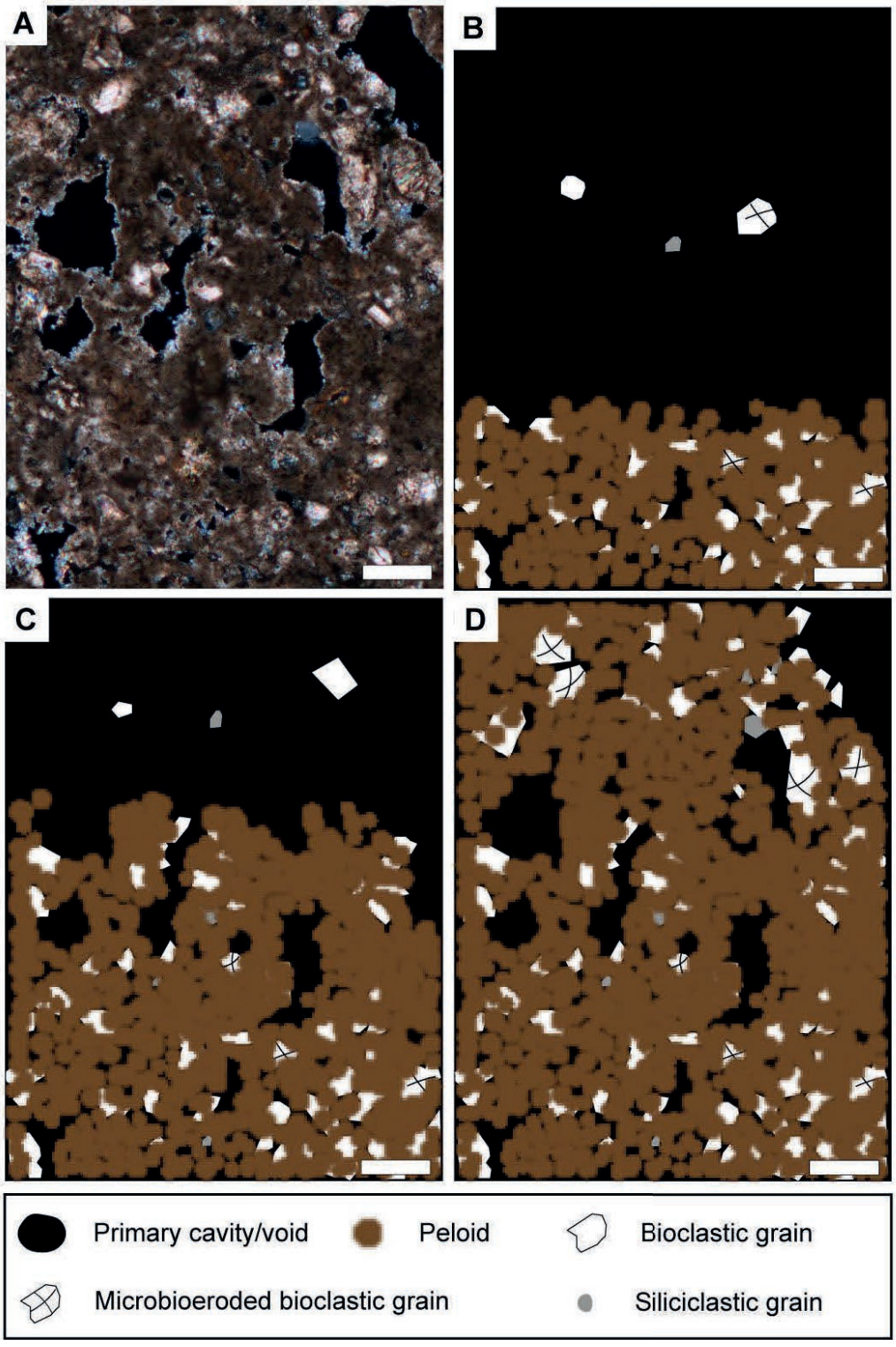


Fig. 12. Microscale evolution of the digitate microfabric of reefal microbial crusts (RMCs). A: close up of mixed peloidal and agglutinated microfabric with irregular and vertical voids (the image identical with Fig. 6F), B: upward accumulation of *in situ* precipitated peloids and detrital grains, C: mixing of peloid deposition parts and non-deposition parts, resulting in the formation of vertically developed voids, D: termination of accumulation of peloids and detrital grains. Scale bar = 100 μm.

Table 1. Distribution of microbioerosion traces observed in etched surfaces of slab samples from core NH4. P: present. Photic zonation criteria are based on Heindel *et al.* (2009b).

	Ichnotaxa	***Fascichnus dactylus***	***Eurygonum nodosum***	***Scolecia filosa***	***Scolecia serrata***	**Scolecia**	**Unknown**
	Photic zonation	**Shallow**	**Shallow**	**Euphotic,**	**Aphotic to**	**cf.*serrata***	**trace**
		II to III	**III to deep**	**dysphotic to cryptophotic**	**cryptophotic**	**Unknown**	
NH4-13-01	Bioclasts in reefal microbial crusts		P		P		
	Cavity in coral skeleton			P			
	Crustose coralline algae and encrusting foraminifers	P	P	P			
	Coral skeleton			P			
NH4-13-02	Bioclasts in reefal microbial crusts			P	P		P
	Cavity in coral skeleton						
	Crustose coralline algae and encrusting foraminifers						
	Coral skeleton					P	
NH4-16	Bioclasts in reefal microbial crusts	P	P	P			P
	Cavity in coral skeleton			P			
	Crustose coralline algae and encrusting foraminifers	P		P			
	Coral skeleton	P	P	P			

Sample	Ichnotaxa	*Fascichnus dactylus*	*Eurygonum nodosum*	*Scolecia filosa*	*Scolecia serrata*	Scolecia cf.*serrata*	Unknown trace
	Photic zonation	**Shallow II to III**	**Shallow III to deep**	**Euphotic, dysphotic to**	**Aphotic to cryptophotic**	**Unknown**	
NH4-17	Bioclasts in reefal microbial crusts			P	P		P
	Cavity in coral skeleton	P			P	P	
	Crustose coralline algae and encrusting foraminifers						
	Coral skeleton			P			
NH4-23	Bioclasts in reefal microbial crusts			P			P
	Cavity in coral skeleton		P	P			P
	Crustose coralline algae and encrusting foraminifers						
	Coral skeleton			P			

Table 2. Results of radiocarbon (^{14}C) ages in coral skeleton and reefal microbial crusts (RMCs) from core NH4. ^{14}C age offset indicates an age difference between corals and RMCs. EFC: encrusting foraminiferal crust.

Sample ID	Depth (m)	Material	Lab code	^{14}C age (yr BP)	^{14}C age offset (yr)	δ13C (‰)	Calibrated age 2σ range	Mean (Cal yr BP)
NH4-13-R	5.04–5.15	RMC	YAUT-042304	6381 ± 43		2.16 ± 1.15	6944–6689	6818
NH4-16-R	5.33–5.44	RMC	YAUT-042305	6488 ± 44		-1.71 ± 1.14	7122–6822	6952
NH4-16-C	5.33–5.44	Coral	YAUT-042306	6759 ± 44	271	-0.24 ± 0.70	7370–7158	7260
NH4-17-R	5.51–5.58	RMC	YAUT-042309	6351 ± 44		'0.57 ± 1.34	6910–6659	6784
NH4-17-C	5.51–5.58	Coral	YAUT-042311	6975 ± 44	624	-1.71 ± 0.82	7553–7365	7453
NH4-23-R	6.38–6.48	EFC	YAUT-042312	6670 ± 44		1.26 ± 1.21	7273–7025	7175
NH4-23-C	6.38–6.48	Coral	YAUT-042313	6745 ± 47	75	-0.88 ± 1.78	7368–7146	7246

After the encrustation of foraminifers and metazoans, the primary cavities were gradually covered by *in situ* precipitated peloids with trapped detrital grains. These peloids and detrital grains were accumulated on the microtopography of underlying substrates by encrusting organisms, exhibiting planner to wavy outer surfaces (Fig. 11B). Then, the accumulation of peloids and detrital grains stopped during some period (Fig. 11C). This non-deposition time and the restart of accumulation may cause the formation of laterally aligned voids (Fig. 11D). The authors speculate that the repeated occurrences of laterally aligned voids may imply the intermittent pauses of peloidal formation. Thereafter, peloids were gradually accumulated with trapped detrital grains on the irregular outer surfaces (Fig. 12B). This may cause the irregular mixing of peloid deposition parts and non-deposition parts, resulting in the formation of vertically developed voids and digitate outer surfaces (Fig. 12C). Microbialite formation finally terminated probably due to unfavourable conditions for peloidal precipitation (Fig. 12D).

Montaggioni & Camoin (1993) and Camoin & Montaggioni (1994) also recognised a two-layered microfabric succession within relatively thick RMCs with laminated and digitated mesofabrics. The lower layer consists of millimetre to centimetre thick laminated crusts that have little lateral persistence. Its internal fabric comprises clotted to dense micrite exhibiting planar to wavy laminae. The upper layer forms the bulk of the micritic crusts and exhibits a mottled to clotted thrombolite-like internal fabric. These micritic masses are generally surrounded by isolated to interconnected irregular shaped voids (Camoin & Montaggioni, 1994). These similar observations between this study and previous studies suggest a common vertical development process of RMCs irrespective of their thickness and mesofabrics.

Camoin & Montaggioni (1994) interpreted the two-layered microfabric succession of Tahitian RMCs as differences in the composition of microbial communities. Westphal *et al.* (2010) speculate that the transition from laminated to dendritic microbialites possibly reflects the decreasing water circulation as the macroporosity of the reef framework progressively became less permeable. The observations herein do not contradict these two possibilities and gradual changes in both environments and microbial communities in primary cavities are probably attributed to the two-layered microfabric succession.

Role of sulfate reduction

Based on previous studies on the nuclei of peloids (Chafetz, 1986; Reitner *et al.*, 2000; Shiraishi *et al.*, 2017) and lipid biomarker and stable sulfur isotope studies (Reitner *et al.*, 2000; Heindel *et al.*, 2010; Heindel *et al.*, 2012; Gischler *et al.*, 2017; Braga *et al.*, 2019), we infer that peloids are probably formed by coccoid sulfate-reducing bacteria. Bacterial degradation of EPS and coral mucus within microbial mats results in anoxic environments, which may cause $CaCO_3$ dissolution by fermentation and sulfide oxidation (Visscher & Stolz, 2005). In more anoxic environments, sulfate reduction occurs, causing increases in pH and alkalinity relative to aerobic respiration (Visscher & Stolz, 2005; Warthmann *et al.*, 2015) and induces $CaCO_3$ precipitation, especially in case that the electron donors are hydrogen and formate (Gallagher *et al.*, 2012, 2014). The precipitation of calcium carbonate occurs around the coccoid sulfate-reducing bacterial EPS, resulting in peloidal formation. Bacterial biofilms also result in trapping and binding detrital grains fallen into the primary cavities.

Microscale laminations observed in the lower part of RMCs resulting from the presence of laterally aligned voids inside dense peloidal aggregates (Fig. 11) are comparable with ToF-SIMS analysis by Heindel *et al.*

(2012), which showed the alternation of dark organic-rich layers and light carbonate-rich layers in laminated reefal microbialites. The dark layer is enriched in carbohydrates which are common constituents of bacterial EPS and coral mucus, while the light layer is enriched in carbonate and depleted in oxygen-containing organics. The carbonate-rich layer corresponds to dense peloidal aggregates, while the carbohydrate-rich layer may correspond to laterally aligned voids in this study. The presence of laterally aligned voids may imply the intermittent pauses of peloidal formation. This pause may be caused by the episodic inflow of oxic interstitial water into the primary cavities by the pumping action of strong waves. Oxic interstitial water disrupts sulfate reduction and hence peloidal formation, resulting in the formation of laterally aligned voids.

On the other hand, the irregular and vertical distribution of peloids and voids in the upper part of RMCs are probably attributed to the gradual closedness of primary cavities (Figs 10 and 12). As the primary cavities become gradually closed by reef development, both interstitial water circulation and light levels would be progressively reduced (Westphal *et al.*, 2010), resulting in decreasing sulfate ion supply. Stagnant interstitial water results in heterogeneous anoxic environments and irregular bacterial biofilm distributions within the primary cavities. Decreasing sulfate ion supply may also be insufficient for sulfate reduction. These cause irregular peloidal accumulation, which is finally terminated by closing cavities. Therefore, the two-layered microfabric succession observed in RMCs may reflect spatial-temporal oxic/anoxic variations in interstitial water and the degree of sulfate ion supply during the gradual closing of primary cavities. Microbial communities and net community metabolism may also change along with the gradual closing of primary cavities, which need further studies.

CONCLUSIONS

Macroscale and microscale fabrics of reefal microbialites obtained in a middle Holocene reef core drilled off Okinawa Island, south-west Japan, were observed using light and scanning electron microscopy with energy dispersive X-ray spectroscopy. The age offsets between corals and RMCs were measured by ^{14}C ages. Based on the petrographic observations and ^{14}C ages, the authors have interpreted the macroscale evolution of primary cavities and the microscale evolution of IBFM and RMCs as follows:

1. Following middle Holocene transgression, coralgal reef frameworks developed vertically in a high-energy, shallow-water environment and underlying corals died due to piling up of new coral colonies. The dead coral surfaces were encrusted with CCA, encrusting foraminifers and metazoans, indicating gradual changes to light-deficient environments in the primary cavities. Dead coral skeleton and CCA were bioeroded by macroborers and microborers in light-deficient and mesotrophic environments in the primary cavities. As reef frameworks further developed upward, primary cavities became cryptophotic, stagnated, semi-closed environments. IBFM partially or totally infills inside the cavities of bioeroded coral skeleton and intraskeletal voids soon after the bioerosion. Coevally, surfaces of primary cavities were covered with RMCs. Then primary cavities were totally closed and microbialite development terminated within a few hundred years after the death of underlying coral colonies. The inferred macroscale evolution was driven in response to progressive changes from a photic, well-circulated, oligotrophic, open environment to a cryptophotic, stagnated, mesotrophic, closed environment in the primary cavities associated with middle Holocene transgression and reef formation.

2. IBFM and RMCs are composed of peloids (spherical micritic clots), voids and

detrital grains (bioclastic and siliciclastic). Peloids are primary, *in situ* precipitated deposits associated with microbial activities. Voids are primary pores and are formed with active *in situ* peloid accumulation. Bioclastic and siliciclastic detrital grains are allochthonous. Micro-bioeroded bioclasts are fallen from bioeroded upper reef surfaces and accumulated into primary cavities during microbialite formation.

3. IBFM geopetally infilled inside bioeroded cavities soon after the bioerosion of coralgal reef frameworks. IBFM formation terminated when the cavities were totally infilled with peloids and/or conditions favouring peloid precipitation changed.

4. RMCs have a two-layered microfabric succession, which is composed of the alternation of dense peloidal aggregates and laterally aligned voids in the lower part and the mixing of peloidal aggregates and irregularly and vertically developed voids in the upper part. The authors speculate that repeated occurrences of laterally aligned voids in the lower part may imply the intermittent pauses of peloidal formation. Peloid accumulation on the irregular outer surfaces probably results in the formation of vertically developed voids and digitate outer surfaces in the upper part.

5. Peloids are probably formed by coccoid sulfate-reducing bacteria in anoxic environments developed by the degradation of bacterial biofilms and organic matters within primary cavities, allowing sulfate reduction and increasing alkalinity, therefore carbonate precipitation. The two-layered microfabric succession observed in RMCs may reflect spatial-temporal oxic/anoxic variations in interstitial water and the degree of sulfate ion supply by the gradual closing of primary cavities.

ACKNOWLEDGEMENTS

We thank Masaaki Chinen for cast preparation techniques. We also thank Center for Research Advancement and Collaboration, University of the Ryukyus for the use of SEM-EDX. This work was partly supported by JSPS KAKENHI Grant Numbers JP25242026, JP16H02940, JP16H06309, JP16H06022, JP18K18787 and 21H04379.

REFERENCES

Braga, J.C., Puga-Bernabéu, Á., Heindel, K., Patterson, M.A., Birgel, D., Peckmann, J., Sánchez-Almazo, I.M., Webster, J.M., Yokoyama, Y. and **Riding, R.** (2019) Microbialites in Last Glacial Maximum and deglacial reefs of the Great Barrier Reef (IODP Expedition 325, NE Australia). *Palaeogeogr. Palaeoclimatol. Palaeoecol.*, **514**, 1–17.

Cabioch, G., Camoin, G., Webb, G.E., Le Cornec, F., Garcia Molina, M., Pierre, C. and **Joachimski, M.M.** (2006) Contribution of microbialites to the development of coral reefs during the last deglacial period: Case study from Vanuatu (S-W Pacific). *Sed. Geol.*, **185**, 297–318.

Camoin, G., Cabioch, G., Eisenhauer, A., Braga, J.C., Hamelin, B. and **Lericolais, G.** (2006) Environmental significance of microbialites in reef environments during the last deglaciation. *Sed. Geol.*, **185**, 277–295.

Camoin, G. and **Seard, C.** (2011) Genesis of microbialites as contemporaneous framework components of deglacial coral reefs, Tahiti (IODP 310): COMMENT. *Facies*, **58**, 163–165.

Camoin, G.F., Gautret, P., Montaggioni, L.F. and **Cabioch, G.** (1999) Nature and environmental significance of microbialites in Quaternary reefs: the Tahiti paradox. *Sed. Geol.*, **126**, 271–304.

Camoin, G.F. and **Montaggioni, L.F.** (1994) High energy coralgal-stromatolite frameworks from Holocene reefs (Tahiti, French Polynesia). *Sedimentology*, **41**, 655–676.

Chafetz, H.S. (1986) Marine peloids; a product of bacterially induced precipitation of calcite. *J. Sed. Res*., **56**, 812–817.

Chazottes, V., Cabioch, G., Golubic, S. and **Radtke, G.** (2009) Bathymetric zonation of modern microborers in dead coral substrates from New Caledonia – Implications for paleodepth reconstructions in Holocene corals. *Palaeogeogr. Palaeoclimatol. Palaeoecol*., **280**, 456–468.

Fujita, K., Sasaki, T., Koyano, S., Chinen, M., Hongo, C., Webster, J.M. and **Iryu, Y.** (2020) Reefal microbial crusts found in Middle Holocene reef from Okinawa Island, the Ryukyu Archipelago. *Galaxea, Journal of Coral Reef Studies*, **22**, 9–25.

Gallagher, K.L., Dupraz, C. and **Visscher, P.T.** (2014) Two opposing effects of sulfate reduction on carbonate precipitation in normal marine, hypersaline and alkaline environments: COMMENT. *Geology*, **42**, e313–e314.

Gallagher, K.L., Kading, T.J., Braissant, O., Dupraz, C. and **Visscher, P.T.** (2012) Inside the alkalinity engine: the role of electron donors in the organomineralization potential of sulfate-reducing bacteria. *Geobiology*, **10**, 518–530.

Gischler, E., Heindel, K., Birgel, D., Brunner, B., Reitner, J. and **Peckmann, J.** (2017) Cryptic biostalactites in a submerged karst cave of the Belize Barrier Reef revisited: Pendant bioconstructions cemented by microbial micrite. *Palaeogeogr. Palaeoclimatol. Palaeoecol*., **468**, 34–51.

Gischler, E., Hudson, J.H. and **Pisera, A.** (2008) Late Quaternary reef growth and sea level in the Maldives (Indian Ocean). *Mar. Geol*., **250**, 104–113.

Glynn, P.W. (1997) Bioerosion and coral-reef growth: A dynamic balance. In: *Life and Death of Coral Reefs* (Ed. C. Birkeland), Chapman & Hall, New York, 68–95.

Heindel, K., Birgel, D., Brunner, B., Thiel, V., Westphal, H., Gischler, E., Ziegenbalg, S.B., Cabioch, G., Sjövall, P. and **Peckmann, J.** (2012) Post-glacial microbialite formation in coral reefs of the Pacific, Atlantic and Indian Oceans. *Chem. Geol*., v. **304**–**305**, p. 117–130.

Heindel, K., Birgel, D., Peckmann, J.R., Kuhnert, H. and **Westphal, H.** (2010) Formation of deglacial microbialites in coral reefs off Tahiti (IODP 310) involving sulfate-reducing bacteria. *Palaios*, **25**, 618–635.

Heindel, K., Westphal, H. and **Wisshak, M.** (2009a) Data report: bioerosion in the reef framework, IODP Expedition 310 off Tahiti (Tiarei, Maraa and Faaa sites). In: *Proceedings of IODP* (Eds G.F. Camoin, Y. Iryu, D.B. McInroy and the Expedition 310 Scientists), **310**, Integrated Ocean Drilling Program Management International, Inc., Washington, DC, doi:10.2204/iodp.proc.310.201.2009.

Heindel, K., Wisshak, M.A.X. and **Westphal, H.** (2009b) Microbioerosion in Tahitian reefs: a record of environmental change during the last deglacial sea-level rise (IODP 310). *Lethaia*, **42**, 322–340.

Humblet, M., Webster, J.M., Yokoyama, Y., Braga, J.C., Fujita, K., Iryu, Y., Fallon, S.J. and **Thompson, W.G.** Reef growth history at intermediate to mesophotic depths since the end of the Last Glacial period along the Great Barrier Reef shelf edge. In: *Coral Reefs and Sea-Level Change: Quaternary Records and Modelling* (Eds G.F. Camoin and N. Hallmann), *Int. Assoc. Sedimentol. Spec. Publ*., **49** (this volume), 189–214.

Iryu, Y., Matsuda, H., Machiyama, H., Piller, W.E., Quinn, T.M. and **Mutti, M.** (2006) Introductory perspective on the COREF Project. *Island Arc*, **15**, 393–406.

Jell, J.S. and **Webb, G.E.** (2012) Geology of Heron Island and adjacent reefs, Great Barrier Reef, Australia. *Episodes*, **35**, 110–119.

Kan, H. (2011) Ryukyu Islands. In: *Encyclopedia of Modern Coral Reefs: Structure, Form and Process* (Ed. D. Hopley), Springer Netherlands, Dordrecht, p. 940–945.

Kawana, T. (2011) History of coral-reef formation, earthquakes and tsunami in the Ryukyu Archipelago. In: *Ryukyu Archipelago in prehistoric and primitive ages* (Eds H. Takamiya and S. Ito), Rokuichi Shobo, Tokyo, p. 63–86.

Kempe, S. (1990) Alkalinity: The link between anaerobic basins and shallow water carbonates? *Naturwissenschaften*, **77**, 426–427.

Lyons, W.B., Long, D.T., Hines, M.E., Gaudette, H.E. and **Armstrong, P.B.** (1984) Calcification of cyanobacterial mats in Solar Lake, Sinai. *Geology*, **12**, 623–626.

Macintyre, I.G. (2011) Submarine lithification. In: *Encyclopedia of Modern Coral Reefs: Structure, Form and Process* (Ed. D. Hopley), Springer Netherlands, Dordrecht, p. 1052–1058.

Macintyre, I. and **Marshall, J.** (1988) Submarine lithification in coral reefs: some facts and misconceptions. *Proceedings of 6th International Coral Reef Symposium, Townsville*, **1**, 263–272.

Montaggioni, L.F. and **Camoin, G.F.** (1993) Stromatolites associated with coralgal communities in Holocene high-energy reefs. *Geology*, **21**, 149–152.

Patterson, M.A., Webster, J.M., Hutchings, P., Braga, J.-C., Humblet, M. and **Yokoyama, Y.** (2020) Bioerosion traces in the Great Barrier Reef over the past 10 to 30 kyr. *Palaeogeogr. Palaeoclimatol. Palaeoecol*., **542**, extent: 109503.

Reimer, P.J., Bard, E., Bayliss, A., Beck, J.W., Blackwell, P.G., Bronk Ramsey, C., Buck, C.E., Cheng, H., Edwards, R.L., Friedrich, M., Grootes, P.M., Guilderson, T.P., Haflidason, H., Hajdas, I., Hatté, C., Heaton, T.J., Hoffmann, D.L., Hogg, A.G., Hughen, K.A., Kaiser, K.F., Kromer, B., Manning, S.W., Niu, M., Reimer, R.W., Richards, D.A., Scott, E.M., Southon, J.R., Staff, R.A., Turney, C.S.M. and **van der Plicht, J.** (2013) IntCal13 and Marine13 radiocarbon age calibration curves 0-50,000 years cal BP. *Radiocarbon*, **55**, 1869–1887.

Reitner, J. (1993) Modern cryptic microbialite/metazoan facies from Lizard Island (Great Barrier Reef, Australia) formation and concepts. *Facies*, **29**, 3–39.

Reitner, J., Thiel, V., Zankl, H., Michaelis, W., Worheide, G. and **Gautret, P.** (2000) Organic and biogeochemical patterns in cryptic microbialites. In: *Microbial Sediments* (Eds R.E. Riding and S.M. Awrami), Springer-Verlag, Berlin, Heidelberg, p. 149–160.

Riding, R. (2000) Microbial carbonates: The geological record of calcified bacterial–algal mats and biofilms. *Sedimentology*, **47**, 179–214.

Riding, R. (2011) Reefal microbial crusts. In: *Encyclopedia of Modern Coral Reefs: Structure, Form and Process* (Ed. D. Hopley), Springer Netherlands, Dordrecht, 911–915.

Riding, R., Liang, L. and **Braga, J.C.** (2014) Millennial-scale ocean acidification and late Quaternary decline of cryptic bacterial crusts in tropical reefs. *Geobiology*, **12**, 387–405.

Seard, C., Camoin, G., Yokoyama, Y., Matsuzaki, H., Durand, N., Bard, E., Sepulcre, S. and **Deschamps, P.** (2011) Microbialite development patterns in the last deglacial reefs from Tahiti (French Polynesia; IODP Expedition #310): Implications on reef framework architecture. *Mar. Geol*., **279**, 63–86.

Shiraishi, F., Hanzawa, Y., Okumura, T., Tomioka, N., Kodama, Y., Suga, H., Takahashi, Y. and **Kano, A.** (2017) Cyanobacterial exopolymer properties differentiate microbial carbonate fabrics. *Scientific Reports,* **7**, p. 11805, doi:10.1038/s41598-017-12303-9.

Visscher, P.T. and **Stolz, J.F.** (2005) Microbial mats as bioreactors: populations, processes and products. In: *Geobiology: Objectives, Concepts, Perspectives* (Ed. N. Noffke), Elsevier, Amsterdam, p. 87–100.

Warthmann, R.J., Camoin, G., McKenzie, J.A. and **Vasconcelos, C.** (2015) Geomicrobiology of carbonate microbialites in the Tahiti reef. *Geol. Soc. London Spec. Publ*., **418**, 287, doi:10.1144/SP418.8.

Webb, G.E. (1996) Was Phanerozoic reef history controlled by the distribution of non-enzymatically secreted reef carbonates (microbial carbonate and biologically induced cement)? *Sedimentology*, **43**, 947–971.

Webb, G.E., Baker, J.C. and **Jell, J.S.** (1998) Inferred syngenetic textural evolution in Holocene cryptic reefal microbialites, Heron Reef, Great Barrier Reef, Australia. *Geology*, **26**, 355–358.

Westphal, H., Heindel, K., Brandano, M. and **Peckmann, J.** (2010) Genesis of microbialites as contemporaneous framework components of deglacial coral reefs, Tahiti (IODP 310). *Facies*, **56**, 337–352.

Yokoyama, Y., Miyairi, Y., Matsuzaki, H. and **Tsunomori, F.** (2007) Relation between acid dissolution time in the vacuum test tube and time required for graphitization for AMS target preparation. *Nuclear Instruments and Methods in Physics Research Section B: Beam Interactions with Materials and Atoms*, **259**, 330–334.

Yoneda, M., Uno, H., Shibata, Y., Suzuki, R., Kumamoto, Y., Yoshida, K., Sasaki, T., Suzuki, A. and **Kawahata, H.** (2007) Radiocarbon marine reservoir ages in the western Pacific estimated by pre-bomb molluscan shells. *Nuclear Instruments and Methods in Physics Research Section B: Beam Interactions with Materials and Atoms*, **259**, 432–437.

IAS (2022) Coral Reefs and Sea-Level Change: Quaternary Records and Modelling, 69–100

New insights on the Late Quaternary evolution of Abrolhos Reefs, eastern Brazilian shelf

VIEIRA, L.S.[†‡], BASTOS, A.C.[‡*], DECHNIK, B.[‡], BRAGA, J.C.[§], MOURA, R.L.[¶], D'AGOSTINI, D.P.[‡], MORAES, F.C.[ǀ] and WEBSTER, J.M.[#]

[†]*Graduate Program Ocean and Earth Dynamics, LAGEMAR, Fluminense Federal University, Niterói, RJ, 24210-346, Brazil.*
[‡]*Geosciences Marine Lab, Oceanography Department, Federal University of Espirito Santo, Vitoria, ES, 29075-910, Brazil.*
[§]*Department of Estratigrafia and Paleontology, University of Granada, Granada, 18010, Spain.*
[¶]*Biology Institute of SAGE/COPPE, Federal* University *of Rio de Janeiro, RJ, 21944-970, Brazil.*
[ǀ]*Instituto de Pesquisa Jardim Botânico do Rio de Janeiro, RJ, 22460-030, Brazil.*
[#]*Geocoastal Research Group, School of Geosciences, University of Sydney, NSW, 2006, Australia.*
[*]*Corresponding author Alex Cardoso Bastos, alex.bastos@ufes.br, Oceanography Department, Federal University of Espirito Santo, Av. Fernando Ferrari, 514, Goiabeiras, Vitoria, ES 29075-910, Brazil.*

ABSTRACT

The Abrolhos shelf, in the eastern Brazilian margin, encompasses the largest reef province in the South Atlantic, characterised by low coral diversity and a high level of endemism. Knowledge gaps about how the Abrolhos coastal reefs evolved, during the post LGM and MIS 6/MIS 5, favoured a paradigm that is revisited in the light of new data. Here, new data from two new, long boreholes (20 and 50 m-long) are presented in order to investigate and provide new insights into the evolution of two shallow reefs on the Abrolhos Shelf during the late Pleistocene and Holocene epochs. Results show that Holocene and Pleistocene reefs grew on highly turbid waters with a significant terrigenous sediment input. Corals and CCA assemblages were identified as main framework builders of Abrolhos inner-shelf reefs since the Pleistocene. No clear shallowing upward sequence of reef builders was observed, which differs from other reef sequences all over the world. In terms of Holocene reef growth, Pedra Grande and Coroa Vermelha reefs turned on roughly coevally at different depths and with different coral assemblages. Pedra Grande reef started growing circa 6.8 kyr BP in a water depth approximately 10 m deeper than Coroa Vermelha, which started growing around 6.4 kyr BP, but Coroa Vermelha turned off at around 4 kyr BP, while Pedra Grande kept growing until around 1.2 kyr BP. This novel reef stratigraphy data provided a new insight on the evolution of the Abrolhos coastal reefs, showing that different environmental and topographic controls could have acted spatially in different ways. Coroa Vermelha reef seems to have started its growth as a result of a topographic high control. Pedra Grande reef seems to be connected to a broader submerged reef setting and started to grow in deeper water depths. The presence of three reef arcs in Abrolhos is proposed, including a submerged reef arc.

©2022 International Association of Sedimentologists

Keywords: Holocene reef growth, Pleistocene reefs, sea-level changes, Abrolhos Reefs, South Atlantic.

INTRODUCTION

Reef growth and demise are directly related to sea-level changes and climatic variability (Woodroffe & Webster, 2014; Camoin & Webster, 2014). A reef response to sea-level fluctuations is dictated, in general, by the relationship between rates of reef growth and accommodation space. This follows the simple reef response model proposed by Neumann & Macintyre (1985) and Davies *et al.* (1985). Reefs can respond by keeping up, catching up or giving up in relation to sea-level change. However, reef growth patterns can be more complex than a simple model of vertical filling of available accommodation space; and responses such as backstepped and lateral growth or progradation are also present worldwide (Schlager, 2005; Montaggioni, 2005; Woodroffe & Webster, 2014; Gischler & Hudson, 2019). Nonetheless, reef turn on and turn off could also be a consequence of other variables, such as climate variability (e.g. sea water temperature) and changes in palaeo-water quality as a result of sediment and nutrient flux (Schlager, 1981; Dechnik *et al.*, 2019).

Quaternary reef evolution in relation to sea-level cycles has been widely studied throughout the Indo-Pacific and Caribbean, where extensive reef systems are located (Abbey *et al.*, 2011; Blanchon *et al.*, 2003; Flamand *et al.*, 2008; Webster *et al.*, 2004; Woodroffe *et al.*, 2010; Gischler, 2015). In a global context, reef coverage in the South Atlantic province is poor when compared to the Indo-Pacific and Caribbean (Bastos *et al.*, 2018). The Abrolhos shelf, located in the eastern Brazilian margin, encompasses the largest reef province in the South Atlantic, characterised by coastal reefs, extensive submerged pinnacles and reef banks (Moura *et al.*, 2013; Ferreira *et al.*, 2020).

Leão *et al.* (2003) summarised reef evolution in the Brazilian shelf by describing four stages, namely: reef initiation and establishment (7 to 5 kyr BP), rapid upward reef accretion (5 to 4 kyr BP), lateral growth (4 to 2 kyr BP) and reef degradation (2 kyr to present). Based on relative sea-level (RSL) curves for the Brazilian east coast (Martin, 2003; Angulo & Lessa, 1997), Leão *et al.* (2003) argued that the first stage occurred during the last phase of shelf flooding (between 8 to 7 kyr BP), until sea-level reached the present level. Holocene reefs developed over older Pleistocene reef tops and the oldest radiocarbon date (7148 cal yr BP) was obtained at approximately 10.5 metres below sea-level (mbsl). The second stage was characterised by a vigorous and rapid vertical growth (up to 7 mm yr^{-1}) of the reef structure during the peak of the Holocene maximum sea-level in the South Atlantic, when sea-level reached up to 2 to 5 m above present sea-level (PSL) at circa 5000 to 5800 years BP (Angulo *et al.* 2006). The third and fourth stages occurred during the sea-level fall phase, when upward reef growth was limited by accommodation space and reefs started to grow laterally, then a wide turn-off of coastal reefs was observed. The lateral growth would also be an explanation for the typical mushroom shape of the Abrolhos pinnacles (Leão & Ginsburg, 1997) that were described by Hartt (1870) as 'chapeirões'. These stages are described based on stratigraphic studies and radiocarbon dating from coastal reefs. Dechnik *et al.* (2019), using short cores and 62 radiocarbon dates in the Abrolhos coastal reefs, found that Abrolhos reefs turned off during the Late Holocene. These authors identified a reef growth hiatus between ~3.7 and 2.5 kyr BP, probably the consequence of sea-level instabilities and/or climate variability during

the Late Holocene (sea-level fall from ~3.7 kyr BP and a small rise between 2.5 to 2 kyr BP).

This current model of Holocene reef evolution in the Abrolhos was proposed and discussed based on a single core (15 m-long at Coroa Vermelha reef, Leão & Ginsburg, 1997). As a result, a significant question still remains about the Pleistocene reefs along the Brazilian coast, as so few data are available. Leão (1982) identified a Pleistocene/Holocene boundary surface at approximately 13 m-deep in Coroa Vermelha (Abrolhos). The surface was defined by a discontinuity in a seismic refraction section and by a macroscopic analysis of the core showing 'an abrupt change to altered reef limestone' with 'diagenetic features' in pre-Holocene rocks. Leão (1982) described a ~2 m-long record of a pre-Holocene reef as a Holocene fauna composition replication. The occurrence of Pleistocene reefs along the Brazilian coast was confirmed by Bernat *et al.* (1983) and Martin *et al.* (1988). These authors dated four coral samples collected from a quarry (3 to 6 m above sea-level) located approximately 400 km north from Abrolhos (Ilhéus, Bahia State), recording U/Th dates ranging from 116,000 to 142,000 years. These results indicate that reefs probably developed along the Brazilian coast during the previous interglacial interval, equivalent to the Holocene Reef, or Marine Isotopic Stage 5e (MIS 5e).

Leão (1982) identified the endemic coral *Mussismilia braziliensis* as the main reef framework builder in the Abrolhos coastal reefs. More recently, Bastos *et al.* (2018) suggested that bryozoans played a major role as reef builders during the Late Holocene (~2000 yr BP) in the Abrolhos outer arc pinnacles. These authors have also argued that the mushroom shape of pinnacles could be related to the typical low disturbance regime of the South Atlantic, with very rare tropical storms and hurricanes. The lack of major high wave/wind energy events, compared to the Caribbean and Indo-Pacific, may have preserved this odd shape in the South Atlantic.

Only recently, new cores and drills have been collected in order to better understand the reef framework and temporal changes in reef growth and composition (Bastos *et al.*, 2018; Dechnik *et al.*, 2019). The gaps in knowledge about how the Abrolhos coastal reefs evolved during the post LGM (MIS 2/MIS 1), and MIS 6/MIS 5, favoured a paradigm that has to be revisited in light of new data. Herein, the authors present data from two new, long boreholes (20 and 50 m-long) in order to investigate and provide new insights into the evolution of two shallow reefs on the Abrolhos Shelf, east Brazil, during the latest Pleistocene and Holocene epochs. The authors' specific objectives are: 1) to establish spatial and temporal variations in Abrolhos Holocene reef turn on; 2) to define and discuss variations in reef stratigraphy, coralgal assemblages and accretion rates; and 3) to identify any compositional differences between Holocene and Pleistocene MIS 5 reef units to determine to what extent reef communities were able to re-establish themselves.

METHODS

Study area

The Abrolhos Continental Shelf (ACS) is a part of the eastern Brazilian Shelf, located between latitudes 17^0 20' to 18^0 10'S and longitudes 38^0 35' to 39^0 20'W. The ACS marks an enlargement of the eastern Brazilian shelf due to the presence of an extensive magmatic province formed by Palaeocene-Eocene volcanic activity (Sobreira & França, 2006). The shelf is 200 km-wide, whereas the inner shelf (<30 m water depth) is around 75 km-wide. The largest reef system of the Abrolhos, unique along the Brazilian shelf in

the South Atlantic, is established and has evolved on the ACS.

The Abrolhos emergent and quasi-emergent reefs are distributed in two main arcs parallel to the coast: the inner or coastal arc and the outer arc (Leão & Ginsburg, 1997; Fig. 1). The inner arc is subjected to high turbidity levels from input of local river terrigenous sediment sources. The Caravelas, Mucuri and Nova Viçosa rivers are the major rivers in the Abrolhos reef area.

These reefs are known as Nova Viçosa (NV), Coroa Vermelha (CV), Sebastião Gomes (SG) and Paredes. Moura *et al.* (2013) and Ferreira *et al.* (2020) show the extensive distribution of submerged reefs across the entire shelf, forming distinct morphologies, such as pinnacles and reef banks, ranging from shallow water depths (5 m) to deeper than 50 m. Fig. 1 illustrates the different morphology of the submerged reefs mapped by Moura *et al.* (2013) and Ferreira *et al.* (2020).

The total spatial coverage of Abrolhos reefs is estimated to be around 8800 km^2 (Moura *et al.*, 2013). It is also important to highlight that the Abrolhos shelf, mainly the outer shelf, is a carbonate province dominated by rhodolith beds (Amado Filho *et al.*, 2012; Moura *et al.*, 2013), encompassing an area of ~20,900 km^2. Only 18 scleractinian coral species inhabit the Brazilian coral reefs (Leão *et al.*, 2003). In comparison to the Caribbean, this is a low coral diversity province and six of the main Brazilian coral reef builders are endemic: *Mussismilia braziliensis, Mussismilia hispida, Mussismilia harttii, Favia leptophylla, Siderastrea stellata* and *Favia gravida*. The reefs are dominated by massive and encrusting forms; and there is a lack of branching forms, which are dominant in the Caribbean and Indo-Pacific reefs (Laborel, 1969, Leão *et al.*, 2003; Francini-Filho *et al.*, 2013).

The oceanographic conditions are mild, including the predominant north-east winds mainly during summer and strong south/south-east winds during winter storms. Sea surface temperature (SST) ranges between 24 and 28.5 °C (Ghisolfi *et al.*, 2015); however, during climate events, such as an El Nino event, SST can be higher than 29 °C, leading to mass coral bleaching, as reported by Teixeira *et al.* (2019). Tidal regime is semi-diurnal with a spring tidal range of 2.6 m. The Brazil Current is the dominant geostrophic current in the region, flowing southward at an average speed of ~0.7 knots (Ghisolfi *et al.*, 2015).

Sampling

Reef composition and stratigraphy are based on a series of cores recovered from the reef flats using a rotary drill. Core barrel recovery was taken at every 1.5 m. Two distinct reefs were drilled in the inner arc: the (1) Pedra Grande Reef (PG), from the reef flat at Paredes Reef, and the (2) Coroa Vermelha Reef (CV), also on its reef flat (Fig. 1). Active coral growth occurs on PG reef, composed of semi-coalesced reef tops completely submerged at low tide. In contrast, no living corals are observed on the CV reef flat, which is composed of mud with a sandy carbonate cay located at its centre. Maximum drilling depth at PG reef was 20 m, whereas the drilling reached 50 m. In this study, only the Holocene and Late Pleistocene (probably MIS 5e) reef portions are investigated, i.e. the entire 20 m in PG and 25 m in CV. Below the Late Pleistocene reef (CV ~25 m, MIS 5e), the core is composed of different units of siliciclastic and carbonate sediments. A total core recovery was 15.5% at PG and 33% at CV, although each core barrel had its recovery percentage, as shown in Fig. 2. Low recovery of these boreholes is probably the result of common cavities and abundant unlithified sediments, as has been reported in previous studies of the area (Leão, 1982 and

Bastos *et al.*, 2018). Table 1 summarises the main relevant information about reef cores and stratigraphy.

Reef stratigraphy, including drilling advance and recovery, is presented following Webster *et al.* (2011). The recovered material is stacked up and placed at the top of the core interval. The vertical error is considered to be the barrel length (1.5 m). Although this is a very conservative approach, it also minimises interpretation errors, since the authors have identified different recovery rates throughout the core. The reef stratigraphy results highlight the reef composition, so recovery rates for each barrel are annotated in the stratigraphic section.

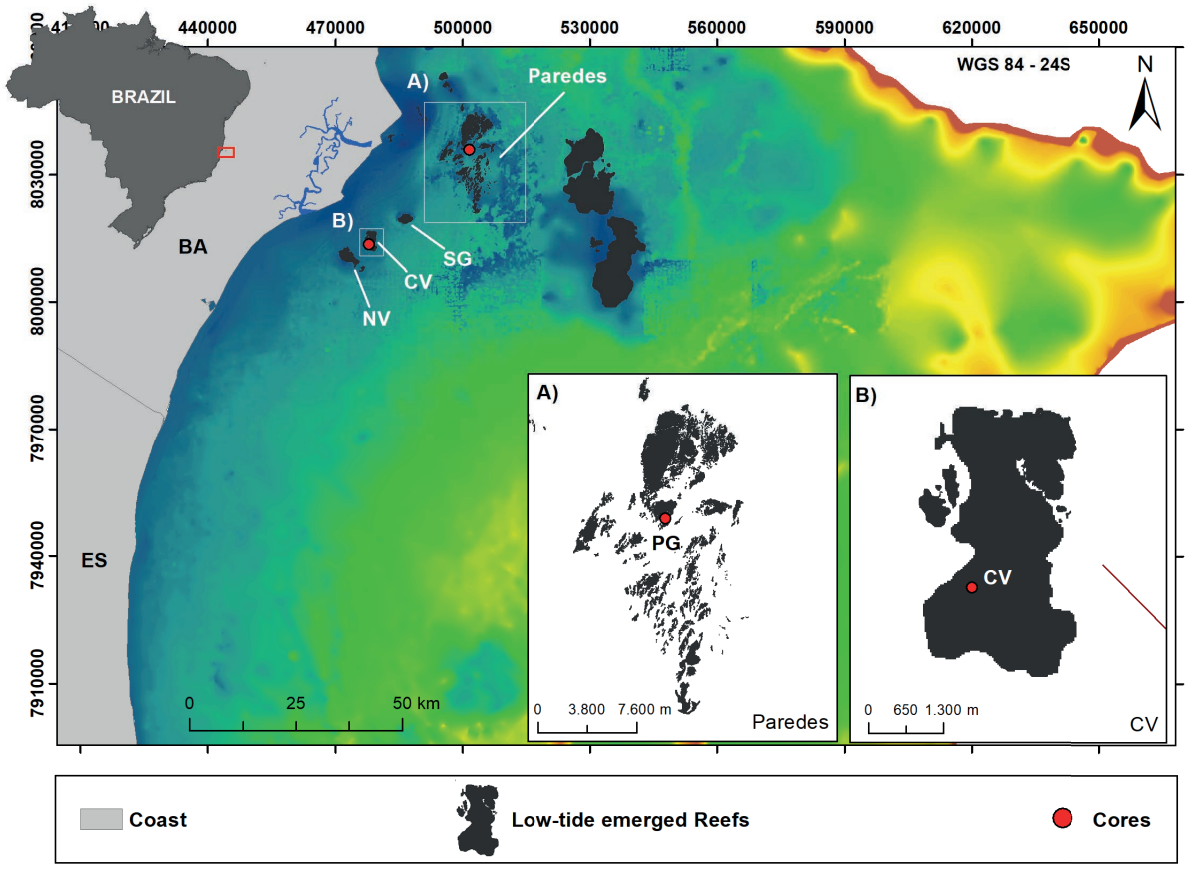


Fig. 1. Study area at Abrolhos Shelf. The emergent and quasi-emergent reefs are highlighted in black. Nova Viçosa (NV), Coroa Vermelha (CV), Sebastião Gomes (SG) and Paredes comprise the inner arc (Leão & Ginsburg, 1997). The location of both reef cores (CV and PG) are indicated by the red dots. A) Close up of the Paredes reef flat, with the drilling location of Pedra Grande reef core (PG, red dot); B) Close up of the Coroa Vermelha reef flat, with the drilling location of Coroa Vermelha reef core (CV, red dot).

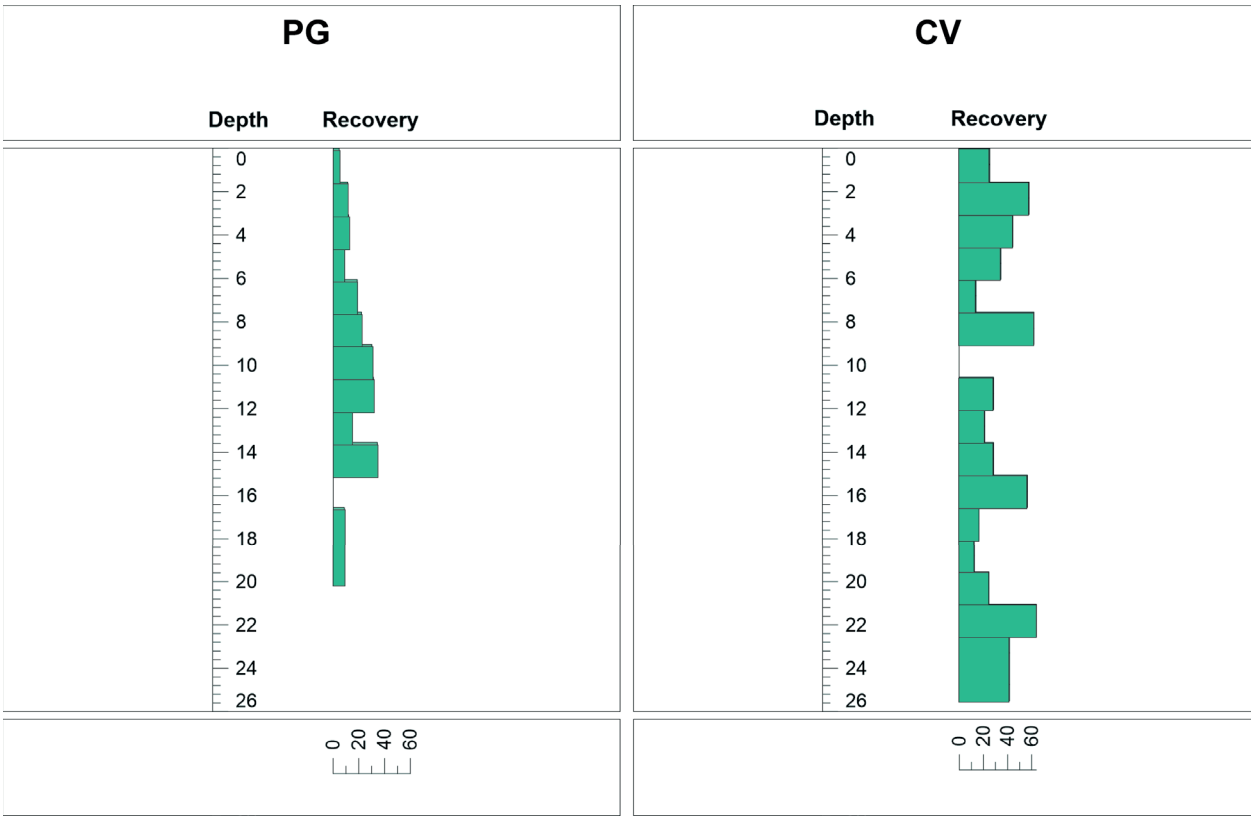


Fig. 2. Percentage of core recovery for each 1.5 m-long core barrel – PG and CV.

Laboratory analyses

Reef cores were sectioned longitudinally for macroscopic and microscopic compositional analyses by high resolution photography and petrographic techniques.

The lithologic description follows Webster *et al.* (2011), including the relative position (in growth position or displaced) of the components. Major and minor components were identified, including corals, crustose coralline algae (CCA), bryozoans, molluscs, polychaetes, foraminifera, amongst others, and carbonate facies were described. Nineteen reef sections were sub-sampled for 27 x 46 mm petrographic thin sections. Thin sections were produced at National Petrographic Services Inc. (USA) using blue epoxy resin impregnation. Fossil component taxonomy, diagenetic characteristics including dissolution, crystallisation of aragonite and overall fossil preservation were described using the thin sections.

Nine samples from the Holocene interval, interpreted as in original growth position (i.e. *in situ*), were sent for radiocarbon dating (^{14}C) at the Center for Applied Isotope Studies (CAIS), University of Georgia, using Accelerator Mass Spectrometry (AMS). Dates are reported as calendar years BP ('present' = 1950 CE) using the 2 sigma confidence interval. Calibration was carried out using Calib 7.1 available at http://calib.qub.ac.uk/calib. The Marine13 calibration curve was applied assuming a global marine reservoir effect of 400 yr and a Delta R of 98±80 (average value for the four closest localities) for regional correction.

Six scleractinian coral samples from both cores were analysed by X-Ray Diffraction (XRD) to identify the percentage of aragonite *vs*. low-magnesium calcite. The combination

of ^{14}C dating and XRD results, along with lithologic and stratigraphic observations, were also used to define the Holocene-Pleistocene boundary.

Reef accretion rates (VA) were calculated using mean calibrated radiocarbon ages and the stacked core sample depths. The computation considered the total Holocene length (reef fragments and hiatuses) between the oldest age and the top of each core. To provide a consistent methodology, the considered present age has been the same as used in ^{14}C dating. All the processed data, including core composition, ^{14}C results and reef accretion rates were compiled in Adobe Illustrator CC 2017 software.

The morphologic analyses of the continental shelf were made based on Bastos *et al.* (2015); and side scan sonar data by Moura *et al.* (2013) and Ferreira *et al.* (2020) were also included in this study.

Reef stratigraphy – Holocene stage/age

In a discussion paper of Holocene stages, Walker *et al.* (2012) argued that the Holocene Epoch can be subdivided into Early, Middle and Late Holocene. This subdivision is based on climate changes worldwide and consists of: Early Holocene 11.7 kyr to 8.2 kyr BP; Middle Holocene 8.2 kyr to 4.2 kyr BP; and Late Holocene from 4.2 kyr BP until now (Walker *et al*., 2012). The 2021 version of the International Chronostratigraphic Chart presents the Holocene Epoch divided into 3 stages/ages, named as: Greenlandian (Early Holocene); Northgrippian (Middle Holocene); and Meghalayan (Late Holocene). All the three ages follow the time intervals proposed by Walker *et al.* (2012). This study uses Late Pleistocene, Early, Middle and Late Holocene to describe the reef stratigraphy ages.

RESULTS

Reef composition

Pedra Grande Reef (PG)

PG reef presented a typical modern coralgal framework, with small colonies of bryozoans, sponge/mollusc borings and carbonate sediment infilling (Figs 3 and 4). In terms of the main framework builders, four scleractinian coral species (*Montastraea cavernosa*, *Mussimilia harttii*, *Porites* sp. and *Siderastrea stellata*), one of hydrocoral (*Millepora* sp.*)* and 6 CCA species (*Harveylithon* gr. *munitum, Lithophyllum* sp., *Lithophyllum* gr. *pustulatum, Dawsoniolithon* gr. *conicum, Porolithon* gr. *onkodes* and *Melyvonnea erubescens*) were recognised (Table 2).

In general, from the base to the top of the drilled sequence, an alternation of coral, CCA and coralgal framework has been observed. From 10.5 m to the top of the core sequence, in terms of facies, floatstones intercalate with boundstones. In detail, the core sequence can be described in terms of 5 sections summarised below:

Holocene Section 1 (20 to 16.5 m): This section at the base of the PG core sequence is composed predominately by *in situ* coral framework facies (*Montastraea cavernosa*). The corallites of *in situ* colonies are horizontal, meaning that these colonies probably grew on the reef wall, as usually observed in the Abrolhos reefs (Francini-Filho *et al.*, 2013).

Holocene Section 2 (15 to 10.5 m): This section is predominantly composed of boundstone facies with varying composition. The section starts with a framework predominantly composed of CCA with small bryozoan colonies and sediment infilling. At approximately 13 m, the boundstone facies becomes dominated by scleractinian corals (*Siderastrea stellata*, *Porites* sp*.)* and hydrocorals (*Millepora* sp.), still with common CCA. Towards the top of this

section (11 m), *in situ Montastraea cavernosa* colonies reappear, with horizontal corallites, forming a boundstone with other scleractinian corals such as *Porites* sp. and *Siderastrea stellata.*

Holocene Section 3 (10.5 to 9 m): This section marks a significant change in reef facies, as it is predominantly composed of an unconsolidated floatstone. The sediment is basically formed by carbonate clasts (fragments of shells, CCA, corals). *Siderastrea stellata, Mussismilia harttii* and *Millepora* sp. were recognised as the main rubble components.

Holocene Section 4 (9 to 4.5 m): This section is characterised by a boundstone facies resembling Section 2. It is a coralalgal framework facies, but in this section the species *Mussismilia harttii* and *Montastraea cavernosa* are the most frequent corals.

Holocene Section 5 (4.5 to 0 m): This section is marked by two *in situ* colonies of *Porites* sp. intermingled with floatstone facies. A colony of *Porites* sp. occurs at the reef top. The floatstone consists of biogenic carbonate fragments and rubble of *Siderastrea* sp. and *Millepora* sp.

Table 1. Main core metadata including geographic coordinates, core recovery, ^{14}C and XRD sampling depths and ranges and the main stratigraphic units.

Core Settings	**PG**	**CV**
Geographic location (LONG/LAT)	-38.9864 / -17.7643	-39.2094 / -17.9658
Maximum drilling depth (m)	20	50
Investigated drilling interval (m)	0 - 20	0 - 25.5
Recovery (%)	15.5	33
^{14}C dated sample depth (m)	0, 1.5, 8.0, 11.5, 13.5, 18.0	0, 4.5, 10.5
XRD data sample depth (m)	7.5, 13.5, 16.5	0, 12.0
Calendar ^{14}C age range (yr)	1145-6785	4442-6406
Reef Unit interval (m):		
Unit 1	0 - 20	0 - 13.5
Unit 2	-	13.5 - 25.5

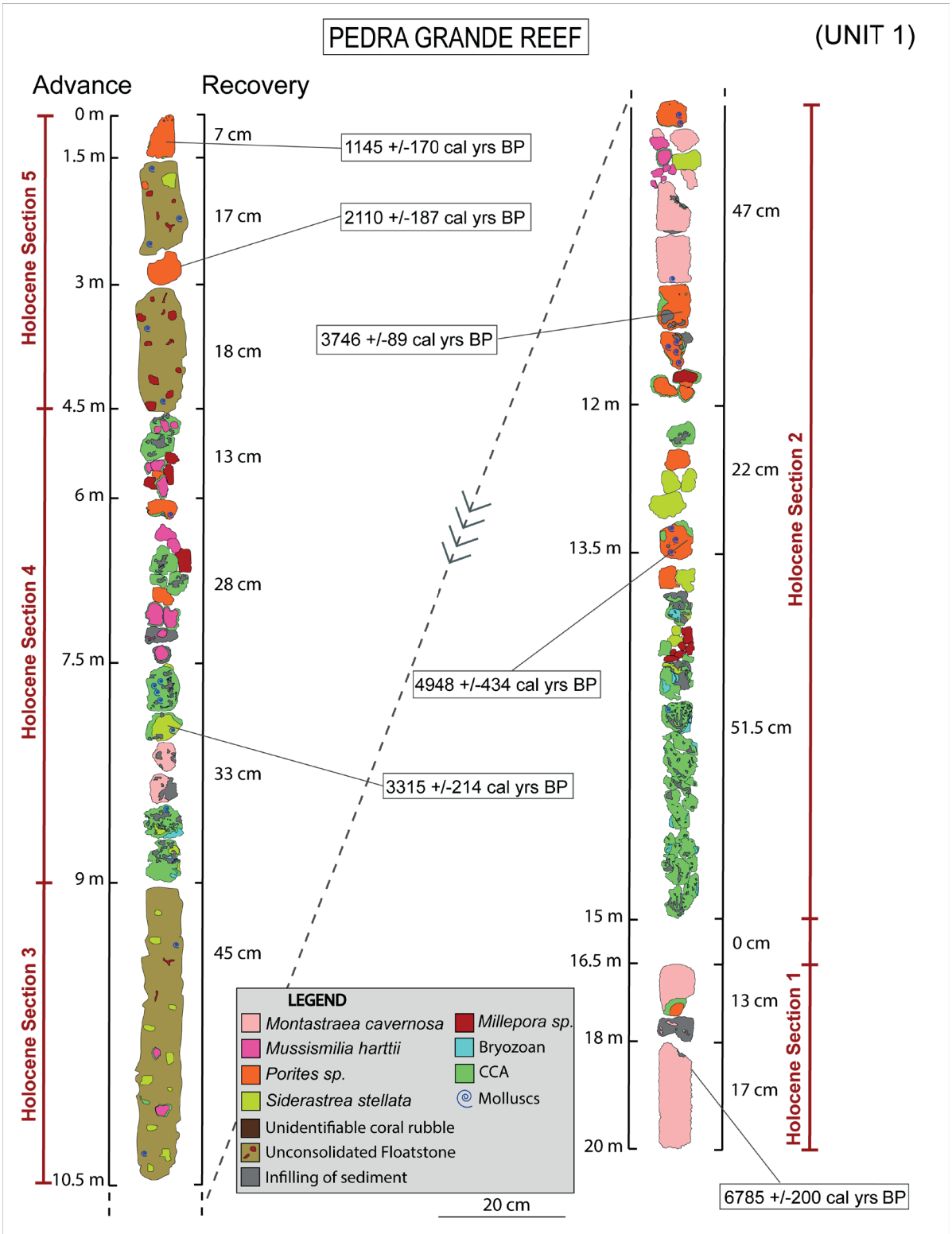


Fig. 3. PG reef core composition and radiocarbon dates. It is important to note that drilling advance intervals are not in the same vertical scale. Recovery information is displayed on the right side, including zero recovery. The diagram aims to produce a detailed stratigraphic image of the composition of the drilled and recovered sections. All the depths are corrected based on drilling data. Radiocarbon dates are shown as calendar years BP.

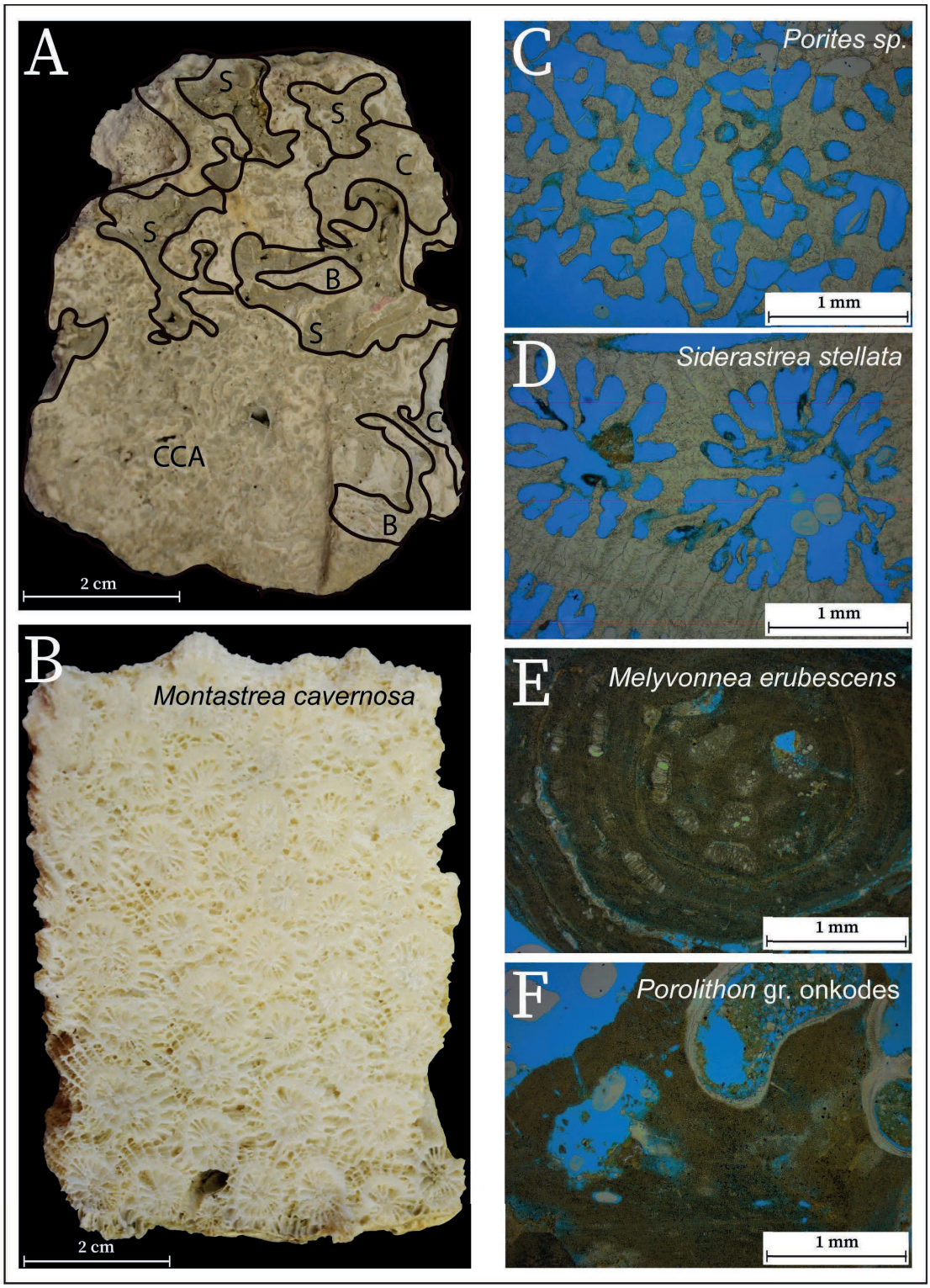


Fig. 4. Images showing the main examples of PG reef core composition. A) hand specimen showing crustose coralline algae (CCA), bryozoan (B), coral (C) and sediment (S) (Section 2); B) *Montastraea cavernosa* hand specimen (Section 1) and petrographic thin sections images of C) *Porites* sp., D) *Siderastrea stellata*, E) crustose coralline algae (CCA), section of *Melyvonnea erubescens* with several thalli showing numerous conceptacles; and F) CCA, section of *Porolithon* gr. *onkodes* associated with vermetid gastropods.

Table 2. Main reef framework builders of CV and PG cores. Note that reef composition, mainly coral taxonomy, between 25.5 to 13.5 m was somehow compromised due to carbonate recrystallisation. These parts of the core were classified as unidentified coral rubble and this might have influenced the final coral genus and species list. Unit 1 – Holocene reef; Unit 2 – Pleistocene reef.

Organism	**CV**		**PG**
	Unit 1	**Unit 2**	**Unit 1**
Rhodophyta			
Corallinales			
Corallinaceae			
Lithophyllaceae			
Amphiroa sp.		x	
Harveylithon gr. *munitum*	x		x
Lithophyllum sp.			x
Lithophyllum gr. *pustulatum*	x	x	x
Paulsilvella sp.	x		
Dawsoniolithon gr. *conicum*			x
Porolithon gr. *onkodes*	x	x	x
Spongites sp.		x	
Hapalidiales			
Melyvonnea erubescens	x		x
Chlorophyta			
Bryopsidales			
Halimeda sp.	x	x	
Cnidaria			
Hydrozoa			
Milleporidae			
Millepora sp.	x	x	x
Anthozoa			
Montastraeidae			
Montastraea cavernosa	x		x
Faviidae			
Favia gravida	x	x	
Mussismilia harttii	x		x
Poritidae			
Porites sp.	x		x
Siderastreidae			
Siderastrea stellata	x	x	x

Coroa Vermelha Reef (CV)

The CV reef base is situated on top of a siliciclastic mudstone, at 25.5 m depth. The core stratigraphy can be described as two major reef units (Unit 1 and Unit 2). These units were defined based on the significant evidence of diagenetic changes that occur at 13.5 m in the CV core (these diagenetic changes were not observed in PG). Based on this evidence, the authors have interpreted that the diagenetic change marks the Holocene/Pleistocene (MIS 5e) boundary surface, such that Unit 1 is the Holocene reef, whilst Unit 2 is the Late Pleistocene reef. XRD results indicate a change in mineralogical composition at the 13.5 m boundary between Units 2 and 1, from low-magnesium calcite to aragonite, corroborating the definition of a Pleistocene/Holocene boundary (see text below and Table 3).

In general, the CV reef core is characterised by floatstones, coral framework and reef rubble with infilling sediments. Although the composition of CV reef was dominated by floatstone facies of coral rubble, the taxonomy of the potential main reef framework builders was possibly defined as such. Five scleractinian coral species (*Favia gravida, Montastraea cavernosa, Mussismilia harttii, Porites* sp. and *Siderastrea stellata*), one hydrocoral (*Millepora* sp.) and eight CCA were identified (*Amphiroa* sp*., Harveylithon* gr. *munitum, Lithophyllum* gr. *pustulatum, Paulsilvella* sp*., Porolithon* gr. *onkodes, Spongites* sp. and *Melyvonnea erubescens*) together with the green alga *Halimeda* sp. (Table 2 and Fig. 5). *Millepora* sp. had the highest occurrence throughout the floatstone, except in the core top, where *in situ* colonies of scleractinian corals, such as *Montastraea cavernosa, Mussismilia harttii* and *Siderastrea stellata* dominated. In addition, serpulids and molluscs were observed as the main bioerosion agents.

Floatstone dominated the facies comprising the entire CV reef sequence, with intercalated coral and coralgal rudstones together with infilling sediments (Figs 5 and 6). The core sequence can be described in terms of the 7 sections below for the Pleistocene and Holocene reefs.

Late Pleistocene Section A (25.5 to 21 m): This section is the potential MIS 5e Pleistocene reef initiation defined by a floatstone facies intercalating a coral rubble interval. At the base of the reef sequence, the floatstone presents a laminar dark structure and coral/reef fragments in the floatstone were unidentifiable. From 23 to 22.5 m, a coral rubble facies is mostly composed by unidentifiable clasts, but a few were identified as *Porites* sp. and *Mussismilia harttii*. A floatstone facies with possible fragments of *Siderastrea stellata* predominates from 22.5 to 21 m.

Late Pleistocene Section B (21 to 16.5 m): This section shows a mixed floatstone/coral rubble facies with *Siderastrea stellata* up to 18 m. The top of the section (18 to 16.5 m) is composed of fragments of *Siderastrea stellata* and *Mussismilia harttii*.

Late Pleistocene Section C (16.5 to 13.5 m): In this section, the floatstone facies predominates and the fossil preservation allowed a better identification of the coral pieces. *Millepora* sp. was widespread in the floatstone facies. A few samples of *Mussismilia harttii* and CCA were observed in the reef/coral rubble facies. The top of this section marks the end of the interpreted Pleistocene (MIS5e) reef sequence.

Holocene Section 1 (13.5 to 10.5 m): The first record of the CV Holocene reef is defined by a floatstone facies with *Millepora* sp. rubble. To the top of the section, the floatstone is intercalated with *Siderastrea stellata* and *Mussismilia harttii* boundstones, giving place to a 30 cm-thick rubble interval composed of *Millepora* sp.

Holocene Section 2 (10.5 to ~6 m): There was no sample recovery between 10.5 to 9 m. This section recorded a change from floatstone to a coral rubble facies towards the top. The floatstone and the rubble show the predominant presence of the hydrocoral *Millepora* sp., *Siderastrea stellata, Mussismilia harttii* and *Porites* sp. are also observed, mainly toward the top of the section.

Holocene Section 3 (~6 to 1.5 m): This section is basically defined by a floatstone facies. Compared with the other floatstone facies in the Pleistocene and Holocene sections, fossil components are more diverse in this section, including bryozoans, CCA and molluscs. Fragments of *Millepora* sp. (abundant), *Siderastrea stellata, Porites* sp. and *Favia gravida* were also identified. The coral rubble size tends to increase towards the top of the section.

Holocene Section 4 (1.5 to 0 m): The reef top is composed of *in situ* colonies of *Siderastrea stellata, Mussismilia harttii* and *Montastraea cavernosa.* This is the first and only identified record of *Montastraea cavernosa* in the CV reef sequence.

^{14}C dating, low-magnesium calcite percentage and accretion rates

Two different reef units were distinguished based on the difference of low-magnesium calcite/aragonite content. Unit 1 presents a low-magnesium calcite content ranging from 0.2 to 5.5% and Unit 2 has low-magnesium calcite contents reaching around 99.5% (Table 3). Pedra Grande core (PG) comprised only Unit 1, whereas Coroa Vermelha core (CV) encompassed the two units. A shift in low-magnesium calcite content at 13.5 m in CV reef core, from <5 to 99.7%, marks the beginning of Unit 2. Due to the high low-magnesium calcite contents in Unit 2, no ^{14}C or U/Th dating was attempted in that unit. As mentioned above, the boundary between the two units is interpreted as the Pleistocene/Holocene boundary.

Radiocarbon dating results show that Unit 1, in both reefs, developed during the Middle Holocene (CV) and Middle-Late Holocene (PG) (Table 3), with ages ranging from 6785 ± 200 cal yr BP to 1145 ± 170 cal yr BP. The oldest dated reef sample was obtained in PG at 18 m depth (6785 ± 200 cal yr BP, with 99.7% of aragonite) (Table 3; Fig. 3). In CV reef, the oldest Holocene dated sample (6406 ± 205 cal yr BP, with 97.2% of aragonite) was obtained at 10.5 m depth (Fig. 5). ^{14}C dates at the top of the cores were very different in PG and CV. In PG, the 0 to 1.5 m depth interval yielded a calendar age of 1145 ± 170 yr BP, whilst CV presented a calendar age of 4442 ± 220 yr BP, for the same depth interval. Table 3 shows all the ^{14}C dates and composition of the dated material.

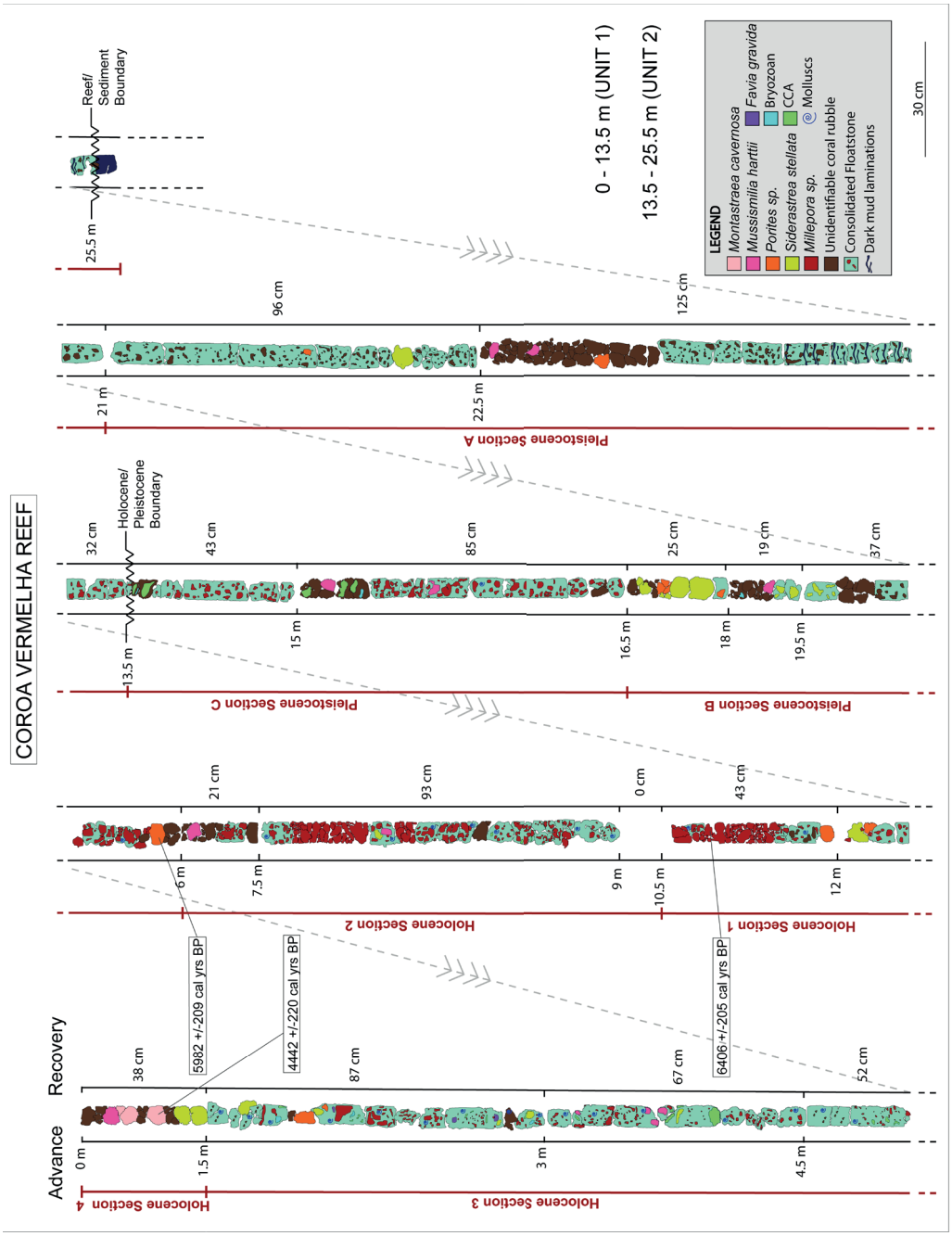


Fig. 5. CV reef core composition and radiocarbon dates. Important to note that drilling advance intervals are not in the same vertical scale and recovery information is displayed on the right side, including zero recovery. The diagram aims to produce a detailed stratigraphic image of the composition of the drilled and recovered sections. All the depths are corrected based on drilling data. Radiocarbon dates are shown as calendar years BP.

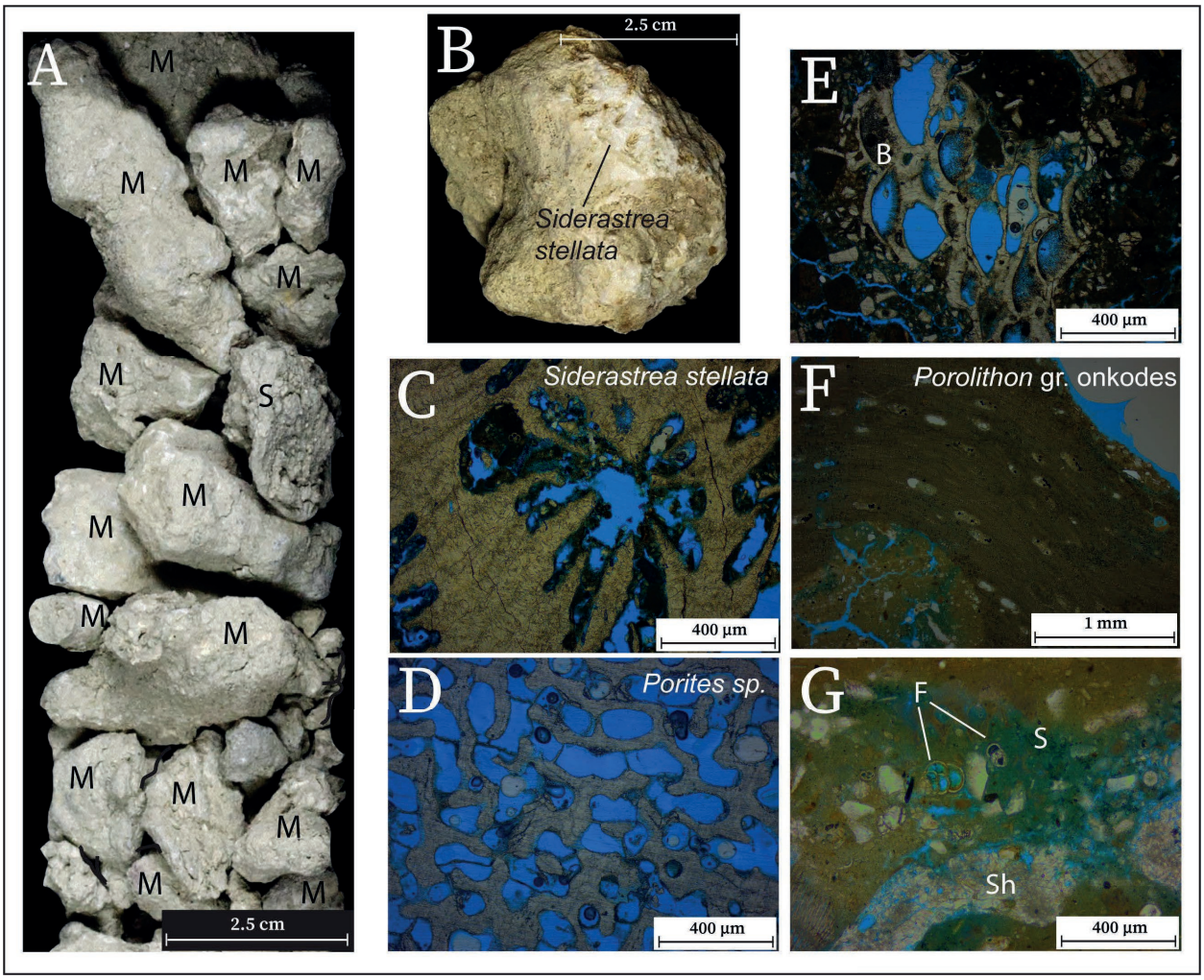


Fig. 6. Reef composition: Examples from CV reef core. A) hand specimens of *Millepora* sp. fragments (M); B) hand specimens of *Siderastrea stellata* and petrographic thin sections images of C) *Siderastrea stellata*, D) *Porites* sp., E) Bryozoan (B), F) CCA, section of *Porolithon* gr. *onkodes* showing numerous conceptacles and trichocyte fields and G) mix of sediments (S), mollusc shell (Sh) and foraminifera (F).

Table 3. Radiocarbon dates, composition of the dated material, accretion rates and XRD results for PG and CV cores.

Reef	Sample ID	Depth (m)	^{14}C Age (^{14}C yr BP)	2σ Calib-ration (Cal BP)	ΔR	Coral Taxonomy	Context	Accretion rates (m ky^{-1})		XRD Arago-nite (%)	XRD Calcite (%)
Pedra Grande	PG 0-1.5 m	0	1620+/-25	1145+/-170	98+/-80	*Porites* sp.	*In situ* (top of Core)	3.2	4.4		
	PG 1.5-3 m	1.5	2520+/-25	2110+/-187		*Porites* sp.	*In situ* (near to the top of the Core)				
	PG 6-7.5 m	7.5	–	–		*Mussismilia harttii*	*In situ* (middle of the Core)			74.5	25.5
	PG 7.5-9 m	8	3530+/-25	3315+/-214		*Siderastrea stellata*	*In situ* (middle of the Core)				
	PG 10.5-12 m	11.5	3780+/-25	3746+/-89		*Porites* sp.	*In situ* (middle of the Core)				
	PG12-13.5 m	13.5	4820+/-20	4948+/-434		*Porites* sp.	*In situ* (middle of the Core)			94.5	5.5
	PG 16.5-18 m	16.5	–	–		*Montastraea cavernosa*	*In situ* (near to the bottom of the		2.1	99.8	0.2
	PG 18-20 m	18	6370+/-20	6785+/-200		*Montastraea cavernosa*	*In situ* (bottom of the Core)				
Coroa Vermelha	CV 0-1.5 m	0	4420+/-25	4442+/-220	98+/-80	*Montastraea cavernosa*	*In situ* (top of the Core)	5.3		97.0	2.9
	CV 4.5-6 m	4.5	5700+/-25	5982+/-209		*Porites* sp.	*In situ* (near to the top of the Core)				
	CV 10.5-12 m	10.5	6050+/-20	6406+/-205		*Millepora* sp.	*In situ* (10.5-12 m interval)				
	CV 12-13.5 m	12	–	–		*Siderastrea stellata*	*In situ* (12-13.5 m interval)			97.2	2.8
	CV 15-16.5 m	15	–	–		*Mussismilia harttii*	*In situ* (15-16.5 m interval)			0.2	99.8

Vertical accretion (VA) rates of the Holocene reefs were determined using radiocarbon ages *versus* core depth. Average rates were 5.3 m kyr^{-1} for CV reef and 3.2 m kyr^{-1} for PG reef. In PG two different intervals of growth were identified: i) from 6785 ± 200 to 3746 ± 90 yr BP (between 18 m and 11.5 m depth) accretion rate was 2.1 m kyr^{-1}; and ii) from 3746 ± 90 to 1145 ± 170 yr BP (between 11.5 m depth and the reef top), accretion rate rose to 4.4 m kyr^{-1} (Fig. 7).

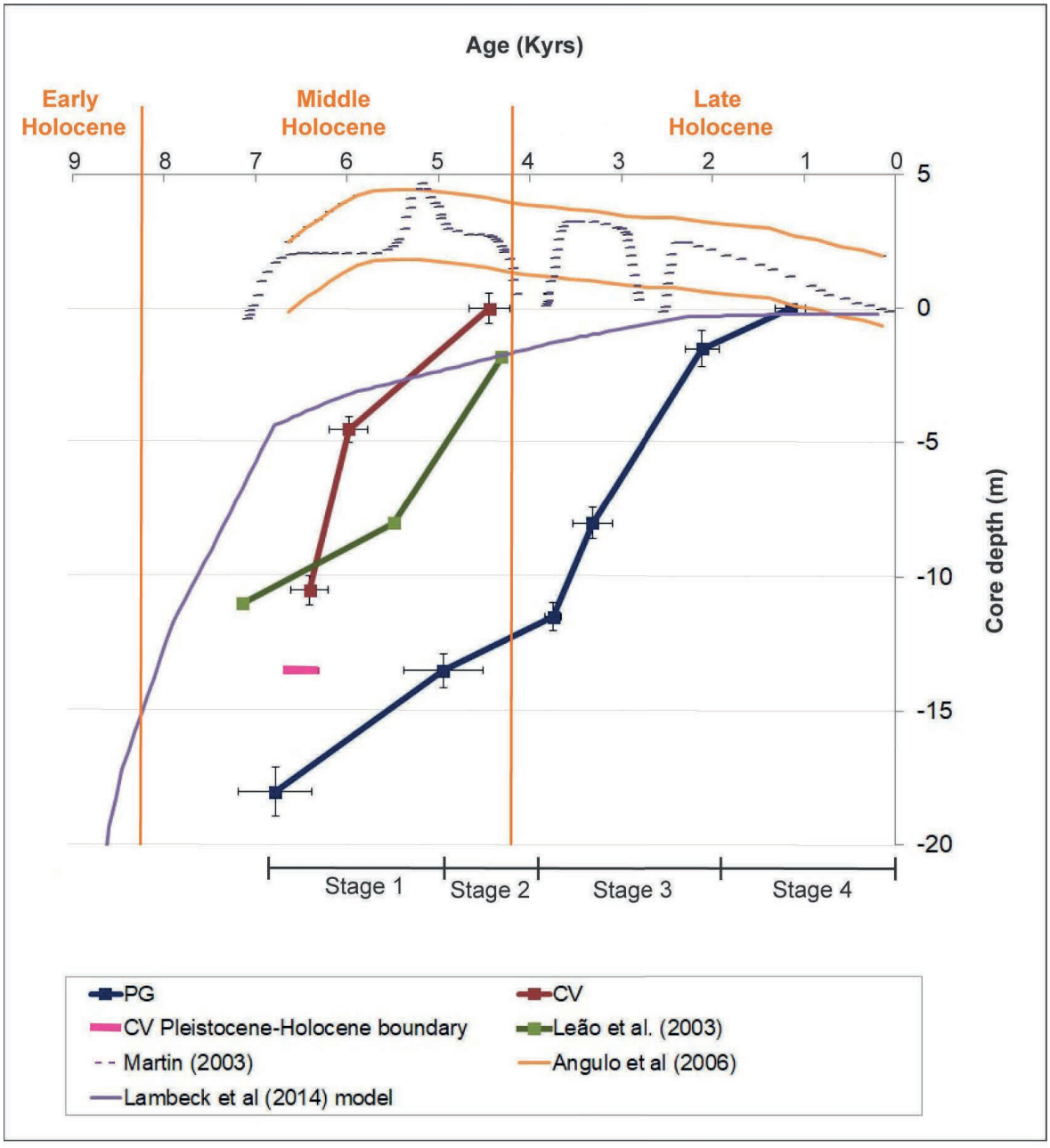


Fig. 7. Age *vs* Depth plot showing ^{14}C and depth data from CV reef (red), PG reef (blue) and Leão *et al.* (2003) (green – CV reef). Angulo *et al.* (2006), Martin (2003) and Lambeck *et al.* (2014) sea-level curves are presented. The Holocene reef stages described by Leão *et al.* (2003) are indicated at the bottom of the plot. The formal subdivision of the Holocene of Walker *et al.* (2012) is indicated. The vertical error was based on the sampling barrel length (1.5 m, see Methods).

DISCUSSION

A synthesis of published radiocarbon dates and core log datasets (Leão, 1982), available seabed morphology and high-resolution seismic data (D'Agostini *et al.*, 2015; Bastos *et al.*, 2015; Ferreira *et al.*, 2020) is combined with the authors' new findings in order to revisit and discuss the evolution of the Abrolhos coastal reefs since the Late Pleistocene. Three main topics are discussed to shed new light on the evolution of the largest reef complex in the South Atlantic: 1) The framework composition of the Late Pleistocene reef Unit 2 in CV, compared to the Middle/Late Holocene units in both CV and PG; 2) Middle Holocene reefs turn on and off in the Abrolhos coastal reefs and their changing growth rates; and 3) the influence of shelf morphology on reef evolution.

Middle/Late Holocene and Pleistocene reef units: framework

The Brazilian coral fauna displays low diversity, lacks branching acroporids common in most Caribbean and Indo-Pacific reefs and the major reef frame builders (in terms of corals) are endemic and evolved from an isolated Palaeogene/Neogene coral fauna (Leão, 1982; Leão & Ginsburg, 1997, Leão *et al.*,2003). According to these authors, in the Abrolhos coastal reefs, coral species are also well adapted to high levels of turbidity (Leão & Ginsburg, 1997).

No major differences were observed between the Middle/Late Holocene and Late Pleistocene coralgal reef compositions obtained from the CV and PG cores. However, the Late Pleistocene reef showed a coral diversity slightly lower than that of CV Middle Holocene reef; and the CCA assemblage is slightly different. This can be a taphonomic bias since most coral fragments in the Late Pleistocene interval were unidentifiable. Also, no major differences in reef composition were observed between Unit 1 in PG and CV (considering only the Middle Holocene reef). The main variations between sites are the different levels of sediment influence recorded by the proportion of floatstone facies along the cores. Dechnik *et al.* (2021) have indicated a spatial assemblage shift in the Abrolhos coastal reefs after a major reef growth turn off between ~3.7 to 2.5 ka. A distinct shift in the dominant reef assemblage from *Mussismilia* to more stress-tolerant *Siderastrea* was defined by these authors using 23 short cores (1 m-long).

In terms of the known reef framework builders in the Abrolhos coastal reefs, the main coral species were observed in the studied cores (Table 1), except for *M. brazilliensis*, which was reported by Leão (1982) and Leão & Ginsburg (1997) in CV. Dechnik *et al.* (2021) have also shown a great variability in coral framework species in CV, including *M. brazilliensis*. The authors of this paper have described the occurrence of six coral species in the reef framework and recognised ten different coralline algae. The scleractinian corals *F. gravida* and *S. stellate* are the most common coral species along the Brazilian coast, found even in tide and shallow pools on the top of reef flats (Leão *et al.*, 1997). They are considered to be very resistant to temperature/salinity/turbidity variations (Leão *et al.*, 2003). In a similar way, *M. harttii* and *Porites* sp. are adapted to moderate/high turbidity (Leão *et al.*, 1997), occupying the reef edge/top with large colonies (Correia, 2010; Leão *et al.*, 1997). The hydrocoral *Millepora* sp., in turn, forms large colonies in shallow reefs worldwide, where they occupy a variety of substrates and produce morphologically complex skeletons (Edmunds, 1999). According to Leão *et al.* (1997), their occurrence is common in water depths shallower than 15 m and they form the edge of reef tops in the mushroom-like pinnacles of Abrolhos. As a matter of comparison, this zone is normally occupied

by *Acropora palmata* in the Caribbean Reefs (Oliveira *et al.*, 2008; Leão, 1982; Leão *et al.*, 1997; Leão *et al.*, 2003; Hopley, 2011; Montaggioni & Braithwaite, 2009; Lighty *et al.*, 1982; Toscano & Macintyre, 2003; Gischler *et al.*, 2010).

Montastraea cavernosa occupies a distinct reef habitat different from that of other sclerectinian and hydrocorals in the cores. It is usually found in more shaded areas of the reef and in Abrolhos, it occurs either as the dominant coral species in the pinnacle walls or in deeper reefs (>20 m) (Francini-Filho *et al.*, 2013; Moura *et al.*, 2013). In both PG and CV reefs, it was found growing together with other corals throughout the cores. Its presence can be explained by the different stages recorded during the reef evolution, or even by a high level of turbidity that reduced light intensity on the top of the reef. This might explain the occurrence of *M. cavernosa* close to the core top in CV.

In terms of reef flora, CCA make a very important framework builder in the South Atlantic shallow reefs (Amado Filho *et al.*, 2018; Figueiredo *et al.*, 2008). Amado Filho *et al.* (2018) reports that CCA, on average, account for 20% of the benthic cover in Abrolhos reefs. In this study, the authors recognised 10 coralline algal taxa across the two cores (Table 1). According to Jesionek *et al.* (2016) and Amado-Filho *et al.* (2018), *Porolithon gr. onkodes* and *Melyvonnea erubescens* live between 2 and 5 m of depth in the Abrolhos Shelf, whilst *Dawsoniolithon* gr. *conicum* (as *Pneophyllum conicum*) can be observed above 15 m. *P. gr. onkodes* lives in habitats directly exposed to sunlight and *D.* gr. *conicum* on the pinnacle walls (Jesionek *et al.*, 2016, Amado-Filho *et al.*, 2018). All of them were identified as important encrusting species in the reef cores, although some differences were observed in terms of species occurrence between the cores (Table 2). The PG and CV reef framework compositions are similar to typical modern Abrolhos shallow benthic reef communities (less than 10 to 12 m-deep) (Francini-Filho *et al.*, 2013; Moura *et al.*, 2013).

In terms of reef facies, the Middle Holocene PG reef received lower levels of sediment influx than the Middle Holocene CV reef, in which floatstone facies predominate. The PG reef is composed of boundstone from the base, at 20 m, up to around 10.5 m in depth. Floatstones, intercalated with boundstones, occur along the top two sections of the core, which is Late Holocene and therefore cannot be compared with the Middle Holocene. The CV reef, on the contrary, shows high levels of sedimentation in both units along the majority of the core length. This was also observed by Leão (1982) and Leão & Ginsburg (1997) for the CV Middle Holocene reef. Comparing the Pleistocene and Holocene units, the only major variation is an increase in boundstone or reef rubble facies in the Middle/Late Holocene unit. Therefore, the CV grew in high turbidity conditions during both the Pleistocene and Holocene, with possible periods of less turbidity in the Holocene. The occurrence of black mud layers at the base of the Pleistocene unit is also an indication of terrigenous sediment input.

The CV core shows that the main Abrolhos framework builders did not change considerably from the Late Pleistocene, probably MIS 5e reef (Unit 2), to the Middle Holocene (Unit 1). Studies of Quaternary reefs in the Great Barrier Reef (Dechnik *et al.*, 2017, Tager *et al.*, 2010), Kenya (Crame, 1981), Belize (Gischler, 2007), Barbados (Mesolella, 1967, Mesolella *et al.*, 1970) and New Guinea (Pandolfi, 1996, Tager *et al.*, 2010) have also revealed striking similarities between framework builders, especially in the coral fauna, in the Holocene and late Pleistocene.

Furthermore, no shallowing upward reef assemblage sequence was clearly observed

along both cores, even at PG, where Middle Holocene coral was recorded at 18 m depth. In this aspect, the Abrolhos reefs diverge from Indo-Pacific and Caribbean Holocene reefs (Hopley *et al.*, 2007; Hopley, 2011; Montaggioni & Braithwaite, 2009; Woodroffe & Webster, 2014) in which, when reefs approach sea-level, the coral assemblage shifts to more robust high energy, shallow water species. A possible explanation for the Abrolhos reefs not showing a shallowing upward coral sequence could be the low coral diversity in the Brazilian margin, which is typically dominated by shallow water species adapted to high turbidity and shadow zones. The low hydrodynamic energy could also be responsible for the lack of trends in these reefs, as no substantial change in energy conditions took place when approaching sea-level.

This finding raises a question about the Holocene evolution of the two reef arcs on the Abrolhos Shelf, inner and outer arcs. Bastos *et al.* (2018) found that bryozoans, alongside with coralgal assemblages, dominate the reef framework in the Abrolhos outer arc for the last 2 kyr, while in the inner arc a coralgal assemblage dominates the Late Pleistocene/Holocene reef framework (this study and Leão, 1982). The different reef composition in the two arcs can be explained by a set of habitat characteristics such as higher turbidity levels along the inner arc and a lower turbidity level and seasonal high productivity along the outer arc, including the distance from the coast (Bastos *et al.*, 2018). In general, abundant bryozoans are absent in deposits with high siliciclastic input (Novak *et al.*, 2013; Santodomingo *et al.*, 2015).

The Holocene reef evolution and the changing accretion rates

Montaggioni (2005) compiled 684 reef accretion rates around the Indo-Pacific province to contrast the main reef evolution between regions. Montaggioni (2005) argued that reefs can respond differently to sea-level rise, as accretion rates are dependent on the main framework builder. Thereby, relative sea-level changes, water depth, hurricane/cyclone frequency and water-energy conditions can be important reef drivers.

The Middle/Late Holocene Abrolhos coastal reefs started growing after 7000 yr BP, when the inner shelf was completely drowned during the last deglaciation and mean sea-level was close to PSL (Leão & Ginsburg, 1997; sea-level curve by Angulo *et al.*, 2006). The new information brings complexity to an Abrolhos evolution model; the study results of the PG and CV reefs show a different growth pattern and timing. Although the oldest coral ages in both sites have a similar age, their initial depths are different. It has a major implication for determining reef turn-on palaeo-depths for the Abrolhos reefs. The Holocene/Pleistocene boundary at CV was observed at around 13 m and the oldest coral age (6406 ± 205 cal yr BP) was obtained at around 10.5 m. In PG, this boundary was not reached in the core and the oldest coral age was obtained at 18 m depth (6785 ± 200 cal yr BP). So, there is a roughly 8 m difference between PG and CV, which means that CV was closer to PSL around this age, while PG was completely submerged. This is supported by the coral colony dated in PG (*M. cavernosa*), which occurs in more shaded or deeper areas in Abrolhos, in contrast with the *Millepora sp* dated in CV.

RSL curves for the eastern Brazilian coast show that sea-level reached the PSL around 7,000 years BP and the Holocene maximum sea-level stage occurred around 5000 to 5800 years BP (Angulo *et al.*, 2006), followed by a slow and continuous fall of the sea-level curve in the last 4900 years. Martin (2003) suggests that the sea-level fall phase was interrupted by two major sea-level

fluctuations (falls, see Fig. 7). Leão *et al.* (2003) calculated a maximum accretion rate of around 6.7 m kyr^{-1} at Coroa Vermelha Reef during a rapid accretion phase, between 5000 to 4000 yr BP. The results presented here show an average accretion rate of 5.3 m kyr^{-1} in CV and 3.2 m kyr^{-1} in PG. However, comparing only the same Holocene time interval, the CV Middle Holocene Reef accretion rates are 5.3 m kyr^{-1}, while in PG the rates are 2.1 m kyr^{-1}. PG Late Holocene Reef accretion rates reach up to 4.4 m kyr^{-1}, double the rate for the Middle Holocene reef accretion in PG and comparable with CV rates.

CV Reef grew for only around 2500 years, before it turned off around 4000 yr BP, as observed herein (4442 +/- 220 cal yr BP), by Leão *et al.* (2003) and by Dechnik *et al.* (2019) (3730 cal yr BP). The turn off of CV Reef could have been caused by a decrease in accommodation space due to a fall in relative sea-level, as proposed by Martin (2003) and Dechnik *et al.* (2019), around 4000 years, close to the boundary of Middle-Late Holocene, as well as perhaps by an increase in sediment input during the sea-level fall, following the maximum sea-level stage (~5000 to 5800 yr BP). Andrade *et al.* (2003), studying the evolution of the Caravelas coastal plain, identified an increase in sediment input associated with the initiation of a second Caravelas river mouth nearby Nova Viçosa (the closer coastal portion to CV reef). The resulting coastal progradation was also mapped by D'Agostini *et al.* (2015) using seismic data. These authors mapped seismic units showing inclined reflectors dipping towards the coastal reefs, south of the Caravelas river mouth. None of those studies has an absolute dating for the coastal progradation but a relative dating shows that it most probably occurred following the maximum sea-level stage (5000 to 5800 yr BP; D'Agostini *et al.*, 2015).

During the interval when the CV Reef turned on, grew and turned off, the PG reef grew at a slower rate (2.1 m kyr^{-1}), about twice as low. When CV turned off, the closest reef record data at PG (3746 +/- 90 cal yr BP at 11.5 m), places the reef close to 11 m depth. After reaching the depth of ~11 to 10.5 m, PG accretion rates in the Late Holocene increased to 4.4 m kyr^{-1} (from 3746 +/- 90 cal yr BP to 1145 +/- 170 cal yr BP), until it reached mean sea-level. This means that PG grew around 10.5 m in 2300 years, showing a behaviour very similar to the accretion rates observed for the Middle Holocene in CV. This faster accretion phase is associated with the occurrence of floatstone facies during the Late Holocene at PG core. Moreover, the reef hiatus mentioned by Dechnik *et al.* (2019) does not seem to have limited the growth of PG reef. On the contrary, the possible fall in sea-level around 3700 yr BP that these authors suggest, or any climate oscillation, could have triggered the increase in PG reef accretion rates.

The coral framework assemblage can also influence reef accretion rates, as proposed by Montaggioni (2005) in the Indo-Pacific reefs. Although reef accretion and coral growth rates are not necessarily coupled (Gischler & Hudson, 2019; Roff, 2020), higher accretion rates were generally recorded in cores containing a greater proportion of branching growth forms (Montaggioni, 2005). In CV, the main coral builder observed in the Middle Holocene was branching *Millepora* sp. (despite the unidentifiable coral fragments), whilst in PG coral framework in the Middle and Late Holocene was dominated by domal species.

The fact that PG reached the mean sea-level around 1200 yr BP seems not to have totally shut down the reef, as occurred in CV around 4000 yr BP. This can explain the distinct morphology between the two reef flats. PG is probably still accreting laterally and its quasi-emergent pinnacles are still

growing. The CV and PG reefs turned on at different depths and have grown independent of each other over the last 6000 yr, despite being located less than 35 km apart (Figs 1 and 7); and the PG reef flat morphology represents a younger reef phase than the CV turn off.

Reef composition and radiocarbon dating data also suggest that no subsidence changes from the Middle to the Late Holocene have driven changes of the reef species distribution, since all the biota assemblage is common to modern shallow and reefal environments. The scarcity of age data from the Late Pleistocene Unit prevents any assessment of the influence of subsidence in reef development.

In addition, it is reasonable to consider that CV reef flat is under an erosive process after reaching sea-level. However, considering that the reef turned off around 4000 yr BP and the reef flat is emergent during low tide (tidal range ~2 m), erosion was not significant enough to bias the 4000 yr turn off event reported in different studies (Leão *et al.*, 2003; Dechnik *et al.*, 2019). Also, the Abrolhos reefs are situated in a 'low energy' environment, as discussed by Bastos *et al.* (2018), as no major tropical storms or hurricanes reach this region.

The shelf morphology as a driver of reef evolution in Abrolhos

Since Hartt (1870) and Laborel (1969), the Abrolhos reefs have been described as unique when compared to other main reef provinces worldwide. The low coral diversity and high endemism, but also the mushroom-like pinnacle morphology, represent distinct traits. The Abrolhos shelf is also different from well-known carbonate platform models, as it does not fit to classic ramp or rimmed shelf models, being more like an open carbonate platform with inner shelf reefs and outer shelf rhodolith beds (Moura *et al.*, 2013; Bastos *et al.*, 2015). The role played by bryozoans as reef builders in the outer arc Abrolhos reefs (Bastos *et al.*, 2018) make these reefs unique as well. This work brings a new insight to the Holocene reef evolution in this carbonate-dominated shelf.

The data obtained in the PG reef has brought a new piece to the Abrolhos reef growth puzzle. The two drilled sequences presented in this study show that the coastal reefs may have turned on at the same time but their growth started from different water depths and their occurrence or distribution are not necessarily controlled by a topographic high, as suggested by Leão & Ginsburg (1997) and D'Agostini *et al.* (2015).

Reef distribution in the Abrolhos Shelf has always been presented and discussed as two reef arcs (Leão, 1982; Leão & Ginsburg, 1997; Leão *et al.*, 2003; Moura *et al.*, 2013; Bastos *et al.*, 2018; Ferreira *et al.*, 2020). The inner arc is formed by coastal patch reefs, forming reef flats during low tides (Fig. 1). The outer arc is mainly composed of a high number of large pinnacles that are partially exposed during low tides. In between the two arcs, lies the so-called Abrolhos Channel.

However, revisiting the high-resolution morphology map around the Abrolhos arcs (using the Bastos *et al.*, 2015 dataset) and combining it with available and published side scan sonar images (Moura *et al.*, 2013 and Ferreira *et al.*, 2020) from the Abrolhos Channel, and shallow seismic lines, the authors can suggest that shelf morphology has played an important role in reef evolution and that the PG Reef is morphologically different from the other 3 coastal reefs in the inner arc.

Fig. 8 shows a detailed bathymetric map of the inner shelf depicting the Paredes/Pedra Grande reef and the submerged reefs mapped by Ferreira *et al.* (2020). In this map, the Paredes/PG reef is adjoined by extensive submerged pinnacles and bank reefs (see side scan sonar images in Fig. 8) set in an almost

north-south direction (between the two known arcs). This reef set is composed by a huge complex of submerged and emergent reefs that include the emergent Paredes/PG reef in its northern boundary.

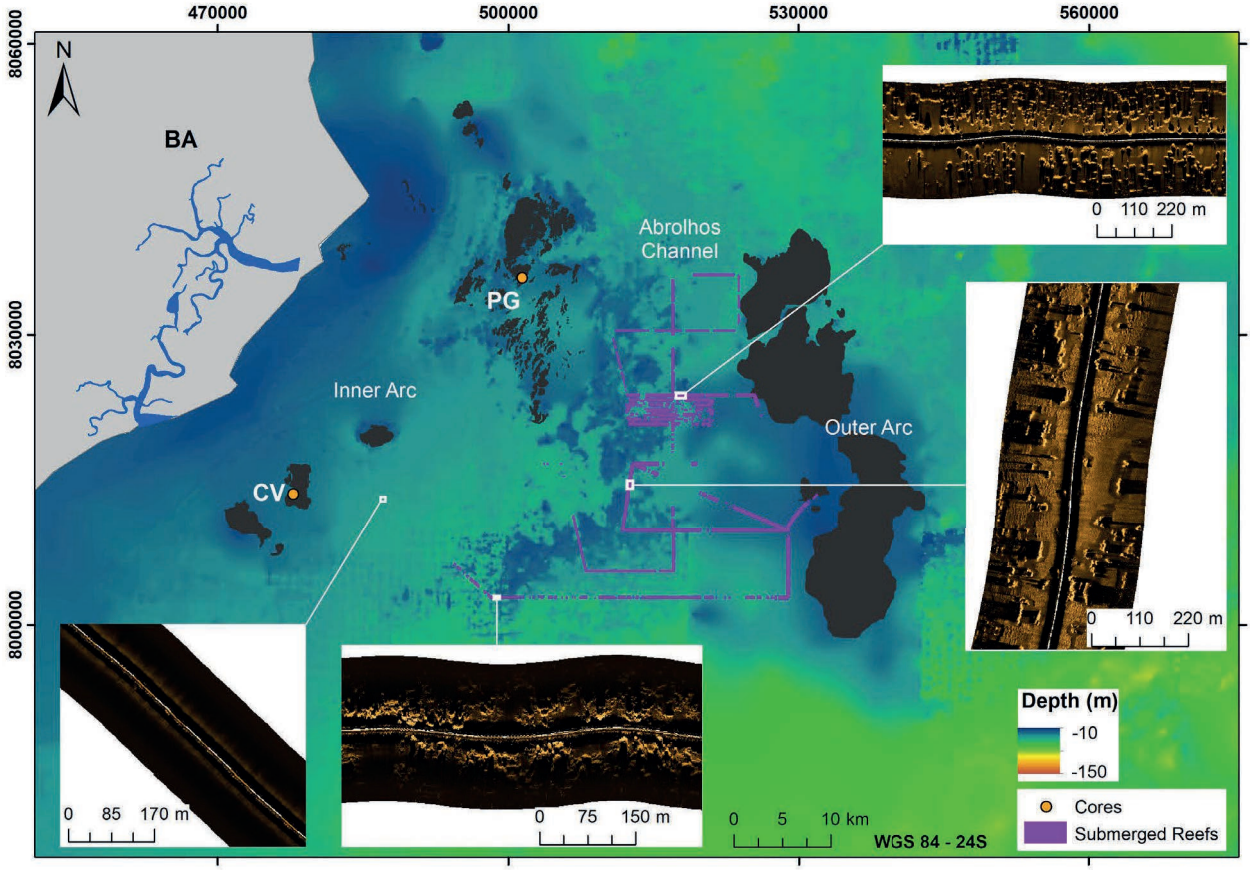


Fig. 8. Abrolhos bathymetric map (dataset from Bastos *et al.* 2015, Moura *et al.* 2013 and Ferreira *et al.* 2020). Black polygons represent quasi-emergent and emergent reefs between the reef arcs. The yellow dots show the location of both reef cores (CV and PG). Purple lines are side scan sonar tracks. Submerged reefs are illustrated in the acoustic images showing distinct reef morphologies. By association, the authors interpret that the irregular darker blue contours in the Abrolhos Channel represent the distribution of submerged reefs.

The bathymetric transects presented in Fig. 9 show the morphological heterogeneity across the Abrolhos reef arcs. Transect A crosses the Paredes/PG reef showing the continuity of a reef topography characterised by submerged irregular peaks, ending at the outer arc, where bathymetric data does not exist as the pinnacles are emergent (Fig. 9). The cross shelf bathymetric transects B and C (Fig. 9) evidenced a distinct seabed morphology setting when compared to Paredes/PG. The seabed morphology surrounding SG, CV and NV (Figs 1 and 8) is flat and resembles a coastal sediment wedge that was observed in the seismic stratigraphic units mapped by D'Agostini *et al.* (2015). Submerged reefs appear at the end of transects B and C (Fig. 9), approximately 10 to 15 km offshore from CV and SG. These reefs represent the southernmost end of the reef complex that emerges as the Paredes reef.

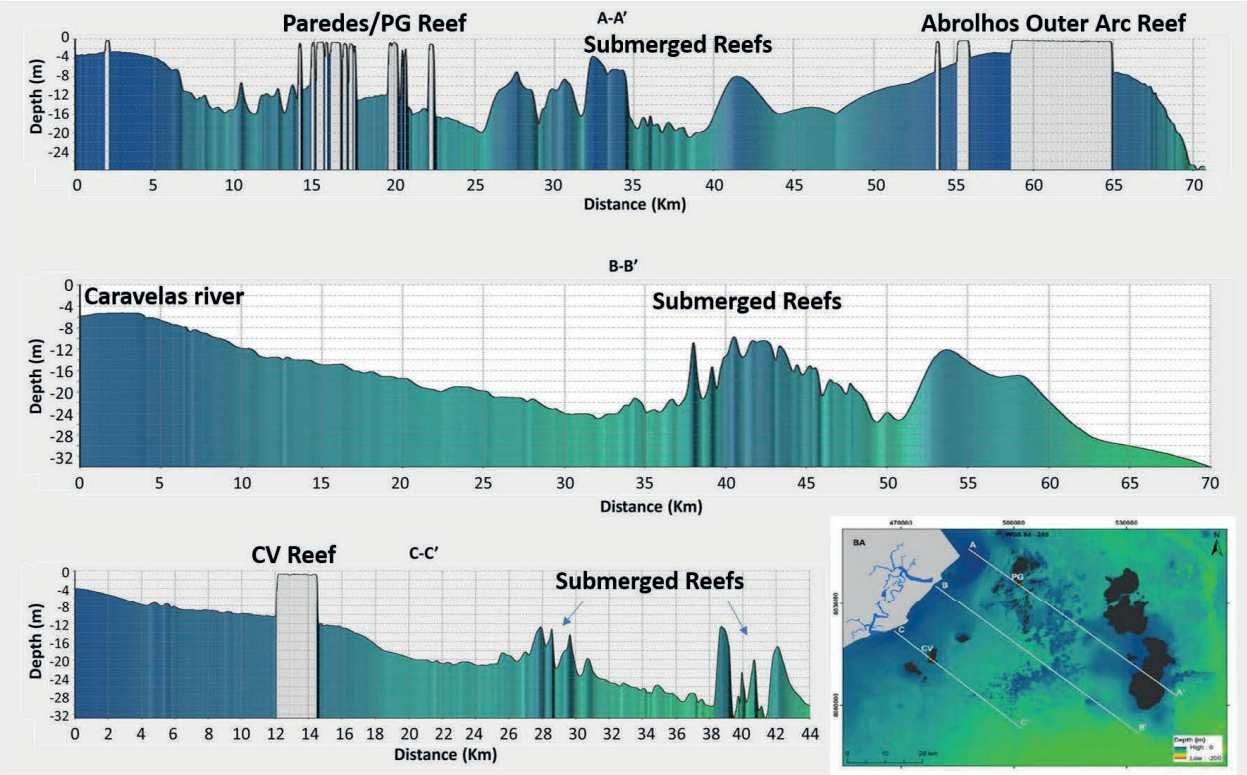


Fig. 9. Cross shelf bathymetric transects of Abrolhos Inner Shelf. Transect A-A' crosses the Paredes/PG reef showing the continuity of a reef irregular bathymetry ending at the outer arc; and transects B-B' and C-C' on smoother seabed bathymetry near the coast; and an irregular one in the end. In yellow is pointed the location of both reef cores (CV and PG). (Modified from Bastos *et al.*, 2015).

Seismic and reef stratigraphic evidences provided by Leão & Ginsburg (1997) and D'Agostini *et al.* (2015) suggest that the three coastal reefs (SG, CV and NV), located to the south of the Caravelas river, have developed on the top of a topographic high, forming small and isolated patch reefs, with extensive reef flats during low tides. Seismic refraction data collected at the top of CV (Leão & Ginsburg, 1997), combined with CV Reef stratigraphy (Leão & Ginsburg, 1997 and the present study) show that the Pleistocene-Holocene boundary surface occurs at a depth ranging from 12.7 to 13.5 m below the reef. D'Agostini *et al.* (2015) have mapped this boundary surface in the seismic reflection data collected in between the coastal reefs. The seismic data interpreted and published by D'Agostini *et al.* (2015) is shown in Fig. 10.

The erosive surface, S1, is interpreted as the exposure surface formed after MIS5, following the beginning of the general sea-level fall, throughout part of late MIS5, MIS4, MIS3, MIS2 and Early Holocene MIS1. During this period, the Abrolhos coastal reef region was fully exposed and any Late Pleistocene reef or sedimentary deposit was exposed to erosion and/or karstic processes (D'Agostini *et al.*, 2015; Leão & Ginsburg, 1997). This surface represents the top of the Late Pleistocene reef. The authors have defined two main seismic units above S1: Sq 2, interpreted as a sea-level rise/channel infilling facies; and Sq 4, interpreted as the combination of maximum sea-level and slow sea-level fall during the Late Holocene and the Middle Holocene. The depth of S1 varies considerably as a result of

erosion (incised channels) or limestone dissolution. In general, the depth of S1 observed by D'Agostini *et al.* (2015), in relation to the position of the coastal reefs (NV, CV and SG), is around 18 to 20 m-deep. Considering the depth of the Pleistocene-Holocene boundary obtained from the CV cores and comparing with S1 mean depth, the Middle Holocene reef unit started to grow on top of S1 around 5 to 7 m higher than the adjacent area between the reefs, suggesting the presence of a topographic high. Transect A, in Fig. 10, is the only seismic data closer to the Paredes and PG reef. Seismic stratigraphy shows a coastal-sediment prograding wedge reaching the inner coastal reefs. Offshore from the coastal reefs, S1 presents a general dip reaching around 25 to 28 m-deep (not considering the bottom of the shelf valleys), with a maximum sea-level fall sediment deposit on top, described as a non-reef transition from the coastal reefs to the Abrolhos Channel submerged reefs. The same pattern is observed in the bathymetric transects B and C, shown in Fig. 9. The exception for this pattern is the transect across the Paredes/PG reef, where no non-reef transition is observed.

Thus, combining the radiocarbon dating and accretion rates with the seabed morphology discussed above and the seismic lines shown in Fig. 10, the authors can establish that the three Abrolhos smaller patch reefs (NV, CV and SG) were directly influenced by an antecedent topography, as proposed by Leão & Ginsburg (1997) and shown by the depth of the Late Pleistocene exposed surface mapped by D'Agostini *et al.* (2015). However, the Paredes/PG Reef is morphologically different from the other three patch reefs and its evolution during the Middle and Late Holocene was not necessarily influenced by any specific topographic high as the one observed in CV. The PG reef started to grow in deeper water than CV, changing its accretion rates much probably as a function of water depth.

Moreover, the morphology of the emergent Paredes/PG reef is adjoined by a submerged or quasi-emergent reef complex formed by pinnacles and bank reefs. This is interpreted herein as one reef set that forms an intermediate arc that is partially submerged and partially emergent. The reason for that is not necessarily a specific topographic high, but the irregular shelf morphology and the associated reef accretion rates. The authors' data show a 6800 years old coral, in PG, at 18 m depth, when the sea-level was very close to the PSL. Looking at the bathymetric map and transects, it is clear that many pinnacles or bank reefs occur around this depth or shallower. This shows that part of these reefs could not keep up with sea-level rise rates and it is possible that the oscillation/sea-level fall observed around 3700 years BP favoured an increase in accretion rates for the reefs closer to the coast or that had already reached a minimum depth (~11 m) that allowed them to keep up with a following sea-level rise (at 2.5 to 2 kyr), as proposed by Dechnik *et al.* (2019). A large number of reefs in the Abrolhos Channel drowned at about 12 m below modern sea-level (Fig. 9); most probably they could not keep up during the Late Holocene as the PG reefs did during this time by increasing their accretion rates.

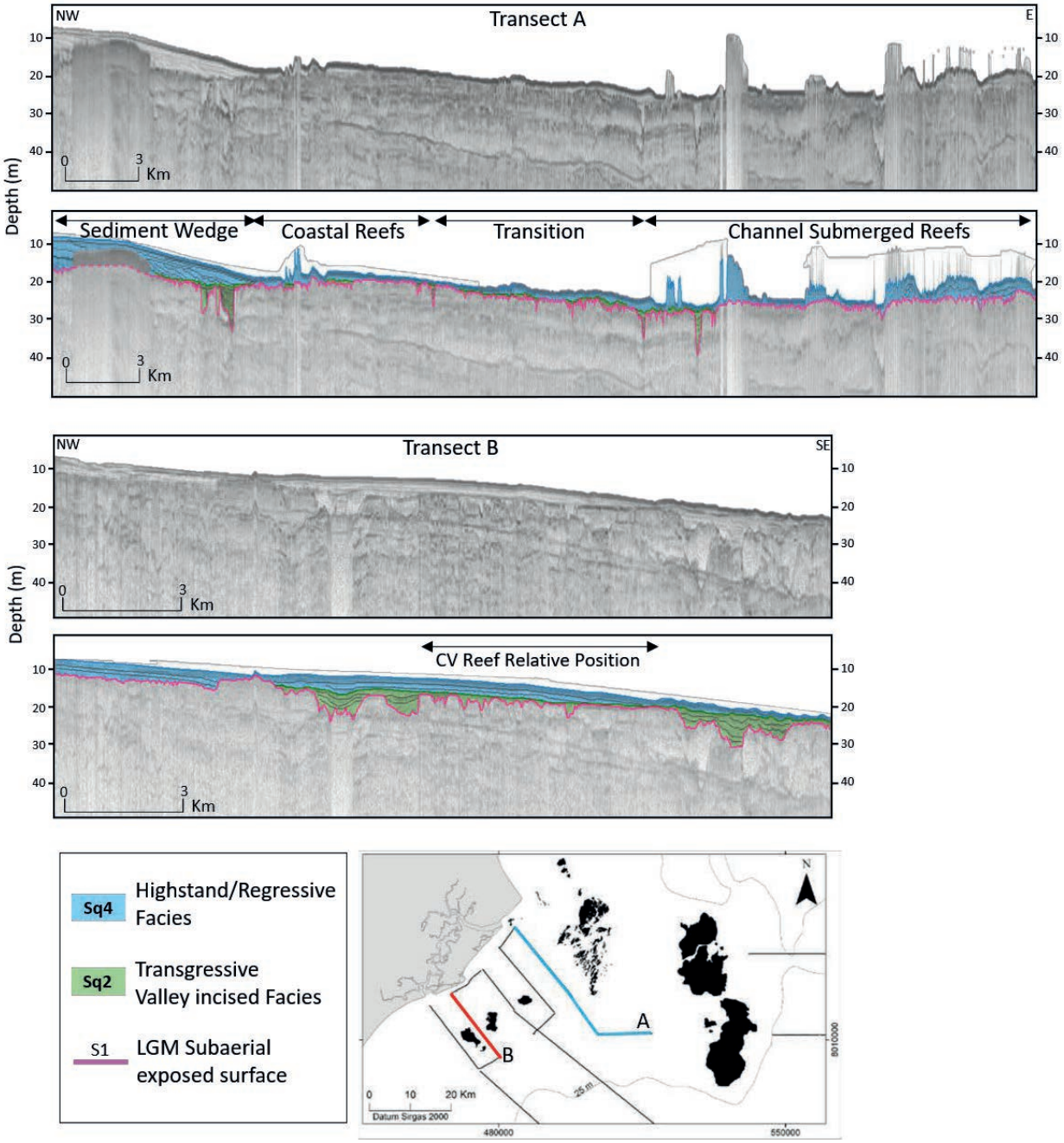


Fig. 10. Seismic data and interpretation based on D'Agostini *et al.* (2015) and Bastos *et al.* (2015). The seismic section was acquired using a Boomer source operating at 250J. Red line in the map inset represents Transect B, located close to CV reef. The blue line is Transect A, collected southward from the Paredes/PG reef.

CONCLUSIONS

This study has provided a new insight on the evolution of Abrolhos coastal reefs based on new reef-stratigraphy data, radiocarbon ages and a compilation of seismic, bathymetric and published data. On this basis the authors conclude the following:

1. Middle and Late Holocene and Late Pleistocene reefs are not very different in terms of reef composition and environmental setting. Both grew on highly turbid waters, with a significant terrigenous sediment input. Corals and CCA assemblages were identified as main framework builders of Abrolhos inner-shelf reefs since the Late Pleistocene. No clear shallowing upward sequence of reef builders was observed, which differs from other reef sequences all over the world.

2. The typical low coral diversity in the Brazilian margin, high turbidity levels, lack of hydrodynamic energy, distinctive reef morphology and coral habitats (reef tops and walls) are possible explanations for the lack of shallowing upward trends and absence of any builder assemblage shift during sea-level rise.

3. Although the Late Pleistocene surface was not recovered in the PG drilled sequence, the PG and CV reefs most probably turned on roughly coevally at different depths and with different coral assemblages. The PG reef started growing, in a water depth approximately 10 m deeper than the CV, circa 6.8 kyr BP. The reefs have grown independently from each other over the last ~ 6 kyr, despite being located less than 35 km apart. In terms of coral growth, CV started growing around 6.4 kyr BP but turned off around 4 kyr. In contrast the PG kept growing until around 1.2 kyr BP. No climate variability or sea-level fall during the Late Holocene negatively affected the PG reef growth, while CV turned off.

4. PG initiation was probably not controlled by a clear palaeo-topographic high, as is the case for CV. The PG reef could have grown on lower relief substrates but this could not be imaged in the seismic lines. The PG/Paredes reef seems to be connected to a broader reef setting that extends to submerged reef banks and pinnacles and which started to grow in deeper water depths, in the order of 20 m below sea-level. The PG/Paredes reef may be considered as an intermediate arc that is partially submerged and partially emergent.

5. Reef distribution in the Abrolhos shelf could be described as three reef arcs with different morphologies: the inner one is composed by patch reefs NV, CV and CG (around 10 km from the coast) forming extensive reef flats during low tides; the intermediate one, composed by a complex of submerged and emerged pinnacles/reef banks (Paredes/PG is a part of it), and the outer arc, characterised by a complex of isolated pinnacles, around 70 km from the coast.

ACKNOWLEDGEMENTS

The project was funded by CAPES-IODP Brazil (0565/2015), CAPES Ciências do Mar and PetroRio ANP grants. LSV received a CAPES-IODP-Brazil PhD scholarship. BD received a CAPES-IODP-Brazil pos-doc fellowship. JMW and JCB were International Visiting Researchers at UFES and JBRJ, supported by CNPq/CAPES Science Without Borders program. RLM and ACB acknowledge individual grants from CNPq (PQ fellowship). We are thankful to Zá Cajueiro for providing invaluable field support. We also thank ICMBio for research permits. We thank Gilberto Amado-Filho (in memoriam) for his inspiration and incentive to study the Abrolhos reefs.

REFERENCES

Abbey, E., Webster, J.M. and **Beaman, R.J.** (2011) Geomorphology of submerged reefs on the shelf edge of the Great Barrier Reef: The influence of oscillating Pleistocene sea-levels. *Mar. Geol.*, **288**, 61–78.

Amado-Filho, G.M., Bahia, R.G., Mariath, R., Jesionek, M.B., Moura, R.L., Bastos, A.C., Pereira-Filho, G.H. and **Francini-Filho, R.B.** (2018) Spatial and temporal dynamics of the abundance of crustose calcareous algae on the southernmost coral reefs of the western Atlantic (Abrolhos Bank, Brazil). *Algae*, **33**(1), 85–99.

Amado-Filho, G.M., Moura, R.L., Bastos, A.C., Salgado, L.T., Sumida, P.Y., Guth, A.Z., Francini-Filho, R.B., Pereira-Filho, G.H., Abrantes, D.P., Brasileiro, P.S., Bahia, R.G., Leal, R.N., Kaufman, L., Kleypas, J.A., Farina, M. and **Bahia, R.G.** (2012) Rhodolith beds are major CaCO3 bio-factories in the tropical South West Atlantic. *PloS One*, **7**(4), e35171, 6pp.

Angulo, R.J. and **Lessa, G.C.** (1997) The Brazilian sea-level curves: a critical review with emphasis on the curves from Paranaguá and Cananéia Regions. *Mar. Geol.,* **140**, 141–166.

Angulo, R.J., Lessa, G.C. and **Souza, M.T.** (2006) A critical review of mid- to late-Holocene sea-level fluctuations on the eastern Brazilian coastline. *Quatern. Sci. Rev.*, **25**, 486–506.

Bastos, A.C., Moura, R.L., Moraes, F.C., Vieira, L.S., Braga, J.C., Ramalho, L.V., Amado-Filho, G.M., Magdalena, U.R. and **Webster, J.M.** (2018) Bryozoans are major modern builders of south Atlantic oddly shaped reefs. *Scientific Reports/Nature*, **8**, article 9638, 1–11.

Bastos, A.C., Quaresma, V.S., Marangoni, M.B., D'Agostini, D.P., Bourguignon, S.N., Cetto, P.H., Amado Filho, G.M., Moura, R.L. and **Collins, M.** (2015) Shelf morphology as an indicator of sedimentary regimes: A synthesis from a mixed siliciclastic-carbonate shelf on the eastern Brazilian margin. *J. South Am. Earth Sci.,* **63**, 125–136.

Bernat, M., Martin, L., Bittencourt, A. and **Vilas Boas, G.** (1983) Datations Io-U du plus haut niveau marin du dernier interglaciaire sur la côte du Brésil. Utilisation du 229 Th comme traceur. *C.R. Acad. Sc. Paris*, **296**, Serie II, 197–200.

Blanchon, P. and **Blakeway, D.** (2003) Are catch-up reefs an artefact of coring? *Sedimentology,* **50**, 6, 1271–1282.

Camoin, G. and **Webster, J.M.** (2014) Coral reefs and sea-level change. In: *Earth and Life Processes Discovered from Subseafloor Environments: A Decade of Science Achieved by the Integrated Ocean Drilling Program (IODP)* (Eds R. Stein, D. Blackman, F. Inagaki and H. Larsen), *Developments in Marine Geology*, **7**, 395–432.

Correia, M.D (2010) Scleractinian corals (cnidaria: Anthozoa) from reef ecosystems on the Alagoas Coast, Brazil. *J. Mar. Biol. Assoc. UK,* **91**, 659–668.

Crame, J. (1981) Ecological stratification in the Pleistocene coral reefs of the Kenya coast. *Palaeontology,* **24**, 609–646.

D´Agostini, D.P., Bastos, A.C. and **Reis, A.T.** (2015) The modern mixed carbonate–siliciclastic Abrolhos shelf: Implications for a mixed depositional model. *J. Sed. Res.*, **85**, 124–139.

Davies, P.J., Marshall, J.F. and **Hopley, D.** (1985) Relationships between reef growth and sea level in the Great Barrier Reef. *Proceeding of the 5th International Coral Reef Congress,* Tahiti, **3**, 95–103.

Dechnik, B., Bastos, A.C., Vieira, L.S., Webster, J.M., Fallon, S., Yokoyama, Y., Nothdurft, L., Sonborn. K., Batista, J., Moura, R. and **Amado-Filho, G.** (2019) Holocene reef growth in the tropical southwestern Atlantic: Evidence for sea level and climate instability. *Quatern. Sci. Rev.*, **218**, 365–377.

Dechnik, B., Bastos, A.C., Vieira, L.S., Webster, J.M., Fallon, S., Yokoyama, Y., Braga, J.C., Pereira, M.A., Nothdurft, L., Sanborn, K., Moura, R.L. and **Amado-Filho, G.** (2021) Environmental controls on Holocene reef development along the eastern Brazilian margin. *Coral Reefs*, **40**, 1321–1337.

Dechnik, B., Webster, J.M., Webb, G.E., Nothdurft, L., Dutton, A., Braga, J.C., Zhao, J.X., Duce, S. and **Sadler, J.** (2017) The evolution of the Great Barrier Reef during the Last Interglacial Period. *Global Planet. Change*, **149**, 53–71.

Edmunds, P.J. (1999) The role of colony morphology and substratum inclination in the success of *Millepora alcicornis* on shallow coral reefs. *Coral Reefs,* **18**, 133–140.

Ferreira, L.C., Bastos, A.C., Amado Filho, G.M, Leite, M.D.A., Boni, G.C., Moraes, F.C., Secchin, N., Vieira, L.S., Bahia, R., Oliveira, N., Quaresma, V.S. and **Moura, R.L.** (2020) Submerged reefs in the Abrolhos shelf: Morphology and habitat distribution. In: *Seafloor Geomorphology as Benthic Habitat: GeoHab Atlas of seafloor geomorphic features and benthic habitats* (Eds P. Harris and E. Baker), Elsevier, 519–532.

Figueiredo, M.A.O., Horta, P.A., Pedrini, A.G. and **Nunes, J.M.C.** (2008) Benthic marine algae of the coral reefs of Brazil: A literature review. *Oecologia Brasil*, **12**, 258–269.

Flamand, B., Cabioch, G., Payri, C. and **Pelletire, B.** (2008) Nature and biological composition of the New Caledonian outer barrier reef slopes. *Mar. Geol.,* **250**, 157–179.

Francini-Filho, R.B., Coni, E.O.C., Meirelles, P.M., Amado-Filho, G.M., Thompson, F.L., Pereira-Filho, G.H., Bastos, A.C., Abrantes, D.P., Ferreira, C.M., Zibran, F.Z., Guth, A.Z., Simida, P.Y.G., Oliveira, N.L., Kaufman, L., Minte-Vera, C.V. and **Moura, R.L.** (2013) Dynamics of coral reef benthic assemblages of the Abrolhos Bank, eastern Brazil: Inferences on natural and anthropogenic drivers. *PLoS One,* **8**, e54260, 1–12.

Ghisolfi, R.D., Silva, M.P., Santos, F.T., Servino, R.N., Cirano, M. and **Thompson, F.L.** (2015) Physical forcing mechanisms controlling the variability of chlorophyll-a over the Royal-Charlotte and Abrolhos Banks-Eastern Brazilian Shelf. *PLoS One,* **10**, e0117082, 1–21.

Gischler, E. (2007) Pleistocene facies of Belize barrier and atoll reefs. *Facies*, **53**, 27–41.

Gischler, E. (2015) Quaternary reef response to sea-level and environmental change in the western Atlantic. *Sedimentology*, **62**, 429–465.

Gischler, E., Ginsburg, R.N., Herrle, J.O. and **Prasad, S.** (2010) Mixed Carbonates and Siliciclastics in the Quaternary of Southern Belize: Pleistocene Turning Points in Reef Development Controlled by Sea-Level Change. *Sedimentology,* **57**, 1049–1068.

Gischler, E. and **Hudson, J.H.** (2019) Holocene tropical reef accretion and lagoon sedimentation: A quantitative approach to the influence of sea-level rise, climate and subsidence (Belize, Maldives, French Polynesia). *The Depositional Record*, **5**, 515–539.

Hartt, C.F. (1870) *Geology and physical geography of Brazil. Boston, Fields*. Osgood & Co. 620pp.

Hopley, D. (2011) *Encyclopedia of modern coral reefs*. Springer Science + Business Media, 1226pp.

Hopley, D., Smithers, S.G. and **Parnell, K.E.** (2007) *The geomorphology of the Great Barrier Reef: Development, diversity and change*. Cambridge University Press, Cambridge, 39pp.

Jesionek, M.B., Bahia, R.G., Hernández-Kantún, J.J., Adey, W.H., Yoneshigue-Valentin, Y., Longo, L.L. and **Amado-Filho, G.M.** (2016) A taxonomic account of non-geniculate coralline algae (Corallinophycidae, Rhodophyta) from shallow reefs of the Abrolhos Bank, Brazil. *Algae*, **31**, 4, 317–340.

Laborel J.L. (1969) Madréporaires et hydrocoralliaires récifaux des côtes brésiliennes. Systématique, écologie, repartition vertical et Géographie. Ann. Inst. *Oceanogr. Paris*, **47**, 171–229.

Leão, Z.M.A.N. (1982) *Morphology, geology and developmental history of the southernmost coral reefs of Western Atlantic, Abrolhos bank, Brazil*. University of Miami, 240pp.

Leão, Z.M.A.N. and **Ginsburg, R.N.** (1997) Living reefs surrounded by siliciclastic: The Abrolhos coastal reefs, Bahia, Brazil. *Coral Reef Symposium*, **2**, 1767–1772.

Leão, Z.M.A.N., Kikuchi, R.K.P. and **Engelberg, E.F.** (1997) *Internet guide to the corals and hydrocorals of Brazil*. http://www.cpgg.ufba.br/guia-corais/

Leão, Z.M.A.N., Kikuchi, R.K.P. and **Testa, V.** (2003) Corals and coral reefs of Brazil. In: *Latin America Coral Reefs* (Ed. J. Cortéz), Elsevier Science, 9–45.

Lighty, R.G., Macintyre, I.G. and **Stuckenrath, R.** (1982) Acropora palmata reef framework: A reliable indicator of sea-level in the western Atlantic for the past 10,000 years. *Coral Reefs*, **1**, 2, 125–130.

Martin, L. (2003) Holocene sea-level history along Eastern-Southeastern Brazil. *Anuário do Instituto de Geociências-UFRJ,* **26**, 13–24.

Martin, L., Suguio, K. and **Flexor, J.M.** (1988) Hauts niveaux marins pleistocenes du llltoral breslllen. *Palaeogeogr. Palaeoclimatol. Palaeoecol.*, **68**, 231–239.

Mesolella, K.J. (1967) Zonation of uplifted Pleistocene coral reefs on Barbados, West Indies. *Science,* **156**, 638–640.

Mesolella, K.J., Sealy, H.A. and **Matthews, R.K.** (1970) Facies geometries within Pleistocene reefs of Barbados, West Indies. *AAPG Bull.,* **54**, 1899–1917.

Montaggioni, L.F. (2005) History of Indo-Pacific coral reef systems since the Last Glaciation: Development patterns and controlling factors. *Earth Sci. Rev.*, **71**, 1–75.

Montaggioni L.F. and **Braithwaite, C.J.R.** (2009) Quaternary coral reef systems. *Dev. Mar. Geol*., Elsevier, 533pp.

Moura, R.L., Secchin, N.A., Amado-Filho, G.M., Francini-Filho, R.B., Freitas, M.O., Minte-Vera, C.V., Teixeira, J.B., Thompson, F.L., Dutra, G.F., Sumida, P.Y.G., Guth, A.Z., Lopes, R.M. and **Bastos, A.C.** (2013) Spatial patterns of benthic megahabitats and conservation planning in the Abrolhos Bank. *Cont. Shelf Res.*, **70**, 109–117.

Neumann, A.C. and **Macintyre, I.** (1985) Reef Response to Sea Level Rise: Keep-up, catch-up or give-up. *Proceedings of the 5th International Coral Reef Congress*, Tahiti, **3**, 105–110.

Novak, V., Santodomingo, N., Rosler, A., Di Martino, E., Braga, J.C., Taylor, P.D., Johnson, K.G. and **Renema, W.** (2013) Environmental reconstruction of a late Burdigalian (Miocene) patch reef in deltaic deposits (East Kalimantan, Indonesia). *Palaeogeogr. Palaeoclimatol. Palaeoecol.,* **374**, 110–122.

Oliveira, M.D.M., Leão, Z.M.A.N. and **Kikuchi, R.K.P.** (2008) Cultivo de Millepora alcicornis como uma ferramenta para restauração e manejo dos Ecossistemas Recifais do nordeste do Brasil. *Revista da Gestão Costeira Integrada,* **8**, 183–201.

Pandolfi, J. (1996) Limited membership in Pleistocene reef coral assemblages from the Huon Peninsul, Papua New Guinea: Constancy during global change. *Paleobiology*, **22**, 153–176.

Roff, G. (2020) Reef accretion and coral growth rates are decoupled in Holocene reef framework. *Mar. Geol.*, **419**, 1–7.

Santodomingo, N., Novak, V., Pretovic, V., Masshall, N., Diu Martino, E., Capelli, E.G., Rosler, A., Reich, S., Brage, J.C., Renema, W. and **Johnson, K.G.** (2015) A diverse patch reef from turbid habitats in the middle Miocene (East Kalimantan, Indonesia). *Palaios,* **30**, 128–149.

Shackleton, N.J. (2000) The 100,000 year ice-age cycle identified and found to lag temperature, carbon dioxide and orbital eccentricity. *Science*, **289**, 1897–1902.

Schlager, W. (1981) The paradox of drowned reefs and carbonate platforms. *Geol. Soc. Am. Bull.*, **92**, 197–211.

Schlager, W (2005) Carbonate sedimentology and sequence stratigraphy. *SEPM Concepts in Sedimentology and Paleontology*, **8**. 199pp.

Sobreira, J.F.F. and **França, R.L.** (2006) Um modelo tectono-magmático para a região do Complexo Vulcânico de Abrolhos. *Bol. Geoci. Petrobras*, **14**, 143–147.

Tager, D., Webster, J.M., Potts, D.C., Renema, W., Braga, J.C. and **Pandolfi, J.M.** (2010) Community dynamics of Pleistocene coral reefs during alternative climatic regimes. *Ecology*, **91**, 191–200.

Teixeira, C.D., Leitão, R.L.L., Ribeiro, F.V., Moraes, F.C., Neves, L.M., Bastos, A.C., Pereira-Filho, G.H., Kampel, M., Salomon, P.S., Sá, João A, Falsarella, L.N., Amario, M., Abieri, M.L., Pereira, R.C., Amado-Filho, G.M. and **Moura, R.L.** (2019) Sustained mass coral bleaching (2016–2017) in Brazilian turbid-zone reefs: taxonomic, cross-shelf and habitat-related trends. *Coral Reefs,* **38**, 801–813.

Toscano, M.A. and **Macintyre, I.G.** (2003) Corrected western Atlantic sea-level curve for the last 11,000 years based on calibrated 14C dates from *Acropora palmata* framework and intertidal mangrove peat. *Coral Reefs,* **22**, 257–270.

Walker, M.J.C., Berkelhammer, M., Björck, S., Cwynar, L.C., Fisher, D.A., Long, A.J., Lowe, J.J., Newnham, R.M., Rasmussen, S.O. and **Weiss, H.** (2012) Formal subdivision of the Holocene Series/Epoch: a Discussion Paper by a Working Group of INTIMATE (Integration of ice-core, marine and terrestrial records) and the Subcommission on Quaternary Stratigraphy (International Commission on Stratigraphy). *J. Quatern. Sci.,* **27**, 649–659.

Webster, J.M., Clague, D.A., Riker-Coleman, K., Gallup, C., Braga, J.C., Potts, D, Moore, J.G., Winterer, E.L. and **Paull, C.K.** (2004) Drowning of the –150 m reef off Hawaii: a casualty of global meltwater pulse 1A? *Geology*, **32**, 249–252.

Webster, J.M., Yokoyama, Y. and **Cotterill, C.** (2011). *Proceedings of the Integrated Ocean Drilling Program/IODP. Great Barrier Reef Environmental, Expedition 325 Scientists*, IODP, 39pp.

Woodroffe, C.D., Brooke, B.P., Linklater, M., Kennedy, D.M., Jones, B.G., Buchanan, C., Mleczko, R., Hua, Q. and **Zhao, J.** (2010) Response of coral reefs to climate change: Expansion and demise of the southernmost Pacific coral. *Geophys. Res. Lett.*, **37**, L15602, 1–6.

Woodroffe, C.D. and **Webster, J.M.** (2014) Coral reefs and sea-level change. *Mar. Geol.,* **352**, 248–267.

IAS (2022) Coral Reefs and Sea-Level Change: Quaternary Records and Modelling, 101–140

Late Pleistocene-Holocene Evolution of Malé Island (North Malé Atoll Rim, Republic of Maldives)

TUĞBA YILDIRIM[*†], ANDRÉ W. DROXLER[†], EBERHARD GISCHLER[‡], DAVID F. NAAR[§], YUSUKE YOKOYAMA[ǀ], PAOLO MONTAGNA[¶] and EDWIGE PONS-BRANCHU[a]

[*]*TPAO (Turkish Petroleum Corporation), Research and Development Center, Ankara, Turkey.*
[†]*Department of Earth, Environment and Planetary Sciences, Rice University, Houston, TX 77005, USA.*
[‡]*Institut für Geowissenschaften, J.W. Goethe-Universität, Altenhöeferallee 1, 60438 Frankfurt am Main, Germany.*
[§]*College of Marine Science, University of South Florida, St. Petersburg, FL, USA, 33701.*
[ǀ]*Atmosphere and Ocean Research Institute, University of Tokyo, Kashiwa, Japan.*
[¶]*Istituto di Scienze Polari (ISP), Consiglio Nazionale delle Ricerche (CNR) Via Gobetti 101, 40129 Bologna.*
[a]*Laboratoire des Sciences du Climat et de l'Environnement LSCE/IPSL, CEACNRS UVSQ, Université Paris-Saclay, Avenue de la Terrasse, Gif-sur-Yvette, 91198 Île-de-France, France.*

ABSTRACT

Malé, the capital of the Republic of Maldives, is established on an island of about 6.8 square kilometres, with a maximum relief of 2.7 m and a population of 236,000 inhabitants. It is amongst the most densely populated areas on Earth and located virtually at sea-level. This study focuses on the late Pleistocene-Holocene evolution of Malé island that recently formed as part of the discontinuous North Malé Atoll rim. Understanding the formation of Malé Island is relevant in predicting its future in the context of accelerating rates of sea-level rise in the next centuries due to anthropogenic global warming. Analyses of two boreholes up to 35 m-long, published information from additional boreholes drilled on Malé Island and a high-resolution multi-beam bathymetric survey acquired along its upper slopes and deep surroundings were available for this study. Two distinct sedimentary units were recovered from the boreholes. Facies analyses of the lower unit reveal an overall deepening coralgal reef that accumulated probably during the previous interglacial (Marine Isotope Stage = MIS 5e) and which was subsequently altered by meteoric diagenesis during a 100 kyr-long time of exposure. The upper unit consists of Holocene unconsolidated coralgal accumulation, unconformably overlying the lower karstified coralgal MIS 5e unit. The upper unit, protected behind a karstified late Pleistocene reef, was initiated at ~8200 yr BP and vertically grew 25 m-high until 6510 yr BP in the northern part of the Malé Island area, which at the time was a karstified limestone island with a central geomorphological depression. The narrow, 30 to 35 m-deep, newly formed central faro lagoon started to fill ~5500 yr BP, when a reef initiated on top of the southern highest Pleistocene karstified reef and sea-level rise stalled. The infilling of the faro lagoon was completed ~4500 yr BP. An island formed that was flanked on its south side by a shallow lagoon and surrounded by a reef flat. Through several phases of land reclamation since the

©2022 International Association of Sedimentologists

1950s, the shallow lagoon was infilled and the reef flat buried with sand and rubble to form Malé Island as it is known today.

Keywords: Maldives, Holocene, Pleistocene, Facies, Island Formation

INTRODUCTION

The Archipelago of the Maldives, visible in its entirety only on satellite images, stretches north-south on almost 8 degrees of latitude in the equatorial Indian Ocean, south-west of India (Fig. 1A). The archipelago consists of either a single or double chain of large and small atolls and oceanic reef platforms. Their coralgal reef rims barely reach sea level, rarely exposed as small islands forming the very tip of one of the largest Cenozoic carbonate platforms still thriving today (Fig. 2). The Maldives carbonate platform, 820 km and 130 km in length and width, respectively, grew 2 to 3 km-thick in the last 55 My on top of a subsiding exposed oceanic basaltic plateau, as the central part of the Chagos-Laccadives Ridge (Aubert & Droxler, 1992, 1996; Purdy & Bertram, 1993; Belopolsky & Droxler, 2003, 2004; Droxler & Jorry, 2021, Figs 1 and 2). The visible part of the modern Maldives platform consists of 14 large and 7 small atolls as well as 4 reef-fringed islands (Naseer & Hatcher, 2004; Gischler *et al.*, 2014; Fig. 1A). North Malé Atoll, located along the eastern chain of the archipelago, belongs to the group of larger atolls (Fig. 1B). The depths of the North Malé Atoll lagoon range between 46 and 64 m, averaging about 50 m (Droxler, 2012). This lagoon water depth range is very similar to the range observed in South Malé atoll lagoon (Betzler *et al.*, 2016a). Both North and South Malé Atoll lagoons are surrounded by a discontinuous rim that consists of several circular reefs usually less than 3 or 4 km in diameter, surrounding a shallow lagoon of depths generally less than 20 m, in the Maldives referred to as faros (Agassiz, 1902; Perry *et al.*, 2013). Some of the faro lagoons have been infilled and small islands have emerged on these platforms. The islands are unconsolidated accumulations of detrital sediments (Kench *et al.*, 2005). One of them is Malé Island (Fig. 1C).

The long-term edification of the Maldives platform was influenced first by the tectonic deformation of a subsiding, initially exposed Chagos-Laccadives volcanic plateau, part of the Island Réunion Hotspot track (Duncan *et al.*, 1990; Aubert & Droxler, 1992, 1996; Belopolsky & Droxler, 2003, 2004). Then, long term subsidence and sea-level fluctuations at different time scales, in addition to monsoon generated currents, influenced the edification of the Maldives carbonate platform (Aubert & Droxler, 1992, 1996; Belopolsky & Droxler, 2003, 2004; Betzler *et al.*, 2009, 2012, 2016 a, b, 2017; Lüdmann *et al.*, 2013, 2018; Figs 2A and 3). The morphology of the modern atolls, such as North Malé Atoll, is regarded as the ultimate late Quaternary phase of the 55 My-long platform evolution (Figs 1C and 2B), linked to its long-term exposure since the onset of the major Northern Hemisphere glaciations about 2.7 to 2.6 Ma, interrupted by successive re-floodings or submergence during short term interglacial sea-level highstands, in particular in the past 450 kyr since Marine Isotope Stage (MIS) 11 (Aubert & Droxler, 1992, 1996; Belopolsky & Droxler, 2003, 2004; Droxler *et al.*, 2011; Droxler & Jorry, 2021; Fig. 3A). This model, based on the long term evolution of the Maldives carbonate platform, is also well illustrated in a study from the smaller carbonate platform of Moruroa Atoll (Central Pacific), where a series of boreholes drilled in its lagoon and along its rim recovered, unconformably overlying a Pliocene flat-

topped platform, vertically stacked interglacial reef units spanning MIS 9 (possibly MIS 11) to MIS 1 that are individually separated by distinct exposure horizons during intervening glacial sea-level falls and lowstands (Braithwaite & Camoin, 2011; Montaggioni *et al.*, 2015; Droxler & Jorry, 2021).

In the last 130 kyr, and in the context of this model, it is expected that two short re-flooding intervals, during which coralgal sedimentation occurred, corresponding to interglacial MIS 5e and Holocene MIS 1, should be separated by a long term 80 to 100 kyr-long exposure horizon (Fig. 3B and C). In the Maldives, these two re-flooding intervals have been recovered in boreholes drilled on Rasdhoo and Baa atoll (also named Maalhosmadulu, Fig. 1A) rims where Holocene coralgal reef formation was re-initiated on top of MIS 5e positive reliefs of antecedent karstic morphologies formed during a long-term exposure interval spanning from MIS 4 to MIS 2 (Gischler *et al.*, 2008; Kench *et al.*, 2009; Fig. 3B and C). In addition to partial dissolution as the immediate results of exposure and effects on aragonite and HMC-rich metastable coralgal interglacial accumulation, specific diagenetic pathways are expected to imprint the exposed accumulation as well. Although, the Holocene successions of the Maldives western atolls, Rasdhoo and Ari Atolls, are relatively well documented by previous studies and revealed information about the Holocene facies, foraminiferal assemblages (Gischler, 2006; Gischler *et al.*, 2008; Parker & Gischler, 2010), reef growth and morphology of reef islands in the Maldives (Woodroffe, 1992; Kench *et al.*, 2005; East *et al.*, 2018; Kench *et al.*, 2020), the Pleistocene facies and diagenetic transformation of the previous interglacial accumulation is only identified by one study at Rashdoo Atoll (Gischler *et al.*, 2018).

This research focuses on the last 130 kyr-long glacial cycle evolution of Malé Island (Fig. 3B and C), a small component of the North Malé Atoll discontinuous rim (Figs 1C,D and 2B). The study attempts to demonstrate that the construction of the discontinuous North Malé Atoll rim segments, such as Malé Island, consists of intermittent short intervals of coral reef edification during peak interglacials, separated by relatively long periods of partial dissolution during glacial and subglacial exposure, in particular when sea-level fell below the average depths of North Malé Atoll lagoon (46 to 64 m). Samples from two 22 m-long and 35 m-long boreholes, drilled on Malé Island by the Environmental Research Center (ERC), are available for this study, in addition to information from additional boreholes drilled throughout the island from geotechnical surveys prior to the construction of the protection wall surrounding the island (JICA, 1992; Riyaz & Park, 2009), several high-rise pre-construction reports (Riyaz, 2007) and the data gathered after the slope failure in 2002 in the north-eastern corner of Malé Island. On a transect down the upper slope, exposed along a scar of the slope failure, some corals were picked by scuba divers for later analysis. Moreover, a detailed multi-beam bathymetric map is available for the upper slopes and deep surroundings along and adjacent to the margins of Malé Island (Rovere *et al.*, 2018; Droxler *et al.*, 2011).

Firstly, this study focuses on analysing the lower lithified sedimentary unit encountered in borehole ERC BH-01. In this unit, facies analyses should reveal information on the initial coralgal reef accumulation and characterise the potential succession of depositional environments, most probably during the previous interglacial interval MIS 5e in a segment of the North Malé Atoll rim. The diagenetic alteration of the Pleistocene deposits, in particular through meteoric diagenesis, is expected to have imprinted the

primary interglacial coralgal accumulation during the 100 kyr-long exposure triggered by a systematic sea-level fall subsequent to MIS 5e (Fig. 3B).

Secondly, the chronological evolution, based upon U/Th and radiocarbon ages, of the Holocene unlithified coral sand upper unit including fossils of corals, calcareous algae, molluscs and benthic foraminifers, unconformably overlying the lower MIS 5e coralgal rock unit, is expected to shed information on the timing of the Holocene re-flooding, the re-establishment and evolution of Malé Island itself and to a large extent the North Malé Atoll rim.

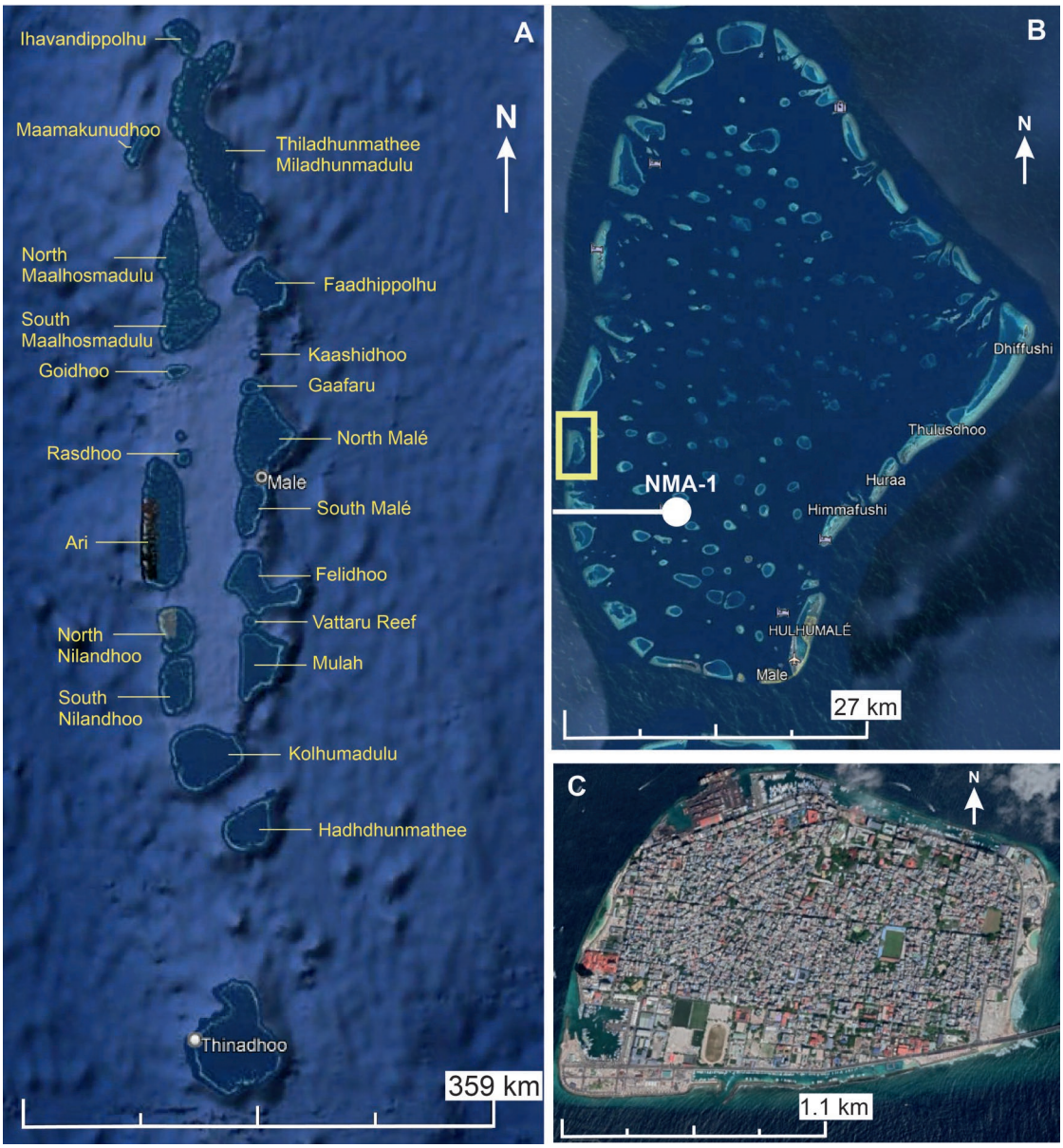


Fig. 1 A) Google Earth® image of the Maldives archipelago in which North Malé Atoll is located. B) Satellite image of North Malé Atoll showing the location of NMA-1 well; white line shows the Shell seismic profile included in Fig. 2A. Yellow rectangle locates the small atoll (faroo) part of the modern discontinuous rim that could be used as an analogue for Malé Island MIS 5e reef morphology (see Fig. 6). C) Google Earth® image of the Malé Island showing the high population density.

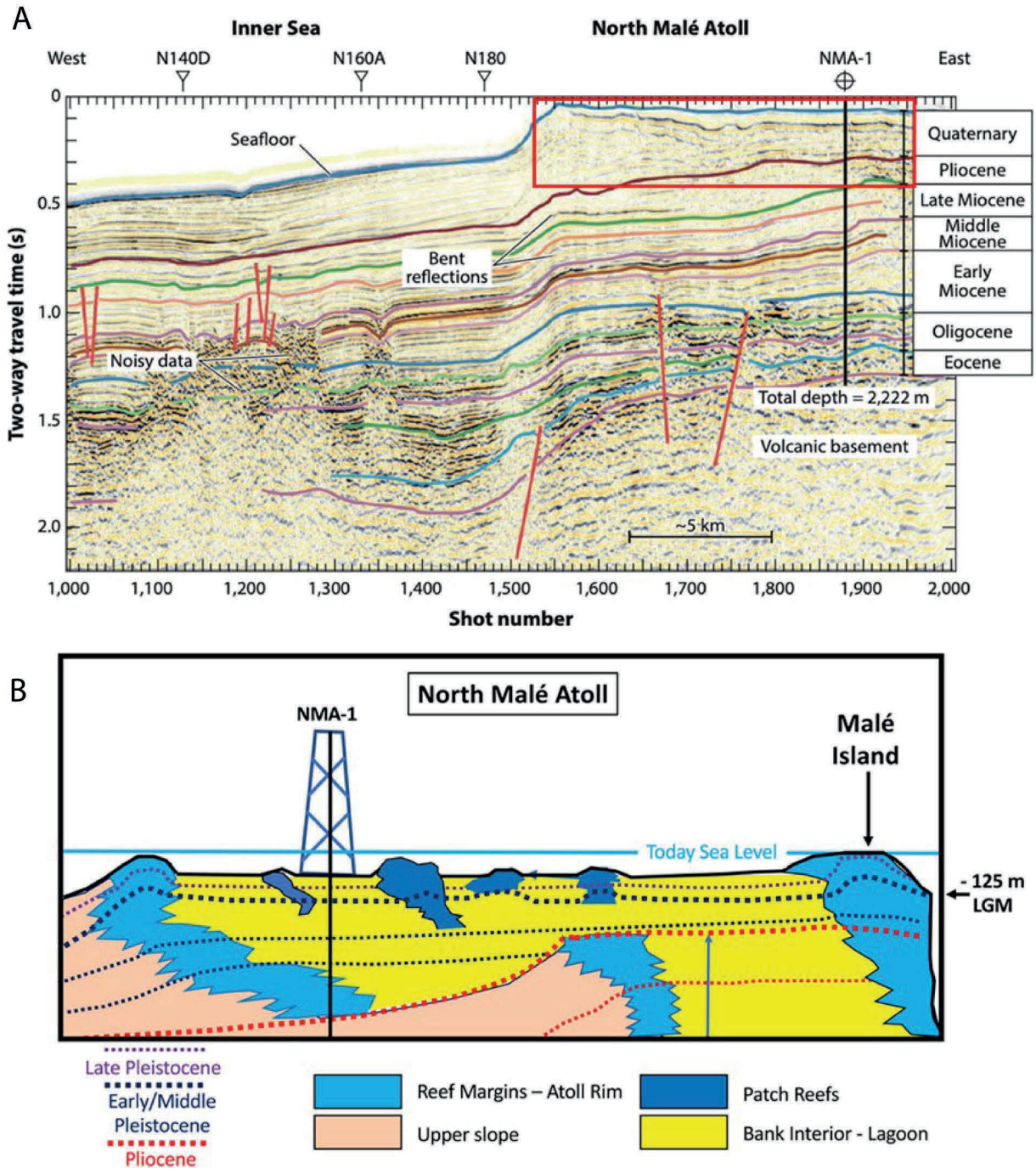


Fig. 2 A) Elf NMA-1 well, located on Shell seismic line E310NMA, was drilled in the lagoon of North Malé Atoll reaching the volcanic plateau on top of which the 2222 m-thick carbonate platform was established in the past 55 My. Red rectangle locates the illustration shown in B. B) The modern atolls are part of the last phase of the carbonate platform evolution triggered by high amplitude sea-level changes during the late Quaternary (Belopolsky & Droxler, 2004; Droxler & Jorry, 2021).

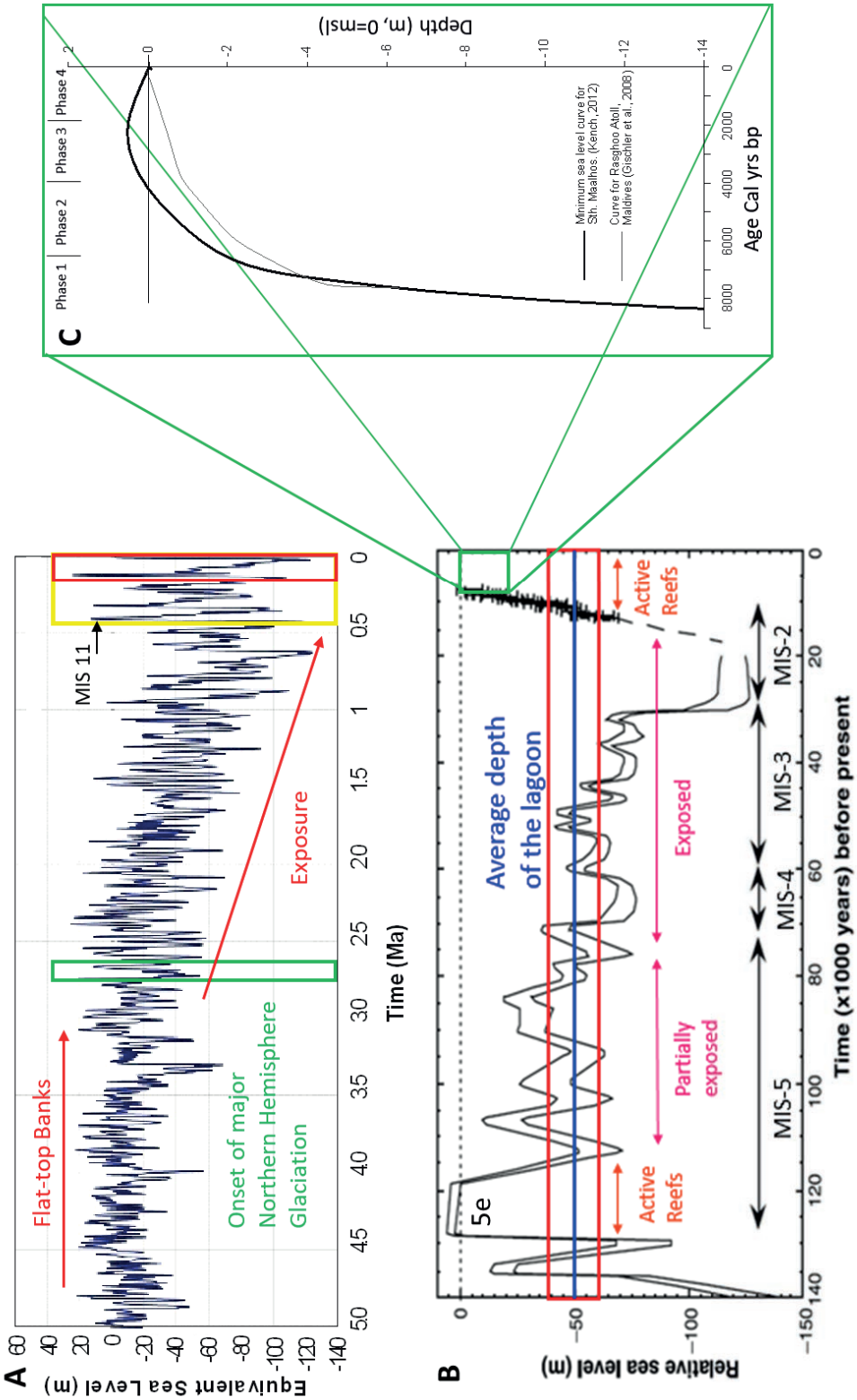


Fig. 3 A) Oxygen isotopic-based sea-level estimate for the past 5 My (Modified from Miller, 2020). Yellow rectangle shows the initiation of modern atoll development since the mid-Brunhes. Red rectangle identifies the Last Interglacial cycle shown in B. B) Sea-level history for the last full glacial cycle from interglacial Marine Isotope Stage 5e to MIS 1, Holocene (Modified from Lambeck & Chappell, 2001). **C)** Maldive sea-level curve for the last 9000 yr (Kench *et al.*, 2009).

MALDIVES GEOGRAPHICAL, CLIMATIC AND OCEANIC SETTINGS

The Maldivian Archipelago consists of 21 major circular to elongate atolls forming either a single or double chain extending from 7°06' N (Ihavandiffulu Atoll) to 0°42' S (Addu Atoll) and lies in between 72°32' E and 73°46' E with an area of over 100,000 km^2. Only an infinitesimal portion of the atoll rims are exposed and have formed small islands or sand shoals. The average elevation of the islands in the Republic of Maldives is 1.5 m above sea-level and the land surface totals 298 km^2 (Aubert & Droxler, 1996). The Maldives Inner Sea lies between the central double atoll chain (5°30' N and 2°30' N) and ranges in water depths between 200 to 600 m (Aubert & Droxler, 1992; Belopolsky & Droxler, 2004). On the oceanic oriental and occidental sides of the archipelago's large atolls, water depths reach more than 2500 m (Aubert & Droxler, 1992 and 1996; Purdy & Bertram, 1993; Belopolsky & Droxler, 2003 and 2004; Droxler & Jorry, 2021).

North Malé Atoll, located along the east central side of the archipelago, covers approximately 1565 km^2 with common lagoon depths ranging between ~46 and 64 m (Naseer & Hatcher, 2004). On its south-eastern corner, North Malé Atoll's discontinuous rim includes three main islands; Malé, Funadhoo and Hulhule Islands. Malé Island covers approximately 6.8 km^2 and, with an official population of 236,000 (Statistics Bureau, 2020), has one of the highest population densities on Earth.

Annual water temperatures range from 28° to 30°C (Gischler, 2006) and annual air temperatures oscillate between 27 to 28°C, barely affected by seasonal variation (Purdy & Bertram, 1993). The Maldives experiences a tropical and monsoon-dominated climate with two distinct monsoon seasons. The wet summer monsoon season occurs from April to November with accompanying south-westerly winds; and the dry winter monsoon season spans from December to March with north-easterly winds (Gischler, 2006; Gischler *et al.*, 2008). However, atmospheric data sets, recorded on the British Hydrographic Office Indian Ocean Routing Charts 5126-1, demonstrate that winds blow stronger and more frequently in an easterly direction. The monthly rainfall on the island averages 162.3 mm (JICA, 1992). Ocean surface currents are influenced by the monsoonal switch of the wind directions; westerlies during winter monsoons and easterlies during summer monsoons (Owen *et al.*, 2011; Fig. 4). Tidal range over Malé and nearby islands ranges from 0.3 to 0.7 m (Coleman, 2000).

MALDIVES GEOLOGICAL SETTINGS

Eocene to Pliocene evolution

The 850 km-long Maldivian Archipelago represents the ultimate growth phase of one of the largest modern Earth Cenozoic carbonate platforms. It grew in the past 55 to 57 My on a subsiding and initially exposed volcanic plateau, part of the Laccadive-Chagos aseismic submarine ridge, the expression of the Réunion Island hot spot track (Duncan *et al.*, 1990; Aubert & Droxler, 1992, 1996; Belopolsky & Droxler, 2003, 2004).

A late Paleocene–early Eocene volcanic tectonized plateau served as a foundation for the edification of a 2 to 3 km-thick carbonate platform made of neritic and upper bathyal limestone and dolostone sequences (Aubert & Droxler, 1992, 1996; Belopolsky & Droxler, 2003, 2004). The overall sequence stacking geometry in the Maldives carbonate platform was mostly influenced by sea-level variations since the early Eocene (Aubert & Droxler, 1996; Belopolsky & Droxler, 2003, 2004; Tcherepanov *et al.*, 2008). However, starting in the middle Miocene, sediment lateral transports, linked to strong monsoon-

generated ocean currents, have influenced, in addition to sea-level fluctuations, the accumulation of the Neogene sequences (Betzler *et al.*, 2009, 2012; 2016 a, b, 2017; Lüdmann *et al.*, 2013, 2018). A series of early/late Pliocene small neritic carbonate platforms in the Maldives, during a period of stable warm climate and low amplitude sea-level fluctuations, became systematically flat-top banks (Aubert & Droxler, 1996; Belopolsky & Droxler, 2003, 2004; Droxler & Jorry, 2021).

Quaternary atoll rim evolution and island formation

Due to a series of island reclamation phases that started as early as 1950, the exposed surface of Malé Island has dramatically increased to its present size (Fig. 5B). The original Malé island (about half in surface area of the current island) was originally surrounded by a shallow lagoon bounded by horseshoe shaped reef flats (Fig. 5A). However, to accommodate the increasing population on the island, some parts of the reef and lagoon were reclaimed and the topography was changed (JICA, 1992; Fig. 5B). The reclamation project by JICA (Japan International Corporation Agency) was carried out along the western and southern margins of the island (JICA, 1992).

Seismic profiles within the atolls themselves of the Maldives Archipelago, across their margins and some flat-topped drowned banks, clearly illustrate that modern atolls in the Maldives Archipelago have grown during the last 500,000 years on top of flat-topped banks (Aubert & Droxler, 1996; Belopolski & Droxler, 2003, 2004; Droxler & Jorry, 2021; Fig. 2).

After the onset of major Northern Hemisphere glaciations at about 2.7 to 2.6 Ma, sea-level fluctuation amplitudes have systematically increased and their frequencies decreased through the Quaternary, triggering long exposure intervals. As a result, the neritic carbonate system in the Maldives became highly karstified, in particular during the early Pleistocene and early Brunhes. Since the mid Brunhes (around MIS 11), and in the past approximately 450 kyr, five 100 kyr-long glacial cycles with maximum sea-level amplitude of about 120 m became well established (Miller *et al.*, 2020; Droxler & Jorry, 2021). During this last 450 kyr interval, the karstified bank top was reflooded only for 10 to 20 kyr-long intervals separated by 100 kyr long periods of exposure. It is inferred that, during the late Quaternary interval, modern atoll morphologies were formed not only in the Maldives but also worldwide (Aubert & Droxler, 1996; Droxler *et al.*, 2011; Droxler & Jorry, 2021). The Holocene reef growth in the past 10 to 8 kyr, established on top of the karstified atoll rim of the previous MIS 5e interglacial, corresponds to the last phase of four to five vertically stacked neritic limestones separated by distinct exposure horizons (Braithwaite & Camoin, 2011; Droxler & Jorry, 2021; Fig. 3).

Via U/Th, Gischler *et al.* (2008, 2018) dated karstified limestone rock samples underlying the Holocene reefs of Rasdhoo Atoll, located in the central western part of the Maldives (Fig. 1a), as between 137 and 114 kyr BP, or previous peak interglacial MIS 5e. Based on these ages and Pleistocene elevation relative to sea-level, late Quaternary subsidence was estimated to range from 90 to 160 mm kyr^{-1}. Similarly, U-series dating of limestone samples were dated from a core drilled through the current reef flat surface at South Maalhosmadulu, also known as Baa Atoll (Fig. 1A), which yielded a minimum age of 122+7.0 kyr, confirming also a last peak interglacial (Kench *et al.*, 2009; Kench, 2012). The Holocene reef growth initiation through re-flooding the top of the last MIS 5e peak interglacial, partially dissolved atoll rim through karstification, is

relatively contemporaneous within the Maldives, at least based upon two studies, 8100 kyr BP in Baa Atoll (Kench *et al.*, 2009; Kench, 2012) and 8500 kyr BP in Rasdhoo Atoll (Gischler *et al.*, 2008).

Based on the similarities among the lithologies recovered in boreholes from Malé Island, Rasdhoo and Baa Atolls, together with coral sands overlying karstified limestone, the authors assume that the evolution models developed by Gischler *et al.* (2008), Kench *et al.* (2009) and Kench (2012) are applicable to the evolution of Malé Island and can explain the rim formation of the major atolls in the Maldives Archipelago – and most probably all modern atolls around the world (Droxler & Jorry, 2021).

The north-eastern and eastern margins of Malé Island are characterised by a series of slope failures (Fig. 6B). The most recent of which occurred in 2002 (Riyaz & Park, 2009; Fig. 6B). Observations, mostly through scuba diving, following the 2002 slope failure when an important jetty in the harbor disappeared overnight, illustrated that 2~3 m-thick tightly consolidated coral rocks and rubbles on the surface were underlain by a 4~6 m-thick weakly cemented layer, loose gravel and sand in water depths ranging between ~4 to 35 m. A distinct field of large fallen reef blocks is observed at the toe of the slope in depths ranging between 30~40 m (Riyaz & Park, 2009). The collapsed parts of the reef along the upper slope of Malé Island are observed only along its north-eastern and eastern margins, exposed to the strongest tidal currents, eroding continuously along the toe of slope the weakly-cemented layers of rock, coral sand and rubble, therefore triggering failures of its upper slopes. In the area of the 2002 upper slope failure in the north-eastern corner of Malé Island, radiocarbon dating of corals exposed on the sea floor indicates rapid vertical growth (aggradation) of an 18 to 20 m-thick reef section from 8200 to 6510 yr (Riyaz & Park, 2009; Fig. 3C).

MATERIALS AND METHODS

Data sets

In order to understand the late Pleistocene-Holocene evolution of Malé Island, samples were collected from two 22 m and 35 m-long boreholes drilled across the island by the Environmental Research Center (ERC), currently the Environmental Protection Agency (EPA) of the Republic of Maldives (Fig. 5A and Table 1). ERC BH-01 was drilled in the south central part of the island at 4°10'22.21" N and 73°30'33.24" E and recovered a 22.9 m-thick section, the upper 10 m consisting of unconsolidated sediments overlying 12.90 m of carbonate rock. ERC BH-02, drilled on the north-east part of the island at 4°10'37.14" N and 73°31'6.62" E, recovered 35.45 m-long un-consolidated sediments and did not reach down to the rock surface. ERC BH-03 was drilled on the north-east of the island at 4°10'38.21" N and 73°31'4.55" E, recovering 27 m of un-consolidated sediments and 3 m-long rock samples at the base. ERC BH-04 was drilled at 4°10'38.96" N and 73°30'55.46" E, recovering 35 m, including 25.70 m of Holocene unconsolidated coral sand and 9.30 m of late Pleistocene limestone. Holiday Inn BH-02 penetrated into 24.00 m of Holocene coral sands and 26.00 m of late Pleistocene limestone. Samples were taken at 0.5 to 1 m intervals down the cores. In this research, 27 unconsolidated sediment samples and 30 rock samples from ERC BH-01 and ERC BH-03 were studied in great detail. Sample names show the core names and the depth interval of the samples taken from the core.

Additional borehole data sets were available from the JICA seawall construction project and from geotechnical reports for the Holiday Inn and Traders Hotels construction planning. Information from those projects was combined in this study. Scuba diving surveys along the western margin of Malé

Island revealed a series of notches, variable in size, occurring at depths between 5 and 15 m (JICA, 1992). In addition, many cores, drilled by JICA on the southern and western parts of Malé Island, recovered a late Pleistocene surface at 10 to 13 m below modern sea-level. However, on the north side of the island no Pleistocene limestone was recovered in the JICA boreholes as deep as 38 m (JICA, 1992; Fig. 5A). Three geotechnical boreholes were drilled in the northern central margin of Malé Island prior to the building of the 15-storey high Holiday Inn Hotel by ELS Amin International Pvt. Ltd. in September, 2006 (Fig. 5A). Riyaz (2007) documented the borehole depths and described the recovered Holocene and late Pleistocene sedimentary units. Geotechnical drilling for the preparation of the Traders Hotel building was performed by Asia Georesearch Agency Corporation Pte. Ltd (AGA) at 10 different locations in the south-eastern part of Malé Island. Core holes penetrated into 12 m-thick Holocene sediments that consist of fine to medium unconsolidated gravely to silty coral sands underlain by late Pleistocene altered limestone.

Additionally, a high resolution, multi-beam bathymetric map was acquired on the upper slopes and North Malé Atoll lagoon deep surrounding Malé Island in August 2008, using a University of South Florida (USF) Kongsberg Simrad EM 3000 (300 kHz), funded by ERC and USF. The USF survey covers the upper slopes all around Malé Island from minimum water depths of about 1 to 2 m to maximum water depths of nearly 200 m along its southern margin (Rovere *et al.*, 2018; Droxler & Jorry, 2021; Fig. 6). In addition, the survey extends about 1 km west and 600 m north of Malé Island and covers the channels separating Malé from Funadhoo and Hulhule Islands and also Malé from Villingili Islands.

Methodologies

29 late Pleistocene rock samples from ERC BH-01 were cut vertically to locate a series of 29 thin sections. The 3 x 4 cm thin sections were produced at Goethe University in Frankfurt, Germany. The thin sections were studied under a Leica petrographic microscope using a Prior J0415G point counter to quantify different components. A minimum of 300 points were counted per thin section on a two dimensional grid. Counting was performed with regard to different grain types, cements, porosity and mud. According to the chart of Van Der Plas & Tobi (1965), absolute error for each grain, cement, pore space or mud with an abundance of 50% was 6%; and with an abundance of 10% was 3.5% (N=300). To determine the different facies occurring in the late Pleistocene samples, point counting data sets were analysed via cluster analysis by running PAST software (Hammer *et al.*, 2001). Facies are classified according to Dunham's classification (1962).

Unconsolidated Holocene samples were dry-sieved in order to separate the fine (<63 μm) sediment fraction from the coarse (>63 μm) fraction. The coarse fraction was disintegrated in a buffered solution of phosphate (pH 7.5) for a day. After washing the samples over a 63 μm screen, they were left in an oven to dry. The coarse and fine fractions were weighed. In order to separate different sizes of the coarse material, dried samples were sieved through a set of three 125 μm, 500 μm and 2 mm screen sieves. The fraction between 500 μm and 2 mm in size was observed under a binocular microscope to identify the benthic foraminifer assemblages and pick a series of foraminifer tests for radiocarbon analyses.

Benthic foraminifer assemblage analysis was performed along the ERC BH-01 and ERC BH-03 cores. Foraminifers were hand-picked with a thin brush out of 27 loose sediment samples between the 0.5 and 2 mm size fraction using a binocular microscope.

At least 300 specimens were picked from each sample when possible and identified according to the different genera. Each individual foraminifer test from the various genera was counted and the data sets were standardised to obtain percentage abundance for statistical analyses. Eight *Amphistegina* tests were picked in 27 samples from ERC BH-01 and ERC BH-03. The foraminifer tests in each sample were packed in a small glass vial, mixed with methanol and cleaned in a Branson 2200 Ultrasonic Cleaner. Once cleaned, all foraminifer samples were separated in glass vials. The samples were analysed with accelerator mass spectrometry (AMS) radiocarbon dating at the Atmosphere and Ocean Research Institute, Department of Earth and Planetary Sciences, University of Tokyo, Japan. Results were calibrated with software CALIB 7.0.2 by using Marine 13 data; a reservoir correction of 132 ± 25 yr was applied as a best approximation of reservoir effect for the central Indian Ocean (Southon *et al.*, 2002; Kench *et al.*, 2005, 2009). Uranium/Thorium (U/Th) age determination was performed on two well preserved coral samples from 25 to 27 m depth of BH-03 at the University of Bologna, Italy.

The mineralogy of late Pleistocene and Holocene carbonates was determined by X-Ray Diffraction (XRD) analyses (Milliman, 1974, pp 21–29) and the relative abundance of the three main carbonate minerals, aragonite, high magnesium calcite (HMC) and low magnesium calcite (LMC), were identified. 29 late Pleistocene rock samples and one Holocene coral sample were cut and powdered with a Rocklabs crusher. 160 mg sample powders was mixed with 40 mg Corundum (Al_2O_3) powder. 2 ml of acetone was added to the powder mixture, which was homogenised with an ultrasonic bath for approximately 10 seconds. Samples were left to dry overnight. Dried powdered samples were packed into the sample holders. Samples were analysed using a PANALYTICAL X'Pert Pro at Goethe University (Frankfurt, Germany), with a Cu X-ray tube and scanning through a range of 18 to 35 degrees 2-theta. Step interval was set to 0.008 degrees 2-theta and a dwell time of 30 seconds.

Thirty unlithified Holocene samples, 5 coarse and 5 fine fractions from ERC BH-01, in addition to 10 coarse and 10 fine fractions from ERC BH-03, were powdered using a mortar and pestle. Powdered samples were analysed at Rice University with a Rigaku D/Max Ultima II Powder XRD 6s scanning the same 2-theta angle range, 18–35 degrees. Step width was set to the 0.01 degrees 2-theta and counting time of 0.5 seconds. Raw data was studied by MDI Jade 2010 Software (Material Data Inc., Livermore, CA, USA) to determine different carbonate phases considering 2-theta and d-spacing of different carbonate minerals defined by Milliman (1974). The relative weight percentages of different carbonate phases are calculated by applying Rietveld Refinement.

U/Th age determination was performed on two well preserved coral samples (99.8% aragonite) from 25 to 27 m depth of BH-03 at the Laboratoire des Sciences du Climat et de l'Environnement in Gif-sur-Yvette (France), following the analytical procedures reported in Douville *et al.* (2010) and Pons-Branchu *et al.* (2014). Briefly, Uranium and thorium isotopes were determined simultaneously using a ThermoScientific Neptune^{Plus} multi-collector-ICP-MS.

The ^{238}U-^{230}Th ages were calculated from measured atomic ratios through iterative age estimation (Ludwig & Titterington, 1994), using published ^{230}Th, ^{234}U and ^{238}U decay constants (Jaffrey *et al.*, 1971; Cheng *et al.*, 2013). Due to the high values for $^{230}Th/^{232}Th$ ratio (>3900), no correction was applied for the non-radiogenic ^{230Th} fraction. In fact, a correction for initial ^{230}Th would be minor

where a $^{230}Th/^{232}Th$ activity ratio of 20 is not exceeded (McCulloch *et al.*, 2010).

The initial $\delta^{234}U$ values for these coral samples are similar (within error) to that of modern sea water (146.8±0.1‰) (Anderson *et al.*, 2010), suggesting a 'closed-system behaviour' of the corals and reliable U-Th ages.

RESULTS

The lower Pleistocene rock unit in boreholes ERC BH-01 and ERC BH-03 is made of white, medium grained, highly fractured and porous coral limestones. The overlying Holocene sediment unit consists of fine to medium-sized sand with coral, calcareous-algal and shell fragments.

Late Pleistocene unit

Late Pleistocene top surface

Based on the multiple boreholes drilled on Malé Island, some by ERC and some for pre-building construction studies and the sea wall construction project operated by JICA, the top surface of the late Pleistocene karstified limestones was roughly determined. Fig. 6A illustrates that the depth of the late Pleistocene limestones is approximately 10 to 13 m along the south and south-west parts of the island. On the other hand, the ERC, Holiday Inn Hotel and JICA boreholes on the north part of the island recovered 25 to 30 m-thick Holocene sediments as a minimum. The top of the late Pleistocene karstified unit is recovered at a depth of 27 m in ERC BH-03 and 24 to 26 m in the Holiday Inn Hotel cores. Based upon the information gathered in the available cores, the late Pleistocene top surface on the northern part of the island is much deeper than the surface along its southern part and forms a much narrower and deeper ridge than on the southern part of the island (Fig. 6A).

Late Pleistocene highs probably occur in the vicinity of Malé island as well. Gaadhoo Koa channel, the sea floor of the deep area separating Malé to Hulhule islands, ranges in water depths from -40 to -60 m. Due to strong currents, the channel floor is chiefly devoid of loose sediments and displays irregular morphologies, including a series of fully enclosed, 20 m-deep, round to oval depressions unfilled by sediment. These resemble typical karst dissolution morphologies aligned along pre-existing fractures (Droxler, 2012; Rovere *et al.*, 2018; Fig. 6B).

Moreover, on the south-western part of the bathymetric map of Malé Island and deep surroundings, in particular along the margin of North Malé atoll, between Malé and Villingili Islands (Fig. 6A), several topographic highs rise 25 to 30 m above the surrounding lagoon floor. These late Pleistocene highs are at similar elevations as the late Pleistocene surface top under the western and southern parts of Malé Island or approximately 10 to 13 m of water depth. The reported depth of a series of notches on the western margin of the island are for the shallowest at approximately 10 m (JICA, 1992) and the deepest at about 20 to 25 m below modern sea-level (MFR, 2009; Rovere *et al.*, 2018) and may correspond to the late Pleistocene surface at 10 to 13 m and 25 m, respectively, observed in the boreholes on Malé Island.

Borehole analyses

Thin Sections: The skeletal grains of late Pleistocene rocks include aragonite-producing corals, molluscs and green algae, *Halimeda*; HMC-producing coralline algae (red algae) and echinoderms; as well as LMC-producing benthic foraminifers. Grains are strongly dissolved and altered in borehole ERC BH-01; most of the aragonite-producing grains are either dissolved or neomorphosed. Primary porosity is poorly preserved, secondary porosity is mostly moldic and vuggy. Grains are highly cemented with

blocky calcite cement (calcite spar). Epitaxial cement is rarely present around echinoderm grains. Dogtooth and meniscus cements are uncommon occurrences. None of the samples are cemented with fibrous aragonite cement. Caliche occurs in the deepest part of ERC BH-01. Micrite envelopes, outlining the former aragonite or HMC grains which were dissolved or replaced by calcite spar, are common in the deepest samples of ERC-01. All samples include mud, which frequently forms peloidal texture (Fig. 7).

Point counting analysis: The skeletal grains are composed, in order of decreasing abundance, of coralline algae, foraminifers (benthic foraminifers including encrusting forms), corals, molluscs, echinoderms and *Halimeda*. Secondary porosity is more abundant than primary porosity and reaches up to 29.33%.

The percentage distribution of individual components relative to depth in borehole ERC BH-01 show different trends (Fig. 8). The percentage abundance of aragonite-producing grains, such as corals (r = 0.62), *Halimeda* (r = 0.65) and molluscs (r = 0.27), decrease upwards in the core, whereas the abundance of LMC-producing benthic foraminifers (r = -0.54) and HMC-producing grains such as coralline algae (r = -0.3) and echinoderms (r = -0.57) increases up the core. The percentage abundance of blocky calcite cement also increases (r = -0.56) from bottom to top. On the other hand, the abundance of secondary porosity (%) shows a weak increase (r = -0.46), whereas mud content slightly decreases up the core.

Microfacies analysis: Microfacies were defined by cluster analysis according to the abundance of different grains also considering mud presence as a cement and/or sediment. Different grain percentages were compiled to run a cluster analysis which reveals 4 different microfacies:
1) Coralline algae-dominated mixed skeletal grainstone/packstone, 2) Coralline algal grainstone/packstone, 3) Coral-algal grainstone/packstone; and 4) *Halimeda* grainstone/packstone (Fig. 9).

Coralline algae-dominated mixed skeletal grainstone/packstone facies underlies the Holocene deposits and alternates with other facies in borehole ERC BH-01 (Fig. 10). The abundant grain type is coralline algae with an average abundance of 13.63%, the other constituent grains in decreasing order are foraminifers (7.66%), molluscs (3.68%), echinoderms (3.48%), corals (1.59%) and *Halimeda* (0.42%). Primary porosity is poorly preserved (1.33%) and secondary porosity is higher than in the other facies with a mean percentage abundance of 24.15%. This facies is highly cemented with calcite spar (16.52%) and mud abundance amounts to 26.35% on average (Fig. 7).

Coralline algal grainstone/packstone is dominated by coralline algae (red algae) with an average percentage abundance of 35.0%. Other grains include corals (5.0%), foraminifers (4.46%), echinoderms (2.93%); and minor contributions of *Halimeda* (0.73%) and molluscs (1.20%). Secondary porosity approximates 18.73% and grains are cemented with granular to blocky calcite cement around 13.06%. Mud presence of this facies is approximately 17.40% (Fig. 7). In addition, caliche occurs in the deeper parts of ERC BH-01, concentrated in coral-algal grainstone/packstone facies (Fig. 7)

Coral-algal grainstone/packstone facies is dominated by corals and coralline algae with a mean abundance of 11.2% and 12.83%, respectively. Other constituents include 5.36% of *Halimeda*, 4% of molluscs, 4.11% of foraminifers and 2.93% of echinoderm grains. The other characteristics of this facies is the presence of caliche averaging 11.55%, reaching up to 25.66%. Caliche is concentrated between 18.3 to 22.9 m depth in ERC BH-01. Mud percentage is 18.0% (Fig. 7).

Halimeda grainstone/packstone facies was recovered at the bottom of borehole ERC BH-01 at approximately 22.9 m depth (Fig. 10). This facies includes 32.33% of *Halimeda* as a dominant grain type with a minor amounts of corals (4.0%), coralline algae (8.33%), molluscs (5.66%), foraminifers (1.33%) and echinoderms (1.0%), on average. Primary porosity is preserved up to 11.66% and secondary porosity is 12.33%. Blocky calcite cement is the major cement type averaging 8.33%. Mud is also present at 14.33% (Fig. 7).

Carbonate mineralogy: Late Pleistocene samples in ERC BH-01, on average, consist of 95.7% LMC and 4.3% aragonite (Table 1). High percentages of aragonite in ERC BH-01 are preserved up to 30% in the deepest part of the core and decrease up the core. Aragonite occurrence also demonstrates the correlation with aragonite-producing grains such as corals and *Halimeda*, which are also abundant in the deepest parts of the ERC BH-01. On the other hand, LMC mineralogy percentages increase reaching 100% at the top of the ERC BH-01 (Fig. 10).

The mean percentages of aragonite and calcite phases of late Pleistocene facies were also calculated. *Halimeda* grainstone/packstone facies includes 30% of aragonite and 70% of LMC. Coral-algal grainstone/packstone facies includes 8.43% of aragonite and 91.57% of LMC. The shallowest facies, Coralline algae-dominated mixed grainstone/packstone facies mineralogically consists of 1.76% of aragonite and 98.24% of LMC. Coralline algal grainstone/packstone facies includes 3.36% of aragonite and 96.64% of LMC.

According to acquired knowledge from the thin section analyses, all Pleistocene samples have been strongly altered and dissolved during diagenesis. Dissolution patterns are visible in all samples and forming mostly moldic and vuggy porosity (Figs 7). Dissolution of aragonite and HMC grains were mostly followed by neomorphism, a change from metastable phases to a stable phase (Flügel, 2004: p. 70).

Holocene unit

Holocene accumulation was initiated at 10 m below sea-level (mbsl) in cores ERC BH-01 and 27 mbsl in ERC BH-03. On the contrary to the cemented and altered Pleistocene limestones, the Holocene unit includes unconsolidated, largely unaltered sediments including corals and coralline algae fragments, *Halimeda*, benthic foraminifers and molluscs. Loose Holocene sediments are white in colour and common throughout the ERC BH-01 and ERC BH-03 cores. However, the deepest two Holocene samples in borehole ERC BH-01 are slightly brownish in colour, which may be due to reworking and mixing of Holocene sediment with material from the underlying late Pleistocene unit.

Holocene carbonate mineralogy

The XRD data sets revealed that the mineralogy of the unconsolidated Holocene succession is very different from the one observed in the late Pleistocene karstified limestones. Other than the altered late Pleistocene limestones, the Holocene samples are not or only slightly altered because their carbonate mineralogy includes higher percentages of aragonite and HMC.

Holocene unlithified samples are mostly made of aragonite and HMC, with a minor amount of LMC. Ten metres of the Holocene succession in ERC BH-01 includes on average 48.42% of aragonite, 28.7% of HMC and 22.9% of LMC in fine fraction, in addition to 51.19% of aragonite, 18.73% of HMC and 29.88% of LMC in coarse fraction (Fig. 10). The Holocene succession in ERC BH-03 includes mean amounts of 69.04% of aragonite, 29.25% of HMC, 1.71% of LMC in fine fraction and 76.34% of aragonite,

23.55% of HMC and 0.11% of LMC in coarse fraction (Table 2).

Holocene benthic foraminifer assemblage analysis

Amongst the constituent grains of the Holocene unit, this study focused on the benthic foraminifera. In total, 8 different genera were identified including *Amphistegina, Calcarina, Textularia, Sorites, Heterostegina, Elphidium, Quincueloqulina* and *Spiroloculina*. The abundance data reveals two dominant genera with higher percentages; *Amphistegina* and *Calcarina* (Table 3). The entire borehole located just behind the modern active reef, ERC BH-01, includes 45.05% of *Amphistegina* and 31.56% of *Calcarina* from the narrow range of coarse fraction. Moreover, ERC BH-03, located at the north-eastern side of the island, includes 33.47% of *Amphistegina* and 44.03% of *Calcarina*. Other genera show much lower abundances in both boreholes.

The plots of the two dominant foraminifer genera in borehole ERC BH-01 show opposing trends with core depth (Fig. 12). The abundance of the *Amphistegina* genus percentages in borehole ERC BH-01 increase ($r = -0.89$), whereas the abundance of *Calcarina* genus percentages decrease up the core ($r = 0.67$). The abundance of the *Amphistegina* and *Calcarina* abundance in ERC BH-03 does not significantly vary up the core (for depth *versus* genus correlation, r value for Amhistegina: -0.52, for Calcarina: 0.14), but reciprocal dominance of these two genera for a certain depth is still noticeable (r value for two genera is -0.89).

Holocene succession and timing

Uranium/thorium dating of two coral samples, most probably faviid corals, from the deepest part of the core BH-03, at 25 and 27 mbsl, revealed ages of 7420 and 7120 cal yr BP, respectively (Table 4). Moreover, in ERC BH-03, radiocarbon dating of benthic foraminifers, overlying the interval where the coral samples were analysed for U/Th dating, revealed ages at average depths as follows: 5535 ± 88 cal yr BP at 25.23 mbsl, 5483 ± 93 cal yr BP at 13.73 mbsl, 4516 ± 114 yr at 9.23 mbsl and 718 ± 73 cal yr BP at 2.23 mbsl. Four calibrated radiocarbon ages from ERC BH-01 range between 3478 ± 88 cal yr BP at 8.48 mbsl, 4021 ± 107 cal yr BP at 5.48 mbsl, 3537 ± 93 cal yr BP at 3.98 mbsl and 1919 ± 93 cal yr BP at 2.23 mbsl (Fig. 13; Table 5).

During the 2002 upper slope failure along the north-eastern margin of Malé Island (Figs 6B and 13), exposed corals were often massive, thick branching and encrusting (Riyaz & Park, 2009). Based upon radio-carbon ages of those corals (8200 yr BP ~22 mbsl, 7640 yr BP ~18 mbsl, 7150 yr BP ~13 mbsl, 6570 yr BP ~10 mbsl and 6510 yr BP ~3 mbsl), the coralgal reef-accretion rate was calculated as 11.24 m kyr^{-1} during an 1690 year-long interval spanning from 8200 to 6510. Radiocarbon ages of benthic foraminifers in ERC BH-01 and 03 were also used to calculate sedimentation rates. Data from ERC BH-01 revealed a rate of 1.55 m kyr^{-1} in a 2102 year-long time interval from 4021 to 1919 years spanning 4 m of cores from 6 to 2 mbsl. Data from ERC BH-03 revealed much higher sedimentation rates around 16 m kyr^{-1} for a 1019 year-long interval from 5535 to 4516 years. The upper part accreted around 2 m kyr^{-1} during 3800 year-long interval from 4516 to 718 yr BP.

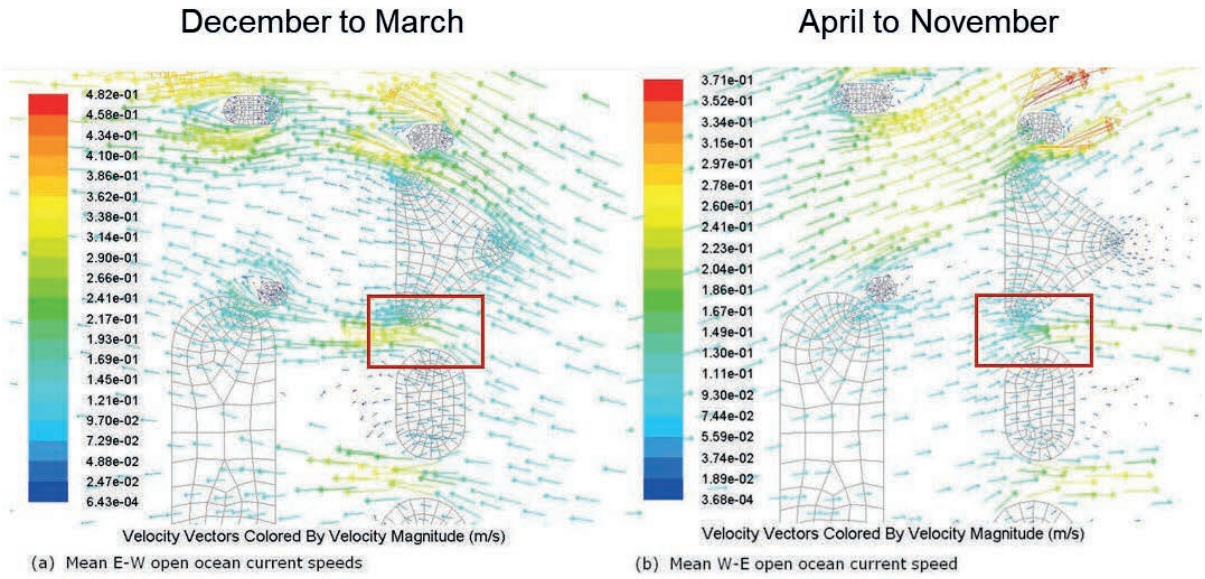


Fig. 4 Monsoonal switch of ocean current directions in the central part of the Maldives. Red rectangles locate the ocean current switch in the channel separating North Malé from South Malé Atolls, north of which Malé Island is located (Owen *et al.*, 2011).

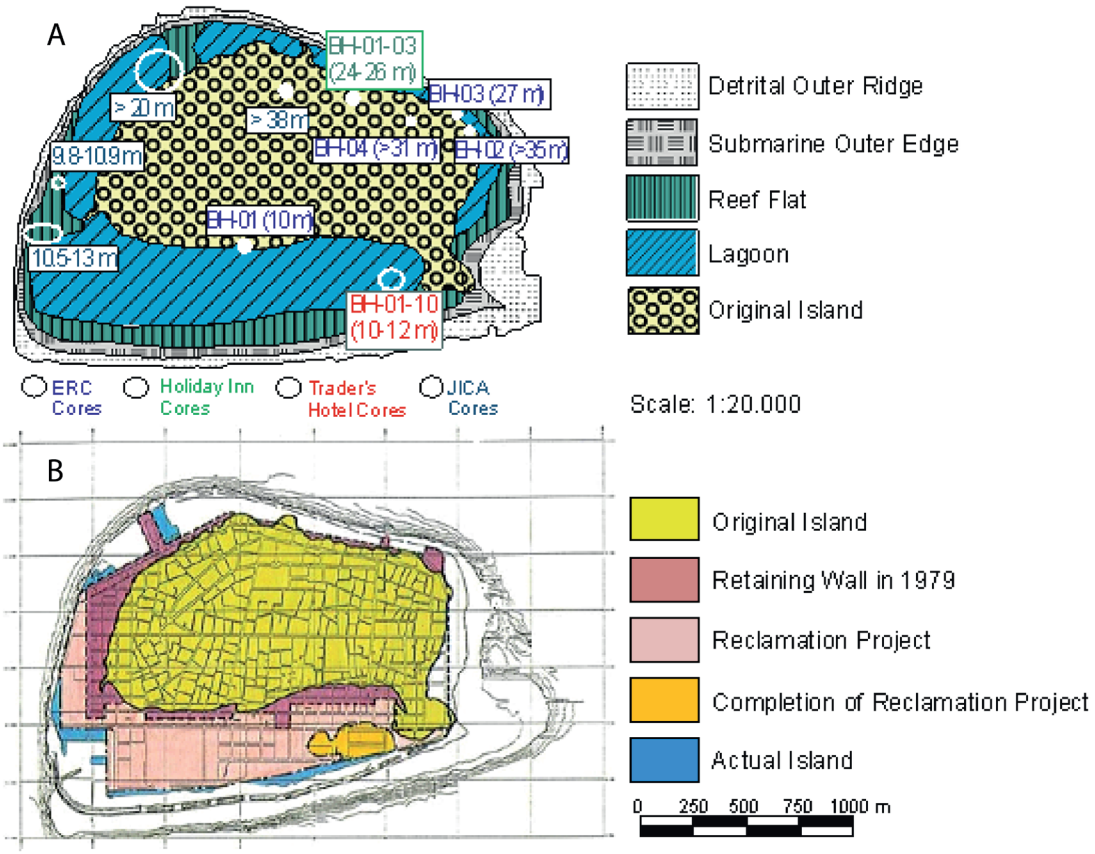


Fig. 5 A) Map showing the original physiography of Malé Island with its reef flats and lagoon prior to reclamation (Redrawn from MFR, 2009). Available boreholes drilled on Malé Island are located. Numbers beside the circles identifying core locations show the depth of the Pleistocene limestone unit top. **B)** The progress of land reclamation on Malé Island since the 1950s (Modified from JICA, 1992).

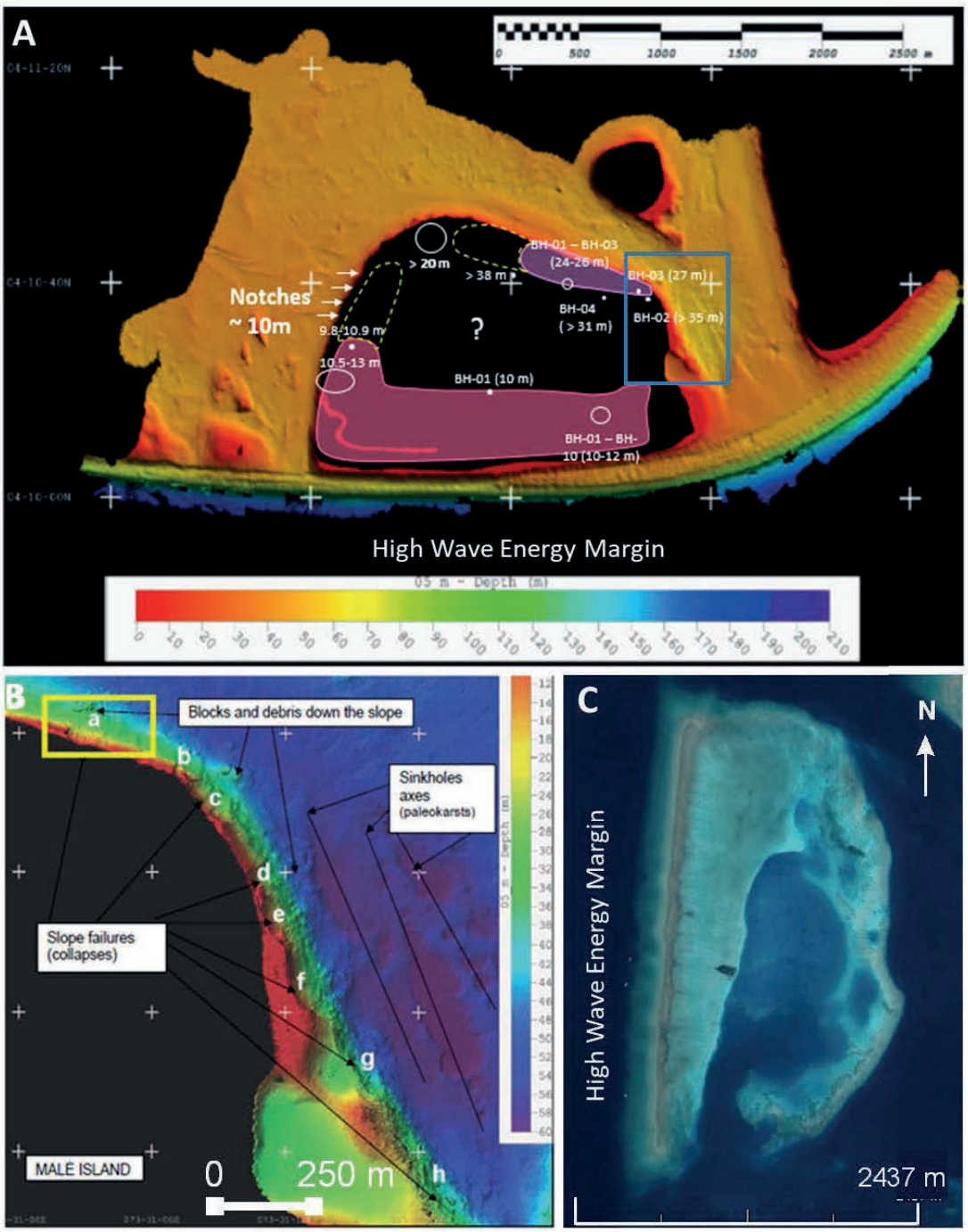


Fig. 6 A) Multi-beam bathymetric maps of the deep surroundings of Malé Island. Existing boreholes on Malé Island (Fig. 5) show the elevation of late Pleistocene karstic topography as pink shaded areas, with its possible extension in the yellow dash line areas. Blue rectangle locates the bathymetric details shown in b. B) North-eastern margin of Malé Island where eight slope failures (a to h) are clearly identified; clear karstic flooded morphologies are also observed as a series of sinkholes aligned along some fractures on the sea floor of Gaadhoo Koa channel, the deep area separating Malé and Hulhule islands. The 'a' slope failure, located in the yellow rectangle, corresponds to the February 2002 slope collapse event (Riyaz & Park, 2009). C) The Pleistocene MIS 5e morphology under Malé Island can be visualised as the small atoll (referred to as faro) shown in the figure, a part of the modern North Malé Atoll discontinuous western rim (Location of modern faro is shown in Fig. 1B).

Table 1. Microfacies of Pleistocene limestone samples derived from point counting analysis and based on cluster analysis tree diagram.

BH-01 depth (mbsl)/ sample number	Coral	Coral-line algae	Halimeda	Mollusc	Foram-inifera	Echino-derm	?	Primary porosity	Secondary porosity
Coralline algal grainstone/packstone									
10.5-11.5/2	0.66	31.33	0.33	1.66	5.33	5.66	0.66	0.33	15
10.5-11.5/3	1	40	0.33	1.33	3.66	3.33	0	0	26.66
11.5-13.4/1	4.33	24.66	0.33	0.33	6.66	2	0	1	20.33
11.5-13.4/6	6	43	2.66	2	5.33	3.66	0	1	12
16.5-18.3/3	13	36	0	0.66	1.33	0	0	1	19.66
Mean	5.00	35.00	0.73	1.20	4.46	2.93	0.13	0.67	18.73
Coral-algal grainstone/packstone									
11.5-13.4/2	9.66	15.33	0	1.33	8	2	0.66	4.66	18.33
18.3-20.1/2	12.33	5.33	4	9.33	4	0	0.66	3.33	11.33
20.1-21.9/3	5.33	18.66	5.66	4	4	0	0.66	4	23.33
20.1-21.9/4	5.66	11.33	14.66	3.33	3	1.33	1	4	16
21.9-22.9/1	11.6	12.66	1.33	0.66	1.66	0	1	1.33	10
21.9-22.9/3	23	13.66	6.66	5.33	4	1.66	0.66	4.33	17.66
Mean	11.26	12.83	5.39	4.00	4.11	0.83	0.77	3.61	16.11
Coralline algae-dominated mixed skeletal grainstone/packstone facies									
10.5-11.5/1	1	15.33	0.66	4.33	5.66	8	0	0	18.33
10.5-11.5/4	3	14.66	0	5	5.66	7	0	0	25.33
10.5-11.5/5	2	18.33	0	2.66	4.33	10.66	0	0	22.33
11.5-13.4/1	4.33	24.66	0.33	0.33	6.66	2	0	1	20.33
11.5-13.4/3	0.66	20.33	0	2.33	9.33	4.66	1	1.66	26
11.5-13.4/8	0.66	10.66	1.33	4.33	10.33	2.66	0	0.66	29.33
11.5-13.4/9	0	9.33	0	2.33	8.66	0.33	0	1	26.66
11.5-13.4/10	0	8.33	0.33	2	11.66	1.66	0.33	0	29
11.5-13.4/11	3.66	11.66	1.33	2.33	11.33	3	0.66	0.66	22
13.4-14.31/1	0	21.66	0.33	3.66	11.33	2.66	1.33	0	15
13.4-14.31/2	2.33	18	0.66	3.66	9	0.33	0.33	1.66	27.33
13.4-14.31/3	1.33	17	0	2.33	11.33	2.66	0	0.66	21.33
13.4-14.31/4	1.66	9.33	0.66	8	8.66	6.33	0.66	0.66	22.33
13.4-14.31/5	1	9.66	0.66	4.66	5	1.33	0.66	0.66	24.66
13.4-14.31/9	2	12	0	6.66	4.33	3	0.66	0	21.66
13.4-14.31/12	0.66	4.66	1.33	4.33	3.66	1.33	0.33	0.33	34
13.4-14.31/13	1.66	10.33	0	3	6	2.66	0.33	0.33	26.33
13.4-14.31/14	2.66	9.33	0	4.33	5	2.33	0.66	1.33	22.66
Mean	1.59	13.63	0.42	3.68	7.66	3.48	0.39	0.59	24.15
Haimeda grainstone/packstone									
>22.8/1	4	8.33	32.33	5.66	1.33	1	0	11.66	12.33

Granular/ blocky calcite cement	Epit-axial cement	Dog-tooth cement	Meniscus cement	Fibrous aragonite cement	Caliche	Peloidal mud	Arago-nite %	Calcite %
Coralline algal grainstone/packstone								
18.66	0.66	0	0	0	0	19.66	0.0	100.0
10.66	0.66	0	0	0	0	12.33	2.4	97.6
20	0	0	0	0	1	19.33	4.8	95.2
12	0.33	0	0	0	0	12	7.3	92.7
4	0	0	0	0	0.66	23.66	2.3	97.7
13.06	0.33	0.00	0.00	0.00	0.33	17.40	3.36	96.64
Coral-algal grainstone/packstone								
18.66	0	0	0	0	0.66	20.66	0.0	100.0
4.33	0	0	0	0	10.33	35	6.9	93.1
10.66	0	0	0	0	5.66	18	6.0	94.0
9	0	0	0	0	25.66	5	10.3	89.7
17.33	0	0	0	0	25.33	17	19.3	80.7
9	0	0	0	0	1.66	12.33	8.1	91.9
11.50	0.00	0.00	0.00	0.00	11.55	18.00	8.43	91.57
Coralline algae-dominated mixed skeletal grainstone/packstone facies								
23.66	0	0	0	0	2.66	20.33	0.0	100.0
21.33	2	0	0	0	0	16	2.2	97.8
20.66	1	0	0	0	0	18	2.5	97.5
20	0	0	0	0	1	19.33	4.8	95.2
13	0	0	0	0	1	20	0.0	100.0
14	0	0	0	0	0	26	2.0	98.0
25	0	0	0	0	7	19.66	2.2	97.8
18	0.33	0.33	0	0	0.33	27.66	0.0	100.0
18	1	0	0	0	1	23.33	2.4	97.6
18.33	0.33	0	0	0	1.33	24	1.9	98.1
9	0	0	0	0	1.33	26.33	4.8	95.2
9	0	0	0	0	1	33.33	0.0	100.0
18.66	2.66	0	0	0	0	20.33	2.2	97.8
18.33	0.33	0	0	0	0.66	32.33	2.2	97.8
12	0.33	0		0	0	37.33	0.0	100.0
11.66	0	0	0	0	0	37.66	2.5	97.5
9	0	0	0	0	0.33	40	0.0	100.0
17.66	0.33	0.33	0	0	0.66	32.66	2.1	97.9
16.52	0.46	0.04	0.00	0.00	1.02	26.35	1.76	98.24
Haimeda grainstone/packstone								
8.33	0	0	0	0	0.66	14.33	30.0	70.0

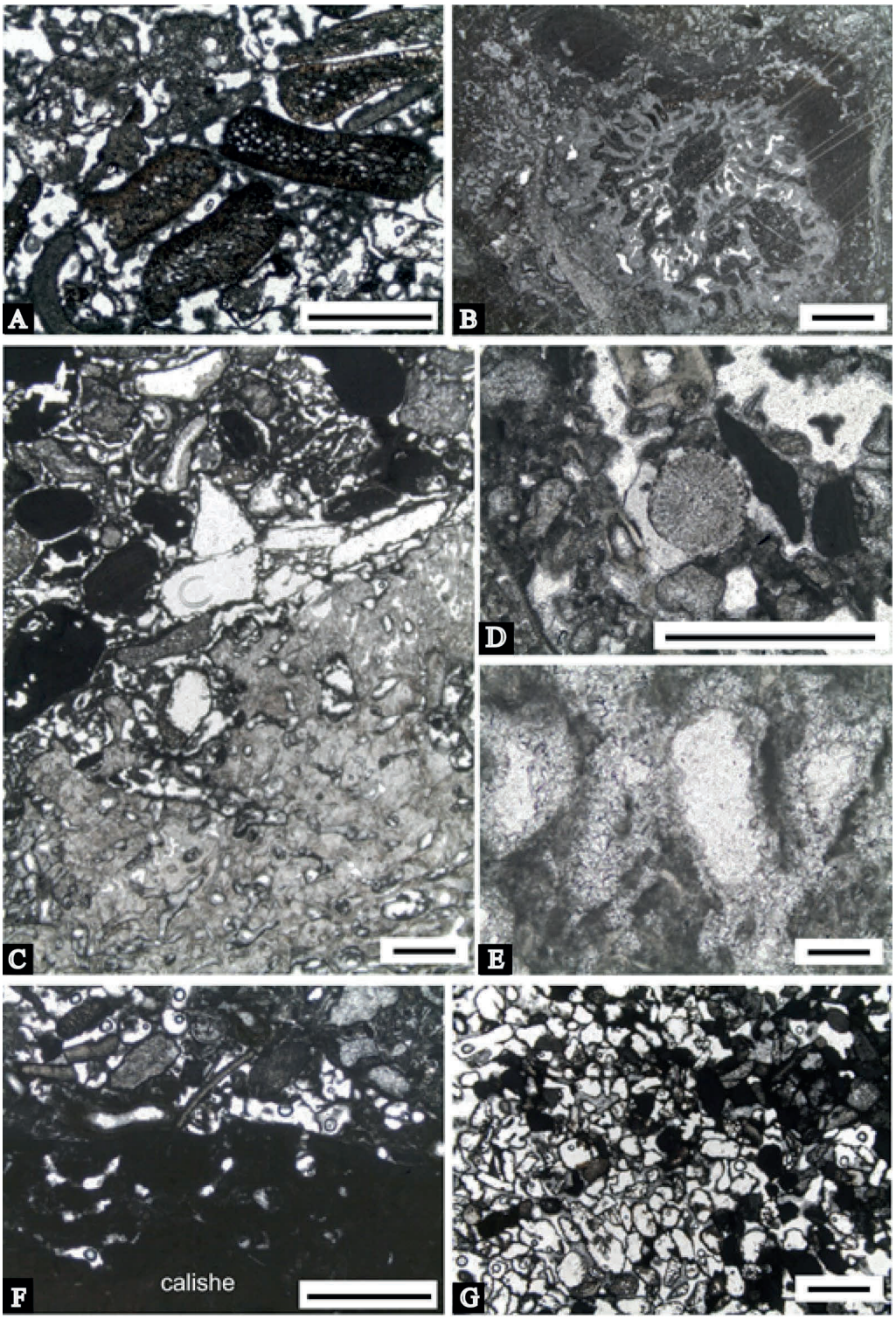


Fig. 7 Thin section micrographs of Pleistocene limestones from ERC BH-01 showing particular features under plain light (Scale bar is 1 mm) A) *Halimeda* grainstone/packstone, depth >22.8 mbsl. B) Coralline algal grainstone/packstone depth 10.5 to 11.5 mbsl. C) Coral-algal grainstone/packstone, depth 21.9 to 22.9 mbsl. D) Echinoderm with epitaxial cement in the middle, 10.5 to 11.5 mbsl. E) Moldic porosity, blocky calcite cement and mud, 11.5 to 13.4 mbsl. F) Caliche formation, 20.1 to 21.9 mbsl. G) Coralline algae fragments and numerous molds of dissolved grains with micrite envelopes, 20.1 to 21.9 mbsl.

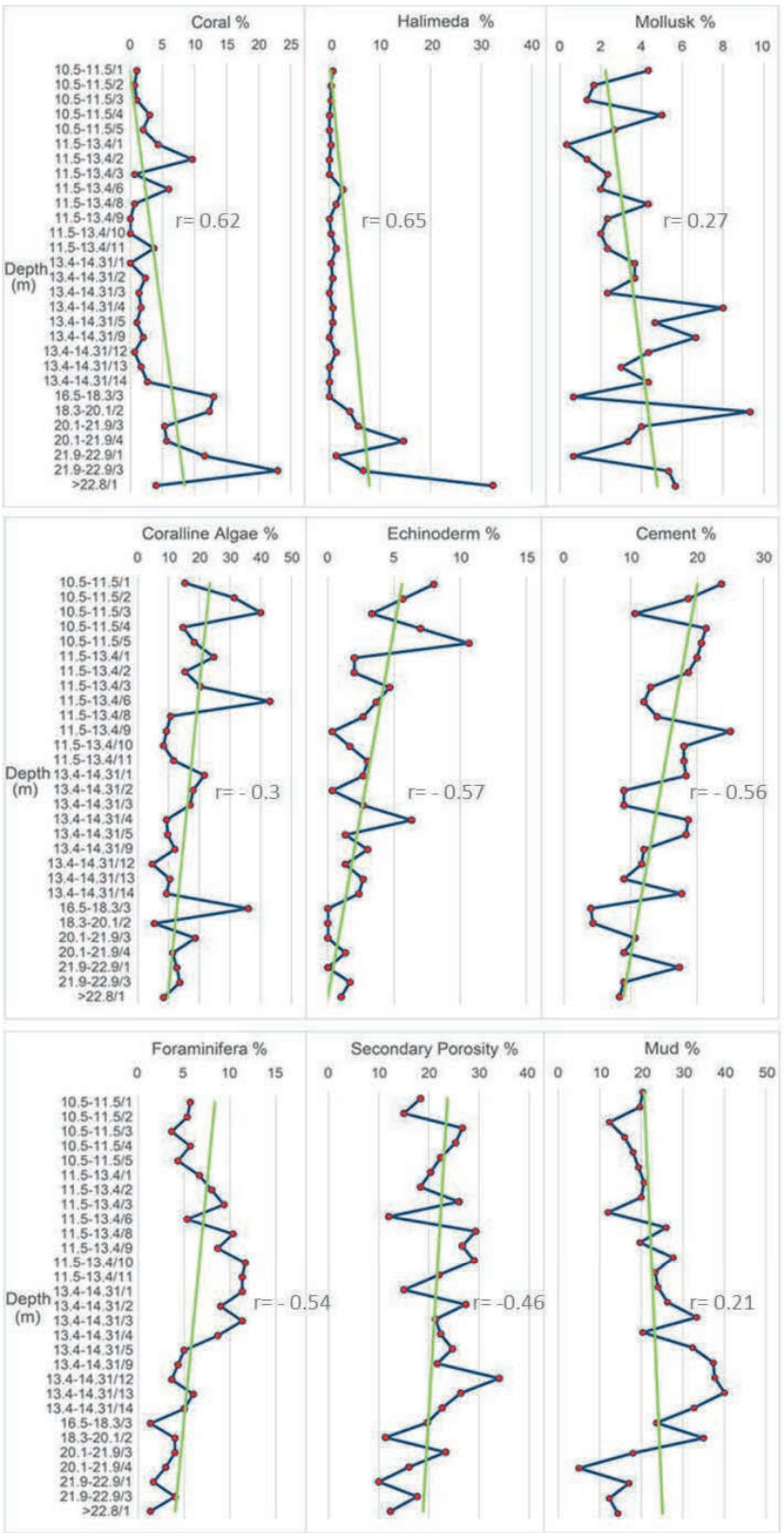


Fig. 8 Plots of point counting analysis. Plots show the percentage distribution of components in relation with depth (Numbers after slash symbol refers to different samples ordered with depth. Green lines are linear trend lines).

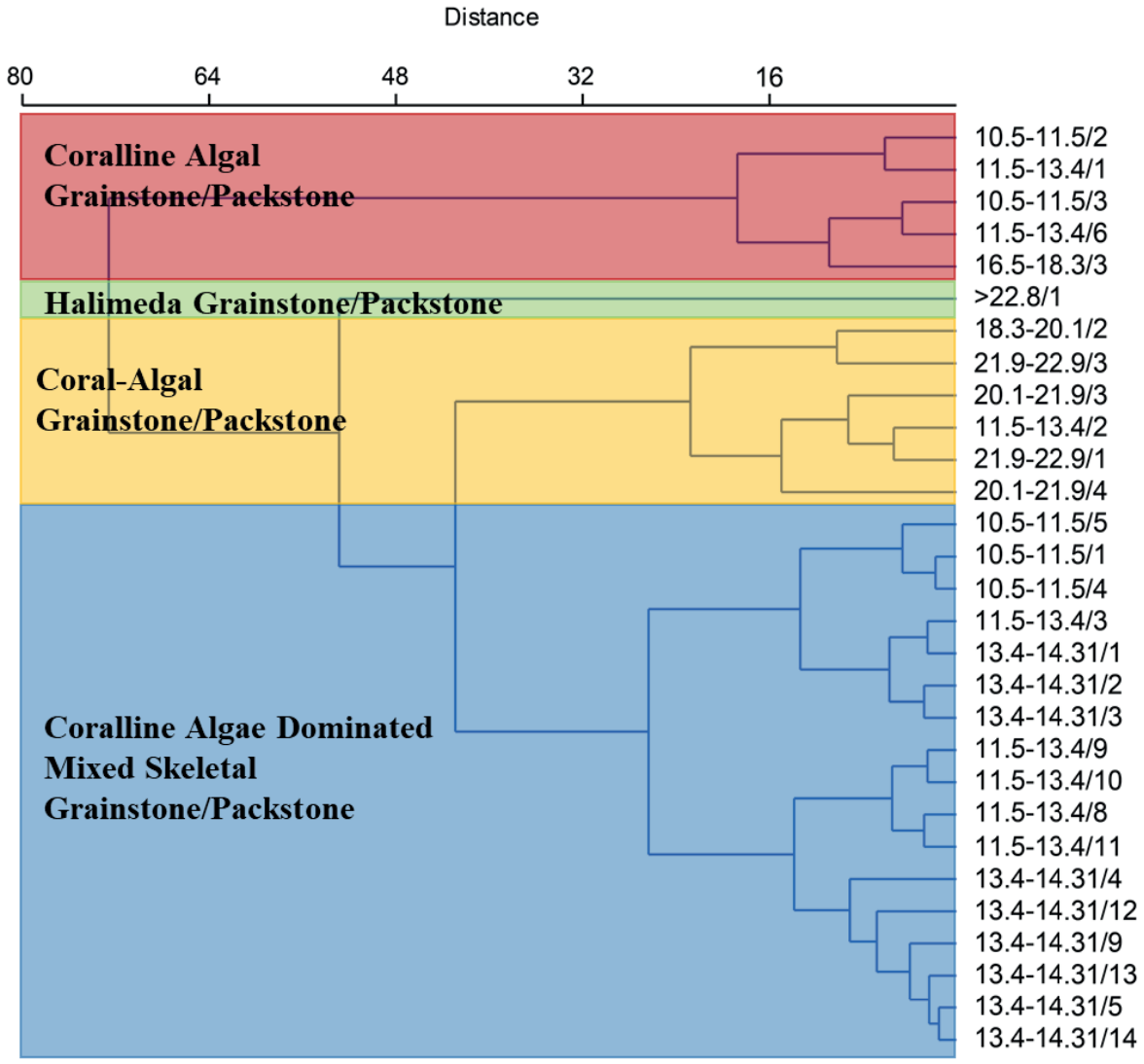


Fig. 9 Tree diagram of cluster analysis produced by the PAST software based on different skeletal grains including coral, red algae, mollusc, foraminifer, echinoderm and *Halimeda.* (Ward's method).

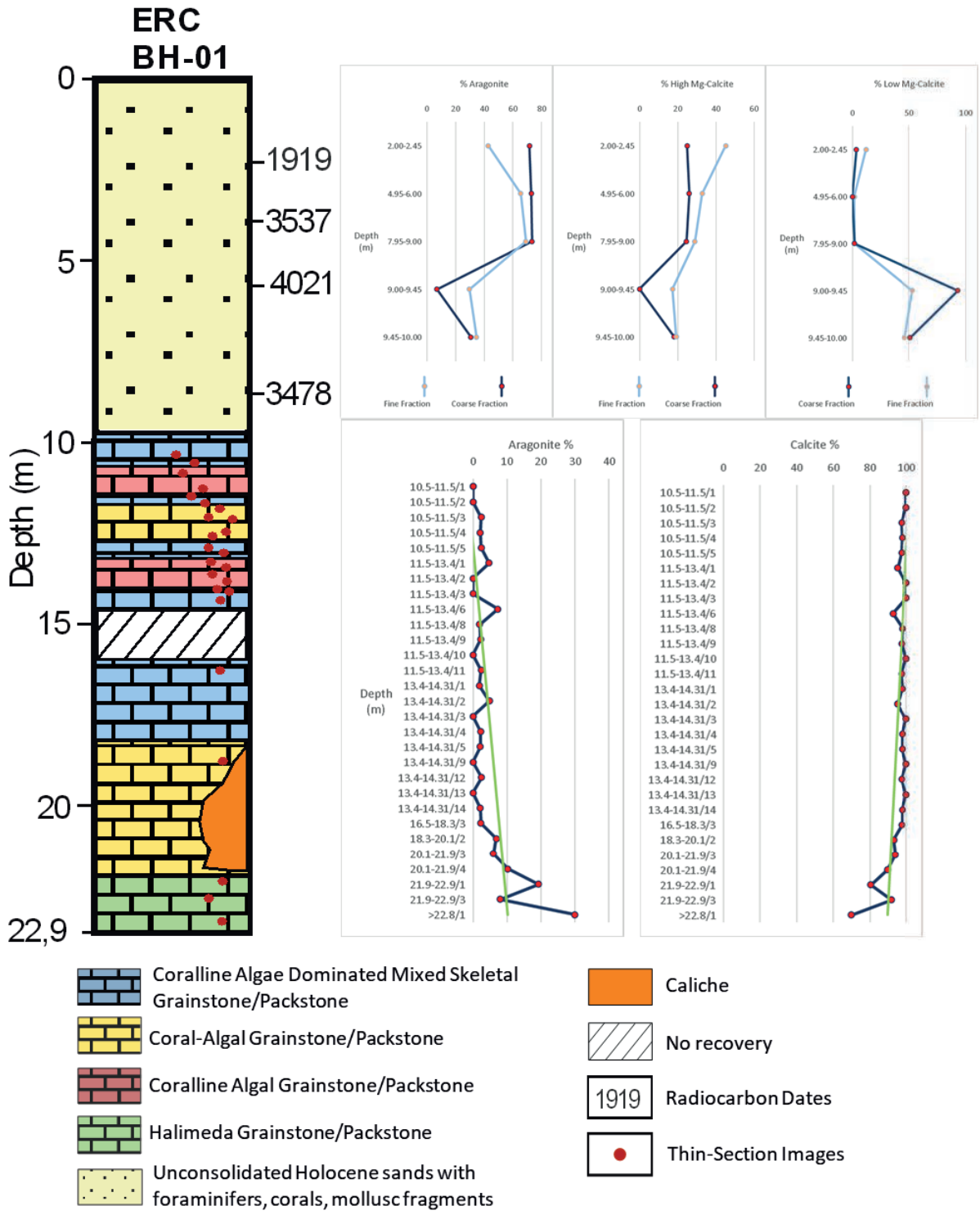


Fig. 10 Stratigraphic column of core ERC BH-01 illustrating late Pleistocene and Holocene deposits in relation with depth. Late Pleistocene facies are overlaid by unconsolidated Holocene deposits. Graphs show the Holocene and Pleistocene mineralogy of ERC BH-01, respectively. Radiocarbon ages (cal yr BP) of the Holocene samples are also shown.

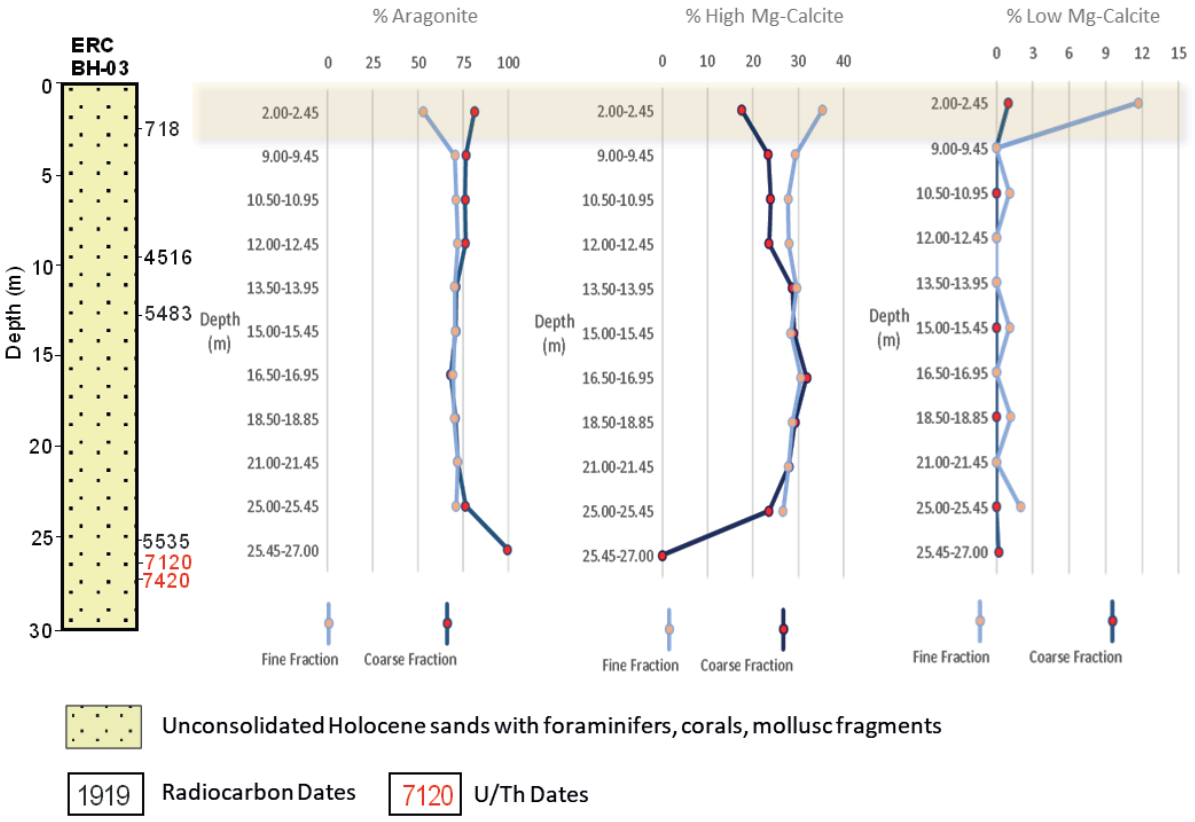


Fig. 11 Graphs showing the mineralogy of both fine and coarse fractions from BH-03 down the borehole. Shaded levels point to the relatively altered top sample, probably affected by infilling of older material during island reclamation. Radiocarbon and U/Th dates in cal yr BP are included to add a chronology to the observed trends on the right side of the figure.

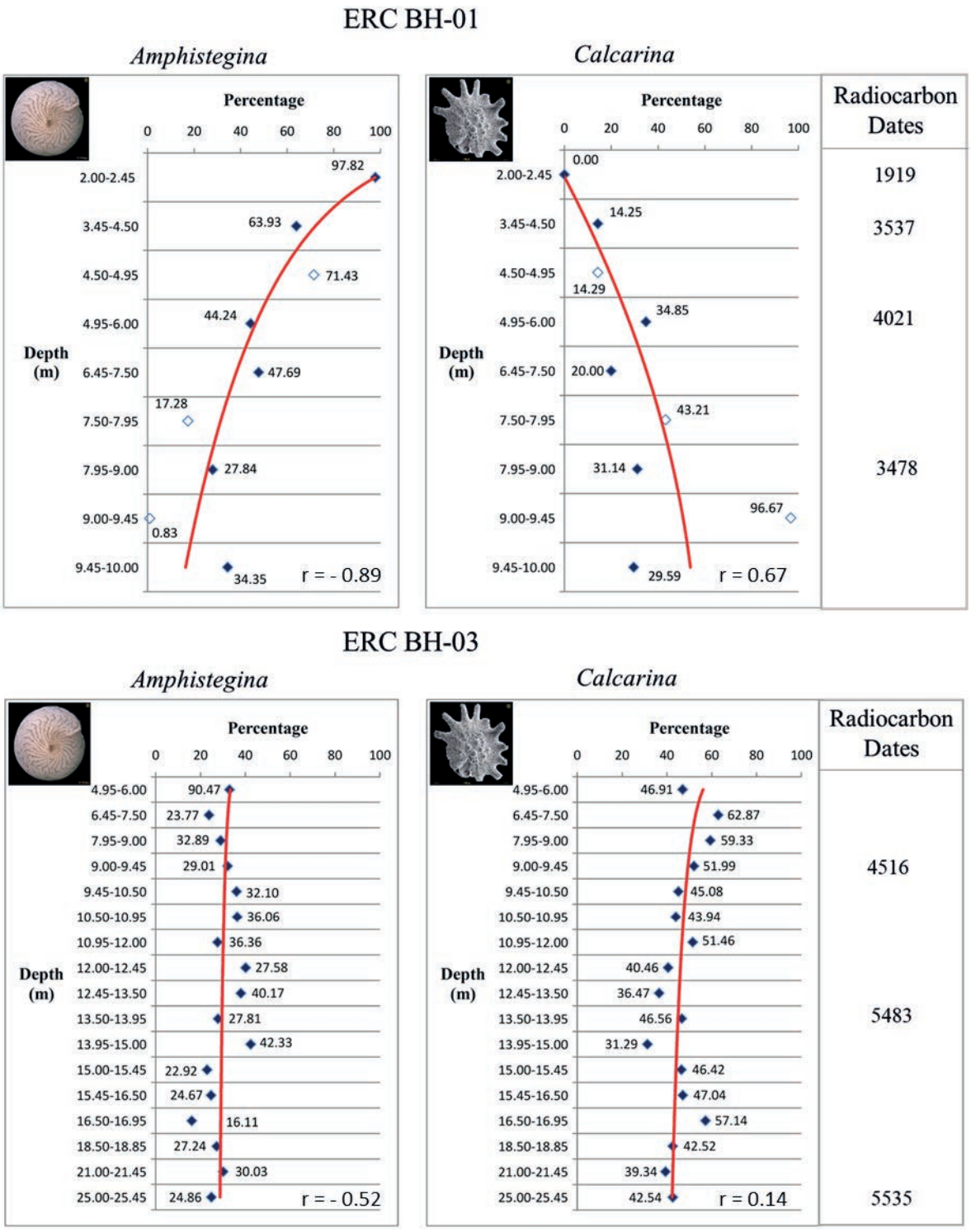


Fig. 12 Abundance and depth relation of two dominant benthic foraminifer genera in ERC BH-01 and ERC BH-03. Empty diamonds refer to foraminifer counts less than 300 (Foraminifer images from www.foraminifera.eu[3]). Radiocarbon dates in cal yr BP are included to add a chronology to the observed trends. Filled diamonds refer to samples more than 300 counts, unfilled diamonds are the samples which have less than 300 counts).

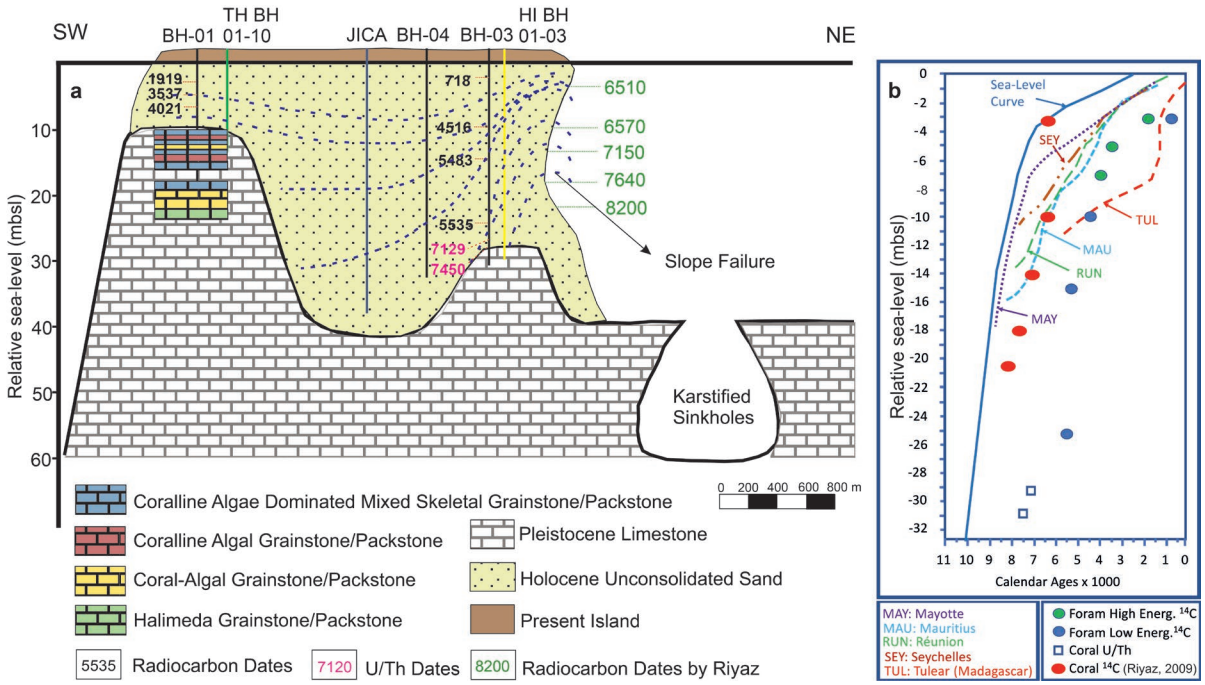


Fig. 13 A) Conceptual model along a south-west to north-east transect across Malé Island (for borehole locations refer to Fig. 5A), along with three ERC boreholes. Additional boreholes are projected on a transect (TH: Trader's Hotel, HI: Holiday Inn; JICA: Japan International Cooperation Agency). Existing radiocarbon dates from the area of the 2002 upper slope failure are shown in green (Riyaz, 2007; Riyaz & Park, 2009). The results from this study of coral U/Th ages (in pink) and benthic foraminifer radiocarbon ages (in black) were plotted. Interpreted Holocene architecture is drawn by blue isochrones. B) Flooding history above the Pleistocene topography under Malé Island is illustrated based on a sea-level curve for the last 10 kyr (Modified from Kench *et al.*, 2009), extended to about 30 kyr ago based on Zinke *et al.*, 2005. Note the vertical dimension in B is about 2X the vertical dimension in A. The dated samples of corals and benthic foraminifers, analysed in this study, at different core depths along Malé Island boreholes and slope transect along the scare of a slope failure (Riyaz, 2007), are plotted in Fig. 13B. The figure offers a comparison with Holocene sea-level curves for the Western Indian Ocean. Reconstructed reef-growth curves (dashed lines) based on boreholes from Mayotte, Mauritius, Reunion, Mahé (Seychelles) and Tulear (Toliara), Madagascar and the inferred sea-level curve (full line; see text for references). Synthetic sea-level curve reconstructed from the data obtained in Mayotte Island, including submersible surveys, reef and lagoon drilling (modified from Zinke *et al.* 2005).

DISCUSSION

Facies and diagenesis

Analyses of boreholes scattered across Malé Island demonstrate that the late Pleistocene rim of North Malé Atoll, at the location of the modern Malé Island, is asymmetrical, broader and shallower in the southern and south-western side the Island, then relatively deeper and narrower in the northern part of the island. The late Pleistocene, most probably MIS 5e, topography can be visualised as a small atoll, often referred to as a faro (Agassiz, 1902), analogous to the faro illustrated in Fig. 6C, a part of the modern North Malé Atoll discontinuous western rim (Fig. 1B). On the bathymetric map of Malé Island, between Malé and Hulhule Islands, irregular morphologies, such as 20 m-deep unfilled round to oval depressions reaching as deep as 60 mbsl, are typical karst dissolution morphologies aligned along pre-existing fractures. They were formed during

successive exposures of Malé Island and North Malé atoll and are linked to intervals of sea-level lowstands below the atoll margin. Moreover, positive geomorphological reliefs 25 to 30 m, a few of them 10 m, above the surrounding lagoon floor of Malé Island are visible on the south-western part of the bathymetric map. These are interpreted as karstic towers and potentially represent late Pleistocene, partially dissolved MIS-5e patch reefs, on top of which live coralgal reefs are thriving (Fig. 6A; Rovere *et al.*, 2018). The Pleistocene MIS 5e morphology under Malé Island can be visualised as the small faro shown in the Fig. 6C, a part of the modern North Malé Atoll discontinuous western rim (Fig. 1B). The late Pleistocene surface under Malé Island is analogous to the surface underlying Rasdhoo Atoll, displaying a similar asymmetry; shallower in the western part facing the open ocean and, therefore, high energy conditions and deeper along the northern, southern and eastern margins (Gischler *et al.*, 2008).

Pleistocene facies identified in this study show similarities with the facies identified by Gischler *et al.* (2018) at Rashdoo Atoll. In their study, facies are also grain-supported and include coral, coralline algae, *Halimeda* and benthic foraminifers. Likewise, Pleistocene facies of Malé Island seem to have counterparts in the Indo-Pacific region (Woodroffe *et al.*, 1991; Montaggioni, 2005; Dutton *et al.*, 2015). Similarly, coralline algal facies are dominant in windward reef crests and reef flats; coral facies are highly encrusted by crustose corallines and bored by sponges. On the other hand, *Halimeda*-rich facies are identified also in Indo-Pacific lagoonal environments (Montaggioni, 2005). *Halimeda*-rich mollusc wackestones were recovered in Pleistocene Belize (Atlantic) lagoonal patch reef cores as well (Gischler, 2007). The trends of skeletal grains acquired by point-counting analysis shows that facies including coral and *Halimeda* are present at the bottom part of the ERC BH-01 and they are almost absent at the uppermost parts of the borehole (Figs 8 and 10). Instead of coral and green algae comprising facies, the facies turn into coralline algae-dominated facies up the core ERC BH-01 (Fig. 10). Change in the dominance of grain types may be explained by a change in water depth or by a change in circulation,. Coralline algae could indicate a relatively deep water setting in the deepest parts of the photic zone where the light is reduced (Coleman, 2000, p. xiii). The same author also explains that the green algae, *Halimeda*, favours the maximum light in the photic zone, in other words, it prefers the shallowest depths. Therefore, the dominance of *Halimeda* and corals in the bottom of ERC BH-01 and the dominance of coralline algae facies in the upper parts of the borehole may be reflecting a deepening upward sequence (Fig. 10). A taxonomic identification of the coralline algae involved would be necessary to validate this assumption. Alternatively, the described facies change could indicate a transition from conditions of restricted to more open circulation. In the western Atlantic, atoll lagoons with restricted water circulation are commonly densely populated by *Halimeda* (Milliman, 1974; Gischler & Lomando, 1999). Finally, caliche is interpreted as a sign of subaerial exposure and the occurrence of caliche might correspond to a transition between two vertically stacked interglacial highstand facies (Braithwaite & Camoin, 2011). The presence of caliche in the deepest parts of ERC BH-01 may imply such a transition from one interglacial facies to another or at least two depositional, suborbital phases during the late Pleistocene interglacial, MIS-5e? (Thompson & Goldstein, 2005).

As the origin of mud has been an issue for carbonate sedimentologists for a long time, in this study both origins of mud as a cement and sediment were considered and facies were identified in this context as grain-

stone/packstone facies (Fig. 9). Facies analyses revealed that Pleistocene facies are grain-supported and largely include skeletal grains; in cases they contain mud. Therefore, the authors' observations herein support the contention of deposition in high-energy environments, regulated by the monsoons (Aubert & Droxler, 2006; Belopolsky & Droxler, 2004; Betzler *et al.*, 2009, 2012, 2016b, 2017; Lüdmann *et al.*, 2013, 2018). Diagenetic patterns of the Pleistocene facies in this study include cementation in the meteoric environment during approximately 100 kyr exposure since the dominant cement type is blocky calcite spar, which typically forms in the meteoric phreatic environment (Longman, 1980; Fig. 7). Aragonite cement is also defined by the same author as a sign of marine diagenesis; however, none of the rocks are cemented with aragonite needles. Micrite envelopes are conspicuous mostly in the deeper part of the borehole around former aragonite and HMC grains that have been dissolved or recrystallised to calcite (Fig. 7). This distribution is probably not a real trend, but rather an observational artefact.

Since aragonite and HMC are metastable minerals (Flügel 2004: p. 70), the XRD analyses of the Pleistocene facies also demonstrate the diagenetic alteration during the ~100 kyr-long (MIS 5d-MIS 2) exposure (Fig. 10). As aragonite mineralogy is poorly preserved, it can be concluded that the Pleistocene facies have been mostly dissolved or neomorphosed; the absence of HMC mineralogy is easily explained through dissolution and recrystallisation. In borehole ERC BH-01 LMC percentage is very high throughout all the Pleistocene facies and increases up core ERC BH-01 due to the closer proximity of meteoritic fluids in the upper part of the late Pleistocene sequence (Fig. 10). The absence of aragonite marine cementation demonstrates that the Pleistocene facies were either not affected by marine diagenesis or the marine diagenetic products were largely removed in the meteoric realm. Therefore, diagenetic diversity of the late Pleistocene at Malé Island is relatively low, especially when compared with the diagenetic diversity from other similar late Pleistocene facies such as the ones in Belize (Gischler, 2007), French Polynesia (Braithwaite & Camoin, 2011) and the Great Barrier Reef (Gischler *et al.*, 2013).

The Holocene samples under Malé Island are very different when compared with the underlying late Pleistocene limestones. Rather than being altered and cemented limestones, Holocene samples include unconsolidated coral sands with skeletal grains. The lack of cementation in Holocene deposits is explained by relatively rapid rise in sea-level, which probably resulted in limited time available for cementation (Gischler *et al.*, 2008). The graphs on Figs 10 and 11 show that aragonite and HMC are the dominant minerologies in ERC BH-01 and ERC BH-03. The oldest Holocene samples in ERC BH-01 were most probably affected through contamination by the underlying altered sediments below 9 m. The XRD results show that this particular Holocene sample is not well preserved because the aragonite and HMC percentages are lower than in the other Holocene samples (Fig. 10). Mixing and reworking of sediments at the north-eastern side of the island might have occurred due to either strong currents or bioturbation that could explain the age reversal (3478 yr BP) for the sample between 7.95 and 9.00 mbsl in ERC BH-01. This age is considered unreliable. In addition, the mineralogy of ERC BH-03 is relatively constant through the borehole; however, the shallowest sample includes higher amounts of LMC (Fig. 11). Dating analysis also revealed a relatively young age (718 yr BP) for the top sample of the ERC BH-03, which might have been affected by infilling with modern material during the island reclamation project.

Model of Malé Island accretion

Fig. 13 illustrates that the Holocene deposition was established on top of karstified Pleistocene limestones, which were probably deposited during MIS 5e. Late Pleistocene reef elevation some 10 to 30 m below modern sea-level would indicate subsidence rates in the range of approximately 0.08 to 0.24 m kyr^{-1}, i.e. in the same order of magnitude of previously calculated rates (Gischler *et al.*, 2018). Coral U/Th-ages and radiocarbon dates of foraminifers are included in the figure along with drawn interpreted isochrones. Holocene reefs under Malé Island grew using the antecedent Pleistocene topography as substratum and also as a protection. Firstly, the Holocene reef initiation occurred along the northern side of the Malé Island around 8200yr BP and vertically aggraded until 6510 yr BP (Riyaz & Park, 2009), creating a relatively deep, narrow and partially enclosed lagoon between the Holocene coral reef and the Pleistocene reef remnant along the southern margin of North Malé atoll. The Holocene reef accretion rate is calculated as 11.24 m kyr^{-1} between 8200 to 6510 yr BP from the coral ages analysed by Riyaz & Park (2009). Gischler *et al.* (2008) calculated even faster accretion rates from Rasdhoo Atoll, even higher than 15 m kyr^{-1} from 8500 to 7500 yr BP with a sudden decrease to 2 m kyr^{-1} from 7500 to 6000 yr BP. Since 6 kyr ago, when sea-level rise stalled or continued to slowly rise to present sea-level (Gischler *et al.*, 2008), reef accretion rates between 6000 to 3000 yr BP dramatically decreased in the Maldives and elsewhere in the Indo-Pacific (Montaggioni, 2005). Based upon dating corals and micro atolls by the radiocarbon method, Kench *et al.* (2009) found evidence that sea-level had risen slowly between 6000 to 4500 yr BP, even exceeding the present sea-level by about 0.5 ± 0.1 m at 2100 yr BP and then falling to its present level. A decrease in the rate of the sea-level rise caused lateral transport of reef rim-derived material into adjacent small atoll lagoons that became either fully or partially filled (Kench *et al.*, 2005; Kench, 2012; Purdy & Gischler, 2005; Gischler, 2006; Perry *et al.*, 2013; Klostermann & Gischler, 2015). It is clearly demonstrated that the late Quaternary coral reef developments from several islands in the West Indian Ocean are similar to the ones observed in the Maldives (Fig. 13B; Camoin *et al.*, 1997; Camoin *et al.*, 2004; Montaggioni & Martin-Garin in their 2020 review). The modern reefs in the West Indian Ocean initially grew from about 10,000 to 9600 yr BP with rates of vertical reef accretion ranging 0.2 to about 10 m kyr^{-1}. The sea-level curves, based on the vertical reef-accretion and lagoon-deposition in the West Indian Ocean, display, as in the Maldives, a rapid rise in sea-level at rates averaging 6 mm yr^{-1} between 10,000 and 7500 to 7000 yr BP, with a stabilisation at the present position around 2500 to 3000 yr BP (from La Réunion Island, Montaggioni, 1976; from La Réunion, Mayotte and Seychelles islands, Dullo *et al.*, 1996; from several localities in the south-western Indian Ocean, Camoin *et al.*, 1997; 2004; from Mauritius Island, Montaggioni & Faure, 1997; from Chagos Island, Eisenhauer *et al.*, 1999; a review from islands in the West Indian Ocean, Montaggioni & Martin-Garin, 2000; from the Mayotte Lagoon, Zinke *et al.*, 2005; from Mahé Island in the Seychelles, Woodroffe *et al.*, 2015; Fig. 13B).

Holocene reefs under Malé Island reached about 2 m below modern sea-level approximately 6000 years ago. The U/Th results of the oldest and deepest corals from BH-03 revealed an age of 7420 and 7120 yr, respectively. These U/Th-ages, radiocarbon dating of corals from Malé Island by Riyaz & Park (2009) and the variation in benthic foraminifer occurrence discussed below also demonstrates rapid infilling of the Malé Island Holocene lagoon with sediments shed from the northern Holocene reef, which had

grown almost to sea-level. It is obvious from the coral ages that the Holocene reef on the northern side of the island is older than the reef on the southern side.

In southern part of Malé Island, a coralgal reef established itself between 5000 and 4000 yr BP on top of a highest late Pleistocene karst remnant topography in the highest energy environment and then grew relatively slowly to present sea-level (Fig. 13). In other words, the Holocene reef on the northern side started to establish itself and grew until about 6000 years ago then, until about 4500 years ago, it shed sediments towards the centre of the faro to fill its lagoon. Once the lagoon was almost completely filled with sediment and, therefore, very shallow, the Malé island formation was initiated. Based on the radiocarbon dates from the two cores, ERC BH-01 and BH-03, it is inferred that the island formation started after 4500 yr BP as the Holocene reef started to keep up with the sea-level rise and the sedimentation rates decreased to 1.5 to 2.0 m kyr^{-1}, i.e. an order of magnitude lower than the rates of 10 to 16 m kyr^{-1} before 4500 yr. Likewise, Kench (2012) explained faro lagoon infilling at the reef islands of Baa atoll to have started during the mid-Holocene about 5000 yr BP. The results herein are consistent with the findings of Perry *et al.* (2013) who found that island formation is affected by the size of the island lagoon and its water depth because infilling time is correlated with the morphology of the island.

The dominant taxa of foraminifera picked from the Holocene samples include *Amphistegina* and *Calcarina*. They occur along with other grains, such as corals, *Halimeda*, red algae and molluscs. Previously, the species of these two genera, *Amphistegina* and *Calcarina*, were interpreted to be the characteristic of two different reef assemblages with abundant coral, *Halimeda* and red algae from Rasdhoo and Ari atolls (Parker & Gischler, 2011). This interpretation also explains the dominance of these two genera in ERC BH-01 and BH-03 boreholes from Malé Island, part of the North Malé Atoll discontinuous rim. A clear trend of two most dominant genera, increasing *Amphistegina* and decreasing *Calcarina*, can be observed in ERC BH-01 in the last 4000 yr BP. Data from core ERC BH-03 do not show particular trends between the two genera prior to 4500 yr BP, the time of lagoon infilling. As ERC BH-03 is located at the north-eastern side of Malé Island in a protected narrow deep lagoon between the late Pleistocene karstified elevated remnant of the MIS-5e reef and the newly established mid Holocene reef (Fig. 13), the fast sedimentation infilling the lagoon, approximately 16 m-thick during a 1000 yr-long period (from 5535 to 4516 yr BP), explains the lack of trend until 4500 yr BP at this site. During the last 4000 yr BP, in ERC BH-01, the two dominant genera show clear opposite trends, *Amphistegina* increases while *Calcarina* decreases up the core. Opposing trends of the most dominant foraminifer taxa might be related to changes in environmental factors, such as energy level. Fujita *et al.* (2008) concluded that *Amphistegina* species are more vulnerable to high energy environments due to weak pseudopodial attachments, whereas *Calcarina* is better adapted to high energy conditions, because of its ability to attach itself to the substratum. Therefore, trends of *Amphistegina* and *Calcarina* up the cores and their reciprocal relation throughout borehole ERC BH-01 can be explained by a slight decrease in water energy during the last 4000 years.

CONCLUSIONS

- This study was based on a series of boreholes drilled throughout Malé Island and a detailed multi-beam bathymetric map for the deep surroundings and margins of Malé Island. It tests the model that the accretion of the discontinuous North Malé Atoll rim was intermittent. Short intervals of coral reef edification during peak interglacials are separated by relatively long periods of partial dissolution during glacial and subglacial exposure, in particular when sea-level fell below the average depths of North Malé Atoll lagoon (46 to 64 m) and reached lowstands of 120 to 130 m below present sea-level (Rovere *et al.*, 2018). The late Quaternary evolution of North Malé Atoll rim was studied at the location of Malé Island where it includes two distinct sedimentary units: a lower unit made of late Pleistocene karstified coralgal limestone and an upper unit, unconformably overlying the late Pleistocene limestone, consisting of unaltered and unconsolidated Holocene sediments.
- Based on the multiple boreholes, the elevation of the top surface of the late Pleistocene limestones was estimated. The late Pleistocene rim topography can be visualised as a small atoll, often referred to as faro, comparable to a part of the modern North Malé Atoll discontinuous western rim, as an analogue. Several boreholes recovered across Malé Island showed that the top surface of late Pleistocene highstand depositions is ~10 mbsl along the southern and south-western part and >25 mbsl in the northern part of the island.
- A 12 m-thick lower late Pleistocene unit (most probably corresponding to the last interglacial MIS 5e) was recovered in ERC BH-01 in which 4 different microfacies were identified from bottom to top 1) *Halimeda* grainstone/packstone, 2) Coral-algal grainstone/packstone, 3) Coralline algae grainstone/packstone; and 4) Coralline algae-dominated mixed skeletal grainstone/packstone. The vertical succession of these 4 microfacies may be interpreted as a deepening upward sequence, as reflecting an increase in circulation, or caused by stacked units separated by subaerial exposure.
- The late Pleistocene interglacial coralgal unit was diagenetically altered in the meteoric environment during a 100 kyr-long exposure (MIS 4 to MIS 2). Diagenetic features include selective grain dissolution, blocky calcite cementation and neomorphism. The carbonate mineralogy of late Pleistocene samples in ERC BH-01 (95.7% LMC and 4.3% aragonite) clearly resulted from an alteration of the original composition. Dissolution features are also visible on the bathymetric map as karst morphologies; for example, a series of karstic depression or dolines, reaching in depth as much as 60 mbsl, are clearly observed in the channel between Malé and Hulhule Islands; and a series of positive reliefs, interpreted as karstic towers, occur in the channel between Malé and Villingili Islands.
- The upper Holocene unconsolidated coralgal reef, overlying the karstified coralgal MIS 5e lower unit, was initiated at ~8200 kyr BP and grew vertically 25 m-high until 6510 ky BP, protected behind a karstified late Pleistocene reef remnant. A small, 30 to 35 m-deep, newly formed lagoon started to fill up only at ~4500 kyr BP, when sea-level rise stalled and a reef initiated on top of the highest elevated Pleistocene karstified reef along the southern part of Malé Island. In contrast to the altered late Pleistocene limestones, the Holocene succession was not or only slightly altered because its carbonate mineralogy includes higher percentages of aragonite and HMC, the original mineralogy produced by neritic carbonate

grains. Benthic foraminifer assemblages of two dominant genera, *Amphistegina* and *Calcarina*, support the deposition in high energy environments and the reciprocal relationship of the two dominant genera might be related to a slight energy decrease during the late part of the Holocene, i.e. the last 4000 years.

ACKNOWLEDGEMENTS

The senior author is grateful to the Turkish Petroleum Corporation (TPAO) for granting a full funding scholarship for a Master's degree at Rice University and support to publish this article. Dr. Rainer Petschick at Goethe University in Frankfurt (Germany) is thanked for making the XRD analyses. The multibeam data sets presented in this article were acquired by co–principal investigators A.W.D. and D.F.N., with extensive field and data-processing support from Brian Donahue at the University of South Florida, St. Petersburg. The different research programs in the Maldives through the years would not have happened without the personnel from the Environmental Research Center (now the Environmental Protection Agency [EPA] of the Republic of Maldives). Special thanks go to Gordon Ewers and Aishath Farhath Ali for their logistic assistance and to Hussain Ibrahim for his assistance at sea with the captain and crew from the EPA. Multibeam funding was provided by the EPA and the University of South Florida. Special thanks to Ahmad Naseem, Dr. Shiham Adam, Dr. Ibrahim Mohamed, Dr. Mahmood Riyaz and Dr. Abdulla Naseer for their invaluable support in Malé and to the National Science Foundation for a grant (0729070) awarded to A.W.D.

Table 2. XRD Analyses results of Holocene deposition including both fine (<63 μm) and coarse (>63 μm) fractions.

BH-01	**Fine Fraction**			**Coarse Fraction**		
Depth (mbsl)	**% Aragonite**	**%High Mg-Calcite**	**%Low Mg-Calcite**	**% Aragonite**	**%High Mg-Calcite**	**%Low Mg-Calcite**
2.00–2.45	42.9	45.2	11.9	71.7	24.9	3.4
4.95–6.00	65.6	32.8	1.6	73.05	26.05	0
7.95–9.00	69.2	29	1.8	73.5	24.6	1.8
9.00–9.45	29.7	17.3	53	7	0	93
9.45–10.00	34.7	19.2	46.2	30.7	18.1	51.2
Mean	48.42	28.7	22.9	51.19	18.73	29.88
BH-03						
Depth (mbsl)	**% Aragonite**	**%High Mg-Calcite**	**%Low Mg-Calcite**	**% Aragonite**	**%High Mg-Calcite**	**%Low Mg-Calcite**
2.00–2.45	53	35.3	11.7	81.4	17.6	1
9.00–9.45	70.6	29.4	0	76.6	23.4	0
10.50–10.95	71.1	27.8	1.1	76.1	23.9	0
12.00–12.45	72	28	0	76.4	23.6	0
13.50–13.95	70.3	29.7	0	71.3	28.7	0
15.00–15.45	70.5	28.4	1.1	70.9	29.1	0
16.50–16.95	69.4	30.6	0	68.1	31.9	0
18.50–18.85	70.1	28.7	1.2	70.7	29.3	0
21.00–21.45	72.1	27.9	0	72	28	0
25.00–25.45	71.3	26.7	2	76.4	23.6	0
25.45–27.00				99.8	0	0.2
Mean	69.04	29.25	1.71	76.34	23.55	0.11

Table 3. Foraminifer counts of different benthic foraminifers from ERC BH-01 and BH-03. Section 1.

BH-01 >0.5mm <2mm Depth (mbsl)	***Amphi-stegina***	***Text-ularia***	***Calc-arina***	***Elphi-dium***	***Hetero-stegina Depressa***	***Sorites***	***Quinquel-oculina***	***Spirol-oculina***	***?***	**Total**
2.00-2.45	314	6	0	1	0	0	0	0	0	321
3.45-4.50	296	4	66	5	4	79	6		3	463
4.50-4.95	5	0	1	0	0	1	0	0	0	7
4.95-6.00	146	5	115	10	10	39	2	0	3	330
6.45-7.50	62	13	26	7	10	11	0	0	1	130
7.50-7.95	14	7	35	4	4	11	4	2	0	81
7.95-9.00	93	38	104	30	16	27	11	6	9	334
9.00-9.45	1	2	116	1	0	0	0	0	0	120
9.45-10.00	101	9	87	17	15	45	11	4	5	294

BH-3 >0.5mm <2mm Depth (mbsl)	***Amphi-stegina***	***Text-ularia***	***Calc-arina***	***Elphi-dium***	***Hetero-stegina Depressa***	***Sorites***	***Quinquel-oculina***	***Spirol-oculina***	***?***	**Total**
2.00-2.45	76	1	1	1	4	1	0	0	0	84
4.95-6.00	101	144	19	6	14	13	4	0	6	307
6.45-7.50	73	193	7	9	11	8	2	1	3	307
7.95-9.00	112	229	14	5	11	4	4	0	7	386
9.00-9.45	113	183	12	0	11	16	6	0	11	352
9.45-10.50	132	165	17	9	13	11	5	1	13	366
10.50-10.95	96	116	12	0	18	9	6	0	7	264
10.95-12.00	104	194	16	8	24	10	13	2	6	377
12.00-12.45	139	140	19	2	18	13	6	0	9	346
12.45-13.50	125	120	26	15	10	10	14	0	9	329
13.50-13.95	89	149	20	10	11	16	17	0	8	320
13.95-15.00	138	102	25	19	13	5	12	0	12	326
15.00-15.45	80	162	15	19	8	21	32	2	10	349
15.45-16.50	75	143	14	15	8	20	27	0	2	304
16.50-16.95	53	188	10	15	6	22	32	1	2	329
18.50-18.85	82	128	13	10	10	27	14	0	17	301
21.00-21.45	100	131	18	3	20	32	7	1	21	333
25.00-25.45	90	154	21	16	14	30	24	1	12	362

Table 3, Section 2.

BH-01 >0.5mm <2mm Depth (mbsl)	**% *Amphi-stegina***	**% *Text-ularia***	**% *Calc-arina***	**% *Elphi-dium***	**% *Hetero-stegina***	**% *Calc-arina***	**% *Sorites***	**% *Quinquel-oqulina***	**% *Spirol-oculina***	**% ?**
2.00-2.45	97.82	1.87	0.00	0.31	0.00	0.00	0.00	0.00	0.00	0.00
3.45-4.50	63.93	0.86	14.25	1.08	0.86	14.25	17.06	1.30	0.00	0.65
4.50-4.95	71.43	0.00	14.29	0.00	0.00	14.29	14.29	0.00	0.00	0.00
4.95-6.00	44.24	1.52	34.85	3.03	3.03	34.85	11.82	0.61	0.00	0.91
6.45-7.50	47.69	10.00	20.00	5.38	7.69	20.00	8.46	0.00	0.00	0.77
7.50-7.95	17.28	8.64	43.21	4.94	4.94	43.21	13.58	4.94	2.47	0.00
7.95-9.00	27.84	11.38	31.14	8.98	4.79	31.14	8.08	3.29	1.80	2.69
9.00-9.45	0.83	1.67	96.67	0.83	0.00	96.67	0.00	0.00	0.00	0.00
9.45-10.00	34.35	3.06	29.59	5.78	5.10	29.59	15.31	3.74	1.36	1.70
Mean	45.05	4.33	31.56	3.37	2.94	31.56	9.84	1.54	0.63	0.75
BH-3 >0.5mm <2mm Depth (mbsl)	**% *Amphi-stegina***	**% *Text-ularia***	**% *Calc-arina***	**% *Elphi-dium***	**% *Hetero-stegina***	**% *Calc-arina***	**% *Sorites***	**% *Quinquel-oqulina***	**% *Spirol-oculina***	**% ?**
2.00-2.45	90.48	1.19	1.19	1.19	4.76	1.19	1.19	0.00	0.00	0.00
4.95-6.00	32.90	46.91	6.19	1.95	4.56	6.19	4.23	1.30	0.00	1.95
6.45-7.50	23.78	62.87	2.28	2.93	3.58	2.28	2.61	0.65	0.33	0.98
7.95-9.00	29.02	59.33	3.63	1.30	2.85	3.63	1.04	1.04	0.00	1.81
9.00-9.45	32.10	51.99	3.41	0.00	3.13	3.41	4.55	1.70	0.00	3.13
9.45-10.50	36.07	45.08	4.64	2.46	3.55	4.64	3.01	1.37	0.27	3.55
10.50-10.95	36.36	43.94	4.55	0.00	6.82	4.55	3.41	2.27	0.00	2.65
10.95-12.00	27.59	51.46	4.24	2.12	6.37	4.24	2.65	3.45	0.53	1.59
12.00-12.45	40.17	40.46	5.49	0.58	5.20	5.49	3.76	1.73	0.00	2.60
12.45-13.50	37.99	36.47	7.90	4.56	3.04	7.90	3.04	4.26	0.00	2.74
13.50-13.95	27.81	46.56	6.25	3.13	3.44	6.25	5.00	5.31	0.00	2.50
13.95-15.00	42.33	31.29	7.67	5.83	3.99	7.67	1.53	3.68	0.00	3.68
15.00-15.45	22.92	46.42	4.30	5.44	2.29	4.30	6.02	9.17	0.57	2.87
15.45-16.50	24.67	47.04	4.61	4.93	2.63	4.61	6.58	8.88	0.00	0.66
16.50-16.95	16.11	57.14	3.04	4.56	1.82	3.04	6.69	9.73	0.30	0.61
18.50-18.85	27.24	42.52	4.32	3.32	3.32	4.32	8.97	4.65	0.00	5.65
21.00-21.45	30.03	39.34	5.41	0.90	6.01	5.41	9.61	2.10	0.30	6.31
25.00-25.45	24.86	42.54	5.80	4.42	3.87	5.80	8.29	6.63	0.28	3.31
Mean	33.47	44.03	4.72	2.76	3.96	4.72	4.56	3.77	0.14	2.59

Table 4. U/Th dating analysis results of two samples from BH-03.

Sample code	**Lab code LSCE**	**^{238}U (µg/g)**		**^{232}Th (ng/g)**		**$\delta^{234}U_m$**		**(^{230}Th/^{232}Th)**		**(^{230}Th/^{238}Th)**		**Age (ka)**		**$\delta^{234}U_{(0)}$**	
BH-03_1	**5305**	**3.517**	**±0.004**	**0.209**	**±0.0004**	**143.6**	**±1.1**	**3,920**	**±10**	**0.0755**	**±0.00020**	**7.45**	**±0.028**	**146.7**	**±1.1**
BH-03_2	**5306**	**2.763**	**±0.003**	**0.051**	**±0.0001**	**145.3**	**±1.1**	**12,053**	**±39**	**0.0725**	**±0.00024**	**7.129**	**±0.031**	**148.2**	**±1.1**

Table 5. Radiocarbon ages of Holocene sediment accumulation deposition determined using benthic foraminifer, *Amphistegina*. Conventional radiocarbon ages have been calibrated to calendar year BP by using CALIB 7.0.2 software with the Marine13 data set and 132+25 Delta-R value for the central Indian Ocean reservoir effect (Southon *et al.*, 2002; Kench *et al.*, 2005; Kench *et al.*, 2009)

Sample	Average depth (mbsl)	^{14}C age (yr BP)	Error +/-	One sigma/1	One sigma/2	Calibrated ^{14}C age (cal yr BP)	Error +/-
BH-01_2.00-2.45	2.23	2440	70	1826	2011	1919	93
BH-01_3.45-4.50	3.98	3770	70	3444	3629	3537	93
BH-01_4.95-6.00	5.48	4140	70	3914	4127	4021	107
BH-01_7.95-9.00	8.48	3720	70	3390	3566	3478	88
BH-03_2.00-2.45	2.23	1300	75	645	791	718	73
BH-03_9.00-9.45	9.23	4500	75	4402	4630	4516	114
BH-03_13.50-13.95	13.73	5250	80	5390	5576	5483	93
BH-03_25.00-25.45	25.23	5310	80	5447	5622	5535	88

REFERENCES

Agassiz, A. (1902) An expedition to the Maldives. *Am. J. Sci*., **13**, 297.

Andersen, M.B., Stirling, C.H., Zimmermann, B. and **Halliday, A.N.** (2010) Precise determination of the open ocean ^{234}U/^{238}U composition. *Geochem. Geophys. Geosyst*., **11**, Q12003, doi:10.1029/2010GC003318.

Aubert, O. and **Droxler, A.W.** (1992) General Cenozoic Evolution of the Maldives Carbonate System (Equatorial Indian Ocean). *Bull. Centres Rech. Explor.-Prod. Elf Aquitaine*, **16**, 113–136.

Aubert, O. and **Droxler, A.W.** (1996) Seismic stratigraphy and depositional signatures of the Maldives carbonate system (Indian Ocean). *Mar. Petrol. Geol*., **13**, 503–536.

Belopolsky, A.V. and **Droxler, A.W.** (2003) Imaging Tertiary carbonate system—the Maldives, Indian Ocean: insights into carbonate sequence interpretation. *The Leading Edge*, **22**, 646–52.

Belopolsky, A.V. and **Droxler, A.W.** (2004) Seismic expressions of prograding carbonate bank margins: Middle Miocene, Maldives, Indian Ocean. *AAPG Mem*., **81**, 267–90.

Betzler, C., Eberli, G.P. and **Alvarez Zarikian C.A.** (2016a) *Expedition 359 Preliminary Report: Maldives Monsoon and Sea Level*. College Station, TX: Int. Ocean Discov. Program. doi: 10.14379/iodp.pr.359.2016

Betzler, C., Eberli, G.P., Kroon, D., Wright, J.D., Swart, P.K., Nath, B.N., Alvarez-Zarikian, C.A., Alonso-García, M., Bialik, O.M., Blättler, C.L., Guo, J.A., Haffen, S., Horozal, S., Inoue, M., Jovane, L., Lanci, L., Laya, J.C., Mee, A.L.H., Lüdmann, T., Nakakuni, M., Niino, K., Petruny, L.M., Pratiwi, S.D., Reijmer, J.J.G., Reolid, J., Slagle, S.L., Sloss, C.R., Su, X., Yao, Z. and **Young, J.R.** (2016b) The abrupt onset of the modern South Asian Monsoon winds. *Sci. Rep*., **6**, 29838. doi: 10.1186/s40645-018-0165-x

Betzler, C., Eberli, G.P., Zarikian, C., Garcia, A., Montserrat & Bialik, Or & Blättler, Clara & Guo, J.A. & Haffen, S. & Horozal, Senay & Inoue, Mayuri & Jovane, Luigi & Kroon, Dick & Lanci, Luca & Laya, Juan Carlos & Ling, Anna & Lüdmann, Thomas & Nakakuni, Masatoshi & Bejugam, Nagender & Niino & Young (2017) Expedition 359 summary. In: *Maldives Monsoon and Sea Level, MS 359-101*, Proc. Int. Ocean Discov. Program Vol. **359**. College Station, TX: Int. Ocean Discov. Program. 10.14379/iodp.proc.359.101.2017.

Betzler, C., Fürstenau, J., Lüdmann, T., Hübscher, C., Lindhorst, S., Paul, A., Reijmer, J.J.G. and **Droxler, A.W.** (2012) Sea-level and ocean-current control on carbonate platform growth, Maldives, Indian Ocean. *Basin Res*., **25**, 172–196. doi: 10.1111/j.1365-2117.2012.00554.x

Betzler, C., Hübscher, C., Lindhorst, S., Reijmer, J.J.G., Romer, M., Droxler, A.W., Fürstenau, J. and **Lüdmann. T.** (2009) Monsoon-induced partial carbonate platform drowning (Maldives, Indian Ocean). *Geology*, **37**, 867–870.

Braithwaite, C.J.R. and **Camoin, G.F.** (2011) Diagenesis and sea-level change: lessons from Moruroa, French Polynesia. *Sedimentology*, **58**, 259–284. doi: 10.1111/j.1365-3091.2010.01182.x

Camoin G.F., Colonna, M., Montaggioni, L.F., Casanova, J., Faure, G. and **Thomassin, B.A.** (1997) Holocene sea-level changes and reef development in the southwestern Indian Ocean. *Coral Reefs*, **16**, 247–259.

Camoin, G.F., Montaggioni, L.F. and **Braithwaite, C.J.R.** (2004) Late glacial to post glacial sea levels in the Western Indian Ocean. *Mar Geol*., **206**, 119–146.

Cheng, H., Edwards, R.L., Shen, C.C., Polyak, V.J., Asmerom, Y., Woodhead, J., Hellstrom, J., Wang, Y., Kong, X., Spötl, C., Wang, X. and **Alexander Jr, E.C.** (2013) Improvements in ^{230}Th dating, ^{230}Th and ^{234}U half-life values and U–Th isotopic measurements by multi-collector inductively coupled plasma mass spectrometry. *Earth Planet. Sci. Lett.*, **371-372**, 82–91.

Coleman, N. (2000) Marine life of the Maldives. Atoll Editions, Australia.

Douville, E., Sallé, E., Frank, N., Eisele, M.H., Pons-Branchu, E. and **Ayrault, S.** (2010) Rapid and accurate U-Th dating of ancient carbonates using inductively coupled plasma-quadrupole mass spectrometry. *Chem. Geol*., **272**, 1–11.

Droxler, A.W. (2012) Sea level induced slope and atoll lagoon sea floor morphologies around Malé Island and Goidhoo Atoll (Republic of Maldives). *Quatern. Int*., **279-280**, 124.

Droxler, A.W. and **Jorry, S.J.** (2021) The Origin of Modern Atolls: Challenging Darwin's Deeply Ingrained Theory. *Annu. Rev. Mar. Sci*., **13**, 537–573, https://doi.org/10.1146/annurey-marine-122414-034137.

Droxler, A.W., Naar, D.F., Donahue, B.T., Flury, F. and **Zuhair, M.** (2011) Sea Level Induced Slope and Atoll Lagoon Sea Floor Morphologies around Malé Island and Goidhoo Atoll (Republic of Maldives). In: *Abstract and Program, XVIII INQUA Congress, Bern (Switzerland)*.

Dullo, W.C., Eisenhauer, A., Heiss, G.A., Wischow, D., Camoin, G.F., Colonna, M. and **Montaggioni, L.F.** (1996) Coral and reef growth in the western Indian Ocean (La Réunion, Mayotte and Seychelles). In: *Global and regional controls on biogenic sedimentation I* (Eds J. Reitner, F. Neuweiler and F. Gunkel),

Reef Evolution Sb2, Göt- tingen, pp 23–27.

Duncan, A.R., Backman, J., Peterson, L. and **Shipboard Party** (1990) The volcanic record of the reunion hotspot. In: *Proceedings of the Ocean Drilling Program, Scientific Results*, **115**, 507–517.

Dunham, R.J. (1962) Classification of carbonate rocks according to depositional texture. In: *Classification of Carbonate Rocks - a Symposium* (Ed. W.E. Ham), *AAPG Mem*., **1**, 108–121.

Dutton, A., Webster, J.M., Zwartz, D., Lambeck, K. and **Wohlfarth, B.** (2015) Tropical tales of polar ice: evidence of last interglacial polar ice sheet retreat recorded by fossil reefs of the granitic Seychelles islands. *Quatern. Sci. Rev*., **107**, 182–196.

Eisenhauer, A., Heiss, G.A., Sheppard, C.R.C. and **Dullo, W.C.** (1999) Reef and island formation and late Holocene sea-level changes in the Chagos islands. In: *Ecology of the Chagos Archipelago* (Eds C.R.C. Sheppard and M.R.D. Seaward), Linnean Society Occasional Publications, **2**, 21–33.

Flügel, E. (2004) *Microfacies of Carbonate Rocks*, Springer, Berlin.

Fujita, K., Osawa, Y., Kayanne, H., Ide, Y. and **Yamano, H.** (2009) Distribution and sediment production of large benthic foraminifers on reef flats of the Majuro Atoll, Marshall Islands. *Coral Reefs*, **28**, 29–45. doi: 10.1007/s00338-008-0441-0

Gischler, E. (2006) Sedimentation on Rasdhoo and Ari Atolls, Maldives, Indian Ocean. *Facies*, **52**, 341-360.

Gischler, E. (2007) Pleistocene Facies of Belize barrier and atoll reefs. *Facies*, **53**, 37–41. doi: 10.1007/s10347-006-0086-9.

Gischler, E., Droxler, A., Thomas, A.L., Webster, J.M., Yokoyama, Y. and **Schöne, B.R.** (2013) Microfacies and diagenesis of older Pleistocene (pre-LGM) reefal deposits, Great Barrier Reef, Australia (IODP Expedition 325). *Sedimentology*, **60**, 1432–1466.

Gischler, E., Hudson, J.H. and **Pisera, A.** (2008) Late Quaternary reef growth and sea level in the Maldives (Indian Ocean). *Mar. Geol*., **250**, 104–113.

Gischler, E., Humblet, M., Braga, J.C. and **Eisenhauer, A.** (2018) Last Interglacial Reef Facies and Late Quaternary Subsidence in the Maldives, Indian Ocean. *Mar. Geol*., **406**, 34–41.

Gischler, E. and **Lomando, A.J.** (1999) Recent sedimentary facies of isolated carbonate platforms, Belize-Yucatan system, Central America. *J. Sed. Res*., **69**, 747–763.

Gischler, E., Storz, D. and **Schmitt, D.** (2014) Sizes, shapes and patterns of coral reefs in the Maldives, Indian Ocean: the influence of winds, storms and precipitation on a major tropical carbonate platform. *Carbonates Evaporites*, **29**, 73–87.

Hammer, O., Harper, D.A.T. and **Ryan P.D.** (2001) PAST: paleontological statistics software package for education and data analysis. *Palaeont. Electronica*, **4**, 1–9.

Jaffey, A., Flynn, K., Glendenin, L., Bentley, W. and **Essling, A.** (1971) Precision measurement of half-lives and specific activities of ^{235}U and ^{238}U. *Phys. Rev*., **5**, 1889–1906.

Japan International Cooperation Agency (JICA) (1992) The Development Study on the Seawall Construction Project for Malé Island in the Republic of Maldives, *JICA Summary Report*, **52**, https://openjicareport.jica.go.jp/pdf/11017894_01.pdf

Kench, P.S. (2012) The geomorphology of Baa (South Maalhosmadulu) Atoll and its reef islands. *Atoll Res. Bull*. **590**, 1–29.

Kench, P.S., McLean, R.F. and **Nichol, S.L.** (2005) New model of reef-island evolution: Maldives, Indian Ocean. *Geology*, **33**, 145–148. doi: 10.1130/G21066.1

Kench, P.S., Smithers, S.G., McLean, R.F. and **Nichol, S.L.** (2009) Holocene reef growth in the Maldives: Evidence of a mid-Holocene sea-level highstand in the central Indian Ocean. *Geology*, **37**, 455–458. doi: 10.1130/G25590A.1

Klostermann, L. and **Gischler, E.** (2015) Holocene sedimentary evolution of a mid-ocean atoll lagoon, Maldives, Indian Ocean. *Int. J. Earth Sci*., **104**, 289**–**307.

Lambeck, K. and **Chappell, J.** (2001) Sea level change through the last glacial cycle. *Science*, **292**, 679-685. doi: 10.1126/science.1059549

Longman, M.W. (1980) Carbonate diagenetic textures from nearsurface diagenetic environments. *AAPG Bull*., **64**, 461–487.

Lüdmann, T., Betzler, C., Eberli, G.P., Reolid, J., Reijmer, J.J.G., Sloss, C.R., Bialik, O.M., Alvarez-Zarikian, C.A., Blättler, C.L., Guo, J.A., Horozal, S., Jovane, L., Lanci., L., Mee, A.L.H., Nakakuni, M., Nath, B.N., Niino, K., Petruny, L.M., Slagle, A.L., Su, X., Swart, P.K., Wright, J.D., Yao, Z. and **Young, J.R.** (2018) Carbonate delta drift: a new sediment drift type. *Mar. Geol*., **401**, 98–111.

Ludwig, K. and **Titterington, D.** (1994) Calculation of ^{230}Th/U isochrons, ages and errors. *Geochim. Cosmochim. Acta*, **58**, 5031–5042.

Lüdmann, T., Kalvelage, C., Betzler, C., Fürstenau, J. and **Hübscher, C.** (2013) The Maldives, a giant isolated carbonate platform dominated by bottom currents. *Mar. Petrol. Geol*., **43**, 326–340.

McCulloch, M., Taviani, M., Montagna, P., Correa, M., L., Remia, A. and **Mortimer, G.** (2010) Proliferation and demise of deep-sea corals in the Mediterranean during the Younger Dryas. *Earth Planet. Sci. Lett*., **298**, 143–152.

MFR Report (2009) *Malé Reef Slope Collapse Engineering Geology Assessment Phase 1*.

Miller, K.G., Browning J.V., Schmelz, W.J, Kopp, R.E., Mountain, G.S. and **Wright, J.D.** (2020) Cenozoic sea-level and cryospheric evolution from deep-sea geochemical and continental margin records. *Amer. Assoc. Advancement Sci*., **6**, 20 eaaz1346. https://doi.org/10.1126/sciadv.aaz1346.

Milliman, J.D. (1974) *Marine Carbonates*. Springer, New York.

Milliman, J.D., Freile, D., Steinen, R.P. and Wilber, R.J. (1993) Great Bahama Bank aragonitic muds: Mostly inorganically precipitated, mostly exported. *J. Sed. Petrol*., **63**, 589-595.

Montaggioni, L.F. (1976) Holocene submergence in Reunion Island. *Ann. S. Afr. Mus.*, **71**, 69–75.

Montaggioni, L.F. (2005) History of Indo-Pacific coral reef systems since the last glaciation: Development patterns and controlling factors. *Earth-Sci. Rev*., **71**, 1–75. doi: 10.1016/j.earscirev.2005.01.002

Montaggioni, L.F., Borgomano, J., Fournier, F. and **Granjeon, D.** (2015) Quaternary atoll development: new insights from the two-dimensional stratigraphic forward modelling of Mururoa island (central Pacific Ocean). *Sedimentology*, **62**(2), 466–500.

Montaggioni, L.F. and **Faure G**. (1997) Response of reef coral communities to sea-level rise: a Holocene model from Mauritius (Western Indian Ocean). *Sedimentology*, **44**, 1053–1070.

Montaggioni, L.F. and **Martin-Garin, B.** (2020) Quaternary development history of coral reefs from West Indian islands: a review. *Int. J. Earth Sci*., **109**, 911–930. https://doi.org/10.1007/s00531-020-01839-3

Naseer, A. and **Hatcher, B.G.** (2004) Inventory of the Maldives coral reefs using morphometrics generated from Landsat ETM+ imagery. *Coral Reefs*, **23**, 161–168.

Owen, A., Kruijsen, J., Turner, N. and **Wright, K.** (2011) *Marine Energy in the Maldives*. Center for Understanding Sustainable Practice, Robert Gordon University, Aberdeen, Scotland.

Parker, J.H. and **Gischler, E.** (2011) Modern Foraminiferal distribution and diversity in two atolls from the Maldives, Indian Ocean. *Mar. Micropal*. **73**, 30–49.

Perry, C.T., Kench, P.S., Smithers, S.G., Yamano, H., O'Leary, M. and **Gulliver, P.** (2013) Time scales and modes of reef lagoon infilling in the Maldives and controls on the onset of reef island formation. *Geology*, **41**, 1111–1114. doi: 10.1130/G34690.1

Pons-Branchu, E., Douville, E., Roy-Barman, M., Dumont, E., Branchu, P., Thil, F., Frank, N., Bordier, L. and **Borst, W.** (2014) A geochemical perspective on Parisian urban history based on U-Th dating, laminae counting and yttrium and REE concentrations of recent carbonates in underground aqueducts. *Quatern. Geochron*., **24**, 43–54.

Purdy, E.G. and **Gischler, E.** (2005) The transient nature of the empty bucket model of reef sedimentation. *Sed. Geol*., **175**, 35–47.

Riyaz, M. (2007) *Environment Impact Assessment Report for Development of Holiday Inn Geoenvironmental and Geotechnical Aspects, Ameeneege, Malé Maldives, (Part I)*, http://saruna.mnu.edu.mv/xmlui/handle/123456789/7325.

Riyaz, M. and **Park, K.** (2009) *Final Report, Geotechnical Investigation of Malé NE Reef Slope Collapse*. Asian Institude of Technology, Bangkok, Thailand.

Robbins, L.L., Tao, Y. and **Evans, C.A.** (1997) Temporal and spatial distribution of whitings on Great Bahama Bank and a new lime mud budget. *Geology*, **25**, 947–950.

Rovere, A., Khanna, P., Bianchi, C., N., Droxler, A.W., Morri C. and **Naar, D.** F., 2018, Submerged reef terraces in the Maldivian Archipelago (Indian Ocean), *Geomorphology*, **317**, 218–232.

Schroeder, J.H. (1972) Calcified filaments of an endolithic alga in recent Bermuda reefs. *Neues Jb. Geol. Paläontol. Abh*., **1972**, 16–33.

Southon, J., Kashgarian, M., Fontugne, M., Metivier, B. and **Yim, W.** (2002) Marine reservoir corrections for the Indian Ocean and southeast Asia. *Radiocarbon*, **44**, 167–180.

Tcherepanov, E.N., Droxler, A.W., Lapointe, P. and **Mohn K.** (2008) Carbonate seismic stratigraphy of the Gulf of Papua mixed depositional system: Neogene stratigraphic signature and eustatic control. *Basin Res*., **20**, 185–209. doi: 10.1111/j.1365-2117.2008.00364.x

The Foraminifera.eu Project: https://foraminifera.eu/

Thompson, W.G. and **Goldstein, S.L.** (2005) Open-System Coral Ages Reveal Persistent Suborbital Sea-Level Cycles. *Science*, **308**, 401–404. doi: 10.1126/science.1104035

Van Der Plas, L. and **Tobi, A.C.** (1965) A chart for judjing the reliability of point counting results. *Amer. J. Sci*., **263**, 87–90.

Woodroffe, C.D. (1992) Morphology and evolution of reef islands in the Maldives. In: *Proc. 7th Int. Coral Reef Symp., Guam*, **2**, 1217–1226.

Woodroffe, C.D., Veeh, H.H., Falkland, A., McLean, R.F. and **Wallensky, E.** (1991) Last interglacial reef and subsidence of the Cocos (Keeling) Islands, Indian Ocean. *Mar. Geol*., **96**, 137–143.

Woodroffe, S.A., Long, A.J., Milne, G.A., Bryant, C.L. and **Thomas, A.L.** (2015) New constraints on late Holocene eustatic sea-level changes from Mahé Seychelles. *Quatern. Sci. Rev*., **115**, 1–16.

Zinke, J., Reijmer, J.J.G., Taviani, M., Dullo, W.C. and **Thomassin, B.A.** (2005) Facies and faunal assemblage changes in response to the Holocene transgression in the Lagoon of Mayotte (Comoro Archipelago, SW Indian Ocean). *Facies*, **50**, 391–40.

IAS (2022) Coral Reefs and Sea-Level Change: Quaternary Records and Modelling, 141–171

Shelf-edge deglacial reef establishment and subsequent partial demise: Response to distinct pulses of sea-level rise associated with environmental changes

BRANDON B. HARPER[*], ANDRÉ W. DROXLER[*], JODY M. WEBSTER[†], PAOLO MONTAGNA[‡,§], YUSUKE YOKOYAMA[¶], MARC HUMBLET[‖], STÉPHAN J. JORRY[#], LUC BEAUFORT[a], KAZUYO TACHIKAWA[a], EDOUARD BARD[a] and EDWIGE PONS-BRANCHU[b]

[*]*Department of Earth Science, Rice University, 6100 Main Street, Houston, TX 77005, USA (e-mail: brandon.b.harper@gmail.com).*
[†]*Coastal Research Group, School of Geosciences, University of Sydney, NSW, 2006, Australia.*
[‡]*Istituto di Scienze Polari, Consiglio Nazionale delle Ricerche, Via Gobetti 101, 40129, Bologna, Italy.*
[§]*Lamont Doherty Earth Observatory of Columbia University, 61 Route 9W, Palisades, NY 10964, USA.*
[¶]*Atmosphere and Ocean Research Institute, Department of Earth and Planetary Sciences, University of Tokyo, 5-1-5 Kashiwanoha, Chiba 277-8564, Japan.*
[‖]*Department of Earth and Planetary Sciences, Nagoya University, Nagoya 464-8601, Japan.*
[#]*IFREMER, Department of Marine Geosciences, BP 70, 29280, Plouzané, France.*
[a]*Aix Marseille Université, CNRS, IRD, INRAE, Coll. France, CEREGE, Aix-en-Provence, France.*
[b]*Laboratoire des Sciences du Climat et de l'Environnement, CNRS-CEA-UVSQ, UMR 8212, 91198, Gifsur-Yvette Cedex, France.*

ABSTRACT

The partial melting of Earth's bi-polar ice sheets since the Last Glacial Maximum (LGM) has translated into a ~120 m amplitude stepwise sea-level rise punctuated by three major meltwater pulses that were tracked and recorded with some of the best accuracy by coral reefs. However, the initial meltwater pulse marking the end of the LGM, at 19 ka, is anchored in only two palaeo reefs (Barbados, Great Barrier Reef). Here, the authors present the analysis of a coralgal reef that thrived along the south-east Papua New Guinea Peninsula outer shelf during this initial pulse. In the cone of a piston core, a shallow *Goniastrea retiformis* coral colony was retrieved at 111 m below present sea-level and uranium/thorium dated to 19.4 ka BP. This colony had been buried beneath the debris of a proximal coralgal reef before its partial drowning at 14.5 ka BP. Seismic survey data suggest that the reef edifice was established directly on the eroded top of a lowstand shelf-edge delta, partially drowned and then back-stepped towards the south-east in response to three distinct deglacial sea-level pulses and stepwise increases of water column turbidity.

©2022 International Association of Sedimentologists

INTRODUCTION

Coral reef response to sea-level fluctuations and environmental changes

Scleractinian corals have been the primary frame builders of tropical reefs since the Oligocene (Macintyre, 1988; Kiessling, 2009). Understanding past coral reef demise sheds light on the challenges faced by modern and future reefs. Today, as in the past, tropical reefs are challenged by significant sea-level rise pulses and environmental changes that threaten their ability to maintain healthy development and vertical growth potential to keep up with sea-level rise (Schlager, 2005; Carpenter *et al.*, 2008). Tropical corals occupy the upper part of the euphotic zone, as their symbiotic relationship with algae (zooxanthellae) depends on sunlight (Pearse & Muscatine, 1977). This reliance on sunlight places tropical corals at special risk for weakening or demise during periods (i.e. pulses) of rapid sea-level rise and intense environmental changes such as poisoning by increased land-based sediment and/or nutrient input, increasing water temperature and reducing sea water pH (Carpenter *et al.*, 2008; Burke *et al*., 2011). Shallow-water coral species, living very near the sea surface, are commonly used to track sea-level (Woodroffe & Webster, 2014). Their aragonite skeletons can be accurately dated using uranium/thorium and radiocarbon techniques and they are, therefore, widely used as sea-level proxies (Fairbanks, 1989; Bard *et al.*, 1990; Chappell & Polach, 1991; Camoin, 2012; Deschamps *et al*., 2012; Abdul *et al*., 2016; Yokoyama *et al*., 2018; Braga *et al*., 2022 this issue).

During early deglacial sea-level rise, low latitude coral reefs commonly established themselves on former siliciclastic glacial lowstand coastlines. Once flooded, the fluvial plain became a continental shelf with siliciclastics constrained to an up-dip position along the new coastline (Droxler & Jorry, 2013). Coral accretion rates depend on the amount of light they receive and the positive relief above the sea floor (Schlager, 1981; Hallock & Schlager, 1986; Montaggioni, 2005). More sunlight is available for photosynthesis at shallow-water depths. Likewise, corals growing in elevated positions encounter less turbid water, providing greater access to sunlight and reduced risk of sediment burial (Hallock & Schlager, 1981). Shallow reefs (<5 m) accrete from 1 to 10 mm yr^{-1}, while deeper reefs (>10 m) accrete at a lower rate of <1 mm yr^{-1} (Schlager, 1981; Schlager, 2005; Montaggioni, 2005; Humblet *et al*., 2022 this issue). Reefs respond to sea-level rise by 'keep-up, catch-up or give-up' (Neumann & Macintyre, 1985) depending on the reef's growth-potential rates relative to the rates of sea-level rise. Modern coral reefs are examples of those that have kept up or caught up to the last deglacial sea-level rise. Back-stepping is a characteristic response of the partial give-up (drowning) of reefs in response to rapid sea-level rise to secure positions in an up-dip position where the environmental conditions are more favourable and/or the rates of sea-level rise have decreased (Blanchon & Shaw, 1995; Schlager, 2005). As globally observed through the latter part of the last deglaciation (Webster *et al.*, 2004a; Schlager, 2005; Webster *et al*., 2018), reefs that cannot keep up with sustained high rates of sea-level rise will partially drown and back-step when they are dropped below their critical depth (Schlager, 1981; Hallock & Schlager, 1986; Webster *et al.*, 2004a; Webster *et al*., 2018; Schlager, 2005).

Reefs in a give-up mode follow a typically observed pattern of shallow-water, usually monospecific, framework corals replaced with increasingly diverse, deeper-water coral assemblages (Camoin *et al*., 1999; Webster *et al*., 2004a) and ultimately capped by benthic

encrustation (e.g. coralline algae and microbialite; Neumann & Macintyre, 1985; Webster *et al*., 2004a; Schlager, 2005). The reefs then fully drown when the carbonate neritic accretion ceases. Though rapid rates of sea-level rise alone can be sufficient to drown reefs (Kim *et al.*, 2012), unfavourable environmental factors (e.g. increased turbidity) can weaken framework corals, reducing their growth-rate potential and increase their susceptibility to drowning (Schlager, 1981; Neumann & Macintyre, 1985; Hallock & Schlager, 1986; Woolfe & Larcombe, 1999; Schlager, 2005).

Partially drowned reefs along the shelf edge of the south-eastern Papuan Peninsula, Papua New Guinea (Figs 1 and 2), have recorded the response of a coralgal reef system to the stepwise high amplitude sea-level rise since the Last Glacial Maximum (LGM). Three successive phases of reef growth exhibit partial drowning and back-stepping that coincide with established major meltwater pulses (MWPs) – 19 kyr MWP (Yokoyama *et al.*, 2000; Hanebuth *et al.*, 2000), MWP-1A (Deschamps *et al*., 2012; Carlson & Clark, 2012) and MWP-1B (Bard *et al*., 1990; Alley *et al*., 2005; Abdul *et al*., 2016; Fig. 3) – and represent possible responses of the present reef system to current and future environmental changes. The initial MWP, marking the very beginning of the last deglaciation at the end of the LGM, occurred at ~19 ka with a rise of ~5 to 10 m (Bard *et al*., 1990; Yokoyama *et al*., 2000; Clark *et al*., 2004; Bard *et al*., 2010; Carlson & Clark, 2012). A sea-level rise of ~12 to 22 m is calculated for MWP-1A, well constrained from 14.65 to 14.3 ka (Carlson & Clark, 2012; Deschamps *et al*., 2012). MWP-1B occurs at 11.3 ka (Fairbanks, 1989; Bard *et al*., 1990; Carlson & Clark, 2012; Abdul *et al*., 2016), though its existence or amplitude is questioned (Bard *et al*., 2010). Results from IODP Expedition 325 based on two transects of boreholes offshore the nearby Great Barrier Reef, summarised in Webster *et al*. (2018) and Yokoyama *et al.* (2018), suggest a gradual rise in sea-level during MWP-1B. Uncertainty of the precise timing and amplitude of the 19 kyr MWP remains. Apart from Barbados, (Bard *et al*., 1990) and the Great Barrier Reef (Webster *et al*., 2018; Yokoyama *et al.,* 2018), corals have not been used to constrain the 19 kyr MWP (Yokoyama & Esat, 2011). This study adds additional coral reef data recovered along a 14 m-long core – MD05-2945 (abbreviated MD-45) (8.625800° S, 146.209000° E) – retrieved 98 m below present sea-level (Beaufort *et al.*, 2005). This core recovered a coralgal section covered by marine sediment, recording the initial deglacial reef growth phase and which provides accurate depths and ages for this initial deglacial MWP marking the end of the LGM.

Gulf of Papua mixed system

The Gulf of Papua (GoP) shelf comprises the northernmost extent of the Great Barrier Reef (GBR) to the south and the less well-studied, although extensive, barrier reef lining the southern shelf edge of Papua New Guinea's (PNG) Papuan Peninsula (Fig. 1). The GBR and the South Papuan Peninsula Barrier Reef (SPPBR) form an extensive tropical mixed siliciclastic-carbonate depositional system stretching from central Queensland, Australia, to the tip of the Papuan Peninsula, PNG (Harris *et al*., 1996; Tcherepanov *et al*., 2008; Droxler & Jorry, 2013). The disconnection between the northern extremity of the GBR and the north-western extremity of the SPPBR occurs within the GoP, where large volumes of siliciclastics are dumped by several important rivers that drain the PNG highlands (Milliman, 1995; Harris *et al*., 1996), including the Fly River, forming a large prograding mud clinoform (Harris *et al*., 1996; Walsh & Nittrouer, 2003; Slingerland *et al*., 2008; Howell *et al*., 2014). The clockwise gyre in the GoP (Andrews &

Clegg, 1989; Slingerland *et al*., 2008) transports fine sediment from the muddy inner shelf towards the narrowing shelf along the Papuan Peninsula, where much of the sediment is transported to the slope of the Pandora Trough (Wolanski & Alongi, 1995; Walsh & Nittrouer, 2003; Muhammad *et al*., 2008; Howell *et al*., 2014) near the western edge of the SPPBR. The northern side of the Papuan Peninsula is currently experiencing complex tectonism due to arc-continent collision of several microplates, resulting in uplift of the Papuan Peninsula and Huon Peninsula and deepening of the Solomon Sea (Wallace *et al*., 2004). In contrast, the GoP margin is remarkably and unexpectedly stable, exhibiting little tectonic activity and relatively slow subsidence since the Pliocene (Bird, 2003; Tcherepanov *et al*., 2008). The shelf break along the Papuan Peninsula, depth of -125 m (Figs 2 and 3; Daniell, 2008; Droxler & Jorry, 2013), attests to the lack of subsidence since the LGM.

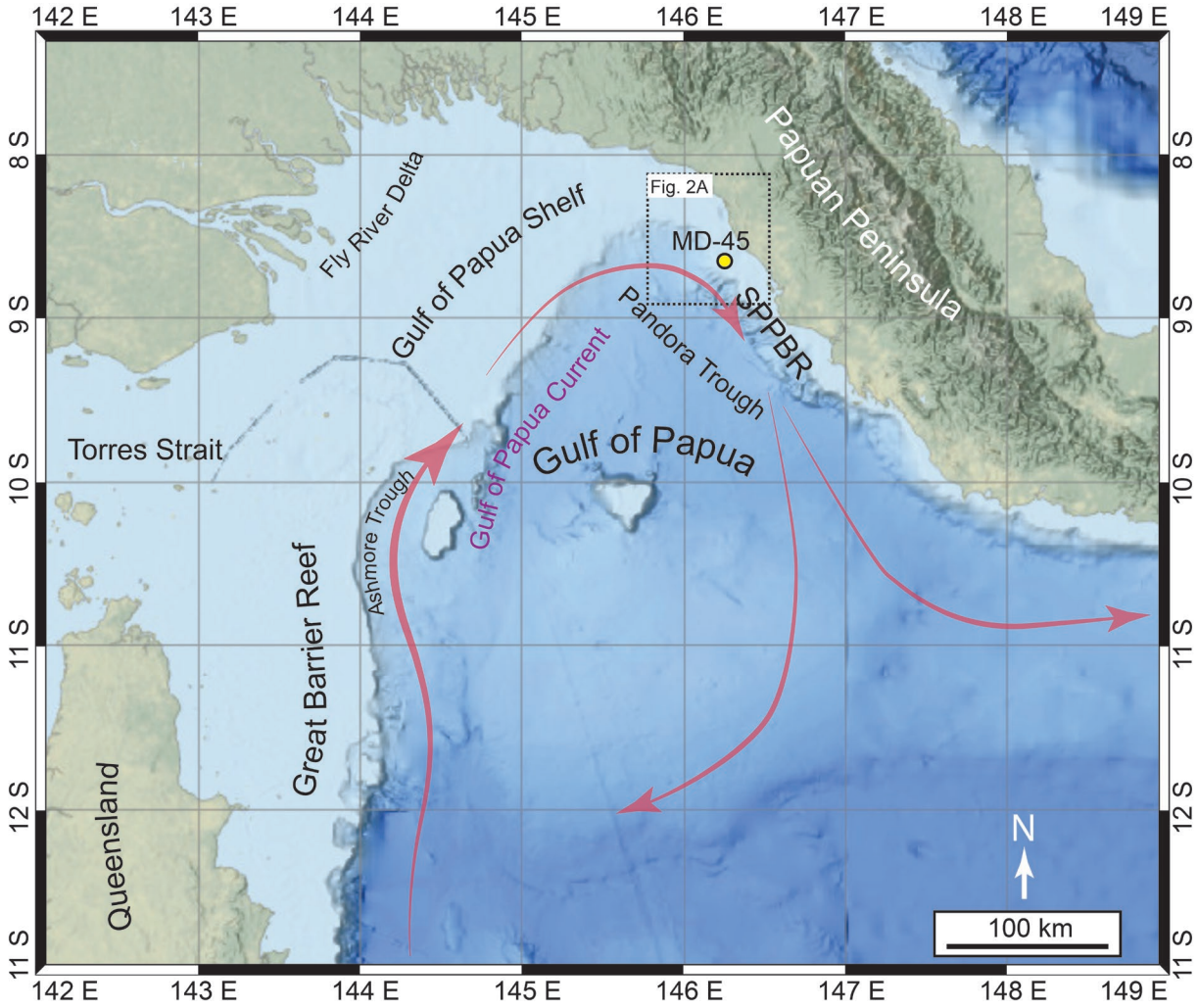


Fig. 1. Map of the Gulf of Papua. Shades of blue from light to dark indicate increasing water depth. Important geographical features and locations related to this study are identified: Great Barrier Reef (GBR), Gulf of Papua Shelf, South Papuan Peninsula Barrier Reef (SPBBR). Also shown with red arrows is the general position of the Gulf of Papua Current (GPC; Steinberg, 2007). The inset box identifies the location of the map in Fig. 2A. Map from GEBCO (2019).

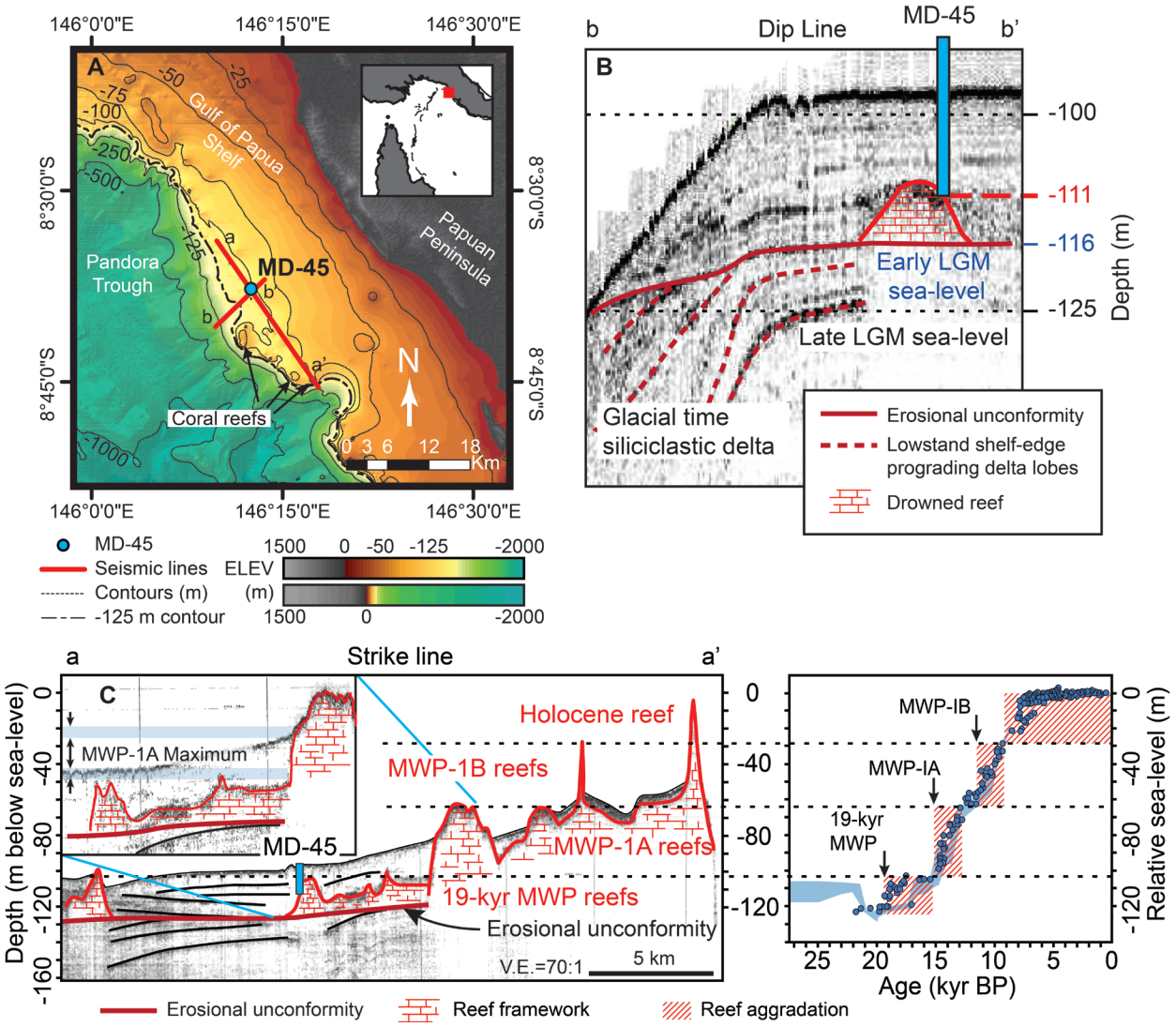


Fig. 2. Back-stepping reefs along the Papuan Peninsula. (A) Bathymetric map of the Gulf of Papua Shelf along the Papuan Peninsula displaying the location of seismic lines and core MD-45. (B) Seismic dip line with reef edifice established on a lowstand delta. Siliciclastic sediments appear to be below the incipient reef at a depth of ~-116 m (early LGM sea-level; Yokoyama *et al.*, 2018), dropping further to -125 m during LGM time. Location of MD-45, striking the buried reef. (C) Seismic strike line displaying established reef on LGM unconformity and a series of partial drowning and back-stepping reefs coincident with depths of meltwater pulses identified on sea-level data during the last deglaciation (Alley *et al.*, 2005). Figure parts (A) and (B) modified from Droxler & Jorry, 2013.

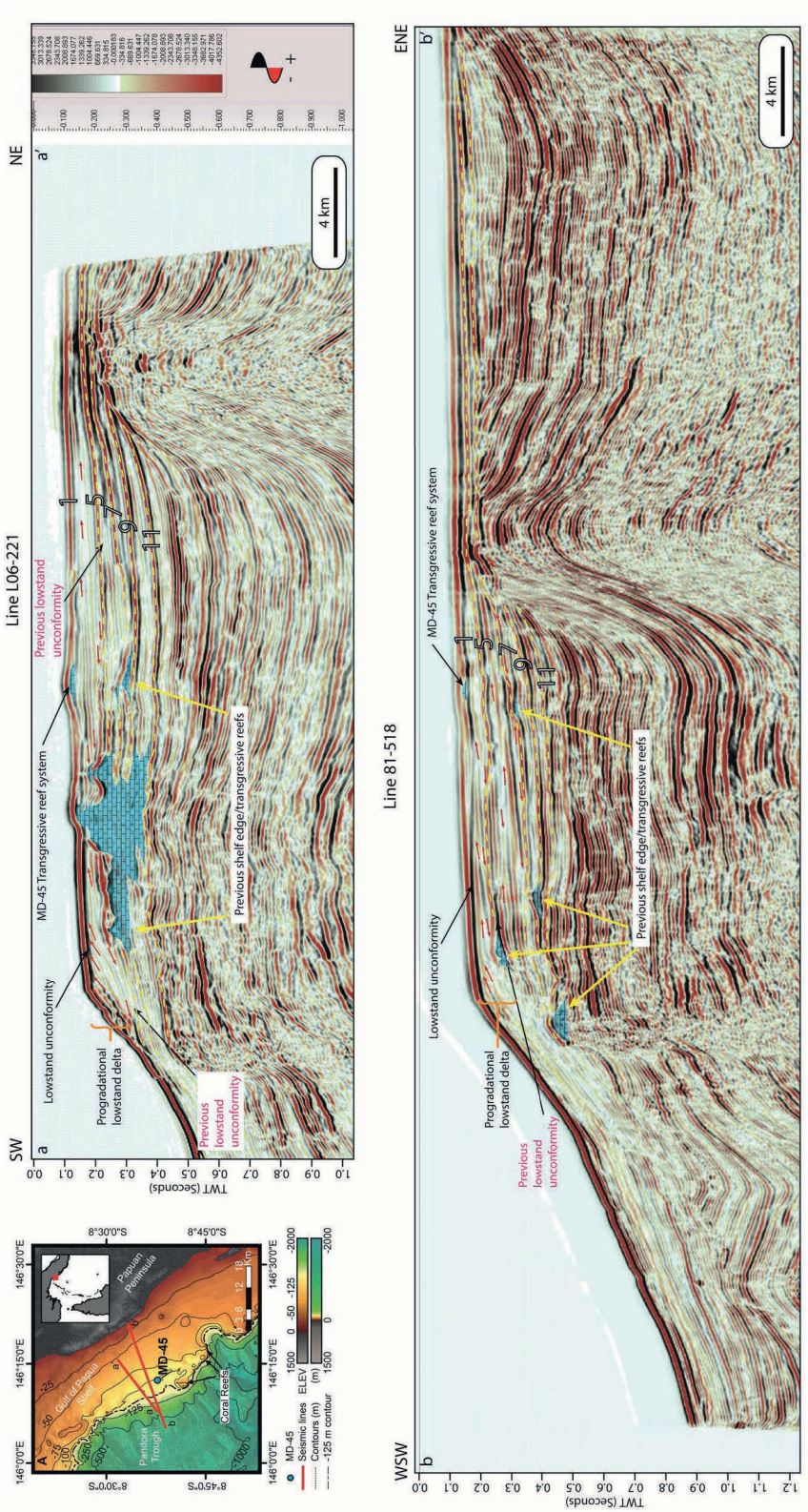


Fig. 3. Seismic dip-lines traversing the South-western Papuan Peninsula Shelf north of the MD-45 hole location. Interpreted on these lines are the transgressive shelf edge-reefs (emphasised by blue block fill) associated with previous glacial-interglacial transitions. Seismic reflection terminations indicated with red arrows show the downlap, onlap and truncations that identify glacial lowstand unconformities that may be associated with previous glacials. Line L06-221 shows successive reefs building on top of previously exposed reefs, while Line 81-518 only intersects reefs that are more isolated and rather shows establishment on siliciclastic substrate. This pattern of transgressive reef development suggests the transgressive reef development and demise seen at the MD-45 location is not unique along this margin but is repeated through successive glacial-interglacial cycles. An important observation is that the reefs were established during a period of tectonic quiescence, as indicated by the onlap of relatively gentle dipping reflections terminating against older, folded and eroded reflection packages. Number labels relate to surfaces potentially corresponding to Marine Isotope Stages. Seismic data provided by Fugro Multi Client Services.

DATA AND METHODS

Advanced piston core MD05-2945 (MD-45) and two 3.5 kHz seismic lines were acquired during the PECTEN (2005) and PANASH (2004) cruises aboard the R/V *Marion Dufresne* and the R/V *Melville,* respectively. The two seismic lines (a strike and a dip) intersect at the location of MD-45. The seismic lines were interpreted to identify reefs, erosional surfaces, internal siliciclastic depositional architecture and overlying sediments. Core sediment samples and coralgal detritus were characterised by identification of coral species and analysis of sediment properties, such as grain-size (fine and coarse fractions separation at 62 micron), carbonate content, X-ray fluorescence (XRF) core scanning, marine grain assemblages, and terrigenous mineral assemblages. Sediment ages were established with AMS radiocarbon and U/Th dating.

Core and sample preparation

MD-45 was sampled extensively, with 2 cm-thick plugs taken at 10 cm intervals within the upper 6 m. Additional plugs and 75 coralgal rubble samples were taken within the lower 8 m. Samples were oven-dried at 70 °C for 24 hours and then weighed to obtain dry weight, disassociated in a phosphate buffered solution (pH 7.5) for 24 hours and then washed over a 63 μm sieve to separate fine fraction (<63 μm) from coarse fraction (>63 μm). The coarse fraction (>63 μm) was oven-dried at 70 °C and then weighed and subtracted from the bulk weight to determine coarse and fine sediment percentages. The fine fraction was allowed to settle in a 2000 mL beaker and was then dried and collected for carbonate content analysis. Fine-grained particles were allowed to settle and the bulk of the water was then removed via siphon; the remaining water was allowed to evaporate and the sediment was dried, collected and stored in plastic vials. The dried coarse fraction was split with a micro-splitter, producing two equal portions, one archived and the other sieved with 300 and 250 μm meshes to produce three grain-size portions. The 300 and 250 μm portion was examined using a Wild Heerbrugg stereomicroscope to extract planktic foraminifera for foraminiferal biostratigraphy and radiocarbon dating. Coralgal clasts were cleaned using buffered (7.5 pH) de-ionised water. Some clasts were cut and sent for U/Th dating, for ease of identification. All coralgal clasts were photographed at high resolution for coral identification to establish trends in assemblages of coralgal debris over time. The taxonomic nomenclature of scleractinian corals follows Veron (2000) and later modifications by Huang *et al*. (2014, 2016).

Carbonate content was measured from the fine fraction. Approximately 0.5 g of sediment was made into powder with a mortar and pestle and analysed for carbonate content following Müller & Gastner's (1971) 'Karbonat-Bombe' method, with modifications: 0.5 g of material instead of 1 g of material and 10 ml 20% 2.3 N HCl instead of 5 ml concentrated HCl were used. Resulting pressure was compared with a reference curve generated from varying amounts of pure carbonate, recalibrated every 5 samples to account for ambient lab pressure variability.

Only the upper 7 m were smooth enough for XRF elemental analysis using an ITRAX core scanner at the Centre Européen de Recherche et d'Enseignement de Géosciences de l'Environnement (CEREGE, France). After smoothing the surface of sediments, the core was scanned at 5 mm spatial resolution under the condition of 30 kV and 30 mA, with 15 seconds of exposure time with a Cr tube as the X-ray source. As coarse coral fragments prevented making a smooth surface and, because of the soupy nature of sediments, XRF scanning was not carried out for the lower 7 m of the

core. In this study, the authors report strontium intensity as a proxy for aragonite (Croudace & Rothwell, 2015), and therefore fine neritic carbonate material, whilst silicon and potassium XRF intensities are used as a proxy for terrigenous input.

Three coral samples at depths – Core Catcher, 1385 to 1395 cm and 1130 to 1135 cm – were analysed for U/Th dating. Two samples obtained from a *Globigerinoides ruber* and *sacculifer* mix, six from fragments of *Turritella cingulifera*, one *Rosalina praegeri* and seven larger benthics (*Marginopora vertebralis*) were analysed for AMS radiocarbon dating at the University of Tokyo (Japan).

U/Th dating

Uranium and thorium isotopes were analysed at the Laboratoire des Sciences du Climat et de l'Environnement (LSCE) in Gif-sur-Yvette (France). Small skeletal fragments were extracted from three coral samples and carefully cleaned using a handheld fine diamond saw to remove sediment-filled cavities or bio-eroded zones. The fragments were examined using a binocular microscope to ensure against the presence of other visible contaminants and finally crushed into a coarse-grained powder with an agate mortar and pestle. The coral material was transferred to acid-cleaned Teflon beakers, ultrasonicated in MilliQ water, rinsed twice and then leached with 0.1N HCl. The clean samples were dissolved in 3 to 4 ml diluted HCl (~10%), equilibrated with a mixed $^{236}U/^{233}U/^{229}Th$ spike and then the U and Th fractions were separated using UTEVA resin (Eichrom Technologies, USA). The U and Th separation and purification followed a slightly modified procedure (Douville *et al.*, 2010).

Uranium and thorium isotopes were determined simultaneously using a ThermoScientific Neptune^{Plus} multicollector-ICP-MS following the protocol developed at LSCE (Pons-Branchu *et al.*, 2014). The ^{238}U-^{230}Th ages were calculated from measured atomic ratios through iterative age estimation (Ludwig & Titterington, 1994), using published ^{230}Th, ^{234}U and ^{238}U decay constants (Jaffrey *et al.*, 1971; Cheng *et al.*, 2013; Extended Data Table 1). Due to the high values for $^{230}Th/^{232}Th$ ratio (>4000) no correction was applied for the non-radiogenic ^{230}Th fraction. In fact, a correction for initial ^{230}Th would be minor where a $^{230}Th/^{232}Th$ activity ratio of 20 is not exceeded (McCulloch *et al.*, 2010).

The initial $\delta^{234}U$ values for these coral samples are slightly lower than for that of the modern sea water (146.8 ± 0.1‰) (Anderson *et al.*, 2010), which is commonly used as a reference for the detection of 'closed-system behaviour' of the coral. Specifically, a substantially different $\delta^{234}U_{initial}$ than that of the modern sea water value (e.g. 7‰ higher or lower; Robinson *et al.*, 2006), most probably points towards open system behaviour. However, several publications have suggested that sea water $\delta^{234}U$ was systematically lower during the Glacial period compared to the Holocene (Esat & Yokoyama, 2006). These coral samples grew during an early stage of the deglaciation. The $\delta^{234}U_{initial}$ *vs.* ages show a near perfect correlation ($r^2 = 0.99$), indicating that these corals might have recorded a rapid change of the sea water $\delta^{234}U$.

AMS radiocarbon dating

Samples were collected from 18 locations throughout the core for AMS radiocarbon dating at the University of Tokyo (Japan): three from *Globigerinoides ruber* and *sacculifer* mix (size range >250 µm), six from fragments of *Turritella cingulifera*, one *Rosalina praegeri* and seven larger benthic foraminifers (*Marginopora vertibralis*) (Table 1). All samples were washed with methanol in a sonic bath to remove adhered debris. Ages were reported for 13 of the 18

samples as five samples were not able to be analysed accurately. Ages were corrected for marine reservoir effects using an average of three samples ($\Delta R = -176$, $\sigma = 56$) from Murray Island in the Torres Strait (Hua *et al*., 2020), obtained through the Marine20 database and then converted to cal-BP using CALIB 8.20 (Stuiver *et al*., 2021).

Diffractometric analysis

Part of the cleaned coarse-grained powder of each coral sample was used for diffractometric analysis. The samples were further crushed with a mortar and the fine powder was mounted on a silicon zero background sample holder. The X-ray powder diffraction data were recorded on a Panalytical θ-θ diffractometer at the Department of Geosciences of the University of Padova (Italy). The High Score Plus program was used for phase identification and quantitative analysis by Rietveld refinement (Rietveld, 1967). Refined parameters comprise scale factors, zero-shift, background, lattice constants and profile parameters (Gaussian and Lorentzian coefficients).

X-ray diffractometric results show that the three coral samples analysed contain very small amounts of calcite (Supplemental Fig. 1), suggesting that the adopted sub-sampling strategy, which consisted of carefully selecting and cleaning the skeletal fragments, was successful in isolating mostly the pristine portion of the aragonite coral skeleton.

Based on A) the small % of calcite within the skeleton, B) the initial $\delta^{234}U$ values close to modern sea water, C) the concentrations of uranium similar to those found in modern tropical corals; and D) the detrital ^{232}Th concentration lower than 0.4 ppb, the U/Th ages can be considered reliable.

RESULTS

MD-45 core data

Faunal analysis: coral

Core MD05-2945 (MD-45), retrieved at the intersection between the strike and dip seismic lines (Fig. 2), struck the side of the buried reef at a depth of -111.3 m below the sea surface (Beaufort *et al*., 2005). The cone of the piston core barrel dislodged and recovered part of a *Goniastrea retiformis* coral colony (11 cm in height and 7 cm in width) in growth position at the base of a 14.3 m-long core (Beaufort *et al*., 2005). Growth position was indicated by upward facing corallites and the freshly broken surface at the base of the colony fragment. The remainder of the core consisted of coralgal debris capped with a siliciclastic mud sequence (Fig. 4A). Overlying this basal colony is an assemblage of coralgal debris displaying an abrupt change from *Goniastrea* (Fig. 4E), *Favites abdita* (Figs 4D, 5B, and 5F), *Acropora* (Fig. 5E and H), *Galaxea* (Fig. 5C) and *Lobophyllia*? (Fig. 4C) to *Montipora* (Fig. 6C, E, G and I), *Porites* (Fig. 6E and G), *Echinophyllia* (Fig. 6B, D and I), and Agariciidae (Fig. 6E), with increasing amounts of coralline algae and digitate microbialites at ~10.75 mbsf (metres below sea floor, or core depth; Figs 7A, B and 4). A complete list of identified coral fragments can be found in Fig. 7 and images of selected samples in Figs 6 and 7. By 6.5 mbsf, coralgal debris is largely absent; only occasional small grains remain, giving way to siliciclastic sand and a 3.5 m-thick mud interval (4.5 to 1 mbsf; Fig. 4A). The authors have identified coral assemblage as a way to best assess palaeo-depth of the reef system (Braga *et al*., this issue).

The *G. retiformis* framework coral observed at the base of the core is a species known to occupy the shallow reef-crests and intertidal zone (Fig. 4B and E; Webster *et al*., 1998; Veron, 2000; Dutton *et al*., 2015;

Vyverberg *et al*., 2018). Although *G. retiformis* can be found in a wide range of depths (0 to 30 m; Hibbert *et al*., 2016; Loya *et al*., 2019), it is commonly observed in high-energy, intertidal reef-flats and reef-edges (Veron, 2000; Golbuu & Richmond, 2007). Modern examples from the Seychelles and Japan suggest that this species occurs most commonly at depths of 0 to 2 m (Vyverberg *et al*., 2018) and 0 to 5 m (Iryu *et al*., 1995; Webster *et al*., 1998; Sugihara *et al*., 2003), respectively. A planula larvae recruitment study in Guam by Golbuu & Richmond (2007) indicated that *G. retiformis* is generally limited to 0 to 10 m depth. This basal framework coral is covered by ~1 m of *Goniastrea, Favites abdita and Galaxea* fragments (Figs 4B, 5 and 7).

From 13 to 10.75 mbsf, *Acropora* (Fig. 5H) and merulinids (Fig. 5A) (esp. *F. abdita,* Fig. 5B) become the dominant assemblage with *Astreopora* (Fig. 5I)*, Stylophora* (Fig. 5D) and *Galaxea* (Fig. 5C) also present (Figs 4B, 5 and 7). Although all these taxa are found from shallow to deep mesophotic reef settings, the dominance of *Acropora* and *F. abdita* and the presence of *Stylophora*, suggest a shallow reef environment (Veron, 2000). The median and average depth of *F. abdita* for occurrences of this species reported over the period 1990-2021 and listed in the OBIS database (N = 294) is 3 m and 4.4 m, respectively (OBIS, 2021). *F. abdita* is a dominant species of the 'domal coral assemblage' defined in Braithwaite & Montaggioni (2007) occurring down to 25 m. *Stylophora*, particularly *S. pistillata*, prefers shallow, high-energy environments that may be periodically exposed and is common at water depths of 0 to 6 m (Veron, 2000; Montaggioni, 2005; Montaggioni & Braithwaite, 2009). In contrast, *Galaxea astreata* prefers reef settings protected from strong wave energy and can be found over a broad depth range down to 65 m (Veron, 2000; Muir & Pichon, 2019). This assemblage of corals is similar to recent work from the GBR that has a depth range of 0 to 30 m, but more probably between 0 to 10 m (Humblet *et al*., 2019). Based on the bulk of this assemblage, the coral debris is probably derived from a nearby shallow-water, reef-flat to upper-slope environment (0 to 20 m, possibly 0 to 10 m). However, the presence of *Galaxea* does increase the uncertainty that corals which more often occupy shallow-water environments are much more common.

At 10.75 mbsf, there is a major shift to foliaceous and encrusting corals – agariciids, *Echinophyllia*, *Montipora* and *Porites* (Figs 4B, 6 and 7) – ending with a final encrusting *Echinophyllia* at 6.5 mbsf. Agariciids (including, *Pachyseris speciosa*; Fig. 6E and I), *Montipora* and *Porites,* are all commonly found in a wide range of depths and reef habitats, from back-reef, lagoon, to reef slope (Veron, 2000). *Echinophyllia echinata* and *aspera* prefer lower reef slopes and low energy lagoons (Veron, 2000). The assemblage composed of lamellar agariciids, particularly *Leptoseris* and *Pachyseris*, *Echinophyllia* and *Montipora* is indicative of reef slope settings >20 m-deep, or shallower but more sheltered or poorly lit reef environments (Montaggioni, 2005; Braithwaite & Montaggioni, 2009). Laminar *Porites* and/or *Montipora* and agariciids indicate deeper fore-reef slope settings in deglacial reef sequences in Tahiti (Abbey *et al*., 2011) and the GBR province (Webster *et al*., 2018; Humblet *et al*., 2019). *Lobophyllia* (Fig. 6F) also is more commonly found in low energy environments such as protected reef slopes and lagoons (Veron, 2000). Lastly, the observed *Fungiidae* (Fig. 6B) corals are solitary and commonly occupy soft, low-energy substrate (Veron, 2000). Additionally, these corals are more often encrusted with microbialites, some digitate in nature. Altogether, there are a wide variety of depths and habitats that can be occupied by this coral assemblage; however, many of the

corals distinctly prefer low-energy environments, which suggests the environment was probably deeper-water forereef slope (>20 m).

Faunal assemblages: non-coral

Non-coral tests and fragments, including shallow benthic gastropods, pelecypods, echinoids and occasionally larger benthic foraminifers (*Marginopora vertebralis*) are common within the lower 8 m. *Marginopora vertebralis* is often found living amongst modern coral reef, including the GBR (Ross, 1972; Lee *et al*., 2016; Renema, 2018). There is a unique 1 m-thick (6.3 to 7.2 mbsf) interval dominated by the benthic gastropod *Turritella cingulifera*. In the top 6.5 mbsf, planktic foraminifera replace larger benthic foraminifera (Fig. 4A). A conspicuous 3.5 m-thick mud interval, beginning at 4.5 mbsf, has instead a large amount of framboidal and agglutinated pyrite clusters, with planktic foraminifera largely absent. The top 1 m is rich in planktic foraminifera, with minor amounts of pteropods, benthic foraminifera, gastropods, pelecypods, and echinoids spines and plates (Fig. 4A).

Lithologies: grain-size

MD-45 displays a stepped, fining upward trend, a change in mineralogy and reduced neritic carbonate input. The basal 3 m of the core is dominated by large coralgal clasts with <25% fines (<63 µm mud) (Fig. 4A). From 11.25 to 7.00 mbsf, coralgal clasts still dominate, with fines increasing to ~40%. Coralgal clasts become significantly smaller and less common after 7 mbsf, as fines increase to 55% for 0.5 m before increasing to 70 to 90%. At this point, coralgal material is sparse and only present as granule and sand-sized grains. A uniform interval from 4.5 to 1 mbsf consists of >98% fine mud (Fig. 4A). Throughout the core, coarse sediments are consistently observed to be carbonate grains.

Lithologies: carbonate content

Through time, carbonate content becomes less concentrated within both the bulk and fine fractions. Bulk carbonate is ~90% at the base, declining gradually to ~80% at 7.4 mbsf before dropping to between 10 and 30% at 6.0 mbsf for the remainder of the core (Fig. 4A). Fine carbonate follows a similar declining upward trend, although at much lower levels, never exceeding 40% (Fig. 4A). This decrease in carbonate content up-core is observed within the elemental data obtained from X-ray fluorescence (XRF) core scans (Fig. 4A). Bulk carbonate content is reciprocal to the fine fraction; and the lack of carbonate in the fines indicates that siliciclastic mud becomes increasingly dominant up core (Fig. 4A).

Lithologies: XRF counts and mineralogy

The coarse nature and large clasts in the lower core limited XRF core scanning to the upper 7 m (Fig. 4A). XRF elemental counts of calcium (Ca), strontium (Sr), silicon (Si) and potassium (K) are shown in Fig. 4A. Sr and Ca counts decline significantly at the mud interval, with a recovery in the top 1 m, where Ca counts increase more significantly than Sr counts. K and Si increase to a maximum by the beginning of the mud interval then slowly decline by ~40% at the surface (Fig. 4A). To better understand aragonite content within the upper 7 m, the authors normalised Sr to K (Sr/K) and Ca (Sr/Ca) to show the drop in aragonite relative to siliciclastics at 6 mbsf and the major decline in aragonite *vs*. pelagic carbonate at 4.5 mbsf, respectively (Fig. 4A).

Radiometric dating

Twenty-one samples were radiometrically dated and corrected, using Intcal20 and local Marine20 correction of $\Delta R = -176$, $\sigma = 56$ (see Methods), to calendar year BP (Table 1) to determine the age of core sediments and the timing of sediment facies transitions at

MD-45. Three U/Th dates were acquired from corals (Fig. 4C, D and E), starting with the basal *G. retiformis* colony (14.3 mbsf, 19.4 kyr BP, Fig. 4E), *F. abdita* (.13.85 mbsf, 18.4 kyr BP, Fig. 4D) and *Lobophyllia?* (11.3 mbsf, 16.9 kyr BP, Fig. 4C). High aragonite content of dated corals (>98%) indicates good candidates for accurate dating. Eighteen larger benthic foraminifers, planktic foraminifer, pelecypod and gastropod samples were analysed for AMS ^{14}C dates to fill in the gaps between the dated corals and to bracket important intervals (Fig. 4A, Table 1). Additionally, the basal *G. retiformis* colony U/Th date was confirmed by an 18.9 kyr BP AMS ^{14}C date (Francis, 2007). Three ^{14}C dates do not appear in chronologic order; however, they are within acceptable margins of error. One ^{14}C date from *Marginopora vertebralis* (large benthic foram) at 13.25 mbsf (18,815 ± 155 cal yr BP) is older than the more accurate U/Th date of *F. abdita* at 13.85 mbsf (18,405 ± 107 yr BP) (Fig. 4A, Table 1).

INTERPRETATION

The sequential deepening of core MD-45 is evidenced by the coralgal and non-coralgal assemblages, sediment grain-size, mineralogy and composition. The coral assemblages present within debris recovered in the lower 8 m of MD-45 are consistent with a deepening succession typical of reef drowning (Webster *et al*., 2004a), where shallow-water corals are replaced by deeper-water corals up core. The non-coralgal assemblages also display a deepening upward sequence as they transition from shallow-water benthic species to include planktic foraminifera and pteropods up core.

Grain-size and type variation also indicate deepening upwards throughout the core. The shift from coarse-grained coralgal debris in the lower part of the core to finer-grained sand, silt and clay-sized particles is indicative of a change from a shallow high-energy environment to a deeper low-energy environment. Mineralogy of fine-grained sediments is not directly measured but rather indicated by elemental proxies obtained by XRF core scanning. Calcium and strontium are excellent proxies for carbonates. Strontium is a particularly good proxy for aragonite (Rothwell *et al*., 2006), as Sr substitutes more easily for Ca in aragonite than within calcite (Boardman & Neumann, 1984). Silicon and potassium are common constituents of siliciclastics but not carbonates. Elemental proxies indicate a transition from shallow-water carbonates to fine-grained siliciclastics and a decrease in neritic reef sediment supply.

These observations within the MD-45 core are consistent with drowning and back-stepping observed on the 3.5 kHz seismic lines (Fig. 2). Accurate radiometric dating of core material coupled with the greater morphologic context, as defined by the interpreted seismic lines, allow interpretation of reef development along this part of the SPPBR as it relates to stepwise sea-level rise during the last deglaciation. The nearby central GBR exhibits a similar pattern of reef establishment, growth and back-stepping related to punctuated sea-level rise (Webster *et al.*, 2018). There, three reef packages have been identified that are related to the three main episodes of deglacial sea-level rise: Reef 3a (21 to 17 ka, up to -105 m), Reef 3b (17 to 13 ka, up to -88 m) and Reef 4 (13 to 10 ka, up to -55 m) (Webster *et al.*, 2018; see their Fig. 4).

LGM lowstand shelf edge delta

The initial phase along the SPPBR deglacial reef formed on an early LGM prograding siliciclastic delta at about 116 m below sea-level, corresponding to sea-level plateauing at 113 m (±6 m), from 30 ka to 21.5 ka (Yokoyama *et al*., 2018). The top of the early LGM shelf-edge delta was partially eroded

and ultimately established itself along the shelf break during the latest part of LGM when sea-level fell as much as 20 m to ~-125 or -130 m centred at 21.5 ka (Yokoyama *et al*., 2018; Figs 2B, 8C and D). Extensive seismic lines throughout the GoP show that part of the SPPBR shelf edge and outer shelf has been tectonically inactive since the middle Pleistocene (Mid-Brunhes) and the inner shelf since the last interglacial highstand, with very low rates of subsidence (Tcherepanov *et al*., 2008; Tcherepanov *et al*., 2010; Fig. 4), verified by the ~-125 m position expected of the present shelf break (Fig. 2B). Two thrusted ridges are clearly visible in Fig. 3, indicating the margin was once active. The outboard ridge pins the location of stacked shelf-edge reefs and the divergent nature of sediment reflectors overlying the folds indicate the margin has not experienced thrusting or inversion during the time of the reef-building events since the Mid-Brunhes. The inner ridge has onlapping strata and is capped by a tectonically undeformed package from the last interglacial highstand.

Reef establishment, 19 kyr MWP

The *Goniastrea retiformis* of the initial reef phase is a coral species commonly observed in very shallow reef settings less than 5 m-deep (Veron, 2000). Though *G. retiformis* may live in greater water depths, it has been used as an excellent proxy of sea-level (Webster *et al*., 1998; Dutton *et al*., 2015; Vyverberg *et al*., 2018), as previously discussed. This specimen was dated to 19.4 kyr BP U/Th age and 18.9 cal kyr BP AMS ^{14}C date (Francis, 2007) and was recovered at 111.3 mbsl. This means that by 19.4 to 19.0 ka sea-level may have risen from 125 to 111 mbsf, an amplitude of ~14 m. It is important to note that this is a minimum calculation of sea-level rise and that the coral may have lived at greater depths. While it is probable that the *G. retiformis* colony lived at shallow palaeo-water depths, there is no conclusive evidence to suggest it lived at mean sea-level. Additionally, tectonic subsidence/uplift may have affected the present depth of the buried reef, though these effects are expected to be minimal. Uplift is seen as improbable as high-quality seismic lines do not indicate evidence of uplift or inversion within the recent past (Fig. 3). Regardless, 14 m of sea-level rise is consistent with published records of the 19 kyr MWP (Yokoyama *et al*., 2000; Hanebuth *et al*., 2000; Hanebuth *et al*., 2006; Ishiwa *et al*., 2019). This coral-based dating of the 19 kyr MWP is well within the published non-coral estimates of a 10 to 15 m rise at 19.1 ka (Yokoyama *et al*., 2000; Ishiwa *et al*., 2019), a 10 m rise at 19.6 to 18.8 ka (Hanebuth *et al*., 2006), a 10 m rise at ~19 ka (Hanebuth *et al*., 2000) and an abrupt 10 to 15 m rise in global sea-level at 19 ka (Clark *et al*., 2004). The results of this study would strengthen the conclusion by Clark *et al*. (2004) that sea-level rose abruptly after 19 ka by 10 to 15 m.

However, in reviewing the overall lines of evidence published until 2012 and summarised in their fig. 10, Carlson & Clark (2012) concluded that, as in Yokoyama *et al*. (2000), the LGM lowstand was terminated by a maximum rise of 10 m between 19.4 and 19 ka, suggesting 8 to 16 mm yr^{-1} as the range of rates of sea-level rise during the initial 19 kyr meltwater pulse. Moreover, as a challenge, recent results of IODP research offshore the Great Barrier Reef indicate that this initial MWP may have been a more subdued and gradual 3.5 mm yr^{-1} (from 21 to 16.5 ka) than previously coral and non-coral-based studies have suggested (Yokoyama *et al*., 2018). Webster *et al*. (2018) also identified reef growth during the initial stage of deglaciation as defined by Reef 3a from the GBR. There they observed initial accretion rates of 3.9 to 4.4 mm yr^{-1} slow to 1.8 mm yr^{-1} at 19.22 ± 0.01 ka following the

MWP. Regardless of the absolute rate of sea-level rise during this 19 kyr MWP, what is clear is that a reef was established during the last deglaciation and accreted as sea-level rose from LGM levels to at least ~111 mbsl by 19.4 ka, with approximately 5 additional metres of aggradation by 17 ka (Fig. 2). This is consistent with the establishment and demise of Reef 3a from the GBR.

Back-stepping and partial drowning, MWP-1A

The seismic strike line (Fig. 2C) illustrates through time a series of back-stepping and partial drownings of the SPPBR. Three distinct reef terraces are observed (Figs 2C and 4). The 19 kyr MWP initial reef generation clearly shows a pattern of rim keep-up simultaneously with partial drowning and back-stepping towards the south-east (Figs 2C and 8B). Back-stepping first occurs with reef-top terminations at a depth of ~103 mbsl (Figs 2B and 2C), approximately consistent with the depth (105 mbsl) at the onset of MWP-1A (Deschamps *et al*., 2012). Back-stepping allowed the reef to in part survive the high amplitudes (14 to 18 m) and rates (~46 ± 6 mm yr^{-1}) of sea-level rise during MWP-1A (Deschamps *et al*., 2012). Continued vertical accretion of an additional 20 m occurred away from the shelf edge during the Bølling/Allerød (B/A), forming a broad and 10 km-long barrier reef over the next 3 kyr (Figs 2C and 8B). Webster *et al*. (2018) also observed GBR back-stepping and accretion in Reef 3b at similar depths (-105 to -85 m) during MWP-1A.

The partial drowning and back-stepping of this initial reef phase is clearly observed and well dated by MD-45 sediments (Fig. 4B). Reef drowning results in a change in coralgal assemblages, reflecting a relative increase in water depth occurring at core depth (~10.75 mbsf). Shallow-water, often mono-specific, corals that once dominated the shallow-reef framework become first partially and then fully replaced by deeper lower-energy corals (Blanchon & Shaw, 1995; Webster *et al*., 2004a; Blanchon *et al*., 2009). Finally, the corals are increasingly encrusted with and replaced by coralline algae, microbialites, bryozoans and benthic foraminifera (Marshall *et al*., 1998; Webster *et al*., 2004b; Fig. 4B). The coral debris in the lower 7.5 m of MD-45, therefore, display a clear deepening/drowning pattern, beginning with a shallow *Goniastrea* framework coral covered by debris from shallow/upper fore-reef corals (*Faviids*, *Galaxea*; Figs 4B, 5 and 7), moving to a more varied assemblage (acroporids, *Faviids*; Fig. 5) and lastly undergoing a major change to encrusting/foliaceous corals (agariciids, *Echinophyllia*, *Montipora*, poritids, etc.) and an increase in encrusting coralline algae and digitate microbialites (Figs 4B and 6). This assemblage trend represents a change in water depth from near 0 to over 20 to 30 m. A significant change in sediment composition occurs at 6.25 mbsf. The fine fraction increases from 40 to 80%, while bulk carbonate content decreases from 60 to 20% (Fig. 4A). Additionally, the decrease of Sr counts and the Sr/K ratio (coral reef-derived aragonite proxies; Fig. 4A) and the increase in siliciclastics (from K) coincide with the end of coralgal clasts above the well-dated *T. cingulifera* interval (15.3 to 14.6 cal kyr BP, Fig. 4A, Table 1). The *T. cingulifera* interval age dates are near to but largely pre-date the beginning of MWP-1A. The greatest sedimentological changes occur immediately after the dated interval. Date ranges of two of the samples are 15.05 to 14.61 cal kyr BP and 15.11 to 14.70 cal kyr BP, possibly contemporaneous with the initiation of MWP-1A at 14.65 ka (Deschamps *et al*., 2012).

The MD-45 reefs are amongst the most proximal to the large PNG siliciclastic sources (Fig. 2A). This is reflected at MD-45,

where siliciclastics are the most significant fine fraction component, at first quite low in the lower 7 m, then significantly increasing to dominate the bulk fraction through time (Fig. 4A) – possibly a sign of increasing turbidity in the water column. Whether increased turbidity resulted in shoaling of the coral growth critical depth (Hallock & Schlager, 1986) is unclear, but improbable, during MWP-1A. However, partial drowning occurred at each of the major MWPs during the last deglaciation, followed by reef keep-up and accretion in a back-stepped location during periods characterised by a lower rate of sea-level rise (Figs 2C and 8B). The presence of fine siliciclastic mud with the coralgal debris in the lower 7 m of the core suggests that the reef was able to cope with some turbid water and even accrete upward, as nearly 3 m of shallow-water coralgal material accumulated at the base of core MD-45. Additionally, during MWP-1A sea-level rose 14 to 18 m in less than 500 years, or 46 mm yr^{-1} (Deschamps *et al*., 2012); rates that are at least an order magnitude higher than current rates of 3.1 ± 0.4 mm yr^{-1} (Thompson *et al*., 2019). The incipient reef was rapidly covered by nearly 25 m of water, probably below a drowning depth suggested for low visibility/turbid water (Hallock & Schlager, 1986) and, in response, a portion of the reef drowned, with the surviving portion continuing to grow in a back-stepping fashion (Figs 2C and 8B). Webster *et al.* (2018) reported rapid sea-level rise (27 to 30 mm yr^{-1}) as a major factor, along with regional sediment flux, in the demise of nearby GBR Reef 3b (17 to 13 ka). As the rate of sea-level rise decreased, the surviving reef continued to accrete by about 20 m in its south-eastern portion during the B/A interval (Figs 2 and 8B).

MWP-1B sea-level rise and increased water column turbidity

A 3.5 m-thick (>98%) fine-grained siliciclastic mud unit (4.5 to 1 mbsf) is well developed in MD-45. The mud package is bracketed by two AMS dates. An articulated (both valves intact, suggesting little to no transport or reworking) pelecypod was dated (11.73 ± 0.19 cal kyr BP) immediately below the mud package (4.6 mbsf) and the *G. ruber/sacculifer* sample was dated (6.32 ± 0.30 cal kyr BP) immediately above (0.9 mbsf). It is inferred that the start of the mud package is synchronous with the 11.3 ka MWP-1B at Papeete (Bard *et al*., 2010) and Barbados (Fairbanks, 1989; Bard *et al*., 1990). Abdul *et al*., (2016) places MWP-1B at 11.45 ka BP at Barbados. The importance of MWP-1B as a high amplitude sea-level rise event is still unresolved (Abdul *et al*., 2016; Bard *et al*., 2016) and may not be a significant factor in direct reef drowning of the GBR or SPPBR (Webster *et al*., 2018).

The 3.5 m-thick fine siliciclastic sediment layer may be explained by a number of related factors. Beginning at ~12 to 11 ka, Indo-Australian monsoon intensity increased until ~4 to 5 ka (Haberle *et al*., 2001; Magee *et al*., 2004; Griffiths *et al*., 2009; Mooney *et al*., 2011; Denniston *et al*., 2013). Griffiths *et al*. (2009) linked the greatest amount of precipitation intensity from 11 to 7 ka to the flooding of the Sunda and Sahel shelves. Thomas *et al*., (2018) identified an order of magnitude increase in the amount of pollen and charcoal delivered to the nearby Ashmore Trough beginning at MWP-1B. Elevated monsoon intensity resulted in increased weathering and the transport of PNG continental material to the GoP. Additionally, increased flooding of the GoP shelf led enhanced tidal energy to rework shelf siliciclastics (Harris *et al*., 2005) and allowed the clockwise intrashelf current (Fig. 1) to establish and transport sediment more effectively towards the SPPBR and MD-45

reef location (Wollanski & Alongi, 1995; Slingerland *et al.*, 2008; Howell *et al*., 2014; Thomas *et al*., 2018). Muhammad *et al.* (2008) recorded fine-grained siliciclastics entering the Pandora Trough directly to the west of this location. The dates bracketing the mud interval (11.7 to 6.3 cal kyr BP) are consistent with work by Griffiths *et al.* (2009), indicating that the mud interval is probably the result of shelf flooding, monsoon intensity, sediment reworking and improved shelf-sediment transport.

This partial drowning and back-stepping event was even more severe than observed during MWP-1A, as shown in the seismic (Figs 2C and 8A). Nearby, GBR Reef 4 (13 to 10 ka) experienced a similar demise. Webster *et al*. (2018) recorded that Reef 4 experienced relatively low rates of sea-level rise (4 mm yr^{-1}) and massive sediment influx (3 x LGM-Holocene levels), thought to be related to shelf reflooding processes. At this time, large pulses of siliciclastic sediment probably had a significant effect, leading to the most dramatic reef demise and back-stepping event of the SPPBR. It is probable that increasing sea-level during MWP-1B and beyond, interacting with regional physiography, had a more significant impact than actual rates of sea-level rise.

Regardless of the magnitude of sea-level rise during this time, it is clear from the mud interval in MD-45 (Fig. 4A) and the final major terrace displayed in the seismic (Fig. 2C) that there was a significant environmental change. This second back-stepping event corresponds to the demise of a major portion of the reef at ~60 mbsl and the persistence of the more modest, active modern reef (Figs 2C and 8A) seismic imaged (Fig. 2C) as two narrow peaks (an artifact of the high vertical exaggeration [70:1] of the seismic representation). Terraces (Reef 4) that formed in the GBR (Webster *et al.*, 2018) from 13 to 10 ka with a sea-level rise from ~88 to ~55 mbsl, drowned terraces from the Gulf of Mexico (57.5 to 61.8 mbsl, ~11.5 ka; Khanna *et al.*, 2017), submerged Maldives terrace 'T3' (58.8 ± 3.8 mbsl; Rovere *et al*., 2018) and a 55 to 60 mbsl terrace at the Abrolhos shelf, Brazil (Cetto *et al*., 2021) are at similar levels to the back-stepping terrace (60 to 65 mbsl) along the SPPBR. It appears that it is not uncommon for terraces related to back-stepping to be formed at this level and time.

The effects of the sea-level-shelf interactions initiated during MWP-1B are also significant in the deglacial sedimentary accumulation on the shelf edge, upper slopes and in the troughs of the GoP. Bank-derived fine aragonite, after disappearing in the slope periplatform sediments during the exposure MIS 4-MIS 2 interval of the GBR and offshore atolls, is re-initiated at ~11.5 ka, which is the time of the reef reflooding in the GoP (Francis, 2007; Mallarino *et al*., 2021). A clear switch from siliciclastic to calcareous turbidites is also dated at ~11.5 ka in several cores recovered from the Pandora Trough (Jorry *et al*., 2008; Jorry *et al*., 2010). At the same time as the MWP-1B, significant modification of benthic foraminifer assemblage occurred in the upper slopes and shelf edge of Ashmore Trough (Carson *et al*., 2008; Mallarino *et al*., 2021). During the last 6.3 kyr, sea-level stabilised and monsoon intensity declined (Haberle *et al*., 2001; Magee *et al*., 2004; Griffiths *et al*., 2009; Denniston *et al*., 2013), resulting in suitable conditions for the reef to grow to its south-east back-stepped position at present day.

Table 1. Radiometric age dates for MD-45 samples. All dated samples with core depth [cm below sea floor (cmbsf)], specimen name and age, either AMS ^{14}C or U/Th. Three coral samples were dated using U/Th. Remainder of samples (benthic and planktonic foraminifera, gastropods and pelecypod) dated using AMS ^{14}C. It was not possible to date five samples due to low sample quality and these are labelled N/A. Basal colony AMS ^{14}C age from Francis (2007).

Table 1. Radiometric Age Dates

Sample		Uncorrected Age (kyr BP)		Age (cal kyr BP)
Depth (cmbsf)	Specimen	U/Th	AMS ^{14}C	AMS ^{14}C
1-2	*Globigerinoides ruber/sacculifer*		1,855 ± 160	1,445 ± 195
10-12	*Globigerinoides ruber/sacculifer*		2,390 ± 170	2,070 ± 230
90-92	*Globigerinoides ruber/sacculifer*		6,315 ± 30	6,765 ± 105
460-462	articulate pelecypod		10,430 ± 85	11,730 ± 190
630-632	*Turritella cingulifera*		N/A	N/A
640-642	*Turritella cingulifera*		12,925 ± 95	14,905 ± 205
660-662	*Turritella cingulifera*		N/A	N/A
670-672	*Turritella cingulifera*		12,890 ± 100	14,830 ± 220
680-682	*Turritella cingulifera*		13,170 ± 95	15,225 ± 175
707-713	*Turritella cingulifera*		N/A	N/A
717-722	*Marginopora vertebralis*		13,230 ± 100	15310 ± 180
737-742	*Marginopora vertebralis*		N/A	N/A
930-933	*Marginopora vertebralis*		13,640 ± 100	15,845 ± 185
980-985	*Marginopora vertebralis*		N/A	N/A
1020-1027	*Rosalina praegeri*		13,585 ± 95	15,780 ± 180
1064-1067	*Marginopora vertebralis*		13,665 ± 345	15,870 ± 470
1130-1135	*Lobophyllia?*	16,923 ± 64		
1268-1273	*Marginopora vertebralis*		14,970 ± 110	17,530 ± 200
1325-1330	*Marginopora vertebralis*		16,135 ± 110	18,815 ± 155
1385-1395	*Favites abdita*	18,405 ± 107		
Core Base	*Goniastrea retiformis*	19,396 ± 48	16,210 ± 35*	18,890 ± 115

**age from Francis, 2007*

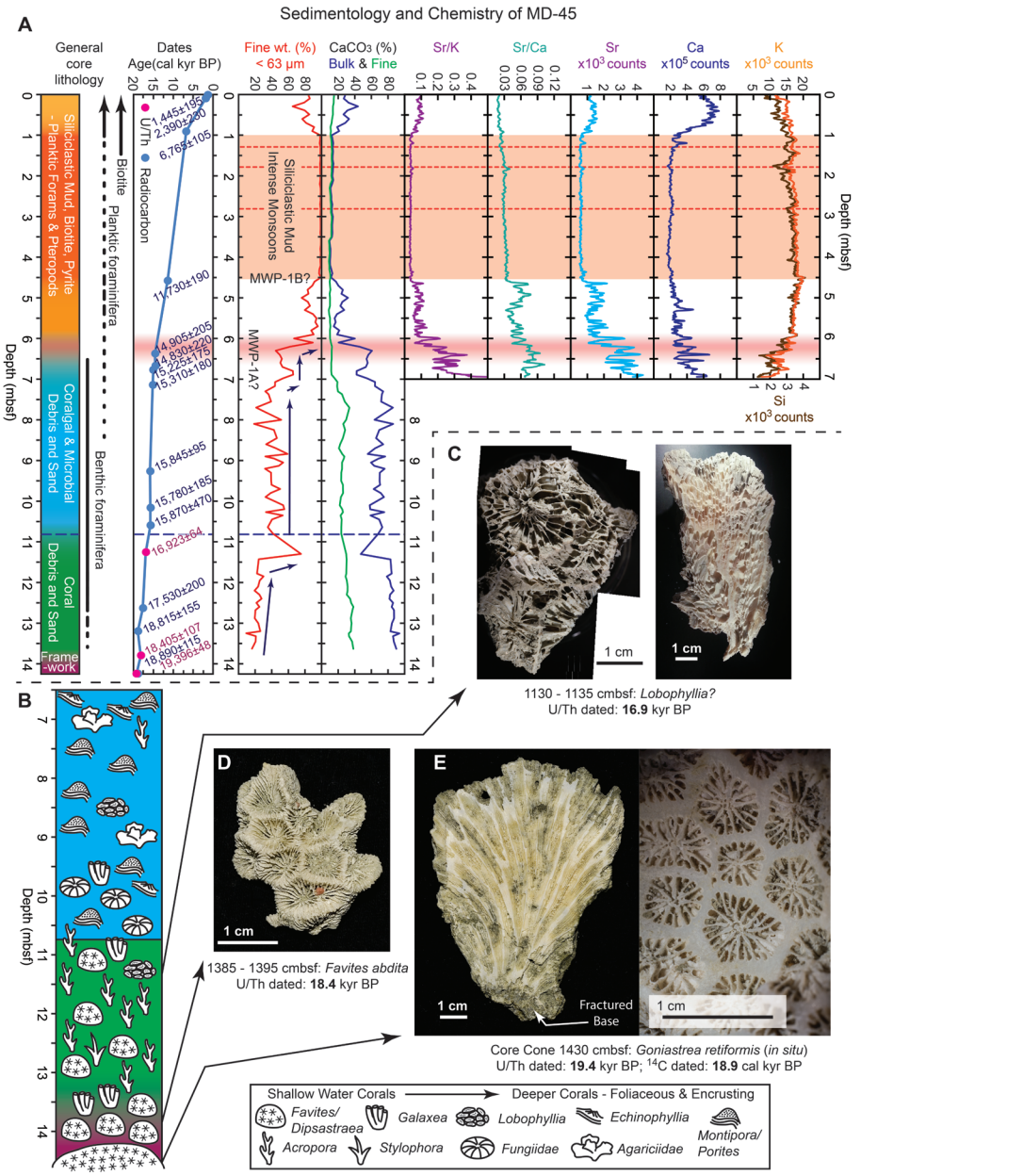


Fig. 4. MD-45 sediment variations. (A) General core lithology with colour variations shows changes in sediment components: violet = framework coral, green = shallow-water coralgal assemblage, blue = deeper-water coralgal assemblage, orange = fine siliciclastics and foraminifera, red = siliciclastic mud. Biostratigraphy defined by presence and/or absence of larger benthic foraminifera and planktic foraminifera. Radiometrically dated sediments in time and depth: pink circles = U/Th-dated corals; blue circles = radiocarbon-dated larger benthic foraminifera, planktic foraminifera, gastropods and pelecypods. Core sediment properties: fine weight percent, bulk and fine carbonate content, Sr/K ratio, Sr/Ca ratio, Sr counts, Ca counts, Si counts, K counts. A pink box represents a fine-grained siliciclastic mud interval tied to increased monsoon intensity initiated during MWP-1B. Red dashed lines indicate potential large-scale variations in monsoon intensity. The diffuse pink band represents a major change from reef-dominated sediments to siliciclastic-dominated sediments during MWP-1A. (B) Bottom 8 m of MD-45, displaying coralgal facies [colours same as (A)] and the relative locations of commonly observed coral fragments. (C) Image of coral fragment dated by U/Th. (D) Image of coral fragment dated by U/Th. (E) Image of piece of framework coral broken off and recovered in the core cone and dated by U/Th.

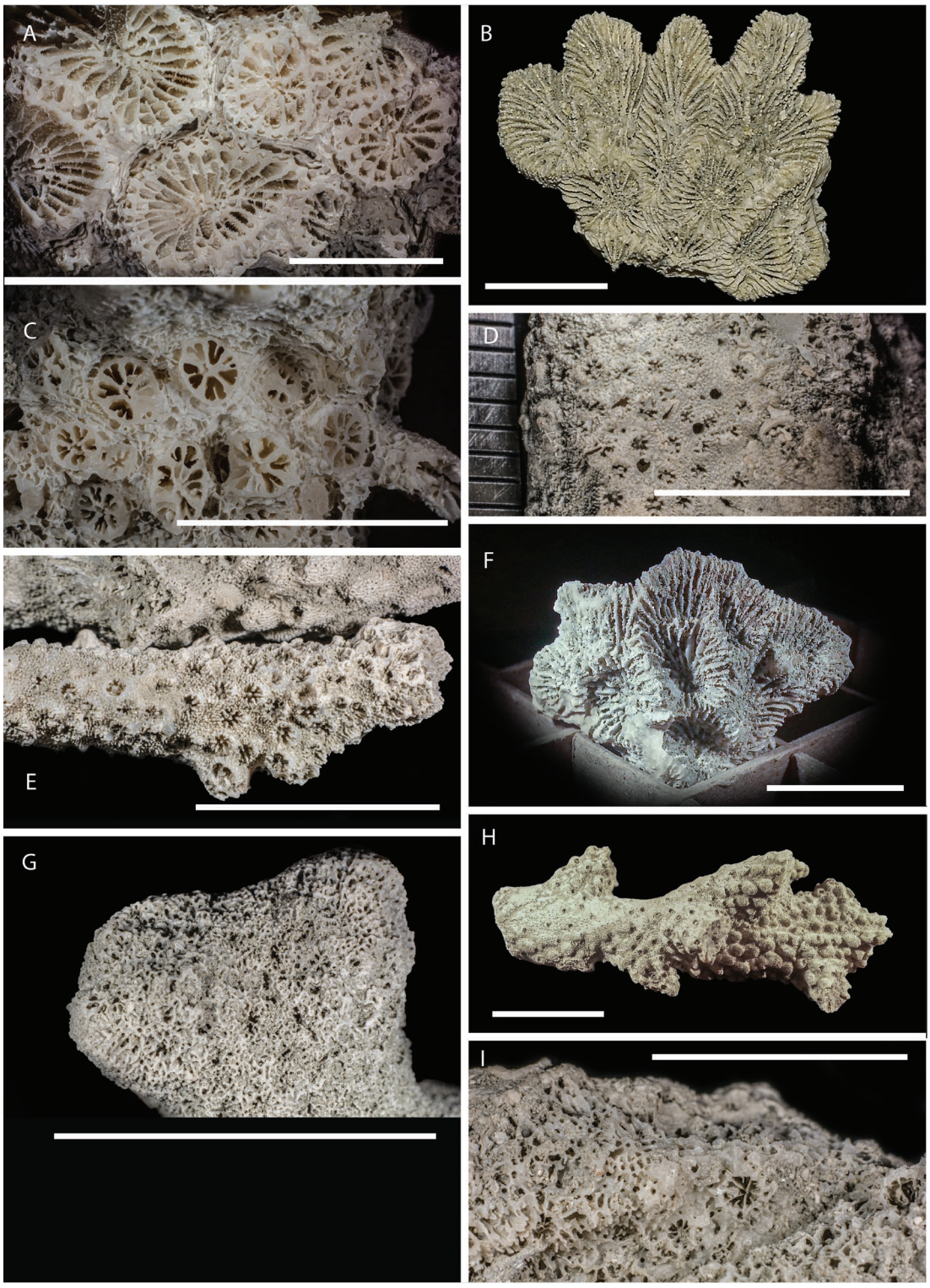


Fig. 5. A selection of debris clasts from shallow-water corals (core depth: 1175 to 1430 cm). Scale bar is 1 cm in length. (A) 1415 cm: *Dipsastraea*. (B) 1400 cm: *Favites abdita*. (C) 1350 cm: *Galaxea astreata*. (D) 1300 cm: *Stylophora*. (E) 1300 cm: fine branching *Acropora*. (F) 1268 cm: flat bifacial *Favites abdita*. (G) 1220 cm: branching/columnar *porites*. (H) 1220 cm: fine branching *Acropora*. (I) 1120 cm: *Astreopora*. Additional coral images from this section are displayed in Fig. 4.

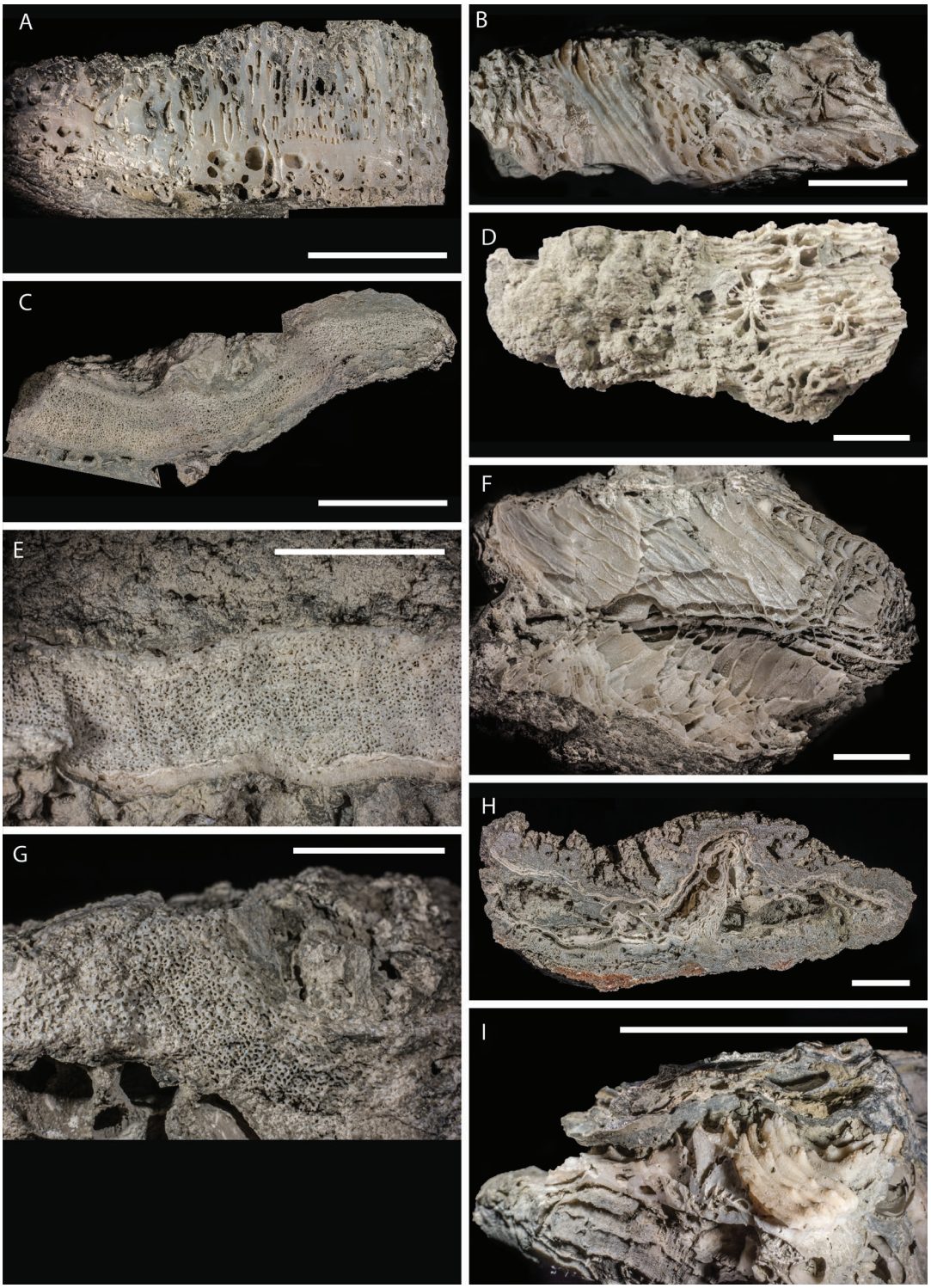


Fig. 6. A selection of debris clasts from deeper-water corals (core depth: 650 to 1175 cm). Scale bar is 1 cm in length. (A) 1020 cm: small (9 to 10 cm in diameter) *Fungiidae*. (B) 980 cm: *Echinophyllia aspera?*. (C) 970 cm: thin encrusting *Montipora*. (D) 960 cm: foliaceous *Echinophyllia echinata*. (E) 888 cm: thin *Agariciidae* encrusted with *Porites* or *Montipora*, encrusted by microbialite. (F) 868 cm: branch of *Lobophyllia*. (G) 810 cm: *Porites* or *Montipora* encrusted (undifferentiated) by microbialite. (H) 690 cm: foliaceous *Pachyseris speciosa* encrusted in digitate microbialite. (I) 650 cm: foliaceous *Echinophyllia echinata?* encrusted by thin *Montipora (sp?)*.

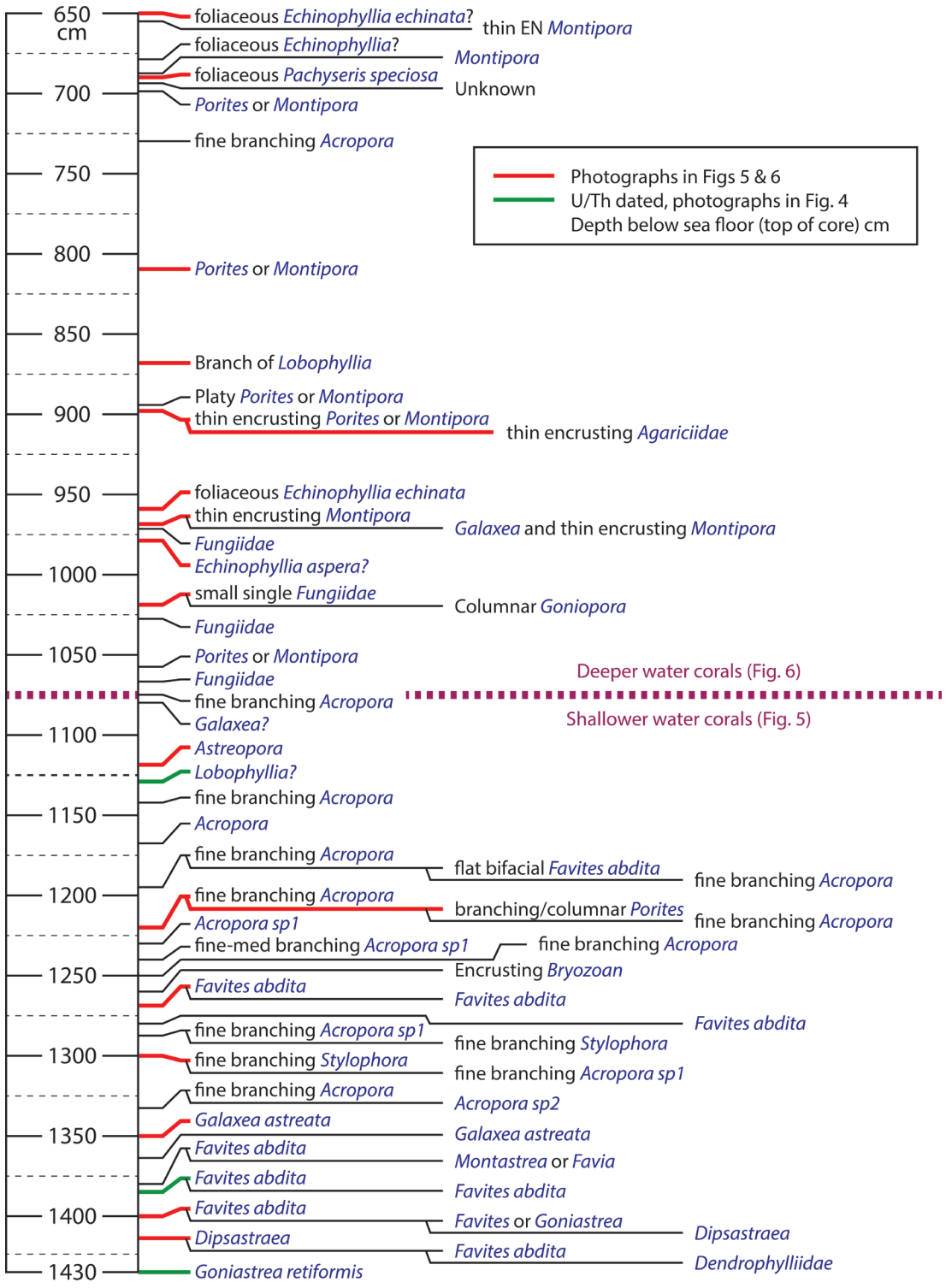


Fig. 7. List of corals identified in the MD-45 core arranged by depth below sea floor (cm). Some sample depths had more than two different corals present. Coral names appear in blue italic font. Red leader lines indicate corals that are shown in Figs 5 and 6. Green leader lines indicate corals that were U/Th dated. *Acropora* species were quite common throughout the core but were difficult to identify to the species level. *Acropora sp1* and *sp2* were both identified as different species.

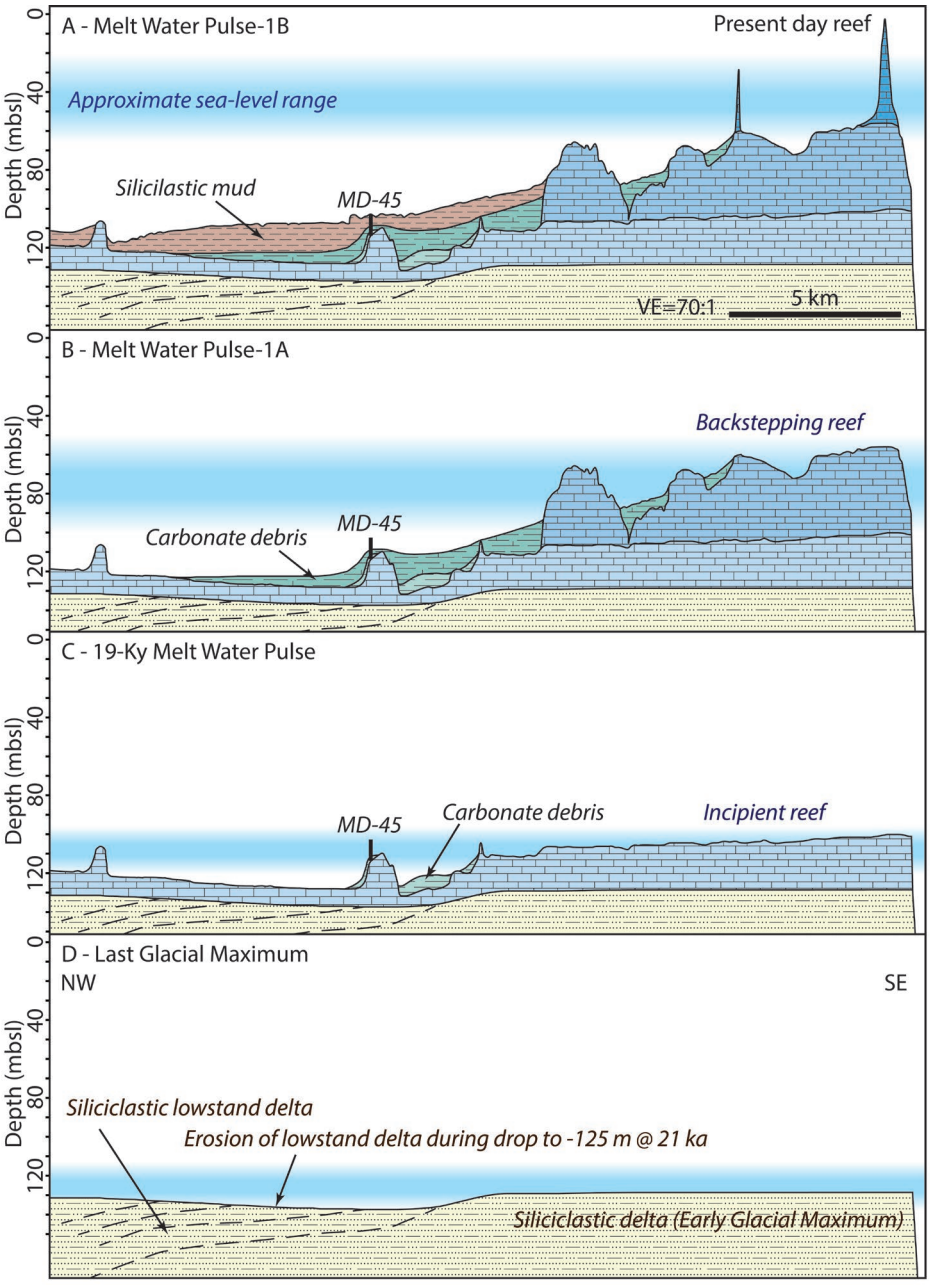


Fig. 8. Diagrams illustrating the SPPBR initiation and back-stepping interpreted to have occurred during sea-level rise following the LGM. Location in Fig. 2A same as Fig. 2C seismic line. Approximate sea-level is indicated by the diffuse blue bar. (A) Last Glacial Maximum: siliciclastic lowstand delta interpreted to have prograded over a series of previous transgressive reefs (Fig. 3). (B) 19 kyr MWP: sea-level rise of ~10 to 15 m immediately following the LGM resulted in insipient reef growth on the lowstand delta. It was at this time that the reef sampled by MD-45 was established and grew at or very near sea-level. Locally, carbonate debris began to accumulate on and around these reefs. (C) MWP-1A: rapid sea-level rise resulted in the drowning of the reef towards the north-west and back-stepping towards the south-east to occur. During this time of sea-level rise and subsequent pause, vertical aggradation also occurred along with the accumulation of reef adjacent coralgal debris. (D) MWP-1B: this MWP was probably not significantly rapid but resulted in climate change that increased sediment flux to the GoP. This led to the poisoning of the reef with only small, isolated pinnacles persisting to present day. A thick siliciclastic mud blanket is seen deposited on much of the early reef and the MD-45 location.

Deglacial transgressive reefs farther back in time

The results of thorough study of core MD-45, integrated with the overall geometry of the north-western extremity of the SPPBR observed in the strike and dip of 3.5 kHz seismic lines, offer clear examples of transgressive shelf-edge reef establishment, growth and stepwise demise. In summary, the evolution of the SPPBR shelf edge was clearly influenced by the last deglacial-punctuated sea-level rise and, in particular, by the three main MWPs, in addition to contemporaneous enhanced turbidity in the water column through an increased flux of fine siliciclastics, specifically during MWP-1B. By interpreting a grid of conventional industrial seismic lines along the southern Papuan Peninsula, it is clear that the last deglacial shelf-edge reef is not a first occurrence but rather a cyclic pattern of such reef growth, probably tied to the well-established, unusually high-amplitude sea-level transgressions along this margin, which are linked to pronounced glacial to interglacial transitions during the Mid-to-Late Brunhes (Droxler & Jorry, 2013).

A series of buried transgressive shelf-edge reefs are clearly identified in seismic lines imaging the north-west extremity of the SPPBR (Fig. 3). The precise ages of these previous transgressive shelf-edge reefs are unknown due to lack of direct sampling. However, in counting down the four to five seismic sequences, (defined by distinct trough-over-peak reflections at top and base with internal prograding reflections, Fig. 3A), the oldest observed shelf-edge reef could be linked to the MIS-12/MIS-11 transgression. It is possible that this oldest observed reef could be associated with an older interglacial such as MIS-13 or MIS-15. Recent barrier reefs were probably well established by MIS-11 but possibly as early as MIS-15, such as the GBR (Webster & Davies, 2003; Humblet & Webster, 2017) and other barrier reefs along the mixed carbonate siliciclastic margins of New Caledonia, the Florida Keys and Belize (Droxler & Jorry, 2013 and references therein). Webster & Davies (2003) noted that the nearby GBR was probably established and re-established multiple times during the last 500 kyr as a result of flooding and reflooding of the GBR shelf. The pattern along the GBR margin and other mixed margins as mentioned above is observed along the SPPBR as well. Thus, this study brings additional lines of evidence to better illustrate the common global pattern of periodic transgressive shelf-edge reef establishment along tropical mixed carbonate-siliciclastic shelf margins triggered by their periodical reflooding during the last four to five high-amplitude, deglacial-punctuated sea-level rises since the Mid-Brunhes.

When present, transgressive reef growth would probably initiate on previous reef substrate as observed in the GBR (Webster *et al*., 2018). Where siliciclastic input is significant, it may be more probable that coralgal reefs have a difficult time persisting (Hallock & Schlager, 1986). In cases where previous transgressive and highstand reefs do not create a significant edifice for re-establishment, or in the case of siliciclastic burial, re-establishment is likely to occur on elevated sedimentary features, such as shelf-edge deltas (Droxler & Jorry, 2013).

CONCLUSIONS

Seismic images anchored by the MD-45 core (Figs 4 and 7) and detailed sedimentology, chemical, lithologic, stratigraphic and biostratigraphic analyses show the establishment of a reef on a lowstand shelf-edge delta during early deglacial times and its back-stepping response to dramatic environmental changes since the LGM. The seismic illustrates the back-stepping

evolution of shelf-edge coralgal reefs associated with well-established deglacial meltwater pulses.

The fact that data have been obtained from the early deglaciation at MD-45, a generally data-poor period, is significant. The MD-45 core uniquely samples the initial coralgal reef established during the 19 kyr MWP. The well-dated (19 to 17 kyr BP) coralgal assemblage that accumulated on top of the initial reef phase shows a distinct transition from shallow-water framework corals to deeper-water foliaceous corals because of partial reef drowning and back-stepping associated with MWP-1A (14.65 ka). Subsequently, a thick siliciclastic mud interval was deposited during the time when the reef partially drowned and back-stepped because of sea-level and shelf reflooding – leading to increased turbidity when monsoons, initiated during MWP-1B (11.3 ka), intensified. Finally, this reef system exhibits how modern coralgal reefs may respond to environmental stressors such as rapid sea-level rise, turbidity, and changes in water chemistry and temperature. This pattern is not unprecedented and may be quite common in tropical mixed carbonate/siliciclastic systems and continue in response to growing climate and environmental changes.

ACKNOWLEGEMENTS

Regional seismic lines were provided by Fugro Multi Client Services, Inc. in Houston, Texas (USA). Core and 3.5 kHz seismic were acquired during the 2005 PECTEN research cruise aboard the R/V Marion Dufresne, funded by the IMAGES program and TOTAL.

This research was greatly aided in part with financial support by the NSF; TOTAL (Cecile Pabian-Goyheneche, Patrick Sorriaux and Aurelien Virgone) which provided the major financial support through a grant to Rice University (André W. Droxler) and internal funding from Rice University to Brandon B. Harper, including the Mills Bennett Fellowship.

REFERENCES

Abbey, E., Webster, J.M., Braga, J.C., Jacobsen, G., Thorogood, G., Thomas, A., Camoin, G. and **Reimer, P.** (2013) Deglacial mesophotic reef demise on the Great Barrier Reef. *Palaeogeogr. Palaeoclimatol. Palaeoecol.*, **392**, 473–494.

Abbey, E., Webster, J.M., Braga, J.C., Sugihara, K., Wallace, C.C., Iryu, Y., Potts, D.C., Done, T.J., Camoin, G.F. and **Seard, C.** (2011) Variation in deglacial coralgal assemblages and their paleoenvironmental significance: IODP Expedition 310, "Tahiti Sea Level". *Global Planet. Change*, **76**, 1–15.

Abdul, N.A., Mortlock, R.A., Wright, J.D. and **Fairbanks, R.G.** (2016) Younger Dryas sea level and meltwater pulse 1B recorded in Barbados reef crest coral *Acropora palmata*. *Paleoceanography*, **31**, 330–344.

Adey, W.H., Townsend, R.A. and **Boykins, W.T.** (1982) The Crustose Coralline Algae (Rhodophyta: Corallinaceae) of the Hawaiian Islands. Smithson. *Contrib. Mar. Sci*., **15**, 74pp.

Alley, R.B., Clark, P.U., Huybrechts, P. and **Joughin, I.** (2005) Ice-sheet and sea-level changes. *Science*, **310**, 456–460.

Andersen, M.B., Stirling, C.H., Zimmermann, B. and **Halliday, A.N.** (2010) Precise determination of the open ocean $^{234}U/^{238}U$ composition. *Geochem. Geophys. Geosyst.*, **11**, Issue 12, https://doi.org/10.1029/2010GC003318

Andrews, J.C. and **Clegg, S.** (1989) Coral Sea circulation and transport deduced from modal information models. Part A. Oceanographic Research Papers. *Deep-Sea Res*., **36**, 957–974.

Bard, E., Hamelin, B. and **Delanghe-Sabatier, D.** (2010) Deglacial Meltwater Pulse 1B and Younger Dryas Sea Levels revisited with boreholes at Tahiti. *Science*, **327**, 1235–1237.

Bard, E., Hamelin, B., Deschamps, P. and **Camoin, G.** (2016) Comment on "Younger Dryas sea level and meltwater pulse 1B recorded in Barbados reefal crest coral Acropora palmata" by N.A. Abdul *et al*. *Paleoceanography*, **31**, 1603–1608.

Bard, E., Hamelin, B., Fairbanks, R.G. and **Zindler, A.** (1990) Calibration of the ^{14}C timescale over the past 30,000 years using mass spectrometric U-Th ages from Barbados corals. *Nature*, **345**, 405–410.

Beaufort, L. (2005) *MD148/PECTEN cruise, RV Marion Dufresne*. Institut Polaire Français, Plouzané, 81 pp. https://doi.org/10.17600/5200080

Bird, P. (2003) An updated digital model of plate boundaries. *Geochem. Geophys. Geosyst.*, **4**, 1–52.

Blanchon, P. and **Shaw, J.** (1995) Reef drowning during the last deglaciation: evidence for catastrophic sea-level rise and ice-sheet collapse. *Geology*, **23**, 4–8.

Blanchon, P., Eisenhauer, A., Fietzke, J. and **Liebetrau, V.** (2009) Rapid sea-level rise and reef back-stepping at the close of the last interglacial highstand. *Nature*, **458**, 881–884.

Boardman, M.R. and **Neumann, A.C.** (1984) Sources of periplatform carbonates: northwest Providence Channel, Bahamas. *J. Sed. Petrol.*, **54**, 1110–1123.

Braga, J.C., Humblet, M., Ramos, D.A.E., Dechnik, B. and **Webster, J.M.** (2022) Quaternary coral, coralline algal and vermetid assemblages as sea-level indicators: a review. In: *Coral Reefs and Sea-Level Change: Quaternary Records and Modelling* (Eds. G.F. Camoin and N. Hallmann), *Int. Assoc. Sedimentol. Spec. Publ.*, **49**, 1–38.

Burke, L., Reytar, K., Spalding, M. and **Perry, A.** (2011) *Reefs at risk revisited*. World Resources Institute, Washington, D.C., 114 pp.

Cabioch, G., Montaggioni, L.F., Faure, G. and **Ribaud-Laurenti, A.** (1999) Reef coralgal assemblages as recorders of paleobathymetry and sea-level changes in the Indo-Pacific province. *Quatern. Sci. Rev.*, **18**, 1681–1695.

Camoin, G.F., Gautret, P., Montaggioni, L.F. and **Cabioch, G.** (1999) Nature and environmental significance of microbialites in Quaternary reefs: the Tahiti paradox. *Sed. Geol.*, **126**, 271–304.

Camoin, G.F., Seard, C., Deschamps, P., Webster, J.M., Abbey, E., Braga, J.C., Iryu, Y., Durand, N., Bard, E., Hamelin, B., Yokoyama, Y., Thomas, A.L., Henderson, G.M. and **Dussouillez, P.** (2012) Reef response to sea-level and environmental changes during the last deglaciation: Integrated Ocean Drilling Program Expedition 310, Tahiti Sea Level. *Geology*, **40**, 643–646.

Carlson, A.E. and **Clark, P.U.** (2012) Ice sheet sources of sea level rise and freshwater discharge during the last deglaciation. *Rev. Geophys.*, **50**, 1–72.

Carpenter, K.E., Abrar, M., Aeby, G., Aronson, R.B., Banks, S., Bruckner, A., Chiriboga, A., Cortés, J., Delbeek, J.C., DeVantier, L., Edger, G.J., Edwards, A.J., Fenner, D., Guzmán, H.M., Hoeksema, B.W., Hodgson, G., Johan, O., Licuanan, W.Y., Livingstone, S.R., Lovell, E.R., Moore, J.A., Obura, D.O., Ochavillo, D., Polidoro, B.A., Precht, W.F., Quibilan, M.C., Reboton, C., Richards, Z.T.,

Rogers, A.D., Sanciangco, J., Sheppard, A., Smith, J., Stuart, S., Turak, E., Veron, J.E.N., Wallace, C., Weil, E. and **Wood, E.** (2008) One-third of reef-building corals face elevated extinction risk from climate change and local impacts. *Science*, **321**, 560–563.

Cetto, P.H., Bastos, A.C. and **Ianniruberto, M.** (2021) Morphological evidences of eustatic events in the last 14,000 years in a far-field site, East-Southeast Brazilian continental shelf. *Mar. Geol.*, **442**, 106659.

Chappell, J. and **Polach, H.** (1991) Post-glacial sea-level rise from a coral record at Huon Peninsula, Papua New Guinea. *Nature*, **349**, 147–149.

Cheng, H., Edwards, R.L., Shen, C.C., Polyak, V.J., Asmerom, Y., Woodhead, J., Hellstrom, J., Wang, Y., Kong, X., Spötl, C., Wang, X. and **Alexander Jr, E.C.** (2013) Improvements in ^{230}Th dating, ^{230}Th and ^{234}U half-life values and U–Th isotopic measurements by multi-collector inductively coupled plasma mass spectrometry. *Earth Planet. Sci. Lett.*, **371**–**372**, 82–91.

Clark, P.U., McCabe, A.M., Mix, A.C. and **Weaver, A.J.** (2004) Rapid rise of sea level 19,000 years ago and its global implications. *Science*, **304**, 1141–1144.

Daniell, J.J. (2008) Development of a bathymetric grid for the Gulf of Papua and adjacent areas: a note describing its development. *J. Geophys. Res.*, **113**, F01S15.

Denniston, R.F., Wyrwoll, K.H., Polyak, V.J., Brown, J.R., Asmerom, Y., Wanamaker Jr, A.D., LaPointe, Z., Ellerbroek, R., Barthelmes, M., Cleary, D., Cugley, J., Woods, D. and **Humphreys, W.F.** (2013) A stalagmite record of Holocene Indonesian-Australian summer monsoon variability from the Australian tropics. *Quatern. Sci. Rev.*, **78**, 155–168.

Deschamps, P., Durand, N., Bard, E., Hamelin, B., Camoin, G., Thomas, A.L., Henderson, G.M., Okumo, J. and **Yokoyama, Y.** (2012) Ice-sheet collapse and sea-level rise at the Bølling warming 14,600 years ago. *Nature*, **483**, 559–564.

Douville, E., Sallé, E., Frank, N., Eisele, M.H., Pons-Branchu, E. and **Ayrault, S.** (2010) Rapid and accurate U-Th dating of ancient carbonates using inductively coupled plasma-quadrupole mass spectrometry. *Chem. Geol.*, **272**, 1–11.

Droxler, A.W. and **Jorry, S.J.** (2013) Deglacial origin of barrier reefs along low-latitude mixed siliciclastic and carbonate continental shelf edges. *Annu. Rev. Mar. Sci.*, **5**, 65–90.

Dutton, A., Webster, J.M., Zwartz, D., Lambeck, K. and **Wohlfarth, B.** (2015) Tropical tales of polar ice: evidence of Last Interglacial polar ice sheet retreat recorded by fossil reefs of the granitic Seychelles islands. *Quatern. Sci. Rev.*, **107**, 182–196.

Esat, T.M. and **Yokoyama, Y.** (2006) Variability in the uranium isotopic composition of the oceans over glacial–interglacial timescales. *Geochim. Cosmochim. Acta*, **70**, 4140–4150.

Fairbanks, R.G. (1989) A 17,000-year glacio-eustatic sea level record: influence of glacial melting rates on the Younger Dryas event and deep-ocean circulation. *Nature*, **342**, 637–642.

Francis, J.M. (2007) *Late Quaternary sediment dispersal and accumulation on slopes of the Great Barrier Reef mixed siliciclastic-carbonate depositional system, Gulf of Papua, Papua New Guinea and North Queensland Margin, Australia*. Rice University, 304 pp.

GEBCO Bathymetric Compilation Group 2019 (2019) The GEBCO_2019 Grid – a continuous terrain model of the global oceans and land. *British Oceanographic Data Centre, National Oceanography Centre, NERC, UK*.

Golbuu, Y. and **Richmond, R.H.** (2007). Substratum preferences in planula larvae of two species of scleractinian corals, Goniastrea retiformis and Stylaraea punctata. *Mar. Biol.*, **152**, 639–644.

Griffiths, M.L., Drysdale, R.N., Gagan, M.K., Zhao, J.X., Ayliffe, L.K., Hellstrom, J.C., Hantoro, W.S., Frisia, S., Feng, Y.X., Cartwright, I., St. Pierre, E., Fischer, M.J. and **Suwargadi, B.W.** (2009) Increasing Australian-Indonesian monsoon rainfall linked to early Holocene sea-level rise. *Nature Geosci.*, **2**, 636–639.

Grigg. R.W. and **Epp, D.** (1989) Critical depth for the survival of coral islands: effects on the Hawaiian Archipelago. *Science*, **243**, 638–641.

Haberle, S.G., Hope, G.S. and **van der Kaars, S.** (2001) Biomass burning in Indonesia and LoPapua New Guinea: natural and human induced fire events in the fossil record. *Palaeoceonogr. Palaeoclimatol. Palaeoecol.*, **171**, 259–268.

Hallock, P. and **Schlager, W.** (1986) Nutrient excess and the demise of coral reefs and carbonate platforms. *Palaios*, **1**, 389–398.

Hanebuth, T., Stattegger, K. and **Grootes, P.M.** (2000) Rapid flooding of the Sunda Shelf: a late-glacial sea-level record. *Science*, **288**, 1033–1035.

Hanebuth, T.J.J., Stattegger, K. and **Bojanowski, A.** (2009) Termination of the Last Glacial Maximum sea-level lowstand: the Sunda-Shelf data revisited. *Global Planet. Change*, **66**, 76–84.

Harris, P.T., Pattiaratchi, C., Keene, J.B., Dalrymple, R.W., Gardner, J.V., Baker, E., Cole, A.R., Mitchell, D., Gibbs, P. and **Schroeder, W.W.** (1996) Later Quaternary deltaic and carbonate sedimentation in the Gulf of Papua foreland basin: response to sea-level change. *J. Sed. Res.*, **66**, 801–819.

Hibbert, F.D., Rohling, E.J., Dutton, A., Williams, F.H., Chutcharavan, P.M., Zhao, C. and **Tamisea, M.E.** (2016) Coral indicators of past sea-level change: A global repository of U-series dated benchmarks. *Quatern. Sci. Rev.*, **145**, 1–56.

Hua, Q., Ulm, S., Yu, K., Clark, T.R., Nothdurft, L.D., Leonard, N.D., Pandolfi, J.M., Jacobsen, G.E. and **Zhao, J.** (2020) Temporal variability in the Holocene marine radiocarbon reservoir effect for the Tropical and South Pacific. *Quatern. Sci. Rev*., **249**, 106613.

Huang, D., Benzoni, F., Fukami, H., Knowlton N., Smith N.D. and **Budd, A.F.** (2014) Taxonomic classification of the reef coral families Merulinidae, Montastraeidae and Diploastraeidae (Cnidaria: Anthozoa: Scleractinia). *Zoological Journal of the Linnean Society*, **171**, 277–355.

Huang, D., Arrigoni, R., Benzoni F., Fukami H., Knowlton N., Smith N.D., Stolarski J., Chou, L.M. and **Budd, A.F**. (2016). Taxonomic classification of the reef coral family Lobophylliidae (Cnidaria: Anthozoa: Scleractinia). *Zool. J. Linn. Soc.*, **178**, 436–481.

Humblet, M. and **Webster, J. M.** (2017) Coral community changes in the Great Barrier Reef in response to major environmental changes over glacial-interglacial timescales: *Palaeogeogr. Palaeoclimatol. Palaeoecol.*, **472**, 216–235.

Humblet, M., Webster, J.M., Yokoyama, Y., Braga, J.C., Fujita, K., Iryu, Y., Fallon, S.J. and **Thompson, W.G.** (2022) Reef growth history at intermediate to mesophotic depths since the end of the Last Glacial period along the Great Barrier Reef shelf edge. In: *Coral Reefs and Sea-Level Change: Quaternary Records and Modelling* (Eds. G.F. Camoin and N. Hallmann), *Int. Assoc. Sedimentol. Spec. Publ.*, 49, 189–214.

Iryu, Y., Takahashi, Y., Fujita, K., Camoin, G., Cabioch, G., Matsuda, H., Sato, T., Sugihara, K., Webster, J.M. and **Westphal, H.** (2010) Sea level history recorded in the Pleistocene carbonate sequence in IODP Hole 310-M0005D, off Tahiti. *Island Arc*, **19**, 690–706.

Ishiwa, T., Yokoyama, Y., Okuno, J., Obrochta, S., Uehara, K., Ikehara, M. and **Miyairi, Y.** (2019) *A sea-level plateau preceding the Marine Isotope Stage 2 minima revealed by Australian sediments*. Sci. Rep., **9**, 6449. https://doi.org/10.1038/s41598-019-42573-4

Jaffey, A., Flynn, K., Glendenin, L., Bentley, W. and **Essling, A.** Precision measurement of half-lives and specific activities of ^{235}U and ^{238}U. *Phys. Rev.*, **5**, 1889–1906.

Khanna, P., Droxler, A.W., Nittrouer, J.A., Tunnell Jr, J.W. and **Shirley, T.C.** (2017) Coralgal reef morphology records punctuated sea-level rise during the last deglaciation. *Nature Comms*., **8**, 1046.

Kiessling, W. (2009) Geologic and biologic controls on the evolution of reefs. *Annu. Rev. Evol. Syst.*, **40**, 73–92.

Kim, W., Fouke, B.W., Petter, A.L., Quinn, T.M., Kerans, C. and **Taylor, F.** (2012) Sea-level rise, depth-dependent carbonate sedimentation and the paradox of drowned platforms. *Sedimentology*, **59**, 1677–1694.

Lee, J., Cevasco, M., Morales, J., Billick, M., Fine, M. and **Levy, O.** (2016) Variation among the Marginopora vertebralis collected from the Great Barrier Reef, Australia. *J. Foramin. Res.*, **46**, 201–219.

Loya, Y., Puglise, K.A. and **Bridge, T.** (2019) *Mesophotic Coral Ecosystems*. Springer International Publishing, **12**, 1003 pp.

Ludwig, K. and **Titterington, D.** (1994) Calculation of ^{230}Th/U isochrons, ages and errors. *Geochim. Cosmochim. Acta*, **58**, 5031–5042.

Macintyre, I.G. (1988) Modern coral reefs of Western Atlantic: new geological perspective. *AAPG Bull.*, **72**, 1360–1369.

Mallarino, G., Francis, J., Jorry, S., Daniell, J., Droxler, A.W., Dickens, G.R., Beaufort, L., Bentley, S., Opdyke, B. and **Peterson, L.** (2021) Time-scale dependent sedimentary record during the past 130 ka from a tropical mixed siliciclastic-carbonate shelf edge and slope: Ashmore Trough (southern Gulf of Papua). *Sedimentology*, **68**. 10.1111/sed.12867

Marshall, J.F., Tsuji, Y., Matsuda, H., Davies, P.J., Iryu, Y., Honda, N. and **Satoh, Y.** (1998) Quaternary and Tertiary subtropical carbonate platform development on the continental margin of southern Queensland, Australia. In: *Reefs and carbonate platforms in the Pacific and Indian Oceans* (Eds G.F. Camoin and P.J. Davies) *Int. Assoc. Sedimentol. Spec. Publ.*, **25**, 163–195.

McCulloch, M., Taviani, M., Montagna, P., Correa, M.L., Remia, A. and **Mortimer, G.E.** (2010) Proliferation and demise of deep-sea corals in the Mediterranean during the Younger Dryas. *Earth Planet. Sci. Lett.*, **298**, 143–152.

Milliman, J.D. (1995) Sediment discharge to the ocean from small mountainous rivers: the New Guinea example. *Geo-Mar. Lett.*, **15**, 127–133.

Montaggioni, L.F. (2005) History of Indo-Pacific coral reef systems since the last glaciation: development patterns and controlling factors. *Earth-Sci. Rev.*, **71**, 1–75.

Montaggioni, L.F. and **Braithwaite, C.J.R.** (2009) *Quaternary Coral Reef Systems: History, development processes and controlling factors*. 1st ed., Elsevier Science Ltd., 532 pp.

Muhammad. Z., Bentley, S.J., Febo, L.A., Droxler, A.W., Dickens, G.R., Peterson, L.C. and **Opdyke, B.N.** (2008) Excess ^{210}Pb inventories and fluxes along the continental slope and basins of the Gulf of Papua. *J. Geophys. Res.*, **113**, F01S17.

Muir, P.R. and **Pichon, M.** (2019) Biodiversity of reef-building, scleractinian corals. In: *Mesophotic coral ecosystems* (Eds Y. Loya, K.A. Puglise and T.C.L. Bridge), *Springer, New York*, 589–620.

Müller, G. and **Gastner, M.** (1971) The 'Karbonat-Bombe', a simple device for the determination of carbonate content in sediment, soils and other materials. *PANGAEA*, **10**, 466–469.

Neumann, A.C. and **Macintyre, I.** (1985) Reef response to sea level rise: keep-up, catch-up or give-up. In: *5th International Coral Reef Congress Tahiti, Proceedings* (Eds C. Gabrie, J.L. Toffart and B. Salvat), **3**, 105–110.

OBIS (2021) Ocean Biodiversity Information System. *Intergovernmental Oceanographic Commission of UNESCO*, www.obis.org.

Pearse, V.B. and **Muscatine, L.** (1971) Role of symbiotic algae (zooxanthellae) in coral calcification. *Biol. Bull.*, **141**, 350–363.

Pons-Branchu, E., Douville, E., Roy-Barman, M., Dumont, E., Branchu, P., Thil, F., Frank, N., Bordier, L. and **Borst, W.** (2014) A geochemical perspective on Parisian urban history based on U-Th dating, laminae counting and yttrium and REE concentrations of recent carbonates in underground aqueducts. *Quatern. Geochron.*, **24**, 43–54.

Renema, W. (2018) Morphological diversity in the foraminiferal genus *Marginopora*. *PLoS One*, **13**, e0208158.

Rietveld, H.M. (1967) Line profiles of neutron powder-diffraction peaks for structure refinement. *Acta Crystallographica*, **22**, 151–152.

Robinson, L.F., Adkins, J.F., Fernandez, D.P., Burnett, D.S., Wang, S.L., Gagnon, A.C. and **Krakauer, N.** (2006) Primary U distribution in scleractinian corals and its implications for U series dating. *Geochem. Geophys. Geosyst.*, **7**, 1–20.

Ross, C.A. (1972) Biology and ecology of *Marginopora vertebralis* (Foraminiferida), Great Barrier Reef. *J. Protozoology*, **19**, 181–192.

Rothwell, R.G. and **Croudace, I.W.** (2015) Twenty years of XRF core scanning marine sediments: what do geochemical proxies tell us? In: *Micro-XRF Studies of Sediment Cores* (Eds I.W. Croudace and R.G. Rothwell), *Dev. Paleoenviron. Res.*, **25**, 163–195.

Rovere, A., Khanna, P., Bianchi, C.N., Droxler, A.W., Morri, C. and **Naar, D.F.** (2018) Submerged reef terraces in the Maldivian Archipelago (Indian Ocean). *Geomorphology*, **317**, 218–232.

Schlager, W. (1981) The paradox of drowned reefs and carbonate platforms. *GSA Bull.*, **92**, 1971–211.

Schlager, W. (2005) Carbonate Sedimentology and Sequence Stratigraphy. *SEPM Concepts in Sedimentology and Paleontology*, **8**, 210 pp.

Slingerland, R., Driscoll, N.W., Milliman, J.D., Miller, S.R. and **Johnstone, E.A.** (2008) Anatomy and growth of a Holocene clinothem in the Gulf of Papua. *J. Geophys. Res.*, **113**, F01S13.

Steinberg, C. (2007) Impacts of climate change on the physical oceanography of the Great Barrier Reef. In: *Climate Change and the Great Barrier Reef* (Eds J.E. Johnson and P.A. Marshall) *Great Barrier Reef Marine Park Authority & Australian Greenhouse Office*, 51–74.

Stuiver, M., Reimer, P.J. and **Reimer, R.W.** (2021) CALIB 8.2. http://calib.org.

Sugihara, K., Nakamori, T., Iryu, Y., Sasaki, K. and **Blanchon, P.** (2003) Holocene sea-level change and tectonic uplift deduced from raised reef terraces, Kikai-jima, Ryukyu Islands, Japan. *Sed. Geol*., **159**, 5–25.

Tcherepanov, E.N., Droxler, A.W., Lapointe, P., Dickens, G.R., Bentley, S.J., Beaufort, L., Peterson, L.C., Daniell, J. and **Opdyke, B.N.** (2008) Neogene evolution of the mixed carbonate-siliciclastic system in the Gulf of Papua, Papua New Guinea. *J. Geophys. Res.*, **113**, F01S21.

Tcherepanov, E.N., Droxler, A.W., Lapointe, P., Mohn, K. and **Larsen, O.A.** (2010) Siliciclastic influx and burial of the Cenozoic carbonate system in the Gulf of Papua. *Mar. Petrol. Geol.*, **27**, 533–554.

Thompson, P.R., Widlansky, M.J., Leuliette, E., Sweet, W., Chambers, D.P., Hamlington, B.D., Jevrejeva, S., Marra, J.J., Merrifield, M.A., Mitchum, G.T. and **Nerem, R.S.** (2019) Sea level variability and change. In: *State of the Climate in 2018*. (Eds J. Blunden and D.S. Arndt), *Bull. Amer. Meteor. Soc.*, **100**, S84–S86.

Thomas, M.L., Warny, S., Jarzen, D.M., Bentley, S.J., Droxler, A.W., Harper, B.B., Nittrouer, C.A. and **Xu, K.** (2018) Palynomorph evidence for tropical climate stability in the Gulf of Papua, Papua New Guinea, over the latest marine transgression and highstand (14,500 years BP to today). *Quatern. Int.*, **467**, 277–291.

Veron, J.E.N. (2000) *Corals of the World*. Australian Institute of Marine Science, Townsville, Australia, 463 pp.

Vyverberg, K., Dechnik, B., Dutton, A., Webster, J.M., Zwartz, D. and **Portell, R.W.** (2018) Episodic reef growth in the granitic Seychelles during the Last Interglacial: Implications for polar ice sheet dynamics. *Mar. Geol.*, **399**, 170–187.

Wallace, L.M., Stevens, C., Silver, E., McCaffrey, R., Loratung, W., Hasiata, S., Stanaway, R., Curley, R., Rosa, R. and **Taugaloidi, J.** (2004) GPS and seismological constraints on active tectonics and arc-continent collision in Papua New Guinea: Implications for mechanics of microplate rotations in a plate boundary zone. *J. Geophys. Res.*, **109**, B05404.

Walsh, J.P. and **Nittrouer, C.A.** (2003) Contrasting styles of off-shelf sediment accumulation in New Guinea. *Mar. Geol.*, **196**, 105–125.

Webster, J.M., Braga, J.C., Humblet, M., Potts, D.C., Iryu, Y., Yokoyama, Y., Fujita, K., Bourillot, R., Esat, T.M., Fallon, S., Thompson, W.G., Thomas, A.L., Kan, H., McGregor, H.V., Hinestrosa, G., Obrochta, S.P. and **Lougheed, B.C.** (2018) Response of the Great Barrier Reef to sea-level and environmental changes over the past 30,000 years. *Nature Geosci*., **11**, 426–432.

Webster, J.M., Clague, D.A., Riker-Coleman, K., Gallup, C., Braga, J.C., Potts, D., Moore, J.G., Winterer, E.L. and **Paull, C.K.** (2004a) Drowning of the -150 m reef off Hawaii: a casualty of global meltwater pulse 1A? *Geology*, **32**, 249–252.

Webster, J.M., Davies, P.J. and **Konishi, K.** (1998) Model of fringing reef development in response to progressive sea level fall over the last 7000 years—(Kikai-jima, Ryukyu Islands, Japan). *Coral Reefs*, **17**, 289–308.

Webster, J.M., Wallace, L., Silver, E., Applegate, B., Potts, D., Braga, J.C., Riker-Coleman, K. and **Gallup, C.** (2004b) Coralgal composition of drowned carbonate platforms in the Huon Gulf, Papua New Guinea; implications for lowstand reef development and drowning. *Mar. Geol.*, **204**, 59–89.

Wolanski, E. and **Alongi, D.M.** (1995) A hypothesis for the formation of a mud bank in the Gulf of Papua. *Geo-Mar. Lett.*, **15**, 166–171.

Woodroffe, C.D. and **Webster, J.M.** (2014) Coral reefs and sea-level change. *Mar. Geol.*, **352**, 248–267.

Woolfe, K.J. and **Larcombe, P.** (1999) Terrigenous sedimentation and coral reef growth: a conceptual framework. *Mar. Geol.*, **155**, 331–345.

Yokoyama, Y. and **Esat, T.M.** (2011) Global climate and sea level: enduring variability and rapid fluctuations over the past 150,000 years. *Oceanography*, **24**, 54–69.

Yokoyama, Y., Esat, T.M., Thompson, W.G., Thomas, A.L., Webster, J.M., Miyairi, Y., Sawada, C., Aze, T., Matsuzaki, H., Okuno, J., Fallon, S., Braga, J.C., Humblet, M., Iryu, Y., Potts, D.C., Fujita, K., Suzuki, A. and **Kan, H.** (2018) Rapid glaciation and a two-step sea level plunge into the Last Glacial Maximum. *Nature*, **559**, 603–607.

Yokoyama, Y., Lambeck, K., De Deckker, P., Johnston, P. and **Fifield, L.K.** (2000) Timing of the Last Glacial Maximum from observed sea-level minima. *Nature*, **406**, 713–716.

Supplementary tables and figures for papers in this volume can be found on the IAS website: https://www.sedimentologists.org/books

IAS (2022) Coral Reefs and Sea-Level Change: Quaternary Records and Modelling, 173–188

How reefs drown: A case study from the Northwest Hawaiian Islands

MICHAEL TOOMEY[*,†], MICHAEL SANDSTROM[‡], EVAN MAGETTE[§] and THOMAS CRONIN[1]

[*]*U.S. Geological Survey, Florence Bascom Geoscience Center, Reston, VA, 20192.*
[†]*University of Texas at Austin, Jackson School of Geosciences, Austin, TX, 78712.*
[‡]*Lamont Doherty Earth Observatory, Columbia University, Palisades, NY 10964.*
[§]*Georgia Institute of Technology, School of Earth and Atmospheric Sciences, Decatur, Georgia 30033.*

ABSTRACT

Thousands of deeply submerged seamounts are scattered across ocean basins, many capped by thick successions of reef carbonates accumulated over millions of years prior to island drowning. How conditions sustaining shallow-water reef development at these sites deteriorated is often unclear but could lend insights into the processes that put stress on modern reef communities. Here the authors examine reef drowning in the Northwest Hawaiian Islands, brought on by low rates of carbonate accretion that often occur at mid-latitude (>30°) locations. New strontium-isotope stratigraphy from shallow water carbonates sampled from a 499 m-long boring through Midway Atoll suggest limited accumulation has occurred at the site since the early-Miocene (~16 Ma). The offshore morphology of Midway indicates carbonate production has often been outpaced by wave erosion during the Pleistocene, shifting the island's centre ~3 km to the south-east in the prevailing wave direction and increasing its circularity. Strong wave action and slow reef accretion may also explain development of extensive reef flats on Midway and nearby islands. Similar features are shared with some other carbonate islands at mid-latitudes but are not typical of Central Pacific atolls, more generally, or guyots. Abrupt sea-level rise may therefore provide a more plausible mechanism for atoll/guyot drowning in the geologic past than poor environmental conditions for carbonate accretion as has previously been invoked.

INTRODUCTION

Reefs drown when the rate of relative sea-level rise exceeds that of accretion (Schlager, 1981; Webster *et al.*, 2004). This can occur abruptly through rapid and sustained relative sea-level rise or through slow subsidence combined with a deterioration in the environmental factors that are critical for coral growth. In areas of rapid subsidence, such as along active margins or near hotspots, reef drowning is commonly observed. For example, offshore the 'Big Island' of Hawaii, stair-step flights of drowned reef terraces (up to ~1500 metres below sea-level [mbsl]) record repeated episodes of back-stepping (e.g. Toomey *et al.*, 2013; Webster *et al.*, 2007; Webster *et al.*, 2009) which can be described in four phases: (1) during episodes of abrupt sea-level rise, such as during glacial terminations, reef accretion is typically too slow (~2.5 to 2.85 mm yr^{-1}, Webster *et al.*, 2007) to keep-up with initial rising waters (e.g. >40 mm yr^{-1} during deglacial Meltwater Pulse 1A, Deschamps *et al.*, 2012). (2) Once the reef is submerged at depth (approx-

©2022 International Association of Sedimentologists

imately greater than 30 mbsl) sunlight attenuation through the water column greatly limits coral growth and therefore reef accretion. (3) Ongoing rapid subsidence (~2.5 mm yr^{-1}, Webster *et al.*, 2007) then carries the terrace into deeper water prior to the next glacial lowstand. (4) New reef growth occurs further up-slope during the ensuing sea-level highstand, initiating development of the next terrace. Drowned terraces offshore the Hawaiian Islands of Maui, Lanai, Oahu (e.g. Faichney *et al.*, 2010), the West Indies (Leclerc *et al.*, 2014), and elsewhere (e.g. Papua New Guinea, Webster *et al.*, 2004; Harper *et al.*, 2022), support the key role tectonic subsidence contributes to reef drowning near young volcanic islands or along active margins.

Abrupt sea-level rise has also been invoked to explain the many deeply submerged (>1000 mbsl) flat-topped seamounts, or guyots, occurring on slowly subsiding ocean crust. Bathymetric and seismic features mapped for North Pacific guyots share many morphologic similarities with modern coral atolls such as raised outer island rims (Winterer, 1998). The paradox of drowned reefs, as articulated by Schlager (1981), is that accretion rates at shallow water sites across the tropics (summarised in Montaggioni, 2005) – both recently and probably in the geologic past as well – are at least an order of magnitude faster than typical subsidence rates due to thermal cooling of ocean crust (Stein & Stein, 1992). The geologic record often indicates more parity between long-term reef accumulation rates and subsidence (Schlager, 1981) but this probably reflects a limitation on the creation of accommodation space rather than substantially reduced reef accretion potential itself. In order for sea-level rise alone to drown an atoll – not inhibition of carbonate production, as discussed below – sea-level rise would need to be: (1) much more rapid than reef accretion, (2) of a magnitude sufficient to submerge the reef below the photic zone; and (3) sustained long enough – perhaps millions of years – for relatively slow rates of atoll subsidence to move the island into deeper water and thus prevent re-activation of substantial carbonate production during subsequent sea-level falls.

Despite prevailing greenhouse conditions from the late Cretaceous through the Eocene, when many Pacific guyots are thought to have formed (Wilson *et al.*, 1998), periodic build-up and collapse of ice sheets could have produced episodes of rapid sea-level rise. Coastal onlap records from the New Jersey margin of the United States and elsewhere show evidence of intermittent eustatic sea-level variability between ~100 to 33 Ma that has been attributed to changes in continental ice (Miller *et al.*, 2005; Miller *et al.*, 2020). Spectral analysis of drill cores recovered from Allison and Resolution Guyots, Mid-Pacific Mountains, found depositional variability occurred at a period of ~100 kyrs consistent with eccentricity driven sea-level cycles (Winterer & Sager, 1995 and refs. therein). Drowning of other guyots such as Wodejebato Guyot, Marshall Islands (12° N, 165° E), is thought to have been preceded by a drawdown of sea-level, surface exposure and meteoric diagenesis of platform carbonates which were then capped by manganese-phosphate crusts and pelagic sediments (Camoin *et al.*, 2009). Development of the raised outer rims found on many guyots (Winterer, 1998) may also be tied to repeated episodes of exposure (dissolution) and submersion (reef accretion) as has been found for many modern Pacific atolls (Toomey *et al.*, 2016).

Even modest rates of sea-level rise during glacial retreat could initiate guyot formation if accompanied by a deterioration in the environmental conditions critical to carbonate production.

Wilson *et al.* (1998) suggested guyots drilled as part of ODP legs 143/144 drowned

sequentially while traversing an area marginal for reef growth in the southern tropics (0 to 10° S), not altogether from a singular rise in sea-level. Some of the proposed drivers for atoll drowning/guyot formation in the Pacific: (1) excess nutrients leading to increased bio-erosion and shallowing of the photic zone (Larson *et al.*, 1995), (2) upwelling of anoxic waters produced by Cretaceous mid-plate volcanism (Vogt, 1989); and (3) decreased sea surface temperatures unfavourable for carbonate production (Camoin *et al.*, 2009). Herein the authors examine how similarly unfavourable conditions for carbonate production at mid-latitude has facilitated recent island drowning in the Northwest Hawaiian Islands (NWHI).

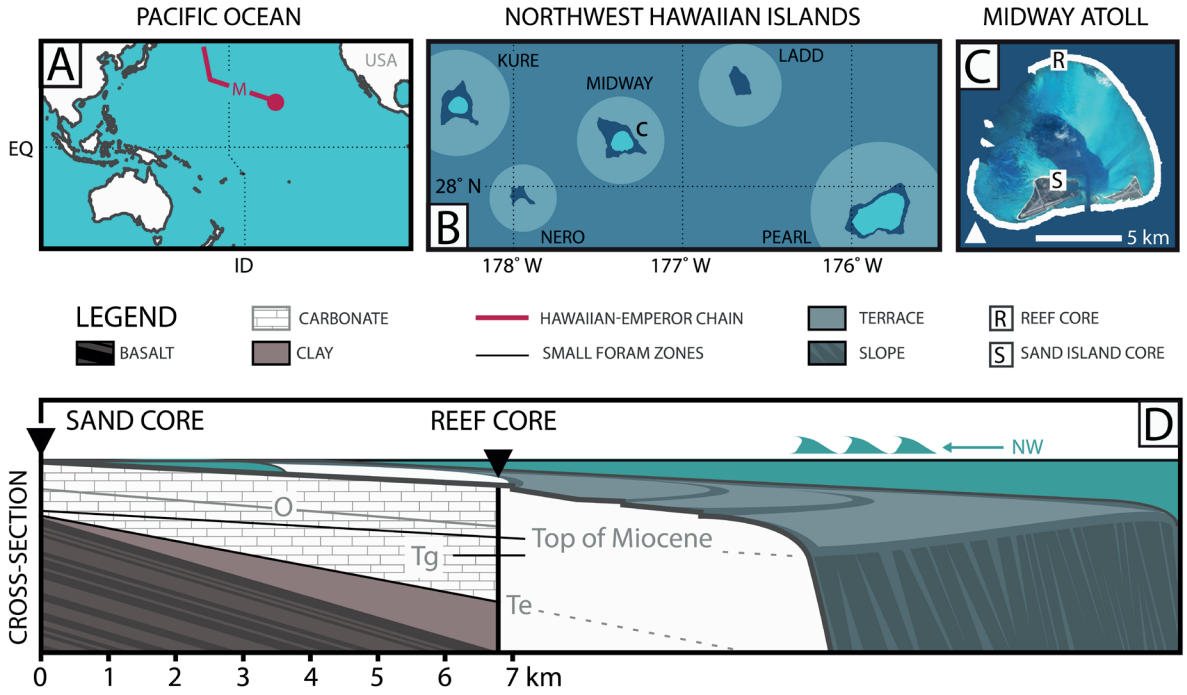


Fig. 1. Geologic setting. (A) Map of the Pacific Ocean. Hawaiian-Emperor seamount chain marked by red line. Location of Midway Atoll and the 'Big Island' shown by 'M' and filled circle, respectively. (B) Midway and surrounding islands. Dark blue outlines 150 mbsl contour of each island while shallow water areas are shown in teal. (C) Satellite image (IKONOS—NOAA) of Midway Atoll. Reef and Sand core sites are given by 'R' and 'S.' (D) Stratigraphy (left) and morphology (right) along a cross-section between core sites. Correlations between boreholes based on biostratigraphic analyses by Holden (Holden, 1976) (Ostracoda) and Todd (Todd & Low, 1970) (smaller foraminifera).

GEOLOGIC SETTING:

In the Hawaiian-Emperor hotspot chain (Fig. 1), marginal reef conditions at high-latitude (>29° N, Grigg, 1982) are thought to drive a transition from atolls and banks at or near sea-level to deeply submerged seamounts. These islands initially formed near the Big Island (20° N, 155° W) before being slowly transported (~8.6 cm yr^{-1}) to the north-west by plate motion (Duncan & Clague, 1985). Over millions of years, fluvial erosion and subsidence have created accommodation space for reef growth, transforming once high volcanic islands into carbonate-capped banks. However, as these islands move progressively north, annual sunlight and water temperature decrease, creating less favourable conditions for carbonate accretion (Grigg, 1982). Reef stress from low SSTs is

probably most acute during glacial intervals, whereas warmer interglacial conditions may allow for accretion in the NWHI (e.g. Siciliano, 2005). However, in net, reef accretion is thought to be outpaced by relative sea-level rise and the combined effects of chemical, physical and biological erosion on geologic timescales (Grigg, 1997; Grigg, 1982).

Two deep drill cores collected at Midway Atoll (Fig. 1) in 1965 (Ladd *et al.*, 1967; Ladd *et al.*, 1970) provide a unique dataset for identifying the timing and mechanisms of atoll drowning in the NWHI. Our analysis and the discussion below will focus on the longer, 499 m-long, 'Reef' core which records the depositional history of Midway since around the end of its shield volcanism stage (~27 Ma, Dalrymple *et al.*, 1977). This core was collected from the northernmost part of the atoll lagoon in ~2 m of water (Ladd *et al.*, 1970). A shorter core was drilled to volcanic bedrock (~150 m) on Sand Island, where seismic data (Shor, 1964) indicated thinning of carbonate deposits. Interpretation of Midway's depositional history – informed by analysis of multi-beam data from the Northwest Hawaiian Islands (Kelley *et al.*, 2015; Smith, 2015) and atoll morphology throughout the Pacific (Andrefouet *et al.*, 2006) – helps to address three primary questions:

1. Is atoll drowning in the Northwest Hawaiian Islands abrupt or gradual?
2. What is the dominant process (e.g. wave erosion, low reef accretion, dissolution) driving guyot formation?
3. Does reef drowning result in unique geomorphic features, as compared to tropical Pacific atolls, in general?

METHODS

The depositional history of Midway atoll was reconstructed using $^{87}Sr/^{86}Sr$ measurements from shallow water carbonates along with existing biostratigraphic data (Cole, 1969; Todd & Low, 1970). Whole-rock samples were collected in 2014 from the Midway 'Reef' drill-core (Ladd *et al.*, 1970) archived at the University of Hawaii Marine Center in Honolulu, Hawaii, United States. Prior to analysis, the outer surface of the sample was removed using a wet saw (e.g. Fig. 2). The remaining material was then ultrasonically cleaned, dried and powdered using a mortar and pestle. Sample quality was also assessed through X-ray diffraction with analytical uncertainty estimated at ± 5% (Toomey *et al.*, 2021). A sample quality rating made using similar visual procedures to Sandstrom *et al*., 2020 is also provided in Table 1. Strontium isotopic measurements were made using a Thermo Scientific Triton Thermal Ionization Mass Spectrometer (TIMS) housed in the Isotope Clean Lab, Jackson School of Geosciences, University of Texas at Austin. The age of each sample (Table 1) was then calculated using the $^{87}Sr/^{86}Sr$ calibration curve of McArthur *et al.* (2001), updated as of 2012 (version 5).

Three metrics – island position, circularity and rim width – were selected to evaluate the effects of submergence on atoll geomorphology: (1) Island position was calculated as the centroid of summit *versus* break-in-slope in order to assess movement through time related to the dominant wave direction. Following the methods similar to Faichney *et al.*, (2010), these features were mapped subjectively in QGIS 3.20 using data from the Northwestern Hawaiian Islands Multibeam Bathymetry Synthesis (Smith, 2015) with the summit and slope break generally following the ~30 and 180 mbsl contours, respectively. (2) Using shapefiles created as part of the Millennium Coral Reef

Mapping Project (MCRMP, Andrefouet *et al.*, 2006), simplified to 100 m resolution, circularity (R_c) was calculated for nearly two hundred atolls in the Central Pacific. Circularity compares an island's area to that of a circle with a perimeter of the same length. Platform shape may reflect reefs under stress. As an island becomes more circular in shape, the area for carbonate production relative to the length of the perimeter exposed to wave action and potential sediment loss is maximised. (3) Average rim width was also approximated for these islands by dividing the area of the rim by the average of each atoll's rim and lagoon perimeters. Islands having highly complex lagoons or those without a defined rim were not included in this analysis.

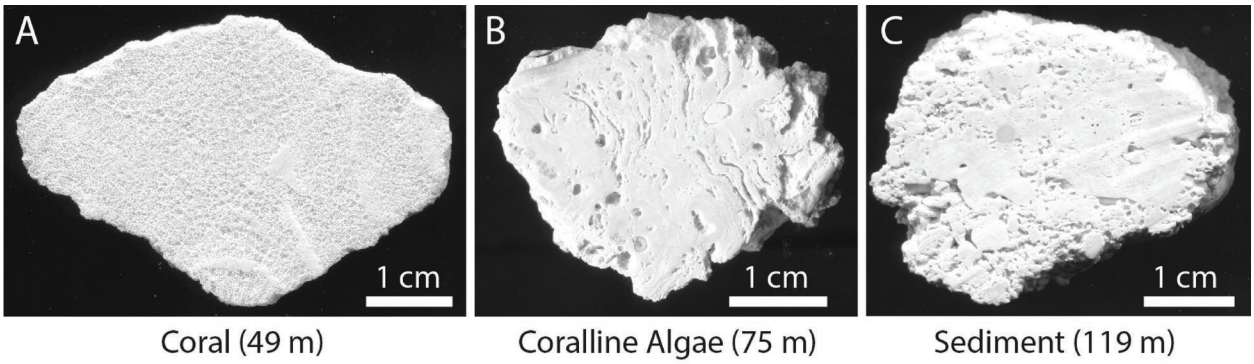


Fig. 2. Optical images of three carbonate samples used for $^{87}Sr/^{86}Sr$ dating. Samples were visually assessed for alteration based on Fe and Mg staining (discolouration), irregularities in mineral structure for biogenic fauna (dissolution, infilling, etching, etc.), microborings and secondary calcite structures. A visual preservation score using '1' for well-preserved, '2' for moderate diagenesis; and '3' for excessive alteration was assigned, similar to Sandstrom *et al.* (2020).

RESULTS AND DISCUSSION

Strontium isotope stratigraphy, as shown in Fig. 3 and reported in Table 1, divides the upper ~220 m of the Reef core into two main units (1A/B, 2) that are generally consistent with existing microfossil (Todd & Low, 1970; Holden, 1976), geochemical (Major & Matthews, 1983; Major, 1984) and sedimentological (Ladd *et al.*, 1970) data. From top to bottom: (Unit 1A) strontium ages of well-preserved corals, sampled between 31 and 55 m, range from 0 to ~0.5 Myr. Depths are referenced to rotary table elevation consistent with the conventions used during the core's collection in 1970 and subsequent publications. At the Reef core site the rotary table was 3 m above mean low water and 5 m above the sediment water interface (Ladd *et al.*, 1970).

The unconsolidated, aragonite rich (93 to 100 %, Table 1), sediments found above 64 m (Ladd *et al.*, 1970) are typical of 'recent' deposits which have had limited, geologic, time to be altered by post-depositional meteoric diagenesis. However, evidence of subaerial weathering horizons was reported at 22, 28 and 46 m in this unit (Ladd *et al.*, 1970), probably reflecting repeated submergence and exposure during high-amplitude mid-late Pleistocene sea-level cycles.

A major solution unconformity at 64 m downcore, indicating a prolonged interval of subaerial exposure, separates this unit (1A) from presumed early Pleistocene carbonates below (Unit 1B). Pleistocene deposition is suggested by $^{87}Sr/^{86}Sr$ analyses of seven carbonate samples between 65 and 127 m depth at Midway (RC) (Table 1).

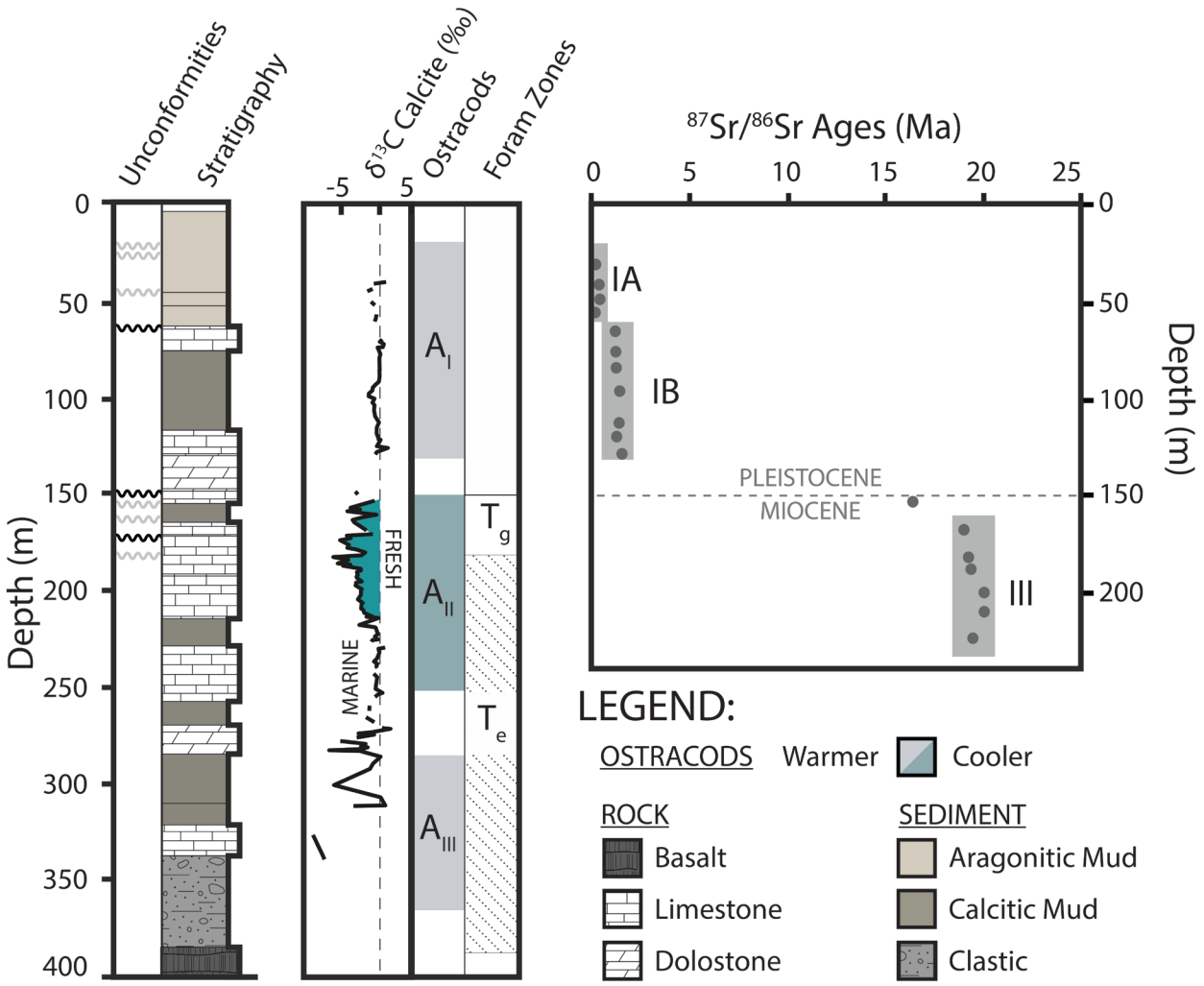


Fig. 3. Stratigraphy and chronology of Midway Reef Borehole. (Left) Unconformities and stratigraphy found in the Midway Reef borehole (Ladd *et al.*, 1970; Major & Matthews, 1983). Well defined and possible unconformities are shown by black and grey wavy lines, respectively. (Middle) $\delta^{13}C$ of calcite data of the 'Reef' core from Major (1984). Ostracode (Holden, 1976) and smaller foraminifera (Todd & Low, 1970) biostratigraphy. (Right) $^{87}Sr/^{86}Sr$ ages from Table 1 grouped into three zones (IA, IB, II).

Although X-ray diffraction analysis (Table 1) shows that these samples have, for the most part, undergone diagenesis, changing from aragonite to calcite, evidence from Enewetak Atoll drill-cores (Ludwig *et al.*, 1988) indicates such alteration probably did not alter their $^{87}Sr/^{86}Sr$ composition. Likewise, visual inspection based on the methods of Sandstrom *et al.*, 2020 indicates two of the Unit 1B samples remain well preserved (Optical imagery score = 1) and therefore probably provide robust $^{87}Sr/^{86}Sr$ ages. Drill core from other atolls across the Pacific (e.g. Enewetak, Quinn *et al.*, 1991; Funafuti, Ohde *et al.*, 2002; Kita Daito Jima, Ohde & Elderfield, 1992) are also 'missing time' during the mid-Pleistocene, probably due to a fall in sea-level between ~1.0 to 0.5 Ma (Rohling *et al.*, 2014) that exceeded the rate of tectonic subsidence during the Mid-

Pleistocene Transition. Lincoln & Schlanger (1987) estimated subsidence at Midway as only ~10 m Myr^{-1} which is roughly comparable to the rate of sea-level fall between approximately 1.0 and 0.6 Ma (Rohling *et al.*, 2014). An early Pleistocene age for Unit 1B is also consistent with foraminiferal (Todd & Low, 1970) and ostracod (Holden, 1976) biostratigraphy which restricts the upper ~150 m of the Reef core to post-Miocene time. Holden (Holden, 1976) also identified *Radimella convoluta* in ostracod zone R1 (21 to 96 m, Fig. 3) which correlates with Pleistocene deposits on Oahu (Resig, 1969).

Seven strontium isotope measurements below 150 m depth (Unit 2) returned ages older than 16 million years (Table 1). Unit 2 strontium ages should be considered suggestive given the high degree of diagenesis amongst these samples (Table 1); however a Miocene age supports observation of diagnostic foraminifera, such as *Austrotrillinia striata* (Cole, 1969; Todd & Low, 1970) within this unit and previous designation of it as Tertiary G/E by Ladd *et al.*, (1970). $^{87}Sr/^{86}Sr$ analysis of carbonates from the base of the Midway section date to 23.5 Ma (Clague *et al.*, 2012). Midway's slope break occurs at roughly the same depth (~150 to 180 mbsl) and the authors of this paper hypothesise that it may represent a geomorphic expression of the Miocene-age deposits around the island.

Taken together, the $^{87}Sr/^{86}Sr$, microfossil and stratigraphic evidence suggests: (1) much of the carbonate section at Midway accumulated during the early-Miocene followed by (2) subaerial exposure and down-wearing due to a sustained fall in eustatic sea-level during the mid to late-Miocene (Miller *et al.*, 2020). Sea-level (SL) fall at Midway is reflected by a lack of deposition and also carbon isotopic evidence (Fig. 3; Major, 1984) of subaerial exposure and alteration of Miocene reef carbonates between ~150 and 200 m. (3) The authors did not find evidence of Pliocene deposition in the $^{87}Sr/^{86}Sr$ data but a thin layer of planktonic foraminifera from 128 to 130 m depth (Todd & Low, 1970) suggests deeper water conditions may have prevailed at Midway from the Late Miocene through Pliocene time. Rapid sea-level rise around 6 Ma (e.g. Miller *et al.*, 2020; Toomey *et al.*, 2016) may have submerged Midway's reefs below the photic zone during the Pliocene. (4) Resumption of shallow water carbonate deposition above 150 m in the Reef core (Unit 1B) coincides with increasingly large drawdowns of sea-level during Pleistocene glacial lowstands (Rohling *et al.*, 2014; Miller *et al.*, 2020) which may have intercepted Midway's submerged platform.

Only about one-third of the much more extensive, presumably Miocene, platform below 150 m is occupied by the current atoll at sea-level (Fig. 4), possibly reflecting deteriorating conditions for carbonate accumulation at Midway as it has migrated north through time. In contrast, reefs at sea-level occupy the very edge of most tropical Pacific atolls, with their shape taking on the irregular plan-form of their volcanic pedestals. While plate motion has carried Midway northwards, the coral belt in the Indo-Pacific has also contracted considerably since the mid-Miocene (Perrin & Kiessling, 2010). Identification of 10 fossil Miocene coral genera at Midway (Unit 2) but only 5 from Pleistocene deposits (Units 1A/B) by Wells (1982) may be indicative of the deterioration of growth conditions brought on by changing climatic conditions between the Miocene and Pleistocene; and also cooler SSTs and less sunlight as Midway migrated to higher latitudes. Likewise, just 9 genera of coral are found at Midway today compared with 15 further south-east in the Hawaiian Islands (Ladd *et al.*, 1970). Even considerably further south at Oahu (21° N) Holocene reef accretion rates are estimated at

less than 1 mm yr^{-1} along wave exposed coasts (Grigg, 1998) compared to the ~5 to 10 mm yr^{-1} typical of reef margins in the tropical Pacific (Montaggioni, 2005 and refs. therein). Differences in wave exposure can probably explain the much more extensive development of Pleistocene reefs along the southern side of the Hawaiian Ridge as well (Faichney *et al.*, 2010).

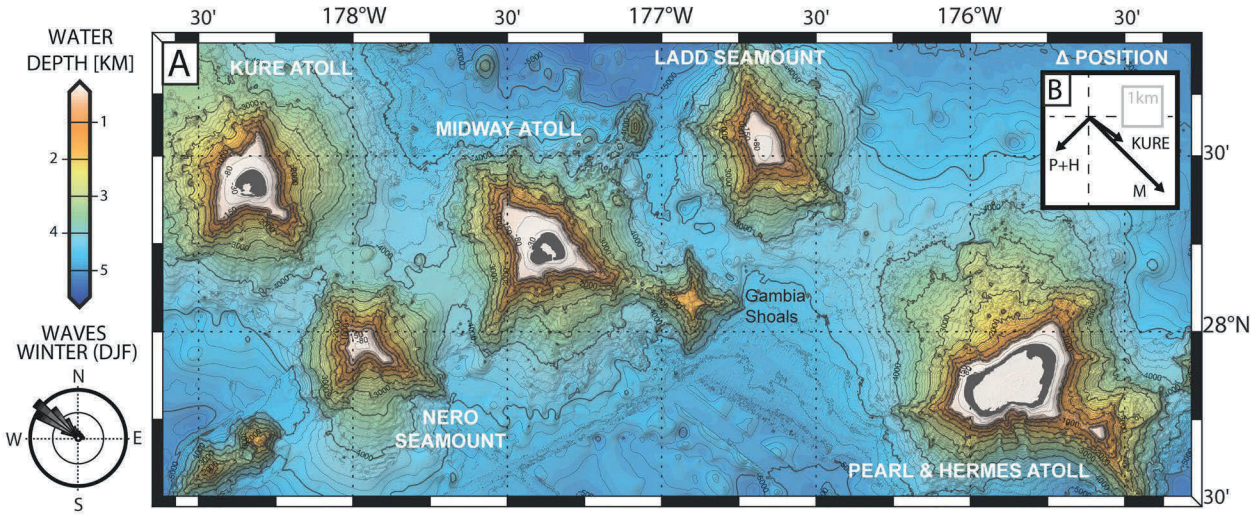


Fig. 4. Bathymetry of the Northwest Hawaiian Islands near Midway: (A) Shaded relief map of the Northwest Hawaiian Islands near Midway Atoll derived from 60 m synthesis of multibeam data for the NWHI made available from the University of Hawaii (Smith, 2015). Water depth colourmap is overlain by contours at 100 m intervals and more frequently at shallow depths. Atoll rims are highlighted in grey. Winter (DJF) wave height data for 28° N, 174° W from U.S. Army Corps of Engineers 1981–2004 hindcast, adapted from Storlazzi *et al.*, (2013). (B) Change in centroid position of island break-in slope (~180 mbsl contour) *vs*. summit (~30 mbsl contour). Nero is shown by dashed grey line due to its unusual shape, which includes a drowned peninsula along its south-east margin causing the apparent translation to the north.

Morphologic observations from Midway suggests carbonate production there has regularly been equalled or outstripped by erosion (physical, chemical and biological) during the Pleistocene. Modern wave data for the Northwest Hawaiian Islands (Fig. 4) shows the largest waves (>5 m) typically arrive from the north-west during winter months (Storlazzi *et al.*, 2013 and refs. therein), probably facilitating the transport of fine-grained sediment to the south-east (e.g. Warner 2016). Export of sediment along Midway's north-western margin could have facilitated a ~6 km break in its rim at the surface. On longer timescales, erosion over many glacial-interglacial cycles probably shifted the island's centre. The centroid of Midway Atoll, near sea-level today, is ~3 km south-east relative to the inferred Miocene platform at the break-in-slope (Fig. 4B). A shift to the south is also observed at Kure and also Pearl & Hermes atolls (Fig. 4).

As wave erosion has competed with reef accretion on the north-west side of Midway during the Pleistocene it has also reshaped the island into a much more circular form (e.g. high R_c). The authors calculate Midway's circularity as 0.89 for the modern surface near sea-level compared to 0.51 for its slope break. Higher R_c with decreasing water depth is also observed for nearby atolls such as Kure and Pearl & Hermes (Fig. 4). Overall, these islands are much more circular than most other atolls in the Central Pacific (Fig. 5). Some of this difference may be explained by flank collapse (e.g. Terry & Goff) but

many of the islands analysed here do not show bites or scars typical of underwater landslides. The authors hypothesise that increased circularity may maximise the area of the island available for potential carbonate production relative to the perimeter exposed to large waves from the North Pacific swell. Due to wave refraction, this mechanism may be more effective for reshaping smaller islands (e.g. Midway *vs*. Pearl and Hermes) with area being weakly correlated (r = 0.2) to circularity in our dataset. For a circle, the ratio of its area to perimeter increases as a function of half the radius, possibly explaining the current submergence (>70 mbsl) of several of Midway's smaller neighbours (e.g. Ladd, Nero) due to increased sediment loss to the fore-reef slope.

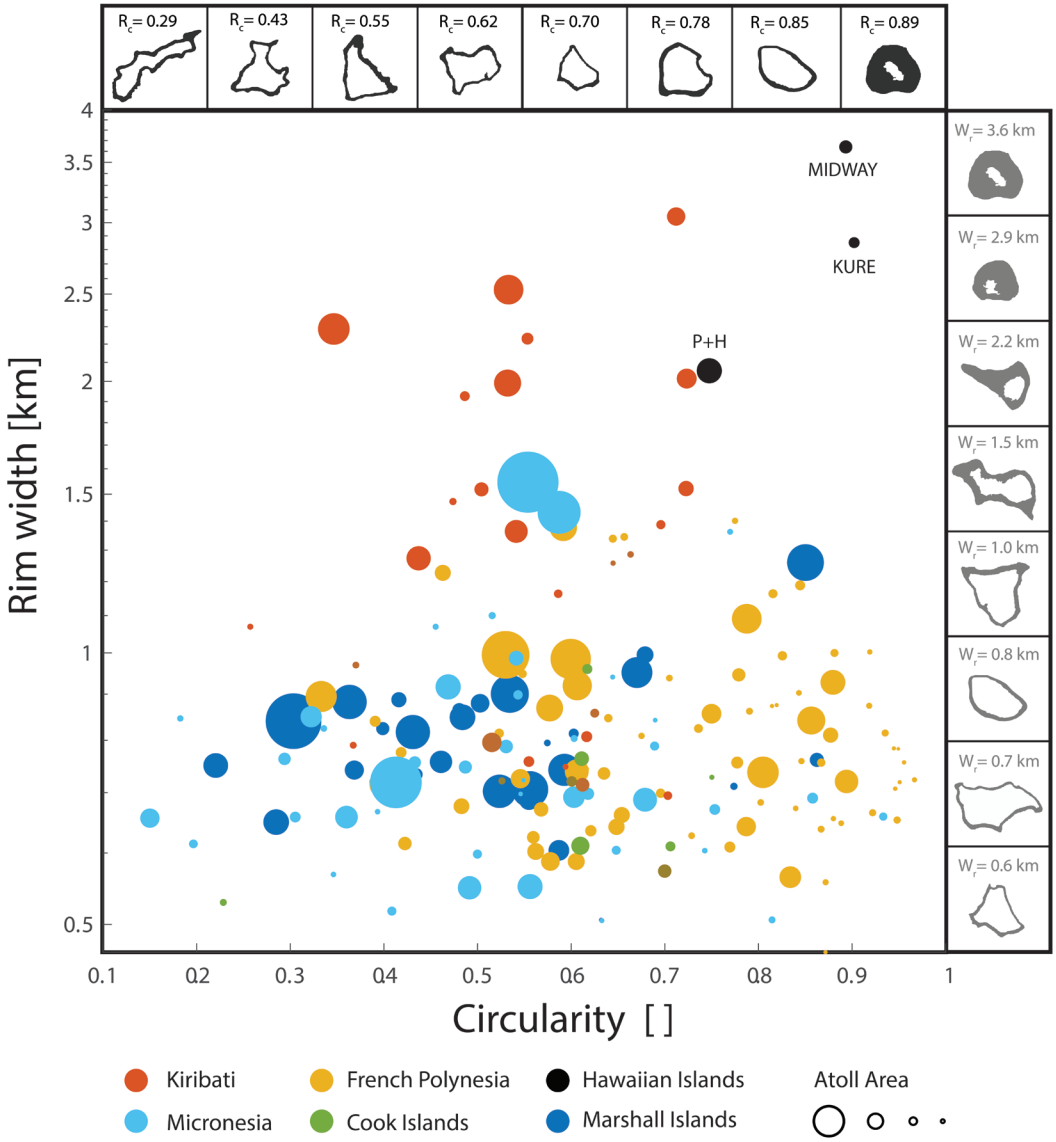


Fig. 5. Geomorphic properties of Central Pacific Atolls. (Top) Spectrum of atoll circularity. Atolls shown from least (left) to most (right) circular: Tarang, Earl Dalhousie, Utirik, Ant, Manihiki, Manuaem Hikueru, and Midway. (Right) Continuum of atolls by reef width going from widest (top) to narrowest (bottom): Midway, Kure, Aranuka, Onotoa, Taka, Marutea, and Tematagi. Atoll area was measured from Millenium Coral Reef Mapping Project shapefiles (e.g. Andrefouet *et al.*, 2006) which are derived from satellite imagery.

Unusually wide atoll rims in the Northwest Hawaiian Islands, as compared with most Central Pacific atolls, could similarly reflect wave stress competing with reef accretion at high latitude. Fig. 5 shows that rims on Pearl & Hermes, Midway and Kure are approximately ~2 to 3 km-wide – roughly triple the mean value for this parameter, 0.9 km – across the 184 other atolls included in this analysis. Wide rims are also seen at other high-latitude atolls such as Middleton and Elizabeth Reefs (~30° S), offshore of Australia's East Coast, as well as Bermuda (32° N) in the North Atlantic. Similar features are also seen at some lower latitudes reefs such as Dongsha Atoll (20° N) in the South China Sea which is influenced by transport of cold water by internal waves (Reid *et al.*, 2019) and frequent tropical cyclones. Environmental conditions at mid-latitudes and elsewhere may promote development of wide reef flats in two ways: (1) conditions for reef accretion that are slower than in the deep tropics could cause them to catch up more slowly to sea-level during deglacial transgressions. As a result, large waves are able to traverse the deep waters along the atoll's rim and deposit sediment closer towards the centre of the island for a longer duration during each glacial transgression. (2) Drier conditions, common at mid-latitudes, in addition to an island's size, may also limit development of deep lagoons (Toomey *et al.*, 2016) leading to more rapid infilling and lateral accretion of reef flats during sea-level highstands.

Evidence of wave-shaped geomorphic features is less apparent in bathymetric data available for older islands in the Hawaiian-Emperor Chain. Recently collected high-resolution multibeam data (Baco *et al.*, 2020) shows highly angular, not circular, planform terraces atop Yuryaku Guyot (32° N, 172° E), located near the bend of the Hawaiian-Emperor Chain. Clague (2010) likened similar terraces on nearby Koko Seamount (35° N, 172° E) to those drowned offshore the 'Big Island' of Hawaii (e.g. Webster *et al.*, 2007) which reflect backstepping of reefs onto higher volcanic terrain during eustatic sea-level rise events. However, decreasing summit depths of three closely spaced, west-to-east oriented, H-E guyots (Kimmei, Antoku, Taisho) (Smoot, 1985) could reflect sequential drowning due to wave exposure. Likewise, high-resolution multibeam from Colahan Seamount (31° N, 176° E; Baco *et al.*, 2020) shows some evidence of decreasing elongation towards its summit (~300 mbsl) but not to the same degree as Midway or its neighbours.

Elsewhere in the Pacific, seismic and bathymetric mapping shows there is little morphologic overlap between Cretaceous guyots and the Northwest Hawaiian Islands. Four Cretaceous guyots near Midway (e.g. Gambia Shoals, Fig. 4), where the Hawaiian and Wentworth chains intersect, are conspicuously flat topped, lacking either the larger terrace steps of the Emperor Seamounts or the wave sculpted geomorphic features of Midway. However, some features could be obscured by more recent pelagic sedimentation. A synthesis of the geomorphic observations for 21 other guyots in the western Pacific by Van Waasbergen & Winterer (1993), based in part on seismic reflection data, shows that the rims of these islands tend to be relatively narrow (~1 km) and occupy positions close to the island edge (~0.5 to 1.0 km), similar to modern atolls (Fig. 5). No preferred orientation of summit morphology was seen on these guyots either (Van Waasbergen & Winterer, 1993), probably indicating constructional reef building processes outpaced erosion by waves or currents. Taken together, morphologic evidence suggests that a gradual onset of marginal conditions for reef accretion, like those seen in the NWHI today, were not the primary driver of guyot formation during the Cretaceous.

Submerged atolls of the western Caroline Islands (~5 to 10° N) may be closer modern analogues to Pacific guyots than Midway. Despite rapid reef accretion elsewhere (~5 to 10 m kyr^{-1}) in the western Pacific (Montaggioni, 2005) and slowing rates of deglacial transgression worldwide during the Holocene (e.g. Bard *et al.*, 1996), many of the Caroline Islands have yet to 'catch-up' to modern sea-level. For example, soundings from Grey Feather Bank (8° N, 149° E) (Shepard, 1970) show water depths in excess of 30 m along stretches of its rim. The Caroline Islands are thought to have experienced extremely high rainfall rates during the last glacial lowstand, resulting in rapid down-wearing of exposed carbonates due to subaerial erosion (Toomey *et al.*, 2016 and refs. therein). During the ensuing transgression after the Last Glacial Maximum, accretion was unable to 'keep-up' with sea-level rise, resulting in many reef builders probably being submerged below the photic zone (>30 mbsl). Extensive subaerial erosion of atolls within the Intertropical Convergence Zone, followed by a rapid and sustained rise in sea-level could, similarly, provide an explanation for how many Cretaceous guyots rapidly drowned while traversing the deep tropics (0 to 10° S) of the Pacific (Wilson *et al.*, 1998).

SUMMARY

Herein the authors demonstrate how marginal conditions for carbonate production and wave erosion have shaped the depositional history of Midway Atoll as plate motion has pushed it to higher-latitude over the past 27 million years. Consistent with previous biostratigraphic investigations of deep borings at Midway, new strontium isotope stratigraphy indicates most of the island's carbonate cap accumulated during the Miocene. A long hiatus followed (~16 Myr) with only limited filling of available accumulation space across Midway's platform since resumption of carbonate deposition during the Pleistocene. Morphological analysis of Midway, as well as nearby islands, indicates Pleistocene reef accretion has often been outstripped by wave erosion, resulting in three distinct features, namely: (1) translation of islands to the south-east (the prevailing wave direction), (2) more circular form; and (3) wider rims than most atolls in the Central Pacific. This same set of features is not seen in a representative sample of western Pacific guyots (Van Waasbergen & Winterer, 1993), indicating their drowning may not be linked to marginal environmental conditions for carbonate production as hypothesised.

ACKNOWLEDGEMENTS

Support for this work was provided by a Distinguished Jackson School of Geosciences Postdoctoral Fellowship from UT Austin (MRT) and the U.S. Geological Survey Land Resources Program (MRT). We would like to acknowledge the School of Ocean and Earth Science and Technology (SOEST) at the University of Hawaii for archiving the Midway core and Staci Loewy (UT Austin) for help analysing the $^{87}Sr/^{86}Sr$ samples presented here. Any use of trade, firm, or product names is for descriptive purposes only and does not imply endorsement by the U.S. Government.

Table 1. Strontium isotope stratigraphy for the Midway 'Reef' boring.

		Metadata		Strontium Isotope Stratigraphy Ages					X-ray Diffraction			Optical
Unit	**Sample name**	**Depth (m)**	**Material**	**$^{87}Sr/^{86}Sr$ (norm. 987)**	**Total 2σ uncertainty**	**Mean SIS Age (Ma)**	**Max. SIS Age (Ma)**	**Min. SIS Age (Ma)**	**Arag-onite (wt.%)**	**Calcite (wt.%)**	**Dolo-mite (wt.%)**	**Imagery score ***
IA	MID_R34	0.0	Coral	0.7091746	0.0000149	0.03	0.48	0.00	95	5		1
	MID_R36	0.0	Coral	0.7091698	0.0000156	0.20	0.63	0.00	98	2		1
	MID_R4	0.0	Coral	0.7091679	0.0000156	0.24	0.68	0.00	100			1
	MID_R6	0.0	Coralline algae	0.7091789	0.0000162	AMSW	0.36	0.00	93	7		1
IB	MID_R11	0.0	Coral	0.7091353	0.0000163	1.04	1.31	0.70	86	14		
	MID_R14	0.0	Coralline algae	0.7091340	0.0000156	1.06	1.32	0.74		100		1
	MID_R37	0.0	Sediment	0.7091325	0.0000152	1.09	1.34	0.79		100		2
	MID_R27	0.0	Coral	0.7091217	0.0000151	1.26	1.54	1.01		100		2
	MID_R66	0.0	Sediment	0.7091234	0.0000152	1.23	1.50	0.98		100		
	MID_R20	0.0	Coralline algae	0.7091311	0.0000152	1.11	1.36	0.82		100		1
	MID_R23	0.0	Sediment	0.7091146	0.0000152	1.38	1.67	1.13		96	4	2
II	MID_R40	0.0	Shell	0.7086991	0.0000151	16.36	16.58	16.13		20	80	1
	MID_R49	0.0	Coral	0.7084901	0.0000154	18.99	19.20	18.77		100		2
	MID_R52	0.0	Coralline algae	0.7084713	0.0000152	19.22	19.46	19.01		94	6	2
	MID_R55	0.0	Coral	0.7084614	0.0000154	19.35	19.62	19.13		100		3
	MID_R58	0.0	Coral	0.7084202	0.0000154	20.03	20.35	19.71		100		3
	MID_R62	0.0	Coral fragments	0.7084201	0.0000155	20.03	20.36	19.71		100		2
	MID_R64	0.0	Sediment	0.7084548	0.0000153	19.45	19.72	19.21		34	66	2

AMSW = above modern sea water $^{87}Sr/^{86}Sr$. *Optical imagery score goes from ‘ 1’ (well-preserved) to ‘ 3’ (significant diagenesis visible), see Sandstrom *et al*., 2020 for details.

REFERENCES

Andrefouet, S., Muller-Karger, F.E., Robinson, J.A., Kranenburg, C.J., Torres-Pulliza, D., Spraggins, S.A. and **Murch, B.** (2006) Global assessment of modern coral reef extent and diversity for regional science and management applications: a view from space. In: *Proceedings of the 10th International Coral Reef Symposium*, **2**, 1732–1745. Japanese Coral Reef Society Okinawa, Japan.

Baco, A.R., Morgan, N.B. and **Roark, E.B.** (2020) Observations of vulnerable marine ecosystems and significant adverse impacts on high seas seamounts of the northwestern Hawaiian Ridge and Emperor Seamount Chain. *Marine Policy*, 103834.

Bard, E., Hamelin, B., Arnold, M., Montaggioni, L., Cabioch, G., Faure, G. and **Rougerie, F.** (1996) Deglacial sea-level record from Tahiti corals and the timing of global meltwater discharge. *Nature*, **382**, 241–244.

Camoin, G., Arnaud-Vanneau, A. and **Bergersen, D.** (2009) Development and demise of mid-oceanic carbonate platforms, Wodejebato Guyot (NW Pacific). In: *Reefs and carbonate platforms in the Pacific and Indian oceans* (Eds G.F. Camoin and P.J. Davies, **71**, 39.

Clague, D.A., Braga, J.C., Bassi, D., Fullagar, P.D., Renema, W. and **Webster, J.M.** (2010) The maximum age of Hawaiian terrestrial lineages: geological constraints from Kōko Seamount. *J. Biogeogr.*, **37**, 1022–1033.

Clague, D.A., Paduan, J.B., Braga, J.C., Humphrey, C., Hinestrosa, G., Fullagar, P.D. and **Smith, J.R.** (2012) Exploring drowned reefs on Gardner Pinnacles. *AGU Fall Meeting Abstracts*, OS51A–1843.

Cole, W.S. (1969) Larger Foraminifera from deep drill holes on Midway Atoll. *US Geol. Surv. Prof. Pap.*, **680**, 1–15.

Dalrymple, G.B., Clague, D.A. and **Lanphere, M.A.** (1977) Revised age for Midway volcano, Hawaiian volcanic chain. *Earth Planet. Sci. Lett.*, **37**, 107–116.

Deschamps, P., Durand, N., Bard, E., Hamelin, B., Camoin, G., Thomas, A.L., Henderson, G.M., Okuno, J. and **Yokoyama, Y.** (2012) Ice-sheet collapse and sea-level rise at the Bølling warming 14,600 years ago. *Nature*, **483**, 559–564.

Duncan, R.A. and **Clague, D.A.** (1985) Pacific plate motion recorded by linear volcanic chains. In: *The ocean basins and margins* (Eds A.E.M. Nairn and F.G. Stehli), Springer, 89–121.

Faichney, I.D., Webster, J.M., Clague, D.A., Paduan, J.B. and **Fullagar, P.D.** (2010) Unraveling the tilting history of the submerged reefs surrounding Oahu and the Maui-Nui Complex, Hawaii. *Geochem. Geophys. Geosyst.*, **11** (7).

Grigg, R.W. (1997) Paleoceanography of coral reefs in the Hawaiian-Emperor Chain–revisited. *Coral Reefs*, **16**, S33–S38.

Grigg, R.W. (1998) Holocene coral reef accretion in Hawaii: a function of wave exposure and sea level history. *Coral Reefs*, **17**(3), 263–272.

Grigg, R.W. (1982) Darwin Point: a threshold for atoll formation. *Coral Reefs*, **1**, 29–34.

Harper, B.B., Droxler, A.W., Webster, J.M., Montagna, P., Yokoyama, Y., Humblet, M., Jorry, S.J., Beaufort, L., Tachikawa, K. and **Pons-Branchu, E.** (2022) Shelf-edge deglacial reef establishment and subsequent partial demise: Response to distinct pulses of sea-level rise associated with environmental changes. *IAS Spec. Publ.* **49**, 173–188 (this volume).

Holden, J.C. (1976) *Late Cenozoic Ostracoda from Midway Island drill holes*. US Government Printing Office.

Kelley, C., Smith, J.R., Miller, J., Tree, J., Boston, B., Garcia, M., Ito, G., Taylor, J., Lichowski, F. and **Wagner, D.** (2015) New insights from seafloor mapping of a Hawaiian marine monument. EOS, **96**, doi:10.1029/2015EO030235.

Kominz, M.A., Browning, J., Miller, K., Sugarman, P., Mizintseva, S. and **Scotese, C.** (2008) Late Cretaceous to Miocene sea-level estimates from the New Jersey and Delaware coastal plain coreholes: An error analysis. *Basin Res.*, **20**, 211–226.

Ladd, H.S., Tracey, J.I. and **Gross, M.G.** (1967) Drilling on Midway Atoll, Hawaii. *Science*, **156**, 1088–1094.

Ladd, H.S., Tracey, J.I. and **Gross, M.G.** (1970) *Deep drilling on Midway atoll*. US Government Printing Office.

Larson, R., Erba, E., Nakanishi, M., Bergersen, D. and **Lincoln, J.** (1995) Stratigraphic, vertical subsidence and paleolatitude histories of Leg 144 guyots. In: *Proceedings of the Ocean Drilling Program. Scientific results*, **144**, 915–933.

Leclerc, F., Feuillet, N., Cabioch, G., Deplus, C., Lebrun, J., Bazin, S., Beauducel, F., Boudon, G., LeFriant, A. and **De Min, L.** (2014) The Holocene drowned reef of Les Saintes plateau as witness of a long-term tectonic subsidence along the Lesser Antilles volcanic arc in Guadeloupe. *Mar. Geol.*, **355**, 115–135.

Lincoln, J. and **Schlanger, S.** (1987) Miocene sea-level falls related to the geologic history of Midway Atoll. *Geology*, **15**, 454–457.

Ludwig, K., Halley, R.B., Simmons, K.R. and **Peterman, Z.E.** (1988) Strontium-isotope stratigraphy of Enewetak Atoll. *Geology*, **16**, 173–177.

Major, R.P. (1984) The Midway Atoll coral cap: Meteoric diagenesis, amplitude of sea-level fluctuation and dolomitization. Dissertation, Brown University.

Major, R.P. and **Matthews, R.** (1983) Isotopic composition of bank margin carbonates on Midway Atoll: amplitude constraint on post-early Miocene eustasy. *Geology*, **11**, 335–338.

McArthur, J.M., Howarth, R. and **Bailey, T.** (2001) Strontium isotope stratigraphy: LOWESS version 3: best fit to the marine Sr-isotope curve for 0–509 Ma and accompanying look-up table for deriving numerical age. *J. Geol.*, **109,** 155–170.

Miller, K.G., Browning, J.V., Schmelz, W.J., Kopp, R.E., Mountain, G.S. and **Wright, J.D.** (2020) Cenozoic sea-level and cryospheric evolution from deep-sea geochemical and continental margin records. *Science Advances*, **6**.

Miller, K.G., Kominz, M.A., Browning, J.V., Wright, J.D., Mountain, G.S., Katz, M.E., Sugarman, P.J., Cramer, B.S., Christie-Blick, N. and **Pekar, S.F.** (2005) The Phanerozoic record of global sea-level change. *Science*, **310**, 1293–1298.

Montaggioni, L.F. (2005) History of Indo-Pacific coral reef systems since the last glaciation: development patterns and controlling factors. *Earth-Sci. Rev.*, **71**, 1–75.

Ohde, S. and **Elderfield, H.** (1992) Strontium isotope stratigraphy of Kita-daito-jima Atoll, North Philippine Sea: implications for Neogene sea-level change and tectonic history. *Earth Planet. Sci. Lett.*, **113**, 473–486.

Ohde, S., Greaves, M., Masuzawa, T., Buckley, H.A., Van Woesik, R., Wilson, P.A., Pirazzoli, P.A. and **Elderfield, H.** (2002) The chronology of Funafuti Atoll: revisiting an old friend. *Proc. Roy. Soc. London. Series A:*

Mathematical, Physical and Engineering Sciences, **458**, 2289–2306.

Perrin, C. and **Kiessling, W.** (2010) Latitudinal trends in Cenozoic reef patterns and their relationship to climate. *Carbonate systems during the Oligocene–Miocene climatic transition. Wiley-Blackwell* (Eds M. Mutti, W.E. Piller and C. Betzler, 17–33.

Quinn, T.M., Lohmann, K. and **Halliday, A.** (1991) Sr isotopic variation in shallow water carbonate sequences: stratigraphic, chronostratigraphic and eustatic implications of the record at Enewetak Atoll. *Paleoceanography*, **6**, 371–385.

Reid, E.C., DeCarlo, T.M., Cohen, A.L., Wong, G.T., Lentz, S.J., Safaie, A., Hall, A. and **Davis, K.A.** (2019) Internal waves influence the thermal and nutrient environment on a shallow coral reef. *Limnol. Oceanogr.*, **64(5)**, 1949–1965.

Resig, J. (1969) Paleontological Investigations of Deep Borings on the Ewa Plain, Oahu. *Hawaii, Hawaii Inst. Geophysics., Univ. Hawaii No. HIG–69-2*.

Rohling, E., Foster, G.L., Grant, K., Marino, G., Roberts, A., Tamisiea, M.E. and **Williams, F.** (2014) Sea-level and deep-sea-temperature variability over the past 5.3 million years. *Nature*, **508**, 477–482.

Sandstrom, M.R., O'Leary, M.J., Barham, M., Cai, Y., Rasbury, E.T., Wooton, K.M. and **Raymo, M.E.** (2021) Age constraints on surface deformation recorded by fossil shorelines at Cape Range, Western Australia. *Geol. Soc. Am. Bull.*, **133**, 923–938.

Schlager, W. (1981) The paradox of drowned reefs and carbonate platforms. *Geol. Soc. Am. Bull.*, **92**, 197–211.

Shepard, F.P. (1970) Lagoonal topography of Caroline and Marshall Islands. *Geol. Soc. Am. Bull.*, **81**, 1905–1914.

Siciliano, D. (2005) Latitudinal limits to coral reef accretion: testing the Darwin point hypothesis at Kure Atoll, Northwestern Hawaiian Islands, using new evidence from high resolution remote sensing and in situ data. Ph.D. Thesis. University of California, Santa Cruz.

Smith, J.R. (2015) Northwestern Hawaiian Islands Multibeam Bathymetry Synthesis: 60-m Bathymetry (Ed U.o.H.a.M.U.H.U.R.L. (HURL), https://www.pacioos.hawaii.edu/metadata/hurl_bathy_60m_nwhi.html.

Smoot, N.C. (1985) Guyot and seamount morphology and tectonics of the Hawaiian—Emperor elbow by multi-beam sonar. *Mar. Geol.*, **64**, 203–215.

Stein, C.A. and **Stein, S.** (1992) A model for the global variation in oceanic depth and heat flow with lithospheric age. *Nature*, **359**, 123–129.

Storlazzi, C.D., Berkowitz, P., Reynolds, M.H. and **Logan, J.B.** (2013) Forecasting the impact of storm waves and sea-level rise on Midway Atoll and Laysan Island within the Papahānaumokuākea Marine National Monument—a comparison of passive versus dynamic inundation models. *US Geol. Surv. Open-File Report*, **1069**.

Todd, R. and **Low, D.** (1970) Smaller foraminifera from Midway drill holes. 2330–7102, US Govt. Print. Off.

Toomey, M., Ashton, A.D. and **Perron, J.T.** (2013) Profiles of ocean island coral reefs controlled by sea-level history and carbonate accumulation rates. *Geology*, **41**, 731–734.

Toomey, M.R., Ashton, A.D., Raymo, M.E. and **Perron, J.T.** (2016) Late Cenozoic sea level and the rise of modern rimmed atolls. *Palaeogeogr. Palaeoclimatol. Palaeoecol.*, **451**, 73–83.

Toomey, M.R., Sandstrom, R.M., Magette, E. and **Cronin, T.M.** (2021) XRD data from Midway Atoll, Reef core. USGS Data Release. https://doi.org/10.5066/P96Q94DY.

Terry, J.P. and **Goff, J.** (2013) One hundred and thirty years since Darwin:'Reshaping'the theory of atoll formation. *The Holocene*, **23**, 615–619.

U.S. Army Corps of Engineers (2011) Wave model hindcast data: Wave Information Studies.

Van Waasbergen, R.J. and **Winterer, E.L.** (1993) Summit geomorphology of western Pacific guyots. *AGU Geophysical Monograph Series*, **77**, 335–366.

Vogt, P. (1989) Volcanogenic upwelling of anoxic, nutrient-rich water: A possible factor in carbonate-bank/reef demise and benthic faunal extinctions? *Geol.l Soc. Am. Bull.*, **101**, 1225–1245.

Webster, J.M., Wallace, L., Silver, E., Applegate, B., Potts, D., Braga, J.C., Riker-Coleman, K. and **Gallup, C.** (2004) Drowned carbonate platforms in the Huon Gulf, Papua New Guinea. *Geochem. Geophys. Geosyst.*, **5**, https://doi.org/10.1029/2004GC000726

Webster, J.M., Wallace, L.M., Clague, D.A. and **Braga, J.C.** (2007) Numerical modeling of the growth and drowning of Hawaiian coral reefs during the last two glacial cycles (0–250 kyr). *Geochem. Geophys. Geosyst.*, **8** (3), DOI: 10.1029/2006GC001415.

Webster, J.M., Braga, J.C., Clague, D.A., Gallup, C., Hein, J.R., Potts, D.C., Renema, W., Riding, R., Riker-Coleman, K., Silver, E. and **Wallace, L.M.** (2009) Coral reef evolution on rapidly subsiding margins. *Global Planet. Change*, **66**.

Wells, J.W (1982) Fossil corals from midway atoll. *US Geol. Surv. Prof. Pap*., 680-G.

Wilson, P.A., Jenkyns, H.C., Elderfield, H. and **Larson, R.L.** (1998) The paradox of drowned carbonate platforms and the origin of Cretaceous Pacific guyots. *Nature*, **392**, 889–894.

Winterer, E. and **Sager, W.** (1995) 31. Synthesis of Drilling Results From the Mid-PACIFIC Mountains: Regional Context and Implications. In: *Proceedings of the Ocean Drilling Program*, **143**, Scientific Results.

Winterer, E.L. (1998) Cretaceous karst guyots: new evidence for inheritance of atoll morphology from subaerial erosional terrain. *Geology*, **26**, 59–62.

IAS (2022) Coral Reefs and Sea-Level Change: Quaternary Records and Modelling, 189–214

Reef growth history at intermediate to mesophotic depths since the end of the Last Glacial period along the Great Barrier Reef shelf edge

MARC HUMBLET[*], JODY M. WEBSTER[†], YUSUKE YOKOYAMA[‡,§,¶,‖,#], JUAN CARLOS BRAGA[a], KAZUHIKO FUJITA[b], YASUFUMI IRYU[c], STEWART J. FALLON[d] and WILLIAM G. THOMPSON[e]

[*]*Department of Earth and Planetary Sciences, Nagoya University, Nagoya 464-8601, Japan.*
[†]*Geocoastal Research Group, School of Geosciences, The University of Sydney, NSW 2006, Australia.*
[‡]*Atmosphere and Ocean Research Institute, The University of Tokyo, Kashiwa 277-8564, Japan.*
[§]*Department of Earth and Planetary Sciences, The University of Tokyo, Tokyo 113-0033, Japan.*
[¶]*Graduate Program on Environmental Sciences, The University of Tokyo, Tokyo 113-0033, Japan.*
[‖]*Japan Agency for Marine-Earth Science and Technology Organization, Biogeochemistry Program, Yokosuka 237-0061, Japan.*
[#]*Research School of Physics, The Australian National University, Canberra, ACT 2601, Australia.*
[a]*Departamento de Estratigrafía y Paleontología, Universidad de Granada, Campus Fuentenueva, 18002, Granada, Spain.*
[b]*Department of Physics and Earth Sciences, University of the Ryukyus, 1 Senbaru, Nishihara, Okinawa 903-0213, Japan.*
[c]*Institute of Geology and Paleontology, Graduate School of Science, Tohoku University, Aobayama, Sendai 980-8578, Japan.*
[d]*Research School of Earth Sciences, The Australian National University, Canberra, ACT 2601, Australia.*
[e]*Woods Hole Oceanographic Institution, Woods Hole, MA 02543, USA.*

ABSTRACT

Reef communities at intermediate (10 to 30 m) and mesophotic (~30 to 150 m) depths occupy large areas of sea floor but little is known about their potential to accrete vertically, their response to sea-level change and other environmental perturbations. In this study, the authors have examined cores from two holes, M0040A and M0041A, drilled by the International Ocean Drilling Program Expedition 325 along the shelf edge of the modern GBR at 131 m water depth. The objective was to investigate reef growth history at palaeo-water depths >20 m over a time period spanning 30,000 years, from the end of the Last Glacial period through the last deglaciation. Based on changes in lithologies and biotic components, and a robust chronostratigraphic framework supported by 47 radiometric ages, the authors have identified two episodes of reef growth, one during Marine Isotope Stage (MIS) 2 and the other at the onset of the deglaciation, both characterised by abundant microbialite crusts and distinct coral assemblages. Palaeo-water depths range from 30 to 60 m and from 20 to 30 m for the MIS 2 and early deglacial reef sections, respectively. The first episode of reef growth documented in the cores initiated at 27 to 25 ka, possibly in response to increased light availability and change in sedimentation resulting from falling sea-level between 32 and 29 ka from MIS 3 and also to low atmospheric pCO_2 at the end of

©2022 International Association of Sedimentologists

the Last Glacial period. Reef accretion was reduced or ceased sometime between 24 and 19 ka, coinciding with the rapid 20 m sea-level fall of the peak Last Glacial Maximum and minima of SSTs. Reef growth resumed at 19.5 to 18.5 ka, influenced by a period of moderate sea-level rise and increasing sea surface temperatures at the onset of the deglaciation. Reef growth termination at ca. 17 ka correlates with a major episode of reef demise previously identified in adjacent mid and outer terrace cores and linked to reduced water quality combined with rapid deglacial sea-level rise. Vertical accretion (VA) rates were calculated based on two methods: linear visual fitting and Bayesian modelling. The findings show that the highest VA rates are associated with microbialite boundstone. Reef ecosystems dominated by microbialite and corals developed at intermediate and mesophotic depths, and grew vertically at maximum rates of 2 to 5 mm yr^{-1} depending on the method used, over a period of rapid environmental change during the transition from MIS 3 to MIS 1. Further study needs to explore the potential of modern-type deep coralgal communities to cope with higher rates of sea-level rise predicted this century.

INTRODUCTION

Mesophotic coral ecosystems (MCEs) refer to benthic communities composed of scleractinian corals, coralline algae and associated species living at depths of 30 to 150 m (Hinderstein *et al.*, 2010). MCE composition and distribution, together with their relationship with shallow coral reef ecosystems, have become the focus of an increasing number of studies over the past twenty years (Loya *et al.*, 2019). These research efforts have led to a better understanding of MCEs, particularly regarding their importance as sanctuaries of biodiversity and their potential role as refuge for shallow reef communities during environmental disturbances and climate change (Pyle & Copus, 2019). In the Great Barrier Reef of Australia (GBR), the extent of deep reef habitats on submerged banks potentially harbouring MCEs is equivalent to that occupied by shallow coral reef communities of the GBR (Harris *et al.*, 2012). The species richness of mesophotic coral communities in the GBR (192 species) amounts to nearly half that of their shallow counterparts (Bridge *et al.*, 2019). The distribution and community structure of MCEs are heterogenous and may be controlled by factors such as water clarity, coastal upwelling and sediment flux (Bridge *et al.*, 2019). Despite a sharp decrease in species richness below 60 m, MCEs at lower mesophotic depths are more extensive and more diverse than was previously thought (Englebert *et al.*, 2017). The widespread occurrences of MCEs in the GBR and elsewhere raises important questions regarding their longevity, their capacity to accrete vertically and cope with long-term climate and sea-level changes, together with their role in shaping sea floor topography. Rapid, high-amplitude glacio-eustatic sea-level fluctuations have exerted a major control on reef growth during the Quaternary (Woodroffe & Webster, 2014). However, there is very little knowledge about how MCEs have responded to long-term environmental changes (Abbey *et al.*, 2013). Unravelling the factors controlling the distribution and development of MCEs constitutes one of the twenty-five key research questions recently identified by mesophotic reef experts (Turner *et al.*, 2019).

A key parameter with regard to MCE's ability to keep up with rapid deglacial sea-level rise is the rate at which they can accrete vertically. Few studies have measured the growth rate of mesophotic corals and even

fewer have assessed net mesophotic reef accretion (Sherman *et al.*, 2019). The amount of photosynthetically active radiation (PAR) is a major factor influencing coral growth rates. As PAR decreases with depth, so does general coral growth rate. At these depths, bioerosion often outpaces coral growth, limiting reef development (Hubbard & Scaturo, 1985; Grigg, 2006; Weinstein *et al.*, 2016). However, the relationship between coral growth rate and depth is not straightforward in all species. Recently, Kahng *et al.* (2020) reported linear extension rates for *Leptoseris* at depths of 70 to 110 m, similar to those in shallow, well-lit environments (i.e. 8 to 25 mm yr^{-1}). Although this reflects horizontal rather than vertical growth, sustained coral growth at mesophotic depths does suggest that some species adapted to low PAR can compensate the effect of bioerosion and maintain their reef-building potential.

Net reef accretion results from the interplay of carbonate production by *in situ* framework builders, mostly corals and coralline algae, sedimentation, precipitation of marine cements, and (bio)erosion (Perry, 2011). Based on a study of variations in coral growth rate at upper mesophotic depths, bioerosion rate and sedimentation along a depth gradient in the US Virgin Islands, Weinstein (2014) estimated potential rates of mesophotic vertical reef accretion at 0.2 to 1.1 mm yr^{-1}, similar to those calculated for modern shallow Caribbean reefs by Perry *et al.* (2013) but significantly lower than typical values of shallow vertical reef accretion rates during the Holocene (i.e. 2 to 7 mm yr^{-1}; Gischler & Hudson, 2019). Fossil mesophotic coral assemblages have been interpreted in Quaternary reef sequences from various geologic settings (Humblet *et al.*, 2009; Webster *et al.*, 2009; Abbey *et al.*, 2011a; Humblet & Iryu, 2014; Humblet *et al.*, 2019) but mesophotic reef growth history remains poorly understood. In submerged fossil reefs of Tahiti and the GBR province, fossil mesophotic coralgal assemblages commonly cap shallow reef sequences, indicating deepening upward (Abbey *et al.*, 2011b; Humblet *et al.*, 2019). Webster *et al.* (2018) calculated vertical accretion rates of these mesophotic intervals accumulated during the last deglacial sea-level rise and obtained values of 0.1 to 3 mm yr^{-1}.

A characteristic shared by fossil MCEs is the predominance of laminar coral growth forms, including corals of the genus *Porites* and *Montipora* and those of the family Agariciidae (Braga *et al.*, 2022). These corals are also typically associated with Hapalidialean coralline algae (e.g. *Lithothamnion* and *Mesophyllum* species; Braga & Aguirre, 2004; Abbey *et al.*, 2013). The analysis of dredged samples from depths of 45 to 130 m along the GBR shelf edge revealed three distinct biotic assemblages, indicating palaeo-water depths of <60 m, <80 to 100 m, and >100 m, respectively, with sample ages clustering around 13 to 10 ka and 8 ka to present (Abbey *et al.*, 2013). The first generation (13 to 10 ka) reflects a deepening and the end at 10 ka coincides with a major episode of reef demise in the GBR, possibly caused by the combination of deglacial sea-level rise and massive sediment flux from the flooded shelf (Abbey *et al.*, 2013; Webster *et al.*, 2018). The age gap between the first and second generation suggests a hiatus of mesophotic coral growth, which resumed at 8 ka as the mesophotic equivalent of the shallow Holocene reef sequence (Abbey *et al.*, 2013).

Surveys of MCEs conducted over the past two decades have shed light on their distribution and composition in different regions of the world (e.g. Armstrong *et al.*, 2006; Kahng & Kelley, 2007; Bridge & Guinotte, 2013; Sinniger *et al.*, 2019; Weinstein *et al.*, 2021). However, understanding of their potential to accrete vertically and the factors controlling their

initiation, growth and demise remains fragmentary. As emphasised by Sherman *et al.* (2019), studies of MCE cores are needed to investigate the long-term growth history of MCEs. To fill in this knowledge gap, the authors have used two distal holes drilled by the International Ocean Drilling Program Expedition 325 (IODP 325) along the shelf edge of the modern GBR (i.e. M0040A and M0041A), which offer a unique window into reef growth history at intermediate (10 to 30 m) to mesophotic (>30 m; i.e. MCE) palaeo-water depths during rapid environmental change, spanning the regression to the Last Glacial Maximum (LGM), the LGM lowstand and the subsequent reef drowning during the deglacial sea-level rise. Specifically, this study aims to achieve the following goals: (1) to reconstruct the history of reef growth and biotic response to rapid sea-level change across the LGM and subsequent deglacial at a deep upper-slope site (i.e. 131 metres below sea-level, mbsl), (2) to determine the composition, age and vertical growth rate of deep (>20 m) reef framework; and (3) to compare the accretion rates of mesophotic and shallow fossil reef sequences.

MATERIAL AND METHODS

Material

The GBR is the largest continuous coral reef system in the World, extending over 2300 km from 24° 30′ S to 9° 30′ S (Hopley *et al.*, 2007). Extensive submerged fossil reef tracts were discovered on the shelf edge at depths of 40 to 110 m, comprising terraces, pinnacles and ridges, interpreted respectively as fringing reefs, patch reefs and barrier reefs (Beaman *et al.*, 2008; Abbey *et al.*, 2011b). These fossil reefs were the target of IODP Expedition 325, which drilled 33 holes along four transects perpendicular to the shelf edge (i.e. transect RIB-02A, NOG-01B, HYD-01C and HYD-02A) at three locations (Ribbon Reef, Noggin Pass and Hydrographers Passage; Webster *et al.*, 2011). The present study focuses on two distal holes on the outer terrace of transect HYD-02A at Hydrographers Passage, i.e. M0040A and M0041A (hereinafter referred to as holes 40A and 41A; Fig. 1A and B). The study area is located along the edge of the continental shelf, offshore Mackay at a latitude of 19° 40′ S (Hinestrosa *et al.*, 2016). At this location, the shelf width is 275 km and the continental slope gradient is ~1° (Hinestrosa *et al.*, 2016). The two holes studied are 10 m apart, were drilled at a depth of 131 m on a ridge between the shelf break and the upper slope and reached a depth of ~20 mbsf (Fig. 1C and D). Average core recoveries of 40A and 41A are 54.6% and 45.5%, respectively, but reach up to 95% in the reef sections.

IODP 325 cores have been the subject of several studies targeting primarily the last 30,000 years. These studies have focused on sea-level and reef growth history (Yokoyama *et al.*, 2018; Webster *et al.*, 2018), changes in key biotic components and processes, such as coralgal assemblages (Humblet *et al.*, 2019), foraminiferal assemblages (Yagioka *et al.*, 2019), microbialite (Braga *et al.*, 2019; Szilagyi *et al.*, 2020), bioerosion (Patterson *et al.*, 2020), as well as sea-surface temperature (SST) reconstruction and palaeoceanography (Felis *et al.*, 2014; Brenner *et al.*, 2020).

Webster *et al.* (2018) define five main reef sequences: (1) an early glacial reef sequence (27 to 22 ka; Reef 2), (2) an LGM-early deglacial reef sequence (22 to 17 ka; Reef 3a), (3) a deglacial reef sequence (17 to 13 ka; Reef 3b), (4) a late deglacial reef sequence (13 to 10 ka; Reef 4) and (5) the modern GBR reef sequence on the shelf (10 ka to the present). The geomorphology of submerged fossil reefs and internal facies architecture reveal a highly dynamic reef growth history largely controlled by eustatic sea-level change and punctuated by five reef death events (Webster *et al.*, 2018). Sea-level fall

to the LGM was not continuous but characterised by a two-step drop, first to -100 m until ca. 30 ka (LGM-a), then, after a period of relative stability, to -118 m, the full extent of the LGM, from 22 to 20.5 ka (LGM-b; Yokoyama *et al.*, 2018). These two episodes of rapid sea-level fall caused the demise of Reef 1 (>30 ka) and Reef 2 by exposure. Deglacial sea-level rise resulted in upslope migration of the reef tract, delineating three successive reef sequences (Reef 3a, 3b and 4), each interrupted by drowning events attributed to the combined effect of rising sea-level and increased shelf-to-basin sediment flux (Webster *et al.*, 2018). This paper examines in detail how this history is reflected in the reef sections of Holes 40A and 41A located on the deep shelf edge along the Great Barrier Reef.

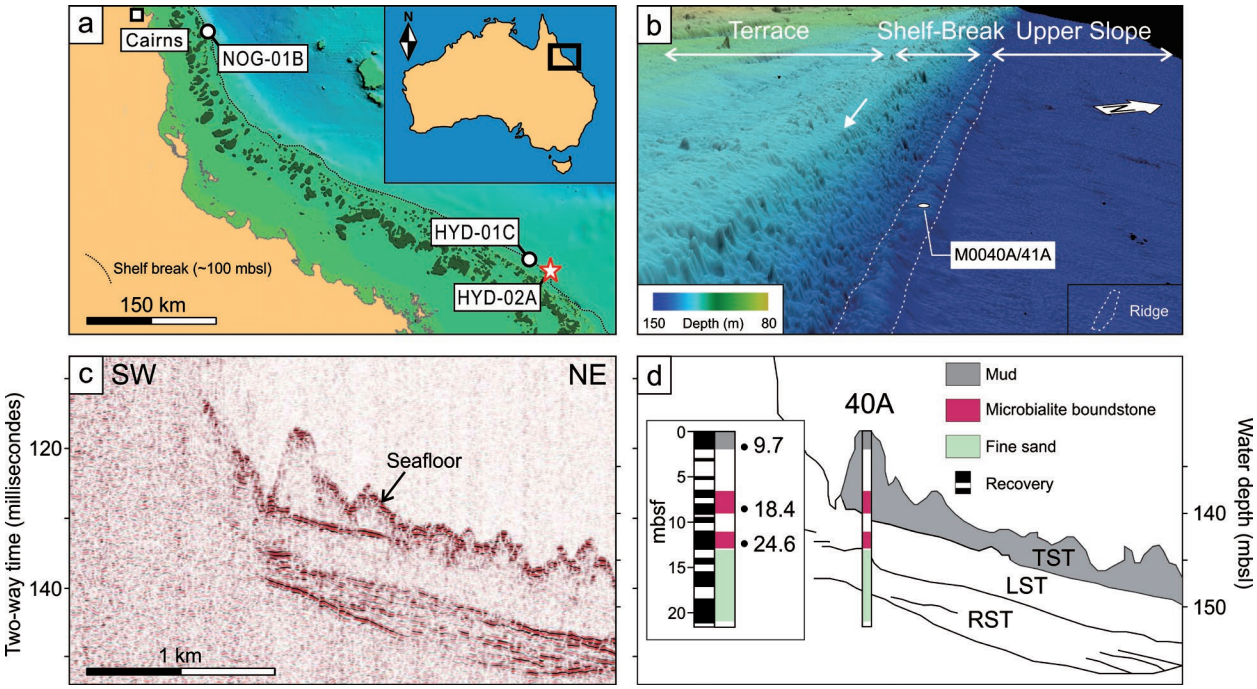


Fig. 1. (a) Location of IODP 325 transects, indicated by black rectangle on inset. The two boreholes described in this study (40A and 41A) were drilled along transect HYD-02A (red star). (b) High-resolution multibeam image of the sea floor at HYD-02A and location of studied boreholes (Hinestrosa *et al.*, 2016). The horizontal distance between the drill site and the slope break (arrow) is 360 m. Note that the two holes 40A and 1A are too close to be distinguishable on the figure. (c) Seismic profile oriented south-west (SW) to north-east (NE), i.e. perpendicular to the shelf break, acquired near Hole 40A drill site; and (d) interpretation of seismic stratigraphic units and preliminary dates published in Hinestrosa *et al.* (2016) and image of Hole 40A to show the correlation between these units and major lithologies and age distributions within the borehole. LST = lowstand system track; mbsf = metres below sea floor; mbsl = metres below sea-level; RST = regressive system track; TST = transgressive system track.

Methods

Cores recovered from Holes 40A and 41A were re-examined at the Center for Advanced Marine Core Research, Kochi Prefecture, Japan. Changes in lithologies and fossil content, particularly trends in taxonomic composition of fossil scleractinian corals, were carefully checked. Each coral was identified at the lowest taxonomic level possible and defined as either *in situ* (IS), not *in situ* (ISX) or status unknown (ISN; Fig. S1), following the criteria for fossil corals in drill cores detailed in Webster *et al.* (2011) and Humblet & Webster (2017). The coral taxonomy follows Veron (2000) with modifications for the family Merulinidae by Huang *et al.* (2014). The guide Humblet *et al.* (2015) was also used to help with the taxonomic identification of fossil corals. More time was dedicated to the description of Hole 40A as this hole displays a better recovery. Basic descriptions of the sedimentary facies and biotic content of Holes 40A and 41A has been published in Webster *et al.* (2011). Information on fossil corals and corallines algae is found in Humblet *et al.* (2019). Large benthic foraminifers and their assemblages were analysed by Yagioka *et al.* (2019).

A total of 47 radiometric ages, comprising 44 radiocarbon ages and 3 U-Th ages, were used to constrain the timing of deposition and correlate variations in sedimentary facies and coralgal assemblages with relative sea-level (RSL) history reconstructed from transect HYD-01C at Hydrographers Passage (Yokoyama *et al.*, 2018). Of these 47 radiometric ages, only 5 were previously published (Webster *et al.*, 2011; Hinestrosa *et al.*, 2016). Ages range from 39 to <9 ka (Table S1). When two or more radiocarbon age measurements were carried out on the same sample, the final age and age uncertainty were obtained by calculating their arithmetic mean. In one instance, one U-Th age and one radiocarbon age were obtained on the same sample (i.e. 325-M0040A-08R-2W 5-8). In this case, the former was selected as the final age of the sample. Sampling for radiometric dating preferentially targeted corals and coralline algae. Less than one gram of pristine material is needed for radiocarbon and U-Th dating. The preservation state of coral skeletons in IODP Expedition 325 cores is extremely good as attested by X-ray diffraction and petrographic analyses of >165 coral samples by Yokoyama *et al.* (2018). Radiocarbon measurements were performed with a Single Stage Accelerator Mass Spectrometer at the Atmosphere and Ocean Research Institute at The University of Tokyo and at the Australian National University (ANU; Table S1). Radiocarbon ages were converted to calendar ages using a local reservoir age of 12 ± 10 yr and calibrated using IntCal 13 and Marine 13 following the method described in Yokoyama *et al.* (2018). Of the three U-Th dates, two have already been published in Webster *et al.* (2011) and Hinestrosa *et al.* (2016); and the new, unpublished date was measured at Woods Hole Oceanographic Institution by multi-collector inductively coupled plasma–mass spectrometry (ICP-MS; Table S1). The detailed description of the U-Th and radiocarbon dating methods are presented in Yokoyama *et al.* (2018, 2019).

The authors have used the radiometric ages to calculate vertical accretion (VA) rates in Holes 40A and 41A and to investigate the relationship between variation in VA rates, sedimentary facies and sea-level change (Table S2). VA rates were determined by visually fitting a line through the data points in the age-depth plot and by calculating the slope of the segments between each successive inflection point, following the method of Webster *et al.* (2018; Fig. 2).

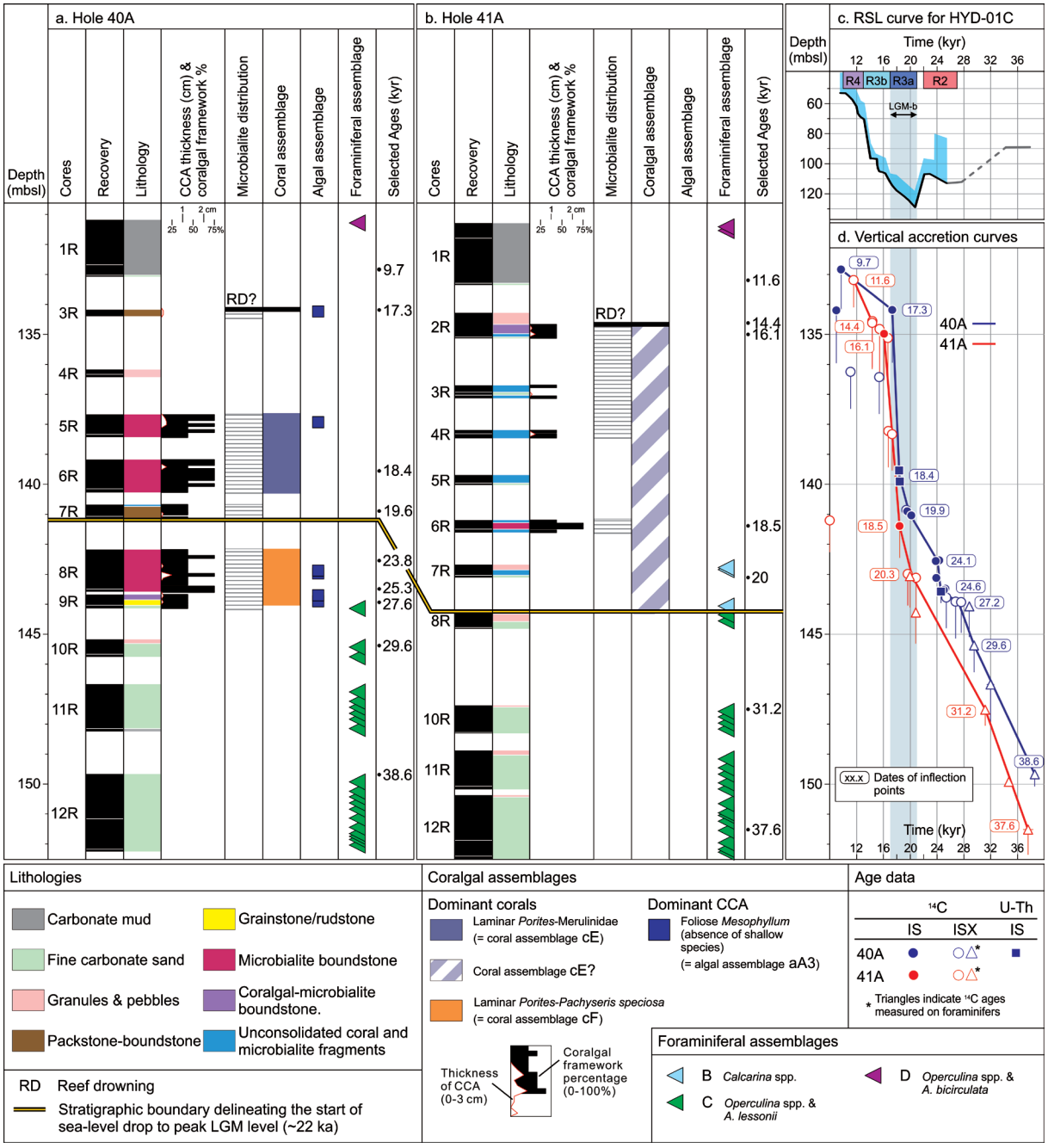


Fig. 2. (a) and (b) Core recovery, major lithologies and microbialite distribution (modified from Webster *et al.*, 2011), coralgal framework abundance, crustose coralline algae (CCA) thickness, coral and algal assemblages (modified from Humblet *et al.*, 2019), foraminiferal assemblages (Yagioka *et al.*, 2019) and selected ages (in kyr CalBP) for Holes 40A and 41A, respectively. The percent volume of coralgal framework and CCA thickness were determined within every 10 cm interval. (c) Relative sea-level (RSL) curve for transect HYD-01C (black line) and segment of the RSL curve obtained for transect NOG-01B with grey line delineating the approximate position of the lower bounds of the MIS 3 RSL position (Yokoyama *et al.*, 2018). Reef sequences (R2, R3a, R3b and R4) are from Webster *et al.* (2018). The light blue vertical band indicates the extent of the Last Glacial Maximum (LGM-b between 22 and 20.5 ka in Yokoyama *et al.*, 2018). (d) Vertical accretion curves reconstructed based on all available ^{14}C and U-Th

age data for Hole 40A (blue) and 41A (red) and dates of inflection points (in squares). For each age-depth data point, the uncertainty on the depth and age is represented by a vertical and horizontal bar, respectively. The latter is not visible when it is smaller than the data point symbol. For detailed information on the dataset used to construct the age-depth plot, see Table S1. CCA, crustose coralline algae; IS, *in situ*; ISX, not *in situ*; LGM = Last Glacial Maximum; mbsl = metres below sea-level; RD = reef drowning; RSL = relative sea-level.

Inflection points were defined preferentially based on *in situ* (IS) corals and coralline algae. Age-depth data used to define inflection points in the basal carbonate sand are derived from samples of the large benthic foraminifer *Operculina* spp., typical of modern shelf slopes, suggesting limited or no transport (Yagioka *et al.*, 2019). Even for inflection points derived from non-*in situ* (ISX) corals and coralline algae, mostly in Hole 41A, similarity in age between stratigraphically close samples support a robust chronology. In order to better constrain the age uncertainties, age models were also produced for the two holes based on Bayesian statistics using the R-based *Bacon* package (Fig. S2; Blaauw *et al.*, 2020) and results were compared with those of the linear visual fit method.

RESULTS

Sedimentary facies and biotic components

The description of sedimentary facies is primarily based on Hole 40A due to its higher core recovery. The cored sections can be divided into five main intervals characterised by distinct lithologies and biotic assemblages (Figs 2 and 3). From the bottom to the top of Hole 40A, these five lithofacies are: (1) unconsolidated fine carbonate sand from 152 to 146.5 mbsl, (2) microbialite boundstone containing *in situ* laminar *Porites* and *Pachyseris speciosa* from 143.5 to 142 mbsl, (3) packstone-boundstone with microbialite encrusting bioclasts from 141 to 140.5 mbsl, (4) microbialite boundstone containing *in situ* laminar *Porites* and Merulinidae from 140 to 134.3 mbsl; and (5) unconsolidated carbonate mud from 133 to 131 mbsl. The succession of sedimentary facies and biotic components are described in detail below, starting from the bottom of Hole 40A.

Fine carbonate sand

The fine carbonate sand interval between 152 and 146.5 mbsl shows an increase up-core in the abundance of coarse sand-size and granule-size bioclasts, including mollusc shell fragments and abundant large benthic foraminiferal tests (compare Fig. 3A and B; Webster *et al.*, 2011). Grain-size measurements conducted by Yagioka *et al.* (2019) indicate a high average mud content of 56% (in weight). The foraminiferal assemblage, described by Yagioka *et al.* (2019), is characterised by *Operculina* spp. and *Amphistegina lessonii* (assemblage C; Fig. 2). The fine sand transitions above 146.5 mbsl in core 10R to coarse sand and granules composed of mollusc shell fragments, foraminiferal tests, echinoid spines and *Halimeda* segments (Webster *et al.*, 2011). There is a sharp increase in the proportion of sand and gravel relative to mud above 147 mbsl (Yagioka *et al.*, 2019). At ~144 mbsl the core is characterised by a ~20 cm-thick interval of bioclastic grainstone and rudstone. Bioclasts include bryozoans, corals, molluscs, foraminiferal tests and *Halimeda* (Fig. 3C). The bottom and top of this interval is heavily bored by *Entobia* (Fig. S4A). *Trypanites* borings are also common. Borings in the grainstone/rudstone interval are not limited to individual bioclasts and penetrate the sedimentary fabric, suggesting that bioerosion occurred when the sediment was already indurated. Microbialite content increases sharply above this interval and the lithology transitions to boundstone.

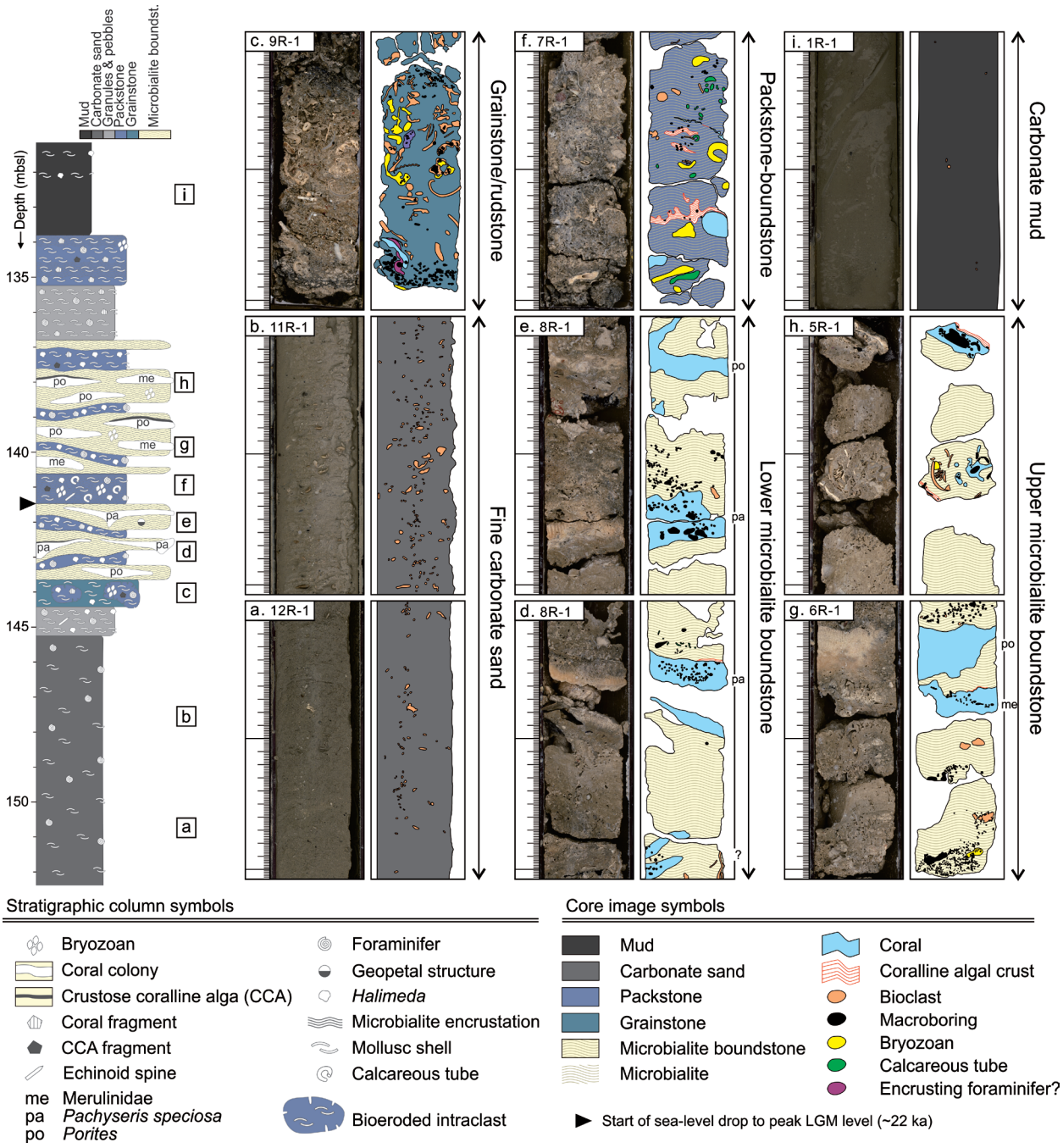


Fig. 3. Schematic lithostratigraphic column of Hole 40A and images of representative core sections showing the major lithofacies, as well as sketches of these sections highlighting the main components.

Lower microbialite boundstone

Microbialite boundstone occurs between 143.5 and 142 mbsl (hereinafter referred to as 'lower microbialite boundstone'; Fig. 3D and E). The dominant coral taxa are laminar *Porites* and *Pachyseris speciosa*, 1 to 2 cm in thickness (assemblage cF of Humblet *et al.*, 2019). Coral clasts include *Tubipora*, *Porites*, Acroporidae and Agariciidae. Associated coralline algae comprise *Lithoporella* and *Lithophyllum* gr. *prototypum* (assemblage aA3 of Humblet *et al.*, 2019) and form thin

crusts no more than a few millimetres thick (Fig. S4B). Other biotic components are fragments of bryozoans and mollusc shells. There are multiple horizons of heavily bored microbialite crusts and corals, mainly by *Entobia* (Fig. S4C). Bioerosion in microbialite crusts suggests microbialite formation at or near sediment-water interface, a style of microbialite formation previously described by Braga *et al.* (2019), as well as enough exposure time for macroboring organisms to colonise the substrate. Small calcareous tubes, ~1 and 2 mm in diameter, are abundant at 143.5 and 143.1 mbsl (Fig. S4D). Microbialite crusts can locally reach several centimetres in thickness. Their fabric is mostly structureless (Fig. S4E), but locally shows crude laminations (Fig. S4F) or digitations (Fig. S4H).

Packstone-boundstone

A 50 cm-thick layer of packstone-boundstone composed mainly of microbialite, calcareous tubes, coralline algal crusts and bioclasts is found above the microbialite boundstone between 141 and 140.5 mbsl (Fig. 3F). Bryozoans are common in this layer. Other bioclasts include corals, coralline algae, mollusc shells, echinoid spines and *Halimeda* segments. The abundance of *in situ* calcareous tubes, the presence of thin continuous algal crusts, microbialite and bioclast-filled cavities suggest that this facies can be categorised, at least in part, as a boundstone (Figs S4H and I). However, in this interval corals are only a minor component and mostly occur as clasts, the main framework builders being calcareous tube-forming organisms, microbialite and coralline algae (including *Mesophyllum* gr. *funafutiense*). The calcareous tubes associated with this facies are mostly Serpulidae; smaller tube-forming encrusting calcareous foraminifers, i.e. nubecularids or spirillinids, have also been identified (Fig. S4I and J).

Upper microbialite boundstone

A second microbialite boundstone occurs between 140 and 134.3 mbsl (hereinafter referred to as 'upper microbialite boundstone'; Fig. 3G and H). As with the lower microbialite boundstone, microbialite is abundant and forms crusts several centimetres in thickness interspersed with *in situ* corals and coralline algae. Coralline algae, including the species *Lithothamnion proliferum*, form thin crusts assigned to the same assemblage aA3 (Humblet *et al.*, 2019). The coral assemblage is distinct from the lower microbialite boundstone and is composed predominantly of *Porites* and Merulinidiae (assemblage cE of Humblet *et al.*, 2019; Fig. S4J). Colonies are significantly thicker than in the lower microbialite boundstone, with transversal sections reaching 5 cm. *Entobia* borings are at places abundant in corals and microbialite crusts but bioerosion appears in general less extensive than in the lower microbialite boundstone. Bioclasts are composed of corals, including *Acropora* and *Seriatopora*, bryozoans, *Homotrema*, sponges and mollusc shells. Microbialite crusts are volumetrically abundant and their fabric is structureless or displays crude laminations.

The transition between the upper microbialite boundstone and the unconsolidated carbonate mud at the top of the hole is not well documented because of poor core recovery. Heavily bored microbialite, corals and coralline algae partially crushed during drilling were recovered at 134.3 mbsl, representing the upper stratigraphic limit of boundstone deposition in Hole 40A. The algal assemblage contains *Mesophyllum* and belongs to the aA3 type (Humblet *et al.*, 2019). Corals cannot be identified due to their poor state of preservation.

Carbonate mud

The carbonate mud interval extends from 133 mbsl to the top of the hole at 131 mbsl. Bioclasts are mostly concentrated at the top of the interval, where sediments become slightly coarser and include *Halimeda* segments, mollusc shells, echinoid spines and foraminiferal tests (Webster *et al.*, 2011). The foraminiferal assemblage, described by Yagioka *et al.* (2019), consists primarily of *Operculina* spp., *Amphistegina bicirculata*, *A. radiata* and includes planktonic forms (assemblage D; Fig. 2). The composition of the modern seabed at Hydrographers Passage between 120 and 140 mbsl is spatially variable and consists of sand, gravel and larger rubble; and live benthos is dominated by azooxanthellate octocorals (Bridge *et al.*, 2011; Renema *et al.*, 2013).

Sedimentary facies of Hole 41A

Variation in sedimentary facies and biotic components cannot be resolved with the same level of detail in Hole 41A due to the lower core recovery. However, the succession of facies is broadly similar to 40A, with the exception of the lower microbialite boundstone, missing in 41A. Similar to Hole 40A, a layer of unconsolidated fine carbonate sand and mud occupies, respectively, the bottom and the top of the hole. The facies between these layers consists of microbialite boundstone containing corals and coralline algae, of which only fragments were recovered. Corals associated with this boundstone include *Porites*, Merulinidae and several other taxa, such as *Leptoseris* and Siderastreidae (Fig. 1S). No *Pachyseris speciosa* was found. Corals are also present in the unconsolidated fine carbonate sand interval and consist of solitary forms, i.e. *Heterocyathus aequicostata*, *Heteropsammia cochlea* and Fungiidae, as well as small fragments of Poritidae, Merulinidae and *Seriatopora*. As with Hole 40A, sediments of the fine sand interval coarsen upward and the proportion of mud decreases up-core relative to that of sand and gravel (Yagioka *et al.*, 2019). The transition between the carbonate sand and microbialite boundstone coincides with a shift in foraminiferal species composition from *Operculina*- to *Calcarina*-dominated assemblage (Assemblage C to B; Yagioka *et al.*, 2019; Fig. 2). In addition, similar to Hole 40A, the top of 41A is characterised by the occurrence of foraminiferal assemblage D (Yagioka *et al.*, 2019; Fig. 2).

Radiometric ages

Carbonate samples recovered from Holes 40A and 41A range in age from 39 to <9 ka, i.e. from the end of Marine Isotope Stage 3 (MIS 3) to the Holocene (Fig. 2; Table S1). The age-depth plot reveals a marked age difference between the two sites, particularly in the lower half of the holes, where at any given depth the age difference between sediments of Holes 40A and 41A is ca. 2 to 4 ka (Fig. 2D).

The fine carbonate sand interval was deposited at the end of Marine Isotope Stage 3 (MIS 3). In Hole 40A, the oldest age of the sandy interval is 38.6 ± 0.45 ka. The transition between the fine sand and the lower microbialite boundstone in this hole occurred at ca. 27 to 25 ka. The bulk of the boundstone accreted between 25.3 to 24.6 and 24.1 ka (i.e. MIS 2) and therefore represents a distal section of Reef 2 (Fig. 2 and Table S2; Webster *et al.*, 2018). In Hole 41A, the age of the sandy interval ranges from 37.6 ± 0.75 to 20.9 ± 0.38 ka (Fig. 2D). The age of the packstone-boundstone that marks the transition between the two microbialite boundstones in 40A is 20.2 to 19.6 ka, therefore placing its deposition timing shortly after the peak LGM (Fig. 2). U-Th ages of 18.4 ± 0.09 ka and 18.5 ± 0.04 ka measured on two corals in the upper microbialite boundstone in 40A constrain the start of its deposition to between 19.5 and 18.5 ka. The

timing of its deposition therefore coincides with that of Reef 3a (Webster *et al.*, 2018). The stratigraphic position of the top of the upper boundstone is unclear due to relatively poor core recovery below the uppermost mud interval. However, boundstone composed of microbialite and coralline algal crusts is present in Hole 40A at ~134 mbsl and microbialite boundstone crushed during coring was also recovered in Hole 41A up to ~135 mbsl. Radiocarbon dating of these horizons yields an age of 16.1 ± 0.19 ka and 17.3 ± 0.22 ka, respectively, suggesting that deposition of microbialite boundstone may have occurred until 16 to 17 ka. The lack of evidence for reef accretion younger than 16 ka suggests that deposition of Reef 3b material at this location, if any, was very limited (Fig. 2). The base of the carbonate mud section was dated based on two samples providing ages of 9.7 ± 0.16 ka and 11.6 ± 0.33 ka in 40A and 41A, respectively. and suggest that the carbonate mud was deposited during the Holocene.

Vertical accretion rates

Visually best-fitted accretion curves for Holes 40A and 41A define seven and five inflection points, respectively (Figs 2 and 4). The general trend delineated by the two curves is roughly sinusoidal in shape, with a sharp increase in VA rates between ca. 20 and ca. 17 ka (Figs 2 and 4). Specifically, sedimentation rates range from 0.1 to 0.6 mm yr^{-1} before 20 ka, corresponding mostly to the deposition of the fine carbonate sand. An exception to this trend is a peak of VA rate at ca. 24 ka, reaching 2 mm yr^{-1}, coinciding with the deposition of the lower microbialite boundstone recovered from 40A (Figs 2 and 4). Values increase between 20 and 17 ka to 5.2 and 2.8 mm yr^{-1} in 40A and 41A, respectively, during the deposition of the upper microbialite boundstone. Lower sedimentation rates of 0.2 to 0.5 mm yr^{-1} are recorded after 17 ka (Figs 2 and 4).

The VA rates calculated based on the Bayesian age-depth models display temporal trends that are similar to those derived from the visual fit method, i.e. VA rates associated with microbialite boundstone tend to be higher compared with other lithologies (Fig. S3). However, mean VA rates derived from the Bayesian age models have maxima of ~2 mm yr^{-1}, significantly lower than peak values derived from the visual fit method. The discrepancy is more pronounced in the interval associated with the upper microbialite boundstone in Hole 40A. This is because the Bayesian age-depth model bypasses a sample used as an inflection point in the visually best-fitted curve of Hole 40A, i.e. sample dated 17.3 ka (Fig. S3A). The scarcity of *in situ* samples at the top of Hole 40A is responsible for the differences between the Bayesian age-depth model and the visual fit method.

DISCUSSION

Palaeoenvironmental variation

The ~20 m sections of unconsolidated carbonate sediments and reef boundstone recovered from Holes 40A and 41A record variation in sedimentation spanning the entire transition from MIS 3 to 1, a period of large and rapid sea-level change. Here, the authors discuss the palaeoenvironmental interpretation of the five main lithofacies identified in Hole 40A in light of the new chronostratigraphic framework presented in this study and the local RSL curve of Yokoyama *et al.* (2018); and using results from previously published analyses of coralgal (Humblet *et al.*, 2019) and foraminiferal assemblages (Yagioka *et al.*, 2019; Fig. 4).

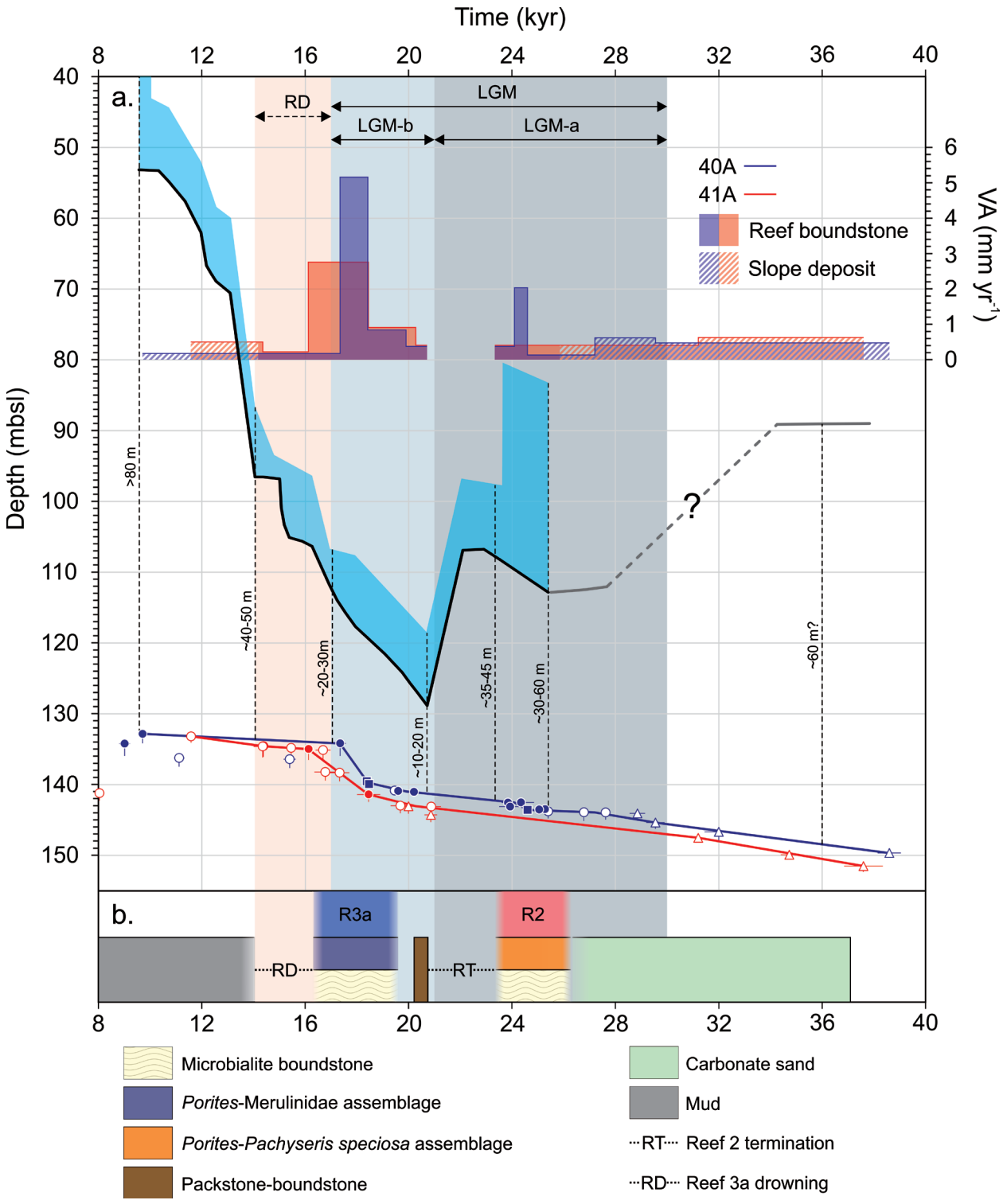


Fig. 4. (a) Relative sea-level (RSL) curve for transect HYD-01C (black line) and segment of the RSL curve obtained for transect NOG-01B (grey line) (Yokoyama *et al.*, 2018), vertical accretion (VA) rates and dated *in situ* samples plotted as a function of age and depth (see Fig. 2 for the meaning of colours and symbols); vertical dashed lines illustrate variation in palaeo-water depths over time. (b) Schematic representation of the depositional history and major facies over the period 8 to 40 ka in Hole 40A.

The unconsolidated fine sand correlated with MIS 3 and recovered in the lower part of Holes 40A and 41A was deposited in the mesophotic zone at depths of 30 to 90 m based on an analysis of foraminiferal assemblages conducted by Yagioka *et al.* (2019) (assemblage C in Fig. 2). This interpretation is consistent with the palaeo-sea-level position derived from the RSL curve of Yokoyama *et al.* (2018) (Fig. 4). In addition, Yagioka *et al.* (2019) measured a coarsening upward with a marked increase in sand and gravel relative to mud content above 147 and 148 m in 40A and 41A, respectively.

Based on this paper's new chrono-stratigraphic framework, the increase in grain size began at ca. 32 ka, coinciding with the sea-level fall leading to LGM-a (32 to 29 ka; Yokoyama *et al.*, 2018; Fig. 4). The assemblage of solitary corals identified in the sandy interval of Hole 41A is also consistent with this interpretation. The association of *Heterocyathus*, *Heteropsammia cochlea* and Fungiidae, specifically *Cycloseris*, is typical of horizontal soft-bottom sediments at >20 m water depth (Veron, 2000).

The carbonate sand transitions to a ~20 cm-thick grainstone/rudstone interval in 40A. Concentrations of *Entobia* borings pervading the sedimentary fabric at the base and top of this layer suggest that it may be a transported block.

The lower microbialite boundstone of Hole 40A, which formed prior to the peak LGM, accreted in the upper mesophotic zone at depth of 30 to 60 m based on palaeo-sea-level position derived from the RSL curve of Yokoyama *et al.* (2018) (Fig. 4). This depth range is consistent with the palaeo-environmental interpretation of the coralgal assemblage in this interval (coral assemblage cF associated with algal assemblage aA3; Humblet *et al.*, 2019). The dominant coral taxa are laminar *Porites* and *Pachyseris speciosa*. *Pachyseris speciosa* is commonly found in the mesophotic zone in various reef provinces (Muir & Pichon, 2019) and both taxa have been described as representative of the upper mesophotic zone in the GBR (Sarano & Pichon, 1988; Bridge *et al.*, 2012). The associated algal assemblage aA3 suggests a water depth >20 m, consistent with a mesophotic setting (Humblet *et al.*, 2019). Microbialite crusts, well developed in this interval, tend to be abundant in LGM and in early-deglacial deep-water reef facies such as in Hole 54B of transect NOG-01B, another distal hole characterised by a high microbialite to corals and coralline algae volume ratio (Braga *et al.*, 2019; Szilagyi *et al.*, 2020).

The packstone-boundstone layer deposited shortly after the sea-level fall of the peak LGM, and recovered from Hole 40A, formed at water depths of 10 to 20 m based on the sea-level reconstruction of Yokoyama *et al.* (2018) (Fig. 4). In this facies, calcareous tubes, microbialite and coralline algae are important components of the framework. Bioclasts, including bryozoans, are more abundant than in the lower microbialite boundstone. One sample of coralline agal crust identified as *Mesophyllum* gr. *funafutiense* suggests a water depth of >20 m, but could be shallower if cryptic or in turbid waters (Humblet *et al.*, 2019). The calcareous tubes associated with this facies include Serpulidae and encrusting foraminifers, probably nubeculariids or spirillinids. In the absence of other diagnostic criteria and accurate taxonomic identification, it is not possible to assign a specific palaeo-depth range to these calcareous tubes. However, three radiocarbon ages obtained in the packstone-boundstone layer firmly constrain its age to 20.2 to 19.5 ka, implying reduced water depth following the 20 m sea-level fall between 21.5 and 20.5 ka (Yokoyama *et al.*, 2018).

The upper microbialite boundstone which formed during the early deglacial sea-level rise accreted at intermediate depths of 20 to

30 m according to the palaeo-water depth range derived from the RSL curve of Yokoyama *et al.* (2018) (Fig. 4). This depth range is consistent with the palaeo-environmental interpretation of the coralgal assemblage in this interval (coral assemblage cE and algal assemblage aA3; Humblet *et al.*, 2019). Algal assemblage aA3 indicates a palaeo-water depth >20 m. The dominant coral taxa, *Porites* and Merulinidae, occur in a wide depth range on modern reefs, but their laminar growth form and the lack of shallow species are consistent with a relatively deep setting. Similar to the lower boundstone of 40A, microbialite crusts are a significant component of the reef framework, consistent with their relatively high abundance in deep fore reef sections of other IODP 325 holes (Braga *et al.*, 2019). The upper microbialite boundstone also shows less macrobioerosion than the lower microbialite boundstone, which is consistent with a shallower palaeo-water depth range, as macrobioerosion tends to increase with depth in MCEs (Weinstein *et al.*, 2019).

The unconsolidated carbonate mud layer at the top of Holes 40A and 41A reflects deepening upward after the end of active reef growth at this location and the deposition of fine shelf slope sediments. Yagioka *et al.* (2019), based on their analysis of the foraminiferal assemblage, assigned a palaeo-water depth of 90 to 130 m to these sediments, in agreement with the RSL curve of Yokoyama *et al.* (2018) (Fig. 4). Similar slope deposits, consisting of calcareous silt with benthic and planktic foraminifera, sponge spicules and pteropod fragments, were recovered by IODP 325 at 170 m water depth 1 km from the shelf edge at Noggin Pass (Hole M0058A; Harper *et al.*, 2015). Closer to the location of Holes 40A and 41A, slope deposits composed of nannofossil ooze were collected by R/V SONNE using a gravity corer from a location at 236 m water depth in the area of Hydrographers Passage (core GeoB 22219-1; Mohtadi *et al.*, 2017).

History of reef growth and demise

Late glacial mesophotic reef growth

Mesophotic reef growth associated with the lower microbialite boundstone initiated between 27 and 25 ka after the sea-level fall of the LGM-a (Fig. 4) and persisted until at least 24 ka. Despite some uncertainty, the timing is roughly similar to that of more proximal sites where reef turn on is dated at 27 ka (Reef 2; Webster *et al.*, 2018). Reef growth initiation may have been promoted by reduced palaeo-water depth during the LGM-a, through (1) increased Photosynthetically Active Radiation (PAR) and (2) change in sedimentation, with the deposition of coarser sediments more suitable for the settlement of coral larvae. Although increased PAR and increased substrate availability can explain the successful recruitment of corals and coralline algae, they do not explain the development of microbialite crusts. Microbialite crust thickness since the LGM shows a negative correlation with atmospheric CO_2 concentrations; and a high carbonate saturation state of sea water during glacial and early deglacial periods has been invoked as an important factor promoting the development of microbialite crusts (Riding *et al.*, 2014; Braga *et al.*, 2019; Szilagyi *et al.*, 2020). Increase in structural complexity and coral cover during reef initiation may in itself promote microbialite crust formation by increasing stable substrate availability and primary pore space (Seard *et al.*, 2011). Decomposition of organic matter in interstitial space between clasts or within the reef framework will probably promote microbialite formation by increasing nutrient concentration (Braga *et al.*, 2019). Specifically in the case of Hole 40A, the colonisation of a sandy substrate by corals during reef turn-on may have created substrate suitable for microbialite formation.

More generally, during sea-level lowstand important sources of nutrients are the rivers draining the exposed continental shelf, which may also have stimulated microbial growth (Braga *et al.*, 2019).

The bulk of the mesophotic reef section recovered in Hole 40A (~1 m in thickness) formed between 25.3 to 24.6 and 24.1 ka. The visually best-fitted accretion curve displays a peak in VA rate of 2 mm yr^{-1} during this interval (Fig. 4), significantly higher than the accumulation rates calculated for the underlying sand in the same hole (i.e. 0.4 to 0.6 mm yr^{-1}). In contrast, the maximum mean VA rate derived from the Bayesian age-depth model is 0.9 mm yr^{-1}, still higher than in the underlying sand section (Fig. S3). Reef growth took place when sea-level was apparently stable (Yokoyama *et al.*, 2018). To the authors' knowledge, this is the first published, direct calculation of the vertical accretion rate of a mesophotic reef which is not part of a drowning sequence. The rates calculated in this study are close to the maximum growth rate potential of modern MCEs estimated by Weinstein (2014), i.e. 1.1 mm yr^{-1} and slightly lower than the maximum rates calculated for mesophotic reef sections of drowning sequences in other IODP 325 holes (i.e. 2.3 to 2.9 mm yr^{-1}; Fig. 5). Those drowning events were probably associated with increased shelf-to-basin sediment flux (Webster *et al.*, 2018) and may not be representative of 'healthy' mesophotic reef growth. Hence, rates of 2 to 3 mm yr^{-1} are probably lower estimates of the maximum growth potential of MCEs. However, direct comparison with the growth potential of modern coralgal frameworks may not be appropriate since the mesophotic reef section of Hole 40A is a microbialite boundstone that has no known equivalent today. In coral-dominated reef frameworks, although the growth rate of non-branching corals tends to decrease with depth (Pratchett *et al.*, 2015), those of species well adapted to mesophotic conditions, such as *Leptoseris*, can remain high and contribute to increase the vertical accretion potential of mesophotic reefs (Kahng *et al.*, 2020).

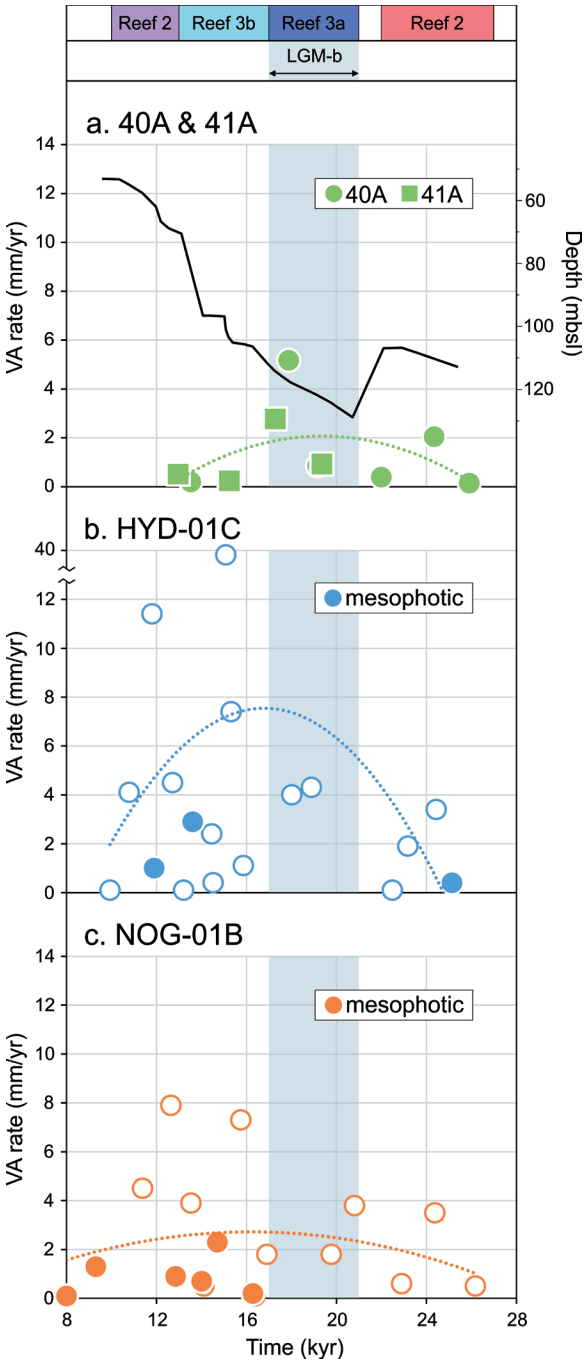


Fig. 5. Values of vertical accretion (VA) rates derived from the visual fit method as a function of time over the period 8 to 40 ka for (a) Holes 40A and 41A, (b) core sections of IODP 325 holes drilled along transect HYD-01C; and (c)

core sections of IODP 325 holes drilled along transect NOG-01B. Values of accretions rates for transects HYD-01C and NOG-01B are from Webster *et al.* (2018).

Mesophotic reef growth continued until at least 24 ka. Limited core recovery does not enable knowledge of exactly when or if reef growth ceased. However, at the very least, reef growth must have slowed considerably as a sample dated 20.2 ka from the packstone-boundstone layer above lies only ~1 m from the top of the lower microbialite boundstone.

At more proximal sites, shallow reef growth was interrupted at ca. 22 ka by the rapid 20 m sea-level fall of the peak LGM to ~120 mbsl. As a consequence, shallow coral facies migrated downslope and reef growth resumed at lower elevations during the early deglacial sea-level rise (Reef 3a; Webster *et al.*, 2018). This paper's authors' dataset shows that limited reef growth, if any, occurred at the location of Hole 40A and 41A between 24 and 19 ka. The 20 m sea-level fall probably negatively affected reef growth. Sea-level fall may translate in cores and outcrops into a succession of coralgal assemblages reflecting a shallowing upward (Webster *et al.*, 1998). However, the lower microbialite boundstone of Hole 40A does not show such a shallowing upward trend. While sea-level fall caused reef demise by exposure in shallow waters, rapid increase in hydrodynamic energy may have limited reef growth on the slope due to wave-induced sediment production and resuspension, or the influence of bottom currents, promoting the formation of unconsolidated substrate (Grossman & Fletcher, 2004). Another detrimental factor could have been lower SSTs during the LGM, particularly at Hydrographers Passage, as SSTs were ~7 to 8° C cooler than present on average at this locality (Felis *et al.*, 2014; Brenner *et al.*, 2020). The rapid transition to the peak LGM is marked by a major change in sedimentation and the deposition of the packstone-boundstone layer rich in serpulid tubes in Hole 40A, followed by the second episode of reef growth at the onset of deglaciation. The singular abundance of serpulid worms may indicate nutrient enrichment (Samini Namin *et al.*, 2010; Le Grand & Fabricius, 2011), perhaps linked to sediment resuspension during sea-level lowstand. The surface on which early deglacial reef growth initiated correlates with a prominent seismic reflector delineating the boundary between the glacial lowstand systems tract and post-glacial transgressive systems tract (i.e. reflector R1) identified by Hinestrosa *et al.* (2016).

There is no evidence for pre-LGM mesophotic reef growth in Hole 41A and sedimentation at this site was characterised by carbonate sand deposition until the LGM. While the rapid sea-level fall of the peak LGM marks the interruption of mesophotic reef growth in Hole 40A, the resulting abrupt shallowing caused a shift in foraminiferal assemblage in Hole 41A (see yellow line in Fig. 2 illustrating the stratigraphic boundary delineating the start of the sea-level fall of the peak LGM in Holes 40A and 41A). The corresponding stratigraphic interval in Hole 40A is dominated by boundstone and was not sampled for foraminiferal analysis and therefore the shift in foraminiferal assemblage in this hole cannot be observed. The absence of mesophotic reef growth in Hole 41A may reflect lateral discontinuity in mesophotic reef facies despite the sites being 10 m apart. In modern reef environments, MCEs commonly display a patchy distribution with areas of relatively high coral cover adjacent to areas of soft sediments largely devoid of macro-benthic life (Frade *et al.*, 2019; Sinniger *et al.*, 2019). Mesophotic growth in 40A probably accentuated the difference in elevation between the two sites (to max. 2 to 3 m), already reflected in the bottom sand section by the age difference existing between them at any given depth.

Early deglacial reef growth

Reef growth resumed after the LGM at ca. 19.5 to 18.5 ka to form the upper microbialite boundstone. Early deglacial reef growth was also delayed at other sites of Hydrographers Passage, whereas reef growth resumed earlier at Noggin Pass, presumably because of a steeper latitudinal SST gradient during the LGM (Humblet *et al.*, 2019).

Early deglacial reef growth associated with the upper microbialite boundstone formed at intermediate depth yields the highest VA rates between 20 and 16 ka (Fig. 4). The visually best-fitted accretion curve produces peak values of 5.2 and 2.8 mm yr^{-1} for Hole 40A and 41A, respectively, whereas maxima of mean VA rates derived from the Bayesian method are 2.2 and 1.7 mm yr^{-1}. The values derived from the visual fit method are similar to accretion rates calculated for early deglacial shallow (<10 m) facies in other IODP 325 holes (i.e. 3.9 to 4.4 mm yr^{-1}; Fig. 5) and are also comparable to values calculated for Indo-Pacific Holocene reef sequences (Dullo, 2005; Gischler & Hudson, 2019) and estimates of reef growth potential for healthy modern shallow coral reefs (Perry & Morgan, 2017). The bulk of the upper microbialite boundstone was probably formed between 19.5 and 17 to 16 ka and hence correlates with Reef 3a of Webster *et al.* (2018). Microbialite is volumetrically abundant. Microbialite crust formation in fore reef settings was coeval with coralgal growth and occurred on the sea floor within the photic zone (Braga *et al.*, 2019; Szilagyi *et al.*, 2020). Hence, microbialite played an important role in sustaining vertical reef accretion during the acceleration of sea-level rise after the LGM at a rate of 3.5 mm yr^{-1} (Yokoyama *et al.*, 2018), sustaining maximum VA rates of 2 to 5 mm yr^{-1}, although these rates are significantly lower than the maximum rates measured in other more proximal IODP 325 core sections (i.e. >10 mm yr^{-1}; Fig. 5).

The formation of the upper microbialite boundstone coincides with the LGM-b between 21 and 17 ka, a period characterised by a moderate 3.5 mm yr^{-1} sea-level rise (Yokoyama *et al.*, 2018). Increasing SST at the onset of the deglaciation may have promoted reef initiation (Felis *et al.*, 2014; Brenner *et al.*, 2020). While sea-level rise stimulates shallow reef growth by increasing substrate availability and accommodation space (Woodroffe & Webster, 2014; Husson *et al.*, 2018; Yokoyama & Esat, 2015; Yokoyama & Purcell, 2021), its impact on reef initiation and reef growth potential at intermediate or mesophotic water depth is less clear. If sea-level rise stimulates growth of depth-generalists in shallow reef settings, then presumably these coral species could colonise deeper habitats where they could contribute to reef initiation. However, even widespread species can display limited genetic connectivity between shallow and deep habitats; and colonisation potential may vary from one species to another (Bongaerts *et al.*, 2017).

Reef growth termination in Holes 40A and 41A at 17 to 16 ka coincides with reef drowning recorded in other holes of the mid and outer terraces and correlates with the reflooding of the inner terrace at 16.5 ka that caused a massive export of terrigenous sediments toward the distal part of the shelf edge (Webster *et al.*, 2018). Acceleration of sea-level rise at 17 ka may have compounded the effect of reduced water quality, particularly at distal sites (Webster *et al.*, 2018; Yokoyama *et al.*, 2018).

Lower values of sedimentation rate averaging 0.3 mm yr^{-1} (visual fit method) and 0.5 to 0.6 mm yr^{-1} (Bayesian method) are recorded after 17 ka and the demise of Reef 3a in shallow waters. The reef framework was ultimately buried by carbonate mud. The accumulation rate of these slope deposits cannot be assessed because one age only was measured in each hole at the base of the

carbonate mud interval, i.e. 9.7 ka and 11.6 ka in 40A and 41A, respectively. However, if a modern age is assumed for the top of the holes, and a constant accumulation rate, rates of 0.17 and 0.16 mm yr^{-1} are obtained in Holes 40A and 41A, respectively. For comparison, the accumulation rate of the top 3 m of Hole 58A based on the age model of Harper *et al.* (2015) is 0.7 mm yr^{-1}.

In conclusion, analysis of the two reef sections in Hole 40A gives insight into the environmental limits of reef growth at intermediate and mesophotic depths under distinct modes of sea-level and climate change. The first episode of reef growth during LGM-a was probably promoted by reduced palaeo-water depth and low pCO_2 and terminated as sea-level rapidly fell to peak LGM level, influenced by increased hydrodynamic energy and minima of sea water temperature. In contrast, the second episode of reef growth during LGM-b occurred under conditions of moderate sea-level rise and increasing sea water temperature at the onset of the deglaciation and ceased as sea-level rise accelerated and sediment flux from the flooded shelf increased. Maxima of VA rates of 2 to 5 mm yr^{-1} (visual fit method) reported here at intermediate to mesophotic depths are comparable to current rates of sea-level rise (3 to 4 mm yr^{-1}), but lower than rates predicted at the end of the century under Representative Concentration Pathway (RCP) 2.6 (4 to 9 mm yr^{-1}) and far below those predicted under RCP8.5 (10 to 20 mm yr^{-1}; Oppenheimer *et al.*, 2019). The findings herein highlight the need to further investigate the potential of deep reef communities to cope with accelerating sea-level rise and their sensitivity to millennial scale environmental change.

CONCLUSIONS

Holes 40A and 41A were drilled 10 m apart at 131 m water depth by IODP Expedition 325 along the shelf edge of the GBR and penetrated ~20 m of unconsolidated carbonate sediments and reef boundstone. In this study, re-examination of their lithologies and biotic components combined with a new robust chronostratigraphic framework supported by 47 radiometric ages are used to explore reef growth history at the distal edge of fossil reef distribution along the GBR shelf. Based on the analysis of this new dataset, the following conclusions can be drawn:

(1) Core sections recovered from Holes 40A and 41A range in age from 39 to <9 ka, thus spanning the transition from MIS 3 to MIS 1.

(2) Five main lithofacies are distinguished in Hole 40A (from bottom to top): (1) unconsolidated fine carbonate sand deposited at the end of MIS 3 between 39 ka and 27 to 25 ka, (2) a lower microbialite boundstone containing laminar *Porites* and *Pachyseris speciosa*, which accreted from 27 to 25 ka to at least 24 ka (MIS 2), (3) packstone-boundstone containing calcareous tubes, coralline algal crusts and microbialite, dated at 20.2 to 19.5 ka, (4) an upper microbialite boundstone containing laminar *Porites* and Merulinidae, which formed between 19.5 to 18.5 ka and 17.3 to 16.1 ka; and (5) unconsolidated carbonate mud of Holocene age.

(3) Lithofacies distribution in Hole 40A is broadly similar to that in Hole 41A, except for the absence of the lower microbialite boundstone of MIS 2 age.

(4) Palaeo-water depth interpretation based on previously published analyses of coralgal and foraminiferal assemblages (Humblet *et al.*, 2019; Yagioka *et al.*, 2019) and sea-level history (Yokoyama *et al.*, 2018) indicates the following ranges: (1) 30 to 90 m for the unconsolidated fine carbonate sand,

(2) 30 to 60 m for the lower microbialite boundstone, (3) 10 to 20 m for the packstone-boundstone, (4) 20 to 30 m for the upper microbialite boundstone; and (5) 90 to 130 m for the unconsolidated carbonate mud.

(5) The first episode of reef growth occurred at mesophotic depth. Initiation at 27 to 25 ka may have been promoted by elevated PAR and change in sedimentation linked to falling sea-level between 32 and 29 ka, as well as low atmospheric pCO_2 at the end of the Last Glacial period. Little or no reef accretion took place between 24 and 19 ka, coinciding with a rapid 20 m sea-level fall of the peak LGM and minima of SSTs.

(6) Reef growth resumed at 19.5 to 18.5 ka during a period of moderate sea-level rise and increasing SSTs at the onset of the deglaciation. The timing of reef growth termination at ca. 17 ka coincides with a major episode of reef demise reported previously from mid and outer terrace cores and linked to increased shelf-to-basin sediment flux compounded by accelerating deglacial sea-level rise (Webster *et al.*, 2018). As a result, reef boundstone is overlain by carbonate mud at the top of the holes, reflecting a deepening and the transition to present-day upper-slope sedimentation.

(7) Maxima of VA rates are reached in reef boundstone sections. The mesophotic reef in Hole 40A yields a peak VA rate of 2 mm yr^{-1} based on the visual fit method and maximum mean VA rate of 0.9 mm yr^{-1} based on the Bayesian age-depth model. The former value is similar to rates calculated for mesophotic reef sections of drowning sequences in other IODP 325 holes. The maxima of VA rates calculated based on the visual fit method for the early deglacial reef section formed at intermediate depth in Holes 40A and 41A are 5.2 and 2.8 mm yr^{-1}, respectively. Maximum of mean VA rates derived from the Bayesian method is ~2 mm yr^{-1} in the two holes. Upper bound estimates of VA rates for the early deglacial reef section (~3 to 5 mm yr^{-1}) are comparable to those of shallower reef facies of the same age from more proximal IODP 325 holes and similar also to Holocene reef sequences of the Indo-Pacific region.

(8) This paper's findings reveal that reef ecosystems at intermediate and mesophotic depths dominated by microbialite and corals were capable to accrete several metres of boundstone at a maximum rate of 5 mm yr^{-1} or less. There is a pressing need to explore the potential of modern-type deep coralgal communities to sustain higher rates of sea-level rise predicted at the end of the century.

ACKNOWLEDGEMENTS

The authors of this study wish to thank the staff of Kochi Core Center, in particular Dr. Yusuke Kubo, IODP curator, for their support during the examination of the cores. This research was funded in part by JSPS Grants-in-Aid for Scientific Research awarded to M.H. (KAKENHI # 18K03824) and Y.Y. (KAKENHI # JP20H00193).

REFERENCES

Abbey, E., Webster, J.M. and **Beaman, R.J.** (2011b) Geomorphology of submerged reefs on the shelf edge of the Great Barrier Reef: The influence of oscillating Pleistocene sea levels. *Mar. Geol.* **288**, 61–78.

Abbey, E., Webster, J.M., Braga, J.C., Jacobsen, G., Thorogood, G., Thomas, A., Camoin G. and **Reimer, P.** (2013) Deglacial mesophotic reef demise on the Great Barrier Reef. *Palaeogeogr. Palaeoclimatol. Palaeoecol.*, **392**, 473–494.

Abbey, E., Webster, J.M., Braga, J.C., Sugihara, K., Wallace, C.C., Iryu, Y., Potts, D., Done, T., Camoin, G. and **Seard, C.** (2011a) Variation in deglacial coralgal assemblages and their paleoenvironmental significance: IODP Expedition 310, "Tahiti Sea Level". *Global Planet. Change*, **76**, 1–15.

Armstrong, R.A., Singh, H., Torres, J., Nemeth, R.S., Can, A., Roman, C., Eustice, R. and **Garcia-Moliner, G.** (2006) Characterizing the deep insular shelf coral reef habitat of the Hind Bank marine conservation district (US Virgin Islands) using the Seabed autonomous underwater vehicle. *Cont. Shelf Res*., **26**, 194–205.

Blaauw, M., Christen, A. and **Aquino, M.** (2020) *Rbacon: Age-Depth Modelling using Bayesian Statistics*. R Foundation for Statistical Computing, Vienna, Austria R package.

Bongaerts, P., Riginos, C., Brunner, R., Englebert, N., Smith, S.R. and **Hoegh Guldberg, O.** (2017) Deep reefs are not universal refuges: reseeding potential varies among coral species. *Science Advances*, **3**, e1602373.

Braga, J.C. and **Aguirre, J.** (2004) Coralline algae indicate Pleistocene evolution from deep, open platform to outer barrier reef environments in the northern Great Barrier Reef margin. *Coral Reefs*, **23**, 547–558.

Braga, J.C., Humblet, M., Ramos, D.A.E., Dechnik, B. and **Webster, J.M.** (2022) Quaternary coral, coralline algal and vermetid assemblages as sea-level indicators: a review. In: *Coral Reefs and Sea-Level Change: Quaternary Records and Modelling. A window into the Future*, IAS Spec. Publ., (this issue).

Braga, J.C., Puga-Bernabeu, A., Heindel, K., Patterson, M.A., Birgel, D., Peckmann, J., Sánchez-Almazo, I.M., Webster, J.M., Yokoyama, Y. and **Riding, R.** (2019) Microbialites in Last Glacial Maximum and deglacial reefs of the Great Barrier Reef (IODP Expedition 325, NE Australia). *Palaeogeogr. Palaeoclimatol. Palaeoecol.*, **514**, 1–17.

Brenner, L.D., Linsley, B.K., Webster, J.M., Potts, D., Felis, T., Gagan, M.K., Inoue, M., McGregor, H., Suzuki, A., Tudhope, A., Esat, T., Thomas, A., Thompson, W., Fallon, S., Humblet, M., Tiwari, M. and **Yokoyama, Y.** (2020) Coral record of Younger Dryas Chronozone warmth on the Great Barrier Reef. *Paleoceanography and Paleoclimatology*, **35** (12) e2020PA003962. https://doi.org/10.1029/2020PA003962

Bridge, T.C.L., Done, T.J., Beaman, R.J., Friedman, A., Williams, S.B., Pizarro, O. and **Webster, J.M.** (2011) Topography, substratum and benthic macrofaunal relationships on a tropical mesophotic shelf margin, central Great Barrier Reef, Australia. *Coral Reefs*, **30**, 143–153.

Bridge, T.C.L., Fabricius, K.E., Bongaerts, P., Wallace, C.C., Muir, P.R., Done, T.J. and **Webster, J.M.** (2012) Diversity of Scleractinia and Octocorallia in the mesophotic zone of the Great Barrier Reef, Australia. *Coral Reefs*, **31** (1), 179–189.

Bridge, T. and **Guinotte, J.** (2013) *Mesophotic coral reef ecosystems in the Great Barrier Reef world heritage area: their potential distribution and possible role as refugia from disturbance*. Research Publication no.109, Great Barrier Reef Marine Park Authority, Townsville.

Bridge, T.C.L., Beaman, R.J., Bongaerts, P., Muir, P.R., Ekins, M. and **Sih, T.** (2019) The Great Barrier Reef and Coral Sea. In: *Mesophotic Coral Ecosystems* (Eds Y. Loya, K.A. Puglise and T.C.L. Bridge), Springer, New York, 351–367.

Dullo, W.C. (2005) Coral growth and reef growth: a brief review. *Facies*, **51**, 33–48.

Englebert, N., Bongaerts, P., Muir, P.R., Hay, K.B., Pichon, M. and **Hoegh-Guldberg, O.** (2017) Lower Mesophotic Coral Communities (60–125 m Depth) of the Northern Great Barrier Reef and Coral Sea. *PLoS ONE*, **12** (2), e0170336.

Eyal, G., Tamir, R. Kramer, N., Eyal-Shaham, L. and **Loya, Y.** (2019) The Red Sea Mesophotic coral ecosystems. In: *Mesophotic Coral Ecosystems* (Eds Y. Loya, K.A. Puglise and T.C.L. Bridge), Springer, New York, 199–214.

Felis, T., McGregor, H.V., Linsley, B.K., Tudhope, A.W., Gagan, M.K., Suzuki, A., Inoue, M., Thomas, A.L., Esat, T.M., Thompson, W.G., Tiwari, M., Potts, D.C., Mudelsee, M., Yokoyama, Y. and **Webster, J.M.** (2014) Intensification of the meridional temperature gradient in the Great Barrier Reef following the Last Glacial Maximum. *Nature Comms*, **5**, 4102.

Frade, P.R., Bongaerts, P., Baldwin, C.C., Trembanis, A.C., Bak, R.P. and **Vermej, M.J.A.** (2019) Bonaire and Curaçao. In: *Mesophotic Coral Ecosystems* (Eds Y. Loya, K.A. Puglise and T.C.L. Bridge), Springer, New York, 149–162.

Gischler, E. and **Hudson, J.H.** (2019) Holocene tropical reef accretion and lagoon sedimentation: a quantitative approach to the influence of sea-level rise, climate and subsidence (Belize, Maldives, French Polynesia). *The Depositional Record*, **5**, 515–539.

Grigg, R.W. (2006) Depth limit for reef building corals in the Au'au Channel, S.E. Hawaii. *Coral Reefs*, **25**, 77–84.

Grossman, E.E. and **Fletcher, C.H.** (2004) Holocene reef development where wave energy reduces accommodation space, Kailua bay, windward Oahu, Hawaii. *USA J. Sed. Res*., **74**, 49–63.

Harper, B.B., Puga-Bernabéu, A., Droxler, A.W., Webster, J.M., Gischler, E., Tiwari, M., Lado-Insua, T., Thomas, A.L., Morgan, S., Jovane, L. and **Röhl, U.** (2015) Mixed carbonate-siliciclastic sedimentation along the Great Barrier Reef upper slope: a challenge to the reciprocal sedimentation model. *J. Sed. Res.*, **85**, 1019–1036.

Harris, P.T., Bridge, T.C.L., Beaman, R.J., Webster, J.M., Nichol, S.L. and **Brooke, B.P.** (2013) Submerged banks in the Great Barrier Reef, Australia, greatly increase available coral reef habitat. *ICES J. Mar. Sci.*, **70**, 284–293.

Hinderstein, L.M., Marr, J.C.A., Martinez, F.A., Dowgiallo, MJ, Puglise, K.A., Pyle, R.L., Zawada, D.G. and **Appeldoorn R.A.** (2010) Theme section on "Mesophotic coral ecosystems: characterization, ecology and management". *Coral Reefs*, **29**, 247–251.

Hinestrosa, G., Webster, J.M. and **Beaman, R.** (2016) Postglacial sediment deposition along a mixed carbonate-siliciclastic margin: new constraints from the drowned shelf-edge reefs of the Great Barrier Reef, Australia. *Palaeogeogr. Palaeoclimatol. Palaeoecol*., **446**, 168–185.

Hopley, D., Smithers, S.G. and **Parnell, K.E.** (2007) *The geomorphology of the Great Barrier Reef: development, diversity and change*. Cambridge University Press, USA.

Huang, D., Benzoni, F., Fukami, H., Knowlton N., Smith N.D. and **Budd, A.F.** (2014) Taxonomic classification of the reef coral families Merulinidae, Montastraeidae and Diploastraeidae (Cnidaria: Anthozoa: Scleractinia). *Zool. J. Linn. Soc*., **171**, 277–355.

Hubbard, D.K. and **Scaturo, D.** (1985) Growth rates of seven species of scleractinian corals from Cane Bay and Salt River, St. Croix, USVI. *Bull. Mar. Sci*., **36**, 325–338.

Humblet, M., Hongo, C. and **Sugihara, K.** (2015) An identification guide to some major Quaternary fossil reef-building coral genera (*Acropora*, *Isopora*, *Montipora* and *Porites*). *Island Arc*, **24**, 16–30.

Humblet, M. and **Iryu, Y.** (2014) Pleistocene coral assemblages on Irabu-jima, South Ryukyu Islands, Japan. *Paleontol. Res*., **18**, 224–244.

Humblet, M., Iryu, Y. and **Nakamori, T.** (2009) Variations in Pleistocene coral assemblages in space and time in southern and northern Central Ryukyu Islands, Japan. *Mar. Geol*., **259**, 1–20.

Humblet, M., Potts, D.C., Webster, J.M., Braga, J.C., Iryu, Y., Yokoyama, Y., Bourillot, R., Seard, C., Droxler, A., Fujita, K., Gischler, E. and **Kan, H.** (2019) Late glacial to deglacial variation of coralgal assemblages in the Great Barrier Reef, Australia. *Global Planet. Change*, **174**, 70–91.

Humblet, M. and **Webster, J.M.** (2017) Coral community changes in the Great Barrier Reef in response to major environmental changes over glacial-interglacial timescales. *Palaeogeogr. Palaeoclimatol. Palaeoecol*., **472**, 216–235.

Husson, L., Pastier, A.M., Pedoja, K., Elliot, M., Paillard, D., Authemayou, C., Sarr, A.C., Schmitt, A. and **Cahyarini, S.** (2018) Reef Carbonate Productivity During Quaternary Sea Level Oscillations. *Geochem. Geophys. Geosyst*., **19**, 1148–1164.

Kahng, S.E. and **Kelley, C.D.** (2007) Vertical zonation of megabenthic taxa on a deep photosynthetic reef (50–140 m) in the Au'au Channel, Hawaii. *Coral Reefs*, **26**, 679–687.

Kahng, S.E., Watanabe, T.K., Hu, H.M., Watanabe, T. and **Shen, C.C.** (2020) Moderate zooxanthellate coral growth rates in the lower photic zone. *Coral Reefs*, **39**, 1273–1284.

Le Grand, H.M. and **Fabricius, K.E.** (2011) Relationship of internal macrobioeroder densities in living massive Porites to turbidity and chlorophyll on the Australian Great Barrier Reef. *Coral Reefs*, **30**, 97–107.

Loya, Y., Puglise, K.A. and **Bridge, T.C.L.**, eds (2019) *Mesophotic Coral Ecosystems*. Springer, New York, 1003 pages.

Mohtadi, M., Beaman, R.J., Boehnert, S., Daumann, M., Floren, V.M., Gould, J.L.A., Hirabayashi, S., Hollstein, M., Kienast, M., Lückge, A., Meyer-Schack, B.I.G., Obrochta, S.P., O'Toole, L.M., Pall, J.R., Renema, W., Rodehutscord, V., Sanborn, K.L., Schade, T., Steinke, S., Webster, J.M., Wenderlich, M.J. and **Yokoyama, Y.** (2017) *R/V SONNE Cruise Report SO256, TACTEAC, Temperature and circulation history of the East Australian Current, Auckland (New Zealand) – Darwin (Australia), 17 April – 09 May 2017*. No. 316, Berichte MARUM – Zentrum für Marine Umweltwissenschaften, Fachbereich Geowissenschaften., Universität Bremen, Bremen, Germany, 81 pages.

Muir, P.R. and **Pichon, M.** (2019) Biodiversity of reef-building, scleractinian corals. In: *Mesophotic Coral Ecosystems* (Eds Y. Loya, K.A. Puglise and T.C.L. Bridge), Springer, New York, 589–620.

Oppenheimer, M., Glavovic, B.C., Hinkel, J., van de Wal, R., Magnan, A.K., Abd-Elgawad, A., Cai, R., Cifuentes-Jara, M., DeConto, R.M., Ghosh, T., Hay, J., Isla, F., Marzeion, B., Meyssignac, B. and **Sebesvari, Z.** (2019) Sea Level Rise and Implications for Low-Lying Islands, Coasts and Communities. In: *IPCC Special Report on the Ocean and Cryosphere in a Changing Climate* (Eds H.-O. Pörtner, D.C. Roberts, V. Masson-Delmotte, P. Zhai, M. Tignor, E. Poloczanska, K. Mintenbeck, A. Alegría, M. Nicolai, A. Okem, J. Petzold, B. Rama, N.M. Weyer), Intergovernmental Panel on Climate Change.

Patterson, M.A., Webster, J.M., Hutchings, P., Braga, J.C., Humblet, M. and **Yokoyama, Y.** (2020) Bioerosion trances in the Great Barrier Reef over the past 10 to 30 kyr. *Palaeogeogr. Palaeoclimatol. Palaeoecol*., **542**, 109503.

Perry, C.T. and **Morgan, K.M.** (2017) Bleaching drives collapse in reef carbonate budgets and reef growth potential on southern Maldives reefs. *Scientific Reports*, **7**, 40581.

Perry, C.T., Murphy, G.N., Kench, P.S., Smithers, S.G., Edinger, E.N., Steneck, R.S. and **Mumby, P.J.** (2013) Caribbean-wide decline in carbonate production threatens coral reef growth. *Nature Comms*, **4**, 1402.

Pyle, R.L. and **Copus, J.M.** (2019) Mesophotic coral ecosystems: introduction and overview. In: *Mesophotic Coral Ecosystems* (Eds Y. Loya, K.A. Puglise and T.C.L. Bridge), Springer, New York, 3–27.

Renema, W., Beaman, R.J. and **Webster, J.M.** (2013) Mixing of relict and modern tests of larger benthic foraminifera on the Great Barrier Reef shelf margin. *Mar. Micropaleontol*., **101**, 68–75.

Riding, R., Liang, L. and **Braga, J.C.** (2014) Millennial-scale ocean acidification and late Quaternary decline of cryptic bacterial crusts in tropical reefs. *Geobiology*, **12**, 387–405.

Samini Namin, K., Risk, M.J., Hoeksema, B.W., Zohari, Z. and **Rezai H.** (2010) Coral mortality and serpulid infestations associated with red tide, in the Persian Gulf. *Coral Reefs*, **29**, 509.

Sarano, F. and **Pichon, M.** (1988) Morphology and ecology of the deep fore reef slope at Osprey Reef (Coral Sea). In: *Proceedings of the 6th International Coral Reef Symposium, Townsville, Australia 8–12 August 1988*, 607–611.

Seard, C., Camoin, G., Yokoyama, Y., Matsuzaki, H., Durand, N., Bard, E., Sépulcre, S. and **Deschamps, P.** (2011) Microbialite development patterns in the last deglacial reefs from Tahiti (French Polynesia; IODP Expedition #310): implications on reef framework architecture. *Mar. Geol*., **279**, 63–86.

Sherman, C.E., Locker, S.D., Webster, J.M. and **Weinstein, D.K.** (2019) Geology and geomorphology. In: *Mesophotic Coral Ecosystems* (Eds Y. Loya, K.A. Puglise and T.C.L. Bridge), Springer, New York, 849–878.

Sinniger F., Harii S., Humblet M., Nakamura Y., Ohba H. and **Prasetia R.** (2019) Ryukyus Islands, Japan. In: *Mesophotic Coral Ecosystems* (Eds Y. Loya, K.A. Puglise and T.C.L. Bridge), Springer, New York, 231–247.

Veron, J.E.N. (2000) *Corals of the World*, 3 vols, Australian Institute of Marine Science, Townsville.

Szilagyi, Zs., Webster, J.M., Patterson, M.A., Hips, K., Riding, R., Foley, M., Humblet, M., Yokoyama, Y., Liang, L., Gischler, E., Montaggioni, L., Gherardi, D. and **Braga, J.C.** (2020) Controls on the spatio-temporal distribution of microbialite crusts on the Great Barrier Reef over the past 30,000 years. *Mar. Geol*., **430**, 106369.

Turner, J.A., Andradi-Brown, D.A., Gori, A., Bongaerts, P., Burdett, H.L., Ferrier-Pagès, C., Voolstra, C.R., Weinstein, D.K., Bridge, T.C.L., Costantini, F., Gress, E., Laverick, J., Loya, Y., Goodbody-Gringley, G., Rossi, S., Taylor, M.L., Viladrich, N., Voss, J.D., Williams, J., Woodall, L.C. and **Eyal, G.** (2019) Key questions for research and conservation of mesophotic coral ecosystems and temperate mesophotic ecosystems. In: *Mesophotic Coral Ecosystems* (Eds Y. Loya, K.A. Puglise and T.C.L. Bridge), Springer, New York, 989–1003.

Veron, J.E.N. (2000) *Corals of the World,* Vol. 1–3. Townsville, Australia, *Aust. Inst. Mar. Sci*.

Webster, J.M., Braga, J.C., Clague, D.A., Gallup, C., Hein, J.R., Potts, D.C., Renema, W., Riding, R., Riker-Coleman, K., Silver, E. and **Wallace, L.M.** (2009) Coral reef evolution on rapidly subsiding margins. *Global Planet. Change*, **66**, 129–148.

Webster, J.M., Braga, J.C., Humblet, M., Potts, D.C., Iryu, Y., Yokoyama, Y., Fujita, K., Bourillot, R., Esat, T.M., Fallon, S., Thompson, W.G., Thomas, A.L., Kan, H., McGregor, H.V., Hinestrosa, G., Obrochta, S.P. and **Lougheed, B.C.** (2018) Response of the Great Barrier Reef to sea level and environmental changes over the past 30,000 years. *Nature Geosci*., **11**, 426–432.

Webster, J.M., Yokoyama, Y., Cotterill, C. and **the Expedition 310 Scientists** (2011) Proceedings of the IODP, 325, Integrated Ocean Drilling Program Management International, Inc, Tokyo.

Weinstein, D.K. (2014) Deep reef bioerosion and deposition: sedimentology of mesophotic coral reefs in the U.S. Virgin Islands. Dissertation, Doctor of Philosophy (PhD), University of Miami.

Weinstein, D.K., Klaus, J.S. and **Smith, T.B.** (2015) Habitat heterogeneity reflected in mesophotic reef sediments. *Sed. Geol*., **329**, 177–187.

Weinstein, D.K., Maher, B. and **Correa, A.M.C.** (2019) Bioerosion. In: *Mesophotic Coral Ecosystems* (Eds Y. Loya, K.A. Puglise and T.C.L. Bridge), Springer, New York, 829–847.

Weinstein, D.K., Sharifi, A., Klaus, J.S., Smith, T.B., Giri, S.J. and **Helmle, K.P.** (2016) Coral growth, bioerosion and secondary accretion of living orbicellid corals from mesophotic reefs in the US Virgin Islands. *Mar. Ecol. Progr. Ser.*, **559**, 45–63.

Weinstein, D.K., Tamir, R., Kramer, N., Eyal, G., Berenshtein, I., Shaker, Y., Loya, Y. and **Torfstein, A.** (2021) Mesophotic reef geomorphology categorization, habitat identification and relationships with surface cover and terrace formation in the Gulf of Aqaba, *Geomorphology*, **379**, 107548.

Woodroffe, C.D. and **Webster, J.M.** (2014) Coral reefs and sea-level change. *Mar. Geol*., **352**, 248–267.

Yagioka, N., Nakada, C., Fujita, K., Kan, H., Yokoyama, Y. and **Webster, J.M.** (2019) Depositional environments beneath the shelf-edge slopes of the Great Barrier Reef, inferred from foraminiferal assemblages: IODP Expedition 325. *Palaeogeogr. Palaeoclimatol. Palaeoecol*., **514**, 386–397.

Yokoyama, Y. and **Esat, T.M.** (2015) Coral Reefs. In: *Handbook of Sea-Level Research* (Eds A. Long, B. Horton and I. Shennan), Wiley, Chichester, 104–124.

Yokoyama, Y., Esat, T.M., Thompson, W.G., Thomas, A.L., Webster, J.M., Miyairi, Y., Sawada, C., Aze, T., Matsuzaki, H., Okuno, J.I., Fallon, S., Braga, J.-C., Humblet, M., Iryu, Y., Potts, D.C., Fujita, K., Suzuki, A. and **Kan, H.** (2018) Rapid glaciation and a twostep sea-level plunge into the Extreme Glacial Maximum. *Nature*, **559**, 603–607.

Yokoyama, Y., Miyairi, Y., Aze, T., Yamane, M., Sawada, C., Ando, Y., De Natris, M., Hirabayashi, S., Ishiwa, T., Sato, N. and **Fukuyo, N.** (2019) A single stage Accelerator Mass Spectrometry at the Atmosphere and Ocean Research Institute, The University of Tokyo. *Nuclear Instruments and Methods in Physics Research Section B: Beam Interactions with Materials and Atoms*, **455**, 311–316.

Yokoyama, Y. and **Purcell, A.** (2021) On the geophysical processes impacting palaeo-sea-level observations. *Geosci. Lett.*, **8**, https://doi.org/10.1186/s40562-021-00184-w

Supplementary tables and figures for papers in this volume can be found on the IAS website: https://www.sedimentologists.org/books

IAS (2022) Coral Reefs and Sea-Level Change: Quaternary Records and Modelling, 215–273

Coral reef development and sea-level changes over the past 50,000 years: new evidence from the north-west shelf of Australia

JODY M. WEBSTER[*], BELINDA DECHNIK[*], KELSEY SANBORN[*], YUSUKE YOKOYAMA[†], JUAN CARLOS BRAGA[‡], WILLEM RENEMA[§], MARC HUMBLET[¶], ROBIN J. BEAMAN[|], LUKE D. NOTHDURFT[#], GREGORY E. WEBB[a], JIAN-XIN ZHAO[a], RICHARD J. MURPHY[*], STEPHEN J. GALLAGHER[b], MICHAEL O'LEARY[c] and VICTORIEN PAUMARD[c]

[*]*Geocoastal Research Group, University of Sydney, Sydney, Australia.*
[†]*Atmosphere and Ocean Research Institute and Department of Earth and Planetary Sciences, The University of Tokyo, Kashiwanoha, Japan.*
[‡]*Departamento de Estratigrafía y Paleontología, Universidad de Granada, Granada, Spain.*
[§]*Naturalis Biodiversity Center, Leiden, The Netherlands & Department of Ecosystem & Landscape Dynamics, Institute for Biodiversity & Ecosystem Dynamics, University of Amsterdam, Amsterdam, The Netherlands.*
[¶]*Department of Earth and Planetary Sciences, Nagoya University, Nagoya, Japan.*
[|]*College of Science and Engineering, James Cook University, Cairns, Queensland, Australia.*
[#]*School of Earth and Atmospheric Sciences, Queensland University of Technology, Brisbane, Australia.*
[a]*School of Earth and Environmental Sciences, The University of Queensland, Brisbane, Australia.*
[b]*School of Geography, Earth and Atmospheric Sciences, The University of Melbourne, Melbourne, Australia.*
[c]*Centre for Energy Geoscience, School of Earth Sciences, The University of Western Australia, Perth, Australia.*

ABSTRACT

Understanding of global sea-level changes and coral reef development is poorly constrained during Marine Isotope Stage 3 (MIS 3; ~60 to 30 ka). Australia's North West Shelf (NWS), at depths of ~50 to 120 m below present sea-level (mbsl), represents an ideal natural laboratory to address these knowledge gaps. In this study, the authors investigate a unique suite of sea-bed rock drill (PROD) cores recovered as part of a geotechnical survey from the NWS ~150 km south-east of Ashmore Reef. Twenty cores, penetrating to 28 m below sea floor, were collected from the top of the now drowned platform complex in similar water depths (74.8 to 81.6 mbsl), forming two transects ~17 km apart. High-resolution 3D seismic and multibeam bathymetry data reveal three distinct, multigenerational platforms that are rimmed by smaller reef terraces and bisected by deeper channels, placing the core transects into a robust, regional geomorphic context that includes a succession of linear palaeo-shorelines and tidal-estuarine channel systems on the adjacent shelf between ~90 to 110 mbsl. The authors have completed detailed logging, high-spatial resolution hyperspectral scanning, petrologic, mineralogic and sedimentary facies analysis of these cores, including a precise palaeoenvironmental reconstruction based on coral, algal and larger benthic foraminifera assemblages; and extensive radiometric dating. The authors have observed a complex suite of

©2022 International Association of Sedimentologists

lithologies including *in situ* coralgal reef frameworks, well-lithified to friable grainstones, packstones and coralline algal floatstone facies separated by at least two major palaeosol horizons. Together with thirty ^{14}C-AMS and closed-system U/Th ages spanning 10.7 to >50 ka, the authors define a complex but consistent record of four distinct chrono-stratigraphic units (Units 1 to 4), representing a repeated succession of shallow reef to deep reef-slope depositional settings as the platforms experienced repeated sea-level oscillations (interstadial/stadial to glacial/deglacial) over the last 75,000 yr. Two distinct phases of shallow-water, high-energy reef development are defined. The age of the older, diagenetically distinct reef unit (Unit 3) is unknown but interpreted to have developed before the MIS 4 lowstand (~65 ka). However, firm chronological constraints on the MIS 3 development of the younger reef unit (Unit 2), place the position of relative sea-level (RSL) between ~63 to 75 $\pm$ 1.8 mbsl by 45.95 to 39.23 $\pm$ 0.2 ka, consistent with other predictions and observations for the region. Following its exposure and demise due to sea-level fall to the Last Glacial Maximum (LGM), the platform system was unable to re-establish fully as it was reflooded during the subsequent deglacial sea-level rise. Deeper reef slope (Unit 1) facies dominate the core tops between ~13.2 to 10.7 ka, representing a major hiatus in shallow-water reef development on the platforms. Deglacial sea-level rise was either too fast and/or other environmental conditions inadequate (i.e. massive riverine sediment flux due to the strengthening Australian summer monsoon and/or reworking of shelf sediments) to allow re-establishment of shallow-water coral reef development on the platforms apart from a few isolated and distal locations (i.e. Ashmore, Cartier, Adele and Scott Reefs).

INTRODUCTION

Considerable progress has been made in understanding the role of coral reef systems as valuable archives of Quaternary sea-level and environmental changes and also how reefs were impacted by these changes (Woodroffe & Webster, 2014; Camoin & Webster, 2015; Gischler, 2015; Braithwaite, 2016). However, major questions still remain about: (1) what processes control high-resolution temporal and spatial variations in reef architecture and composition, particularly in response to millennial scale sea-level and climate changes (Blanchon *et al.*, 2009; Webster *et al.*, 2018), (2) what causes reefs to 'turn-on' or 'turn-off' (i.e. drowning and/or exposure) and what are their climatic and ecologic thresholds (Kiessling *et al.*, 2012; Toth *et al.*, 2015); and (3) how reef communities reassemble following disturbances on interglacial/glacial *vs* inter-stadial/stadial, millennial scales (Tager *et al.*, 2010; Precht & Aronson, 2016). There is an urgent need for further research, not only to decipher processes driving past sea-level and climate change and its geographical variability but also to better understand how coral reefs might respond in the context of future global climate change (Camoin & Webster, 2015).

Marine Isotope Stage 3 (MIS 3; 60 to 29 ka) is characterised by considerable millennial scale global sea-level and climate variability (Siddall *et al.*, 2008; Grant *et al.*, 2012) and therefore represents a key time period to gauge coral reef responses. However, well-dated MIS 3 reef records are rare and mainly limited to rapidly uplifting convergent margins such as the raised reef terraces on the Huon Peninsula, Papua New Guinea (PNG; Yokoyama *et al.*, 2000;

Yokoyama *et al.*, 2001; Chappell, 2002; Cutler *et al.*, 2003), Kikai-jima, Ryukyus (Sasaki *et al.*, 2004), Espiritu Santo and offshore islands, Vanuatu (Fairbanks *et al.*, 2005; Taylor *et al.*, 2005) or the few submerged reefs that have been sampled via scientific drilling or ROV at Barbados (Peltier & Fairbanks, 2006), Ryukyus (Sasaki *et al.*, 2006), Huon Gulf, PNG (Webster *et al.*, 2009), Tahiti (IODP Exp. 310; Thomas *et al.*, 2009) and most recently the Great Barrier Reef (GBR) (IODP Exp. 325; Gischler *et al.*, 2013; Webster *et al.*, 2018; Yokoyama *et al.*, 2018). Unfortunately, these records are either potentially biased by abrupt co-seismic uplift/subsidence events, chronologically poorly constrained, lack sufficient stratigraphic and multi-proxy coralgal data to allow accurate palaeoenvironmental reconstruction, and/or come from only one or few drill/ROV sites and not the closely spaced transects necessary to faithfully reconstruct MIS 3 reef growth modes, architecture and communities (Camoin & Webster, 2015).

Significant advances have been made in reconstructing sea-level changes over the past 150 kyrs using continuous deep-sediment archives (i.e. Grant *et al.*, 2012) and discontinuous fossil coral reefs that can provide more accurate constraints on the vertical position of past sea-level (Woodroffe & Webster, 2014). This has contributed to the understanding of eustatic sea-level (ESL) variability, ice sheet dynamics and global isostatic adjustment (GIA) over the last 150 ka, particular during MIS 5e (Dutton *et al.*, 2015) and the LGM-deglaciation (IODP Exp. 310, 325; Barbados; Deschamps *et al.*, 2012; Abdul *et al.*, 2016; Yokoyama *et al.*, 2018). However, recent reviews of global fossil, coral-based sea-level data (e.g. Dutton & Lambeck, 2012; Medina-Elizalde, 2013; Hibbert *et al.*, 2016) have raised several key issues: (1) the bias towards high sea-level events (i.e. Holocene and MIS 5e highstands), (2) the lack of temporal coverage, particularly during interstadial/stadial and lowstand sea-levels, (3) a major bias towards co-seismically uplifted sites; and (4) ongoing debates about the reliability of the age determinations (Hibbert *et al.*, 2016; Chutcharavan *et al.*, 2018). Indeed, this is the case for MIS 3 where the precise timing, magnitude and rate of sea-level oscillation is still debated (see Siddall *et al.*, 2008 for reviews; Gowan *et al.*, 2021) in part due to the lack of appropriate absolute coral age data. Further, recent observations and models of Northern Hemisphere ice sheets (Pico *et al.*, 2018) suggest higher ESLs during MIS 3 than previously thought, while De Deckker *et al.* (2019) also argued for a rapid and steep drop in ESL, at least 100 mbsl, during MIS 4 between 71 and 59 ka.

Australia‘s North West Shelf (NWS) has a range of complex submerged submarine landscapes, including drowned platforms, terraces, banks, shoals, coastal barriers, dunes, tidal and estuarine channels (Anderson *et al.*, 2011; Brooke *et al.*, 2017; Moore *et al.*, 2017; O’Leary *et al.*, 2020) at depths of ~50 to 120 mbsl, making it an ideal natural laboratory to address these knowledge gaps (Fig. 1A). In recent years, extensive, industry 3D seismic surveys NW of Ashmore Reef have revealed much about the longer-term structural evolution of the margin, including insights about the major controls on distribution and growth of Miocene (Saqab & Bourget, 2016; McCaffrey *et al.*, 2020) and early Pleistocene (Saqab & Bourget, 2015) isolated carbonate build-ups (ICBs) that form the foundations of many of these banks. In parallel, there have been numerous biophysical surveys of the tops of these features, establishing their importance as recent and modern mesophotic reef habitats (Heyward, 1997; Heyward *et al.*, 2010; Anderson *et al.*, 2011). Sediment cores recovered from the adjacent shelf (i.e.

Bonaparte Gulf) have been used to reconstruct the history of MIS 2-deglacial RSL and associated sedimentary environmental changes (Nicholas *et al.*, 2014; Ishiwa *et al.*, 2016; Ishiwa *et al.*, 2019a). However, the lack of rotary drill cores from the adjacent submerged terraces, banks and shoals have left their ages and compositions unknown. Finally, this region of the NWS, directly adjacent to Timor-Leste, represents a key migration pathway for the first humans into Australia (Bird *et al.*, 2018; Fig. 1A). These migration models are based on assumptions that from ~70 to 10 ka, these platforms formed an emergent chain of habitable, resource-rich islands north-west (NW) of Australia. Again, the lack of absolute ages from those now submerged landscapes place uncertainties around palaeoenvironmental reconstructions and timing of occupation (O'Leary *et al.*, 2020).

Here, a unique suite of cores recovered from ~80 mbsl have been investigated as part of a geotechnical survey using a seabed rock drill (PROD) from the top of a drowned platform on the NWS ~150 km south-east (SE) of Ashmore Reef. The authors have combined available multibeam bathymetry and high-resolution 3D seismic data, along with detailed logging, high-resolution hyperspectral scanning, optical and scanning electron microscopy (SEM), sedimentary facies and palaeoenvironmental analyses using coralgal and larger benthic foraminifer assemblages and extensive ^{14}C-AMS and U/Th dating of the cores to: (1) characterise geomorphology of the platforms and adjacent shelf; (2) determine the internal chrono-stratigraphic evolution of the platforms, including succession of facies, mineralogical, diagenetic and palaeoenvironmental changes; (3) provide the first accurate constraints on MIS 3 reef growth and RSL in the region; and (4) discuss the development of the NWS reef and platform system in response to sea-level and associated palaeoenvironmental changes over the past 50,000 yr.

REGIONAL SETTING

The North West Shelf

The North West Shelf (NWS) is a ~2400 km-long physiographic feature (including the continental shelf, outer-shelf and marginal plateaus) located along the north-western margin of Australia that extends from Melville Island in the north-east to the Exmouth Gulf in the south-west (Bradshaw *et al.*, 1988; Purcell & Purcell, 1988; James *et al.*, 2004; Fig. 1A). The NWS includes four sedimentary basins (i.e. Northern Carnarvon, Roebuck, Browse, Bonaparte) and one orogenic belt (i.e. Timor-Banda Orogen; Longley *et al.*, 2002). The NWS experienced a complex tectono-stratigraphic evolution with periods of active rifting, collision and tectonic quiescence varying through time and space (Longley *et al.*, 2002; Marshall & Lang, 2013; Paumard *et al.*, 2018; Paumard *et al.*, 2019a).

The Bonaparte Basin (where the Ashmore Platform is situated) includes a series of Palaeozoic and Mesozoic depocentres and structural highs that developed during a multiphase tectonic history (Mory, 1991; Longley *et al.*, 2002; Marshall & Lang, 2013). In summary, the structural evolution of the Bonaparte Basin comprises: (1) two phases of Palaeozoic extension; (2) one phase of Late Triassic compression; (3) one phase of Mesozoic rifting followed by sea floor spreading; and (4) one phase of Neogene arc-continent collision (Bradshaw *et al.*, 1988; Gunn, 1988; Patillo & Nicholls, 1990; O'Brien *et al.*, 1993; O'Brien *et al.*, 1996; Shuster *et al.*, 1998; Cadman & Temple, 2004; Keep & Haig, 2010; Bourget *et al.*, 2012; Saqab *et al.*, 2017). Cenozoic sedimentation in the Bonaparte Basin evolved from a subtropical carbonate ramp to shallow-water, tropical carbonates

interrupted by brief periods of terrigenous siliciclastic inputs (Apthorpe, 1988; Mory, 1991; Whittam *et al.*, 1996; Longley *et al.*, 2002; Saqab & Bourget, 2016).

Although located at similar latitude to the central and northern Great Barrier Reef (GBR), modern NWS reefs are far less extensive, consisting of series of relatively small isolated shelf edge pinnacle and atoll reefs and inshore fringing reefs (Kordi & O'Leary, 2016). These shelf edge reefs represent the remnants of an extensive Miocene 'Great Barrier Reef' extending from near the equator to 22°S that drowned due to subsidence in the late Miocene (McCaffrey *et al.*, 2020). Last Interglacial (LIG) reefs have been observed on the NWS at Cockatoo Island at a depth of 16 m below the modern fringing reef platform (Solihuddin *et al.*, 2015) and seismically inferred at a depth of 25 m below the modern reef platform on mid-shelf Adele Reef (Solihuddin *et al.*, 2016). These observations, combined with the depth (~26 m) and age of the LIG reef below the modern Scott Reef, suggest that the NWS experienced significant Late Pleistocene subsidence at rates on the order of ~0.2 to 0.45 mm yr^{-1} (Collins *et al.*, 2011; Solihuddin *et al.*, 2016). This is an order of magnitude faster than the Neogene continental-scale subsidence of the northern margin of Australia estimated by Sandiford (2007) at 15 to 20 m myr^{-1}.

Oceanography and climate

At 12°S the Ashmore Platform is on the southerly edge of the West Pacific Warm Pool (WPWP) (Fig. 1) just north of the 28° C sea-surface temperature (SST) isotherm (Gallagher *et al.*, 2009; Rosenthal *et al.*, 2018) downstream of the Indonesian Throughflow (ITF; Gordon, 2005; Gallagher *et al.*, 2017). The ITF is a major arm of the global thermohaline circulation that transports warm waters from the Pacific Ocean into the Indian Ocean, exerting a major control on the distribution of reefs in the eastern margin of the Indian Ocean (Gallagher *et al.*, 2014).

The arid to semi-arid climate of the Australian interior extends to the north-west coast of Australia. To the north, rainfall is variable yet mainly monsoonal, with the dominance of summer rainfall declining sharply towards the south (Sturman & Tapper, 2005). Warm, moist, equatorial air is the major source of monsoonal and cyclonic rain in the north but it is replaced in the south by tropical air from the Indian Ocean also known as the 'pseudo-monsoon' (Gentilli, 1972). During the Austral summer, north-westerly winds bring monsoonal rains (Australian Summer Monsoon – ASM) to the Kimberley region, whereas atmospheric circulation changes in the dry season (Austral winter) bringing south-easterly trade winds and dust from the arid Australian interior.

MATERIALS AND METHODS

Sample sites, bathymetry and seismic data

A recent compilation of available source bathymetry data off northern Australia into a ~100 m pixel digital elevation model (DEM), called the nthaus100 grid (Beaman, 2018), with a $\pm$~2.5 m vertical uncertainty, shows that the drill sites are on a north-west to south-east trending platform near Ashmore Reef in variable water depths from 90 to 50 mbsl (Fig. 1A). Industry 3D seismic surveys, Onnia-1 and Onnia-2, were accessed through Geoscience Australia and provided a high-resolution, spatially contiguous bathymetric dataset covering the Ashmore Platform, with a bin spacing (i.e. spatial resolution) of 12.5 x 12.5 m, for an average vertical resolution of ~15 to 20 m across the study area. Three high-resolution (5 m) multibeam passes across the platform, also included in the nthaus100 grid, provide additional depth ($\pm$~1 m) constraints (Fig. 2) on the geomorphic features described in

section 4.1. Following the methodology detailed by Paumard *et al.* (2019b) and O'Leary *et al.* (2020), the PaleoScan™ sea floor digital elevation model was imported and merged into ArcGIS including ArcMap software for shaded relief/slope analysis that allowed interpretation of the sea floor geomorphology of the region (Fig. 2). The detailed sea floor morphology covers an extensive area of the drowned platforms and surrounding shelf. This map is resolved at much higher resolution compared with the generally sparse bathymetry data available in the region within the nthaus100 grid, which does not include the 3D seismic-derived bathymetry data.

Fig. 3 shows the location of the drill site transects and a comparison of the spatial resolution between the nthaus100 bathymetry (Fig. 3A) and 3D seismic-derived bathymetry (Fig. 3B). The SW transect occupies a more exposed position on the platform(s) compared with the NW transect, based on comparison with modern regional oceanographic conditions (including Ashmore Reef) and the dominant south and south-easterly winds and waves (Berry, 1993; Glenn & Collins, 2005).

Seabed drilling operations and core recovery

Cores were collected between 2006 and 2007 using a seabed drilling system (PROD) as part of a geotechnical survey conducted by PTTEP (PTT Exploration and Production Public Company Limited) Australasia (Fig. 2B). The survey cored and/or penetrated 21 holes from 13 sites along two transects (NW and SW) between 74 and 98 mbsl (Fig. 2) with a maximum penetration of 28 m (Table 1). The drill site water depths, and subsequent sample depths, are not corrected for tide or to any particular datum. However, the maximal tidal range uncertainty ($\pm$ 0.9 to 2 m) was applied for each site based on the day the site was drilled using hindcast tidal predictions from the closest tidal station (AusTides Skua No.4 - Australian_Hydrographic_Office, 2018).

Not all holes were continuously cored; others were subjected to cone penetrometer testing (denoted with the sample suffix 'C'; Table 1) and some recovered sections were unavailable due to subsequent geotechnical testing. This study focusses on 10 holes from 7 sites that had the deepest penetration and highest recoveries from the NW and SW transects (Table 1). Total average core recovery was ~25% including all missing sections (i.e. non-sampled sections, *in situ* cone penetrometer testing and geotechnical testing). However, in this study the authors have focussed their analyses on the most complete holes with commonly > 85% recovery and where the core quality was excellent. Any missing and non-sampled intervals of the core are labelled as 'missing' and indicated on the stratigraphic logs.

Stratigraphic, sedimentary facies and reef assemblage analysis

Cores were logged using a combination of physical core material, computed tomography (CT) scans and petrographic thin sections using established criteria (Abbey *et al.*, 2011; Dechnik *et al.*, 2015; Humblet & Webster, 2017). Four distinct chrono-stratigraphic units and their boundaries were defined, based on major changes in sedimentary facies, biotic assemblages, macro and micro mineralogical and diagenetic characteristics (thin section petrology, scanning electron microscope [SEM], hyperspectral imagery) and available radiometric dating information (details below).

Ten sedimentary facies were identified based on primary framework and detrital fractions following established criteria (Camoin *et al.*, 2007; Dechnik *et al.*, 2015; Table 2; Fig. 4). Corals were identified to generic level or species, where possible, in

well-preserved samples based on modern and fossil taxonomic guides (Veron & Wallace, 1984; Wallace, 1999; Veron, 2000; Budd *et al.*, 2012; Huang *et al.*, 2014; Humblet *et al.*, 2015; Huang *et al.*, 2016; Richards, 2016) (Table 3). Sixty thin sections were used to identify the taxonomic composition of crustose coralline algae (CCA) and larger benthic foraminifers (LBF; Renema, 2010; Renema, 2018; Table 3) and their main assemblages (Table 4). The taxonomic approach and palaeoenvironmental interpretation based on CCA follows the procedure indicated in Humblet *et al.* (2019).

The abundance of vermetid gastropods was tallied into three categories (category 3 = >10, category 2 = 5 to 10 and category 1 = 0 to 5 vermetid individuals per CCA crust) following Dechnik *et al.*, (2017). Coralgal assemblages were defined on the basis of the dominant coral, CCA and LBF types, vermetid gastropod abundance and comparisons with modern depositional environments from Western Australian and the wider Indo-Pacific (see below for supporting references) (Table 4).

Radiometric dating, XRD, SEM and hyperspectral mineralogical analysis

Coral, coralline algal and mollusc samples were chosen from the best preserved sections of the NWS cores for ^{14}C-AMS and U/Th dating. Care was taken to select samples free of obvious diagenetic alteration (e.g. dissolution, staining, sediment fill, minimal secondary cement). Furthermore, thin section petrology, SEM, XRD and hyperspectral data were also used to evaluate the reliability of the resulting ages following recognised methodologies (e.g. Sanborn *et al.*, 2020). Limited reconnaissance ^{14}C dating of a stratigraphically deeper and clearly diagenetically different reef unit was undertaken to confirm that it is older than the radiocarbon dating window (e.g. ~50 ka BP; Stuiver *et al.*, 2020).

All samples for ^{14}C-AMS dating were ultrasonically cleaned in continuously replaced Nano-pure water. The powdered coral, coralline algal and mollusc samples (1 to 2 mg) were prepared using the small-volume graphitisation vacuum line and measured by accelerator mass spectrometry (AMS) at the Analytical Center for Environmental Science, Atmosphere and Ocean Research Institute, University of Tokyo, Japan (Yokoyama *et al.*, 2010; Hirabayashi *et al.*, 2017). All of the radiocarbon dated samples reported herein have undergone a severe acid leach, approximately discarding 30 to 40% of each sample aliquot (Yokoyama *et al.*, 2000; Yokoyama *et al.*, 2007). The ^{14}C ages were converted to calendar ages (ka) with 2σ errors using CALIB.8.1.0 and the Marine20 international calibration datasets (Stuiver *et al.*, 2020), with a weighted mean Delta-R (ΔR) value of 64 ± 39 ^{14}C yr based on the four nearest points (<500 km apart) (Table 5).

Three paired U-Th coral ages were produced at The University of Queensland Radiogenic Isotope Facility (RIF; Table 6 for complete isotope data). Subsamples (~1 g) were taken from corals representing *in situ* growth, then cleaned in an ultrasonic bath. Subsamples were crushed into ~1 mm chips, which were soaked for 24 h in a 15% H_2O_2 solution, sonicated for 15 min and rinsed in milliQ water three times before being dried on a hotplate at 60° C overnight. After this pre-treatment, 0.15 g of the most pristine aragonite fragments were hand selected under optical microscope to be included in U-Th geochemical analysis. Prior to analysis, subsamples were digested in double-distilled HNO_3 and a ^{229}Th-^{233}U mixed tracer was used to spike samples. The three ages were measured in duplicate on a Nu Plasma HRMulti-Collector-Inductively Coupled Plasma-Mass Spectrometer (MC-ICP-MS) in 2019. Details of sample vetting, U-Th geochemical procedures, initial ^{230}Th

corrections and age calculations follow Zhao *et al.* (2009), Clark *et al.* (2014) and Salas-Saavedra *et al.* (2018). Ages were calculated using the program Isoplot 3.75 (Ludwig, 2012) utilising decay constants of Cheng *et al.* (2000). All ages were converted into years BP (relative to 1950) for comparison with ^{14}C dates (Table 5) and are presented in ka BP in this study.

SEM analysis was performed on representative dated coral, coralline algae and mollusc samples using a Hitachi Tabletop SEM at Queensland University of Technology (QUT) (TM3000) and Wenona School (Sydney) (TM4000). Samples were examined to confirm the absence of significant secondary cements, boring, staining, dissolution, recrystallisation and sediment fill (Nothdurft & Webb, 2009; Salas-Saavedra *et al.*, 2018), whilst providing a comprehensive description and catalogue of main diagenetic features and environments (marine, meteoric) observed down hole (Braithwaite & Montaggioni, 2009; Gischler *et al.*, 2013).

With two exceptions, XRD analysis was undertaken on all ^{14}C-AMS and U/Th dated corals to test for low-Mg calcite. Samples ~1 g were hand ground to a powder in an agate mortar and pestle under ethanol. Samples were front-pressed into circular quartz sample holders. Powder X-ray diffraction patterns were acquired using a Malvern PANalytical X'Pert Pro Powder X-ray diffractometer using a cobalt tube (40 kV, 40 mA) in Bragg-Brentano geometry. Patterns were collected over 1 hr from 5 to 90 °2θ at a step size of 0.0167°. Incident optics included 0.04 rad Soller slits, 15 mm mask, 1° anti-scatter slit and 0.25° fixed divergence slit. Receiving optics before the X'Celerator detector were 0.04 rad Soller slits, an Fe kβ filter and a 5.0 mm anti-scatter slit. Samples were spun during data collection at a speed of 2 rps. Rietveld refinement was performed in TOPAS (V5, Bruker). An instrument response function previously determined from NIST SRM660A was used to model kβ radiation and the intrinsic peak shape. Refined parameters included 15 term Chebyshev background, scale factors and unit cell parameters for each phase, specimen displacement and a Lorentzian crystallite size term to account for peak broadening for each phase.

High-resolution (~0.33 mm per square image pixel) hyperspectral data were also acquired in the shortwave infrared (980 to 2500 nm) from 74 representative core sections to map and quantify mineralogic and lithological variations, along with amounts of hydroxyl (OH) and H_2O. Classified images of carbonate (aragonite, calcite and dolomite) were derived using the method of Murphy *et al.* (2017). The shape of primary carbonate absorption at ~2331 nm was used as an indicator to detect subtle changes in carbonate mineralogy across the core sections. The shape of the feature was quantified in terms of its wavelength position, intensity and asymmetry. With increasing intensity of diagenesis and alteration of aragonite to calcite, the shape of the ~2331 nm carbonate absorption changes, specifically: i) wavelength position shifts to longer wavelengths, ii) intensity increases; and iii) the feature becomes more left-asymmetric (as indicated by increasingly negative asymmetry values). Purity or crystallinity of calcite in the sections was quantified as the area of minor (secondary) carbonate absorption at ~1880 nm, which is present only in pure or crystalline calcite. Its area is proportional to the purity/crystallinity of the calcite in the section. The amount of OH and H_2O was quantified as the area of the primary OH and H_2O absorptions at ~1430 and 1930 nm, using the method described by Murphy *et al.* (2021).

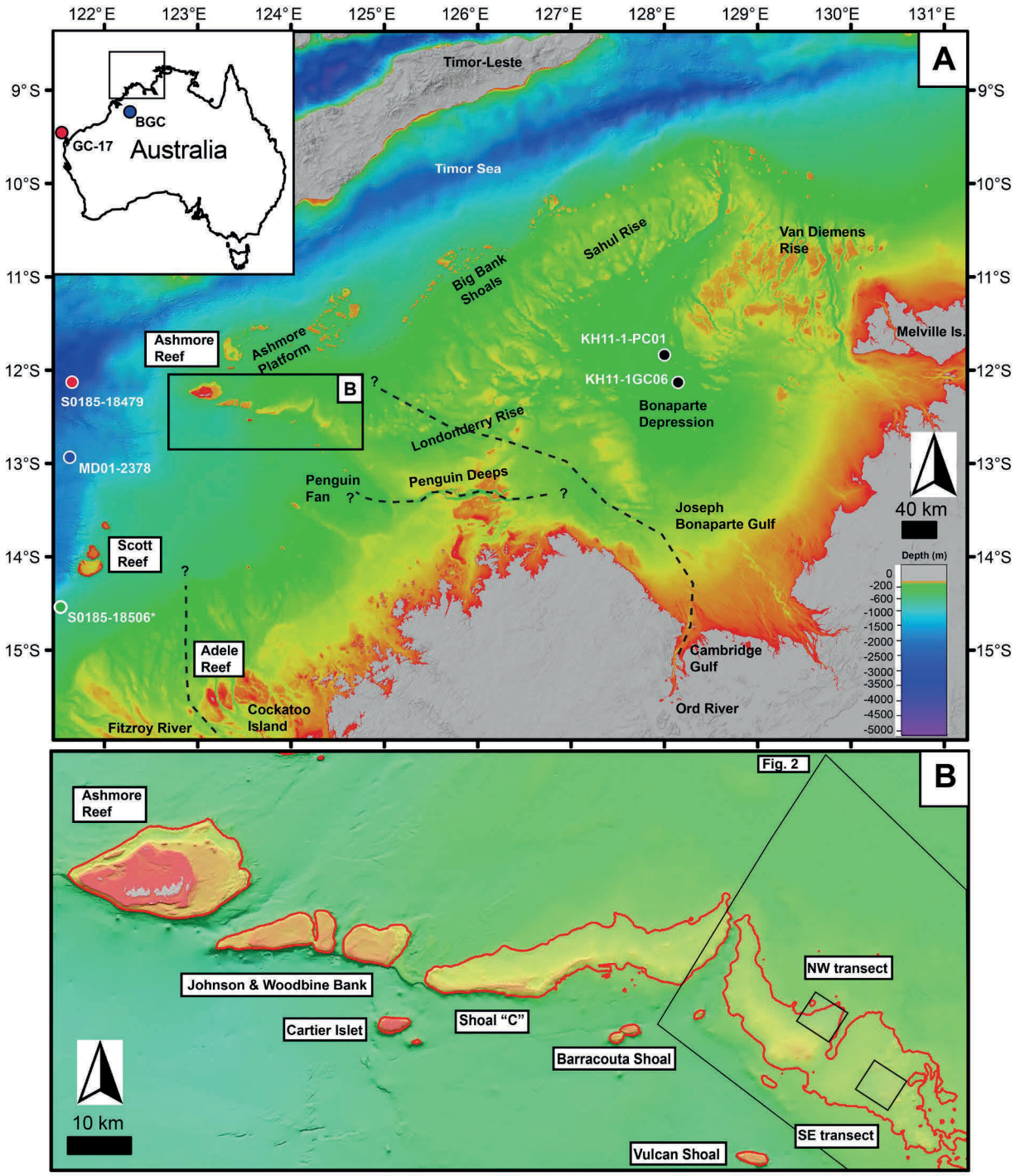


Fig 1. (A) Regional topography and bathymetry map (100 m DEM) showing the location of the main study sites and other locations (marine sediments cores, speleothems) referred to in the study (bathymetry data: Beaman, 2018). The black dash lines represent the interpreted position of the palaeo-Fitzroy and Ord rivers on the NWS during lower sea-levels (after Glenn, 2004; Kuhnt *et al*., 2015). (B) Close-up map showing the geomorphology of the Ashmore platform structure and the location of the NW and SW coring transects (black squares). The larger black polygon represents the wider area shown in Fig. 2 that also incorporates the 3D seismic-derived seabed geomorphology data. The red line represents the -80 m depth contour from the nthaus100 grid.

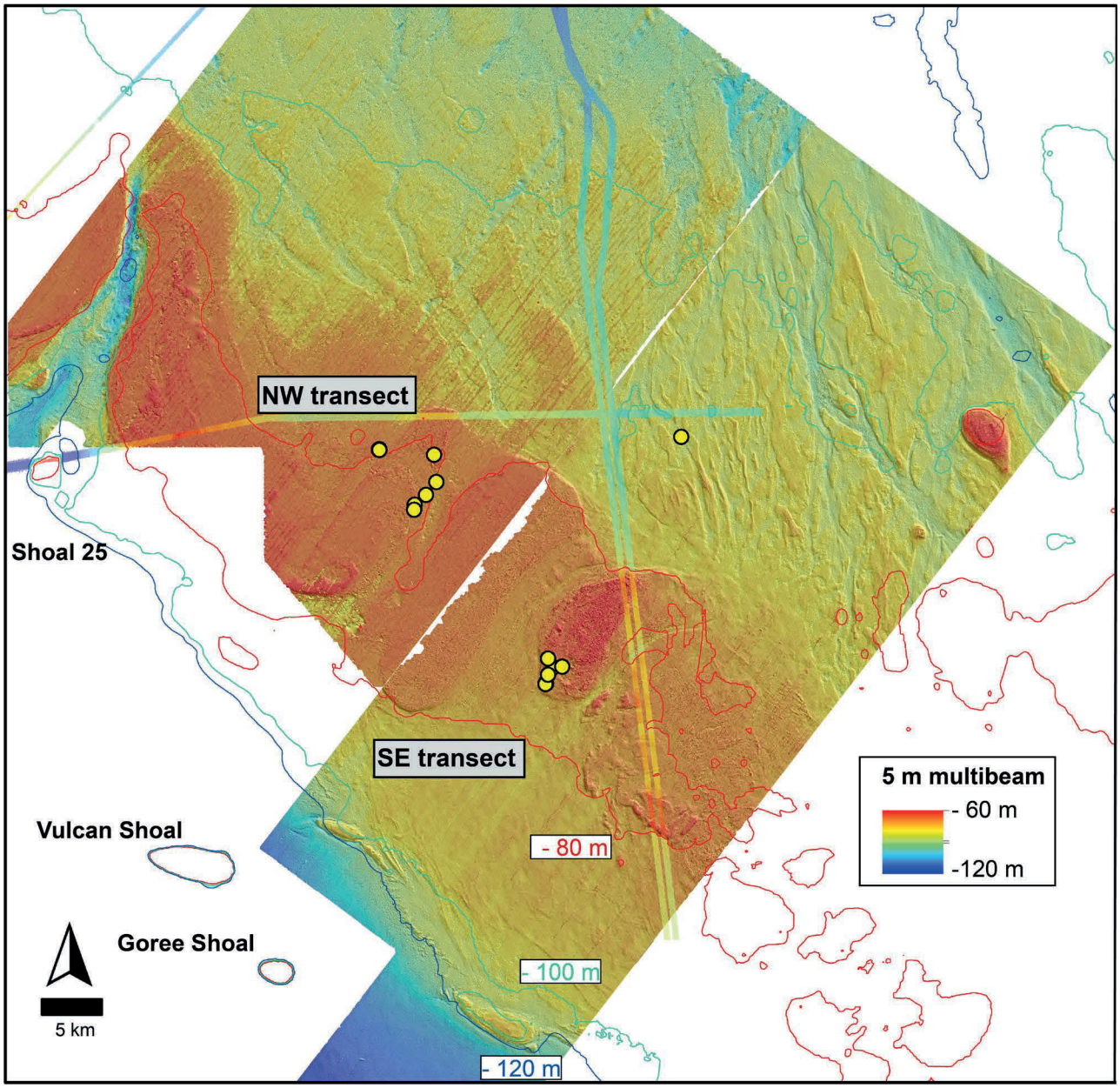


Fig 2. 3D seismic derived seabed geomorphic map of the platform and adjacent region. The limited 5 m gridded multibeam data are also shown.

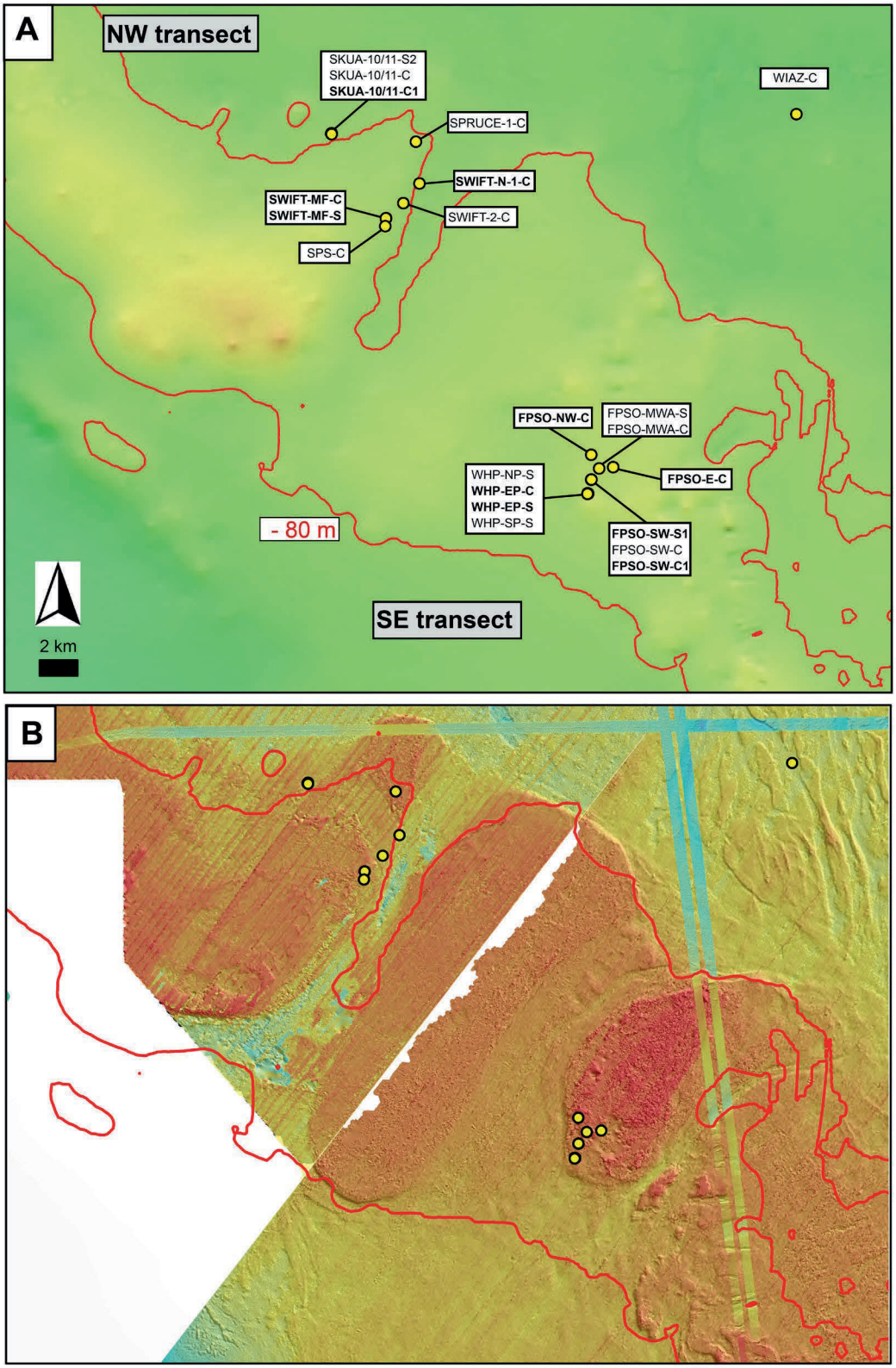


Fig 3. Close-up maps showing NWS core locations forming NW and SW transects. The red line represents the -80 m depth contour. (A) nthaus100 bathymetric grid (Beaman, 2018). (B) 3D seismic-derived bathymetry.

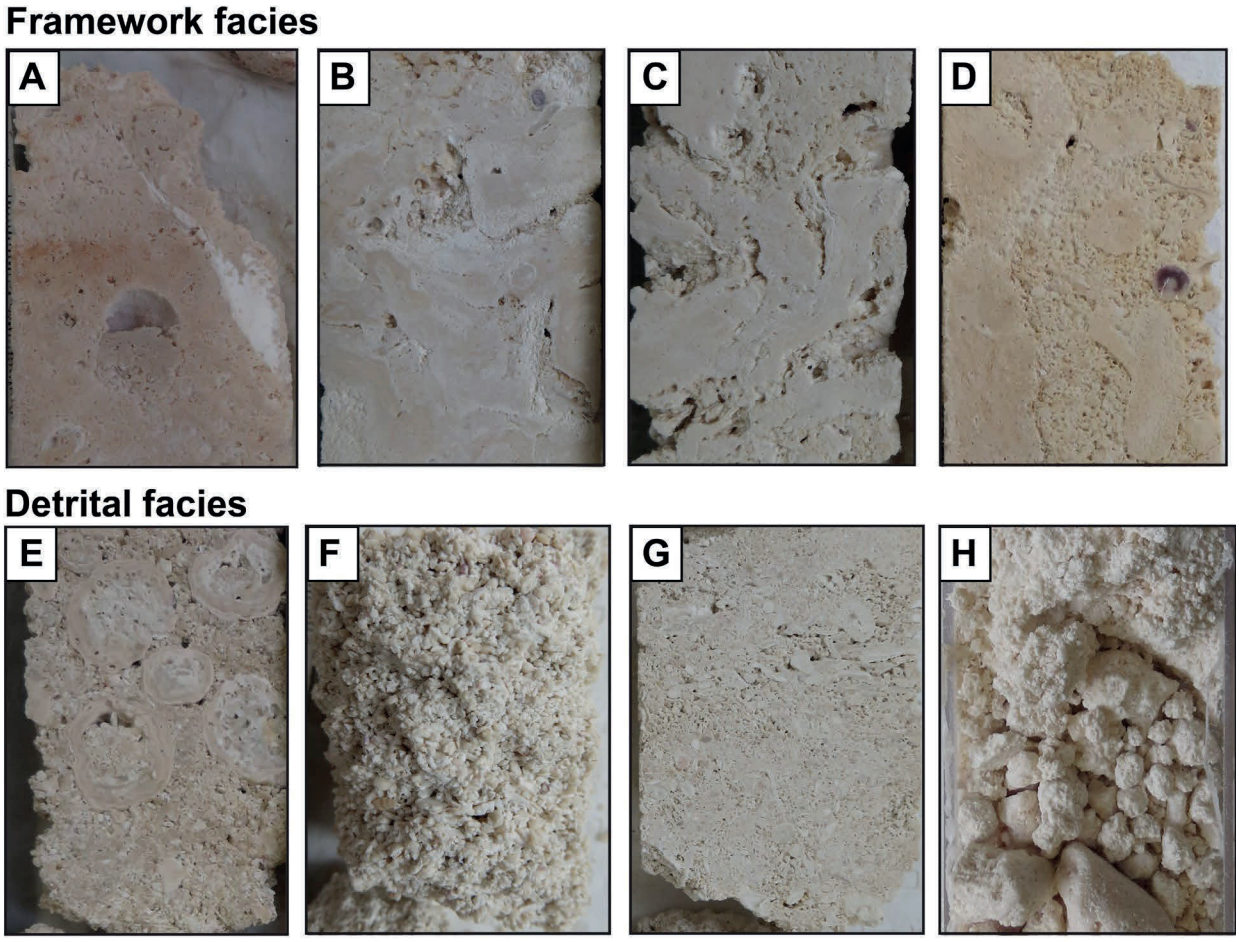


Fig 4. Main lithologies in NWS cores divided into framework and detrital facies. (A) Framestone, massive coral-dominated (SWIFT-N-1-C-2BB1). (B) Framestone, submassive-encrusting coral-dominated (WHP-EP-C-3A). (C) Bindstone, encrusting coralline algal-dominated (FPSO-NW-C-7B). (D) Bafflestone, branching coral-dominated (FPSO-NW-C-1A). (E) Floatstone, rhodolith-dominated (FPSO-NW-C-6A). (F) Grainstone, larger benthic foraminifera-dominated (WHP-EP-C-9A). (G) Packstone-grainstone, larger benthic foraminifera and coralline algal-dominated (WHP-EP-C-7BB1). (H) Unconsolidated coral rubble and carbonate sand (WHP-EP-S-11A). Core diameter is 4.5 cm in all images.

Table 1. Summary of NWS drill site locations and metadata.

Site[a]	Tran-sect	Date	Easting (m)[b]	Northing (m)	Seabed water depth (mbsl)[c]	Tide error +/- (m)[c]	Hole penetr-ation (m)	Total recovered core (m)[d]	Hole penetr-ation (mbsl)
SKUA-10/11-C	NW	29/03/03	654054.99	8617597.95	79.6	1.2	9.6	0.9	89.2
SKUA-10/11-C1	NW	7/04/03	654083.56	8617628.49	81.6	1.6	10.6	2.6	92.2
SKUA-10/11-S2	NW	7/04/03	654080.47	8617576.78	78	1.6	4.4	0.2	82.4
SPRUCE-1-C	NW	29/03/03	658427.9	8617155.61	76.5	1.2	10.5	3.0	87.0
SWIFT-N-1-C	NW	30/03/03	658604.2	8614952.19	81.5	1.4	10.3	3.5	91.8
SWIFT-2-C	NW	8/04/02	657766.92	8613925.37	80.1	0.9	11	2.3	91.1
SWIFT-MF-C	NW	30/03/03	656869.85	8613135.87	78.5	1.4	12.2	2.7	90.7
SWIFT-MF-S	NW	30/03/03	656863.62	8613130.78	76.4	1.4	2.6	0.9	79.0
SPS-C	NW	8/04/03	656825.26	8612726.39	78.3	1.4	10.7	3.1	89.0
WHP-EP-C	SW	31/03/03	667216.09	8598605.28	78.5	1.6	27.15	2.6	105.7
WHP-EP-S	SW	4/04/03	667216.99	8598602	78.2	2.0	27.8	7.1	106.0
WHP-NP-S	SW	5/04/03	667188.09	8598617.69	77.3	1.9	0.6	0.0	77.9
WHP-SP-S	SW	5/04/03	667185.08	8598583.11	78	1.9	0.6	0.0	78.6
FPSO-SW-C1	SW	5/04/03	667380.2	8599333.43	77.3	1.9	22.7	4.6	100.0
FPSO-SW-S1	SW	8/04/02	667385.61	8599336.51	78	0.9	21.3	6.8	99.3
FPSO-SW-C	SW	31/03/03	667380.51	8599337.04	76.7	1.6	0.7	0.0	77.4
FPSO-NW-C	SW	7/04/03	667382.67	8600640.76	78.9	1.6	21.5	4.4	100.4
FPSO-E-C	SW	6/04/03	668511.45	8599985.35	74.8	1.8	21.4	6.1	96.2
FPSO-MWA-C	SW	5/04/03	667792.49	8559927.21	78.6	1.9	10.4	2.9	89.0
FPSO-MWA-S	SW	5/04/03	667791.61	8599922.74	75.9	1.9	0.8	0.0	76.7
WIAZ-C		9/04/02	678082.68	8618484.87	97.5	1.1	11.8	0.0	109.3

[a]Drill sites highlighted in bold are focus of this study. Sites in adjacent rows (e.g. SWIFT-MF-C, SWIFT-MF-F) represent replicate sites given their proximity. Some holes were not continuously cored and were subjected to cone penetrometer testing (denoted with sample sufix code 'C'.

[b]Datum: Geocentric Datum Australia 1994 (GDA94); Coordinates transformed from ITRF2000 to GDA94 Datum using 7-parameter transformation values (Epoch 2007.5). Projection: Map Grid Australia Zone 51, CM 123 degrees East.

[c]Depths are water depths below sea-level (mbsl) of the PROD landing on the seabed and are not corrected for tide or to any particular datum. However, the authors apply the maximum tidal range uncertainty for each site based on the day the site was drilled using hindcast tidal predictions from AusTides Skua No.4 (Australian Hydrographic Office, 2018).

**C= Cone Penetrometer Testing, S =Sampling.

[d]Estimated total recovered core for each site accounting for missing sections (non-sampled sections, *in situ* cone penetrometer testing and further geotechnical testing).

Table 2. Main sedimentary facies observed in the NWS cores.

Facies	Dominant components
Framework facies	
Framestone	*In-situ* coral framework sometimes associated with coralline algal crusts.
Bindstone	Thick coralline algal crusts (>10 mm) commonly binding *in-situ* corals. Vermetid gastropods common.
Bafflestone	Branching coral framework, autochthonously binding grainstone/ packstone sediments between branches.
Detrital facies	
Floatstone	Grainstone/packstone supported matrix with >10% composed of coralline algal, shell & coral fragments >2 mm.
Rhodolith floatstone	Grainstone/packstone supported matrix with ~20 to 40% composed of coralline algal rhodoliths 5 to 20 mm in diameter.
Mollusc floatstone	Grainstone/packstone supported matrix with ~20 to 40% composed of mollusc & gastropod shell fragments >2 mm.
Grainstone	Semi-lithified, grain-supported sediments composed of mainly of larger benthic foraminifera (LBF) with mollusc shell & coral fragment.
Grainstone/ packstone	As above but with ~10 to 20% lime mud in the matrix.
Wackestone	Mud supported with <20% sand sized sediments, with few (<10%) coral fragments.
Coral rubble	Unconsolidated coral clasts sometimes associated with a packstone matrix.

Table 3. Summary of the coral, coralline algal and large benthic foraminifera taxa observed in the NWS cores.

Corals	**Coralline algae**	**Large benthic foraminifera**
Family	Order	Family
ACROPORIDAE	**CORALLINALES**	**NUMMULITIDAE**
Acropora sp.	*Porolithon* gr. *onkodes*	*Heterostegina depressa*
Acropora gr. 21 (*A.humilis*, *A.gemmifera, A. monticulosa) Acropora* gr. 22 (*A. digitifera*)	*Porolithon gardineri* *Amphiroa* sp. *Dawsoniolithon conicum*	*Cycloclypeus carpenteri* *Operculina* sp. (*ammonoides* group)
Acropora gr. 25 *Acropora* gr. 26 (*A. aspera?*)	*Dawsoniolithon* sp. *Harveylithon* gr. *munitum*	Family **CALCARINIDAE**
Acropora gr. 27 (*A. latistella*) *Isopora palifera*	*Harveylithon* gr. *rupestre* *Harveylithon* sp.	*Neorotalia calcar*
Montipora gr. 9 (*M. hispida*?) *Montipora* sp. (encrusting-submassive)	*Hydrolithon boergesenii* *Hydrolithon* sp. *Lithophyllum* gr. *acrocamptum*	*Calcarina hispida* gr. *Calcarina spengleri* *Calcarina mayori*
Family **MERULINIDAE**	*Lithophyllum* gr. *kotschyanum Lithophyllum* gr. *prototypum* *Lithophyllum* gr. *pustulatum*	*Calcarina* indet. *Schlumbergerella floresiana*
Goniastrea gr. 1 *Platygyra sinensis?*	*Lithophyllum* sp. *Neogoniolithon* spp.	Family **AMPHISTEGINIDAE**
Dipsastraea gr. 1 (*D. stelligera*?) *Dipsastraea* gr. 2	Order **HAPALIDIALES**	*Amphistegina lobifera* *Amphistegina lessonii*
Favites gr. 1		*Amphistegina radiata*
Cyphastrea sp.	*Lithothamnion* gr. *proliferum*	
Echinopora sp.	*Lithothamnion* spp.	Family **SORITIDAE**

Family **AGARICIDAE**

Pavona clavus

Pavona explanulata

Family **POCILLOPORIDAE**

Stylophora pistillata

Seriatopora sp.

Family **PORITIDAE**

Goniopora gr. 4

Porites gr. 1 (*P. lutea, P. australensis*?)

Porites gr. 6 (*P. cylindrica, P. nigrescens*)

Porites gr. 4/5

Family **MILLEPORIDAE**

Millepora sp.

Order **SPOROLITHALES**

Sporolithon sp.

Other red algae

Peyssonnelia spp.

Amphisorus sp. 1 (thin)

Amphisorus sp. 2 (thick)

Sorites sp.

Family **PENEROPLIDAE**

Peneroplis cf planatus

Family **ALVEOLINIDAE**

Alveolinella quoyi

Borelis sp.

Other Foraminifera

Sphaerogypsina globulus

Elphidium craticulatum

Table 4. Summary of coral, coralline algal and large benthic foraminifera assemblages in the NWS cores and their probable palaeoenvironmental settings.

Assemblage	Main components	Associated biota	Palaeoenvironmental interpretation
Coralline algae (CCA)			
A1	Thick crusts of *Porolithon* gr. *onkodes*		Shallow, high energy reef settings, 0 to 10 m
A2	*Lithophyllum* spp. (*L.* gr. *kotschyanum, L. gr. acrocamptum*, and *L* gr. *pustulatum*) with associated *Harveylithon* spp. (*H.* gr. *munitum* and *H. gr. rupestre*)		Intermediate reef slope settings, 0 to 30 m
A3	Laminar *Lithothamnion* spp, with associated thin crusts of *Lithophyllum* gr. *pustulatum, Lithoporella* and *Peyssonnelia*		Deeper reef slope, >20 m
Larger benthic foraminifera (LBF)			
LBF1	*Schlumbergerella* sp. and *Amphistegina lobifera* with associated *Amphisorus* sp, *Calcarina hispida*, and *Peneroplis* sp.		Reef crest and flat settings 0 to 10 m
LBF2	*Amphistegina radiata* and *Heterostegina depressa* with associated *Calcarina spengleri* and *Alveolinella quoyi*		Reef slope settings, 5 to 50 m
Coralgal			
C1	*Acropora* (*A. humilis, gemmifera, monticulosa*) (robust corymbose/digitate branching), *Stylophora pistillata* and branching *Porites* (*P. cylindrica, P. nigrescens*), with associated *Isopora palifera* and *Montipora* (sub-massive/encrusting)	A1, LBF1, V3-2	Shallow, very high energy, reef crest-upper slope settings, 0 to 10 m; 0 to 5 m*
C2	*Acropora* (corymbose branching, partially dissolved) and merulinids (*Dipsastraea* gr. 2), with associated *Montipora* (encrusting-sub-massive) and *Seriatopora* (branching)	A2, V1-2	Intermediate reef slope settings, 0 to 30 m
C3	*Acropora* (digitate & robust corymbose branching) and *Porites* gr. 1 (massive)		Shallow, high energy, reef settings, 0 to 10 m

	with associated merulinids *(Dipsastraea* gr. 1)	A1, LBF1, V2	
C4	*Pavona clavus* (columnar), with associated *Acropora* (digitate), *Montipora* (columnar/encrusting), *Pocillopora* (branching) and *Pavona explanulata* (thin encrusting)	A2, LBF1?	Intermediate depth and energy, sheltered back reef settings, >10 to 30 m

RESULTS

Platform and shelf geomorphology

The 3D seismic-derived bathymetry map, with available high-resolution multibeam, reveals extensive new details about the geomorphology of the platform top and surrounding shelf to the NE and SW (Figs 2 and 3). Rather than forming a single continuous platform, the Ashmore Platform is divided into at least three distinct NE/SW trending, oval shaped platforms as much as 22 km-long and 26 km-across, in places rising ~30 m above the surrounding sea floor to ~60 mbsl and separated by channels as deep as ~120 mbsl (Fig. 3B).

Rising from greater than ~95 mbsl, the platforms are rimmed by a series of small but distinct terraces that can be traced continuously as much as 20 km at ~90 mbsl, 80 mbsl, 70 mbsl and a shallowest terrace ~60 mbsl limited to the SE margin. The drill sites are located on the widest 80 m terrace, with the SE transect (FPSO, WHP) located on the seaward edge of the platform, while the NW transect (SWIFT, SKUA) is situated ~10 km back from the seaward SE edge of the larger platform but proximal to the dividing channel (Fig. 3A and B). SE of the platform complex, the sea floor is relatively smooth until ~95 m where it is marked by a succession of ~10 en echelon, linear to arcuate, NW-SE trending ridges down to ~110 m that are ~100 to 300 m-wide and ~400 to 800 m-apart. Just seaward of these ridges are two smaller (4 to 8 km) oval shaped platforms that are rimmed by at least four smaller terraces between ~120 and 100 mbsl. While the tops of these platforms are in deeper water (~90 to 100 mbsl), they are similar in shape to a series of submerged oceanic banks and shoals farther to the SW (e.g. Shoal C, Barracouta shoal, Vulcan shoal, Shoal 25). The Vulcan Shoal, only 8 km away, rises to ~20 to 30 mbsl but also has a distinct step or terrace at ~80 mbsl (Moore *et al.*, 2017; Figs 1B and 2B). In contrast, the shelf geomorphology NE of the main - 80 m platforms and drill transects is distinctly different. There, the sea floor between ~90 and 110 mbsl is characterised by a complex network of NNW trending channels and elongate bank features (~8 to 10 m channel depths) and by the distinct absence of narrow meandering channel or oxbow lake morphologies.

Biologic assemblages and palaeo-environmental settings

Coralline algal assemblages (CCA)

Three distinct coralline algal assemblages (Table 4, Fig. 5) were established in the NWS cores, based on dominant algal genera and, where possible, species. Based on comparisons with their modern CCA counterparts and previously established fossil assemblages from the Indo-Pacific, there are three different palaeoenvironments, ranging from shallow, high-energy (<6 to 10 m), intermediate (0 to 30 m) and definitively deeper reef slope settings (>20 m).

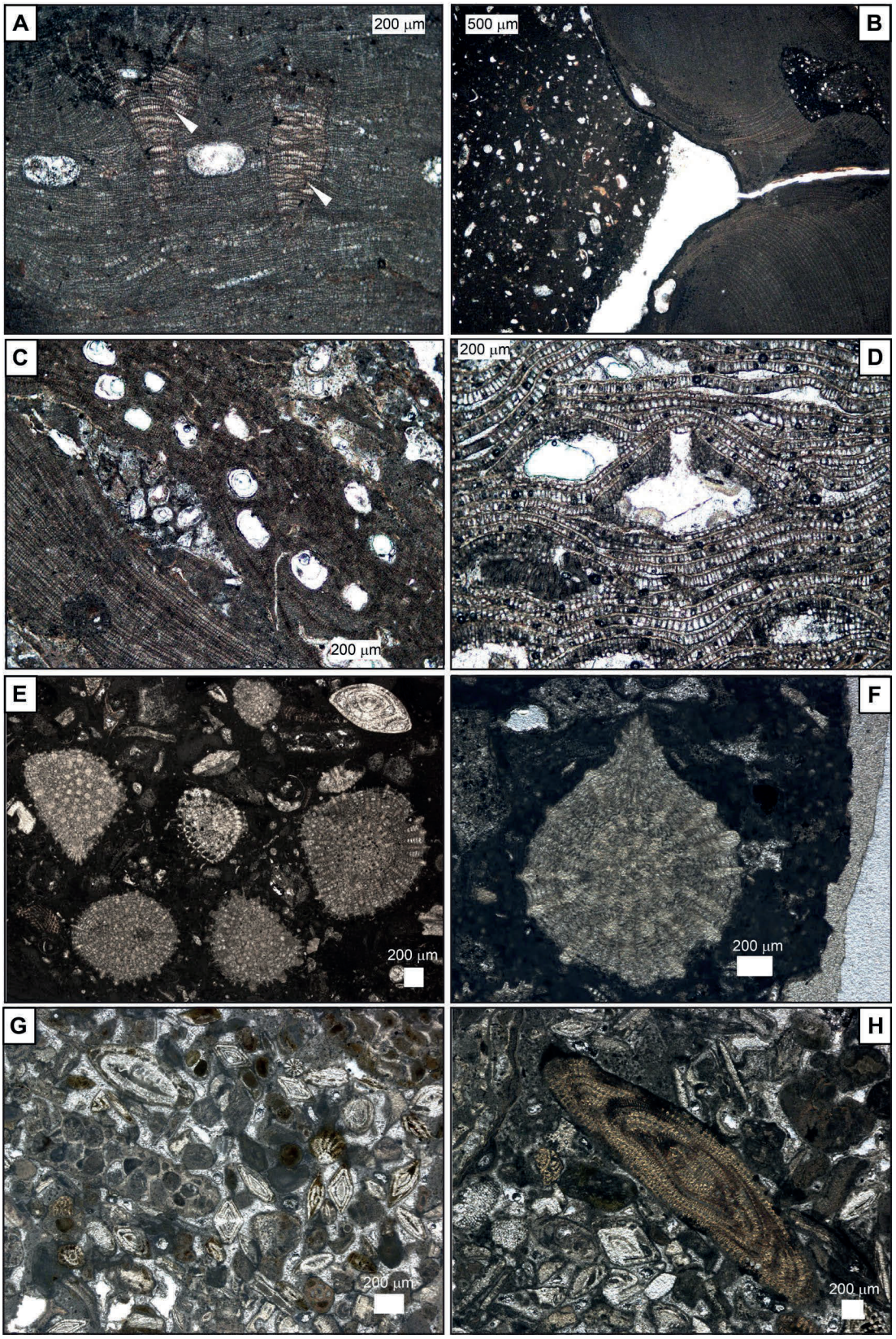


Fig. 5. Thin section images showing the main coralline algal (CCA) and benthic foraminifera assemblages (LBF) in NWS cores. (A) Crust of *Porolithon* gr. *onkodes* with two semi endophytic thalli of *Lithophyllum*

gr. *cuneatum* (white arrow heads) that are characteristic of shallow-water settings (A1 assemblage) (WHP-EP-C-3A). (B) Branches of *Lithophyllum* gr. *kotschyanum* with conceptacles (FPSO-EC-1A); and (C) a crust of Hapalidalean CCA with many conceptacles growing on a *Lithophyllum* crust (bottom left); both are common in shallow to intermediate waters (A2 assemblage) (SWIFT-N1-C-1A). (D) Crust of superimposed applanate branches of *Lithoporella*, typical of deep-water settings (or darkened sites), showing two conceptacles (A3 assemblage) (FPSO-SW-C1-1A). (E) Overview of the *Schlumbergerella floresiana*-dominated assemblage with associated *Amphistegina* spp. (right top corner) typical of shallow-water reef and platform top settings (LBF1 assemblage) (FPSO-EC-1A). (F) Close up showing *Schlumbergerella floresiana* (LBF1 assemblage) (WHP-EP-S-3A). (G) Overview showing *Amphistegina radiata*-dominated assemblage (with *Heterostegina depressa* & a textularid) typical of deeper reef slope settings (LBF2 assemblage) (SKUA-10-11-C1-5A). (H) Close up showing details of the *Amphistegina* spp. assemblage with *Alveolinella quoyi* and *Calcarina* spp. (LBF2 assemblage) (WHP-EP-S-15A).

Algal Assemblage 1 (A1) is dominated by thick, centimetre-scale crusts of *Porolithon* gr. *onkodes* with associated semi-endophytic *Lithophyllum* gr. *cuneatum* (Fig. 5A), thin crusts of *Lithophyllum* gr. *pustulatum* and scattered *Lithophyllum* gr. *prototypum* and *Harveylithon* spp. Living *P.* gr. *onkodes* is common in shallow-water (<10 m), high-energy environments throughout the Indo-Pacific (Adey *et al.*, 1982; Verheij, 1994; Iryu *et al.*, 1995; Cabioch *et al.*, 1999; Payri *et al.*, 2000; Dechnik *et al.*, 2017; Braga *et al.*, 2022). Analogous fossil assemblages dominated by *P.* gr. *onkodes* are similarly characteristic of shallow reef settings in palaeowater depths of <10 m and <6 m where associated with thick algal crusts and abundant vermetid gastropods (Cabioch *et al.*, 1999; Abbey *et al.*, 2011; Camoin *et al.*, 2012; Gischler *et al.*, 2016; Dechnik *et al.*, 2017; Humblet *et al.*, 2019).

Algal Assemblage 2 (A2) is dominated by *Lithophyllum* species (*L.* gr. *kotschyanum, L.* gr. *acrocamptum* and *L.* gr. *pustulatum*) with associated *Harveylithon* (*H.* gr. *munitum* and *H.* gr. *rupestre*) with thin (<0.2 mm) crusts of *Hydrolithon* sp. and minor Hapalidiales (Fig. 5B and C). This assemblage commonly comprises the crusts forming the rhodolith-dominated facies. Fossil assemblages dominated by *Lithophyllum* and *Harveylithon* species with no crusts of *P.* gr. *onkodes* typically occur in shallow to intermediate depths to 30 m throughout the Indo-Pacific (Dechnik *et al.*, 2017). Modern species of *L.* gr. *kotschyanum* in the GBR have a wide depth distribution (0 to 20 m) and *H.* gr. *munitum* was recorded between 9 and 27 m (Dechnik *et al.*, 2017). Thus, the authors suggest that this algal assemblage was probably deposited in shallow to intermediate palaeo-water depths of 0 to 30 m.

Algal Assemblage 3 (A3) is dominated by laminar *Lithothamnion* spp. with associated thin crusts of *Lithophyllum* gr. *pustulatum*, *Peyssonnelia* and *Lithoporella* sp. (Fig. 5D) and characterises many crusts of the rhodolith facies. Modern Indo-Pacific CCA assemblages dominated by *Lithothamnion* and other Hapalidiales are characteristic of relatively deep waters below 20 – 30 m (Adey *et al.*, 1982; Lund *et al.*, 2000; Matsuda & Iryu, 2011; Bassi *et al.*, 2012).

Fossil assemblages dominated by *Lithothamnion* spp. commonly occur in deeper tropical settings (>20 m) or on shaded surfaces within reef frameworks (Webster *et al.*, 2009; Abbey *et al.*, 2011; Humblet *et al.*, 2019). Green calcareous *Halimeda* plates can also be associated with the coralline algal assemblage. Therefore, the authors suggest that this assemblage was deposited on a deeper reef slope in palaeo-water depths >20 m.

Larger benthic foraminifera assemblages (LBF)

The authors recognised 20 taxa of LBFs in thin sections. Community composition is more similar to nearby areas in Indonesia (Renema & Troelstra, 2001; Renema, 2003) than to the West Australia coast (Parker, 2009). The components that most stand out are the calcarinids, especially *Schlumbergerella floresiana* and *Calcarina* spp. (*C. hispida* gr., *C. spengleri, C. mayori*). *Schlumbergerella* have not been observed along the West Australia coast (Parker, 2009; Weinmann *et al.*, 2013) but *S. floresiana* occurs on nearby Ashmore Reef where it is most abundant foraminifer on the modern reef crest and back reef settings (Glenn & Collins, 2005). The foraminifers in the NWS cores can be grouped into two assemblages. Assemblage 1 (LBF1) is dominated by *S. floresiana* and *Amphistegina lobifera*, with associated *Amphisorus* spp., *C. hispida* gr. and *Peneroplis* spp. and is found in 12 thin sections (Fig. 5E and F). These taxa can occur *in situ* on the upper reef slope and reef flat, with a maximum depth of ~20 m, but with the highest densities at 0 to 10 m water depth, particularly on the reef crest when dominated by *S. floresiana.* Assemblage 2 (LBF2) is characterised by *Amphistegina radiata* and *Heterostegina depressa* (Fig. 5G). This assemblage was found in 16 thin sections and can be associated with *C. spengleri* and *Alveolinella quoyi* (Fig. 5H). On reefs in Indonesia the main taxa of this assemblage occur in deeper (coral) reef slope settings with coral rubble covered with crustose coralline algae at a depth range of 5 to 50 m (Renema & Troelstra, 2001).

Coralgal assemblages

Four main coralgal assemblages (Table 4, Fig. 6) were defined based on dominant coral, CCA and LBF compositions, as well as vermetid gastropod abundance. These assemblages represent various palaeo-environments, from very shallow, high-energy reef crests, upper and middle, intermediate-energy slopes, as well as sheltered back reef settings, based on comparisons with their modern counterparts, sedimentary facies associations and previously established fossil assemblages from the Indo-Pacific.

Coralgal assemblage 1 (C1) is the most common assemblage and is dominated by robust branching (corymbose/digitate) *Acropora* (i.e. *A. humilis, A. monticulosa, A. gemmifera*), branching *Stylophora pistillata* and *Porites* (*P. cylindrica, P. nigrescens*), associated *Isopora palifera* (sub-massive/encrusting) and *Montipora* (encrusting/branching) (Fig. 6A to C) with rare massive *Goniastrea, Goniopora* and *Cyphastrea* species. Fossil assemblages dominated by robust *Acropora/Isopora* species are commonly interpreted as growing in high-energy, shallow-water (<10 m) environments, typical of outer reef flats or upper reef slopes (Humblet *et al.*, 2019; Braga *et al.*, 2022). On the north-west Cape of Western Australia acroporids and encrusting *Montipora* commonly occur along shallow reef platforms in water depths of ~2.5 to 5 m, whereas *Porites* species dominate at slightly greater depths of ~4 to 6 m (Twiggs & Collins, 2010). Specifically, modern surveys at Ashmore Reef confirm that several *Acropora* species (i.e. *A. latistella, A. humilis, A. gemmifera*), *Isopora palifera* and *S. pistillata*, *P. cylindrica, P. nigrescens* which characterise this fossil assemblage, are all common in exposed, shallow-water settings <10 m (Kospartov *et al.*, 2006; Richards *et al.*, 2009; Ceccarelli *et al.*, 2011). This assemblage is also associated with shallow CCA (A1), LBF (LBF1) assemblages and abundant vermetid gastropods (mainly abundance category 3, 2) and therefore can be restricted to very shallow, high-energy reef crest-upper slope

settings <5 m deep (Dechnik *et al.*, 2017; Humblet *et al.*, 2019).

Coralgal assemblage 2 (C2) is dominated by corymbose branching *Acropora* spp. and merulinids (*Dipsastraea* gr. 2), with associated *Montipora* (encrusting-sub-massive) and *Seriatopora* (branching) (Fig. 6D). While common, the *Acropora* branches are heavily altered (dissolved/partially dissolved) limiting their taxonomic and morphologic identification. However, significantly, this coral community invariably occurs with relatively thin crusts of intermediate algae (A2) and few vermetid gastropods (category 1, 2), suggesting that this assemblage was deposited in intermediate reef slope settings, across a wide range of water depths (0 to 30 m) (Dechnik *et al.*, 2017; Humblet *et al.*, 2019).

Coralgal Assemblage 3 (C3) is characterised by corymbose/digitate *Acropora*, such as *A. digitifera* and more robust branching species (*A.* gr. 21 - *A. humilis, A. gemmifera, A. monticulosa*) and massive *Porites* (gr. 1 - *P. lutea, P. australiensis*), with associated merulinids (*Dipsastraea* gr. 1) (Fig. 6D). Similar to coralgal assemblage 1 (C1), this assemblage is associated with shallow CCA (A1), LBF (LBF1) assemblages and moderate abundance of vermetid gastropods (category 2) and is interpreted to be characteristic of shallow, high-energy reef settings <10 m (Dechnik *et al.*, 2017; Humblet *et al.*, 2019; Braga *et al.*, 2022).

Coralgal Assemblage 4 (C4) is rare, occurring only at the base of FPSO-E-C core. Columnar *Pavona clavus* (Fig. 6G) dominates this assemblage with associated branching *Acropora (*digitate*), Pocillopora*, encrusting *Montipora* and *Pavona explanulata*. Modern *P. clavus* typically occurs in semi-protected environments over a wide range of water depths (0 to mesophotic depths) (Veron & Pichon, 1979; CoralTraitDatabase, 2020; OBIS, 2020). Specifically, at Ashmore Reef *Pavona clavus* has been observed in lower reef slope and lagoonal environments (Kospartov *et al.*, 2006). The C4 corals are encrusted by thin crusts of intermediate CCA (A2) lacking vermetid gastropods and occur amongst a grainstone/packstone matrix containing the LBFs *Neorotalia calcar* and *Calcarina hispida*, which are characteristic of reef flat, back reef and lagoonal settings at Ashmore Reef (Glenn & Collins, 2005). However, they lack the exposed, reef crest *S. floresiana* most characteristic of LBF1. A broadly similar massive to columnar agariciid (*Gardinoseris planulata, Pavona maldivensis*) fossil assemblage (A3 in Gischler *et al.*, 2016) with similar CCA components occurs in the lower sections of Holocene reefs at Bora Bora where it indicates an intermediate-energy, fore reef environment, or sheltered reef flat or back reef setting (10 to 20 m). Thus, the authors interpret the C4 assemblage as having grown in an intermediate, backreef or lagoonal environment at >10 to 30 m palaeowater depth.

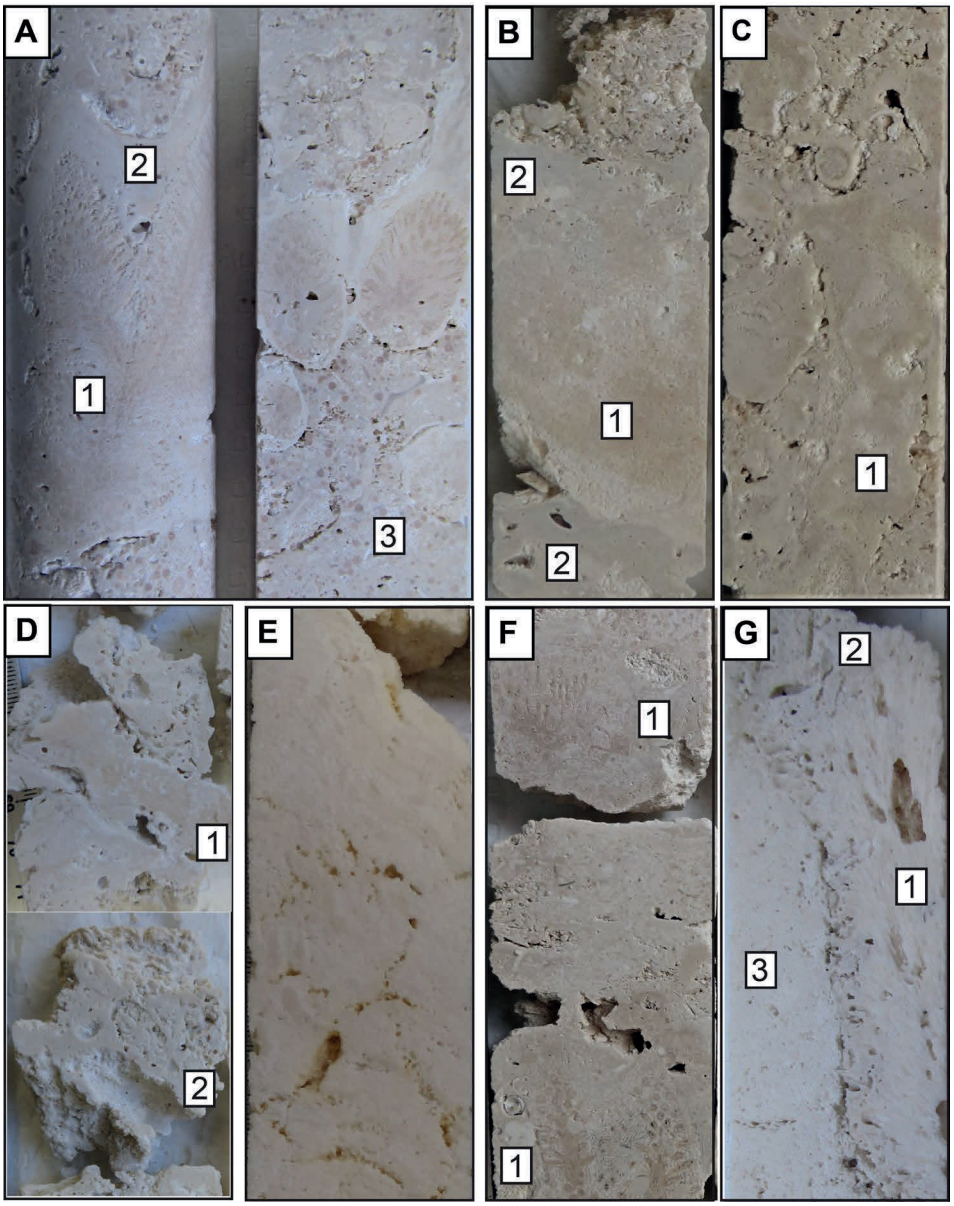


Fig. 6. Main coralgal assemblages observed in NWS cores. (A) Robust branching *Acropora monticulosa* (corymbose/digitate) (1), with branch tips encrusted by thick layers of *Porolithon* gr. *onkodes* (A1) and vermetid gastropods (2) (FPSO-E-C-1A-1) and associated grainstone/packstone sediments dominated by larger benthic foraminifera (*Schlumbergerella floresiana*) (LB1) that is characteristic of shallow, high-energy, upper reef crest-slope settings in <5 m water depths (C1 assemblage). (B) Submassive *Isopora palifera* (1) growing on and encrusted by thick crusts of coralline algae (2) (SWIFT-N-1C-4A) and (C) branching *Montipora* are also characteristic of the C1 assemblage (FPSO-NW-C-3A). (D) Partially (1) (FPSO-SW-S1-6A) to severely dissolved (2) (FPSO-SW-S1-7A) branching *Acropora* sp. covered with thin crusts of A2 coralline algae are characteristic of intermediate reef slope settings in 0 to 30 m water depths. (E) Massive *Porites* (SWIFT-MF-C-10B) and (F) robust branching *Acropora digitifera* (1) (SWIFT-N-1-C-6A) with associated thick crusts of A1 coralline algae that is characteristic of shallow, high-energy reef settings in <10 m water depths (C3 assemblage). (G) Columnar *Pavona clavus* (1) associated thins crusts of A2 coralline algae (2) and grainstone/packstone sediments (3) characteristic of deeper, backreef or lagoonal settings, >10 to 30 m (FPSO-E-C-10A (C4 assemblage). Core diameter is 4.5 cm in all images.

Mineralogical variations, diagenetic characteristics and environments

Visual observation of the cores, thin sections, SEM, XRD and hyperspectral data reveal a diverse suite of characteristics indicating both marine and meteoric diagenesis (Figs 7 to 10). The major downhole patterns are described below. The top few metres of the holes (~75 to 79 mbsl) are characterised by entirely marine diagenetic signatures. SEM and thin sections (Fig. 5B and C) reveal well-preserved coralline algae crusts and other bioclasts. Local minor pore filling cements consist of acicular aragonite, high-Mg calcite scalenohedral crusts and peloids (Fig. 8C), but no meteoric diagenetic overprint was observed. In contrast, both marine and meteoric diagenetic signatures are present from ~80 to 90 mbsl. In some sections aragonite coral microstructure is pristine (Fig. 8A and B), whilst in others a heterogeneous meteoric overprint is characterised by partial dissolution of coral skeletons and replacement with low-Mg calcite cements. Pore-filling cements are predominantly isopachous dogtooth low-Mg calcite, suggesting a meteoric phreatic environment (Fig. 8D to F).

This meteoric overprint and associated mineralogic changes are complex and spatially variable at the core scale with the hyperspectral image and numerical data sets showing many sections where corals are altered to calcite, while others retain their aragonitic skeleton (i.e. $CaCO_3$ classification, feature characteristics, calcite purity; Figs 9 and 10). In these cases, SEM and thin section data clearly show that significant elements of pristine aragonite coral skeletons remain (Fig. 8A and B) consistent with XRD measurements up to 97.5% aragonite from representative corals (Table 6).

However, below ~90 mbsl the meteoric diagenetic signatures become more pervasive and complex. Mouldic porosity is evident in hand specimens from ~90 to 95 mbsl with many dissolved and partially dissolved corals (Figs 6D and 7C). SEM and thin sections show these heterogeneously dissolved and recrystallised corals have been mostly replaced by low-Mg calcite but locally some skeletal aragonite remains (Fig. 8G to J). Low Mg calcite also occurs occluding coral pore spaces and euhedral rhombohedral crystals that are morphologically consistent with dolomite also occur (Fig. 8H and I). These same rhombohedral crystals also partially replace microbial carbonates in some coral pores (Fig. 8J). The presence of dolomite in corals from these depths is supported by hyperspectral data (e.g. Fig. 9B – $CaCO_3$ classification as green pixels in SWIFT-N1-C-6-7) and was confirmed by XRD measurements reporting 11% dolomite.

Two notable palaeosol horizons occur between 79 to 82 mbsl (Fig. 7A and B) and 89 to 92 mbsl (Fig. 7F) marking changes in the down-hole lithologic, mineralogic and diagenetic features described above. These palaeosols consist of reddish-brown grainstone-packstone as much as several cm-thick and multi-layered in some cores. Hyperspectral imaging (Fig. 7I) confirms the abundance of clay (kaolinite) within these layers. Thin section analysis reveals extensive dissolution within these sections and pisoids clearly penetrate into the surrounding carbonate substrate (CCA and LBF packstones), indicating that they post-date these sediments. Hyperspectral proxy imagery and numerical data also record major changes in carbonate mineralogy at or near these two main palaeosol horizons (Figs 9 and 10). This is best observed in FPSO-NW-C-1, SWIFT-N-1-C and SKUA-10/11, which have the highest density of hyperspectral proxy measurements that together suggests that these palaeosol horizons represent major chrono-stratigraphic boundaries (Fig. 10).

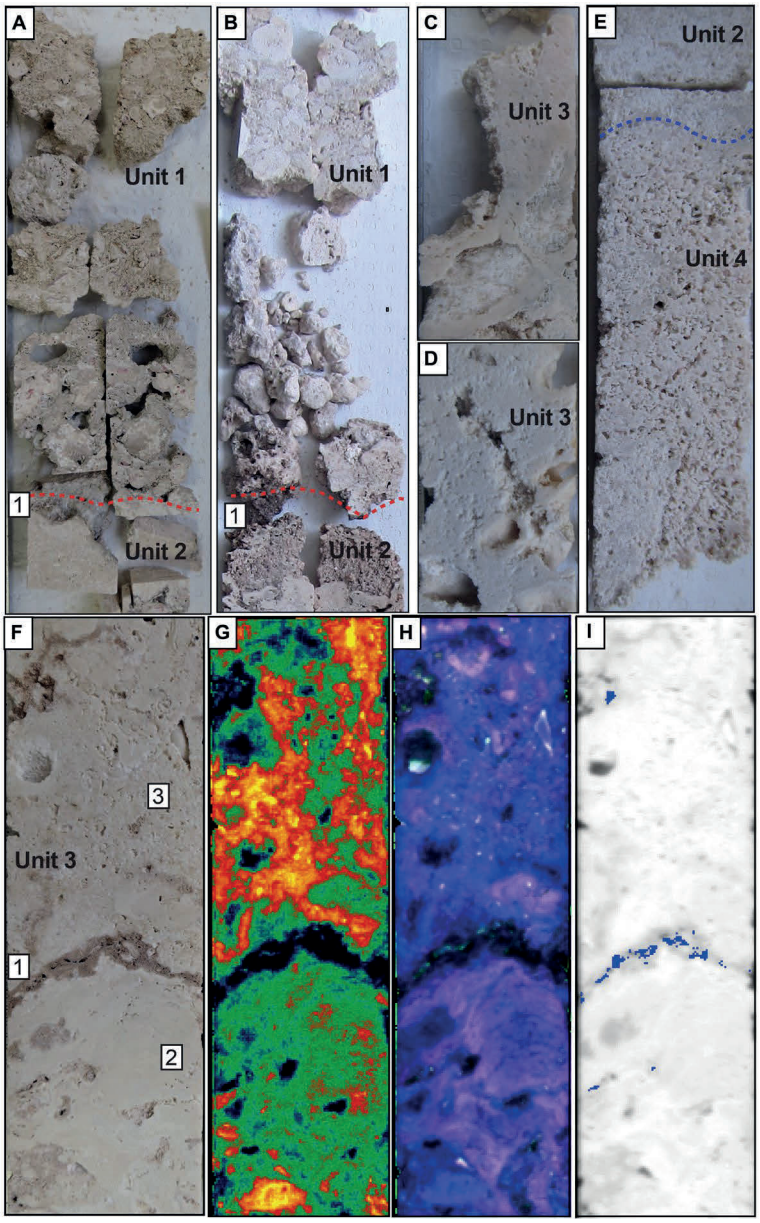


Fig. 7. Representative images showing characteristics of the major chrono-stratigraphic units, their boundaries and macro-scale diagenetic features. (A) and (B) Core images showing the Unit 1 (Rhodolith floatstone-dominated facies) and 2 (Coral framestone-dominated facies) boundary characterised by a distinct palaeosol horizon (1) (SWIFT-N-1-C-1A; FPSO-SW-C1-1A). (C) and (D) Core images of Unit 3 (Coral framestone-dominated facies) characterised by dissolved and partially dissolved (mouldic porosity) robust *Acropora* branches with grainstones/packstones (FPSO-E-C-8A). (E) Core image showing the boundary (dashed line) between Unit 2 and 4 that is marked by a sharp contact and clean grainstones facies that lack corals (FPSO-SW-C1-6A). (F) Core image showing the characteristics of the 2nd major palaeosol marking the Unit 2 and 3 boundary (FPSO-NW-C-7A-2). These multiple red, brown soils layers (1) penetrate into Unit 3, characterised here by thick coralline algal bindstone (2) and (3) packstone facies. The main lithology types, and macro-scale diagenetic features, are accurately discriminated by the high-resolution hyperspectral imagery: (G) calcite purity index, (H) intensity of absorption features of water, OH and carbonate displayed as red, green and blue; (I) clay (kaolinite) mapped from its diagnostic absorption feature at 2207 nm (blue pixels) is clearly visible in the palaeosol. Core diameter is 4.5 cm in all images.

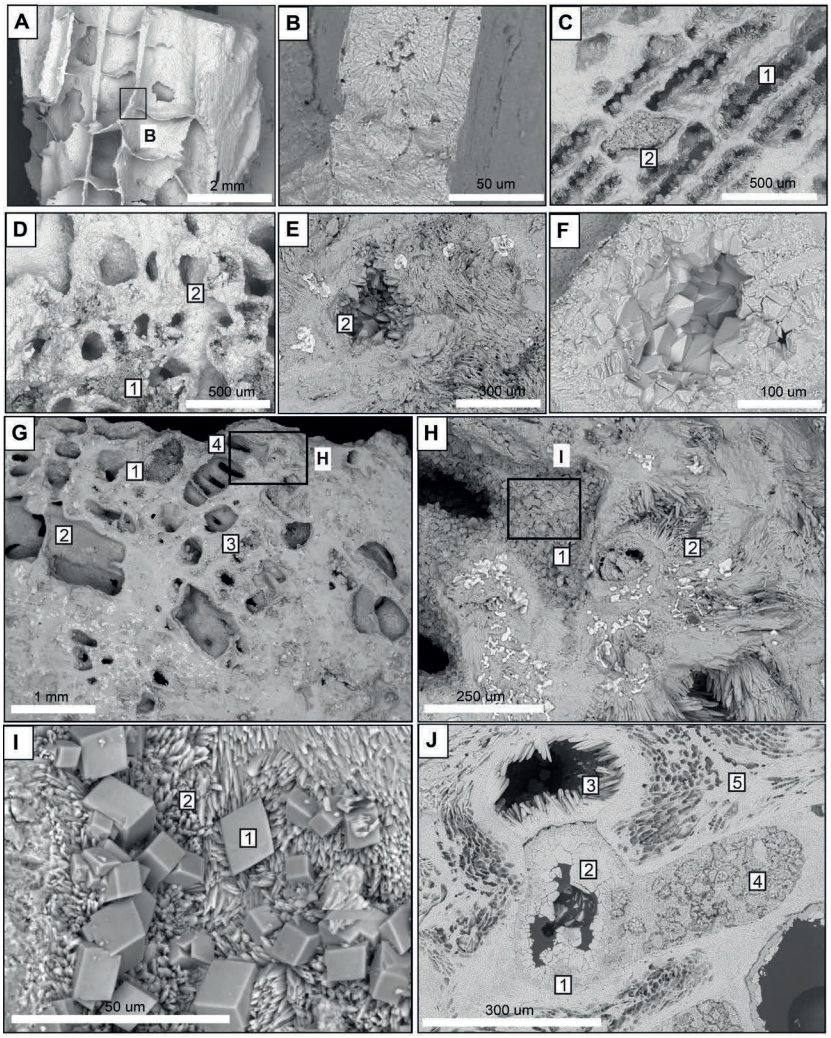


Fig. 8. Representative SEM images showing characteristic, micro-scale features indicative of both marine and meteoric diagenetic environments. (A) Well preserved *Platygyra sinensis* with large open pore spaces, free of internal cements and (B) close up of well-preserved fibrous, coral skeletal microstructure with minor microboring (FPSO-NW-C-1A). (C) *Goniopora* showing key features of marine diagenesis including acicular aragonite fringing cements (1) and peloidal high-Mg calcite (2) within interseptal spaces (SWIFT-N-1-C-1A-3). (D) *Montipora* showing partial dissolution of coral skeleton (1) and blocky, low-Mg calcite meteoric cement (SKUA-10-11-C1-3A1). (E) *Acropora* with pore lined with low-Mg calcite cement (2) as a result of meteoric diagenesis (FPSO-SW-S1-3B). (F) Blocky, low-Mg calcite meteoric cement in *Acropora* (WHP-EP-S-3A-1). (G) *Acropora* skeleton showing various marine and meteoric cements including an aragonite fringe (1), high-Mg calcite peloids (2), low-Mg calcite (3); and dolomite (4) in the region of higher magnification shown as box H (SWIFT-N-1-C-6A). (H) Enlargement showing dolomite cement on aragonite (1) and large secondary acicular aragonite cements (2). Region of higher magnification shown as box I. The bright white material is secondary halite. (I) Enlargement of rhombohedral dolomite cement (1) overlying fine acicular, possibly syntactic aragonite cement (2). (J) Polished SEM image of SWIFT-N-1-C-6A showing complex relationships between different phases of marine and meteoric diagenetic products. Blocky dolomite cement partially replacing or nucleated on high-Mg calcite lining pore in coral skeleton (1), directly overlain by blocky low-Mg calcite cement not quite occluding the pore (2). Secondary acicular aragonite cement lines second pore (3). High-Mg calcite microbialite containing trapped and bound sediment is partially replaced by dolomite in pore (4) and remaining elements of original coral aragonite skeleton (5) have undergone partial dissolution resulting in scalloped pattern.

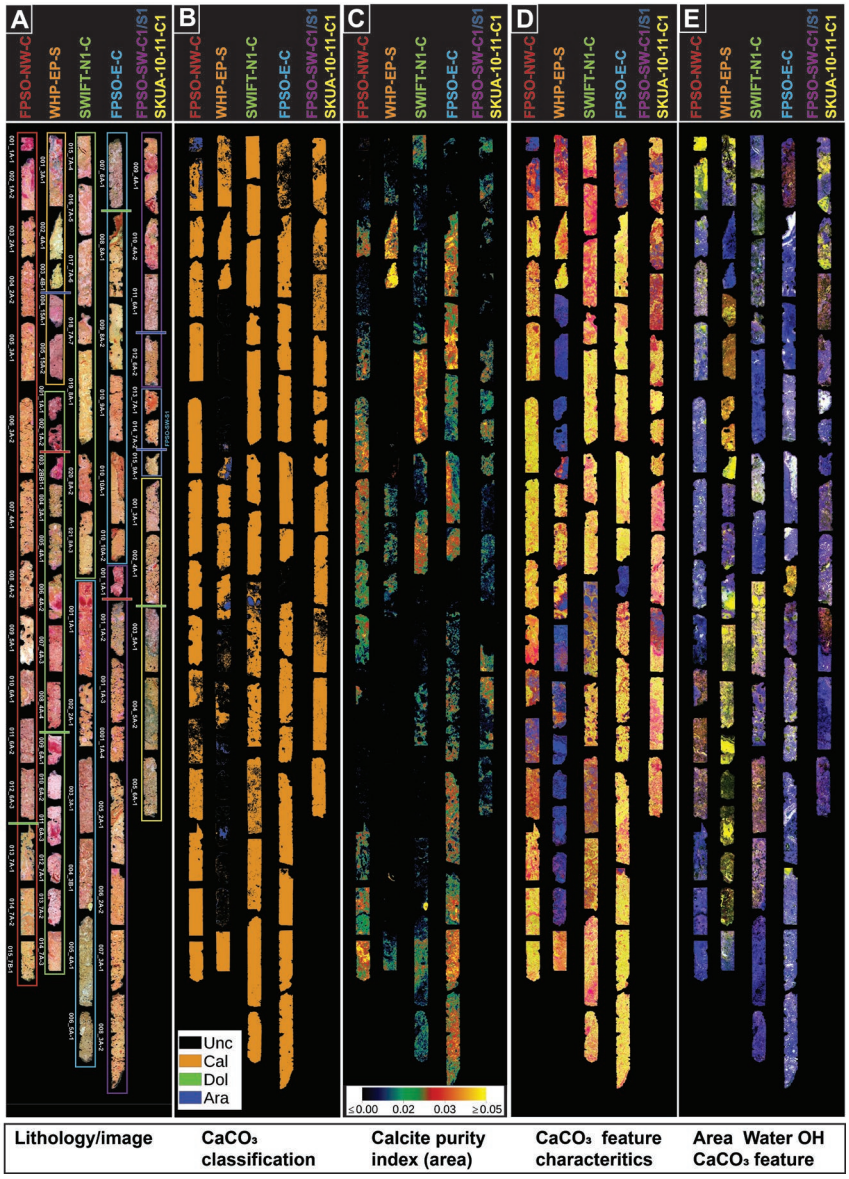


Fig. 9. Representative images showing the major hyperspectral characteristic of NWS shelf cores. (A) False colour composite image showing the main lithologic characteristics of the main sites and representative core section. (B) Classified image of the carbonates (calcite, aragonite, dolomite, unclassified) derived using the method of Murphy *et al.*, (2017). (C) Image showing calcite purity index based on the area of the minor (secondary) carbonate absorption feature at 1880 nm, showing more aragonitic calcite phases (black), poorly crystalline calcite (blue tones) and progressively more crystalline calcite phases (red through yellow tones). (D) Image showing $CaCO_3$ feature characteristics based on the wavelength position, intensity and asymmetry of the primary carbonate absorption feature located at ~2331 nm, displayed as red, green and blue, respectively. The image highlights the primary carbonate phases in the image with red tones indicating less crystalline calcite, green tones indicating crystalline calcite and blue tones indicating aragonite. Intermediate colours represent mixtures of these three phases. (E) Image showing the area of the absorption features of water, OH and carbonate displayed as red, green and blue, respectively. Yellow tones show aragonitic phases, containing large amounts of water and OH. Blue tones highlight more crystalline calcite phases with little or no water absorption, white and reddish tones show carbonate phases with high (white) and low (red tones) water, OH and carbonate absorption, probably transitional between aragonite and calcite.

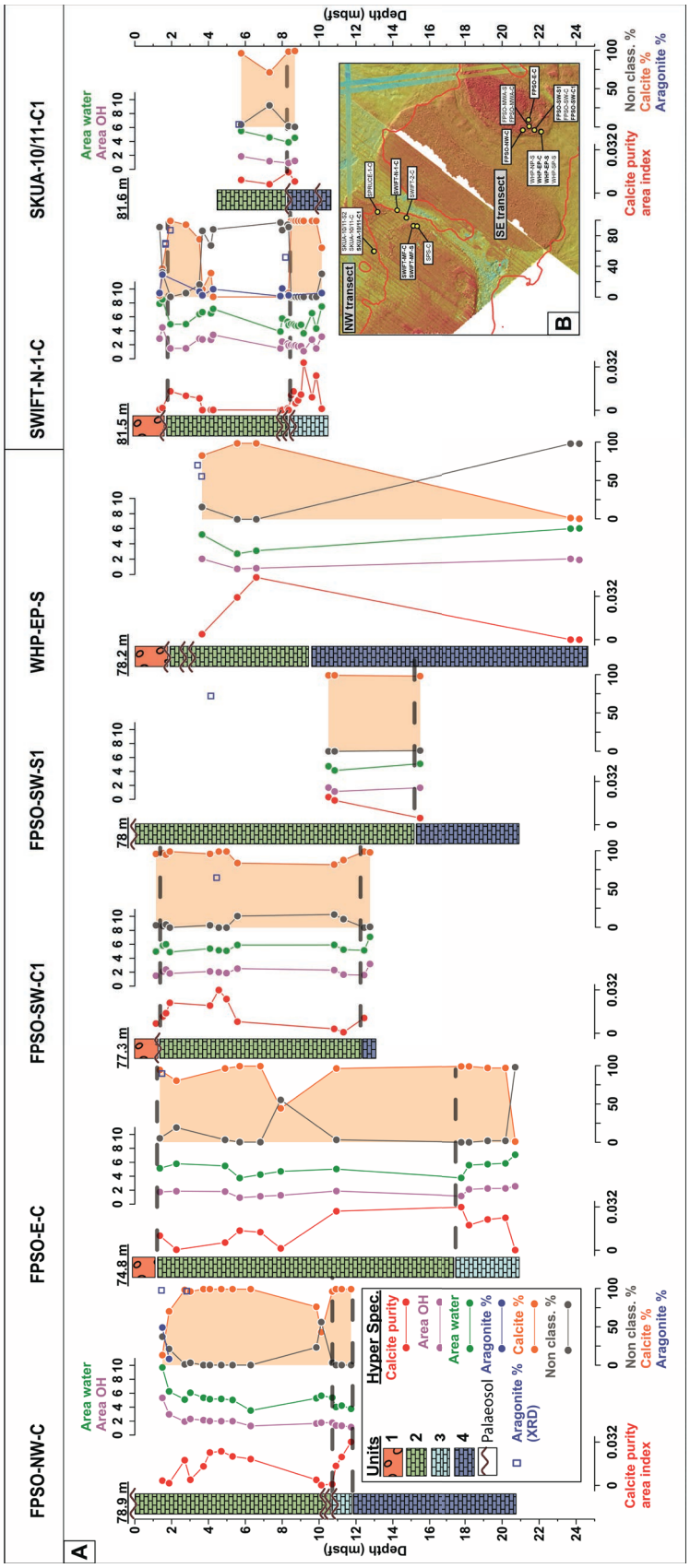


Fig. 10. Hyperspectral proxy data versus depth in representative NWS cores. (A) Simplified logs showing down hole variation in numerical hyperspectral proxy data (calcite purity area index, area of the absorption features of water and OH, carbonate classification based on percent pixels) and XRD (% aragonite – blue squares). The grey dashed lines represent boundaries of the four chronostratigraphic units (Units 1–4) that also correspond to major changes in the hyperspectral proxy data and in some cases are marked by palaeosol horizons. To illustrate the down hole patterns in carbonate classification, the % of pixels classified as calcite are shaded with a light orange fill. (B) Core locations and their geomorphic context on the platforms.

Radiometric dating *vs*. depth

Radiocarbon measurements were made on 24 carbonate samples (corals, coralline algae and molluscs) from core depths of 75.62 to 90.64 mbsl (Fig. 11, Table 5). Calibrated ages range from 10.7 to 44.8 ka, spanning MIS 3 to MIS 1 during the late deglacial. Two samples at the base of SWIFT-MF-C and FPSO-NW-C could not be calibrated because they contain no modern carbon (i.e. they are too old and radiocarbon 'dead'). Four ages from well preserved coralline algae (Fig. 7) from the top 1 m of SWIFT-N-1-C, WHP-EP-C, FPSO-SW-C1 and FPSO-E-C range from 10.4 to 13.1 ka confirming that these rhodoliths are late deglacial in age. Samples below ~81 to 83 mbsl in the coral-dominated sections of the holes down to ~89 mbsl cluster towards the end of MIS 3 and into MIS 2. However, based on SEM, hyperspectral, petrologic and XRD data, some of these samples have undergone varying degrees of meteoric diagenetic alteration, suggesting subaerial exposure. This is clearly illustrated in Fig. 11, showing age versus depth of the coral samples plotted with their corresponding percent aragonite and their relationship to RSL in the region. For example, several coral samples (e.g. SKUA-10-11-C1-3A – 21.3 ka; SWIFT-MF-C-4A – 27.9 ka) plot well above the position of RSL during MIS 2 in the region (Ishiwa *et al.*, 2019a), consistent with their almost entire recrystallisation to calcite based on mineralogical data. Eleven corals in this middle section of the holes range in age between ~27.9 to 39.7 ka with aragonite values between 51.6 and 97.5%. However, the SEM observations, hyperspectral and XRD data also show that this diagenesis is highly variable; and that the authors consider coral samples FPSO-NW-C-1A-1 (97.5%), FPSO-NW-C-2A (96.4%), and less so FPSO-E-C-1A-2 (89.4%) and SWIFT-N-1-C-2BB1 (86.9%), to yield the most reliable ^{14}C-ages of 35.0 to 39.7 ka in these cores. This is consistent with the paired U/Th ages on the same coral samples (FPSO-NW-C-1A-1, FPSO-NW-C-2A, FPSO-E-C-1A-2) that returned three ages between 39.23 and 45.95 ka in MIS 3. These corals were evaluated for ^{232}Th, initial ^{234}U/^{238}U activity ratios (reported as $d^{234}U_i$ in permil) and also for anomalous ^{238}U concentrations, which can indicate detrital Th contamination or open-system diagenesis (Dechnik *et al.*, 2017). These samples passed those criteria and have initial $d^{234}U_i$(‰) values between 141.64 and 142.49 $\pm$ 0.9 to 1.1‰, well within recently published screening tolerances (140 $\pm$ 8‰) (see Chutcharavan *et al.*, 2018 for recent review) for MIS 3 corals (Table 6). Furthermore, samples FPSO-NW-C-1A-1 (39.23 ka) and FPSO-NW-C-2A (44.74 ka) from the same hole, are *in-situ* and in stratigraphic order. The authors also note that the U/Th ages are 2.56 to 7.9 kyr older than their corresponding radiocarbon ages, an offset consistent with other MIS 3 corals from the adjacent uplifted reefs of the Huon Peninsula (Yokoyama *et al.*, 2000). Two coralline algal samples (WHP-EP-S-3A-2, FPSO-NW-C-6A-2) and one mollusc sample (SKUA-10-11-C1-3A2) from this same middle section of the cores gave ^{14}C-ages between 31.5 to 40.2 ka. However, only WHP-EP-S-3A-2 (33.15 ka) is considered moderately reliable based on SEM observations and its consistent stratigraphic position.

Finally, the three samples below ~89 m (SWIFT-N-1-C-6A, SWIFT-MF-C-10B, FPSO-NW-C-7B) are radiocarbon 'dead' and/or XRD and SEM observations confirm they have suffered the most severe diagenetic alteration, including dolomitization (XRD 11.1%) (Figs 7 to 9). Taken together, this indicates the presence of a stratigraphically deeper, coral-dominated section that is both diagenetically distinct and older than 50 ka.

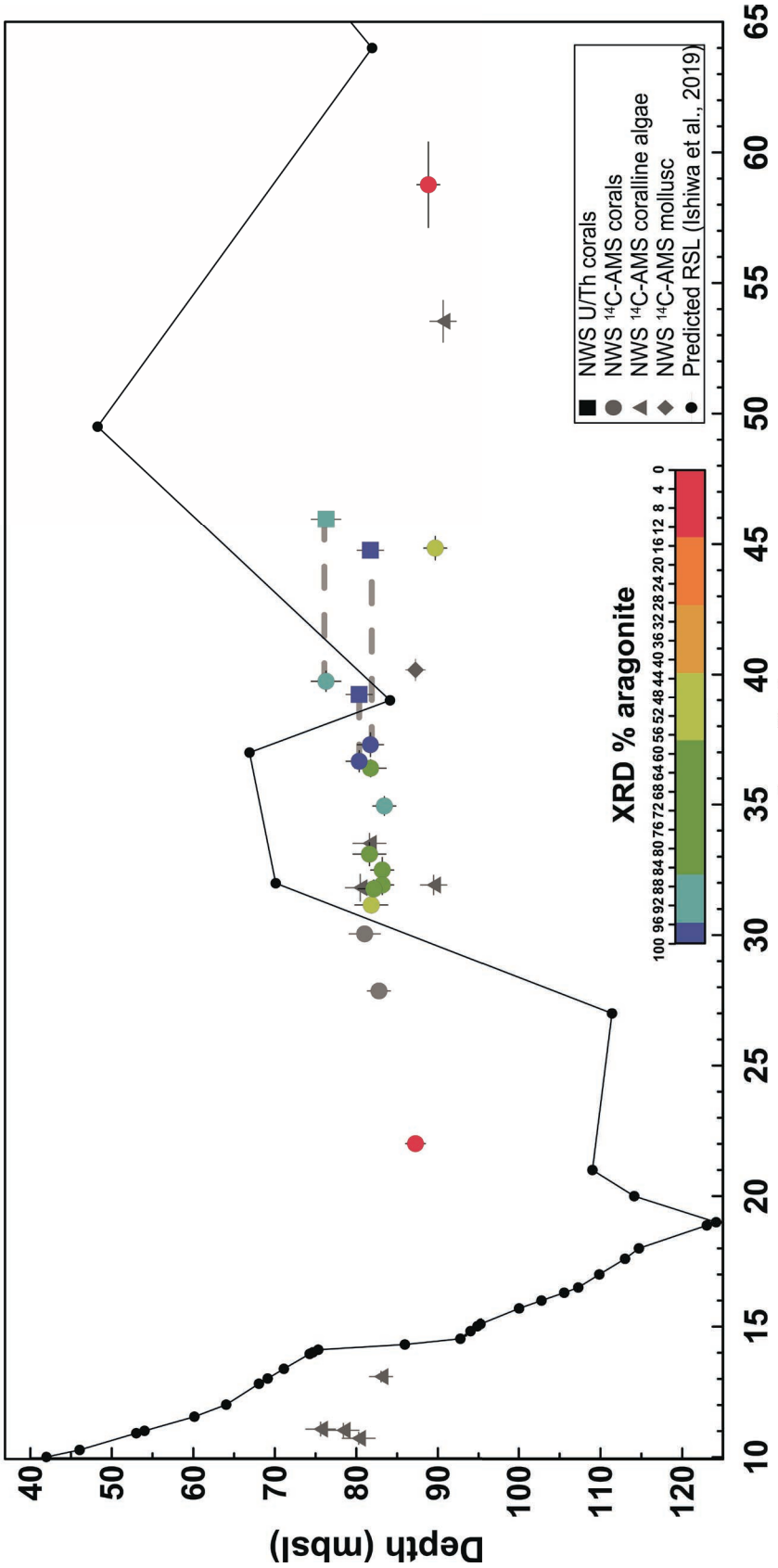


Fig. 11. Summary of age *vs.* depth data from the NWS cores. Sample depths are plotted as metres below sea-level (mbsl) and include the tidal error but are not corrected for regional subsidence. The predicted RSL (black points and line) for the NWS based on GIA modelling is shown for reference (Ishiwa *et al.*, 2019a). In some cases, the size of the symbol is larger than the age error. Coral samples are colour coded with their respective % aragonite as measured by quantitative XRD. The grey dashed lines represent the age offset between closed-system U/Th ages and calibrated ^{14}C-AMS ages on the same coral sample (see Tables 5 and 6 for details). The grey coloured symbols represent samples that lack XRD data.

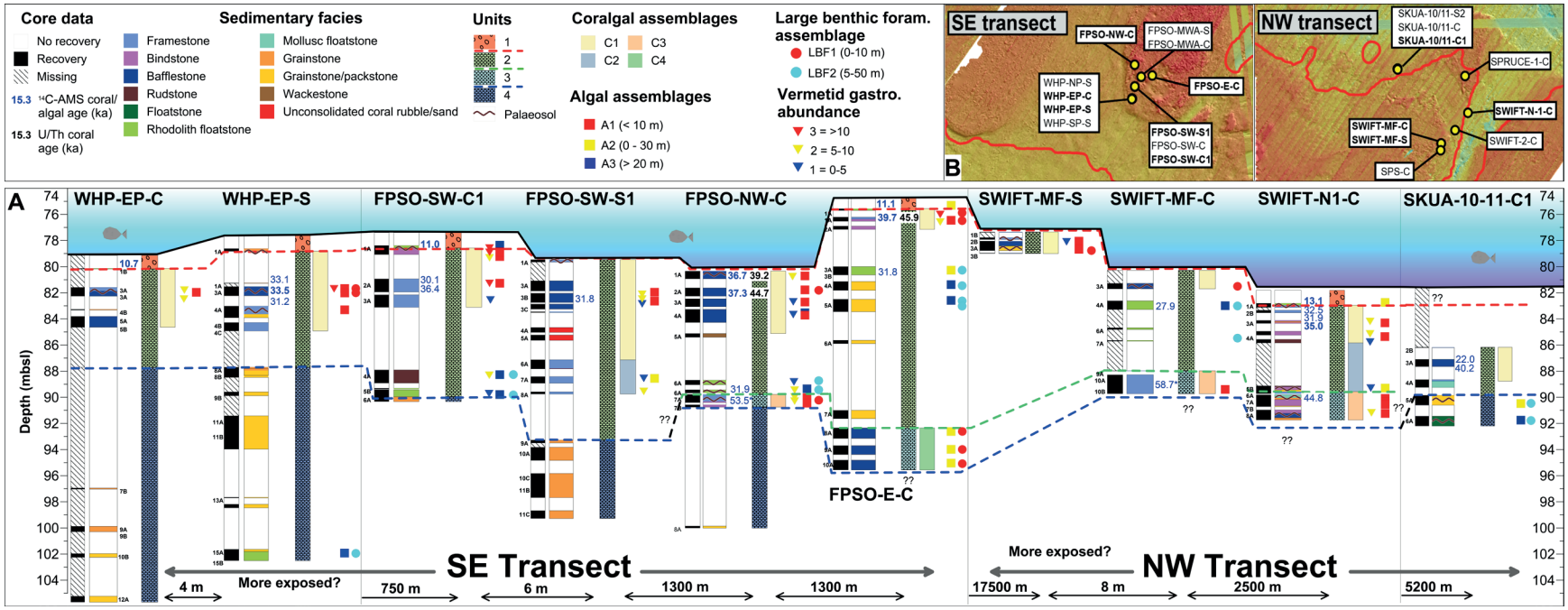


Fig. 12. Summary of sedimentary facies, chrono-stratigraphic units, reef biota and radiometric data for the SE and NW drill transects on the NWS. (B) Simplified stratigraphic sections showing the distribution of recovered core intervals, coral, algal, large benthic foraminifera assemblages, vermetid gastropod abundance, palaeosols horizons and U–Th and ^{14}C-AMS ages (bold values represent reliable ages). The boundaries of the four chrono-stratigraphic units (Units 1 to 4) are represented by the dashed coloured lines. The x-axis represents the distance between the cores and is schematic; (A) gives the actual core locations and their geomorphic context on the platforms.

Table 5 (first section). Radiometric data from the carbonate deposits recovered from the NWS cores.

Sample ID	Lab code	Tran-sect	Depth below sea-level (mbsl)	Tidal depth ±(m)	Dated Lithology	Genera/ lithology
SKUA-10-11-C1-3A1	YAUT-028036	NW	87.25	1.2	Coral	*Montipora*
SKUA-10-11-C1-3A2	YAUT-028037	NW	87.25	1.2	Mollusc	
SWIFT-N-1-C-1A-2	YAUT-028032	NW	83.03	1.4	Coralline algae	Rhodolith
SWIFT-N-1-C-1A-1	YAUT-028031	NW	83.17	1.4	Coral	*Goniopora*
SWIFT-N-1-C-1A-3	YAUT-028033	NW	83.17	1.4	Coral	*Goniopora*
SWIFT-N-1-C-2BB1	YAUT-037437	NW	83.43	1.4	Coral	*Favites* gr. 1
SWIFT-N-1-C-6A	YAUT-037832	NW	89.68	1.4	Coral	*Acropora*
SWIFT-MF-C-4A	YAUT-037438	NW	82.77	1.4	Coral	*Acropora*
SWIFT-MF-C-10B	YAUT-037439	NW	88.83	1.4	Coral	*Acropora*
WHP-EP-C-1BB1	YAUT-028029	SW	80.29	2	Coralline algae	Rhodolith
WHP-EP-S-3A-1	YAUT-028026	SW	81.61	2	Coral	*Acropora*
WHP-EP-S-3A-2	YAUT-028028	SW	81.61	2	Coralline algae	Fragments
WHP-EP-S-3A	YAUT-037829	SW	81.83	2	Coral	*Acropora*
FPSO-SW-C1-1A	YAUT-028023	SW	78.41	1.9	Coralline algae	Rhodolith
FPSO-SW-C1-2A	YAUT-028024	SW	81.02	1.9	Coral	*Acropora*
FPSO-SW-C1-2A	YAUT-037826	SW	81.74	1.9	Coral	*Acropora*
FPSO-SW-S1-3B	YAUT-037828	SW	82.13	1.9	Coral	*Acropora*
FPSO-NW-C-1A-1	YAUT-028025	SW	80.35	1.6	Coral	*Platygyra sinensis*
FPSO-NW-C-2A	YAUT-037836	SW	81.72	1.6	Coral	*Porites*
FPSO-NW-C-6A-2	YAUT-037831	SW	89.48	1.6	Coralline algae	Rhodolith
FPSO-NW-C-7B	YAUT-037833	SW	90.64	1.6	Coralline algae	Rhodolith
FPSO-E-C-1A-1	YAUT-028018	SW	75.62	1.8	Coralline algae	Rhodolith
FPSO-E-C-1A-2	YAUT-028019	SW	76.28	1.8	Coral	*Acropora*
FPSO-E-C-3B	YAUT-037837	SW	80.48	1.8	Coralline algae	Rhodolith

Table 5 (second section). Radiometric data from the carbonate deposits recovered from the NWS cores.

Sample ID	Assem.	XRD[a]	Aragonite	Calcite	Hi-Mg Calcite	Dolomite	SEM	Context info.[b]
SKUA-10-11-C1-3A1	C1	3.3	3.3	93.1	3.6		Y	IS
SKUA-10-11-C1-3A2	C1							NEI
SWIFT-N-1-C-1A-2	A2							IS
SWIFT-N-1-C-1A-1	C1	69.9	69.9	14.2	17.8		Y	IS
SWIFT-N-1-C-1A-3	C1	68.6	68.6	16.1	15.2		Y	IS
SWIFT-N-1-C-2BB1	C1	86.9	86.9	10	3.1		Y	IS
SWIFT-N-1-C-6A	C2	51.6	51.6	17.6	19.7	11.1	Y	IS
SWIFT-MF-C-4A	C1							NEI
SWIFT-MF-C-10B	C3	4.2	4.2	95.8			Y	IS
WHP-EP-C-1BB1	-						Y	IS
WHP-EP-S-3A-1	C1	70.5	70.5	18	11.5			IS
WHP-EP-S-3A-2	C1						Y	IS
WHP-EP-S-3A	C1	56	56	20.5	23			IS

FPSO-SW-C1-1A	A3						Y	IS
FPSO-SW-C1-2A	C1						Y	IS
FPSO-SW-C1-2A	C1	65	65	35			Y	IS
FPSO-SW-S1-3B	C1	72.1	72.1	20.1	7.8			IS
FPSO-NW-C-1A-1	C1	97.5	97.5	1.9	0.7		Y	IS
FPSO-NW-C-2A	C1	96.4	96.4	3.6			Y	IS
FPSO-NW-C-6A-2	A3							IS
FPSO-NW-C-7B	C3						Y	IS
FPSO-E-C-1A-1	-						Y	IS
FPSO-E-C-1A-2	C1	89.4	89.4	5	5.6			IS
FPSO-E-C-3B	-						Y	IS

Table 5 (third section). Radiometric data from the carbonate deposits recovered from the NWS cores.

Sample ID	**Palaeo-water depth max (m)**	**Palaeo-water depth min (m)**	**d^{13}C (‰)**	**±1s**	**^{14}C age (yr BP)**	**±1s**	**Calibrated age (ka)[c]**	**Lower cal. range BP**
SKUA-10-11-C1-3A1	10	0	2.73	1.36	18961	58	22.0	21.707
SKUA-10-11-C1-3A2	10	0	5.74	0.79	36127	175	40.2	39.749
SWIFT-N-1-C-1A-2	30	0	21.1	4.24	11817	51	13.1	12.875
SWIFT-N-1-C-1A-1	5	0	2.19	2.88	29144	110	32.5	32.028
SWIFT-N-1-C-1A-3	5	0	-0.67	3.44	28775	109	31.9	31.564
SWIFT-N-1-C-2BB1	5	0	-3.7	2.5	31429	130	35.0	34.596
SWIFT-N-1-C-6A	30	0	3.6	2.3	43132	293	44.8	44.375
SWIFT-MF-C-4A	10	0	0.3	2.8	24660	86	27.9	27.631
SWIFT-MF-C-10B	10	0	0.9	3.3	58765	1636	58.8	
WHP-EP-C-1BB1	30	0	14.2	3.94	9952	47	10.7	10.486
WHP-EP-S-3A-1	5	0	-4.28	8.52	29548	131	33.1	32.672
WHP-EP-S-3A-2	5	0	3.63	1.98	29900	115	33.5	33.15
WHP-EP-S-3A	5	0	-2.3	5.6	28017	109	31.2	30.95
FPSO-SW-C1-1A	-	>20	19	4.61	10165	51	11.0	10.761
FPSO-SW-C1-2A	5	0	1.49	8.76	26772	116	30.1	29.803
FPSO-SW-C1-2A	5	0	-3.6	3.2	32844	136	36.4	36.08
FPSO-SW-S1-3B	5	0	-6.4	4.1	28653	107	31.8	31.45
FPSO-NW-C-1A-1	5	0	4.19	3.11	33094	144	36.7	36.268
FPSO-NW-C-2A	5	0	10.4	3.1	33602	141	37.3	36.847
FPSO-NW-C-6A-2	-	>20	3.6	4.3	28774	107	31.9	31.563
FPSO-NW-C-7B	10	0	5.3	1.9	53535	796	53.5	
FPSO-E-C-1A-1	30	0	-9.86	2.74	10192	42	11.1	10.804
FPSO-E-C-1A-2	5	0	8.34	3.31	35659	172	39.7	39.344
FPSO-E-C-3B	30	0	8.7	7.4	28687	122	31.8	31.435

Table 5 (fourth section). Radiometric data from the carbonate deposits recovered from the NWS cores.

Sample ID	Upper cal range BP	2s age range (ka)	Lower	Upper	Mean 2s error (kyr)	U-Th age (ka)[d]	±2s (kyr)	U/Th Corrected depth below sea-level (mbsl)[e]	Corrected depth below sea level (mbsl)[e]	Chrono-strat unit
SKUA-10-11-C1-3A1	22.237	21.707-22.237	0.272	0.258	0.26				82.9	2
SKUA-10-11-C1-3A2	40.564	39.749-40.564	0.414	0.401	0.41				79.2	2
SWIFT-N-1-C-1A-2	13.264	12.875-13.264	0.199	0.19	0.19				80.4	1
SWIFT-N-1-C-1A-1	32.971	32.028-32.971	0.478	0.465	0.47				76.7	2
SWIFT-N-1-C-1A-3	32.475	31.564-32.475	0.371	0.54	0.46				76.8	2
SWIFT-N-1-C-2BB1	35.287	34.596-35.287	0.361	0.33	0.35				76.4	2
SWIFT-N-1-C-6A	45.349	44.375-45.349	0.45	0.524	0.49				80.7	3
SWIFT-MF-C-4A	28.211	27.631-28.211	0.247	0.333	0.29				77.2	2
SWIFT-MF-C-10B		-	1.636	1.636	1.64				77.1	3
WHP-EP-C-1BB1	11.014	10.486-11.014	0.229	0.299	0.26				78.1	1
WHP-EP-S-3A-1	33.586	32.672-33.586	0.442	0.472	0.46				75.0	2
WHP-EP-S-3A-2	33.891	33.15-33.891	0.377	0.364	0.37				74.9	2
WHP-EP-S-3A	31.463	30.95-31.463	0.217	0.296	0.26				75.6	2
FPSO-SW-C1-1A	11.215	10.761-11.215	0.261	0.193	0.23				76.2	1
FPSO-SW-C1-2A	30.356	29.803-30.356	0.26	0.293	0.28				75.0	2
FPSO-SW-C1-2A	36.783	36.08-36.783	0.321	0.382	0.35				74.5	2
FPSO-SW-S1-3B	32.142	31.45-32.142	0.336	0.356	0.35				75.8	2
FPSO-NW-C-1A-1	37.059	36.268-37.059	0.401	0.39	0.40	39.23	0.19	72.5	73.0	2
FPSO-NW-C-2A	37.814	36.847-37.814	0.455	0.512	0.48	44.74	0.20	72.8	74.3	2
FPSO-NW-C-6A-2	32.463	31.563-32.463	0.37	0.53	0.45				83.1	2
FPSO-NW-C-7B		-	0.796	0.796	0.80				79.9	3
FPSO-E-C-1A-1	11.234	10.804-11.234	0.262	0.168	0.22				73.4	1
FPSO-E-C-1A-2	40.149	39.344-40.149	0.384	0.421	0.40	45.95	0.22	67.1	68.3	2

FPSO-E-C-3B	32.268	31.435-32.268	0.508	0.533	0.52		74.1	2

[a]XRD value represents the % aragonite content of the measured corals.
[b]Special attention was given to establishing the context of each coral within each cored section. A combination of criteria was used to distinguish in situ corals from allochthonous rubble and/or drilling disturbance. Corals were classified as either *In-Situ* (IS), Not Enough Information (NEI) or Not *In-Situ* (NIS) based on criteria established in Humblet & Webster (2017).
[c]Only the samples in bold gave reliable ages and are plotted on Fig. 13 with the other relevant relative sea level indicators and paleo-oceanographic proxy data from the region.
[d]See Table 6 for the full details of the U/Th data.
[e]The sample depths are corrected to account for the long term subsidence rate (0.2 mm/yr) reported for the region since the Last Interglacial (Collins *et al*., 2011; Solihuddin *et al*., 2016).

Table 6. U-series coral measurements and ages recovered from the NWS cores.

Sample Name	U (ppm)	±2s	^{232}Th (ppb)	2σ	(^{230}Th/ ^{232}Th)	2σ	(^{230}Th / ^{238}U)	2σ	(^{234}U/ ^{238}U)	2σ	Corr. initial (^{234}U/ ^{238}U)[a]	2σ
FPSO-E-C-1A-2	3.5890	0.0019	1.925	0.008	2212	11	0.3910	0.0013	1.1270	0.0007	1.1446	0.0008
FPSO-E-C-1A-2	3.5861	0.0020	1.919	0.007	2213	12	0.3903	0.0017	1.1285	0.0008	1.1462	0.0009
FPSO-NW-C-1A-1	2.4214	0.0013	1.675	0.003	1500	7	0.3420	0.0015	1.1262	0.0009	1.1410	0.0010
FPSO-NW-C-1A-1	2.4196	0.0011	1.684	0.005	1497	7	0.3433	0.0012	1.1273	0.0010	1.1423	0.0011
FPSO-NW-C-2A	3.0382	0.0015	1.714	0.005	2047	11	0.3806	0.0017	1.1245	0.0010	1.1413	0.0011
FPSO-NW-C-2A	3.0384	0.0013	1.709	0.005	2063	9	0.3825	0.0011	1.1266	0.0007	1.1437	0.0008

Table 6 continuation. U-series coral measurements and ages recovered from the NWS cores.

Sample Name	$d^{234}U_i$ (‰)[b]	2σ	Uncorr. ^{230}Th age (ka)[c]	2σ	Corr. ^{230}Th age (ka)	2σ	Age (ka)[d]	2σ	$d^{234}U_i$ (‰)[b]	2σ
FPSO-E-C-1A-2	144.6	0.8	46.06	0.20	46.04	0.20				
FPSO-E-C-1A-2	146.2	0.9	45.87	0.24	45.86	0.24	45.95	0.22	145.41	0.89
FPSO-NW-C-1A-1	141.0	1.0	39.18	0.21	39.16	0.21				
FPSO-NW-C-1A-1	142.3	1.1	39.31	0.16	39.29	0.16	39.23	0.19	141.64	1.07
FPSO-NW-C-2A	141.3	1.1	44.67	0.24	44.66	0.24				
FPSO-NW-C-2A	143.7	0.8	44.84	0.16	44.83	0.16	44.74	0.20	142.49	0.94

[a]Nu Plasma MC-ICP-MS ^{230}Th ages and geochemical data with 2σ errors. Activity ratios calculated using decay constants of Cheng *et al*. (2000). Values have been corrected for laboratory procedural blanks.

[b]$d^{234}U_i$ = [(234U/238U)-1] x 1000. All values meeting screen tolerances for corals 17 to 60 ka (Chutcharavan *et al.*, 2018)

[c]Uncorrected ^{230}Th age calculated using Isoplot 3.75 program (Ludwig, 2012).

[d]Interpreted ages calculated by using mean for the individual sub samples of each coral. Interpreted closed-system ages are highlighted in bold.

NWS chrono-stratigraphic units, biotic distributions and successions

Four chrono-stratigraphic units were defined based on distinct lithologic, reef assemblage, mineralogic and chronologic variations (Fig. 12). Unit 1 is the top-most unit observed at most sites (WHP-EP-C, WHP-EP-S, FPSO-SW-C1, FPSO-E-C, SWIFT-N1-C) forming a 1m-thick deposit at the sea floor that is bounded at its base by a major palaeosol. Comprised of rhodolith floatstone facies, this unit was deposited in intermediate (0 to 30 m) to deeper (>20 m) reef slope settings between 13 and 10 ka. Mineralogical and SEM data confirm that Unit 1 was exposed only to marine diagenesis. Unit 2 was observed across all sites, in rare cases (FPSO-NW-C) directly at the sea floor, and is marked at its top by the first major palaeosol ~79 to 80 mbsl (base of Unit 1). This unit is ~10 to 15 m-thick and characterised by a clear shallowing-upward succession. *In situ*, coralgal-dominated bindstones, framestones and bafflestones are common between ~80 to 90 mbsl and, below this, deeper reef slope, grainstone/packstone, floatstone and rudstone facies occur. Mineralogical and SEM data confirm that Unit 2 was exposed to both marine and meteoric diagenesis but reliable U/Th and ^{14}C-AMS ages from pristine corals span 36.7 to 45.8 ka at the top of this unit. A major change in lithology, assemblage and mineralogic characteristics marks the base of this unit. At sites FPSO-NW-C, FPSO-E-C, SWIFT-C and SWIFT-NI-C the second major palaeosol horizon, consisting of multiple closely spaced but distinct soil layers at the base of the unit ~90 mbsl marks the start of a second coralgal-dominated reef unit (Unit 3). Only present at these four sites, Unit 3 is a second <4 m-thick, coralgal reef-dominated unit composed of bindstones, framestones and bafflestones that were deposited in shallow-water, high-energy (0 to 5 m, reef crest-upper slope) setting, except in FPSO-E-C where deeper, more sheltered back reef settings are implied. Ages range from 44 ka to radiocarbon 'dead' and mineralogical data confirm that this reef unit is heavily diagenetically altered, recording extensive mouldic porosity and, in the case of site SWIFT-N1-C, preserving evidence of dolomitization. At the remaining sites WHP, FPSO-SW-C1, FPSO-SW-S1, FPSO-NW-C and SKUA a final distinct unit was observed based on major lithologic, sedimentary facies and mineralogic characteristics. No age data are available for Unit 4 but it is characterised entirely by detrital facies – grainstones, packstones and floatstones that were probably deposited in deeper (>20 m) platforms settings. Mineralogical and SEM data confirm that Unit 4 also was exposed to both marine and meteoric diagenesis (but no evidence of dolomitization was observed).

DISCUSSION

The history of carbonate platform development on the NWS and its relationship to sea-level and associated palaeoenvironmental changes in the region over the past 75 ka is summarised in Fig. 13. After careful sample screening that accounts for their diagenetic characteristics, stratigraphic context and growth position, the nine most reliable NWS RSL data points (including two categorised as less reliable) are shown in Fig. 13A. The authors discuss the implications of the new NWS reef core and bathymetry data in the context of other published sediment core and speleothem records (sediment flux, sea-surface temperature and precipitation) from the region and confirm the NWS is a highly complex submerged landscape characterised by multi-generational carbonate platform structures adjacent to a diverse system of palaeo-shorelines and tidal-estuarine channels. The shallow, internal chrono-stratigraphic structure of platforms records

coherent successions of shallow to deeper reef and platform facies separated by at least two subaerial exposure surfaces that the authors argue reflect the strong control of millennial-scale RSL variability during MIS 4 and MIS 3. Critically, robust U/Th dating of a shallow-water MIS 3 reef unit provides the first constraints on the magnitude of RSL at this time. Apart from a few isolated and distant locations, shallow-water reef development was never re-established regionally on the platforms.

Regional geomorphic interpretation of the submerged landscapes

Initiation and distribution of ICBs in the western Bonaparte Basin has been discussed in detail by Saqab & Bourget (2015). In short, Mesozoic tectonics, associated with Neogene reactivation, controlled the spatial distribution of ICBs by creating palaeotopographic highs in the region. Regionally, reefs were established on these highs during the MIS 15/16 transition as a result of: (1) high-amplitude sea-level fluctuations associated with the reactivation of the carbonate factory during rapid sea-level rises; and (2) drift currents bringing warm, low-salinity and nutrient-rich waters (i.e. Indonesian Throughflow; Gallagher *et al.*, 2014; Gallagher *et al.*, 2017). The combination of these parameters has shaped the 'carbonate palaeolandscape' of the study area. Once established, these carbonate build-ups acted as palaeotopographic highs that facilitated successive phases of carbonate platform growth, including the latest phase(s) of MIS 4-1 development that are the focus of this study.

The 3D seismic imagery has revealed, in unprecedented detail, a range of submerged landscapes both terrestrial and marine in origin (Figs 2 and 3). During lower glacial sea-levels (i.e. MIS 4 and 2) the platform reefs would have featured as low relief topographic highs (i.e. limestone plateaus) above a broad coastal plain (Ishiwa *et al.*, 2016). The shelf to the south of the platform is relatively narrow (8 to 10 km) and orientated towards prevailing SW swells, which dominate the present-day Western Australian coast. This area of shelf probably represented a wave dominated coastal plain with a series of regressive low relief 4 to 8 m-high ridges orientated perpendicular to the SW currently at depths from ~90 to 110 mbsl. Given the ridge orientation they probably formed under a modal SW wave climate.

The shelf seabed NE of the reef platforms exhibits a much more complex but very shallow seaward sloping surface morphology as compared to the shelf located to the SW of the reef platforms (Fig. 2). The north to north-west aspect means the shelf is protected from long period SW swells and therefore would experience a lower energy, possibly tidally dominated environment. The submerged shelf morphology shows a narrowing and termination of channels up against the northern edge of the reef platforms. The channels that deeply incise the reef platforms were probably subject to strong tidal flows during periods of lower sea-level. A complex system of channel and elongate bank features with a distinct absence of narrow meandering channel or oxbow lake morphology also occurs. Both these observations would point to an estuarine-dominated rather than fluvial-dominated coastal plain. Modern examples of such morphologies occur along the Kimberley coast in the Cambridge and Joseph Bonaparte Gulfs (Fig. 1A) and along the southern Gulf of Carpentaria. These active coastal regions are characterised by large estuarine systems dominated by extensive branching tidal channels, mangrove fringed tidal banks and extensive supratidal salt flats. Based on these modern analogues, the elevations of the inter-channel banks should approximate the intertidal zone and therefore provide a relatively narrow indicative range in which to establish a

palaeo-sea-level datum. High-resolution multibeam bathymetry data show tidal bank elevations ranging between -90 and 100 mbsl (Fig. 2). Given this elevation the timing of estuarine development probably occurred during glacial low stands MIS 4 (De Deckker *et al.*, 2019) and MIS 2 (Ishiwa *et al.*, 2019a).

Chrono-stratigraphic results indicate that the NWS reef development occurred during the MIS 3 interstadial, which separates MIS 2 and 4 glacial lowstands (Sections 5.2 to 5.4 for details). Sea-level rise from MIS 4 and into MIS 3 would have resulted in the flooding of these estuarine deposits to a depth of 20 to 30 m. This would be well within wave base of the long period SW swells and may have reworked these higher energy beach ridge sand deposits and the shelf, SW of the reef platforms. Along the lower energy northern shelf the finer sediments, which probably form the tidal channel-bank deposits, may remain undisturbed below a lower energy (shorter wave period) wave base. However, periodic high-energy wave events such as cyclones, or if the region experienced a macrotidal range similar to today, then the reworking/resuspension of these finer estuarine sediments, may have resulted in a more turbid marine environment, potentially impacting or delaying the re-establishment and growth of corals on these reef platforms. The authors lack sufficient age data to evaluate such a lag but the U/Th data confirm shallow-water, high-energy coral reef growth was established by at least 46 ka.

Chrono-stratigraphic interpretation of the units

The NWS drill transects record four chrono-stratigraphic units (Units 1 to 4; Fig. 12) that are defined by internally consistent lithologic, mineralogic, sedimentary facies, reef assemblages and chronologic changes. Fig. 13A shows the NWS platforms have had a complicated evolution over the past 75,000 yr in response to RSL changes operating at different time scales and magnitudes (interstadial/stadial and glacial/interglacial).

As a result, the platforms are characterised by multiple phases of shallow-water, high-energy interstadial-stadial reef growth and deeper-reef slope and platform deposition, bounded by periods of subaerial exposure that are spatially continuous across and between the platforms. The authors' interpretation of multi-generational reef and platform development on the NWS is consistent with other late Pleistocene studies of raised reefs in the Huon Peninsula (Chappell, 2002) and Barbados (Blanchon *et al.*, 2009) on rapidly subsiding submerged reefs in the Huon Gulf and around Hawaii (Webster *et al.*, 2009); and most recently the MIS 3-deglacial GBR shelf edge reefs sampled during IODP Exp. 325 (Gischler *et al.*, 2013; Webster *et al.*, 2018; Yokoyama *et al.*, 2018) that also record short-term, polycyclic reef deposition (and subaerial exposure) in response to precessional (20 ka) and sub-orbital, millennial timescales.

The complex history and internal architecture of the NWS platforms is visualised in Fig. 13A by plotting their probable subsidence pathway (0.2 m kyr^{-1}; Solihuddin *et al.*, 2016) back through time (sloping green rectangle and lines), with the reliable NWS RSL data (red symbols with corresponding palaeo-water depths – Table 6) and other RSL observations from the region. Unit 1 represents a chronologically well constrained period of deep-water, coralline algal-dominated deposition during a brief ~3 kyr period of the late deglacial (see Section 5.5). Unit 2 represents a significant and well constrained ~>10 kyr phase of shallow-water, high-energy coral reef during MIS 3 before its exposure and demise during the RSL fall to the LGM, which is marked by a major palaeosol horizon (see Section 5.3). Unfortunately, the lack of any reliable age

control for Units 3 and 4 make interpretation of their origins difficult. However, several lines of evidence support the interpretation that Unit 3 represents another distinct albeit brief, phase of shallow-water (<5 m) reef development prior to the MIS 4 lowstand ~65 ka (De Deckker *et al.*, 2019). Firstly, its stratigraphic position just below the deeper reef-slope facies at the base of the well-dated MIS 3 reef (Unit 2) represents a major lithologic and paleoenvironmental change (>20 m palaeowater). Secondly, the development of a second major palaeosol horizon marking this boundary (~90 mbsl), combined with Unit 3's more complex mineralogic variations, including significant dolomitization, suggest it had a very different diagenetic history as compared with Unit 2. The euhedral dolomite cement partly replacing high-Mg calcite microbial sediments is consistent with a more complex diagenetic history. Although the dolomite is yet to be studied isotopically, its sporadic nature and occurrence with preserved aragonite and high-Mg calcite are not consistent with the pervasive dolomitization associated with deeper burial or hydrothermal brines (e.g. Drivet & Mountjoy, 1997) or formation in low-energy, evaporative playa-lagoon-sabkha settings (e.g. McKenzie *et al.*, 1980). Its scattered occurrence in reef facies is most consistent with formation during early sea-level fall when mixing between sea water and subordinate freshwater occurred in a phreatic environment (e.g. Machel & Mountjoy, 1986; Strasser & Strohmenger, 1997). However, additional study is required. The authors are unable to tie Unit 3 to a specific sea-level oscillation but the most probable interpretation is that this reef was deposited before the MIS 4 lowstand ~65 ka when the platform was exposed. However, based on uniform regional subsidence rates and its shallow palaeowater depth (<5 m), it is tantalising to speculate that the Unit 3 reef could have developed during a fall in interstadial to stadial RSL, such as MIS 5c to 5b or MIS 5a to 4 (Fig. 13A). Similarly, the age of Unit 4 is unknown but its stratigraphic position (~88 to 106 mbsl) and palaeoenvironment imply that this unit was deposited on non-reefal and deeper (>20 m) platforms during one or more of the higher, interstadial sea-level intervals such as MIS 5a, 5c or less probably MIS 5e. Despite the significant meteoric diagenetic overprint(s) in Units 4 and 3, and less so Unit 2, the hyperspectral, SEM and thin section analyses confirm the presence of original aragonite coral skeleton that could be targeted for fine scale laser ablation-inductively coupled plasma-mass spectrometry to improve chronological constraints.

MIS 3 reef & platform development and palaeoenvironmental changes

The NWS cores define a new record of MIS 3 reef development on the margin (Fig. 13A). Unit 2 represents a significant 10 to 15 m-thick phase of reef development characterised by a distinct shallowing upwards sequence, from deeper fore-reef slope (>20 m water depth) at its base to very shallow, high-energy reef assemblages (<5 m water depth) at the top (Fig. 12A). Unfortunately, no reliable dates are available for the base of this sequence, so the reef turn-on age is unknown. However, U/Th ages confirm that the reef surface was within ~5 m of RSL by ~46 to 39 $\pm$ 0.2 ka, indicating a significant reduction in accommodation (>15 m) and that active vertical reef accretion took place over a sustained interval of MIS 3 time greater than 7 kyr. Environmental conditions must have been optimal for reef development and this is consistent with regional palaeoceanographic data, which indicate relatively warm and stable (~26 to 27°C) SSTs (Zuraida *et al.*, 2009) and comparatively low precipitation (van der Kaars & Deckker, 2002; van der Kaars *et al.*,

2006) and riverine flux (Stuut *et al.*, 2014) during MIS 3 (Fig. 13A).

Shallowing upwards sequences are common features of Quaternary reef systems but their interpretation is far from straightforward. They may result from the simple vertical infilling of accommodation as the reef adopts a 'catch-up' mode of growth from deeper into shallower water or, alternatively, they may be produced as a consequence of lateral reef progradation (see Camoin & Webster, 2015; Braithwaite, 2016 for recent reviews). Core recovery and age control from the NWS sites are insufficient to distinguish between shallowing upwards caused by catch-up growth in response to periods of stable or falling RSL (Fig. 13A) and lateral progradation of the system during MIS 3. However, the consistency of the shallowing upwards patterns within and between the SE and NW core transects, along with the position of most sites at/near the platform margins (Fig. 12B), argues strongly for a vertical shallowing across the platforms, and probably the entire system, over a sustained period of relatively stable sea-level at this position. This is consistent with recent interpretations of many inferred MIS 3 aged and geomorphically mature coastal landscapes (coastal barrier dunes, lagoonal systems, tidal flats and estuarine channels) that have been preserved at similar depths of 70 to 75 mbsl on the outer shelf further south off Barrow and the Montebello Islands (O'Leary *et al.*, 2020) and elsewhere around Australia (Brooke *et al.*, 2017). The NWS cores provide new evidence for extensive coral reef and carbonate platform development on the outer shelf at a similar time.

New record of MIS 3 RSL on the margin; and comparisons with other records

The NWS cores provide new constraints on RSL during MIS 3 along the margin. While there are relatively few reliable ages and given the platforms' complicated growth and exposure history (Section 5.2) in response to repeated and rapid RSL oscillations over the past ~75 ka, the authors interpret the three *in situ*, closed-system U-Th coral dates from the top of Unit 2 to reflect accurately the minimum position of RSL towards the end of MIS 3 (Fig. 13A). These data, along with the authors' palaeowater depth reconstruction (0 to 5 m) and including the modern tidal error, confirm that RSL was between 63 to 75 ± 1.8 mbsl from 45.95 to 39.23 ka $\pm$ 0.2, assuming a similar constant subsidence rate (0.2 mm yr^{-1}) reported for NWS since the LIG (Collins, 2011; Solihuddin *et al.*, 2016). It is acknowledged that by applying a more conservative palaeowater reconstruction of 0 to 10 m, RSL at this time could have been as high as 58 mbsl. Furthermore, RSL could have been even higher if the authors' interpretation was incorrect that only a little material was eroded away (i.e. is a significant section missing?) during subsequent subaerial exposure and palaeosol formation at the top of the platform when RSL fell to MIS 2 some time after ~30 ka. However, based on interpretation of similar styles of palaeosol formation observed at the top of the LIG (Dechnik *et al.*, 2017) and MIS 3 (Gischler *et al.*, 2013) GBR deposits, the authors consider this improbable. It is also not probable that significant erosion would have occurred during the deglacial reflooding stage, given the level of lithification/ cementation observed in reef Unit 2.

These uncertainties aside, the authors' preferred NWS constraints (63 to 75 ± 1.8 mbsl from 45.95 to 39.23 $\pm$ 0.2 ka) are broadly consistent with recent RSL predictions for the region (Ishiwa *et al.*, 2019a) and observations from reef terraces at the Huon Peninsula (see Hibbert *et al.*, 2016 for original data sources and a new compilation). The authors' data also support recent published observations and models of Northern Hemisphere ice sheets (Carlson *et*

al., 2018; Pico *et al.*, 2018; Dalton *et al.*, 2019) that indicate higher ESLs during MIS 3 than previously thought, based on other records such as the Red Sea isotope record (Grant *et al.*, 2012). The authors acknowledge that there are currently inadequate reliable dates from the NWS cores to constrain MIS 3 RSL further or to accurately date the end of MIS 3. However, they do represent important new MIS 3 RSL reference points with which to connect to the new history of MIS 2 sea-level variations recorded in Bonaparte Gulf sediment cores (Ishiwa *et al.*, 2019a; Fig. 1A). Together the cores imply a drop in RSL of >40 m following the end of MIS 3 to the start of the sea-level plateau at ~26 ka at ~110 mbsl, that preceded the MIS 2 minimum of ~19.7 to 19.1 ka.

Why did the shallow coral reefs fail to re-establish during deglacial-MIS 1?

Core data confirm that shallow-water coral development was unable to re-establish itself as sea-level reflooded the tops of the platforms during the deglacial. Rather, between ~13.2 and 10.7 ka deposition on the platforms was dominated by a relatively thin (~1 m) veneer of deeper, reef slope rhodolith facies (Unit 1). This facies is similar to modern rhodolith habitats that occur in water depths of >20 to 45 mbsl on the tops of adjacent banks and shoals (Barracouta and Vulcan; Heyward *et al.*, 2010), banks further to the north (Van Diemem's Rise; Anderson *et al.*, 2011) and deep fore-reef slopes to the south (Helby Bank and Osprey; Turner *et al.*, 2018). This is entirely consistent with the interpretation that they were deposited in water depths >20 m (Fig. 13A) and is supported by their common occurrence in the latter stages of coral reef and platform drowning in Late Quaternary reefs system around the world (see Webster *et al.*, 2009 for a summary). However, in case of the NWS, based on observations from drill transects, this deep-water facies was deposited directly on top of the subaerial exposure surface marking the demise of the MIS 3 reef unit.

No data are available for the adjacent Ashmore Reef, which grew to present sea-level. However, drilling data from Scott Reef further to the south (Fig. 1A) indicate that reef development occurred from 11.5 ka at a depth of 58 mbsl (Collins *et al.*, 2011). Whilst the authors cannot preclude the existence of shallow-water reef grow at depths between 60 and 75 m, these data raise the obvious question as to why reef development was not able to re-establish itself over a huge >700 km by 300 km region of available substrate provided by the older, MIS 3 reef platforms. Fig. 13C shows the seabed <80 mbsl that roughly estimates the maximum extent of any MIS 3 reefs and carbonate platform systems that would have been available substrates for subsequent deglacial-Holocene reef development. With exception of a select few reefs on the NWS (i.e. Ashmore, Cartier, Scott and Adele reefs) that re-established and were able to 'keep up' or 'catch up' to present sea-level, the authors argue that the combination of the depth of the NWS platforms at ~75 to 80 mbsl, the rate of RSL rise and poor water quality caused by the massive, influx of riverine sediments and/or sediment remobilisation at the time were what impeded reef growth in most areas. These factors are discussed in turn below.

Based on their depths and comparisons with RSL data from the Bonaparte Gulf (Ishiwa *et al.*, 2019a), the NWS platforms would probably have been reflooded by ~14 to 15 ka (Fig. 13A). This is consistent with RSL reconstructions from Sunda Shelf and Tahiti that indicate rapid sea-level rise (40 to 50 mm yr^{-1}), including the meltwater pulse event 1A (MWP-1A) at this time (Hanebuth *et al.*, 2000; Deschamps *et al.*, 2012). Furthermore, IODP Exp. 325 drilling on the GBR, while unable to provide improved constraints on MWP-1A, indicated rapid

RSL rise during this mid-deglacial (~16 to 13 ka) on the order of 20 to 60 mm yr^{-1} (Yokoyama *et al.*, 2018). Therefore, at this crucial time/depth the rate and magnitude of platform flooding may have been too rapid to allow initiation and sustained development of shallow-water reefs. However, significantly, the authors' geomorphic analysis reveals that the NWS platform tops become increasingly shallow if considering a transect towards Ashmore Reef. This implies a classical backstepping of the platform with the final expression of catch-up being Ashmore Reef and Cartier Island, despite the former being rimmed by an extensive sequence of drowned terraces between 70 to 30 mbsl (Glenn *et al.*, 2007). Thus, some other factor(s), perhaps related to their more oceanic and distal position on the outer shelf, may have allowed these few NWS reefs (including Scott and Adele) to reach present level.

The authors' review of the relevant palaeoenvironmental proxy records for the NWS (Fig. 13B) provides additional evidence that, in contrast to MIS 3, oceanographic conditions during the mid-late deglaciation were far from optimal for coral reef development. Land-based speleothems and marine sediment pollen records along the margin confirm that precipitation was very high during the mid-deglacial to the early Holocene (~15 to 8.5 ka; van der Kaars & Deckker, 2002; van der Kaars *et al.*, 2006; Denniston *et al.*, 2013). This is consistent with numerous deep sea marine sediment cores in the region that record a massive increase in riverine sediment input during that period (Stuut *et al.*, 2014; Kuhnt *et al.*, 2015) as a result of a major strengthening of the ASM caused by the southern migration of the Intertropical Convergence Zone (ITCZ; Kuhnt *et al.*, 2015; Ishiwa *et al.*, 2019b).

Significant palaeo-rivers in the region (i.e. palaeo-Fitzroy and Ord rivers, Fig. 1A) may have acted as major sources of riverine sediment at that time. Apart from enhanced riverine input, other oceanographic factors may have contributed to enhanced sediment flux via the resuspension of shelf sediments. For example, numerous large sediment waves, contourites and channels occur along the NWS between 55 to 130 m, where the sea floor may have experienced stronger bottom currents influenced by different internal waves, tides and storms during the mid-deglaciation (16.0 ka and 13.3 ka; Bischoff, 2014; Belde *et al.*, 2017). Poor water quality due to elevated sediment and nutrient flux has been implicated in the degradation and demise of numerous deglacial and Holocene reefs around the world (e.g. Montaggioni, 2005; Gischler, 2015; Webster *et al.*, 2018), but on the NWS it may have impeded re-establishment of shallow-water reef growth on the platforms during deglacial reflooding.

Regardless of which factor(s) (RSL rise rate *vs*. water quality) was most important, compared with the previous phase of high-energy, shallow-water coral reef during MIS 3, the lack of shallow-water reef growth during MIS 1 represents a major hiatus in platform building across the NWS. Excepting a few isolated reefs that were able to reach present sea-level, this vast network of submerged banks and shoals now provide highly important and diverse modern mesophotic reef habitats (Heyward, 1997; Anderson *et al.*, 2011; Moore *et al.*, 2017).

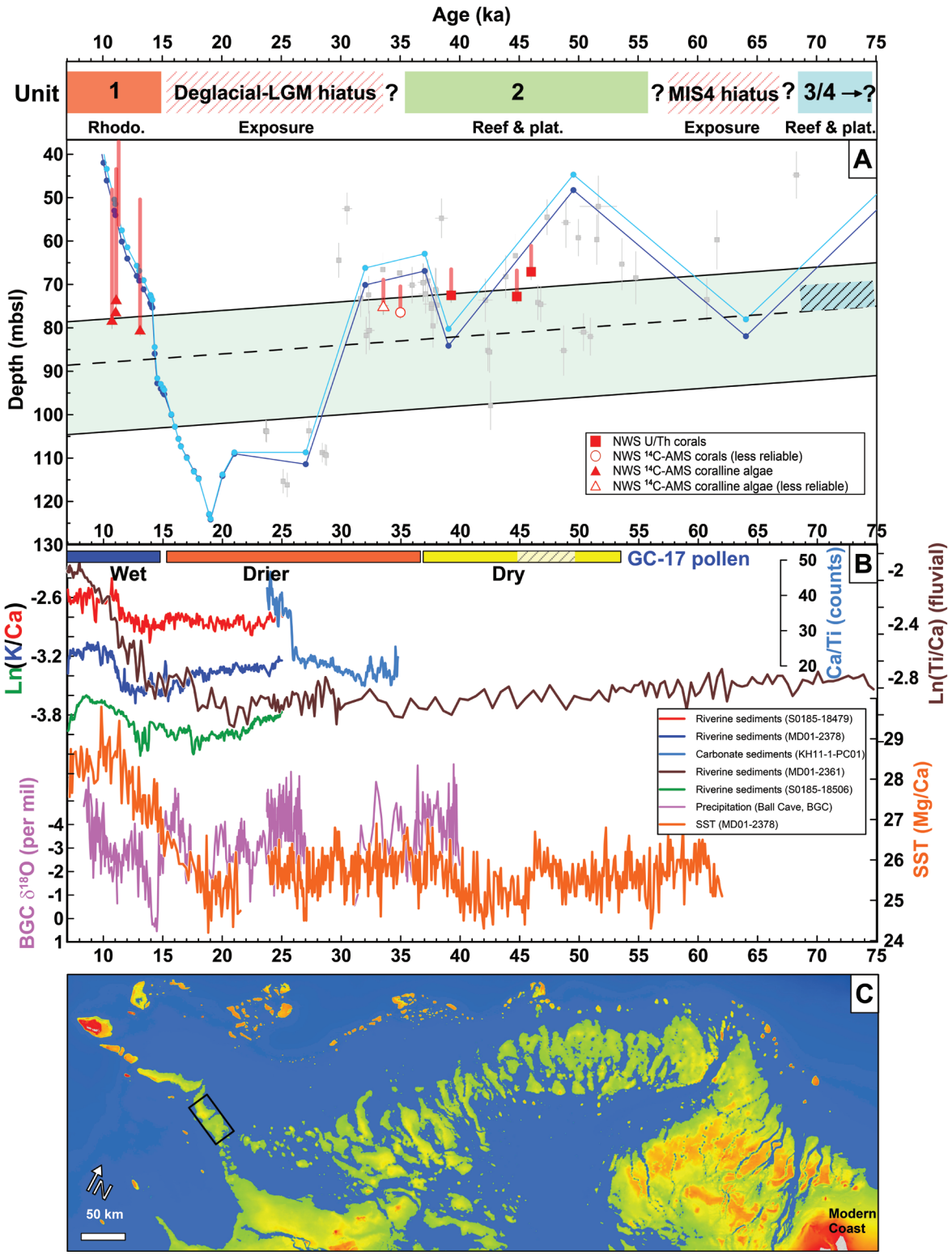


Fig. 13. Summary of the most reliable RSL observations, reef and platform development and relevant palaeoceanographic proxies from the NWS from MIS 4-1. (A) Age versus depth of reliable U/Th and ^{14}C-AMS dates, their relationship with predicted regional RSL (dark blue) and ESL (light blue) (Ishiwa *et al.*, 2019a) as well as regional subsidence (sloping green rectangle and lines) (Solihuddin *et al.*, 2016). The elevations of the NWS RSL data are corrected for regional subsidence and of the samples with paired ^{14}C-

AMS and U/Th ages only the U/Th is plotted (see Table 5). Palaeo-water depths based on reef biotic assemblages are indicated by the vertical red bars. Age and tidal uncertainties are shown or smaller than the plotted symbols. The sloping green rectangle and lines represents the probable subsidence pathway of key platform and chrono-stratigraphic unit depths (-80, -90 (dashed) and -106 mbsl). The temporal distribution of chrono-stratigraphic units (1 to 4) and their interpreted corresponding depositional stage and environment is also shown. The hatched blue rectangle represents one possible depositional depth and time of reef Unit 3; that was subsequently exposed during MIS 4 and then again during MIS 2. RSL coral data (grey squares) from the Huon Peninsula spanning MIS 3-2 are also shown (see Hibbert *et al*., 2016 original data sources). (B) Summary of relevant palaeoenvironmental proxy records for the NWS over the past 75,000 yr. See Fig. 1A for the locations of the marine sediment cores recording regional sea-surface temperatures (SST) (Zuraida *et al*., 2009; Sarnthein *et al*., 2011), riverine sediment input (Stuut *et al*., 2014; Kuhnt *et al*., 2015), carbonate sediment input (Ishiwa *et al*., 2016), pollen composition indicating wet *vs*. dry periods (van der Kaars & Deckker, 2002; van der Kaars *et al*., 2006) and land-based speleothems (Denniston *et al*., 2013) as a proxy for precipitation. Note the wet conditions and high regional, riverine input during from ~15 to 8.5 ka. (C) Visualisation showing the approximate position of the shoreline at 80 mbsl based on an extraction (>80 m blue pixels) of the available bathymetric data (Beaman, 2018) and the detailed study site (black rectangle). The green pixels represent the maximum extent of the reef and carbonate platform system that was growing during MIS 4-3 before being terminated by sea-level fall to MIS 2. Apart from the most offshore areas (Ashmore, Cartier, Adele and Scott Reefs) significant shallow-water coral reef development, at or near sea-level, was never re-established on the majority of these platforms during deglaciation and MIS 1. The position of the modern coastline relative to this -80 m shoreline visualisation is shown in grey (bottom right – Melville Island) and in Fig. 1A.

CONCLUSIONS

The NWS cores, combined with seabed geomorphology data, constrain the history of platform and shelf development as well as sea-level changes over the past 50,000 yr. The authors conclude that:

(1) The 3D seismic-derived and multibeam bathymetry datasets record a complex submerged landscape shaped by changes in sea-level, sediment input and transport pathways, together with carbonate platform development through MIS 4 to 1. Three distinct, multigenerational platforms occur between ~80 to 60 mbsl; these are rimmed semi-continuously by smaller reef terraces and bisected by deeper channels. A succession of linear palaeo-shoreline features to the SW and a complex tidal-estuarine channel system to the NE are interpreted to have formed at lower sea-levels (>90 to 110 m) during MIS 2 and 4 when the platform was exposed.

(2) The two drill transects record four chrono-stratigraphic units (Units 1 to 4) that are defined by internally consistent lithologic, mineralogic, sedimentary facies, reef assemblages and chronologic changes. Despite some missing sections, these units can be correlated up to 17 km between transects and sites at depths of ~75 and 106 mbsl; and reflect a wide range of shallow to deep depositional reef and platform settings.

(3) Chronologic data (^{14}C-AMS, U/Th ages) confirm episodic platform development that spans 10.7 to >50 ka. Repeated facies successions deposited in very shallow, high-energy reef (<5 m) and deeper fore reef slope settings (>20 m), along with clear evidence of meteoric diagenetic alteration (including two palaeosol intervals at ~80 and 90 mbsl and dolomitization at 90 to 92 mbsl in Unit 3) reflect the complex pattern of platform growth and demise (exposure) in response to repeated sea-level fluctuation from MIS 4 to MIS 1.

(4) The authors define a significant 10 to 15 m-thick coral reef-dominated phase of platform development (Unit 2) during MIS 3.

Constrained by the first reliable, closed-system U/Th ages (45.95 to 39.23 ± 0.2 ka) on the NWS, this unit records a clear shallowing upwards sequence based on reef assemblages before subaerial exposure and demise as sea-level fell to the LGM towards the end of MIS 3 ~30 ka. The age of an older, diagenetically distinct reef unit (Unit 3) is unknown but is interpreted to have developed prior to the MIS 4 lowstand ~65 ka.

(5) The NWS chronologic and palaeowater data confirm that the RSL was between ~63 to 75 ± 1.8 mbsl during MIS 3 (45.95 to 39.23 ± 0.2 ka), consistent with RSL predictions for the region and uplifted reef terraces on the Huon Peninsula. This also supports recently published observations and models of Northern Hemisphere ice sheets indicating higher ESLs during MIS 3.

(6) The platform system was unable to fully re-establish itself following reflooding during the deglacial sea-level rise. Deeper reef slope (Unit 1) facies dominate the core tops between ~13.2 to 10.7 ka, representing a major hiatus in shallow-water reef development on the platform. Unlike other margins around the world, deglacial sea-level rise was either too fast and/or other environmental conditions were unfavourable (i.e. massive riverine sediment flux due the changing monsoon and/or resuspension of shelf sediments) to allow re-establishment of shallow water coral reef development apart from on a few isolated and more distal locations (i.e. Ashmore, Cartier, Adele and Scott Reefs). The more distal locations of those reefs may provide support for the adverse water quality hypothesis on the more inshore platforms.

ACKNOWLEDGEMENTS

We thank the PTTEP Australasia for recovering the cores from the NWS and we acknowledge Dr. Alisha Thompson and Wenona School (Sydney, NSW) for the use of their SEM facilities. Financial support for this research was provided by the Australian Research Council (grants DP1094001, DP120101793). We thank Geoscience Australia for providing the 3D seismic data and Eliis for providing the PaleoScan™ software.

REFERENCES

Abbey, E., Webster, J.M., Braga, J.C., Sugihara, K., Wallace, C., Iryu, Y., Potts, D., Done, T., Camoin, G. and **Seard, C.** (2011) Variation in deglacial coralgal assemblages and their paleoenvironmental significance: IODP Expedition 310, "Tahiti Sea Level". *Global Planet. Change*, **76**, 1–15.

Abdul, N.A., Mortlock, R.A., Wright, J.D. and **Fairbanks, R.G.** (2016) Younger Dryas Sea-Level and Meltwater Pulse 1B Recorded in Barbados Reef-Crest Coral Acropora palmata. *Paleoceanography*, **31**, 330–344.

Adey, W.H., Townsend, R.A. and **Boykins, W.T.** (1982) The crustose coralline algae (Rhodophyta: Corallinaceae) of the Hawaiian Islands. *Smithson. Contrib. Mar. Sci*., **15**, 1–74.

Anderson, T., Scott Nichol, L.R., Heap, A.D., Battershill, C., Hughes, M., Vaughn Barrie, P.J.S., Alvarez de Glasby, B., Tran, M., Daniell, J. and **Shipboard Party** (2011) *Seabed Environments of the Eastern Joseph Bonaparte Gulf, Northern Australia*, Aust. Inst. Mar. Sci., 61 pp.

Apthorpe, M.C. (1988) Cainozoic Depositional History of the North West Shelf. In: *The North West Shelf, Australia Symposium* (Eds P.G. Purcell and R.R. Purcell), 1988-08-10, The Petroleum Exploration Society of Australia (PESA), Perth, pp. 55–84.

Australian Hydrographic Office (2018) *Tide Predictions for Australia*.

Bassi, D., Iryu, Y. and **Nebelsick, J.H.** (2012) To Be or Not to Be a Fossil Rhodolith? Analytical Methods for Studying Fossil Rhodolith Deposits. *J. Coastal Res*., **279**, 288–295.

Beaman, R.J. (2018) *High-resolution depth model for Northern Australia - 100 m*. James Cook University, Cairns, Australia. Available at: https://www.deepreef.org/bathymetry/219-nthaus-bathy.html.

Belde, J., Reuning, L. and **Back, S.** (2017) Bottom currents and sediment waves on a shallow carbonate shelf, Northern Carnarvon Basin, Australia. *Cont. Shelf Res*., **138**, 142–153.

Berry, P.E. (1993) Historical background, description of the physical environments of Ashmore Reef and Cartier Island and notes on exploited species. *Records of the Western Australian Museum Supplement*, **44**, 1–11.

Bird, M.I., Beaman, R.J., Condie, S.A., Cooper, A., Ulm, S. and **Veth, P.** (2018) Palaeogeography and voyage modeling indicates early human colonization of Australia was likely from Timor-Roti. *Quatern. Sci. Rev*., **191**, 431–439.

Bischoff, K. (2014) *Controls on the stratigraphic evolution of an isolated carbonate buildup setting: Quaternary example from the Timor Sea (NW Australia)*. The University of Western Australia, 93 pp.

Blanchon, P., Eisenhauer, A., Fietzke, J. and **Liebetrau, V.** (2009) Rapid sea-level rise and reef back-stepping at the close of the last interglacial highstand. *Nature*, **458**(7240), 881–884.

Bourget, J., Ainsworth, R.B., Backé, G. and **Keep, M.** (2012) Tectonic evolution of the northern Bonaparte Basin: impact on continental shelf architecture and sediment distribution during the Pleistocene. *Aust. J. Earth Sci*., **59**(6), 877–897.

Bradshaw, M.T., Yeates, A.N., Beynon, R.M., Brakel, A.T., Langford, R.P., Totterdell, J.M. and **Yeung, M.** (1988) Paleogeographic evolution of the North West shelf region; Evolution paléogéographique de la région de la plateforme nord-occidentale australienne, The North West Shelf, Australia Symposium, 1988-08-10, The Petroleum Exploration Society of Australia (PESA), Perth, pp. 29–54.

Braga, J.C., Humblet, M., Ramos, D.A.E., Dechnik, B. and Webster, J.M. Quaternary coral, coralline algal and vermetid assemblages as sea-level indicators: a review. In: *Coral Reefs and Sea-Level Change: Quaternary Records and Modelling. A Window Into the Future* (Eds G.F. Camoin and N. Hallmann), *Int. Assoc. Sedimentol. Spec. Publ*., **49** (this volume), 1–38.

Braithwaite, C.J.R. (2016) Coral-reef records of Quaternary changes in climate and sea-level. *Earth-Sci. Rev*., **156**, 137–154.

Braithwaite, C.J.R. and **Montaggioni, L.F.** (2009) The Great Barrier Reef: a 700,000 year diagenetic history. *Sedimentology*, **56**(6), 1591–1622.

Brooke, B.P., Nichol, S.L., Huang, Z. and **Beaman, R.J.** (2017) Palaeoshorelines on the Australian continental shelf: Morphology, sea-level relationship and applications to environmental management and archaeology. *Cont. Shelf Res*., **134**, 26–38.

Budd, A.F., Fukami, H., Smith, N.D. and **Knowlton, N.** (2012) Taxonomic classification of the reef coral family Mussidae (Cnidaria: Anthozoa: Scleractinia). *Zool. J. Linn. Soc*., **166**(3), 465–529.

Cabioch, G., Montaggioni, L.F., Faure, G. and **Ribaud-Laurenti, A.** (1999) Reef coralgal assemblage as recorders of paleobathymetry and sea level changes in the Indo-Pacific province. *Quatern. Sci. Rev*., **18**, 1681–1695.

Cadman, S.J. and **Temple, P.R.** (2004) Bonaparte Basin, NT, WA, AC & JPDA. *Australian Petroleum Accumulations Report*, **5**, Geoscience Australia, Canberra.

Camoin, G.F., Iryu, Y., McInroy, D.B. and **Scientists, E.** (2007) Proceedings of the Integrated Ocean Drilling Program Volume 310 Expedition Reports Tahiti Sea Level. *Proceedings of the Integrated Ocean Drilling Program*, **310**, doi:10.2204/iodp.proc.310.101.2007.

Camoin, G.F., Seard, C., Deschamps, P., Webster, J.M., Abbey, E., Braga, J.C., Iryu, Y., Durand, N., Bard, E., Hamelin, B., Yokoyama, Y., Thomas, A.L., Henderson, G.M. and **Dussouillez, P.** (2012) Reef response to sea-level and environmental changes during the last deglaciation: Integrated Ocean Drilling Program Expedition 310, Tahiti Sea Level. *Geology*, **40**(7), 643–646.

Camoin, G.F. and **Webster, J.M.** (2015) Coral reef response to Quaternary sea-level and environmental changes: State of the science. *Sedimentology*, **62**(2), 401–428.

Carlson, A.E., Tarasov, L. and **Pico, T.** (2018) Rapid Laurentide ice-sheet advance towards southern last glacial maximum limit during marine isotope stage 3. *Quatern. Sci. Rev*., **196**, 118–123.

Ceccarelli, D.M., Richards, Z.T., Pratchett, M.S. and **Cvitanovic, C.** (2011) Rapid increase in coral cover on an isolated coral reef, the Ashmore Reef National Nature Reserve, north-western Australia. *Mar. Freshw. Res.*, **62**(10).

Chappell, J. (2002) Sea level changes forced ice breakouts in the Last Glacial cycle: new results from the coral terraces. *Quatern. Sci. Rev*., **21**(10), 1229–1240.

Cheng, H., Edwards, R.L., Hoff, J., Gallup, C.D., Richards, D.A. and **Asmerom, Y.** (2000) The half-lives of uranium-234 and thorium-230. *Chem. Geol*., **169**(1), 17–33.

Chutcharavan, P.M., Dutton, A. and **Ellwood, M.J.** (2018) Seawater 234U/238U recorded by modern and fossil corals. *Geochim. Cosmochim. Acta*, **224**, 1–17.

Clark, T.R., Roff, G., Zhao, J.-x., Feng, Y.-x., Done, T.J. and **Pandolfi, J.M.** (2014) Testing the precision and accuracy of the U–Th chronometer for dating coral mortality events in the last 100 years. *Quatern. Geochronol*., **23**, 35–45.

Collins, L.B. (2011) Geological Setting, Marine Geomorphology, Sediments and Oceanic Shoals Growth History of the Kimberley Region. *J. Roy. Soc. W. Aust*., **94**, 89–105.

Collins, L.B., Testa, V., Zhao, J. and **Qu, D.** (2011) Holocene Growth History and Evolution of the Scott Reef Carbonate Platform and Coral Reef. *J. Roy. Soc. W. Aust*., **94**, 239–250.

CoralTraitDatabase (2020) Coral Trait Database. https://coraltraits.org/

Cutler, K.B., Edwards, R.L., Taylor, F.W., Cheng, H., Adkins, J., Gallup, C.D., Cutler, P.M., Burr, G.S. and **Bloom, A.** (2003) Rapid sea-level fall and deep-ocean temperature change since the last interglacial period. *Earth Planet. Sci. Lett*., **206**, 253–271.

Dalton, A.S., Finkelstein, S.A., Forman, S.L., Barnett, P.J., Pico, T. and **Mitrovica, J.X.** (2019) Was the Laurentide Ice Sheet significantly reduced during Marine Isotope Stage 3? *Geology*, **47**(2), 111–114.

De Deckker, P., Arnold, L.J., van der Kaars, S., Bayon, G., Stuut, J.-B.W., Perner, K., Lopes dos Santos, R., Uemura, R. and **Demuro, M.** (2019) Marine Isotope Stage 4 in Australasia: A full glacial culminating 65,000 years ago – Global connections and implications for human dispersal. *Quatern. Sci. Rev*., **204**, 187–207.

Dechnik, B., Webster J. M., Davies, P.J., Braga, J.C. and **Reimer, P.J.** (2015) Holocene 'turn-on' and evolution of the Southern Great Barrier Reef: Revisiting reef cores from the Capricorn Bunker Group. *Mar. Geol*., **363**, 174–190.

Dechnik, B., Webster, J.M., Webb, G.E., Nothdurft, L., Dutton, A., Braga, J.-C., Zhao, J.-x., Duce, S. and **Sadler, J.** (2017) The evolution of the Great Barrier Reef during the Last Interglacial Period. *Global Planet. Change*, **149**, 53–71.

Denniston, R.F., Wyrwoll, K.-H., Asmerom, Y., Polyak, V.J., Humphreys, W.F., Cugley, J., Woods, D., LaPointe, Z., Peota, J. and **Greaves, E.** (2013) North Atlantic forcing of millennial-scale Indo-Australian monsoon dynamics during the Last Glacial period. *Quatern. Sci. Rev*., **72**(0), 159–168.

Deschamps, P., Durand, N., Bard, E., Hamelin, B., Camoin, G., Thomas, A.L., Henderson, G.M., Okuno, J.i. and **Yokoyama, Y.** (2012) Ice-sheet collapse and sea-level rise at the Bølling warming 14,600 years ago. *Nature*, **483**(7391), 559–564.

Drivet, E. and **Mountjoy, E.W.** (1997) Dolomitization of the Leduc Formation (Upper Devonian), southern Rimbey-Meadowbrook reef trend, Alberta. *J. Sed. Res*., **67**(3), 411–423.

Dutton, A., Carlson, A.E., Long, A.J., Milne, G.A., Clark, P.U., DeConto, R., Horton, B.P., Rahmstorf, S. and **Raymo, M.E.** (2015) Sea-level rise due to polar ice-sheet mass loss during past warm periods. *Science*, **349**(6244), aaa4019.

Dutton, A. and **Lambeck, K.** (2012) Ice Volume and Sea Level During the Last Interglacial. *Science*, 337 (6091), 216–219, DOI: 10.1126/science.1205749.

Fairbanks, R.G., Mortlock, R.A., Chiu, T.-C., Cao, L., Kaplan, A., Guilderson, T.P., Fairbanks, T.W., Bloom, A.L., Grootes, P.M. and **Nadeau, M.-J.** (2005) Radiocarbon calibration curve spanning 0 to 50,000 years BP based on paired 230Th/234U/238U and 14C dates on pristine corals. *Quatern. Sci. Rev*., **24**(16-17), 1781–1796

Gallagher, S.J., Fulthorpe, C.S., Bogus, K.A. and **Scientists, E.** (2017) Expedition 356 Summary. *Proceedings of the International Ocean Discovery Program*, **356**, 43 pp.

Gallagher, S.J., Wallace, M.W., Hoiles, P.W. and **Southwood, J.M.** (2014) Seismic and stratigraphic evidence for reef expansion and onset of aridity on the Northwest Shelf of Australia during the Pleistocene. *Mar. Petrol. Geol*., **57**, 470–481.

Gallagher, S.J., Wallace, M.W., Li, C.L., Kinna, B., Bye, J.T., Akimoto, K. and **Torii, M.** (2009) Neogene history of the West Pacific Warm Pool, Kuroshio and Leeuwin currents. *Paleoceanography*, **24**(1), 1–27.

Gentilli, J. (1972) Australian Climate Patterns. Thomas Nelson, Melbourne, 285 pp.

Gischler, E. (2015) Quaternary reef response to sea-level and environmental change in the western Atlantic. *Sedimentology*, **62**(2), 429–465.

Gischler, E., Hudson, H.J., Humblet, M., Braga, J.C., Eisenhauer, A., Isaack, A., Anselmetti, F.S. and **Camoin, G.F.** (2016) Late Quaternary barrier and fringing reef development of Bora Bora (Society Islands, south Pacific): first subsurface data from Darwin's type barrier-reef system. *Sedimentology*, 1522–1549.

Gischler, E., Thomas, A.L., Droxler, A.W., Webster, J.M., Yokoyama, Y., Schöne, B.R. and **Porta, G.D.** (2013) Microfacies and diagenesis of older Pleistocene (pre-last glacial maximum) reef deposits, Great Barrier Reef, Australia (IODP Expedition 325): A quantitative approach. *Sedimentology*, **60**, 1432–1466.

Glenn, K.C. (2004) *Sedimentary processes during the Late Quaternary across the Kimberley Shelf, Northwest Australia*. PhD Thesis, The University of Adelaide, 266 pp.

Glenn, K.C., Beard, M. and **Pisel., S.** (2007) *Ashmore Reef: from Lead line to LADS*.

Glenn, K.C. and **Collins, D.** (2005) Ashmore Reefs sedimentologic and morphological response to sea level rise. *The Beagle, Records of the Museums and Art galleries of the Northern Territory Supplement*, **1**, 13–29.

Gordon, A.L. (2005) Oceanography of the Indonesian Seas and the throughflow. *Oceanography*, **4**, 14–27.

Gowan, E.J., Zhang, X., Khosravi, S., Rovere, A., Stocchi, P., Hughes, A.L.C., Gyllencreutz, R., Mangerud, J., Svendsen, J.I. and **Lohmann, G.** (2021) A new global ice sheet reconstruction for the past 80 000 years. *Nature Comms*, **12**(1), 1199.

Grant, K.M., Rohling, E.J., Bar-Matthews, M., Ayalon, A., Medina-Elizalde, M., Ramsey, C.B., Satow, C. and **Roberts, A.P.** (2012) Rapid coupling between ice volume and polar temperature over the past 150,000 years. *Nature*, **491**(7426), 744–747.

Gunn, P.J. (1988) Bonaparte Basin: evolution and structural framework. . In: P.G. Purcell and R.R. Purcell (Editors), The North West shelf, Australia. Symposium 1988-08-10, The Petroleum Exploration Society of Australia (PESA), Perth, 275–285.

Hanebuth, T., Stattegger, K. and **Grootes, P.M.** (2000) Rapid Flooding of the Sunda Shelf: A Late-Glacial Sea-Level Record. *Science*, **288**(5468), 1033–1035.

Heyward, A., Moore, C., Radford, B. and **Colquhoun, J.** (2010) Monitoring Program for the Montara Well Release Timor Sea: Final Report on the Nature of Barracouta and Vulcan Shoals. Report prepared by the *Australian Institute of Marine Science* for PTTEP Australasia (Ashmore Cartier) Pty. Ltd.

Heyward, A., Pinceratto, E. and **Smith, L.** (1997) Big Bank Shoals of the Timor sea: an environmental resource atlas. Australian Institute of Marine Science and BHP Petroleum, Townsville, 115 pp.

Hibbert, F.D., Rohling, E.J., Dutton, A., Williams, F.H., Chutcharavan, P.M., Zhao, C. and **Tamisiea, M.E.** (2016) Coral indicators of past sea-level change: A global repository of U-series dated benchmarks. *Quatern. Sci. Rev.*, **145**, 1–56.

Hirabayashi, S., Yokoyama, Y., Suzuki, A., Miyairi, Y. and **Aze, T.** (2017) Short-term fluctuations in regional radiocarbon reservoir age recorded in coral skeletons from the Ryukyu Islands in the north-western Pacific. *J. Quatern. Sci.*, **32**(1), 1–6.

Huang, D., Arrigoni, R., Benzoni, F., Fukami, H., Knowlton, N., Smith, N.D., Stolarski, J., Chou, L.M. and **Budd, A.F.** (2016) Taxonomic classification of the reef coral family Lobophylliidae (Cnidaria: Anthozoa: Scleractinia). *Zool. J. Linn. Soc*., **178**(3), 436–481.

Huang, D., Benzoni, F., Fukami, H., Knowlton, N., Smith, N.D. and **Budd, A.F.** (2014) Taxonomic classification of the reef coral families Merulinidae, Montastraeidae and Diploastraeidae (Cnidaria: Anthozoa: Scleractinia). *Zool. J. Linn. Soc*., **171**(2), 277–355.

Humblet, M., Hongo, C. and **Sugihara, K.** (2015) An identification guide to some major Quaternary fossil reef-building coral genera (Acropora,Isopora,Montipora, andPorites). *Island Arc*, **24**(1), 16–30.

Humblet, M., Potts, D.C., Webster, J.M., Braga, J.C., Iryu, Y., Yokoyama, Y., Bourillot, R., Séard, C., Droxler, A., Fujita, K., Gischler, E. and **Kan, H.** (2019) Late glacial to deglacial variation of coralgal assemblages in the Great Barrier Reef, Australia. *Global Planet. Change*, **174**, 70–91.

Humblet, M. and **Webster, J.M.** (2017) Coral community changes in the Great Barrier Reef in response to major environmental changes over glacial-interglacial timescales. *Palaeogeogr. Palaeoclimatol. Palaeoecol*., **472**, 216–235.

Iryu, Y., Nakamori, T., Matsuda, S. and **Abe, O.** (1995) Distribution of marine organisms and its geological significance in the modern reef complex of the Ryukyu Islands. *Sed. Geol*., **99**(3-4), 243–258.

Ishiwa, T., Yokoyama, Y., Miyairi, Y., Ikehara, M. and **Obrochta, S.** (2016) Sedimentary environmental change induced from late Quaternary sea-level change in the Bonaparte Gulf, northwestern Australia. *Geosci. Lett*., **3**(1).

Ishiwa, T., Yokoyama, Y., Okuno, J., Obrochta, S., Uehara, K., Ikehara, M. and **Miyairi, Y.** (2019a) A sea-level plateau preceding the Marine Isotope Stage 2 minima revealed by Australian sediments. *Sci. Rep*., **9**(1), 6449. DOI:10.1038/s41598-019-42573-4.

Ishiwa, T., Yokoyama, Y., Reuning, L., McHugh, C.M., De Vleeschouwer, D. and **Gallagher, S.J.** (2019b) Australian Summer Monsoon variability in the past 14,000 years revealed by IODP Expedition 356 sediments. *Prog. Earth Planet. Sci*., **6**(1).

James, N.P., Bone, Y., Kyser, T.K., Dix, G.R. and **Collins, L.B.** (2004) The importance of changing oceanography in controlling late Quaternary carbonate sedimentation on a high-energy, tropical, oceanic ramp: north-western Australia. *Sedimentology*, **51**(6), 1179–1205.

Keep, M. and **Haig, D.W.** (2010) Deformation and exhumation in Timor: Distinct stages of a young orogeny. *Tectonophysics*, **483**(1), 93–111.

Kiessling, W., Simpson, C., Beck, B., Mewis, H. and **Pandolfi, J.M.** (2012) Equatorial decline of reef corals during the last Pleistocene interglacial. *Proc. Natl. Acad. Sci. USA*, **109**(52), 21378–21383.

Kordi, M.N. and **O'Leary, M.** (2016) Geomorphic classification of coral reefs in the north western Australian shelf. *Regional Studies in Marine Science*, **7**, 100–110.

Kospartov, M., Beger, M., Ceccarelli, D.M. and **Richards, Z.T.** (2006) *An assessment of the distribution and abundance of sea cucumbers trochus giant clams coral fish and invasive marine species at Ashmore reef national nature reserve and Cartier island marine reserve: 2005, The Department of Environment and heritage*. Report issued by the Department of the Environment and Heritage, Canberra, 298 pp.

Kuhnt, W., Holbourn, A., Xu, J., Opdyke, B., De Deckker, P., Röhl, U. and **Mudelsee, M.** (2015) Southern Hemisphere control on Australian monsoon variability during the late deglaciation and Holocene. Nat Commun, **6**, 5916.

Longley, I.M., Buessenschuett, C., Clydsdale, L., Cubitt, C.J., Davis, R.C., Johnson, M.K., Marshall, N.M., Murray, A.P., Somerville, R., Spry, T.B. and **Thompson, N.B.** (2002) The North West Shelf of Australia - a Woodside perspective. . In: S.J. Moss and M. Keep (Editors), The sedimentary basins of Western Australia 3. Petroleum Exploration Society of Australia., pp. 27–88.

Ludwig, K. (2012) *Isoplot 3.75–4.15: a geochronological toolkit for Microsoft Excel*. Berkeley Geochronology Center Special Publication. Berkeley, California, 75 pp.

Lund, M.J., Davies, P.J. and **Braga, J.C.** (2000) Coralline algal nodules off Fraser Island, eastern Australia. *Facies*, **42**, 25–34.

Machel, H.-G. and **Mountjoy, E.W.** (1986) Chemistry and Environments of Dolomitization - A Reappraisal. *Earth-Sci. Rev.*, **23**(3), 175–222.

Marshall, N.G. and **Lang, S.C.** (2013) A new sequence stratigraphic framework for the North West Shelf, Australia. . In: *The Sedimentary Basins of Western Australia 4* (Eds M. Keep and S.J. Moss), *Proceedings of the Petroleum Exploration Society of Australia Symposium*, pp. 1–31.

Matsuda, S. and **Iryu, Y.** (2011) Rhodoliths from deep fore-reef to shelf areas around Okinawa-jima, Ryukyu Islands, Japan. *Mar. Geol.*, **282**(3-4), 215–230.

McCaffrey, J.C., Wallace, M.W. and **Gallagher, S.J.** (2020) A Cenozoic Great Barrier Reef on Australia's North West shelf. *Global Planet. Change*, **184**. https://doi.org/10.1016/j.gloplacha.2019.103048

McKenzie, J.A., Hsü, K.J., Schneider, J.F., Zenger, D.H., Dunham, J.B. and **Ethington, R.L.** (1980) *Movement of Subsurface Waters Under the Sabkha, Abu Dhabi, UAE and its Relation to Evaporative Dolomite Genesis, Concepts and Models of Dolomitization*. SEPM Soc. Sed. Geol., pp. 20.

Medina-Elizalde, M. (2013) A global compilation of coral sea-level benchmarks: Implications and new challenges. *Earth Planet. Sci. Lett.*, **362**(0), 310–318.

Montaggioni, L.F. (2005) History of Indo-Pacific coral reef systems since the last glaciation: Development patterns and controlling factors. *Earth-Sci. Rev.*, **71**(1–2), 1.

Moore, C., Cappo, M., Radford, B. and **Heyward, A.** (2017) Submerged oceanic shoals of north Western Australia are a major reservoir of marine biodiversity. *Coral Reefs*, **36**(3), 719–734.

Mory, A.J. (1991) Geology of the Offshore Bonaparte Basin, Northwestern Australia. *Geol. Surv. W. Austr. Report*, **29**, 47 pp.

Murphy, R.J., Van Kranendonk, M.J., Baumgartner, R. and **Ryan, C.** (2021) Biogenicity of Spicular Geyserite from Te Kopia, New Zealand: Integrated Petrography, High-Resolution Hyperspectral and Elemental Analysis. *Astrobiology*, 115–135.

Murphy, R.J., Webster, J.M., Nothdurft, L., Dechnik, B., McGregor, H.V., Patterson, M.A., Sanborn, K.L., Webb, G.E., Kearney, L.I., Rintoul, L. and **Erler, D.V.** (2017) High-resolution hyperspectral imaging of diagenesis and clays in fossil coral reef material: a nondestructive tool for improving environmental and climate reconstructions. Geochem. Geophys. Geosyst., 18(8), 3209–3230.

Nicholas, W.A., Nichol, S.L., Howard, F.J.F., Picard, K., Dulfer, H., Radke, L.C., Carroll, A.G., Tran, M. and **Siwabessy, P.J.W.** (2014) Pockmark development in the Petrel Sub-basin, Timor Sea, Northern Australia: Seabed habitat mapping in support of CO2 storage assessments. *Cont. Shelf Res.*, **83**, 129–142.

Nothdurft, L.D. and **Webb, G.E.** (2009) Earliest diagenesis in scleractinian coral skeletons: implications for palaeoclimate-sensitive geochemical archives. *Facies*, **55**(2), 161–201.

O'Brien, G.W., Etheridge, M.A., Willcox, J.B., Morse, M., Symonds, P., Norman, C. and **Needham, D.J.** (1993) The structural architecture of the Timor Sea, North-Western Australia: implications for basin development hydrocarbon exploration. *The APPEA Journal*, **33**(1), 258–279.

O'Brien, G.W., Lisk, M., Duddy, I., Eadington, P.J., Cadman, S. and **Fellows, M.** (1996) Late Tertiary fluid migration in the Timor Sea: A key control on thermal and diagenetic histories? *The APPEA Journal*, **36**(1), 399–427.

O'Leary, M.J., Paumard, V. and **Ward, I.** (2020) Exploring Sea Country through high-resolution 3D seismic imaging of Australia's NW shelf: Resolving early coastal landscapes and preservation of underwater cultural heritage. *Quatern. Sci. Rev.*, **239**, 10.

OBIS (2020) OBIS (Ocean Bioversity Information System). https://obis.org/

Parker, J.H. (2009) Taxonomy of foraminifera from Ningaloo reef, Western Australia. *Assoc. Australs. Palaeontol. Mem.*, **36**. 767–784.

Patillo, J. and **Nicholls, P.J.** (1990) A tectonostratigraphic framework for the Vulcan Graben, Timor Sea region. *APPEA J.*, **30**(1), 27–51.

Paumard, V., Bourget, J., Durot, B., Lacaze, S., Payenberg, T., George, A.D. and **Lang, S.** (2019b) Full-volume 3D seismic interpretation methods: A new step towards high-resolution seismic stratigraphy. *Interpretation*, **7**(3), B33–B47.

Paumard, V., Bourget, J., Lang, S., Wilson, T., Riera, R., Gartrell, A., Vakarelov, B.K., O'Leary, M. and **George, A.** (2019a) Imaging past depositional environments of the North West Shelf of Australia: Lessons from 3D seismic data. In: *The Sedimentary Basins of Western Australia V: Proceedings of the Petroleum Exploration Society of Australia Symposium* (Ed. S.M.M. Keep), Petroleum Exploration Society of Australia., Perth, pp. 30.

Paumard, V., Bourget, J., Payenberg, T., Ainsworth, R.B., George, A.D., Lang, S., Posamentier, H.W. and **Peyrot, D.** (2018) Controls on shelf-margin architecture and sediment partitioning during a syn-rift to post-rift transition: Insights from the Barrow Group (Northern Carnarvon Basin, North West Shelf, Australia). *Earth-Sci. Rev.*, **177**, 643–677.

Payri, C., N'Yeurt, A. and **Orempuller, J.** (2000) *Algues de Polynésie française: Algae of French Polynesia*. Au Vent de Iles, Editions Tahiti, S.N. Des Editions Vilo, 320 pp.

Peltier, W.R. and **Fairbanks, R.G.** (2006) Global glacial ice volume and Last Glacial Maximum duration from an extended Barbados sea level record. *Quatern. Sci. Rev.*, **25**(23–24), 3322–3337.

Pico, T., Birch, L., Weisenberg, J. and **Mitrovica, J.X.** (2018) Refining the Laurentide Ice Sheet at Marine Isotope Stage 3: A data-based approach combining glacial isostatic simulations with a dynamic ice model. *Quatern. Sci. Rev.*, **195**, 171–179.

Precht, W.F. and **Aronson, R.B.** (2016) Stability of Reef-Coral Assemblages in the Quaternary. In: *Coral Reefs at the Crossroads* (Eds D.K. Hubbard, C.S. Rogers, J.H. Lipps, G.D. Stanley Jr.),. Springer, Netherlands: Dordrecht, pp. 155–173.

Purcell, P.G. and **Purcell, R.R.** (1988) The North West Shelf, Australia - An Introduction. In: *The North West shelf, Australia. Symposium*, 1988-08–10 (Eds P.G. Purcell and R.R. Purcell), PESA, Perth, pp. 3–15.

Renema, W. (2003) Larger foraminifera on reefs around Bali (Indonesia). *Zoologische Verhandelingen*, **345**(31), 337–366.

Renema, W. (2010) Is increased calcarinid (foraminifera) abundance indicating a larger role for macro-algae in Indonesian Plio-Pleistocene coral reefs? *Coral Reefs*, **29**(1), 165–173.

Renema, W. (2018) Terrestrial influence as a key driver of spatial variability in large benthic foraminiferal assemblage composition in the Central Indo-Pacific. *Earth-Sci. Rev.*, **177**, 514–544.

Renema, W. and **Troelstra, S.R.** (2001) Larger foraminifera distribution on a mesotrophic carbonate shelf in SW Sulawesi (Indonesia). *Palaeogeogr. Palaeoclimatol. Palaeoecol.*, **175**, 125–146.

Richards, Z. (2016) *The Coral Compactus: Western Australia; Hard Coral Genus Identification Guide*; Version 1.1. Publication URL: http://museum.wa.gov.au/explore/articles/wa-coral-compactus

Richards, Z., Beger, M., Hobbs, J.-P., Bowling, T., Chong-Seng, K. and **Pratchett, M.** (2009) Ashmore reef national nature reserve and Cartier island marine reserve marine survey 2009, Department of the Environment, Water Heritage & the Arts, JCU.

Rosenthal, Y., Holbourn, A.E., Kulhanek, D.K. and **Expedition 363 Scientists** (2018) Western Pacific Warm Pool. *Proceedings of the International Ocean Discovery Program*, **363**. http://publications.iodp.org/proceedings/363/363title.html

Salas-Saavedra, M., Dechnik, B., Webb, G.E., Webster, J.M., Zhao, J.-x., Nothdurft, L.D., Clark, T.R., Graham, T. and **Duce, S.** (2018) Holocene reef growth over irregular Pleistocene karst confirms major influence of hydrodynamic factors on Holocene reef development. *Quatern. Sci. Rev.*, **180**, 157–176.

Sanborn, K.L., Webster, J.M., Webb, G.E., Braga, J.C., Humblet, M., Nothdurft, L., Patterson, M.A., Dechnik, B., Warner, S., Graham, T., Murphy, R.J., Yokoyama, Y., Obrochta, S.P., Zhao, J.-X. and **Salas-Saavedra, M.** (2020) A new model of Holocene reef initiation and growth in response to sea-level rise on the Southern Great Barrier Reef. *Sed. Geol.*, **397**.

https://doi.org/10.1016/j.sedgeo.2019.105556.

Sandiford, M. (2007) The tilting continent: A new constraint on the dynamic topographic field from Australia. *Earth Planet. Sci. Lett*., **261**(1), 152–163.

Saqab, M.M. and **Bourget, J.** (2015) Controls on the distribution and growth of isolated carbonate build-ups in the Timor Sea (NW Australia) during the Quaternary. *Mar. Petrol. Geol*., **62**, 123–143.

Saqab, M.M. and **Bourget, J.** (2016) Seismic geomorphology and evolution of early–mid Miocene isolated carbonate build-ups in the Timor Sea, North West Shelf of Australia. *Mar. Geol*., **379**, 224–245.

Saqab, M.M., Bourget, J., Trotter, J. and **Keep, M.** (2017) New constraints on the timing of flexural deformation along the northern Australian margin: Implications for arc-continent collision and the development of the Timor Trough. *Tectonophysics*, **696–697**, 14–36.

Sarnthein, M., Grootes, P.M., Holbourn, A., Kuhnt, W. and **Kühn, H.** (2011) Tropical warming in the Timor Sea led deglacial Antarctic warming and atmospheric CO2 rise by more than 500yr. *Earth Planet. Sci. Lett*., **302**(3-4), 337–348.

Sasaki, K., Omura, A., Miwa, T., Tsuji, Y., Matsuda, H., Nakamori, T., Iryu, Y., Yamada, T., Sato, Y. and **Nakagawa, H.** (2006) 230Th/234U and 14C dating of a lowstand coral reef beneath the insular shelf off Irabu Island, Ryukyus, southwestern Japan. *Island Arc*, **15**(4), 455–467.

Sasaki, K., Omura, A., Murakami, K., Sagawa, N. and **Nakamori, T.** (2004) Interstadial coral reef terraces and relative sea-level changes during marine oxygen isotope stages 3–4, Kikai Island, central Ryukyus, Japan. *Quatern. Int*., **120**(1), 51–64.

Shuster, M.W., Eaton, S., Wakefield, L.L. and **Kloosterman, H.J.** (1998) Neogene Tectonics greater Timor Sea, offshore Australia: applications for trap risk. *The APPEA Journal*, **38**(1), 351–379.

Siddall, M., Rohling, E.J., Thompson, P.R. and **Waelbroeck, C.** (2008) Marine isotope stage 3 sea level fluctuations: Data synthesis and new outlook. *Rev. Geophys*., 46(RG4003,), doi:10.1029/2007RG000226.

Solihuddin, T., Bufarale, G., Blakeway, D. and **O'Leary, M.J.** (2016) Geomorphology and late Holocene accretion history of Adele Reef: a northwest Australian mid-shelf platform reef. *Geo-Mar. Lett*., **36**(6), 465–477.

Solihuddin, T., Collins, L.B., Blakeway, D. and **O'Leary, M.J.** (2015) Holocene coral reef growth and sea level in a macrotidal, high turbidity setting: Cockatoo Island, Kimberley Bioregion, northwest Australia. *Mar. Geol*., **359**, 50–60.

Strasser, A. and **Strohmenger, C.** (1997) Early diagenesis in Pleistocene coral reefs, southern Sinai, Egypt: response to tectonics, sea-level and climate. *Sedimentology*, **44**, 537–558.

Stuiver, M., Reimer, P.J. and **Reimer, R.W.** (2020) CALIB 8.2 [WWW program] at http://calib.org, accessed 2020-11-12.

Sturman, A. and **Tapper, N.** (2005) *The weather and climate of Australia and New Zealand*. Oxford University Press, Melbourne, 541 pp.

Stuut, J.-B.W., Temmesfeld, F. and **De Deckker, P.** (2014) A 550 ka record of aeolian activity near North West Cape, Australia: inferences from grain-size distributions and bulk chemistry of SE Indian Ocean deep-sea sediments. *Quatern. Sci. Rev*., **83**, 83–94.

Tager, D., Webster, J.M., Potts, D.C., Renema, W., Braga, J.C. and **Pandolfi, J.M.** (2010) Community dynamics of Pleistocene coral reefs during alternative climatic regimes. *Ecology*, **91**(1), 191–200.

Taylor, F.W., Mann, P., Bevis, M.G., Edwards, R.L., Cheng, H., Cutler, K.B., Gray, S.C., Burr, G.S., Beck, J.W., Phillips, D.A., Cabioch, G. and **Récy, J.** (2005) Rapid forearc uplift and subsidence caused by impinging bathymetric features: Examples from the New Hebrides and Solomon arcs. *Tectonics*, **24**(6), TC6005.

Thomas, A.L., Henderson, G.M., Deschamps, P., Yokoyama, Y., Mason, A.J., Bard, E., Hamelin, B., Durand, N. and **Camoin, G.** (2009) Penultimate Deglacial Sea-Level Timing from Uranium/Thorium Dating of Tahitian Corals. *Science*, **324**(5931), 1186–1189.

Toth, L.T., Aronson, R.B., Cobb, K.M., Cheng, H., Edwards, R.L., Grothe, P.R. and **Sayani, H.R.** (2015) Climatic and biotic thresholds of coral-reef shutdown. *Nature Climate Change*, **5**(4), 369–374.

Turner, J.A., Babcock, R.C., Hovey, R. and **Kendrick, G.A.** (2018) Can single classifiers be as useful as model ensembles to produce benthic seabed substratum maps? *Estuar. Coast. Shelf Sci*., **204**, 149–163.

Twiggs, E.J. and **Collins, L.B.** (2010) Development and demise of a fringing coral reef during Holocene environmental change, eastern Ningaloo Reef, Western Australia. *Mar. Geol*., **275**(1–4), 20–36.

van der Kaars, S. and **Deckker, P.** (2002) A Late Quaternary pollen record from deep-sea core Fr10/95, GC17 offshore Cape Range Peninsula, northwestern Western Australia. *Rev. Palaeobot. Palynol*., **120**, 17–39.

van der Kaars, S., De Deckker, P. and **Gingele, F.X.** (2006) A 100 000-year record of annual and seasonal rainfall and temperature for northwestern Australia based on a pollen record obtained offshore. *J. Quatern. Sci*., **21**(8), 879–889.

Verheij, E. (1994) Nongeniculate Corallinaceae (Corallinales, Rhodophyta) from the spermonde Archipelago, SW Sulawesi, Indonesia. *Blumea: Biodiver. Evol. Biogeogr. Plants*, **39**(1/2), 95–137.

Veron, J.E.N. and **Pichon, M.** (1979) Scleractinia of Eastern Australia. Part III Families Agariciidae, Siderastreidae, Fungiidae, Oculinidae, Merlinidae, Mussidae, Pectiniidae, Caryophylliidae, Dendrophylliidae. *Aust. Inst. Mar. Sci. Monogr*., **4**, 422 pp. DOI: https://doi.org/10.5962/bhl.title.60646

Veron, J.E.N. and **Stafford-Smith. M** (2000) *Corals of the world*. Aust. Inst. Mar. Sci. and CRR, 3 vols.

Veron, J.E.N. and **Wallace, C.** (1984) Scleractinia of Eastern Australia. Part V Families Acroporidae. *Aust. Inst. Mar. Sci. Monogr*., **6**, 485 pp.

Wallace, C. (1999) *Staghorn Corals of the World: A Revision of the Genus Acropora*. CSIRO Publishing, 421 pp..

Webster, J.M., Braga, J.C., Clague, D.A., Gallup, C., Hein, J.R., Potts, D.C., Renema, W., Riding, R., Riker-Coleman, K., Silver, E. and **Wallace, L.M.** (2009) Coral reef evolution on rapidly subsiding margins. *Global Planet. Change*, **66**(1–2), 129–148.

Webster, J.M., Braga, J.C., Humblet, M., Potts, D.C., Iryu, Y., Yokoyama, Y., Fujita, K., Bourillot, R., Esat, T.M., Fallon, S., Thompson, W.G., Thomas, A.L., Kan, H., McGregor, H.V., Hinestrosa, G., Obrochta, S.P. and **Lougheed, B.C.** (2018) Response of the Great Barrier Reef to sea-level and

environmental changes over the past 30,000 years. *Nature Geosci*., **11**(6), 426–432.

Weinmann, A.E., Rödder, D., Lötters, S. and **Langer, M.R.** (2013) Heading for New Shores: Projecting Marine Distribution Ranges of Selected Larger Foraminifera. *PLOS ONE*, **8**(4), e62182.

Whittam, D.B., Norvick, M.S. and **Mclntyre, C.L.** (1996) Mesozoic and Cainozoic Tectonostratigraphy of Western ZOCA and Adjacent Areas. *The APPEA Journal*, **36**(1), 209–232.

Woodroffe, C.D. and **Webster, J.M.** (2014) Coral reefs and sea-level change. *Mar. Geol*., **352**, 248–267.

Yokoyama, Y., Esat, T.M. and **Lambeck, K.** (2001) Coupled climate and sea-level changes deduced from Huon Peninsula coral terraces of the last ice age. *Earth Planet. Sci. Lett*., **193**(3-4), 579–587.

Yokoyama, Y., Esat, T.M., Lambeck, K. and **Fifield, L.K.** (2000) Last Ice Age Millennial Scale Climate Changes Recorded in Huon Peninsula Corals. *Radiocarbon*, **42**(3), 383–401.

Yokoyama, Y., Esat, T.M., Thompson, W.G., Thomas, A.L., Webster, J.M., Miyairi, Y., Sawada, C., Aze, T., Matsuzaki, H., Okuno, J.i., Fallon, S., Braga, J.-C., Humblet, M., Iryu, Y., Potts, D.C., Fujita, K., Suzuki, A. and **Kan, H.** (2018) Rapid glaciation and a two-step sea level plunge into the Last Glacial Maximum. *Nature*, **559**, 603–607.

Yokoyama, Y., Koizumi, M., Matsuzaki, H., Miyairi, Y. and **Ohkouchi, N.** (2010) Developing Ultra Small-Scale Radiocarbon Sample Measurement at the University of Tokyo. *Radiocarbon*, **52**(2), 310–318.

Yokoyama, Y., Miyairi, Y., Matsuzaki, H. and **Tsunomori, F.** (2007) Relation between acid dissolution time in the vacuum test tube and time required for graphitization for AMS target preparation. *Nuclear Instruments & Methods in Physics Research Section B-beam Interactions With Materials and Atoms*, **259**, 330–334.

Zhao, J.-x., Neil, D.T., Feng, Y.-x., Yu, K.-f. and **Pandolfi, J.M.** (2009) High-precision U-series dating of very young cyclone-transported coral reef blocks from Heron and Wistari reefs, southern Great Barrier Reef, Australia. *Quatern. Int*., **195**(1-2), 122–127.

Zuraida, R., Holbourn, A., Nürnberg, D., Kuhnt, W., Dürkop, A. and **Erichsen, A.** (2009) Evidence for Indonesian Throughflow slowdown during Heinrich events 3–5. *Paleoceanography*, **24**(2), PA2205.

IAS (2022) Coral Reefs and Sea-Level Change: Quaternary Records and Modelling, 275–317

Neogene and Quaternary reef terraces of Mangaia, Rarotonga and Aitutaki (southern Cook Islands, South Pacific) revisited: gauges of sea-level change and island uplift?

EBERHARD GISCHLER[*], GABRIELA MEYER[†], JUAN CARLOS BRAGA[‡], SYLVIA RIECHELMANN[§], ADRIAN IMMENHAUSER[§#] and ANTON EISENHAUER[¶]

[*]*Institut für Geowissenschaften, Goethe-Universität, Altenhöferallee 1, 60438 Frankfurt am Main, Germany.*
[†]*Institut für Theoretische Physik, Goethe-Universität, Max-von-Laue-Strasse 1, 60438 Frankfurt am Main, Germany.*
[‡]*Departamento di Estratigrafia y Paleontologia, Universidad de Granada, 18002 Granada, Spain*
[§]*Institut für Geologie, Mineralogie und Geophysik, Ruhr-Universität Bochum, Universitätsstrasse 150, 44801 Bochum, Germany.*
[#]*Fraunhofer Research Institution for Energy Infrastructure and Geothermal Systems IEG, Am Hochschulcampus 1, 44801 Bochum, Germany.*
[¶]*GEOMAR, Wischhofstrasse 1-3, 24148 Kiel, Germany.*

ABSTRACT

New sedimentological data of facies and diagenesis as well as chronological data including strontium ($^{87}Sr/^{86}Sr$)-isotope ratios and uranium (U)-series dating, radiocarbon (^{14}C) accelerator mass spectrometry (AMS) dating and biostratigraphy from elevated reef terraces (makatea) in the southern Cook Islands of Mangaia, Rarotonga and Aitutaki contribute to controversial discussions regarding age and sea-level relationships of these occurrences during the Neogene and Quaternary. The oldest limestones of the uplifted makatea island of Mangaia include reef-related facies which are mid-Miocene in age, based on new Sr-isotope and biostratigraphical data. In between these older deposits and the lowest coastal reef terrace of marine isotope stage (MIS) 5e, various older Pleistocene reef-related facies were identified. Based on Sr-isotope ratios, these were deposited during earlier Pleistocene highstands (as old as 2.28 Ma). Rare reef terraces on Rarotonga belong to the Plio-Pleistocene and the late Miocene, according to $^{87}Sr/^{86}Sr$ ratios. The late Miocene age is enigmatic as it exceeds the age of subaerially exposed volcanic rocks of Rarotonga island. The fossil reef could have formed on an older submarine volcanic high that was later displaced by younger volcanism to its present position, or the Sr-age could be too old due to diagenetic resetting. The Plio-Pleistocene Rarotonga reef terraces are overlain irregularly by Holocene reef deposits that are interpreted as storm rubble. Reef terraces on Aitutaki represent evidence of a higher-than-present (up to 1 m) sea-level during the late Holocene, based on ^{14}C AMS age data. They are very similar to elevated late Holocene reefs of adjacent French Polynesia with regard to composition, elevation and age.

©2022 International Association of Sedimentologists

INTRODUCTION

Changes in relative sea-level are of paramount significance for mankind. This holds true especially for those people who live at or close to sea-level. In particular, the mere existence of most of the 58 so-called Small Island Developing States (SIDS) and the 39 members of the intergovernmental organisation of the Alliance of Small Island States (AOSIS) is dependent on sea-level and its fluctuations. The Cook Islands, along with many other, mostly tropical, nations are a member of both SIDS and AOSIS. In light of the predicted rise in sea-level during the 21st century, both the ca 65 million people of the SIDS and the >600 million people, i.e. close to 10% of the world's population, living in coastal areas <10 m above sea-level are threatened to lose their homeland and their livelihood (IPCC, 2014). From a scientific point of view, tropical islands, especially coral-reef islands, are unique dipsticks of late Quaternary sea-level change, which may potentially be used for past sea-level reconstructions that are also essential for future predictions. Therefore, fossil tropical coral reefs elevated above modern sea-level have been used successfully to constrain sea-level fluctuations in the Quaternary (Woodroffe & Webster, 2014; Camoin & Webster, 2015; and references therein).

The most prominent and best studied examples of Quaternary coral reef terraces include Barbados, western Atlantic (Mesolella *et al*., 1969; Schellmann & Radtke, 2004), and the Huon Peninsula, western Pacific (Chappell, 1974; Chappell & Shackleton, 1986), both located in areas of tectonic uplift adjacent to subduction zones. The Cook Islands represent another highly interesting research location as they include a variety of reef and island types including elevated reef deposits reaching as far back as the Miocene, thereby rendering them among the oldest islands on the Pacific lithospheric plate. Inherent problems of using fossil reefs as sea-level gauges may include the taphonomy of reef builders including redeposition (Blanchon & Perry, 2004), the bathymetrical range of depth-indicative corals that may amount to several metres (Abbey *et al*., 2011; Braga *et al*., 2022), uncertainties in the context of glacial isostatic adjustment (GIA) that increase with increasing age of the deposits considered (Dutton *et al*., 2015), lithospheric flexuring and subsidence and uplift in the vicinity of larger volcanic islands (McNutt & Menard, 1978), temporal limitations of U-series and ^{14}C-dating, and finally diagenetic alteration of dated material such as corals the skeletons of which consist of metastable aragonite.

Fossil, exposed coral reefs in the Cook Islands, tropical South Pacific, which represent a far-field site with regard to GIA, have been proven to be useful as Quaternary sea-level gauges and in reconstructions of lithospheric flexure and uplift in the past (e.g. Woodroffe *et al*., 1990, 1991). Still, uncertainty and controversy exist with regard to the age of the reef terraces of the Neogene-Quaternary makatea island of Mangaia, the age of elevated reefs of the volcanic island of Rarotonga and the Holocene sea-level indicators of the almost-atoll Aitutaki. For these reasons, the authors have revisited elevated reef sites in the southern Cook Islands and detailed their occurrences, their petrography and facies; and present new absolute age data using radiogenic Sr-isotope ratios, U-series and ^{14}C AMS dating as well as biostratigraphy.

STUDY AREA

The islands of Mangaia, Rarotonga and Aitutaki belong to the Cook Island archipelago, which comprises fifteen islands, divided into northern and southern groups (Fig. 1). The southern islands, including Mangaia, Rarotonga and Aitutaki, are part of

the Cook-Austral island hotspot chain (Hein *et al*., 1997). The chain appears to have a compound character, though, except for Mangaia, all other islands are too young to agree with a uniform hotspot model (Dickinson, 1998). Rarotonga, the largest and youngest of the Cook Islands, has been put forward as a classical example of causing lithospheric loading, flexuring and uplift of some of the older, surrounding reefs and islands in the southern chain (McNutt & Menard, 1978). However, it was pointed out, and in part with controversial results, that the flexural model does not satisfactorily explain the responses of the southern Cook Islands with regard to their ages and elevations (Lambeck, 1981; Spencer *et al*., 1987, 1988; Woodroffe *et al*., 1991; Dickinson, 1998).

The Cook Islands are located in the trade-wind belt and winds from the south-east and east predominate. Air temperatures range between 22 and 30° C. Annual precipitation amounts to ca. 2000 mm yr^{-1}. It is highest during December to March and ranges from 80 to 260 mm $month^{-1}$ (Stoddart & Gibbs, 1975). Water temperatures in the southern Cook Islands range between 25.5 and 27.3° C. The study area is microtidal with spring tide amplitudes of 0.5 m and neap tide amplitudes of 0.1 m (Stoddart & Gibbs, 1975).

Mangaia (Fig. 2) covers some 52 km^2, rises to 169 m above sea-level and is considered to be the oldest island on the Pacific plate. Mangaia has a central volcanic hill dated to 17.0 to 19.4 Ma, i.e. early Miocene (Dalrymple *et al*., 1975; Turner & Jarrard, 1982), surrounded by a swampy depression where taro is grown and an up to 70 m-high limestone platform of Neogene – Quaternary age, characterising it as a typical makatea island (Cotton, 1969; Wood & Hay, 1970; Stoddart *et al*., 1985). A Miocene age for the oldest limestones on the island is based on the findings of foraminifers belonging to the genus *Lepidocyclina* (Marshall, 1927). Early researchers have agreed on uplift of the island but controversially discussed the origin of the limestone platform. Marshall (1927, 1929) and Davis (1928, p. 403–408) interpreted Mangaia as an uplifted barrier-reef system whereas Chubb (1927) and Hoffmeister (1930) suggested karst erosion as the origin of the geomorphological depression between volcanics and limestone rim. This latter view was convincingly adopted by Wood & Hay (1970), Stoddart *et al*. (1985) and Purdy & Winterer (2006). Mangaia is surrounded by a modern fringing reef. Analyses of the modern reef platform, including elevated micro-atolls, suggest a higher-than-present sea-level during the late Holocene (Yonekura *et al*., 1988). The outer margin of the makatea platform is terraced (Marshall, 1927; Schofield, 1967; Wood, 1967; Wood & Hay, 1970; Ward *et al*., 1971; Stoddart *et al*., 1985). There is an up to 12 m-high lower cliff at the coast. Radiometric dating of this terrace has yielded late Pleistocene (marine isotope stage = MIS 5) ages (Veeh, 1966; Woodroffe *et al*., 1991). From the top of this cliff inland, the terrain rises irregularly to a relatively flat area ca 15 m above sea-level on which the airstrip is built. Further inland, the terrain rises once more to terraces at ca 23 m, 35 m and 55 m, i.e. to the oldest parts of the makatea, which is Miocene in age. The ages of the terrace slope from ca. 9 m to 35 m elevation are largely unknown.

Rarotonga (Fig. 3) is the largest island in the archipelago (67 km^2) and the capital, Avarua, represents the administrative centre of the Cook Islands. The island rises to 640 m above sea-level and is largely volcanic (Marshall, 1930; Wood & Hay, 1970). Exposed volcanic rocks are of Pleistocene age and K-Ar-ages range from 1.19 to 2.27 Ma (Dalrymple *et al*., 1975; Turner & Jarrard, 1982). There is a narrow coastal fringe of volcanoclastic sediments including sands and gravels as well as swamp deposits.

Several rivers drain the mountain range of Rarotonga. The island is completely surrounded by a shallow fringing reef that reaches several hundred metres in width (Lewis *et al*., 1980). Marshall (1930) reported on isolated, low cliffs of fossil reefs with coral heads in growth position on the eastern island side (Matavera, Ngatangiia). Schofield (1970) described another outcrop from Nikao, adjacent to the airport and provided ^{14}C-ages of >48.4 kyr BP and 28.2 kyr BP for Nikao and Ngatangiia, respectively. This author also reported a Holocene age (2.03 kyr BP) for a small reef terrace some 0.9 m above sea-level near Avarua. Stoddart (1972) described another reef terrace on the northernmost sand and rubble island (Motutapu) on the eastern island side and estimated the vertical extension of the Ngatangiia and Motutapu reef terraces as ca 3 m above modern sea-level. The ages of the Rarotonga fossil reef terraces were described as mainly Pleistocene and possibly Holocene (Wood & Hay, 1970) even though reliable Pleistocene ages are lacking. Moriwaki *et al*. (2006) studied various coastal deposits of Rarotonga and obtained three ^{14}C-ages from Holocene corals on top of the Pleistocene reef terrace at Ngatangiia and Motutapu (0.2 to 1.35 m above sea-level) ranging from 584 to 942 yrs BP. Fossil microatolls ca 0.9 m above modern sea-level in Ngatangiia were reported as being 3.0 to 4.3 kyr BP (Chikamori, 1996).

The almost-atoll of Aitutaki (Fig. 4) covers some 98 km^2, which encompasses 16 km^2 for the central volcanic island, 39 km^2 for the surrounding lagoon and 43 km^2 for fringing and barrier reefs (Hein *et al*., 1997). The age of the volcanic rocks ranges between 8.4 and 0.7 Ma and two volcanic phases are distinguished (Dalrymple *et al*., 1975; Turner & Jarrard, 1982). Volcanic rocks occur on the main island, which rises 124 m above sea-level and on two small lagoon islands (Rapota, Moturakau) in the southern part of the platform (Fig. 4). Hein *et al*. (1997) and Gray & Hein (2005) detailed the late Quaternary development of Aitutaki based on the analysis of six core-holes. Volcanic rocks are overlain by 70 m of Pleistocene limestone, which is diagenetically altered and locally dolomitized. Its age is therefore largely unknown. The Holocene deposits are up to 22 m-thick and as old as 7.92 ka (Gray & Hein, 2005). The lagoon is up to 10 m-deep and has an average depth of about 4 m (Gray & Hein, 2005). Modern platform interior sediments contain considerable amounts of non-skeletal carbonate grains (Rankey & Reeder, 2009; Gischler, 2020). The marginal reef of Aitutaki is extensive, well developed and includes from outboard to inboard a reef crest and a pavement colonised by corals and calcareous algae; and with a wide sand apron. The marginal reef is continuous and there are very few shallow and narrow passages. The fifteen motus were mapped by Stoddart & Gibbs (1975), who identified rather extensive limestone terraces ('conglomerate platform') ca 1 m above modern sea-level on the windward island sides. Unlike in a previous observation (Shepard, 1961), these authors did not interpret the conglomerate platform as fossil, elevated reef and also slightly underestimated its elevation (Gibbs *et al*., 1971; Stoddart & Gibbs, 1975). Yonekura *et al*. (1988) and Goodwin & Harvey (2008) reported elevated (up to +0.8 m) microatolls from Aitutaki and Rarotonga dated between 0.36 to 1.8 kyr BP. Allen (1998) suggested a late Holocene sea-level fall based on geoarchaeological investigations along the west coast of Aitutaki.

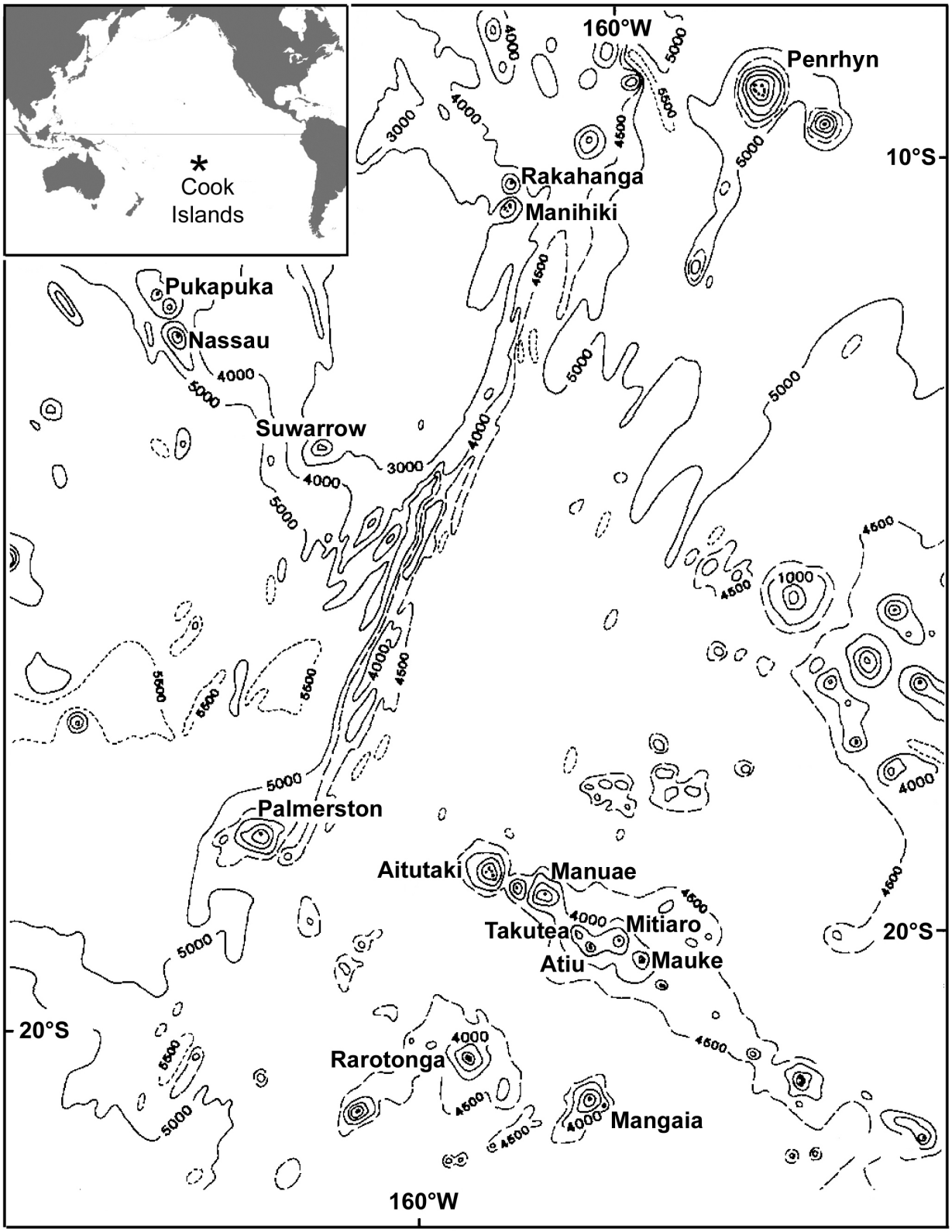


Fig. 1. Map of the Cook Island archipelago including northern and southern chains (modified from Woodroffe *et al*., 1990).

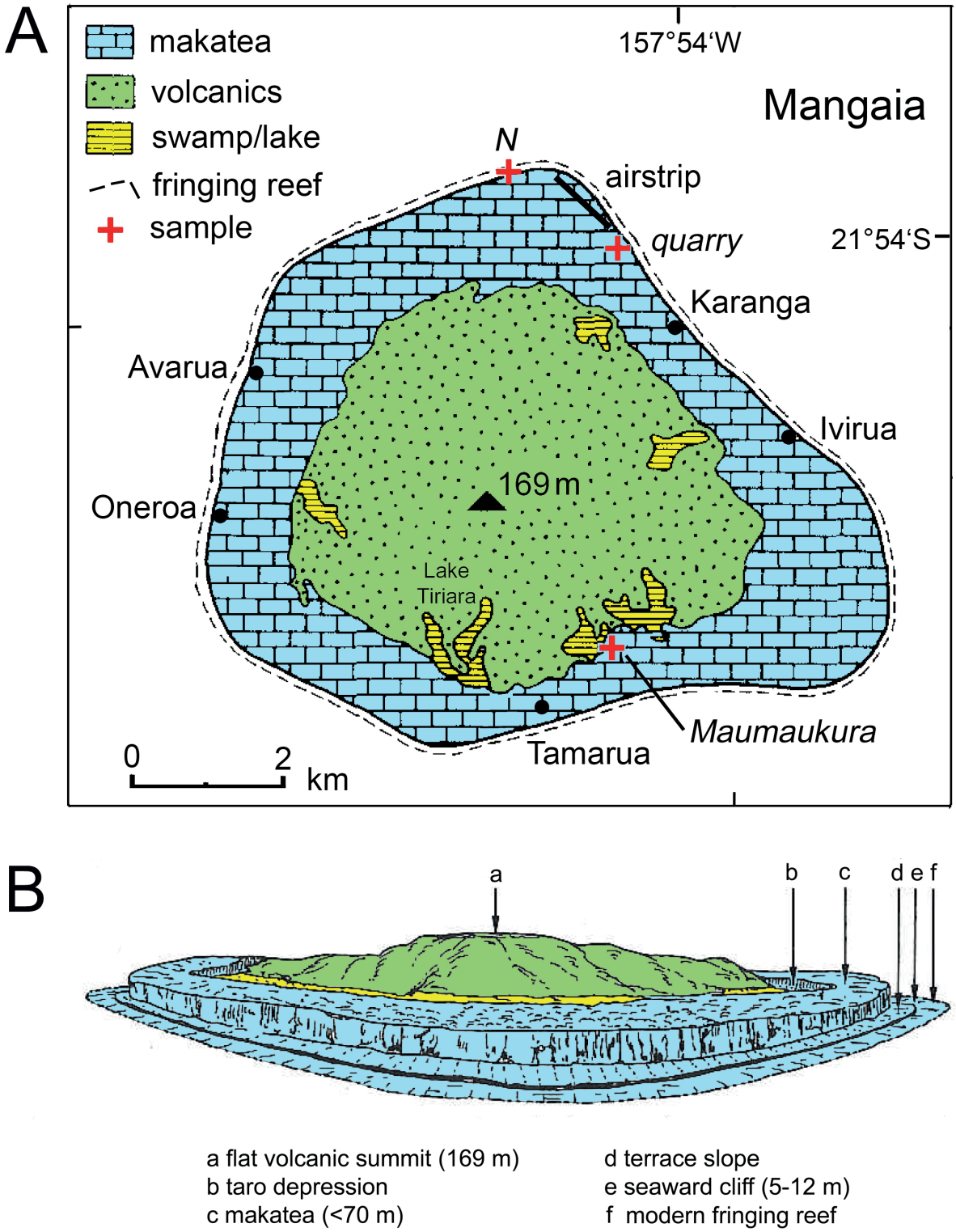


Fig. 2. (A) Map of Mangaia indicating sample locations (modified from Woodroffe *et al*., 1991). (B) Schematic block diagram of Mangaia from Stoddart *et al*. (1985), modified from Marshall (1930).

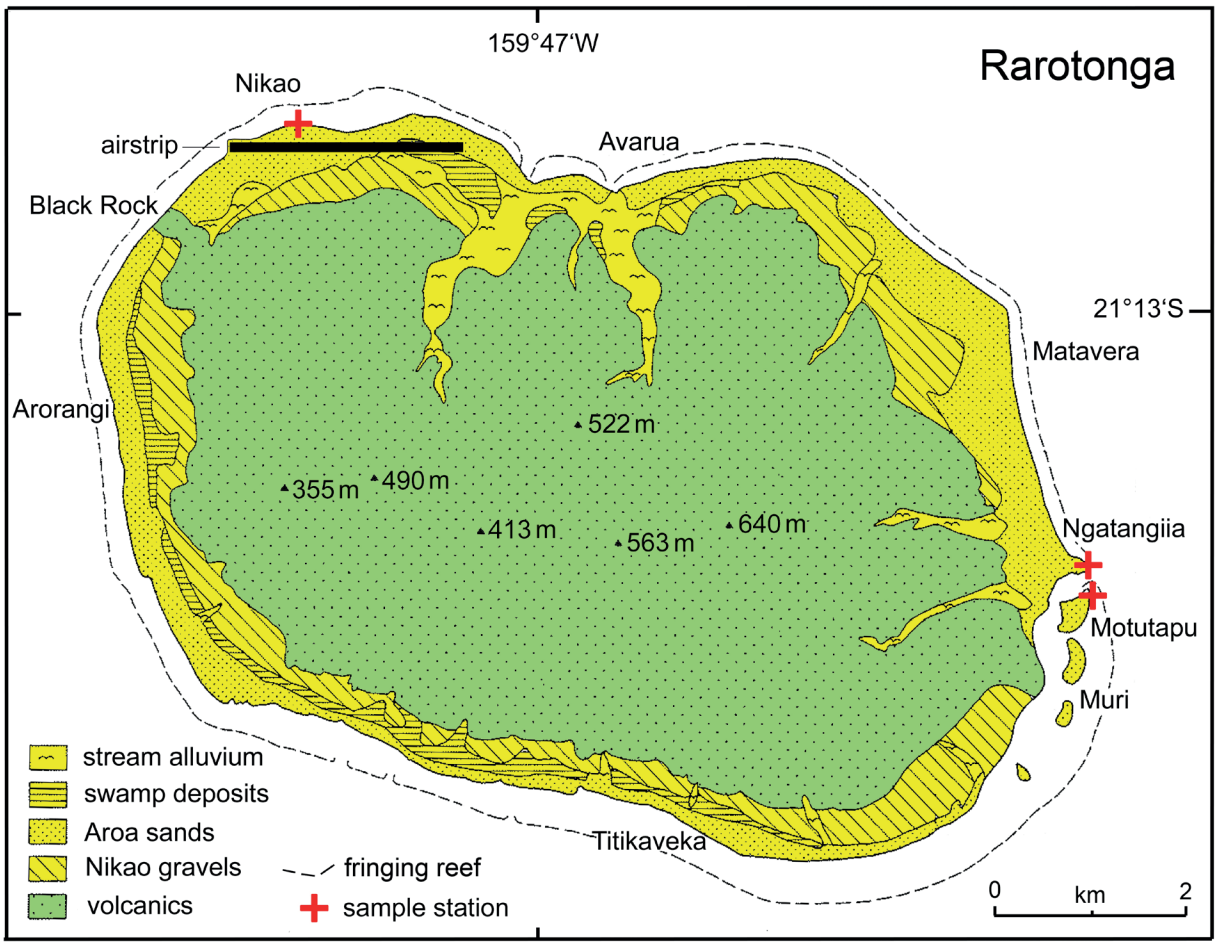


Fig. 3. Map of Rarotonga with sample locations (modified from Stoddart, 1972).

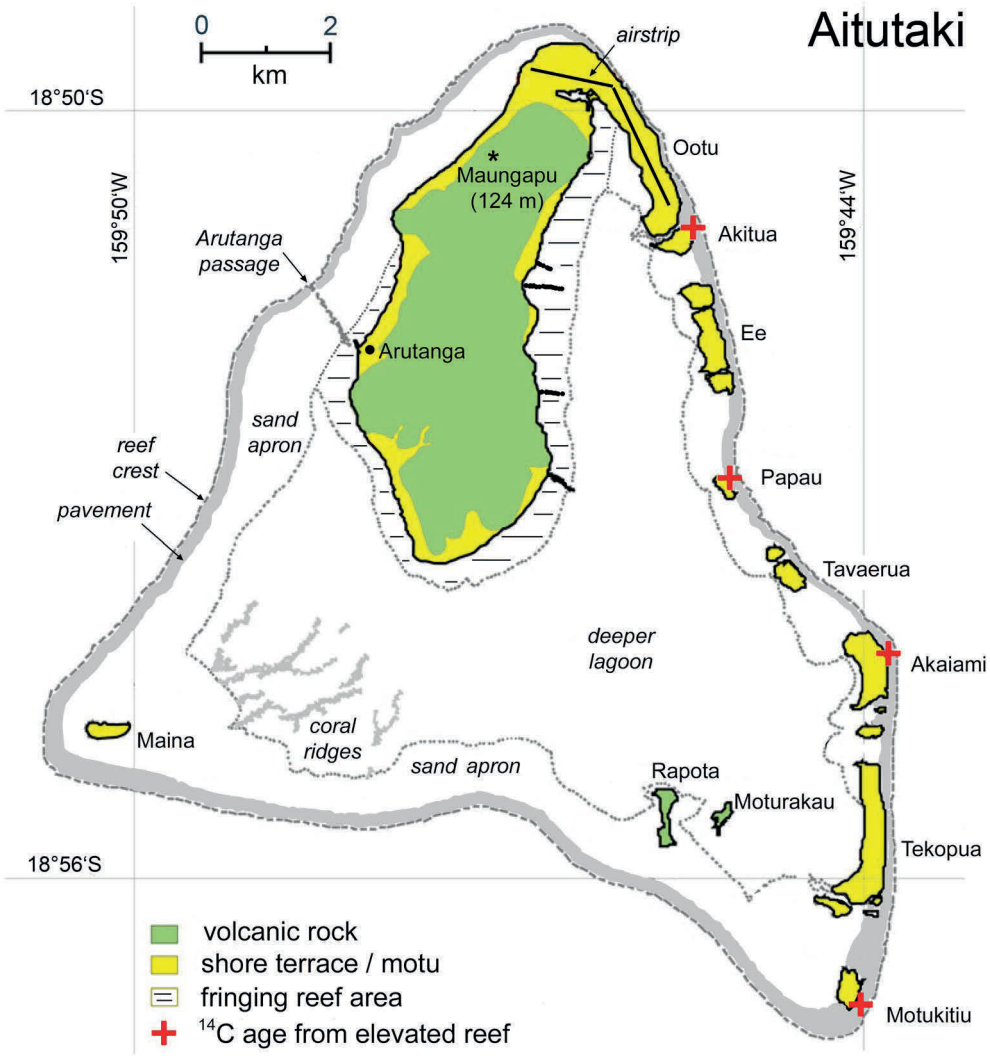


Fig. 4. Map of Aitutaki including sample stations (modified from Forbes *et al*., 2013).

METHODS

The southern Cook Islands of Mangaia, Rarotonga and Aitutaki were visited during July to August 2019 and the coastal geology of the islands was investigated. Print-outs of satellite images (GoogleEarth®) and topographic maps 1:25,000 of the Cook Islands were used (PITopo25-PI-11, -12 and -17; New Zealand Government). Rock and coral samples were collected by means of a hammer and a chisel and their latitudes and longitudes recorded with a Magellan type 2000 GPS (Figs 2 to 4; Table 1). Elevations relative to modern sea-level of the fossil reef sample 'Mangaia North (N)' and the samples from Rarotonga and Aitutaki were estimated with a measuring stick and level. Tide tables (Australian Government, Bureau of Meteorology) were taken into account when estimating elevation above mean sea-level. The authors estimate the accuracy of this method to be within 0.5 m. The elevation of samples from higher positions on Mangaia were estimated by referring to the topographic map 1:25,000 (PITopo25-Pl17). Weathered rock and coral surfaces were removed and clean samples pulverised using mortar and pestle. Relative contents of aragonite, calcite and high-magnesium

calcite were determined using a Panalytical Xpert Pro X-ray diffractometer applying the method of Milliman (1974, p. 24–27). Selected samples were polished and thin-sections studied with a petrographic microscope (Leica DM 2500 M).

Element concentrations (Ca, Mg, Sr, Fe, Mn) were measured using an inductively coupled plasma atomic emission spectrometer (ICP-OES; iCAP 6500 DUO of Thermo Fisher Scientific) at Ruhr-University Bochum. 1.5 mg ± 10% of the sample powder was weighed with a XPR6UD5 Mettler Toledo scale. The sample was dissolved in 1 ml 3M HNO_3 using a dilutor of the type microlab 600 series (Hamilton). Samples were homogenised using a MS2 minishaker (IKA) and reacted for 24 hours at room temperature. Subsequently, 2 ml deionised H_2O were added using once more the microlab 600 series dilutor and then homogenised with the MS2 minishaker. Standards used include BCS-CRM512 (dolomite; Bureau of Analysed Samples Ltd.) and BCS-CRM513 (limestone; Bureau of Analysed Samples Ltd.). The long-term 1s-reproducibility of BCS-CRM512 and BCS-CRM513 are: Ca 0.3 wt.% and 0.5 wt.%, Mg 0.2 wt.% and 14 ppm, Sr 19 ppm and 2 ppm, Fe 8 ppm and 10 ppm and Mn 1 ppm and 2 ppm, respectively (n=66; 2019–2020).

Strontium-isotope analysis ($^{87}Sr/^{86}Sr$) was conducted on 10 bulk rock samples from Mangaia and Rarotonga using thermal ionisation mass spectrometry (TIMS; TI-Box, formerly MAT 262, Spectromat) at Ruhr-University. Samples of the host limestone were selected on polished hand specimens thereby avoiding blocky cement. Samples were obtained with a small hand-held drill (Proxxon). 1 to 4 mg of sample powder was weighed with a XP56 (Mettler Toledo) scale to receive a sample containing ca. 400 ng of Sr. The sample was dissolved using 1 ml of 6M HCl during a 24-hour reaction time at room temperature. Subsequently, samples were dried on a hot plate at 90° C, then re-dissolved in 0.4 ml of 3M HNO_3. Perfluoroalkoxy alkanes (PFA) columns were filled with TrisKem Sr-ion exchange resin (100 to 150 mesh) and the resin was flushed with 1 ml of 0.05 M HNO_3 and conditioned with 3 ml of 3M HNO_3. Subsequently, the 0.4 ml of 3M HNO_3 containing the dissolved sample were put on the column. The matrix was separated with 3.6 ml 3M HNO_3. The Sr-fraction was recovered with 2 ml of deionised H_2O. Samples were evaporated on a hot plate at 90 °C and re-dissolved in 1 ml of H_2O_2-HNO_3 (1:1; 31%:65%) to remove organic remains. Samples were then evaporated on a hotplate at 60 °C and re-dissolved in 0.4 ml of 6M HCl. After evaporation on a hotplate at 90 °C, the samples were again re-dissolved in 1 µl of ionisation-enhancing solution (after Birck, 1986) and loaded on Re single filaments. The loading, column and reagent blanks were <5 pg, <1 ng and <0.01 ppb. The long-term reproducibilities are: NIST NBS 987: $^{87}Sr/^{86}Sr = 0.710242 \pm 0.000001$ 2s SE / ± 0.000031 2s SD (n = 508); USGS EN-1: $^{87}Sr/^{86}Sr = 0.709159 \pm 0.000002$ 2s SE / ± 0.000032 2s SD (n = 421). The $^{87}Sr/^{86}Sr$ data were corrected to the difference between NIST NBS 987 value given by McArthur *et al*. (2001) and the mean value measured in Bochum. The obtained Sr-isotope ratios were used to obtain age ranges based on graphic intercepts with the intrinsic lines around the curve of Farrell *et al*. (1995) for Quaternary samples and graphic intercepts with the curved data cloud of McArthur *et al*. (2001) for Neogene samples. The Sr-isotope method for dating (McArthur *et al*., 2012) has been very useful, including Neogene and Quaternary limestone deposits, as the Sr-curve exhibits variation over time; however, commonly upper and lower bounds of ages are determined that may range hundreds of thousands to a few millions of years.

For U/Th dating, corals from Mangaia and

Rarotonga with no indications of early diagenesis and an aragonite content of >97% were selected. Separation of uranium and thorium from the sample matrix was done using Eichrom-UTEVA resin following the methods of Fietzke *et al*. (2005). Determination of uranium and thorium isotope ratios was done at GEOMAR, Kiel, Germany, using a Thermo Fisher Neptune collector inductively coupled plasma mass spectrometer (MC-ICP-MS; Thermo Fisher Scientific, Waltham, MA, USA) as described by Fietzke *et al*. (2005). For isotope dilution measurements, a combined $^{233}U/^{236}U/^{229}Th$ spike was used. Stock solutions were calibrated for concentration using NIST-SRM 3164 (U) and NIST-SRM 3159 (Th) as combi-spike, calibrated against CRM-145 uranium standard solution (formerly NBL-112A) for uranium isotope composition and against a secular equilibrium standard (HU-1, uranium ore solution) for the precise determination of $^{230}Th/^{234}U$ activity ratios. In clean-room laboratories at GEOMAR, Kiel, usually whole-procedure blank values of this kind of sample were measured between 0.5 pg and 1.0 pg for thorium and between 10 pg and 20 pg for uranium. Both values are in the range typical of this method and the laboratory (Fietzke *et al*., 2005). Based on the $^{230}Th/^{232}Th$ and $^{234}U/^{238}U$ ratios, ages were calculated using the uranium and thorium half-lives of Cheng *et al*. (2000).

Absolute ages of inferred Holocene coral samples from Aitutaki were measured by Beta Analytic Inc., Miami, Florida, by means of accelerator mass spectrometry (AMS). An ΔR-value of -7 ± 40 (reservoir correction, Rarotonga) was used. Ages were calibrated based on the MARINE13 database (Reimer *et al*., 2013).

One sample from the oldest limestone part of the island of Mangaia was treated following the method of Bourdon (1957) in order to obtain planktic foraminifera for age determination.

Table 1. GPS coordinates of studied samples on Mangaia, Rarotonga and Aitutaki.

	Latitude	Longitude	
Rarotonga			
Nikao	21°11.998'S	159°48.632'W	
Ngatangiia	21°14.573'S	159°43.474'W	
Motutapu	21°14.733'S	159°43.421'W	
Mangaia			
Maumaukura	21°56.976'S	157°54.284'W	
North	21°53.487'S	157°54.895'W	
airport quarry	21°54.101'S	157°54.253'W	
Aitutaki			
Akitua	18°50.908'S	159°45.262'W	
Papau	18°52.913'S	159°44.920'W	
Akaiami	18°54.550'S	159°43.665'W	*Porites*
	18°54.589'S	159°43.662'W	*Acropora*
Motukitiu	18°57.017'S	159°43.923'W	

RESULTS

Mangaia

Old makatea

On Mangaia, samples were collected at three locations at different elevations relative to modern sea-level. Samples from the oldest part of the makatea (Fig. 5A, B and F) were collected from a freshly made road outcrop at Maumaukura Lookout near the village of Tamarua (Fig. 2) some 45 m above sea-level. These are very hard, massive, light yellow grainstones and less commonly packstones (Fig. 6E), commonly with a low-magnesium calcite mineralogy (Table 2). Common constituent particles include fragments of coralline algae, coral, mollusc, foraminifera, echinoderms, bryozoa and peloids (Fig. 7). Coralline algae are most common and include the genera *Mesophyllum*, *Harveylithon*, *Lithoporella*, *Sporolithon* and abundant geniculate forms such as *Corallina* and *Jania* (Fig. 8A and B). Fine carbonate detritus is rare. The age-indicative foraminifer *Lepidocyclina* Gümbel 1870 occurs frequently (Fig. 7A and F). The dominant cement is blocky low-magnesium calcite (Fig. 7). Isopachous crusts of lengthy, bladed crystals are also found (Fig. 7D). Age data were obtained via biostratigraphy and Sr-isotope geochemistry. The common occurrence of *Lepidocyclina* suggests an Oligocene to Miocene age (Boudagher-Fadel & Price, 2010). Sr-isotope ratios (Tab. 3) indicate an age range of ca. 11.7 to 15.9 Ma based on the curve presented in McArthur *et al*. (2001), i.e. Langhian to Serravallian or mid-Miocene (Fig. 9). The attempt to recover planktic foraminifera by acid treatment during disintegration was not successful.

Airstrip quarry in the terrace slope

The second location studied is a recently developed quarry near the southern end of the airport (Fig. 2A). The base of the quarry is on the 15 m terrace at the same elevation as the airstrip. The quarry wall is some 10 m-high. It comprises what previous authors have called the terrace slope, a low-angle rise of the topography between 15 and 20 m elevation (Fig. 2B). In the quarry, three rock units (1 to 3) are layered on top of each other with more or less horizontal boundaries clearly visible in the outcrop. However, the boundary between unit 3 and the uppermost unit 4 is not horizontal but undulating with a relief of up to 2 m (Fig. 5E).

Unit 1: The lowermost unit 1 is a hard, buff-coloured grainstone with coral, red algal, mollusc and foraminifer fragments, shells and tests (Figs 6A, 10A and B). Coralline algae include abundant *Porolithon* gr. *onkodes* as well as *Harveylithon* gr. *munitum*, *Lithophyllum* gr. *kotschyanum* and *Lithophyllum* gr. *prototypum*. Bladed cements and blocky, low-magnesium calcite cements are present. Within the carbonate phases, aragonite and high-magnesium calcite are most common (Table 2). The Sr-isotope age range is 1.03 to 1.95 Ma (Fig. 11; Table 3).

Unit 2: The second unit is a partly friable, light buff-coloured, porous coralgal boundstone containing the encrusting foraminifer *Homotrema rubrum*. Coralline algae (*Lithothamnion* sp., *Mesophyllum* sp.) are intergrown with foraminifera and may form a framework of contorted foliose thalli of *Neogoniolithon* sp.; and less commonly *Spongites* sp. containing various foraminifera and serpulids. In this facies, blocky cement predominates (Figs 6B and 10C). It consists of low-magnesium calcite (Table 2) and ranges in age from 0.36 to 1.25 Ma (Fig. 11; Table 3).

Unit 3: This unit is a buff-coloured grainstone with corals, red algae, *Halimeda*, mollusc and foraminifer remains (Figs 6C, 10D and E). Coralline algal fragments include abundant *Porolithon* gr. *onkodes*, *Harveylithon* gr. *munitum*, *Lithophyllum* gr. *kotschyanum*, *Lithophyllum* gr. *prototypum*,

Amphiroa sp. and other geniculate taxa, as well as unidentified Hapalidiales. Diagenetic precipitates show meniscus cements and geopetal features. The carbonate phases include aragonite, low-magnesium and high-magnesium calcite (Tab. 2). The age range is 0 to 0.69 Ma based on Sr-isotopes (Fig. 11; Table 3).

Unit 4: The uppermost unit 4 is a very hard, light-buff packstone to grainstone with abundant coralline algae, coral, mollusc and foraminifer fragments (Figs 6D and 10F). Corallines include abundant geniculate *Amphiroa* sp. and *Corallina*, as well as abundant *Porolithon* gr. *onkodes*, *Lithophyllum* gr. *pustulatum*, *Lithophyllum* gr. *kotschyanum* and *Lithophyllum* gr. *prototypum*. Blocky calcite cement is very common; peloidal cement occurs in places. Samples consists of ca 75% low-magnesium calcite and 25% aragonite (Tab. 2). The age range obtained is 1.16 to 1.88 Ma (Fig. 11; Table 3).

Lower cliff

The third location investigated on Mangaia was the lowest cliff at the northern coast (Figs 2 and 5A to D), rising to ca 8 m above modern sea-level. In the studied area, it exhibits striking spur-and-groove patterns. It is a coral-rich grainstone to boundstone (Fig. 5D) with abundant robust-branching acroporids. Some of the corals escaped diagenetic alteration and consist of >99% aragonite. The U-series age of 127.06 ka obtained from a *Porites* coral collected 2 m above modern sea-level clearly indicates deposition during marine isotope stage 5e (Table 4). The Sr-isotope age range of this sample is 0 to 0.47 Ma (Fig. 12; Table 3).

Rarotonga

Reef terraces on Rarotonga have been studied at three locations including Nikao, Motutapu and Ngatangiia (Fig. 3).

Nikao

The reef terrace investigated at the north-western coast of Nikao, near the airport, extends over ca. 50 m and has an elevation of up to 1.5 m above modern sea-level (Fig. 13C and D). It is a very hard, dark brown coralgal boundstone with large cavities filled by blocky spar (Fig. 14D). In places, branched corals (questionable *Pocillopora* sp.) are preserved *in situ*. Corals are diagenetically altered as seen in the lack of the original fibrous textures now replaced by blocky cement. Identified coralline algae include *Lithothamnion* sp., *Harveylithon* sp., *Lithoporella* sp., *Lithophyllum* gr. *pustulatum*, *Lithophyllum* sp., questionable *Mesophyllum* sp. and geniculates such as *Amphiroa* sp. and *Corallina* sp. (Fig. 8C). The rock is composed of low-magnesium calcite (Table 2). The brown stain probably results from fine volcano-clastic material. In thin-section, abundant coral, coralline algal fragments, dense brownish matrix and blocky low-magnesium calcite can be seen (Fig. 15F). Due to strong diagenetic alteration and the lack of pristine, aragonitic coral material, no U-series dating was attempted. Sr-isotopes ages range between 5.7 and 8.7 Ma, i.e. late Miocene (Fig. 16).

Motutapu and Ngatangiia

At the shore of the northernmost reef island Motutapu and separated by Muri channel close-by on the mainland coast near Ngatangiia, extensive terraces, extending over some 100 m, up to 3 m above modern sea-level, are found (Fig. 13A and B). These are coralgal grainstones, boundstones and packstones, i.e. reef-related facies (Fig. 14A to C). Samples have a brownish stain, which possibly originates from minor amounts of fine volcano-clastic sediment. They contain abundant fragments of coral, coralline algae and *Halimeda* (Fig. 15A to C). Corals include acroporids and *Porites* sp. Coralline algae in a Motutapu sample include abundant

Porolithon gr. *onkodes*, *Lithophyllum* gr. *pustulatum*, *Amphiroa* sp. and *Corallina* sp. In a Ngatangiia sample, thick crusts of *Porolithon* gr. *onkodes* with vermetids, as well as *Dawsoniolithon* sp. and *Jania* were found (Fig. 8D). A second Ngatangiia sample contained *Mesophyllum* gr. *funafutiense*, *Lithophyllum* gr. *prototypum*, *Harveylithon* sp., *Lithoporella* sp., *Amphiroa* sp., *Corallina* sp. and *Jania* sp. Coralline algae and *Halimeda* fragments and platelets, respectively, are preserved in various degrees of diagenetic alteration. Mineralogical composition is characterised by varying amounts of low-magnesium and high-magnesium calcite and the occurrence of blocky low-magnesium calcite cement (Fig. 15B to D) (Table 2).

On the top of the terraces, isolated patches of pristine coralgal grainstones are found that are composed of >99% aragonite (Table 4). A clear and continuous boundary between the older diagenetically altered and the younger, pristine sections is not visible in the outcrop. U-series dating of pristine corals produced late Holocene ages of 0.064 kyr BP and 3.21 kyr BP, respectively (Table 4). Older, diagenetically altered rocks were dated using radiogenic Sr-isotope ratios. Age ranges are Plio-Pleistocene (0.8 to 4.49 Ma) for the two Ngatangiia samples and late Pleistocene (0 to 0.12 Ma) for the Motutapu sample (Figs 17 and 18; Table 3).

Aitutaki

Along the eastern platform margin, on the windward side of the motus of Aitutaki, extensive reef terraces are found which extend from 50 m to more than 300 m in length and up to 50 m width and rise up to 1.0 m above modern sea-level (Fig. 19). The terraces are coral boundstones and grainstones with both *in situ* and redeposited corals. The most common corals include robust acroporids and massive *Porites*. The tops of the latter reach the highest elevations (up to 1.0 m) above sea-level. On four of these motus, pristine coral samples have been collected from reef terraces and radiometrically dated using ^{14}C AMS. All samples are late Holocene in age and range from 1.9 to 5.8 kyr BP (Table 5).

Table 2. Relative amounts of carbonate phases and element concentrations of rock samples from Mangaia and Rarotonga.

Sample	Aragonite	Mg-calcite	Calcite	Ca (ppm)		Mg (ppm)		Sr (ppm)		Fe (ppm)		Mn (ppm)	
	rel. wt.-%	rel. wt.-%	rel. wt.-%	$\bar{x}$	±S	$\bar{x}$	±S	$\bar{x}$	±S	$\bar{x}$	±S	$\bar{x}$	±S
Mangaia													
Maumaukura	0	0	100	387470	3402	4982	23	171.2	1.3	49.4	1.3	39.3	0.2
Airstrip unit 1	59.3	36.7	4	356900	2142	22380	30	2989.0	9.3	9.1	0.9	3.0	0.1
Airstrip unit 2	0	0	100	391300	1739	2812	16	137.4	2.9	49.3	0.8	12.9	0.2
Airstrip unit 3	54.2	9.8	36	374510	4663	7031	48	2496.0	19.4	45.3	1.1	5.7	0.1
Airstrip unit 4	25.5	0	74.5	375830	2939	12660	59	1189.0	2.9	45.2	1.4	13.2	0.1
Mangaia N	99.8	0	0.2	381300	3168	1516	4	7308.0	26.9	12.3	0.7	0.0	0.1
Rarotonga													
Nikao	0	0	100	265640	2125	3202	29	259.7	1.6	1691.0	15.8	29.3	0.2
Ngatangiia 1	3	0	97	378290	5972	6205	24	510.6	2.2	479.5	1.4	38.1	0.2
Ngatangiia 2	4.9	0	95.1	371080	2542	5404	30	526.9	4.1	549.1	1.9	36.6	0.1
Motutapu	29.8	69.4	0.8	326160	3288	40860	345	1619.0	14.9	236.8	1.9	17.7	0.2

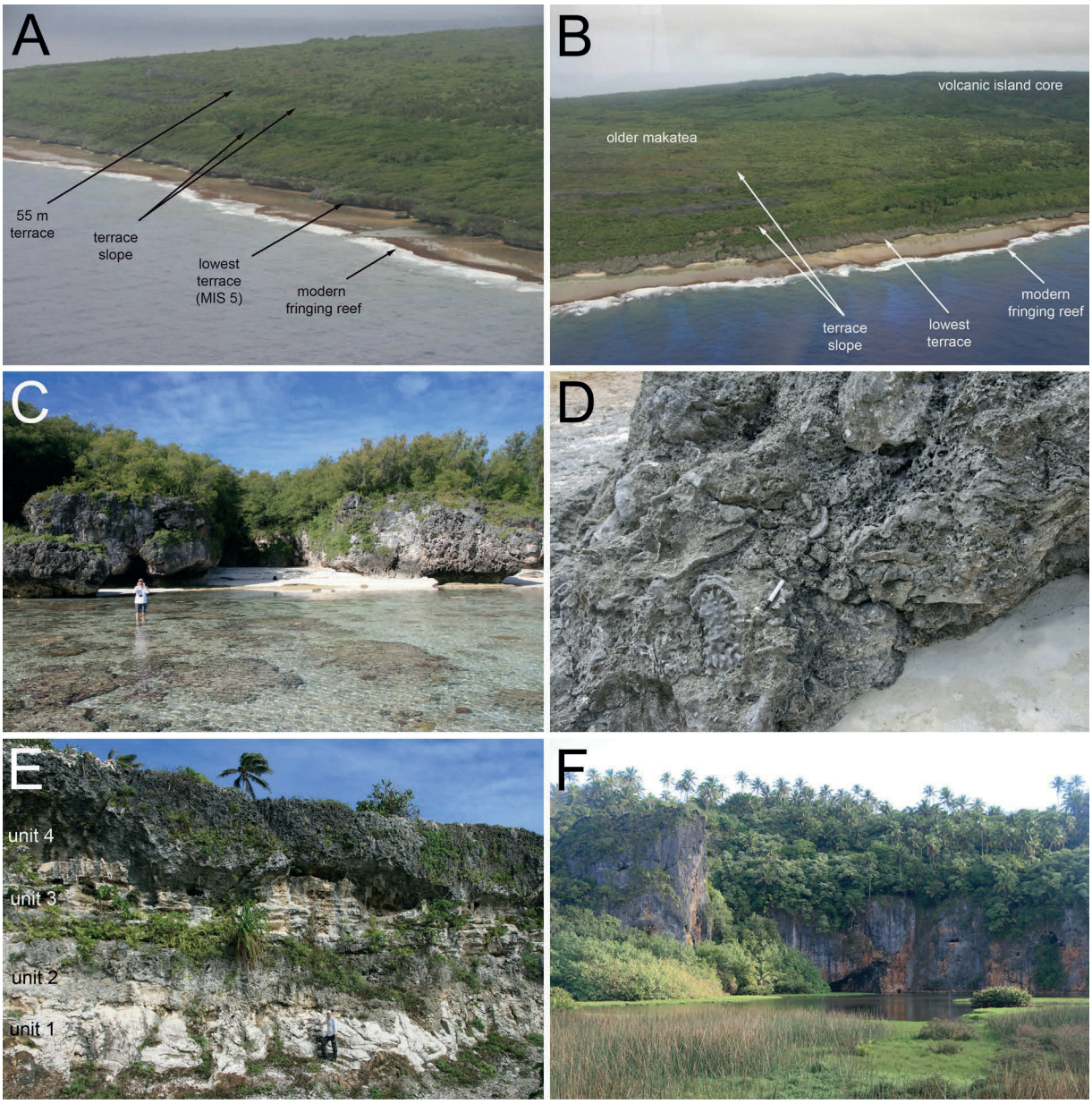


Fig. 5. Photos of reef terraces in Mangaia. (A) Aerial view of south-eastern part of Mangaia looking south. From offshore to inshore, the modern fringing reef, the Pleistocene (MIS 5e) cliff, the 'terrace slope' and the old makatea are seen. (B) Aerial view of southern part of Mangaia looking west. Modern fringing reef, MIS 5e-terrace, terrace slope, old makatea and central volcanic hill are seen. (C) Sample station Mangaia North observed from modern fringing reef. Note the Pleistocene spurs and grooves in the lower terrace. (D) Close-up of MIS 5e-reef limestone with abundant corals. (E) Quarry at the southern end of the airstrip, which is located within the 'terrace slope'. Note the four rock units. (F) Old makatea cliff as seen from the inland swampy depression between volcanic island core and makatea across Lake Tiriara (north-west of Tamarua) looking south.

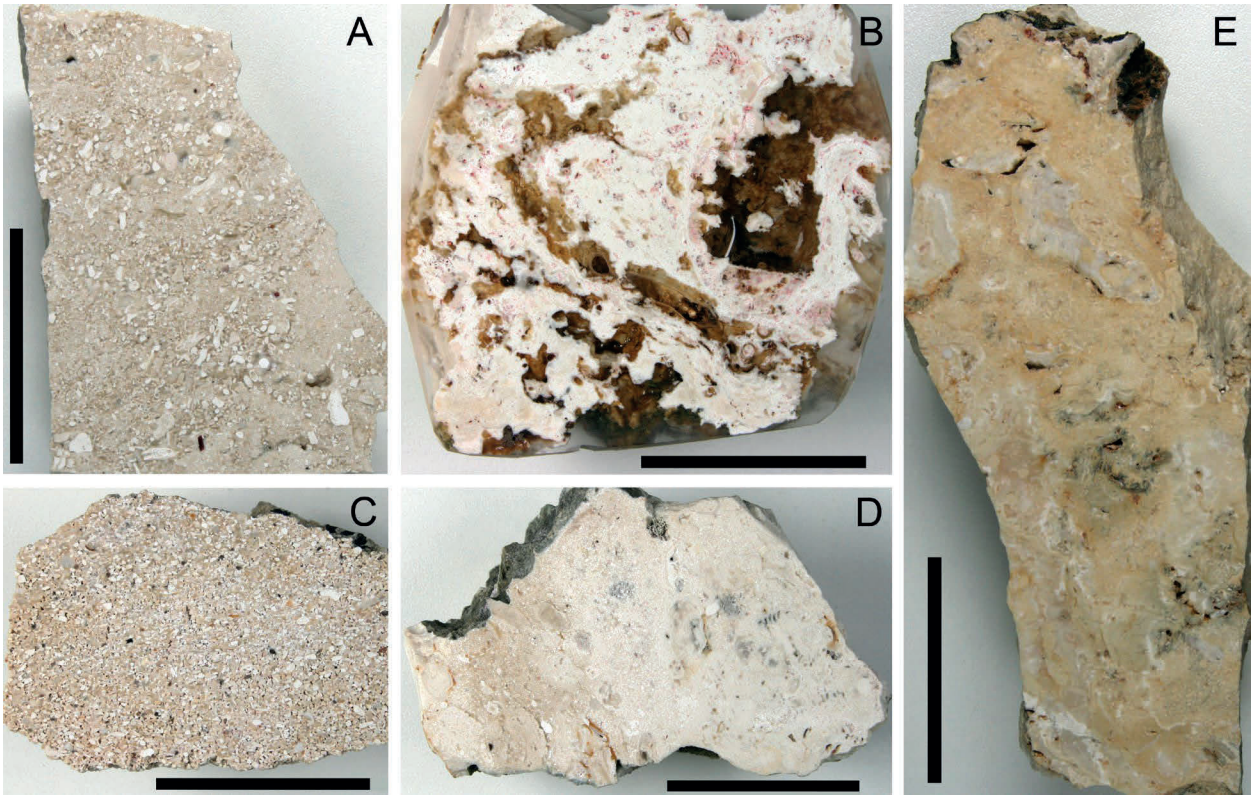


Fig. 6. Polished hand specimens from Mangaia. Scale bar is 5 cm. All samples oriented upward. Images A to D show four Pleistocene units at quarry near airstrip. (A) Lowermost layer (unit 1) in quarry near airstrip is a dense biogenic grainstone. (B) Unit 2 in quarry is a very porous, chalky boundstone. (C) Grainstone, possibly beach-rock, unit 3 in quarry. (D) Uppermost unit 4 in quarry is a dense packstone. (E) Older, Miocene limestone from Maumaukura Lookout near Tamarua.

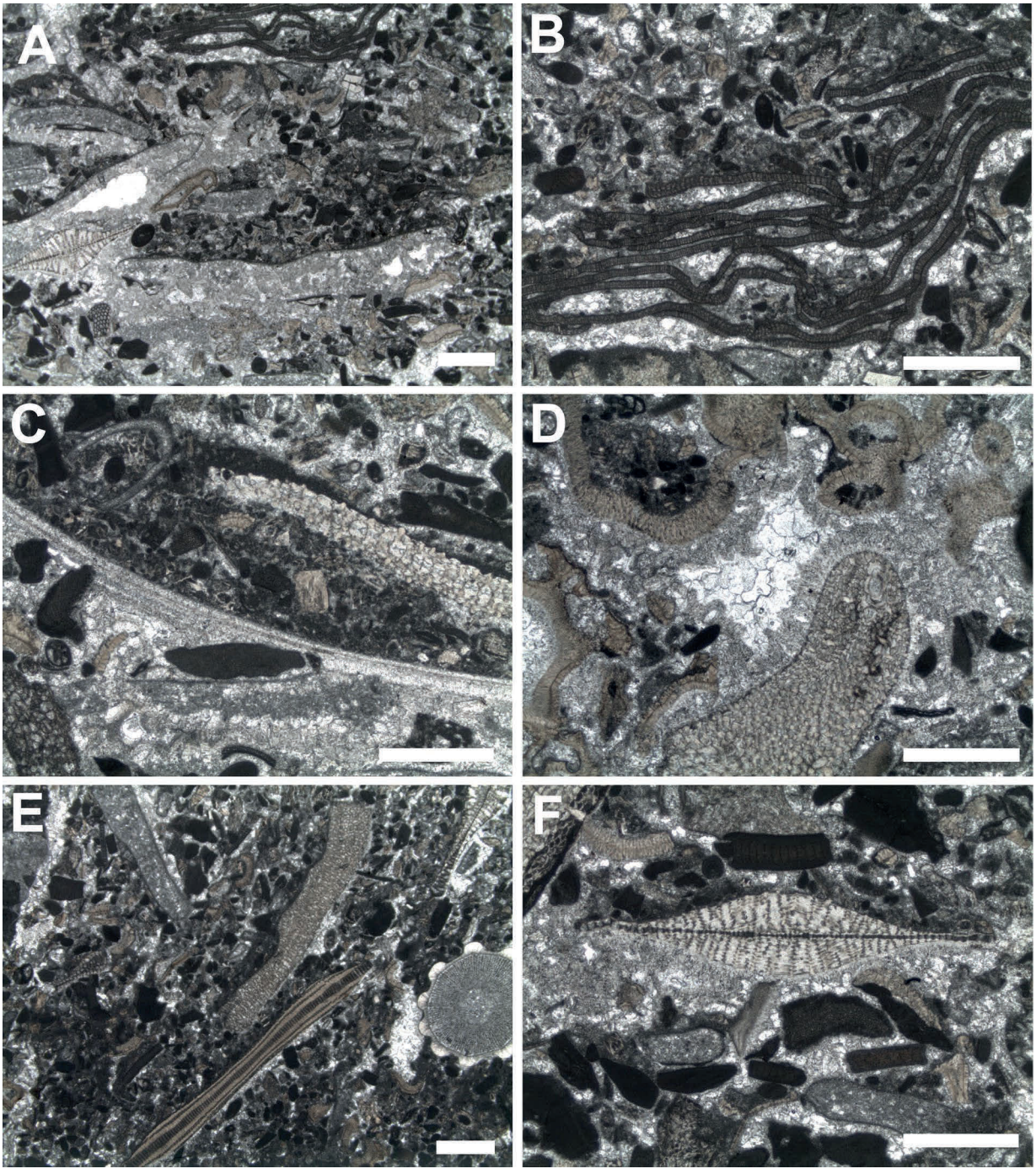


Fig. 7. Thin-section micrographs from old makatea on Mangaia. Scale bar is 1 mm. (A) Grainstone with coralline algae, peloids and foraminifera. Note occurrence of *Lepidocyclina* on left hand side of picture. (B) Close-up of previous image highlighting encrusting coralline algae (*Lithoporella* sp.). (C) Packstone with shell fragments, coralline algae. (D) Encrusting foraminifera and coral fragment. Note early marine cement and younger meteoric (blocky) cement. (E) Packstone with foraminifera (including *Lepidocyclina* in upper right corner of image), coralline algae, echinoderm fragment and abundant peloids. (F) *Lepidocyclina* and coralline algal fragments.

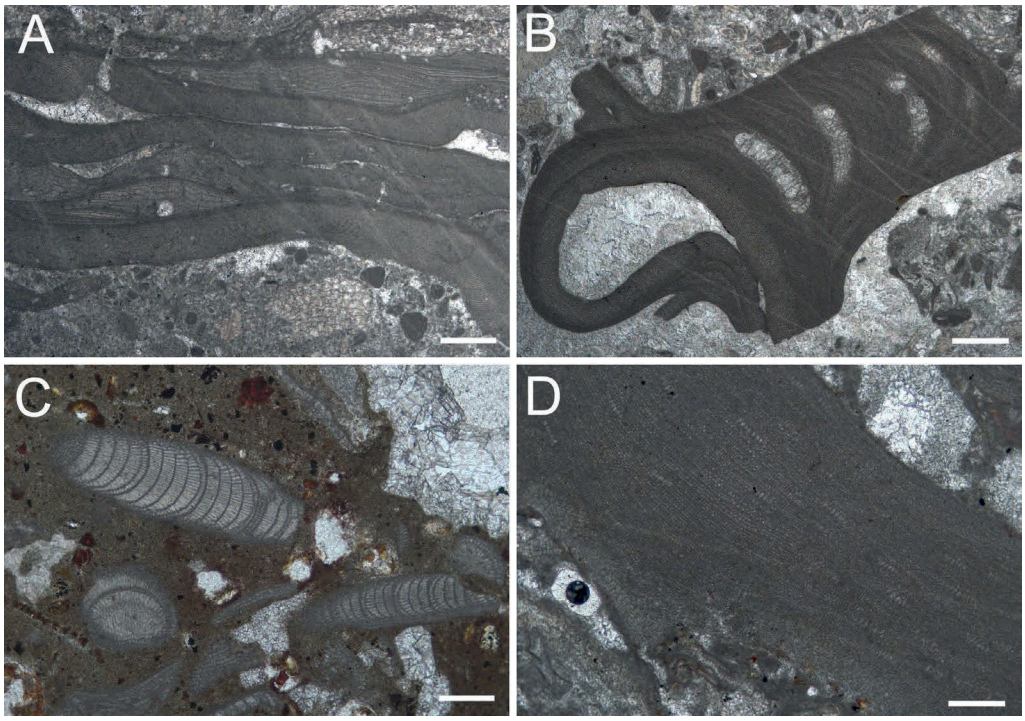


Fig. 8. Thin-section micrographs of crustose coralline algae. A. Maumaukura, Mangaia. Several laminar, foliose thalli of *Mesophyllum* sp. Scale bar is 500 µm. B. Maumaukura, Mangaia. Thallus of *Mesophyllum* sp. (a species different from the one in previous image) with large multiporate conceptacles in a protuberance. Scale bar is 500 µm. C. Nikao, Rarotonga. Several segments of the geniculate coralline *Amphiroa* sp. and fragments of *Lithoporella* sp. (top centre and bottom centre) and other unidentifiable corallines. Scale bar is 200 µm. D. Avana, Rarotonga. Plant of *Porolithon* gr. *onkodes* with characteristic rows of several trichocytes dispersed in the thallus. Scale bar is 200 µm.

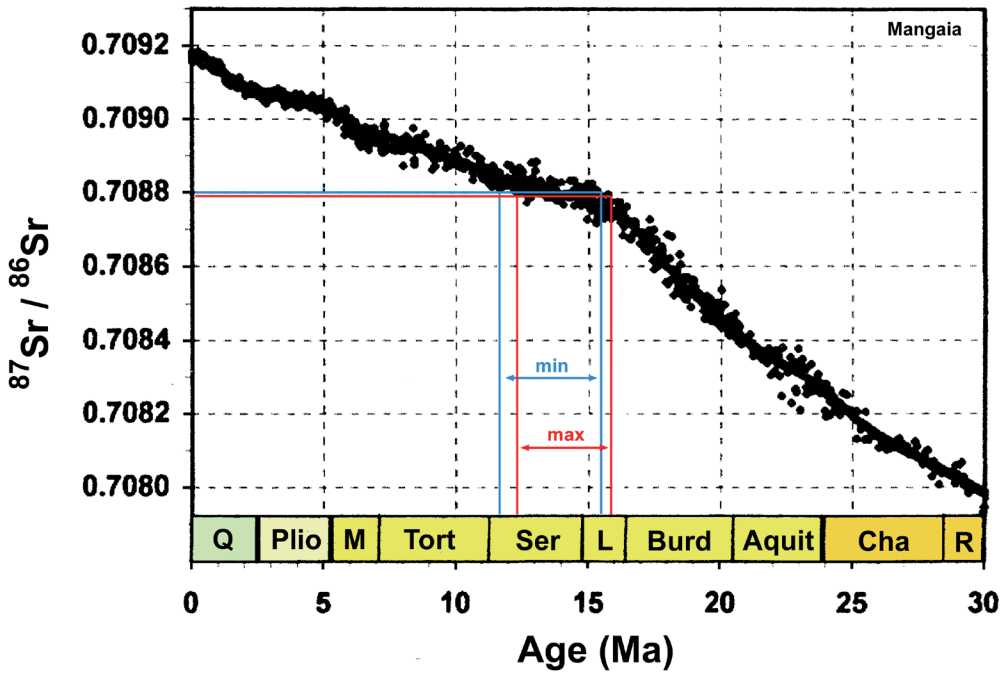


Fig. 9. Sr-isotope age range of sample from older makatea on Mangaia. Sr-isotope curve from McArthur *et al.* (2001). Minimum and maximum Sr-isotope ratios from Table 3 have been used to identify age range.

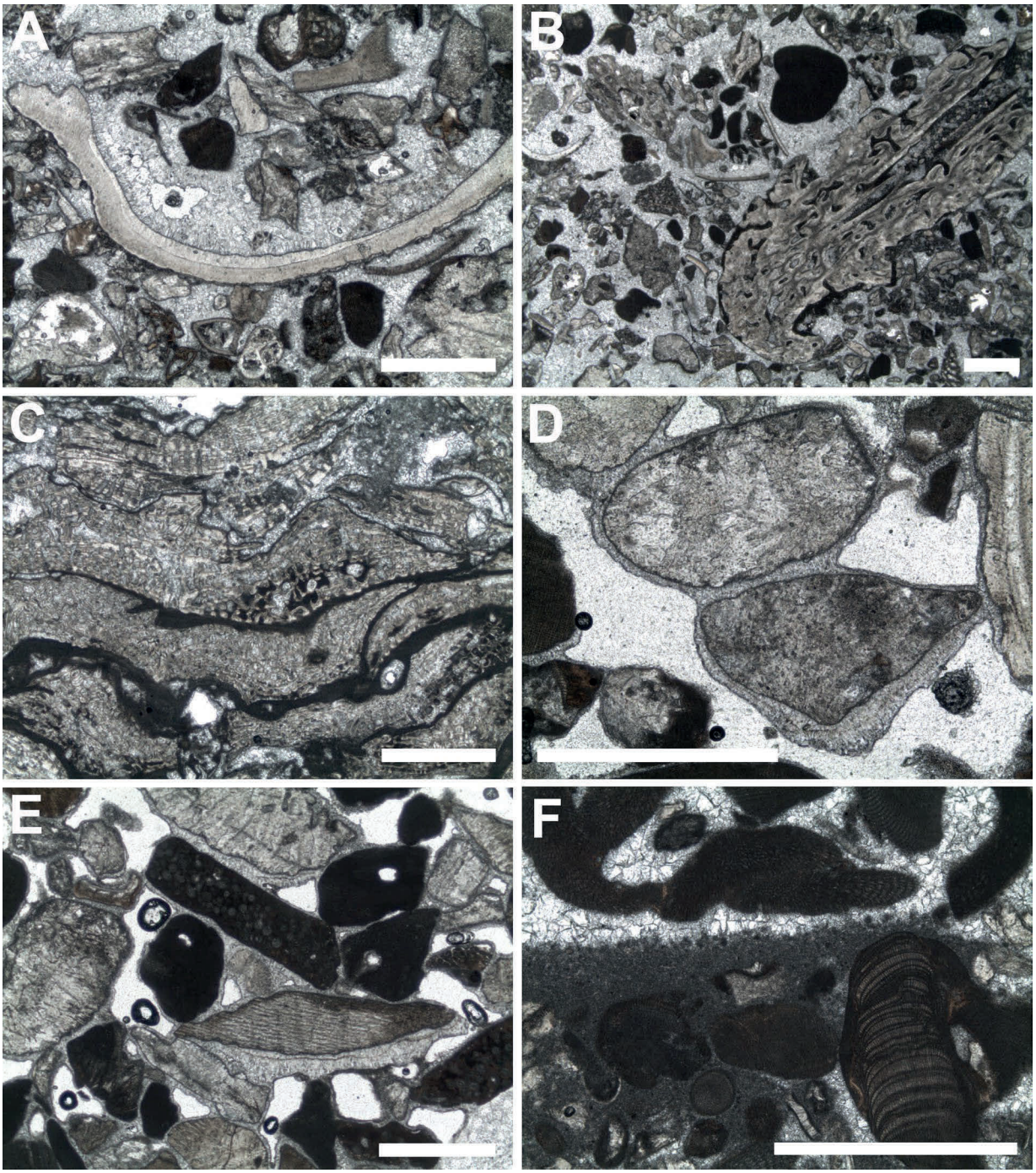


Fig. 10. Thin-section micrographs of limestones from quarry near airstrip on Mangaia. Scale bar is 1 mm. (A) Grainstone with mollusc shells, coralline algal fragments and blocky calcite cement. Unit 1. (B) Coralgal grainstone with blocky cement. Unit 1. (C) Boundstone with alternating platy corals and coralline algae. Unit 2. (D) Coral fragments with vadose cement texture. Unit 3. (E) Coralgal grainstone with meniscus cement texture. Unit 3. (F) Coralline algal fragments (*Amphiroa* at bottom right), peloidal and blocky cements. Unit 4.

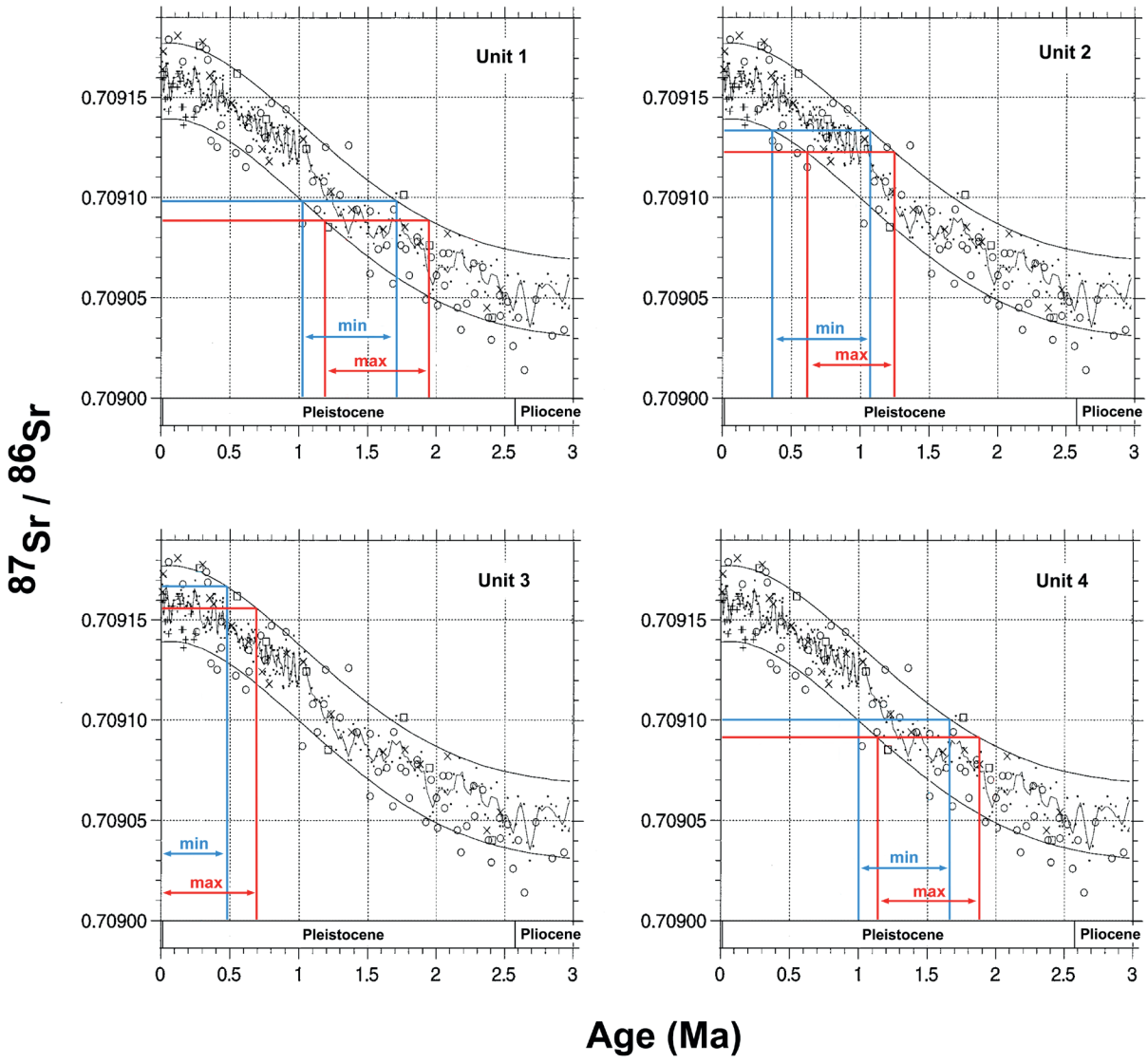


Fig. 11. Sr-isotope age ranges of samples from airstrip quarry in Mangaia. Sr-isotope curve from Farrell *et al*. (1995). Minimum and maximum Sr-isotope ratios from Table 3 have been used to identify age range.

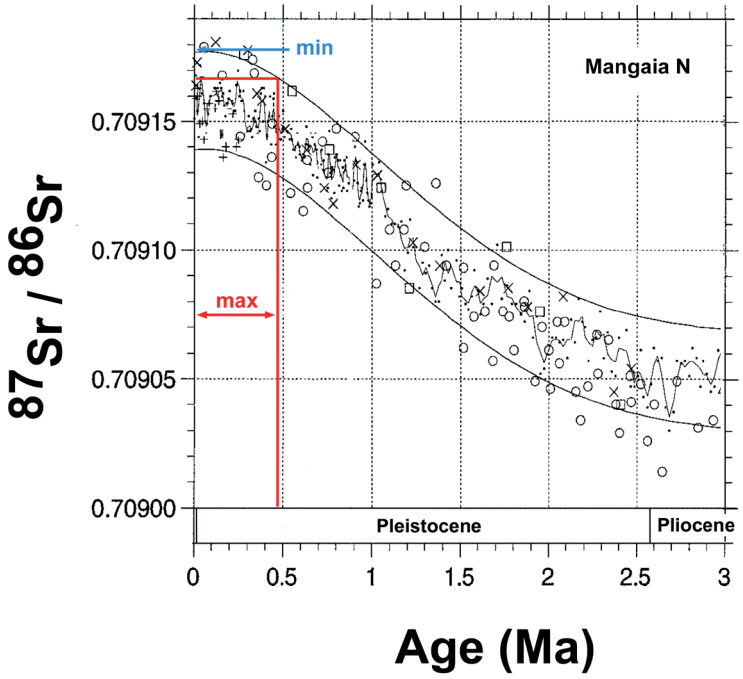


Fig. 12. Sr-isotope age range of Pleistocene coral from Mangaia N. Sr-isotope curve from Farrell *et al*. (1995).

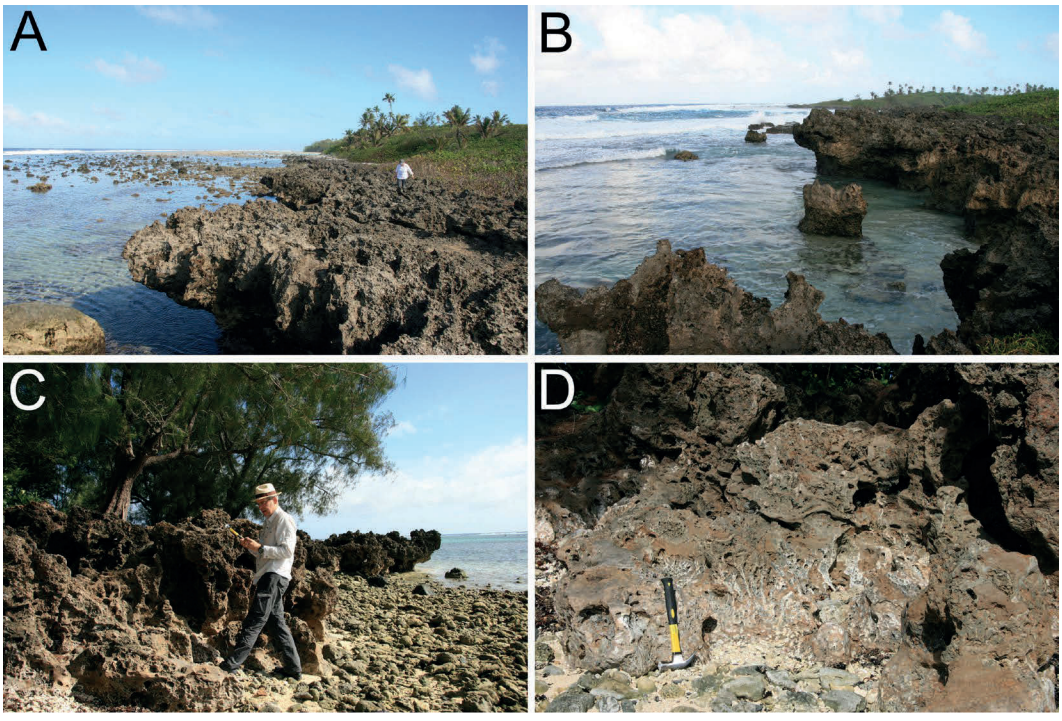


Fig. 13. Photos of reef terraces in Rarotonga. (A) North-eastern corner of Motutapu looking south showing Pleistocene reef terrace that stands some 2 m above modern sea-level. (B) Pleistocene reef terrace at Ngatangiia (looking south) with top some 3 m above modern sea-level. (C) Strongly weathered, fossil reef terrace at Nikao up to 1.5 m above modern sea-level. (D) Close-up of outcrop in C exhibiting fossil corals in growth position and strong weathering of limestone.

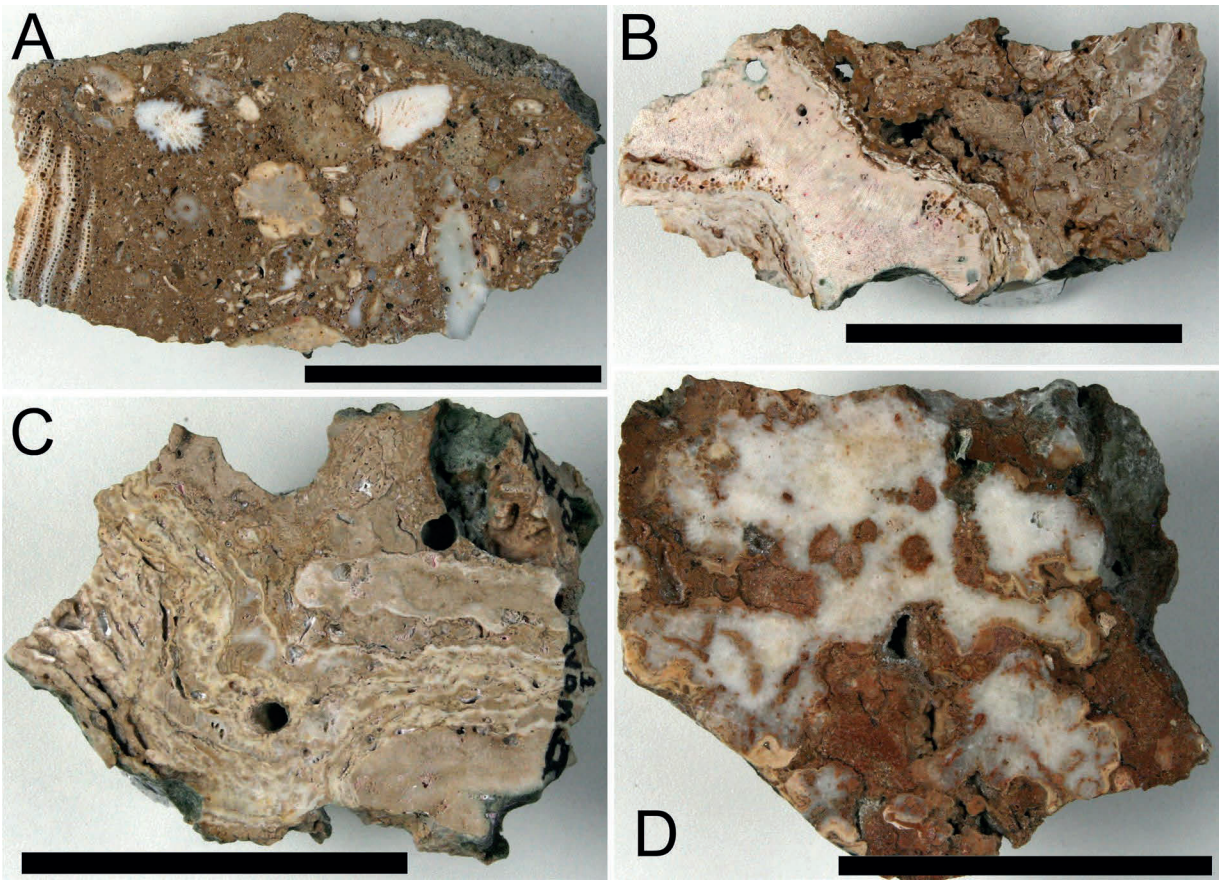


Fig. 14. Polished hand specimens from reef terraces of Rarotonga. Scale bar is 5 cm. All samples oriented upward. (A) Brownish grainstone with coral fragments; Motutapu. (B) Grainstone with large coral and coralline algal fragments; Ngatangiia. (C) Coralgal grainstone to boundstone; Ngatangiia. (D) Strongly altered coral grainstone to boundstone; Nikao.

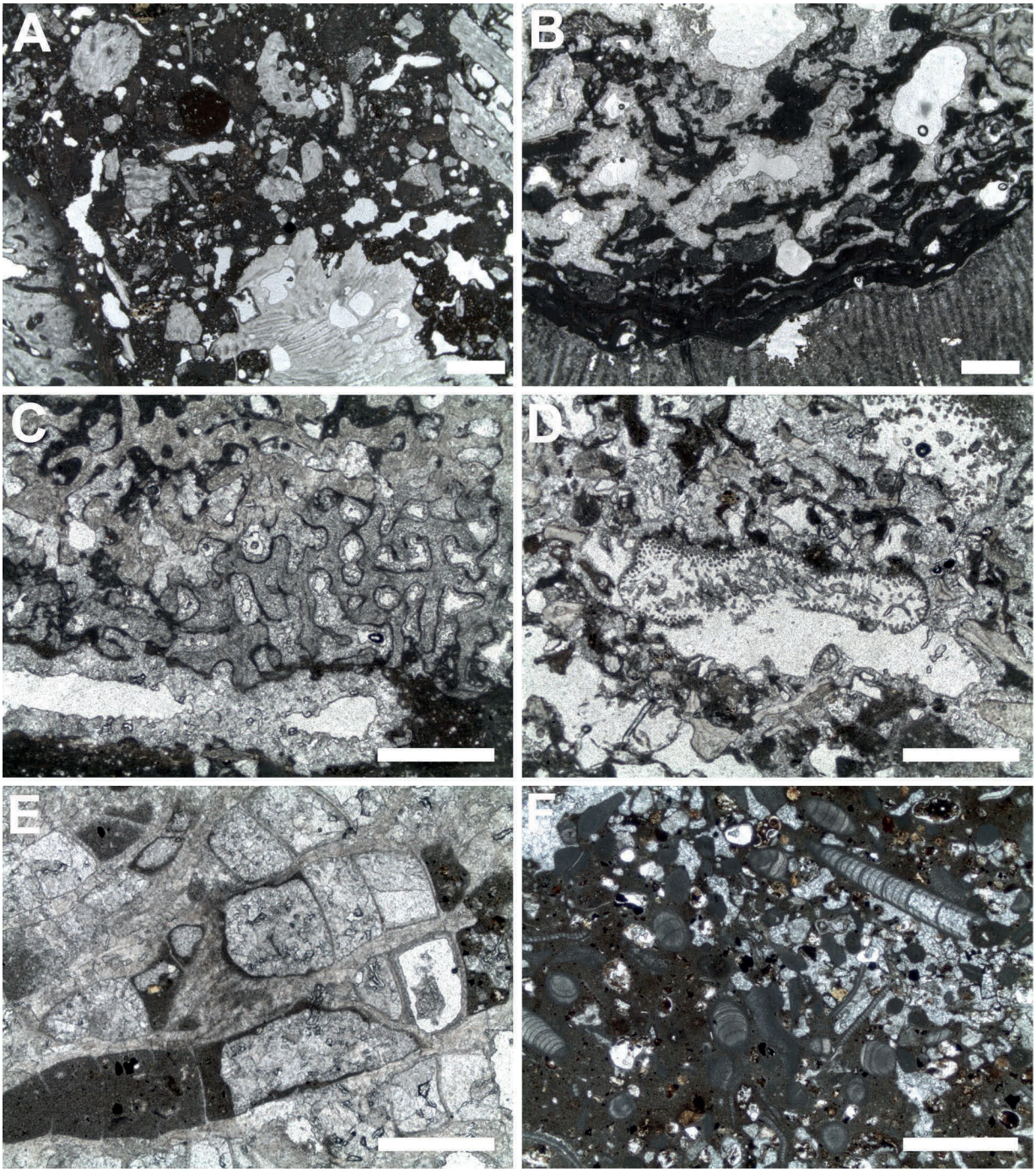


Fig. 15. Thin-section micrographs of limestones from reef terraces of Rarotonga. Scale bar is 1 mm. (A) Holocene coral packstone; Motutapu. (B) Pleistocene coral overlain by diagenetically altered coralline algal crusts; Ngatangiia. Large voids partly filled in with blocky calcite. (C) Recrystallised Pleistocene coral (*Porites*), fine detritus and blocky cement; Ngatangiia. (D) Partly dissolved *Halimeda* platelet in center; Ngatangiia. (E) Diagenetically altered coral and block calcite cement; Nikao. (F) Strongly altered coralgal packstone with geniculate corallines and *Lithoporella*; Nikao.

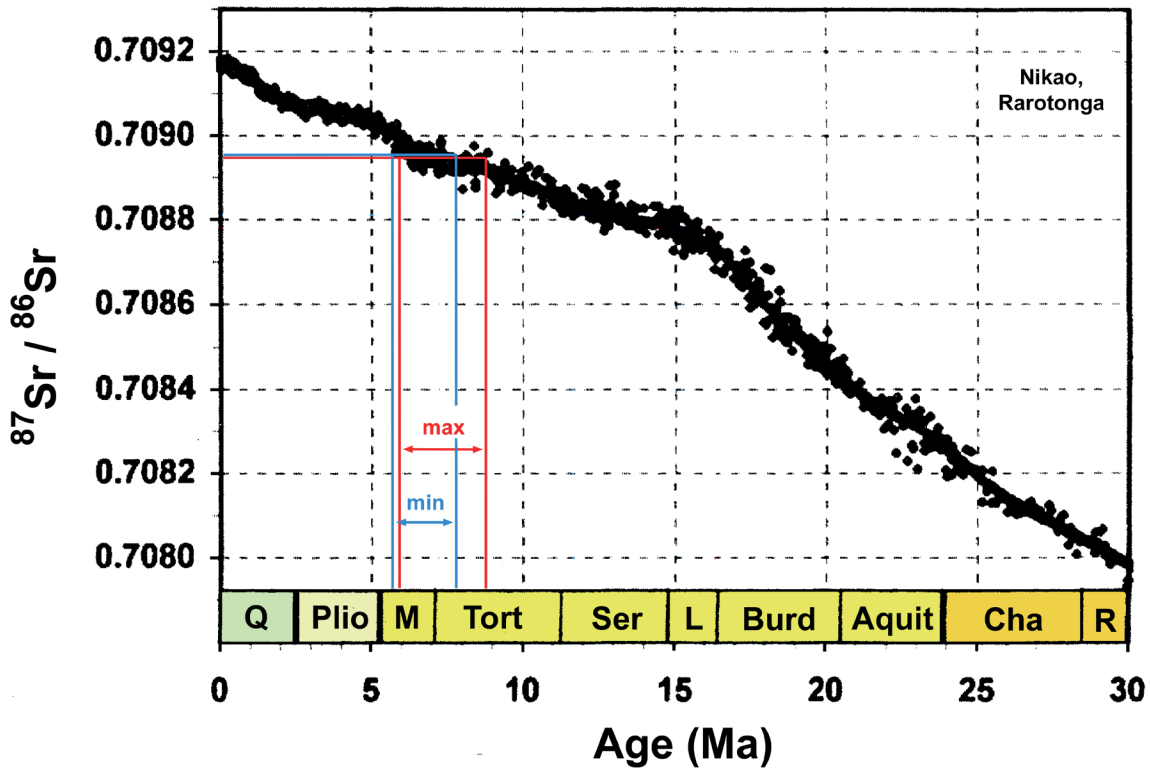


Fig. 16. Sr-isotope age range of sample from Nikao reef terrace, Rarotonga. Sr-isotope curve from McArthur *et al*. (2001).

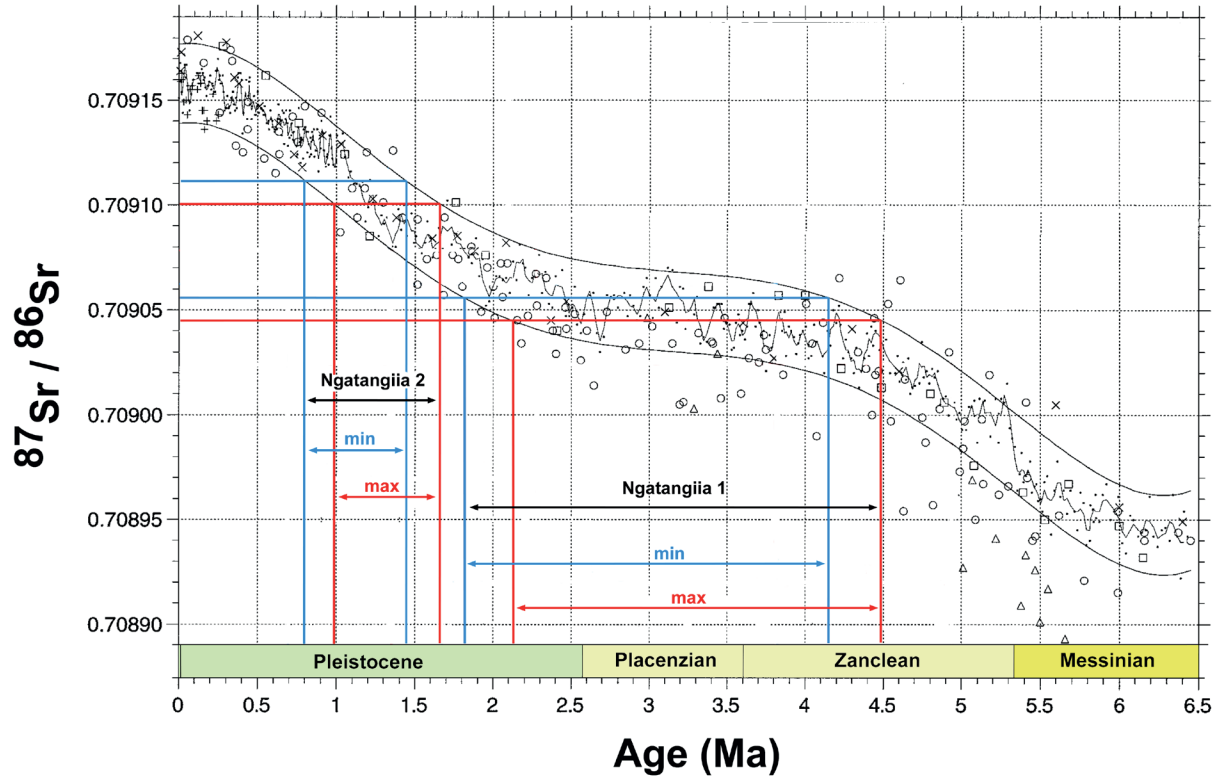


Fig. 17. Sr-isotope age ranges of samples from Ngatangiia, Rarotonga. Sr-isotope curve from Farrell *et al*. (1995).

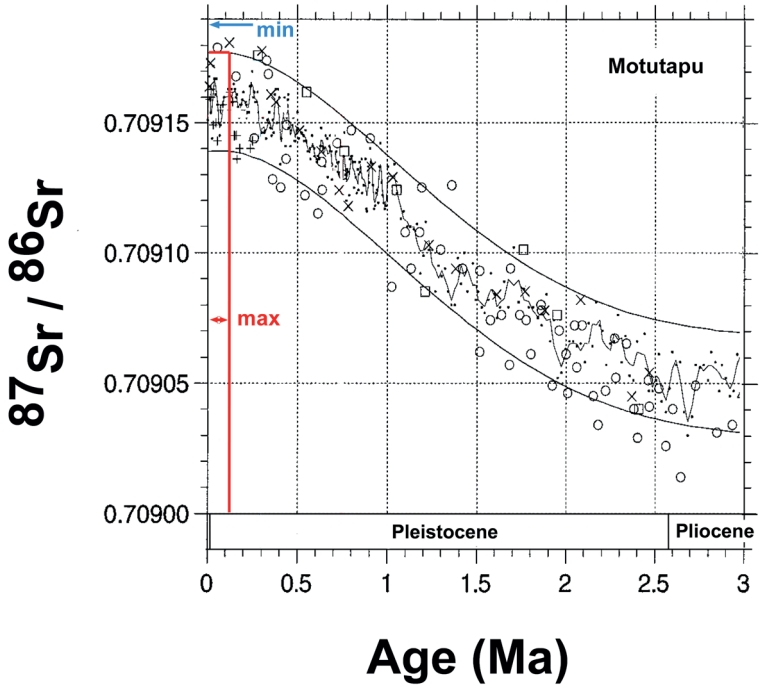


Fig. 18. Sr-isotope age range of sample from Motutapu, Rarotonga. Sr-isotope curve from Farrell *et al*. (1995).

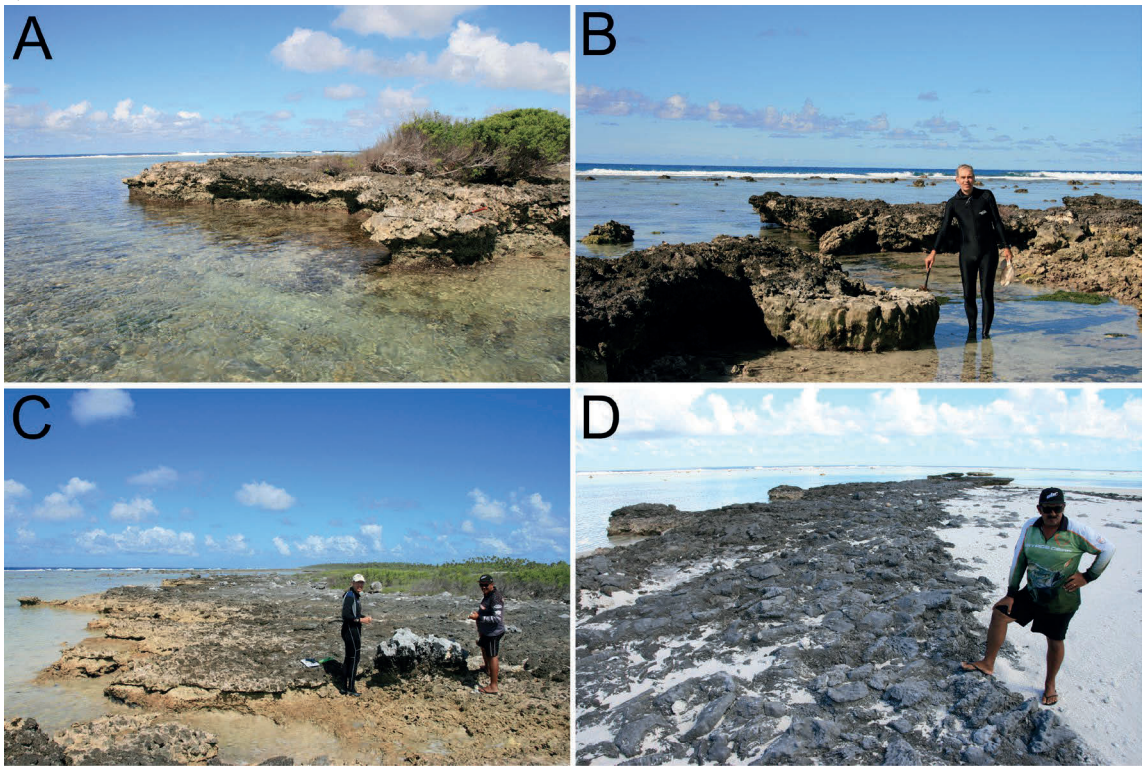


Fig. 19. Photos of reef terraces in Aitutaki. (A) Eastern corner of Motu Akitua (looking to the south-east) with fossil reef terrace. (B) Eastern side of Motu Papau with reef terrace and *in situ*, fossil *Porites* microatoll. (C) Eastern island side of Motu Akaiami with extensive fossil reef terrace. Massive *Porites* coral colony between persons is preserved *in situ*. (D) Reef terrace on south-eastern island side of Motukitiu.

Table 3. $^{87}Sr/^{86}Sr$ ratios and determined ages of bulk samples from Mangaia and Rarotonga.

Sample name	$^{87}Sr/^{86}Sr$ measured	± 2 σ mean	$^{87}Sr/^{86}Sr$ sample corrected to difference: NBS 987 value McArthur *et al.* (2001) and NBS 987 Bochum mean value	$^{87}Sr/^{86}Sr$ min	$^{87}Sr/^{86}Sr$ max	Estimated age (Ma) (based on Farrell *et al.* 1995; McArthur *et al.* 2001)	Mean value (Ma)	
Mangaia								
Maumaukura	0.708790	0.000005	0.708795	0.708790	0.708800	11.7 - 15.9	13.9	Mid Miocene
Airstrip unit 1	0.709082	0.000004	0.709087	0.709083	0.709091	1.03 - 1.95	1.49	MIS 29-71
Airstrip unit 2	0.709124	0.000005	0.709129	0.709124	0.709134	0.36 - 1.25	0.81	MIS 11-37
Airstrip unit 3	0.709158	0.000005	0.709163	0.709158	0.709168	0 - 0.69	0.35	MIS 1-17
Airstrip unit 4	0.709091	0.000005	0.709096	0.709091	0.709101	1.16 - 1.88	1.52	MIS 35-71
Mangaia N	0.709169	0.000005	0.709174	0.709169	0.709179	0 - 0.47	0.24	MIS 1-11
Rarotonga								
Nikao	0.708946	0.000004	0.708951	0.708947	0.708955	5.7 - 8.7	7.2	Late Miocene
Ngatangiia 1	0.709048	0.000004	0.709053	0.709049	0.709057	1.83 - 4.49	3.16	Plio-Pleistocene
Ngatangiia 2	0.709103	0.000005	0.709108	0.709103	0.709113	0.80 - 1.67	1.24	Mid Pleistocene
Motutapu	0.709176	0.000005	0.709181	0.709176	0.709186	0 - 0.12	0.06	MIS 1-5

Table 4. U/Th-ages from coral samples of Mangaia and Rarotonga. n.d.= not detected.

Sample		Ngatangiia, Rarotonga	Motutapu, Rarotonga	Mangaia N
Elevation	m	3	2	2
Coral		*Porites*	*Acropora*	*Porites*
Aragonite	%	99.8	99.8	99.6
age	kyr	0.064	3.205	127.058
±	kyr	0.022	0.044	1.51
^{238}U	ppm	2.8416	3.377	2.3357
±	ppm	0.0091	0.011	0.0047
^{232}Th	ppb	0.179	n.d.	0.326
±	ppb	0.06	0.068	0.067
^{230}Th	ppt	0.032	1.834	29.722
±	ppt	0.011	0.014	0.027
$^{230}Th/^{232}Th$	dpm/dpm	33.82	n.d.	17035.18
±	dpm/dpm	15.91	n.d.	3496.18
$^{238}U/^{232}Th$	dpm/dpm	49191.13	n.d.	22162.43
±	dpm/dpm	16547.72	n.d.	4548.58
$^{230}Th/^{238}U$	dpm/dpm	0.0007	0.0328	0.7687
±	dpm/dpm	0.0002	0.0003	0.0022
$^{234}U/^{238}U$	dpm/dpm	1.142	1.132	1.101
±	dpm/dpm	0.006	0.006	0.004
$^{234}U/^{238}U$ initial	dpm/dpm	1.142	1.133	1.144
±		0.006	0.006	0.005

Table 5. ^{14}C-ages from corals from reef terraces of Aitutaki. pMC = percent modern carbon.

Sample	Elevation (m)	Coral	Aragonite (rel. wt.-%)	Measured age (kyr BP)	±	Age (kyr cal BP)	±
Motu Akitua	0.5	*Acropora*	99.9	3.12	0.03	3.454	0.121
Motu Papau	0.5	*Porites*	99.9	1.89	0.03	1.931	0.135
Motu Akaiami 1	1	*Porites*	99.9	2.28	0.03	2.368	0.168
Motu Akaiami 2	1	*Acropora*	99.8	1.93	0.03	1.987	0.131
Motukitiu	1	*Acropora*	99.9	5.07	0.03	5.854	0.125
Motukitiu	1	*Tridacna*	99.7	0.121 pMC	0.004	0.114 pMC	0.004

DISCUSSION

Neogene reef terraces

Mangaia

The grain-supported facies sampled on the highest and oldest part of the makatea on Mangaia is clearly reef-related. According to Flügel (2004), *Lepidocyclina* is typical of shallow subtidal, moderate-energy lagoonal or back-reef depositional environments. Boudagher-Fadel (2018) characterised *Lepidocyclina* as being not as restricted with regard to occurrence and as being common in reef and fore-reef settings as well. The scarcity of abundant miliolids speaks against a lagoonal setting and the absence of *Amphistegina* against reef or proximal fore-reef environments. Therefore, a somewhat deeper fore-reef setting of 20 to 30 m depth is assumed. The coralline algae have wide palaeobathymetrical ranges of tens-of-metres and lack clear indicators of shallow, high-energy waters. Some taxa such as *Harveylithon* sp. are rare below 30 m depth. Based on the grain-supported textures, the common occurrences of corals, types of coralline algae and the foraminifera, the facies investigated was presumably deposited in a moderately high-energy fore-reef setting no deeper than 30 m. Early marine consolidation is evidenced by lengthy, bladed cements. The relatively long exposure in the meteoric realm explains the predominance of blocky cement in these deposits.

As the biostratigraphic range based on the findings of the foraminifer genus *Lepidocyclina* is Oligocene to Miocene and the Sr-isotope age is mid-Miocene, a mid-Miocene age, i.e. an age range of 12 to 16 Ma is most probable. This would fit to the slightly older K/Ar-age of the underlying volcanics of late early Miocene, i.e. 17 to 19.4 Ma (Dalrymple *et al*., 1975; Turner & Jarrard, 1982). An inferred mid-Miocene age of the makatea would be slightly younger than the suggested age of 17 Ma based on the finding of age-indicative planktonic foraminifera belonging to stratigraphic zones N7/N8, as reported by Yonekura *et al*. (1988). The uplift of Mangaia and other islands in the southern Cooks has been largely attributed to lithospheric loading by Rarotonga even though details of the causes and effects of this process were controversially discussed (McNutt & Menard, 1978; Lambeck, 1981; Spencer *et al*., 1987, 1988). Based on the average age of the Rarotonga volcanic rocks exposed above sea-level and the height of the Mangaia makatea, Stoddart *et al*. (1985) and Woodroffe *et al*. (1991) have estimated the uplift of Mangaia to 0.04 m kyr^{-1}. This is a minimum value based on the fact that parts of the Miocene reef platform have probably been eroded by karst processes. Estimates of erosion rates in Pacific limestone islands in the Marshalls, Kiribati and French Polynesia exhibit a wide range from 0 to 0.2 m kyr^{-1} (Paulay & McEdward, 1990). Stoddart *et al*. (1971) have meticulously assessed the subaerial erosion on the Pleistocene limestone island of Aldabra, Indian Ocean, to 0.005 m kyr^{-1}. Using this value and the average age of the Rarotonga volcanics would result in a reasonable total erosion estimate of 8.65 m for the Mangaia makatea. Woodroffe *et al*. (1991) suggested that on the southern Cook Islands of Atiu, Mitiaro and Mauke the older makatea, that evidently underlies exposed Pleistocene reef limestone, is also of Neogene age; however, absolute or biostratigraphic age data do not exist. Marshall (1930) reports that in contrast to his findings on Mangaia, *Lepidocyclina* does not occur in the older makatea of Atiu, suggesting ages younger than mid-Miocene.

Rarotonga

The Sr-isotope age of the reef terrace of Nikao, northern Rarotonga, suggests a late Miocene age (Fig. 16). This finding is enigmatic as the subaerial portion of

Rarotonga was formed only in the early Pleistocene (1.19 to 2.27 Ma; Turner & Jarrard, 1982). The oldest reliable K-Ar-age reported is >2.27 Ma (minimum age). Older eruptions are possibly of Pliocene age (Wood & Hay, 1970). A possible explanation for the relatively old age of the Nikao reef terrace could be a formation on a submarine high of the volcanic edifice and later displacement by younger volcanic lava flows. Indeed, the coralline algae suggest either a deep or shaded setting in tens of metres of water. The *in-situ* preservation of the branched corals might also hint to a somewhat deeper, lower energy environment. There are no age data from the submarine flanks of the islands and seamounts in the Cook Islands though (Hein *et al*., 1997), which could possibly shed light on this dating problem. An alternative explanation for the late Miocene age could be the strong diagenetic alteration of the Nikao reef terrace, which possibly rendered the Sr-isotope data unreliable. Indeed, Sr-contents are relatively low and Fe-concentrations elevated in this sample hint to strong diagenetic alteration. Signs of dissolution and large amounts of blocky cement in the deposits suggest also a strong influence of meteoric diagenesis. For these reasons, additional age data from this location would be desirable. The two ^{14}C-ages from older reef terraces in Rarotonga reported by Schofield (1970) are at the age limit of the dating method, therefore appear as outliers and should be no longer referred to (Fig. 20).

Pleistocene reef terraces

Rarotonga

The oldest Pleistocene reef terraces are possibly the ones from Ngatangiia on the eastern coast of Rarotonga. The Sr-isotope age ranges are large and reach far into the Pliocene due to a plateau in Sr-isotope reference curves (Farrell *et al*., 1995; McArthur *et al*., 2001); however, early Pleistocene ages of both samples are possible according to the data (Fig. 17) and would fit to the ages of the exposed volcanic rocks (1.19 to 2.27 Ma) that form the volcanic island of Rarotonga. The common occurrence of reef-related corals and the findings of abundant *Porolithon* gr. *onkodes* intergrown with vermetids suggests deposition in very shallow, high-energy waters for the older sample. The apparently younger sample from Ngatangiia is characterised by the occurrence of corallines indicative of lower energy or lower illumination in a somewhat deeper realm of up to 30 m of water. The occurrence of blocky, low-magnesium calcite cements suggests diagenetic alteration in the meteoric realm. Due to the fact that only very wide age ranges are available for the Ngatangiia deposits, any sea-level reconstructions based on these data would not be meaningful. The youngest, late Pleistocene sample from nearby Motutapu was most probably deposited during MIS 5e based on the composition and Sr-age data. Palaeobathymetry data suggests deposition in high-energy, shallow water based on the common occurrence of acroporid corals and the abundance of coralline algal fragments of *Porolithon* gr. *onkodes*. Elevation and age data of this sample suggest that relative sea-level during MIS 5e stood at least 3 m higher than today.

Mangaia

The ages of the terraces on Mangaia, from ca 9 m to ca 35 m elevation, positioned in between the last interglacial and the older, mid-Miocene makatea, have been largely unknown. The new Sr-ages obtained from the recently created airstrip quarry clearly suggest older Pleistocene ages, i.e. as old as 1.95 Ma (Fig. 21, Table 3). All four facies occurring in the quarry are reef-related and show diagenetic indications of post-depositional cementation in the meteoric zone. The coralline algae suggest shallow, high-energy settings for units 1, 3 and 4 based

on the common occurrence of *Porolithon* gr. *onkodes* and a somewhat deeper or shaded, low-energy setting for unit 2. Facies in units 1 to 3 exhibit a deepening and shallowing trend from a shallow, high-energy back-reef (unit 1) to a deeper reef (unit 2) to a littoral or beach facies (unit 3). The vadose cement textures in unit 3 support an interpretation as beach deposit. Other typical indicators of beach deposits such as low-angle bedding or fenestral textures are lacking. Unit 4 is probably once more a shallow, high-energy back-reef facies. Sr-isotope data indicate a Pleistocene age of the described succession within the terrace slope, ranging from ca 1.95 Ma to modern based on Sr-isotope data (Table 3). Units 1 to 3 show a decreasing age trend; however, unit 4 appears to be older, i.e. slightly older than unit 1. This peculiar age 'reversal' and the undulating boundary to the underlying unit 3 suggests units 1 to 3 being Pleistocene facies that were deposited attached to an older, Pleistocene cliff with overhangs (unit 4). Alternatively, the age inversion could be a hint to the reworking of older bioclasts; however, the age difference of units 3 and 4 seems to be too large for such an interpretation.

Six U-series ages of coral samples from Atiu and Mauke islands cluster around ca 200 ka and have been correlated with MIS 7 (Woodroffe *et al*., 1991). These data have shown already that Pleistocene deposits older than MIS 5e are exposed in the southern Cook Islands. However, it is improbable that the youngest unit 3 of the airstrip quarry is age-equivalent to the MIS 7-deposits because the latter have been found to be exposed at lower elevations (below 3 m above modern sea-level) as compared to the MIS-5e terraces (Woodroffe *et al*., 1991). After correction for estimated uplift-rates of 0.011 and 0.007 m kyr^{-1}, respectively (Woodroffe *et al*., 1991), these data plot between ca. -1 m and +1 m relative to modern sea-level, which is well within the supposed high sea-level range of MIS 7 (ca +5 m) based on either deep sea-based or reef-derived datasets (Schellmann & Radtke, 2004; Rohling *et al*., 2009; Rowe *et al*., 2014).

The age of the older makatea on the neighbouring islands of Atiu, Mauke and Mitiaro is apparently younger than Miocene, possibly Pliocene or older Pleistocene, as no *Lepidocyclina* has been recovered and because younger Pleistocene deposits unconformably overlie them. Based on comparisons with the elevation of stranded shorelines in Gippsland, south-eastern Australia, Ward *et al*. (1971) had estimated the ages of the terraces on Mangaia occurring from 15 m to 35 m elevation to range from ca 400 ka to 865 ka, which would fall within the age range of units 2 and 3 as suggested by the new Sr-isotope data. It has to be kept in mind though that there were no absolute age determinations of the older Pleistocene available from Gippsland but only estimated 'altimetric' ages based on elevation. The assumption of Stoddart *et al*. (1985), who considered deposits to ca. +20 m elevation on Mangaia as last interglacial and positioned the Quaternary-Tertiary contact at 14.5 to 18.5 m, can probably not be sustained based on the new data. The erosional terraces of the main volcanic islands of Rarotonga and Aitutaki (Schofield, 1967; Wood & Hay, 1970) could well be additional hints to former, possibly older Pleistocene sea-level positions. However, as no fossil reefs are present that could potentially be dated, the origin of these terraces remains poorly constrained.

The newly obtained MIS 5e-age (127.06 ka) from the lowest terrace on Mangaia ('Mangaia N') at an elevation of +2 m corresponds to some of the previous ages of Woodroffe *et al*. (1991) (Fig. 20, Table 6). The abundance of robust-branching acroporids in this coral-rich facies speaks for a reefal, high-energy and shallow-water depositional environment. A correction for

uplift of the 2 m elevation of the newly dated sample, using the 0.04 m kyr^{-1} estimate of Stoddart *et al*. (1985), would result in a position ca. 3 m below modern level. During this time, i.e. 123 to 129 ka, sea-level was 2 to 3 m above present level according to the compilation of Hearty *et al.* (2007). Hence, the bathymetrical position of the newly dated coral would have been some 5 m below former sea-level. Based on the notion that maximum MIS 5e-sea-level was 6 to 9 m higher than today (Hearty *et al*., 2007; Dutton *et al*., 2015), the elevation of the two MIS 5e-ages of Woodroffe *et al*. (1991) 13 to 15 m above sea-level can be explained only with additional island uplift. Correction for uplift results in sample elevations of 7.6 m and 10.3 m, respectively, with the latter value only slightly exceeding maximum MIS 5e-sea-level. Elevated reefs of MIS 5e-age have been reported from Atiu, Mitiaro and Mauke as well (Fig. 20). The elevation of one of the samples from Atiu corrected for uplift lies slightly above the maximum MIS 5e-sea-level. There are no clear morphological or lithological hints to the existence of older MIS 7 deposits along the lower terrace on Mangaia. Woodroffe *et al*. (1991) reported MIS 7 deposits from the nearby islands of Mauke and Mitiaro that occurred at lower elevation as compared to the MIS 5e reef; however, it was conceded that it was difficult in cases to differentiate between older Pleistocene units.

Veeh (1966) and Woodroffe *et al*. (1991) also reported somewhat younger coral ages from Mangaia with elevations 2 to 11 m above modern sea-level, that can be best assigned to MIS 5c (Fig. 20). Three of the ages lie between 1 and 2 m below modern sea-level, after correction for uplift. One age is still positioned some 7 m above modern sea-level despite uplift correction. Additional MIS 5c-ages have been obtained from Atiu and Mitiaro (Woodroffe *et al*., 1991). After correction for uplift, one of them lies slightly below and four of them several metres above modern sea-level. There are different heights reported for maximum MIS 5c-sea-level. Both deep sea core data and reef terrace data suggests 10 to 20 m below modern level (e.g., Schellmann & Radtke, 2004; Lisiecki & Raymo, 2005; Rohling *et al*., 2009). Based on these observations, it becomes difficult to explain the relatively high elevation of the MIS 5c samples. Either MIS 5c-sea-level stood somewhat higher as suggested, e.g. by Rohling *et al*. (2014) based on data from the eastern Mediterranean Sea, or estimated uplift rates are too small. Dickinson (1998) speculated that continued magmatism below Rarotonga would still inflate the volcanic edifice and cause continued lithospheric flexure in the vicinity to explain excess makatea elevations in the surrounding islands. However, volcanic activity in Rarotonga ceased about a million years ago.

Holocene reef terraces

The new ^{14}C-data from the elevated reef terraces of Aitutaki provide – in combination with existing data from the archipelago – additional evidence for a higher-than-present sea-level during the Holocene (Fig. 22, Table 7). Following the report of Shepard (1961) of an elevated reef 60 cm above sea-level on Aitutaki, this was questioned by Wood & Hay (1970) and Stoddart & Gibbs (1975) who claimed there was no makatea or raised reef on Aitutaki. The latter authors characterised the fossil reef terrace as storm rubble; however, the new age data from elevated, *in-situ* corals ranging from 5.85 to 1.93 kyr BP clearly underline that sea-level stood up to 1.0 m higher during the late Holocene. Stoddart & Gibbs (1975) argued that corals in the elevated Aitutaki reef terraces were principally not *in situ*; however, many coral colonies, especially large, massive *Porites* and robust acroporids in growth position have been identified during this study. Higher-than-present (0.9 to 1.5 m)

Holocene (2.03 kyr BP) sea-level in the southern Cook Islands has also been reported from near Avarua, Rarotonga (Schofield, 1970), even though this outcrop was never relocated by subsequent workers, including this study.

Yonekura *et al.* (1988) analysed elevated microatolls on the modern fringing reef of Mangaia and concluded that sea-level stood up to 1.7 m above modern level during 4.0 to 3.4 kyr BP and fell to present level starting ca 3 kyr BP. The same authors also reported a fossil (1.53 kyr BP) microatoll elevated to 0.4 to 0.5 m above sea-level from Aitutaki, although without noting its location. Goodwin & Harvey (2008) concluded that the Holocene highstand of sea-level in the Cook Islands ceased some 1.5 kyr BP and fell from +1.3 m to +0.45 m by 1 kyr BP, based on the analysis of 3 microatolls from Aitutaki and 6 microatolls from Rarotonga. Woodroffe *et al*. (1990) obtained 6 age dates from corals elevated up to 0.3 m above sea-level ranging in age from 5.59 to 3.35 kyr BP from Mitiaro and Mauke. At the margin of Suwarrow Atoll, northern Cook Islands, Scoffin *et al*. (1985) discovered corals elevated up to 0.5 m above sea-level ranging in age from 4.68 to 2.4 kyr BP.

Most of the elevated latest Holocene corals occurring on top of Pleistocene reef terraces in Rarotonga analysed by Moriwaki *et al*. (2006) and during this study were probably redeposited storm rubble as they are plotting much too high above modern sea-level (Fig. 22). The isolated character of these young corals and coral grainstones lends further evidence to redeposition. The Holocene reef terraces of Aitutaki are very similar to those in French Polynesia (Montaggioni & Pirazzoli, 1984), which indicate that the sea rose above modern level since ca 6 kyr BP, stood at least 1 m above modern level from 5 to 3 kyr BP and then fell to modern level (Rashid *et al*., 2014; Hallmann *et al*., 2018).

CONCLUSIONS

- The Neogene limestone of Mangaia is a mid-Miocene reef facies. In-between these deposits and the MIS 5e-terrace, older Pleistocene reef-related facies (as old as 2.28 Ma) are present. More precise dating of these deposits is required to assign them to discrete sea-level highstands.
- Reef terraces of Rarotonga are possibly late Miocene (Nikao), Plio-Pleistocene (Ngatangiia) and late Pleistocene (Motutapu) based on Sr-isotope ratio age ranges. The late Miocene age of the Nikao sample is enigmatic. Plio-Pleistocene terraces are superimposed by Holocene storm deposits. Additional U-series dating of diagenetically unaltered corals would be desirable to constrain the ages of the older Rarotonga reef terraces.
- The late Holocene reef terraces of Aitutaki indicate a higher-than-present sea-level of at least +1 m. Reef terraces are comparable to similar deposits in adjacent French Polynesia.
- Limitations of this study refer to the fact that older reef terrace deposits without preserved aragonitic coral material had to be dated by the Sr-isotope method, which produced age ranges only. In addition, for the reconstruction of former sea-levels, the erosion rates of elevated reef terraces (makatea) are largely unconstrained; and the influence of processes such as uplift, subsidence and glacial isostatic adjustment on relative sea-level during the older Pleistocene and Neogene are increasingly difficult to estimate with increasing age of the deposits.

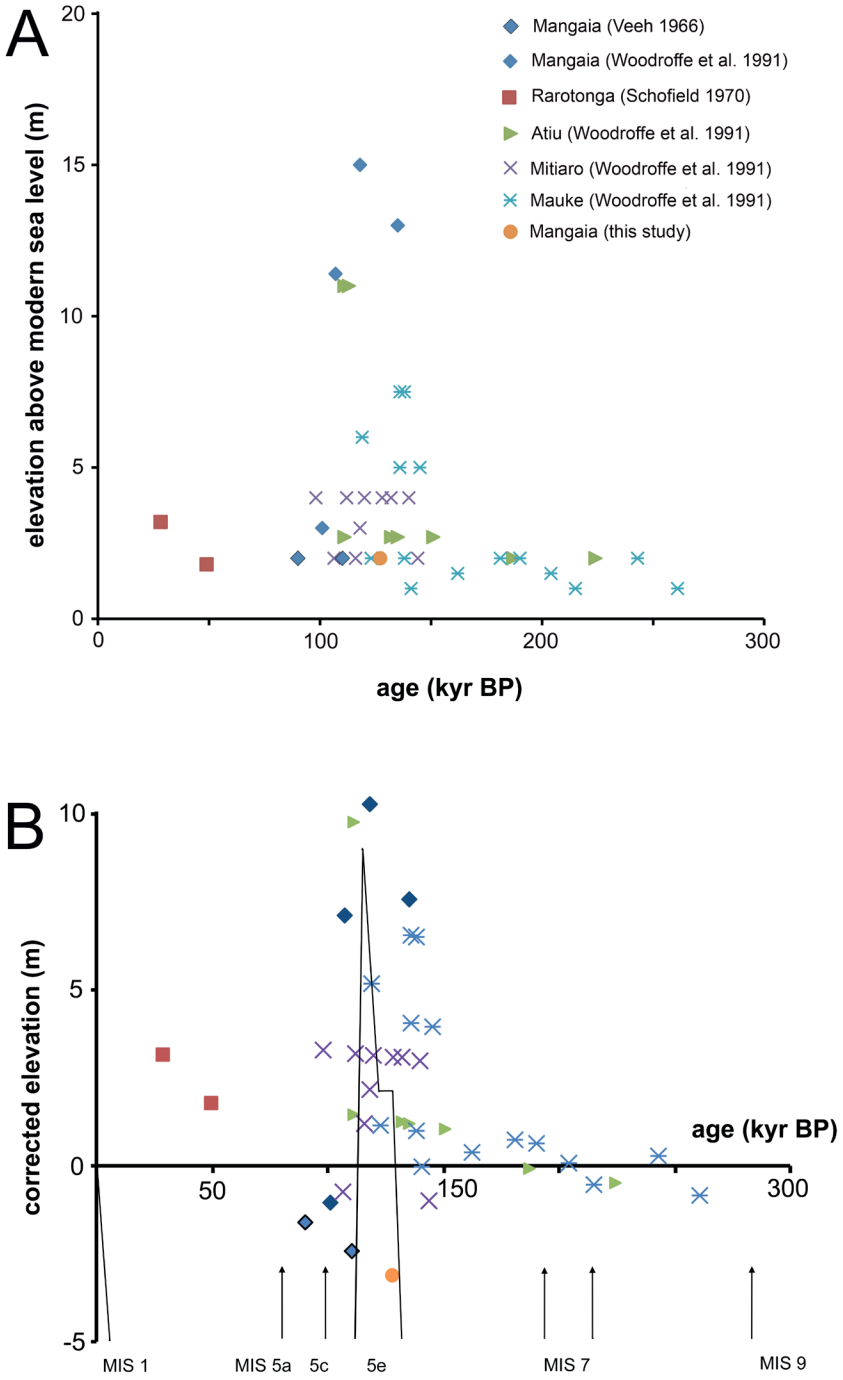


Fig. 20. (A) Coral-based data on Pleistocene sea-level from the southern Cook Islands. Sources include Veeh (1966), Schofield (1970), Spencer *et al*. (1988) and Woodroffe *et al*. (1991). Note that older data point from Schofield (1970) is a minimum age. Data are not corrected for uplift. Highest data points (>10 m) from Mangaia and Atiu may be explained only by uplift, in addition to higher MIS 5e-sea-level. (B) Same dataset corrected for uplift as estimated in Woodroffe *et al*. (1991). Positions of sea-level peaks of MISs 1, 5, 7 and 9 have been indicated. The course of sea-level during MIS 5e is based on the compilation of Hearty *et al*. (2007). Due to controversial data regarding exact maximum sea-levels of MIS 5a, 5c and 7, only arrows have been drawn.

Table 6. Pleistocene coral age data from the southern Cook Islands.

PLEISTOCENE						
Sample	**Coral**	**Elevation (m)**	**ARA (%)**	**Age (kyr BP)**	**Error (kyr)**	**Reference**
Mangaia						
Mang1	*Favia*	2	unknown	90.0	20.00	Veeh (1966)
Mang2	*Leptoria*	2	unknown	110.0	20.00	Veeh (1966)
M2	*Porites*	15	>99	118.0	12.00	Spencer *et al.* (1988); Woodroffe *et al.* (1991)
M3	*Porites*	11.4	>100	107.0	18.00	Spencer *et al.* (1988); Woodroffe *et al.* (1991)
M47	*Porites*	3	>101	101.0	12.00	Spencer *et al.* (1988); Woodroffe *et al.* (1991)
M54	*Porites*	13	>102	135.0	15.00	Spencer *et al.* (1988); Woodroffe *et al.* (1991)
Rarotonga						
Airport	coral	1.8	recryst.	>48.9		Schofield (1970)
Ngatangiia	coral	3.2	recryst.	28.2	0.85	Schofield (1970)
Atiu						
AT2	massive	2	>99	187.0	11.50	Woodroffe *et al.* (1991)
				224.0	19.50	Woodroffe *et al.* (1991)
AT8	*Porites*	2.7	>99	132.0	9.50	Woodroffe *et al.* (1991)
				111.0	7.00	Woodroffe *et al.* (1991)
AT9	*Porites*	2.7	>98	135.0	10.00	Woodroffe *et al.* (1991)
				151.0	11.50	Woodroffe *et al.* (1991)
AT11	massive	11	>99	111.0	6.00	Woodroffe *et al.* (1991)
				113.0	8.50	Woodroffe *et al.* (1991)
Mitiaro						
MT1	faviid	4	>99	128.0	6.00	Woodroffe *et al.* (1991)
				140.0	9.50	Woodroffe *et al.* (1991)
				98.1	5.25	Woodroffe *et al.* (1991)
MT2	faviid	4	>99	112.0	7.00	Woodroffe *et al.* (1991)
				132.0	9.00	Woodroffe *et al.* (1991)
MT9	*Plesiastrea*	4	>98	120.0	6.00	Woodroffe *et al.* (1991)
				132.0	8.50	Woodroffe *et al.* (1991)
MT13	*Porites*	2	>99	116.0	8.00	Woodroffe *et al.* (1991)
				144.0	8.50	Woodroffe *et al.* (1991)
				106.3	5.25	Woodroffe *et al.* (1991)
MT15	*Porites*	3	>98	118.0	7.00	Woodroffe *et al.* (1991)
				118.0	7.00	Woodroffe *et al.* (1991)

Table 6 continuation. Pleistocene coral age data from the southern Cook Islands.

PLEISTOCENE						
Sample	**Coral**	**Elevation (m)**	**ARA (%)**	**Age (kyr BP)**	**Error (kyr)**	**Reference**
Mauke						
MK6	faviid	1	>99	215.0	14.00	Woodroffe *et al.* (1991)
				261.0	44.50	Woodroffe *et al.* (1991)
				141.0	8.85	Woodroffe *et al.* (1991)
MK9	*Porites*	7.5	>98	136.0	9.50	Woodroffe *et al.* (1991)
				138.0	9.50	Woodroffe *et al.* (1991)
MK10	faviid	1.5	>99	204.0	18.00	Woodroffe *et al.* (1991)
				162.0	11.50	Woodroffe *et al.* (1991)
MK14	faviid	2	>99	243.0	22.00	Woodroffe *et al.* (1991)
				190.0	18.00	Woodroffe *et al.* (1991)
				181.2	13.80	Woodroffe *et al.* (1991)
MK15	encrusting	2	>98	123.0	7.50	Woodroffe *et al.* (1991)
				138.0	11.50	Woodroffe *et al.* (1991)
MK16	*Porites*	5	>99	136.0	11.00	Woodroffe *et al.* (1991)
				145.0	9.50	Woodroffe *et al.* (1991)
MK18	*Porites*	6	>98	119.0	7.50	Woodroffe *et al.* (1991)
				119.0	7.00	Woodroffe *et al.* (1991)
Mangaia						
Mangaia N	*Porites*	2	99.6	127.1	1.51	This study

Table 7. Holocene coral age data from the Cook Islands.

HOLOCENE						
Sample	**Coral**	**Elevation (m)**	**ARA (%)**	**Age (kyr BP)**	**Error (kyr)**	**Reference**
Mangaia						
Man3	*Porites*	1.5	100	3.410	0.170	Yonekura *et al.* (1988)
Man4	*Porites*	1	98.5	5.020	0.190	Yonekura *et al.* (1988)
Man7	*Porites*	1.1	100	4.990	0.210	Yonekura *et al.* (1988)
Man13	*Porites*	0.95	100	4.370	0.210	Yonekura *et al.* (1988)
Man15A	*Porites*	1.25	100	3.540	0.190	Yonekura *et al.* (1988)
Man21	*Porites*	1.4	100	3.980	0.180	Yonekura *et al.* (1988)
Rarotonga						
Avarua	coral	0.9	sl. recryst.	2.030	0.060	Schofield (1970)
Ngatangiia	coral	1.35	unknown	0.655	0.162	Moriwaki *et al.* (2006)
Ngatangiia	coral	1.35	unknown	0.584	0.066	Moriwaki *et al.* (2006)
Motutapu	coral	0.2	unknown	0.942	0.105	Moriwaki *et al.* (2006)
Motutapu	coral	0.5	unknown	0.942	0.105	Moriwaki *et al.* (2006)
Black Rock	*Porites*	0.15	unknown	0.260	0.088	Goodwin & Harvey (2008)
Black Rock	*Porites*	0.25	unknown	0.200	0.105	Goodwin & Harvey (2008)
Black Rock	*Porites*	0.35	unknown	0.470	0.081	Goodwin & Harvey (2008)
Black Rock	*Porites*	0.06	unknown	1.000	0.110	Goodwin & Harvey (2008)
Black Rock	*Porites*	0.06	unknown	0.960	0.100	Goodwin & Harvey (2008)
Black Rock	*Porites*	0.15	unknown	0.276	0.135	Goodwin & Harvey (2008)
Black Rock	*Porites*	0.15	unknown	0.150	0.119	Goodwin & Harvey (2008)
Aitutaki						
unknown	elev. reef	0.6	unknown	unknown	unknown	Shepard (1961)
Airport	microatoll	0.45	unknown	1.530	0.210	Yonekura *et al.* (1988)
Ootu	*Porites*	0.8	unknown	1.591	0.107	Goodwin & Harvey (2008)
Ootu	*Porites*	0.6	unknown	1.520	0.117	Goodwin & Harvey (2008)
Ootu	*Porites*	0.8	unknown	1.601	0.104	Goodwin & Harvey (2008)
Mitiaro						
MT17	faviid	0.3	unknown	4.850	0.090	Woodroffe *et al.* (1990)
MT16	faviid	0.3	unknown	4.350	0.090	Woodroffe *et al.* (1990)
MT18	*Porites*	0.3	unknown	4.070	0.080	Woodroffe *et al.* (1990)
MT19	*Porites*	0.3	unknown	5.590	0.090	Woodroffe *et al.* (1990)
MT22	*Porites*	0.3	unknown	4.450	0.080	Woodroffe *et al.* (1990)

Table 7 continuation. Holocene coral age data from the Cook Islands.

HOLOCENE						
Sample	**Coral**	**Elevation (m)**	**ARA (%)**	**Age (kyr BP)**	**Error (kyr)**	**Reference**
Mauke						
MK13	*Porites*	0.2	unknown	3.350	0.080	Woodroffe *et al.* (1990)
Suwarrow						
2	faviid	0.5	unknown	4.650	0.060	Scoffin *et al.* (1985); Woodroffe *et al.* (1990)
23	*Porites*	0.5	unknown	2.000	0.060	Scoffin *et al.* (1985); Woodroffe *et al.* (1990)
25	*Porites*	0.5	unknown	4.680	0.050	Scoffin *et al.* (1985); Woodroffe *et al.* (1990)
26	*Porites*	0.5	unknown	4.460	0.050	Scoffin *et al.* (1985); Woodroffe *et al.* (1990)
3	*Porites*	0.5	unknown	3.560	0.050	Scoffin *et al.* (1985); Woodroffe *et al.* (1990)
62	*Porites*	0.5	unknown	2.620	0.050	Scoffin *et al.* (1985); Woodroffe *et al.* (1990)
63	*Porites*	0.5	unknown	4.310	0.050	Scoffin *et al.* (1985); Woodroffe *et al.* (1990)
4	*Porites* + faviid	0.5	unknown	2.400	0.060	Scoffin *et al.* (1985); Woodroffe *et al.* (1990)
40	faviid	0.5	unknown	2.400	0.060	Scoffin *et al.* (1985); Woodroffe *et al.* (1990)
Aitutaki						
Motu Akitua	*Acropora*	0.5	99.9	3.454	0.03	This study
Motu Papau	*Porites*	0.5	99.9	1.931	0.03	This study
Motu Akaiami 1	*Porites*	1	99.9	2.368	0.03	This study
Motu Akaiami 2	*Acropora*	1	99.8	1.987	0.03	This study
Motukitiu	*Acropora*	1	99.9	5.854	0.03	This study
Rarotonga						
Ngatangiia	*Porites*	3	99.8	0.064	0.02	This study
Motutapu	*Acropora*	2	99.8	3.205	0.04	This study

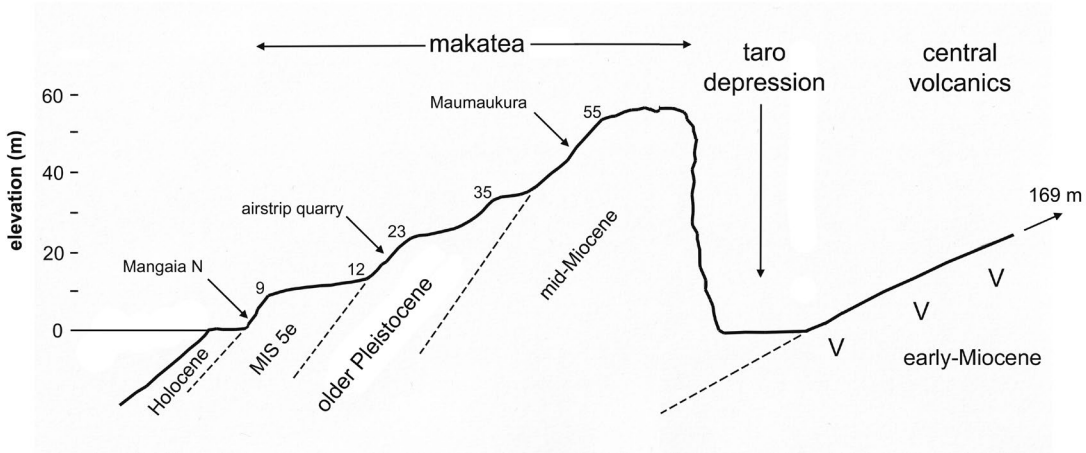


Fig. 21. Schematic and simplified cross-section through the makatea of Mangaia, including ages and age ranges as well as elevations of modern and fossil reef terraces (numbers are in metres) and also including elevations of the three investigated locations. Note that drawing is not to scale as width of makatea is 1 to 2 km. Height of makatea locally reaches up to 70 m.

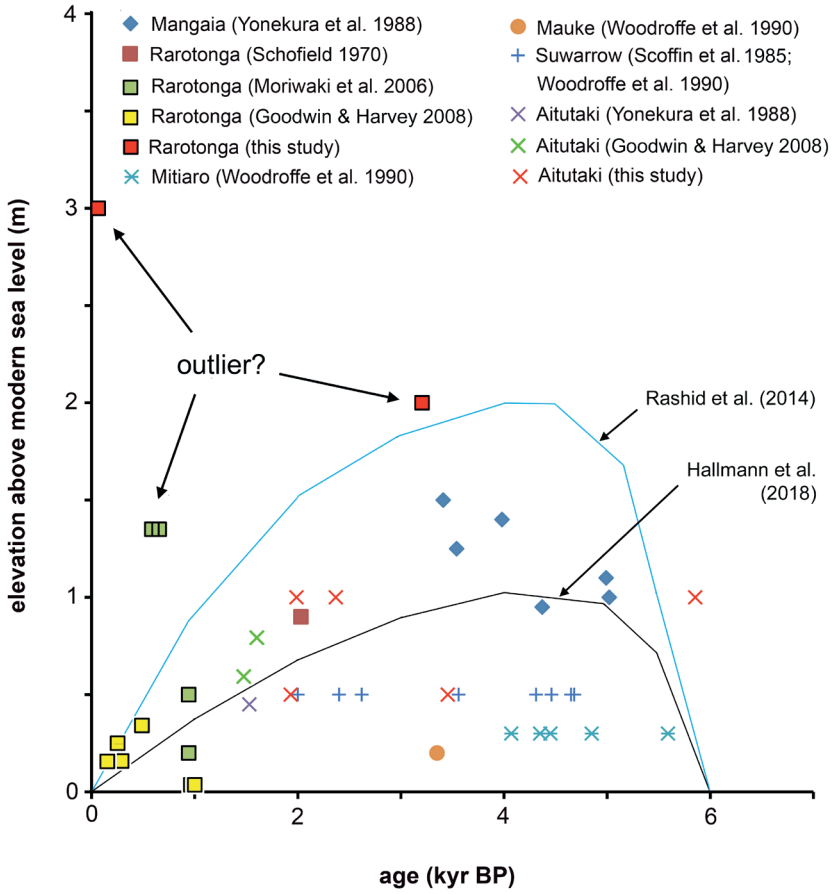


Fig. 22. Coral-based data on Holocene sea-level from the southern Cook Islands. Sources include Shepard (1961), Schofield (1970), Scoffin *et al*. (1985), Yonekura *et al*. (1988) and Woodroffe *et al.* (1990). Intrinsic lines of sea-level data from French Polynesia (Rashid *et al*., 2014; Hallmann *et al*., 2018) are shown for comparison. Data are not corrected for uplift. Some data points from Rarotonga are probably outliers and are probably redeposited storm rubble.

ACKNOWLEDGEMENTS

The authors are grateful to Caroline Pickering for supporting them in many ways during their stay on Mangaia. James Nolan of Wahoo Charters in Aitutaki is thanked for his assistance as a reliable boat captain and field assistant. Rock and coral samples were prepared by Nils Prawitz and Daniel Parwareschnia. Jacques Osthoff photographed polished rock samples. Thin-sections were made by Nils Prawitz. Rainer Petschick ran the X-ray diffractometer. Kathrin Krimmler is thanked for preparing samples for element concentrations and Sr-isotope analyses. Oliver Friedrich (Heidelberg) is thanked for meticulously treating a sample from Mangaia to obtain calcareous microfauna. Two journal reviewers provided helpful comments that improved this paper.

REFERENCES

Abbey, E., Webster, J.M., Braga, J.C., Sugihara, K., Wallace, C., Iryu, Y., Potts, D., Done, T., Camoin, G. and **Seard, C.** (2011) Variation in deglacial coralgal assemblages and their paleoenvironmental significance: IODP Expedition 310, "Tahiti Sea-level". *Global Planet. Change*, **76**, 1–15.

Allen, M.S. (1998) Holocene sea-level change on Aitutaki, Cook Islands: landscape change and human response. *J. Coastal Res.*, **14**, 10–22.

Birck, J.L. (1986) Precision K-Rb-Sr isotopic analysis: application to Rb-Sr chronology. *Chem. Geol.*, **56**, 73–83.

Blanchon, P. and **Perry, C.T.** (2004) Taphonomic differentiation of *Acropora palmata* facies in cores from Campeche Bank reefs, Gulf of Mexico. *Sedimentology*, **51**, 53–76.

Boudagher-Fadel, M. (2018) *Evolution and geological significance of larger benthic foraminifera*. 693 p., UCL Press, London.

Boudagher-Fadel, M. and **Price, G.D.** (2010) Evolution and paleogeographic distribution of the Lepidocyclinids. *J. Foramin. Res.*, **40**, 79–108.

Bourdon, M. (1957) Micropaleontological studies: utilisation of acetic acid during disintegration of hard rocks. *Rev. Inst. Fr. Pétrol.*, **12**, 14–15.

Braga, J.C., Humblet, M., Ramos, D.A.E., Dechnik, B. and **Webster, J.M.** Quaternary coral, coralline algal and vermetid assemblages as sea-level indicators: a review. In: *Coral Reefs and Sea-Level Change: Quaternary Records and Modelling* (Eds G.F. Camoin and N. Hallmann), *Int. Assoc. Sedimentol. Spec. Publ.*, **49** (this volume), 1–38.

Camoin, G.F. and **Webster, J.M.** (2015) Reef response to Quaternary sea-level and environmental changes: state of the science. *Sedimentology*, **62**, 401–428.

Chappell, J. (1974) Geology of coral terraces, Huon Peninsula, New Guinea: a study of Quaternary tectonic movements and sea-level changes. *Geol. Soc. Am. Bull.*, **85**, 553–570.

Chappell, J. and **Shackleton, N.J.** (1986) Oxygen isotopes and sea-level. *Nature*, **324**, 137–140.

Cheng, H., Edwards, R., Hoff, J., Gallup, C., Richards, D. and **Asmerom, Y.** (2000) The half-lives of uranium-234 and thorium-230. *Chem. Geol.*, **169**, 17–33.

Chikamori, M. (1996) Development of coral reefs and human settlement: archeological research in the northern Cook Islands and Rarotonga. *Bull. Indo-Pacific Prehist. Assoc.*, **15**, 45–52.

Chubb, L.J. (1927) Mangaia and Rurutu: a comparison between two Pacific islands. *Geol. Mag.*, **64**, 518–522.

Cotton, C.A. (1969) The pedestals of oceanic volcanic islands. *Geol. Soc. Am. Bull.*, **80**, 749–760.

Dalrymple, G.B., Jarrard, R.D. and **Clague, D.A.** (1975) K-Ar ages of some volcanic rocks from the Cook and Austral Islands. *Geol. Soc. Am. Bull.*, **86**, 1463–1467.

Davis, W.M. (1928) The coral reef problem. *Am. Geog. Soc. Spec. Publ.*, **9**, 596 p.

Dickinson, W.R. (1998) Geomorphology and geodynamics of the Cook-Austral island-seamount chain in the South Pacific Ocean: implications for hotspots and plumes. *Int. Geol. Rev.*, **40**, 1039–1075.

Dutton, A., Carlson, A.E., Long, A.J., Milne, G.A., Clark, P.U., DeConto, R., Horton, B.P., Rahmstorf, S. and **Raymo, M.E.** (2015) Sea-level rise due to polar ice-sheet mass loss during past warm periods. *Science*, **349**, aaa4019-1.

Farrell, J.W., Clemes, S.C. and **Gromet, L.P.** (1995) Improved chronostratigraphic reference curve of late Neogene seawater $^{87}Sr/^{86}Sr$. *Geology*, **23**, 403–406.

Fietzke, J., Liebetrau, V., Eisenhauer, A. and **Dullo, W.C.** (2005) Determination of uranium isotope ratios by multistatic MIC-ICP-MS, method and implementtation for precise U- and Th-series isotope measurements. *Journal of Analytical Atomic Spectrometry*, **20**, 395–401.

Flügel, E. (2004) *Microfacies of Carbonate Rocks*. 976 p.; Springer, Berlin.

Forbes, D.L., James, T.S., Sutherland, M. and **Nichols, S.E.** (2013) Physical basis of coastal adaptation on tropical small islands. *Sustain. Sci.*, **8**, 327–344.

Gibbs, P.E., Stoddart, D.R. and **Vevers, H.G.** (1971) Coral reefs and associated communities in the Cook Islands. In: Fraser, R. (compiler) Cook Bicentenary Expedition in the South-West Pacific. *Bull. Roy. Soc. NZ*, **8**, 91–105.

Gischler, E. (2020) Sediments of the almost-atoll Aitutaki, Cook Islands, South Pacific. *Sed. Geol.*, **403**, 105672.

Goodwin, I.D. and **Harvey, N.** (2008) Subtropical sea-level history from coral microatolls in the southern Cook Islands, since 300 AD. *Mar. Geol.*, **253**, 14–25.

Gray, S.C. and **Hein, J.R.** (2005) Lagoonal reef accretion and Holocene sea-level history from three atolls in the Cook Islands, central South Pacific. *J. Coastal Res.*, Special Issue, **42**, 253–264.

Hallmann, N., Camoin, G., Eisenhauer, A., Botella, A., Milne, G.A., Vella, C., Samankassou, E., Pothin, V., Dussouillez, P., Fleury, J. and **Fietzke, J.** (2018) Ice volume and climate changes from a 6000 year sea-level record in French Polynesia. *Nature Comms*, **9**, 285.

Hearty, P.J., Hollin, J.T., Neumann, A.C., O'Leary, M.J. and **McCulloch, M.** (2007) Global sea-level fluctuations during the last interglacial (MIS 5e). *Quatern. Sci. Rev.*, **26**, 2090–2112.

Hein, J.R., Gray, S.C. and **Richmond, B.M.** (1997) Geology and hydrogeology of the Cook Islands. In: *Geology and Hydrogeology of Carbonate Islands* (Eds H.L. Vacher and T. Quinn), *Dev. Sedimentol.*, **54**, 503–535.

Hoffmeister, J.E. (1930) Erosion of elevated fringing coral reefs. *Geol. Mag.*, **57**, 549–554.

IPCC (2014) *Climate Change 2014: Synthesis Report. Contribution of Working Groups I, II and III to the Fifth Assessment Report of the Intergovernmental Panel on Climate Change* (Eds R.K. Pachauri and L.A. Meyer), IPCC, Geneva, Switzerland, 151 pp.

Lambeck, K. (1981) Lithospheric response to volcanic loading in the southern Cook Islands. *Earth Planet. Sci. Lett.*, **55**, 482–496.

Lewis, K.B., Utanga, A.T., Hill, P.J. and **Kingan, S.G.** (1980) The origin of channel-fill sands and gravels on an algal-dominated reef terrace, Rarotonga, Cook Islands. *South Pacific Marine Geological Notes,* **2**, 1–23.

Lisiecki, L.E. and **Raymo, M.E. (2005)** A Pliocene-Pleistocene stack of 57 globally distributed benthic ^{18}O records. *Paleoceanography*, **20**, PA1003.

Marshall, P. (1927) Geology of Mangaia. *Bulletin Bernice P. Bishop Museum*, **36**, 1–48.

Marshall, P. (1929) Mangaia and Rurutu - a comparison between two Pacific islands. *Geol. Mag.*, **66**, 385–389.

Marshall, P. (1930) Geology of Rarotonga and Atiu. *Bulletin Bernice P. Bishop Museum*, **72**, 1–75.

McArthur, J.M., Howarth, R.J. and **Bailey, T.R.** (2001) Strontium isotope stratigraphy: LOWESS version 3: best fit to the marine Sr-isotope curve for 0-509 Ma and accompanying look-up table for deriving numerical age. *J. Geol.*, **109**, 155–170.

McArthur, J.M., Howarth, R.J. and **Shields, G.A.** (2012) Strontium isotope stratigraphy. In: *The Geological Time Scale* (Eds F. Gradstein, J.G. Ogg, M. Schmitz and G. Ogg), Elsevier, Amsterdam, p. 127–144.

McNutt, M. and **Menard, H.W.** (1978) Lithospheric flexure and uplifted atolls. *J. Geophys. Res.*, **83**, 1206–1212.

Mesolella, K.J., Matthews, R.K., Broecker, W.S. and **Thurber, D.L.** (1969) The astronomical theory of climatic change: Barbados data. *J. Geol.*, **77**, 250–274.

Milliman, J.D. (1974) *Marine Carbonates*. 375 p.; Springer, Berlin.

Montaggioni, L.F. and **Pirazzoli, P.A.** (1984) The significance of exposed coral conglomerates from French Polynesia (Pacific Ocean) as indicators of recent relative sea-level changes. *Coral Reefs*, **3**, 29–42.

Moriwaki, H., Chikamori, M., Okuno, M. and **Nakamura, T.** (2006) Holocene changes in sea-level and coastal environments on Rarotonga, Cook Islands, South Pacific Islands. *The Holocene*, **16**, 839–848.

Paulay, G. and **McEdward, L.R.** (1990) A simulation model of island reef morphology: the effects of sea-level fluctuations, growth, subsidence and erosion. *Coral Reefs*, **9**, 51–62.

Purdy, E.G. and **Winterer, E.L.** (2006) Contradicting barrier reef relationships for Darwin's evolution of reef types. *Int. J. Earth Sci.*, **95**, 143–167.

Rankey, E.C. and **Reeder, S.L.** (2009) Holocene ooids of Aitutaki Atoll, Cook Islands, South Pacific. *Geology*, **37**, 971–974.

Rashid, R., Eisenhauer, A., Stocchi, P., Liebetrau, V., Fietzke, J., Rüggeberg, A. and **Dullo, W.C.** (2014) Constraining mid to late Holocene relative sea-level change in the southern equatorial Pacific Ocean relative to the Society Islands, French Polynesia. *Geochem. Geophys. Geosyst.*, **15**, 2601–2615.

Reimer, P.J., Bard, E., Bayliss, A., Beck, J., Blackwell, P., Ramsey, C., … and **Van der Plicht, J.** [30 authors] (2013) IntCal13 and Marine13 radiocarbon age calibration curves 0–50,000 years cal BP. *Radiocarbon*, **55**, 1869–1887.

Rohling, E.J., Foster, G.L., Grant, K.M., Marino, G., Roberts, A.P., Tamisiea, M.E. and **Williams, F.** (2014) Sea-level and deep-sea temperature variability over the past 5.3 million years. *Nature*, **508**, 477–482.

Rohling, E.J., Grant, K., Bolshaw, M., Roberts, A.P., Siddall, M., Hemleben, C. and **Kucera, M.** (2009) Antarctic temperature and global sea-level closely coupled over the past five glacial cycles. *Nature Geosci.*, **2**, 500–504.

Rowe, M.P., Wainer, K.A., Bristow, C.S. and **Thomas, A.L.** (2014) Anomalous MIS 7 sea-level recorded on Bermuda. *Quatern. Sci. Rev.*, **90**, 47–59.

Schellmann, G. and **Radtke, U.** (2004) A revised morpho- and chronostratigraphy of the late and middle Pleistocene coral reef terraces on southern Barbados (West Indies). *Earth-Sci. Rev.*, **64**, 157–187.

Schofield, J.C. (1967) Pleistocene sea-level evidence from Cook Islands. *J. Geosci. Osaka City Univ.*, **10**, 118–120.

Schofield, J.C. (1970) Notes on late Quaternary sea-levels, Fiji and Rarotonga. *NZ J. Geol. Geophys.*, **13**, 199–206.

Scoffin, T.P., Stoddart, D.R., Tudhope, A.W. and **Woodroffe, C.D.** (1985) Exposed limestones of Suwarrow Atoll (Northern Cook Islands, S.W. Pacifique). *Proceedings 5th International Coral Reef Symposium*, **3**, 137–140.

Shepard, F.P. (1961) Sea-level rise during the past 20,000 years. *Z. Geomorphol.*, N.F., Suppl.vol., **3**, 30–35.

Spencer, T., Stoddart, D.R. and **Woodroffe, C.D.** (1987) Island uplift and lithospheric flexure: observations and cautions from the South Pacific. *Z. Geomorphol,* N.F., Suppl. vol., **63**, 87–102.

Spencer, T., Stoddart, D.R., Woodroffe, C.D. and **Harmon, R.S.** (1988) Lithospheric flexure and raised reef limestones, S. Cook Islands. *Proceedings 6th International Coral Reef Symposium*, **3**, 485–489.

Stoddart, D.R. (1972) Reef islands of Rarotonga. *Atoll Res. Bull.*, **160**, 1–14.

Stoddart, D.R. and **Gibbs, P.E.** (1975) Almost-atoll of Aitutaki: reef studies in the Cook Islands, South Pacific. *Atoll Res. Bull.*, **190**, 1–158.

Stoddart, D.R., Spencer, T. and **Scoffin, T.P.** (1985) Reef growth and karst erosion on Mangaia, Cook Islands: a reinterpretation. *Z. Geomorphol,* N.F., Suppl. vol., **57**, 121–140.

Stoddart, D.R., Taylor, J.D., Fosberg, F.R. and **Farrow, G.E.** (1971) Geomorphology of Aldabra Atoll. *Phil. Trans. Roy. Soc. London*, **B260**, 31–65.

Turner, D.L. and **Jarrard, R.D.** (1982) K-Ar dating of the Cook-Austral Island chain: a test of the hot spot hypothesis. *J. Volcanol. Geoth. Res.*, **12**, 187–220.

Veeh, H.H. (1966) Th^{230}/U^{238} and U^{234}/U^{238} ages of Pleistocene high sea-level stand. *J. Geophys. Res.*, **71**, 3379–3386.

Ward, W.T., Ross, P.J. and **Colquhoun, D.J.** (1971) Interglacial high sea-levels – an absolute chronology derived from shoreline elevations. *Palaeogeogr. Palaeoecol. Palaeoclimatol.*, **9**, 77–99.

Wood, C.P. (1967) Geology of the Cook Islands. *NZ J. Geol. Geophys.*, **10**, 1429–1445.

Wood, C.P. and **Hay, R.F.** (1970) Geology of the Cook Islands. *NZ Geol. Surv. Bull.*, **82**, 1–103.

Woodroffe, C.D., Short, S.A., Stoddart, D.R., Spencer, T. and **Harmon, R.S.** (1991) Stratigraphy and chronology of late Pleistocene reefs in the southern Cook Islands, South Pacific. *Quatern. Res.*, **35**, 246–263.

Woodroffe, C.D., Stoddart, D.R., Spencer, T., Scoffin, T.P. and **Tudhope, A.W.** (1990) Holocene emergence in the Cook Islands, South Pacific. *Coral Reefs*, **9**, 31–39.

Woodroffe, C.D. and **Webster, J.M.** (2014) Coral reefs and sea-level change. *Mar. Geol.*, **352**, 248–267.

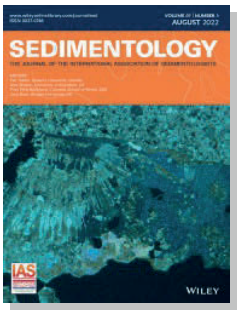
Yonekura, N., Ishii, T., Saito, Y., Maeda, Y., Matsushima, Y., Matsumotu, E. and **Kayanne, H.** (1988) Holocene fringing reefs and sea-level change in Mangaia Island, southern Cook Islands. *Palaeogeogr. Palaeoclimatol. Palaeoecol.*, **68**, 177–188.

International Association of Sedimentologists

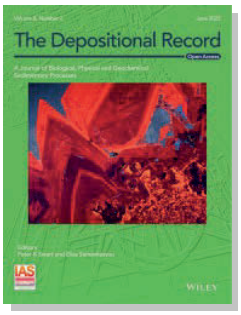
An International Non-Profit Organisation

www.sedimentologists.org

IAS PUBLICATIONS



Leading research journal
No submission fees



Fully Open Access



Leading research journal
No submission fees



Special Publications
Field Guides

IAS membership is open to everybody with an interest in any and all aspects of sedimentology, from modern processes and environments to deep-time rock records. Membership fees are very affordable - far less than for many other Professional geoscience societies

Scan to find out more...

MEMBERSHIP BENEFITS

- ✓**Access to the online version of** Sedimentology, Basin Research, and The Depositional Record, including all issues ever published and early view articles, and to most of the IAS Special Publications
- ✓Option to receive the **printed versions** of Sedimentology and Basin Research at **very favourable rates** and **large discount** on all print versions of IAS Special Publications
- ✓**Discounted subscription** to Journal of Petroleum Geology
- ✓Monthly IAS **electronic newsletter**
- ✓Reduced registration rates for Annual **IAS Regional Meetings**
- ✓Reduced registration rates for the **International Sedimentological Congress** every four years
- ✓Ability to apply for **sponsorship** for thematic meetings, workshops and short courses
- ✓**Early Career Scientists** can apply for **postdoctoral research grants**
- ✓Annual **Institutional grants** for capacity building in low- to middle-income countries
- ✓Access to the **IAS Members Directory** and to a network of IAS **Regional Correspondents**, as well as a **personalised profile space** on the IAS website to interact with other members
- ✓The **Friendship Scheme**, giving free membership to sedimentologists in low- to middle-income countries

ADDITIONAL STUDENT MEMBER BENEFITS

- ✓PhD student members can apply for **travel grants** to attend IAS sponsored meetings
- ✓PhD student members can apply for **research grants**
- ✓Masters student members can apply for dissertation fieldwork awards
- ✓International **Summer Schools** for PhD students with expert leaders in spectacular locations
- ✓**Special lecturer tours** by eminent sedimentologists to give talks and teach short courses

@sedimentologists **@sedimentology** **IAS沉积学之家** **International Association of Sedimentologists**